RECENT DEVELOPMENTS IN NEUROANATOMICAL TERMINOLOGY

EDITED BY: Hans J. ten Donkelaar and Luis Puelles
PUBLISHED IN: Frontiers in Neuroanatomy

frontiers Research Topics

Frontiers Copyright Statement

© Copyright 2007-2019 Frontiers Media SA. All rights reserved.

All content included on this site, such as text, graphics, logos, button icons, images, video/audio clips, downloads, data compilations and software, is the property of or is licensed to Frontiers Media SA ("Frontiers") or its licensees and/or subcontractors. The copyright in the text of individual articles is the property of their respective authors, subject to a license granted to Frontiers.

The compilation of articles constituting this e-book, wherever published, as well as the compilation of all other content on this site, is the exclusive property of Frontiers. For the conditions for downloading and copying of e-books from Frontiers' website, please see the Terms for Website Use. If purchasing Frontiers e-books from other websites or sources, the conditions of the website concerned apply.

Images and graphics not forming part of user-contributed materials may not be downloaded or copied without permission.

Individual articles may be downloaded and reproduced in accordance with the principles of the CC-BY licence subject to any copyright or other notices. They may not be re-sold as an e-book.

As author or other contributor you grant a CC-BY licence to others to reproduce your articles, including any graphics and third-party materials supplied by you, in accordance with the Conditions for Website Use and subject to any copyright notices which you include in connection with your articles and materials.

All copyright, and all rights therein, are protected by national and international copyright laws.

The above represents a summary only. For the full conditions see the Conditions for Authors and the Conditions for Website Use.

ISSN 1664-8714
ISBN 978-2-88963-126-1
DOI 10.3389/978-2-88963-126-1

About Frontiers

Frontiers is more than just an open-access publisher of scholarly articles: it is a pioneering approach to the world of academia, radically improving the way scholarly research is managed. The grand vision of Frontiers is a world where all people have an equal opportunity to seek, share and generate knowledge. Frontiers provides immediate and permanent online open access to all its publications, but this alone is not enough to realize our grand goals.

Frontiers Journal Series

The Frontiers Journal Series is a multi-tier and interdisciplinary set of open-access, online journals, promising a paradigm shift from the current review, selection and dissemination processes in academic publishing. All Frontiers journals are driven by researchers for researchers; therefore, they constitute a service to the scholarly community. At the same time, the Frontiers Journal Series operates on a revolutionary invention, the tiered publishing system, initially addressing specific communities of scholars, and gradually climbing up to broader public understanding, thus serving the interests of the lay society, too.

Dedication to Quality

Each Frontiers article is a landmark of the highest quality, thanks to genuinely collaborative interactions between authors and review editors, who include some of the world's best academicians. Research must be certified by peers before entering a stream of knowledge that may eventually reach the public - and shape society; therefore, Frontiers only applies the most rigorous and unbiased reviews.
Frontiers revolutionizes research publishing by freely delivering the most outstanding research, evaluated with no bias from both the academic and social point of view. By applying the most advanced information technologies, Frontiers is catapulting scholarly publishing into a new generation.

What are Frontiers Research Topics?

Frontiers Research Topics are very popular trademarks of the Frontiers Journals Series: they are collections of at least ten articles, all centered on a particular subject. With their unique mix of varied contributions from Original Research to Review Articles, Frontiers Research Topics unify the most influential researchers, the latest key findings and historical advances in a hot research area! Find out more on how to host your own Frontiers Research Topic or contribute to one as an author by contacting the Frontiers Editorial Office: researchtopics@frontiersin.org

RECENT DEVELOPMENTS IN NEUROANATOMICAL TERMINOLOGY

Topic Editors:
Hans J. ten Donkelaar, Radboud University Medical Center, Netherlands
Luis Puelles, Universidad de Murcia, Spain

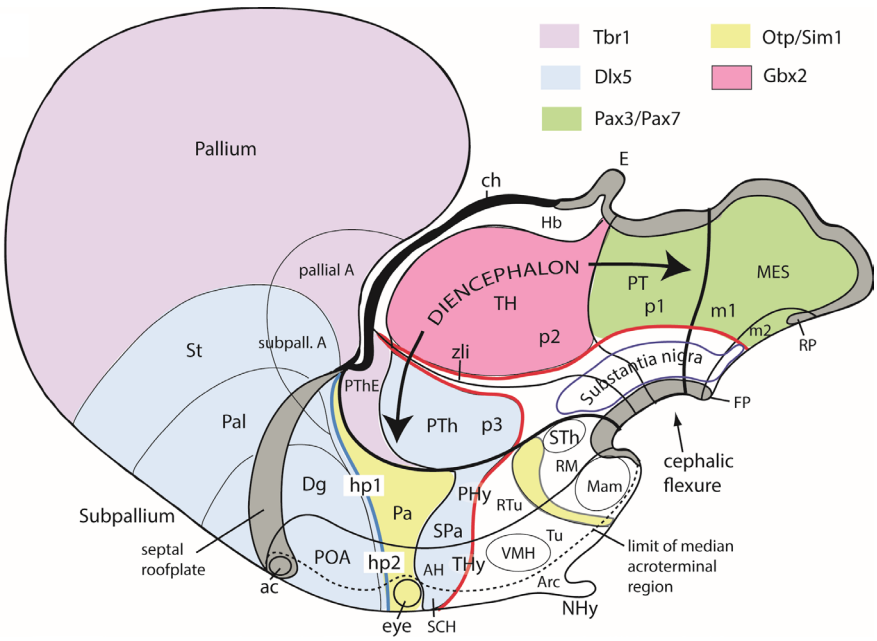

A recent update of the prosomeric approach to the brain.
Image: Figure 10 from Puelles L. (2019).

Puelles L (2019) Survey of Midbrain, Diencephalon, and Hypothalamus Neuroanatomic Terms Whose Prosomeric Definition Conflicts With Columnar Tradition. *Front. Neuroanat.* 13:20.
doi: 10.3389/fnana.2019.00020

The present series of papers are meant to provoke discussion on neuroanatomical terminology. After publication of the Terminologia Neuroanatomica (TNA 2017; http://FIPAT.library.dal.ca), recently ratified by the International Federation of Associations of Anatomists (IFAA), August 9 in London (UK), several neuroscientists were invited to give their views on this new official IFAA terminology. This resulted in 12 papers and one commentary on the following topics: (A) Further development of a developmental ontology; (B) Common terminology for cerebral cortex and thalamus; (C) White matter tracts; and (D) Neuron types. The suggestions made to

improve the TNA will be considered in the next version of the TNA. Neuroanatomical terminology should remain an actively ongoing endeavor and concerns all using this nomenclature, whether in Latin, English or other languages.

Citation: ten Donkelaar, H. J., Puelles, L., eds. (2019). Recent Developments in Neuroanatomical Terminology. Lausanne: Frontiers Media.
doi: 10.3389/978-2-88963-126-1

Table of Contents

CHAPTER D

NEURON TYPES IN THE CENTRAL NERVOUS SYSTEM AND SENSORY ORGANS

frontiers in Neuroanatomy

EDITORIAL
published: 07 August 2019
doi: 10.3389/fnana.2019.00080

Editorial: Recent Developments in Neuroanatomical Terminology

Hans J. ten Donkelaar[1]* *and Luis Puelles*[2]

[1] *Department of Neurology, Radboud University Medical Center, Nijmegen, Netherlands,* [2] *Department of Human Anatomy and Psychobiology, Facluty of Medicine, Universidad de Murcia, Murcia, Spain*

Keywords: terminology, prosomeric model, cerebral cortex, thalamus, neural progenitor cells, neuron types, tracts

Editorial on the Research Topic

Recent Developments in Neuroanatomical Terminology

A recent revision of the terminology of the sections titled the "Central nervous system" (CNS) and the "Peripheral nervous system" (PNS) within the *Terminologia Anatomica* (1998) and the *Terminologia Histologica* (2008) has been posted to the open part of the Federative International Programme for Anatomical Terminology (FIPAT) website (http://FIPAT.library.dal.ca) as the official FIPAT terminology for the nervous system, the *Terminologia Neuroanatomica* (TNA, 2017). A third chapter deals with the sensory organs. The major differences between the TNA and the TA and TH have been outlined in an introductory paper (ten Donkelaar et al., 2017). For an illustrated version of the TNA, see ten Donkelaar et al. (2018).

In general, the TNA uses a more natural hierarchical and embryologically-based classification of brain structures for the prosencephalon (forebrain), following the prosomeric model (Puelles, 2013; Puelles et al., 2013). Neuron types are implemented for all of the sections. Given these novelties, involving a framework change in the prevalent neuromorphological descriptive paradigm (that is, the current prosomeric model vs. Herrick's columnar model), and their potential impact on the future communication of neuroanatomical research results, the scientific community might profit from a wider discussion of the FIPAT's decisions. Accordingly, discussion focused on the following topics:

(A) **Further development of a developmental ontology**. Three papers discuss the further implementation of a developmental ontology into neuroanatomical terminology: (1) The subdivision of the forebrain based on embryological and genoarchitectonic studies; the forebrain is subdivided into the caudal prosencephalon, giving rise to the midbrain-diencephalon (midbrain, pretectum, thalamus with epithalamus, prethalamus, and related tegmental parts), and the rostral prosencephalon, giving rise to the hypothalamus, the eyes, and the entire telencephalon. Puelles' review surveys midbrain, diencephalic, and hypothalamic neuroanatomical concepts and various recent findings whose prosomeric pregnancy conflicts with columnar tradition, leaving a complex scenario with many terminological problems to be gradually resolved within the field. He also contributes an updated prosomeric concept of the diencephalic-telencephalic transition. (2) New definition of midbrain boundaries and corresponding alar subdivisions; the transgenic approach establishes a new concept of the isthmocerebellar or prepontine hindbrain (Watson et al., 2017), conventionally misidentified as a part of the midbrain. Another novel aspect touches the conventional pons, which is subdivided into prepontine, pontine, and retropontine or pontomedullary hindbrain neuromeric domains, restricting the term pons to the basilar part of the pons. The contribution by Watson et al. recommends a new brain stem nomenclature based on developmental gene expression, progeny analysis, and fate mapping. (3) In the TNA,

OPEN ACCESS

Edited and reviewed by:
Javier DeFelipe,
Cajal Institute (CSIC), Spain

***Correspondence:**
Hans J. ten Donkelaar
hans.tendonkelaar@radboudumc.nl

Received: *12 July 2019*
Accepted: *25 July 2019*
Published: *07 August 2019*

Citation:
ten Donkelaar HJ and Puelles L (2019) Editorial: Recent Developments in Neuroanatomical Terminology. Front. Neuroanat. 13:80. doi: 10.3389/fnana.2019.00080

a modernized version of the blood vessels of the brain with clinical subdivisions is included to ensure it contains a more or less complete list of terms for the human nervous system. The paper by Ferran's group attempts a prosomeric molecular-marker analysis of the early vascularization of the embryonic mouse forebrain and presents a tentative topological map relating human brain vessels to specifc segmental and dorsoventral units, also touching on some terminological issues (Puelles et al.).

(B) **Common terminology for cerebral cortex and thalamus**. Three papers deal with aspects of the nomenclature for the cerebral cortex and the thalamus: (1) one aiming for a common terminology for the gyri and sulci of the cerebral cortex (ten Donkelaar et al.); (2) a second on the cytoarchitectonic areas of the gyrus ambiens (Insausti et al.), incorporating the Brodmann area 34 into the entorhinal cortex; and (3) a third on subdivisions for the thalamic nuclei. Mai and Majtanik contributed an extensive review of the various terminologies used for thalamic nuclei, using a new volumetric approach to characterize the significant subdivisions, normalizing the individual thalamus shapes in MNI space, which allows comparison of the nuclear regions delineated by the different authors. Their final scheme of the spatial organization provided the frame for the selected terms for the subdivisions of the human thalamus using on the (modified) terminology of the TNA.

(C) **White matter tracts**. Two papers deal with white matter tracts, which in the TNA follows the Swanson and Bota (2010) classification as central roots, intrinsic tracts, commissural connections and long tracts, divided into ascending and descending tracts: (1) Baud et al. address a new scheme for the representation of white matter in the CNS. In this approach, white matter is directly attached to the CNS, and no longer considered part of the brain segments. The new classification of white matter tracts selects the origin as the primary criterion and the type of tract as the secondary criterion. It follows a top-down approach from telencephalon to spinal cord; (2) Mandonnet et al. discuss the nomenclature of the human white matter association pathways and propose a new nomenclature based on the structural wiring diagram of the human brain; and (3) in a Commentary, Panesar and Fernández-Miranda emphasize that cortical connectivity should be identified on the basis of their origin, termination and axonal properties.

(D) **Neuron types**. In the TNA, the terms for the various types of neurons provided by Bota and Swanson (2007) are used. Three papers deal with aspects of this topic: (1) one on auditory nomenclature, combining name recognition with anatomical description, which should help future generations in learning the structure-function correlates of the inner ear more easily (Fritzsch and Elliott); (2) a second on neural progenitor cell (NPC) nomenclature, including embryonic and adult precursor cells of the cerebral cortex and the hippocampus, increasing our knowledge of what is ultimately most important, i.e., understanding NPC function in the developing as well as in the adult CNS (Martínez-Cerdeño and Noctor); and (3) a major one on neuron names in a gene- and property-based format, with special reference to cortical neurons (Shepherd et al.). Precision in neuron name is increasingly needed now that we are entering a new era in which classic anatomical criteria are only the beginning of defining the identity of a neuron. New criteria include patterns of gene expression, membrane properties, neurotransmitters and neuropeptides, and physiological properties. Related to this topic is (4) a paper on navigating the murine brain aimed toward best practices for determining and documenting neuroanatomical locations in experimental studies (Bjerke et al.).

The suggestions made to improve the TNA will be considered in the next version of the TNA. Neuroanatomical terminology remains an actively ongoing endeavor.

AUTHOR CONTRIBUTIONS

HtD and LP designed the Research Topic, invited contributors and edited most of the manuscripts.

ACKNOWLEDGMENTS

With pleasure, we acknowledge the efforts made by Kathleen Rockland, Marcello Rosa, Alberto Muñoz, Paul Manger, and Javier DeFelipe, editing those manuscripts in which the editors of this Research Topic were involved, and naturally all the reviewers who greatly improved the quality of the manuscripts.

REFERENCES

Bota, M., and Swanson, L. W. (2007). The neuron classification problem. *Brain Res. Rev.* 56,79–88. doi: 10.1016/j.brainresrev.2007.05.005

Puelles, L. (2013). "Plan of the developing vertebrate nervous system. Relating embryology to the adult nervous system," in *Comprehensive Neuroscience*, eds P. Rakic and J. L. R. Rubinstein (New York, NY: Elsevier), 187–209.

Puelles, L., Harrison, M., Paxinos, G., and Watson, C. (2013). Forebrain gene expression domains and the evolving prosomeric model. *Trends Neurosci.* 36, 570–578. doi: 10.1016/j.tins.2013.06.004

Swanson, L. W., and Bota, M. (2010). Foundational model of structural connectivity in the nervous system with a schema for wiring diagrams, connectome, and basic plan architecture. *Proc. Natl. Acad. Sci. U.S.A.* 107, 20610–20617. doi: 10.1073/pnas.1015.128107

ten Donkelaar, H. J., Broman, J., Neumann, P. E., Puelles, L., Riva, A., Tubbs, R. S., et al. (2017). Towards a Terminologia Neuroanatomica. *Clin. Anat*. 30, 145–155. doi: 10.1002/ca.22809

ten Donkelaar, H. J., Kachlik, D., and Tubbs, R. S. (2018). *An Illustrated Terminologia Neuroanatomica: A Concise Encyclopedia of Human Neuroanatomy*. Heidelberg: Springer.

TNA (2017). *Terminologia Neuroanatomica*. Federative International Programme for Anatomical Terminology. Available online at: http://FIPAT.library.dal.ca

Watson, C., Shimogori, T., Puelles, L. (2017). Mouse Fgf8-Cre-LacZ lineage analysis defines the territory of the postnatal isthmus. *J. Comp. Neurol*. 525, 2783–2799. doi: 10.1002/cne.24242

Conflict of Interest Statement: The authors declare that the research was conducted in the absence of any commercial or financial relationships that could be construed as a potential conflict of interest.

Copyright © 2019 ten Donkelaar and Puelles. This is an open-access article distributed under the terms of the Creative Commons Attribution License (CC BY). The use, distribution or reproduction in other forums is permitted, provided the original author(s) and the copyright owner(s) are credited and that the original publication in this journal is cited, in accordance with accepted academic practice. No use, distribution or reproduction is permitted which does not comply with these terms.

frontiers in Neuroanatomy

REVIEW
published: 27 February 2019
doi: 10.3389/fnana.2019.00020

Survey of Midbrain, Diencephalon, and Hypothalamus Neuroanatomic Terms Whose Prosomeric Definition Conflicts With Columnar Tradition

*Luis Puelles**

Departamento de Anatomía Humana y Psicobiología, IMIB-Arrixaca Biomedical Institute, University of Murcia, Murcia, Spain

Recent neuroanatomic concepts and terms referring to the non-telencephalic forebrain are presented and discussed, in context with the present scenario in which the old columnar paradigm is being substituted by the prosomeric model, largely on the basis of novel molecular and experimental evidence.

Keywords: columnar model, prosomeric model, neuroanatomical advances, novel anatomic terms, forebrainterminology, forebrain axis, lamina affixa, thalamo-striatal sulcus

OPEN ACCESS

Edited by:
Alberto Munoz, Complutense University of Madrid, Spain

Reviewed by:
Ramon Anadon, University of Santiago de Compostela, Spain
Fernando Martinez-Garcia, University of Jaume I, Spain
Enrique Saldaña, University of Salamanca, Spain

***Correspondence:**
Luis Puelles
puelles@um.es

Received: *30 October 2018*
Accepted: *04 February 2019*
Published: *27 February 2019*

Citation:
Puelles L (2019) Survey of Midbrain, Diencephalon, and Hypothalamus Neuroanatomic Terms Whose Prosomeric Definition Conflicts With Columnar Tradition. Front. Neuroanat. 13:20. doi: 10.3389/fnana.2019.00020

> "Since some variety, including that of terminology and spelling, may be regarded as the 'spice of life,' I nevertheless prefer to write 'piriform' [instead of 'pyriform] without prejudice to the preference of others"
>
> Kuhlenbeck (1973).
>
> (The Central Nervous System of Vertebrates, Vo l3., Part II., footnote 289, p.668).

INTRODUCTION

Forebrain neuroanatomic terms used widely during the last 100 years are typically adapted to the *columnar model* of the forebrain, which was first proposed by Herrick (1910) in amphibia and reptilia (review in Herrick, 1948), and was later extrapolated to amniote and several anamniote vertebrates by Kuhlenbeck in the twenties, thirties and beyond (review in Kuhlenbeck, 1973). Many other authors also contributed to this development, particularly with work on diverse mammals, converting this model in the predominant neuroanatomic paradigm until its recent decline. Indeed, the advent of brain molecular marker results accruing since the 1980s has increasingly elicited a concern about the lack of explanatory value and scarce present utility of the columnar model. The change is due in essence to the increasing need to have meaningful morphologic interpretations of gene expression patterns and functions in the brain. The columnar model has revealed itself unwieldy and generally unsatisfactory for aiding the spatially-oriented understanding of observed genoarchitectonic patterns, as well as for extracting causal interpretations of experimental developmental results and transgenic mutant phenotypes (**Figures 1A,B, 2–6**).

The literature since 1990 shows practically no example of straightforward application of the columnar model to gene expression or mutant phenotype analysis, and the few instances are considered difficult to understand (e.g., Alvarez-Bolado et al., 1995). It has been less obvious that the capacity of the columnar model to inspire insight on brain functions has also reached a low ebb. This capacity seemed high initially, but it gradually was realized that it stood on a simplistic basis, i.e., Herrick (1910) objective to explain forebrain functions as an extension of brainstem columnar

functions related to visceral and somatic cranial nerve components. This scenario has led to the substitution of the aged columnar model by more powerful segmental brain models. The latter are historically older (see Orr, 1887; McClure, 1890; Locy, 1895; von Kupffer, 1906; Ziehen, 1906), but had practically been relegated to oblivion under the influence of the dominant columnar model. The modern version of such segmental (neuromeric) models is the *prosomeric model* (**Figure 1B**; Puelles and Rubenstein, 1993, 2003, 2015; Rubenstein et al., 1994; Puelles, 2013), which embodies a corrected and expanded version of the earlier neuromeric model of Palmgren (1921) and Rendahl (1924). This model's name derives from *prosomeres*, understood as neuromeric developmental units of the prosencephalon or forebrain (irrespective that the model also deals with rhombomeres in the hindbrain; note the prosomeric forebrain also includes the midbrain, whose prosomeres are also called "mesomeres").

The theoretic underpinnings of forebrain neuromorphology became molecular during the last 40 years, and in so doing registered a readjustment which fundamentally rests on a different axis concept and the role played by neuromeres transverse to that axis (**Figures 2A,B**). This implied a significant paradigm change in brain neuroanatomy that is still being assimilated as new generations of neuroscientists enter the field. The new paradigm is already prevalent in the subfields of developmental and evolutionary/comparative neuromorphology (Puelles et al., 2013, 2018; Nieuwenhuys and Puelles, 2016). Colleagues that do not follow closely the developmental advances accrued in this field may not see yet the reasons why

Abbreviations: 3, oculomotor nerve; 4, trochlear nerve; 5, trigeminal nerve root; 6, abducens nerve root; 7, facial nerve root; 8, cochleovestibular nerve root; ABasM, median anterobasal nucleus; ABasW, anterobasal wing; ac, anterior commissure; AC, nucleus of the anterior commissure; AD, dorsal alar region; AH, anterior hypothalamic nucleus; AHP, peduncular (posterior) part of anterior hypothalamic nucleus; AL, lateral alar region; AP, alar plate; APT, anterior pretectal nucleus; Arc, arcuate nucleus; ArcW, arcuate wing; av, anteroventral thalamic area; AVL, ventrolateral alar region; BI, intermediate basal region; BIC, brachium of the inferior colliculus; BL, lateral basal region; BM, medial basal region; BP, basal plate; BSC, brachium of the superior colliculus; BST, bed nucleus of the stria terminalis (supracapsular); c.p., posterior commissure; Cb, cerebellum; Cd, caudate tail; CERVEL., cerebellum; ch, chorioidal roof; CIC, central nucleus of inferior colliculus; Cn, cuneate nucleus; CnG, central gray; Co, cochlear column; com.post, posterior commissure; CoPT, commissural pretectum; CPa, central part of main paraventricular nucleus; DCIC, dorsal nucleus of inferior colliculus; Dg, diagonal area; DHyB, diencephalo-hypothalamic boundary; Di, diencephalon; Dien, diencephalon; Dk, nucleus of Darkschewitsch; DLTg, dorsolateral tegmental nucleus; DMcP, Dorsomedial core, peduncular part; DMcT, dorsomedial core area, terminal part; DMsP, dorsomedial shell area, peduncular part; DMsT, dorsomedial shell area, terminal part; DPa, dorsal part of main paraventricular nucleus; DpG, deep (central) gray; DPM, dorsal premamillary nucleus; DPML, lateral stratum of DPM; DR, dorsal raphe nucleus; DTg, dorsal tegmental nucleus; DTh, dorsal thalamus; E, epiphysis; e.e., epiphyseal evagination; e.x., habenular commissure; ECIC, external nucleus of inferior colliculus; em.th, eminentia thalami; ep, epiphysis; EPIPH, epiphysis; ETh, epithalamus; f.r., fasciculus retroflexus; FP, floor plate; fx, fornix tract; H, habenula; h.s-t.r., habenulo-subthalamic ridge (zona limitans); hab, habenula; HB, habenula; Hb, habenula; hp1-hp2, hypothalamo-telencephalic prosomeres 1-2; HTh, hypothalamus; hy., hypothalamus; IC, inferior colliculus; IC, interstitial nucleus of Cajal; ICbP, inferior cerebellar peduncle; ICo, intercollicular nucleus; IF, interpeduncular fossa; InG, intermediate gray; IP, interpeduncular nucleus; IR, rostral interstitial nucleus; JcPT, juxtacommissural pretectum; LA, lateral anterior nucleus; lc, lamina cornea (BST); LCh, laterochiasmatic nucleus; LCo, locus coeruleus; LG, lateral geniculate nucleus; LGN, lateral geniculate nucleus; LiC, nucleus linearis caudalis; LLD, dorsal lateral lemniscal nucleus; LLV, ventral lateral lemniscal nucleus; LM, lateral mamillary nucleus; m, mamillary body; m1-m2, mesencephalic prosomeres or mesomeres 1-2; ma, mamillary body; Mam, mamillary body; MB, mamillary body; MCbP, middle cerebellar peduncle; MDB, mesencephalo-diencephalic boundary; ME, median eminence; Med, medulla; Mes, mesencephalon; mesV, mesencephalic trigeminal nucleus; MG, medial geniculate nucleus; mge, medial ganglionic eminence; MHB, midbrain-hindbrain boundary; MM, medial mamillary nucleus (ventral part); MPO, medial preoptic nucleus; MT, medial terminal nucleus; mtg, mamillotegmental tract; mth, mamillothalamic tract; MTu, medial tuberal nucleus; n.h., nucleus habenulae; NA, nuclei of amygdala (medial); NH, neurohypophysis; NHy, neurohypophysis; och, optic chiasma; OPT, olivary pretectal nucleus; ot, optic tract; P.AL., alar plate; P.BAS:, basal plate; p.d.th.m., pars dorsalis thalami (middle part); p.i.d., pars intermedia diencephali (pretectum); p.v.th., pars ventralis thalami; p1–p3, diencephalic prosomeres 1-3; p1PAG, pretectal periaqueductal gray; p1Tg, pretectal tegmentum; p2Tg, thalamic tegmentum; p3Tg, prethalamic tegmentum; Pa, paraventricular hypothalamic area; pa, paraventricular hypothalamic area; PAG, periaqueductal area; Pal, pallidum; pallial A, pallial amygdala; PaR, pararubral nucleus; PB, parabrachial nucleus; PBas, posterobasal nucleus; PBG, parabigeminal nucleus; pc, posterior commissure; pc, posterior commissure; PCMc, magnocellular nucleus of the posterior commissure; PCPc, parvocellular nucleus of the posterior commissure; PcPT, precommissural pretectum; pd, posterodorsal thalamic area; Ped, peduncle; PHTh, posterior hypothalamus; PHy, peduncular hypothalamus; PL.V., floor plate; PLTg, posterolateral tegmental nucleus; pm, perimamillary area; PM, perimamillary nucleus (dorsal premamillary n.); Poa, preoptic area; POA, preoptic area; poa, preoptic area; PPa, peduncular paraventricular area; PPn, pedunculopontine nucleus; PreIsth, preisthmus; pret, pretectum; prm, periretromamillary area; PRM, periretromamillary nucleus; PRML, lateral stratum of PRM; PRuTg, prerubral tegmentum; PSPaZ, peduncular subparaventricular zone; PT, pretectum; pt, pretectum; PTh, prethalamus; pth, prethalamus; PThE, prethalamic eminence; pthe, prethalamic eminence; R, rhombencephalon; r.m., mamillary recess; r0-r11, rhombomeres 0-11; rf, retroflex tract; rf, retroflex tract; Rh, rhombencephalon; rm, retromamillary area; RM, retromamillary area; RMC, magnocellular red nucleus; RML, lateral retromamillary nucleus; RMM, medial retromamillary nucleus; RP, roof plate; RPa, rostral paraventricular area; RPC, parvocellular red nucleus; Rt, reticular nucleus (prethalamus); rtu, retrotuberal area; RTuV, ventral retrotuberal area; RuMc, magnocellular red nucleus; RuPc, parvocellular red nucleus; S.TH.M., sulcus thalami medius; S.THAL.VEN., sulcus thalami ventralis; SbPO, subpreoptic nucleus; SC, spinal cord; SC, superior colliculus; SCbP, superior cerebellar peduncle; SCH, suprachiasmatic nucleus; SCH, suprachiasmatic nucleus; SDD, sulcus diencephali dorsalis; SDM, sulcus diencephali medius; SdV, descending sensory trigeminal nucleus; SDV, sulcus diencephali ventralis; se, septum; Sec.Pros., secondary prosencephalon; SL, sulcus limitans; SNR, substantia nigra; SPa, subparaventricular hypothalamic area; spa, subparaventricular hypothalamic area; SpV, principal sensory trigeminal nucleus; St, striatum; s-t., subthalamus; std, sulcus thalami dorsalis; STh, subthalamic nucleus; stm, sulcus thalami medius; stv, sulcus thalami ventralis; SubB, subbrachial nucleus; subpall. A, subpallial amygdala; tc, tectal commissure; Tel, telencephalon; TG, tectal gray; tg, tegmentum; tgc, tectal gray commissure; Tgp (Fi), fimbria hippocampi; TGPC, tectal gray paracommissural nucleus; Th, thalamus; TH, thalamus; th, thalamus; th.1, thalamic bulge 1 (prethalamus); th.2, thalamic bulge 2 (thalamus); TH.D, dorsal thalamus; TH.V., ventral thalamus; THy, terminal hypothalamus; TPa, terminal paraventricular area; TPCD, tectal paracommissural dorsal nucleus; TPCV, tectal paracommissural ventral nucleus; tpt, tractus peduncularis transversus; tpth, taenia prethalamica; TSO, terminal supraoptic nucleus; TSPaZ, terminal subparaventricular zone; tst, taenia striae terminalis; tth, taenia thalami; Tu, tuberal area; tu, tuberal area; TuSbO, tuberal suboptic nucleus; TuV, tuberal ventral area; U, uncus; v.t., velum transversum; VEL.TR., velum transversum; Vest, vestibular column; VM, ventromedial nucleus; VMH, ventromedial hypothalamic nucleus; VMs, shell of ventromedial nucleus; VPa, ventral part of main paraventricular nucleus; VPM, ventral premamillary nucleus; VTA, ventral tegmental area; VTg, ventral tegmental nucleus; VTh, ventral thalamus; zi, zona incerta (prethalamus); ZIR, rostral zona incerta; zli, zona limitans intrathalamica; Zr, reticular nucleus.

this change to the prosomeric model is convenient and necessary.

A number of columnar neuroanatomic *terms* unfortunately need to be adapted to the logic of the prosomeric model, in order to obtain full fruits of its heuristic potency. Side-by-side comparison of the columnar and prosomeric models shows roughly a 90° difference in the definition of the brain axis in the rostral forebrain, as well as sizeable differences in the rostral and caudal delimitation of the midbrain (**Figures 1A,B**; Puelles and Rubenstein, 2015). Fundamental regions of the forebrain such as midbrain, diencephalon (including pretectum, thalamus and prethalamus), and hypothalamus have now subtly different prosomeric definitions. Therefore, I am not writing about whimsical altering of terminology here or there. We deal with a major paradigmatic change in the whole of neuromorphology produced thanks to the evidence of hundreds of gene markers and a mass of experimental results accrued during the last 40 years. We obviously must argue against the traditional terminological conservativeness of neuroanatomists, but, given that scientists will continue to communicate with each other using words, the consequent adjustments will be accepted sooner or later, as happened with important name changes accepted in the past. For instance, the term "hypothalamus" was a neologism as recently as 1893 (His, 1893), substituting the earlier name of "subthalamus" (Forel, 1877).

It is clear that many forebrain anatomic descriptors (e.g., dorsal, ventral, rostral, caudal, anterior, posterior) need to be adjusted to the different axial reference (**Figures 1A,B**), and some well-known neural structures must be ascribed to natural regions of the brain different than those assumed classically (e.g., the subthalamic nucleus, is a retromamillary derivative found in the retrotuberal basal hypothalamus). One can translate mentally to some extent the new morphologic meaning of the anatomic entities. However, the newer generations will surely prefer more direct and pragmatic general solutions, and I leave aside the important fact that we absolutely will need such solutions in any computerized *ontologies*, since databases are not able to translate mentally. We do not want databases to fix forever the meanings of descriptors, or how we call items in the brain, since terminologies imply theories, hypotheses and assumptions, and these at least will surely change. I believe terminological adaptation to the present paradigm change will emerge gradually, at its own pace, driven by the inevitable semantic needs resulting from continued scientific activity. Old vitiated terms will be found increasingly confusing due to their false implications or assumptions, and will be gradually left aside, to the benefit of more exact alternative terms, wherever they come from. Accordingly, it would be premature at the present time to pretend to offer a fully developed system of solutions to this complex problem (Puelles L. et al., 2012a commented on changes needed for the future hypothalamus concept, whose proposal seems presently impossible; likewise, Puelles, 2016 covered the new midbrain concept, and also proposed some urgent related terminology changes; the present essay will be partly based on these accounts). Probably a diversity of conceivable alternative terms will emerge as more authors start attending to this issue. More and more colleagues will discover that they are being short-changed into confused ideas by the old terminology and/or model. Irrespective that we probably will suffer a transitional chaotic period in semantics (see a remarkable example in Xie and Dorsky, 2017 on the hypothalamus, where both inconciliable columnar and prosomeric models are used at cross-purposes), the new proposals surely will be amply discussed for cogency and usefulness. Eventually, at some point in the future, a new forebrain neuroanatomic nomenclature agreeing or not with the prosomeric model will be convened upon by an international congregation of experts.

The present essay aims to explore in a preliminary way this scenario, first presenting some of the criticisms addressed nowadays to the columnar length axis, which underpin in my opinion the cited paradigm change (**Figures 1A,B**), and then commenting on the nature of the problems raised at each major forebrain region. Selected examples of potentially changeable terms will be discussed. It will be seen that some aspects of neuroanatomic terminology are changing already, or were changed tentatively in recent times, in order to adapt to the new neuromorphological thinking made possible by the prosomeric model (more on this rationale in Puelles E. et al., 2012a; Puelles et al., 2012b, 2013; Puelles L. et al., 2012a; Puelles, 2013; Puelles and Rubenstein, 2015; Nieuwenhuys and Puelles, 2016).

PROBLEMS WITH THE COLUMNAR FOREBRAIN AXIS AND THE DEFINITION OF LONGITUDINAL COLUMNS IN THE FOREBRAIN

In proposing his columnar model Herrick (1910) contradicted widely accepted ideas on the forebrain length axis which had been systematized shortly before by Orr (1887); His (1893, 1895, 1904); Ziehen (1906), and Johnston (1906, 1909). Herrick postulated that the length axis of the brain (and its landmark, the sulcus limitans of His, dividing alar and basal longitudinal zones) might end in the telencephalon, rather than in the preoptic recess, as the earlier authors had uniformly assumed (**Figure 1A**; compare **Figures 2A**, **4**, **6**). The diencephalon of Herrick was thus a full transverse sector of the neural tube intercalated between the telencephalon, rostrally, and the midbrain, caudally, and included ventrally the hypothalamus (M, Di, Tel, HTh; **Figure 1A**, see also **Figure 3**). Herrick's (1910) main interest lay in defining a *dorsoventral* subdivision of the diencephalon into four *longitudinal columns* (*epi*thalamus [ETh], *dorsal* thalamus [DTh], *ventral* thalamus [VTh], and *hypo*thalamus [HTh]; **Figure 1A**). The words in cursive in the previous sentence correspond to descriptors whose morphologic meaning within columnar interpretation applies the columnar axis concept. The referred forebrain domains do not have the same topologic meaning in the prosomeric model (**Figure 1B**). The columnar axis was in any case a theoretic construct, because it was not morphologically visible in terms of landmarks, and, moreover, its assumed straightness was contradicted sharply by the cephalic flexure (**Figures 2**, **3**). In Herrick's subsequent work, and that of many of his followers, the

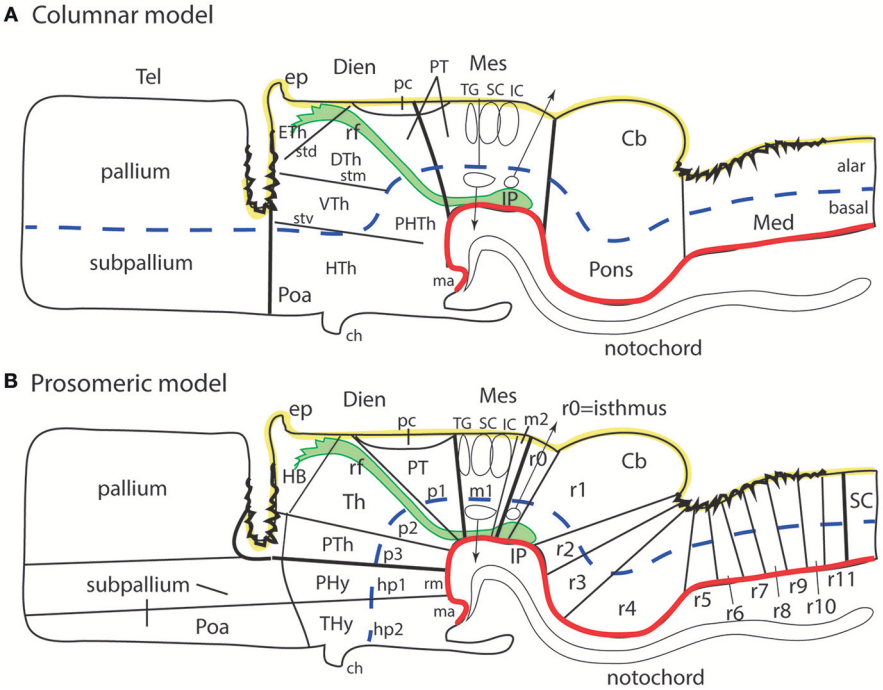

FIGURE 1 | Schematic comparison of the columnar and prosomeric models (original drawing). The same basic drawing shows in both cases telencephalon (Tel), diencephalon (Dien), mesencephalon (Mes), cerebellum (Cb), pons, and medulla (Med), as well as the notochord, the floor plate (as defined molecularly and by a glial palisade; in red), the roof plate inclusive of chorioidal plexi yellow background with black irregular domains, and the alar-basal boundary (thick blue dash line), which divides the alar and basal longitudinal zones. The retroflex tract descending from the habenula to the interpeduncular nucleus (rf, IP; green) is also depicted. Differences between the two schemata refer to the boundaries limiting large regions one from another (thick black lines) and boundaries separating subdivisions (columns or neuromeres), representing either ventricular sulci or ridges (thin black lines). **(A)** Columnar model: Here I used the recent version of the columnar model used by Swanson (2012), because he reasonably accepts a bending of the alar-basal boundary around the cephalic flexure (see blue dash line and its curve parallel to the floor in red); this axis landmark later ascends arbitrarily in front of the ventral thalamus (VTh) into the telencephalon, separating there pallium from subpallium. Note this model includes a tegmental posterior hypothalamus that reaches the midbrain next to the retroflex tract (PHTh), and expands rostrally into the standard hypothalamus (HTh). This model divides the hindbrain merely into medulla and cerebello-pontine complex. The midbrain is larger in this model, because it encompasses isthmic and prepontine formations caudally (including the trochlear nucleus/nerve and the interpeduncular complex; IP), and pretectal formations rostrally (caudal half of pretectum rostral to the tectal gray (TG), and the parvocellular red nucleus -not shown). Note the rostral midbrain limit passes through the middle of the posterior commissure (pc) and is not strictly transversal (= outdated His (1893) limit; compare **Figure 2A**). This model does not postulate a specific limit between the pretectum and the dorsal thalamus and epithalamus, but other columnar sources accept it passes behind the retroflex tract (rf). The columnar diencephalic subdivisions show parallel sulci thalami medius and ventralis (stm, stv) which delimit HTh, VTh, and DTh. The std (sulcus thalami dorsalis) separates DTh from epithalamus (ETh), but it does not course parallel to the others. The topological relationship of these sulci relative to the axial landmark (blue dash line) is variable: the std is parallel to it, thus being the only truly longitudinal diencephalic sulcus in this model; the stm is orthogonal to the axis, while the stv can be seen as parallel to the axial reference ascending into the telencephalon, or as orthogonal to the sulcus limitans. Inconsistently with the supposed longitudinal nature of the DTh and VTh columns, the schema shows that they reach the roof plate at one end and point into the floor plate at the other end. This is why authors such as Kappers (1947) interpreted these "columns" as transversal domains (see **Figure 6A**). The hypothalamus extends beyond the rostral end of the epichordal floor plate at the mamillary body, so that it needs *ad hoc* causal underpinnings for justifying the implied more rostral extent of dorsoventral patterning. **(B)** Prosomeric model: All the neuromeric units are included, highlighting their regular topology with regard to the floor plate (red), the alar-basal boundary (blue), and the roof plate (yellow; note the roof plate extends farther in the telencephalon, along the commissural septum, finally building a roof for the preoptic area (Poa) at the anterior commissure level; this telencephalic roof relationship is also incongruent with the columnar axial concept). The prosomeric model recognizes many more subdivisions in the brainstem, and notably ascribes the pons (r2-r4) to different rhombomeres than the cerebellum (r0, r1), as indicated by fate mapping. The prepontine hindbrain (r0, r1) is thus distinguished from the midbrain, which consequently results reduced in size and contents. The rostral midbrain limit passes behind the posterior commissure. Note the interpeduncular complex now lies in the prepontine hindbrain (IP). The m2 mesomere represents the novel preisthmus concept. As regards the diencephalon, it can be easily seen that basically the same regions are interpreted in a different and more solid topologic framework supported by gene expression patterns. There appears a diencephalic tegmental (basal) region, which contains part of the mesodiencephalic substantia nigra and ventral tegmental area. The hypothalamic floor is restricted to retromamillary and mamillary subdomains (rm, ma). The entire forebrain complex, from secondary prosencephalon to caudal midbrain, is divided into alar and basal territories.

abandonment of His's alar-basal axial sulcal landmark led to parallel underplaying of the important alar-basal histogenetic difference in the diencephalic wall. This is precisely one aspect of reality that genes—particularly *Shh* expressed throughout the forebrain basal plate and various other Shh-related genes (**Figures 5A–C**)—have modernly corroborated, reinforcing our present prosomeric belief that Herrick's "longitudinal columns" actually are *transversal* entities (**Figures 4–6**).

Another relevant point we have learned with the genes in hand is that true regional boundaries of brain progenitor domains

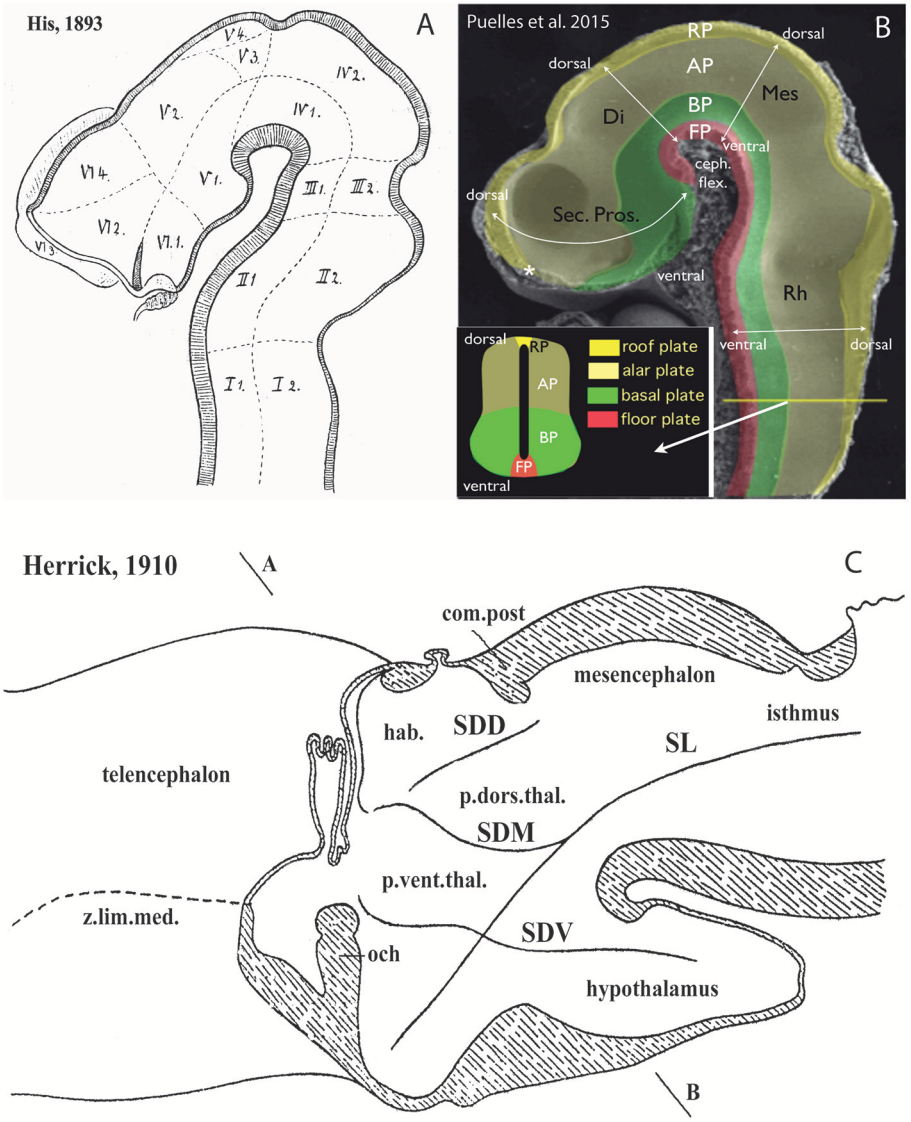

FIGURE 2 | Longitudinal vs. transversal neural tube directions in the conceptions of His (1893) **(A)**; Martínez et al. (2012) and Puelles et al. (2015) **(B)**; and Herrick (1910) **(C)** (no copyright permission required). **(A)** The pioneering view of His (1893) illustrates his original notion of axial longitudinal zones (floor, basal, alar, and roof plates) found throughout the brain; the common alar-basal boundary coincides with his *sulcus limitans*, which represents heterochronic differential neurogenesis prevalent at the basal plate (the sulcus is formed in early human embryos due to intraventricular bulging of the neurogenetically precocious basal plate, i.e., the set of domains I-VI numbered 1; the remaining domains represent the alar plate). A marked cephalic flexure is represented, and the axial landmark zones (floor, basal, alar, and roof plates) all bend around it, indicating a *bent* brain length axis. Theoretically transversal limits between the domains I–VI are also marked. Note the definition of an isthmic segment at the rostral end of the hindbrain (identified as III1 + III2). The midbrain (IV1 + IV2) appears delimited from the diencephalon *sensu stricto* (V1–V4) by a tentative oblique plane (later non-corroborated) that jumps from the middle of the posterior commissure to the mamillary body neighborhood. The hypothalamus was first defined by His in this schema as the sum of the V1 and VI1 domains, both entirely within the basal plate. The boundary separating V from VI has later been validated for the alar domains, but not for the basal ones. V1 underlies the alar "thalamus" and "epithalamus" (thalamic hypothalamus), while VI1 underlies the preoptic recess (optic hypothalamus) as well as the striate and parolfactory bodies (subpallium; VI2, VI3); the subpallium was accordingly held to reach the rostral part of the alar-basal boundary, at the preoptic recess (VI4 represents the telencephalic pallium). **(B)** This image, extracted from book chapters published in 2012 and 2015, shows the prosomeric assumptions about the longitudinal organization of the neural tube in a mouse embryo, which follow closely the model of His. The only difference is that the longitudinal zones are defined by primary early gene markers (rather than secondary differentiation patterns) and the rostral end of the alar-basal limit ends under the prospective optic chiasma, rather than at the preoptic recess (the sulcus limitans only approximates the primary (molecular) alar-basal boundary, due to its tertiary growth-related nature). In this image the floor (FP) is red, the basal plate (BP) green, the alar plate (AP) light yellow, and the roof plate (RP) strong yellow (see also the explanatory inset, a cut at spinal cord level); an asterisk marks the roof's rostral end at the prospective anterior commissure. White arrows indicate the changing dorsoventral dimension due to the cephalic flexure of the brain axis. The floor ends rostrally at the mamillary pouch (correlative with an initial chordal induction and the early position of the notochordal tip). The rostral neural line extending dorsoventrally from the asterisk (roof) to the mamillary body (floor) represents

(Continued)

FIGURE 2 | the novel prosomeric notion of "acroterminal area." **(C)** Modified drawing showing the alternative columnar model of Herrick (1910), as defined in an adult urodele. This initial study of Herrick still admitted the sulcus limitans of His (SL, compare with **A,B**), but no longer depicted it as closely following in curvature the cephalic flexure; it was implied not to represent an axial landmark, and was wholly disregarded in subsequent work. The axial landmark role was assigned to the sulcus diencephali medius (SDM) and sulcus diencephali ventralis (SDV) (otherwise also known as "thalamic" sulci), arbitrarily held to separate "longitudinal columns' identified as hypothalamus, pars ventralis thalami (p.vent.thal.) and pars dorsalis thalami (p.dors.thal.). An additional sulcus nearly orthogonal to the SDM, which separates the habenular region or epithalamus (hab.) from the p.dors.thal, was taken as sulcus diencephali dorsalis (SDD). Note the SDD finishes roughly under the posterior commissure (com.post.), thus implying that the pretectum (not identified) was half epithalamic and half dorsal thalamic. Remarkably, both SDM and SDV are clearly orthogonally disposed relative to the sulcus limitans, as well as to the forebrain roof and floor plates (check also **A,B**), and they are not continuous either with the midbrain or with the telencephalon. Their topology with regard to the cephalic flexure is vaguely represented.

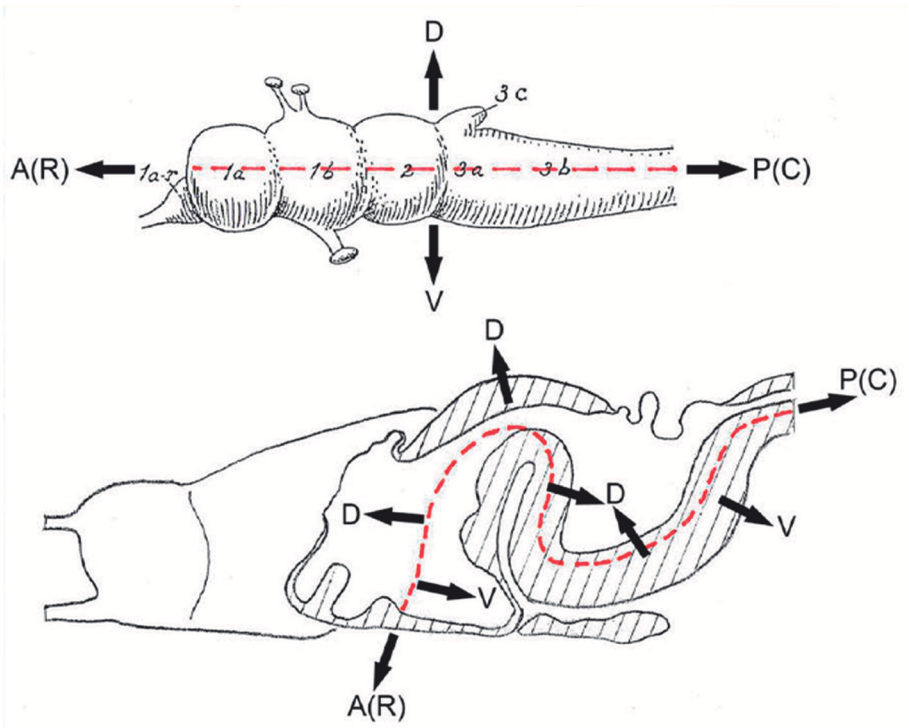

FIGURE 3 | These two schemata are copied from Nieuwenhuys and Puelles (2016) (plate 50) (no copyright permission required). They highlight the crucial difference in the axial morphological reference for the brain used by columnar authors as compared to neuromeric authors following His (1893). The upper *columnar* schema was drawn by Ranson (1928), and it pretended to illustrate how the length axis of a primitive brain (red dashes) passes straightly through the telencephalon (1a), the diencephalon (1b), the midbrain (2), and the hindbrain (3a,3b; 3c is the cerebellum). The tags A(R) and P(C) refer to anterior (rostral) and posterior (caudal), respectively. D and V mark the orthogonal dorsoventral dimension. Remarkably, the cephalic flexure is not represented, though it appears in all vertebrates (an instance of psychological negation). The lower schema represents a gymnophionan (amphibian) brain whose cephalic flexure is extremely marked. The length axis (red dashes) is marked according to *prosomeric* tenets following the observable curvature and ending behind the optic chiasma (the telencephalon is understood as a dorsal outgrowth of the hypothalamic alar plate). As in the upper schema, the AP course of the axis decides what is dorsal (D) or ventral (V).

do not habitually coincide with *ventricular sulci*, much used in standard columnar studies for delimitation. Some of the primary molecular boundaries coincide rather with *ventricular ridges* at early developmental stages, notably those adopting a *transversal interneuromeric topology* [e.g., *Shh*-positive ZLI (zona limitans intrathalamica), pretectal *Pax3* and thalamic *Gbx2*; **Figures 5A,B**, **10**; see Lakke et al. (1988), a scanning electron microscopic analysis in the diencephalon]. In any case, both sulci and ridges of the ventricular surface are understood now as tertiary epiphenomena of the morphogenetic histogenetic differences established first by primary molecular boundaries. Moreover, it is very doubtful that genes can code for a sulcus or a ridge, and, even if they could, mechanistic effects merely *shaping* the ventricular surface do not seem efficient characters for evolutionary selection.

The arbitrary columnar concept of what was "longitudinal" in the diencephalon also caused unexplained "impossible" topologic relationships of the "columns" with the roof and floor plates (**Figures 1A**, **2C**, **4**, **6A,B**), which induced followers of the model to disregard the bending of the brain axis at the cephalic flexure, a constant feature of all vertebrate brains (**Figure 3**). Some ulterior versions of the columnar model did admit the cephalic flexure and part of the sulcus limitans of His (e.g., Kuhlenbeck, 1973; Altman and Bayer, 1988, 1995; Swanson, 2012; concept

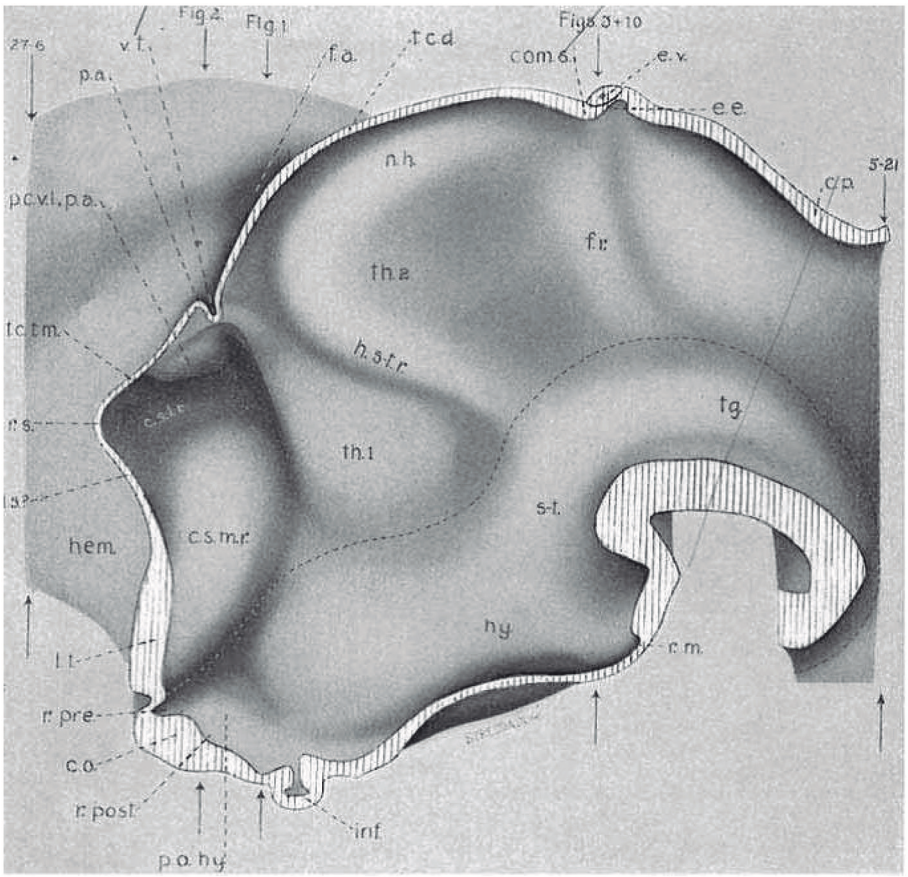

FIGURE 4 | Copy of a reconstruction of the ventricular surface of a 19 mm human embryo published by Bailey (1916) (no copyright permission required). The axial reference is the sulcus limitans of His, an untagged dash line bending around the cephalic flexure and ending rostrally at the preoptic recess (r.pre). Modern versions of this limit, informed by neuronal differentiation markers and genoarchitectonic markers, instead make it end rostrally at the postchiasmatic recess (r.post), thus allowing the eye vesicles and the optic chiasma (c.o.) to represent alar structural elements. Kuhlenbeck proposed another variant with a rostral end of sulcus limitans at the mamillary recess (r.m.; reviewed in Kuhlenbeck, 1973); this option would ascribe the tuberal hypothalamus to the alar plate, but runs counter to early tuberal expression of the *Shh* gene. The standard basal plate zone delimited by the sulcus limitans (check **Figures 2A**,**B**) carries successively the tags for tegmentum (tg; at pretectal and midbrain levels), subthalamus (s-t; at retromamillary level) and hypothalamus (hy; at tuberal level). Bailey (1916) departs here from the original (His, 1893) notion, which completely equates the old subthalamus of Forel (1877) with his hypothalamus (**Figure 2A**). The alar plate region shows two compartments identified as th.1 and th.2, referring to two thalamic regions; according to the columnar model of Herrick (1910), these would be identified respectively as ventral and dorsal thalamus, while in the columnar model they represent the prethalamus and thalamus, respectively. However, the two boundaries that limit the thalamus (dorsal thalamus) are not "longitudinal' sulci, but are identified by Bailey (1916) as *transversal ridges* that converge into the cephalic flexure. Caudally there is a ridge caused by the retroflex tract (f.r.), which we now know courses at the limit between the thalamic and pretectal diencephalic prosomeres (see **Figures 1B**, **5**, **6**); rostrally another transversal ridge (identified as the habenulo-subthalamic ridge, h.s-t.r.) extends from the roof into the sulcus limitans, roughly pointing to the basal area identified as "subthalamus." This ridge corresponds to the zona limitans intrathalamica of Rendahl (1924) and Gilbert (1935). The prethalamus (ventral thalamus) area is limited rostrally by a shallow sulcus that might correspond to Herrick's sulcus diencephali ventralis. It does not extend beyond the sulcus limitans and corresponds to what more modern columnar authors have identified as sulcus hypothalamicus of Monro, the supposed continuation of a partially bent columnar axis into the telencephalon (**Figure 1A**). This so-to-speak "innocent" reconstruction done outside of any school shows that the same morphology has been interpreted as "longitudinal" or as "transversal" depending of the axis accepted by the authors.

represented in **Figure 1A**), but inconsistently maintained the belief that diencephalic columns were longitudinal.

As regards the theoretically straight length axis of Herrick (1910), it was rarely discussed that there is very poor developmental support for its telencephalic ending. Modern molecular embryology highlights instead the relevant axial causal role of the notochord in establishing the *neural floor plate*, which in its turn induces in antagonistic interaction with roof plate morphogens the *basal plate* and the *alar-basal boundary* or sulcus limitans (see Puelles L. et al., 2012a; **Figures 2B**, **5A–C**). Note the notochord (and accordingly the floor plate) ends rostrally under the mamillary hypothalamic pouch (Ma; **Figures 1A,B**, **6A**; additional molecular evidence in Puelles L. et al., 2012a; Puelles and Rubenstein, 2015). There is no analogous causal underpinning for the postulated columnar brain axis extending hypothetically into the telencephalon; compare (**Figures 1A,B**). Swanson (2012, 2018) holds speculatively that the *columnar* basal hypothalamus

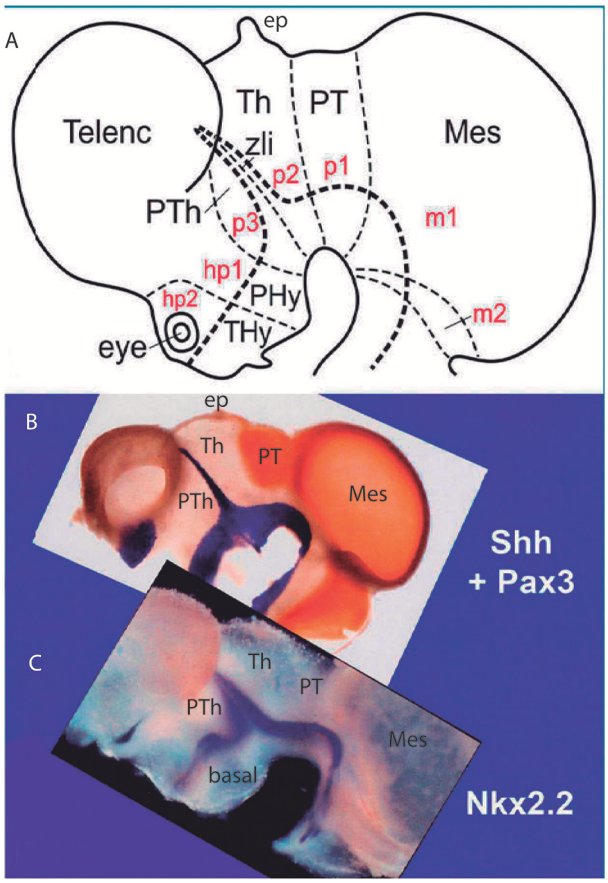

FIGURE 5 | Original images from chick embryo brains illustrating molecular support for the longitudinal axial landmarks postulated in the prosomeric model (no copyright permission required). **(A)** Schematic view of the prosomeric forebrain, with the mesencephalic m1 and m2 mesomeres, the diencephalic pretectal, thalamic and prethalamic prosomeres p1–p3, and the hypothalamo-telencephalic prosomeres hp1 and hp2. The molecular alar-basal boundary curves around the cephalic flexure and associates to an orthogonal spike limiting the thalamus (Th; alar p2) from prethalamus (PTh, alar p3). This spike is known since Rendahl (1924) as the zona limitans intrathalamica (zli), which is understood nowadays as a *mid-thalamic secondary organizer* that releases diffusible SHH and WNT signals contributing to inner regionalization of Th and PTh, possibly also of pretectum (PT) (see Puelles and Martinez, 2013). The midbrain is organized instead by FGF8 signals spreading from the *isthmic organizer*, found just caudal to m2 (preisthmus) (review in Puelles, 2017). The *peduncular* and *terminal* segmental parts of the hypothalamus are also identified (PHy, THy); the corresponding hypothalamo-telencephalic prosomere hp1 extends into the evaginated telencephalic hemisphere, while hp2 ends in the subpallial preoptic area (unmarked). **(B)** Wholemount of a chick embryo double reacted for *Shh* mRNA *in situ* hybridization (blue signal) and immunoreaction against the protein transcription factor coded by *Pax3* (brown signal). The Shh signal clearly delineates the floor and basal longitudinal zones of the whole forebrain (secondarily there appears a downregulation of this signal at the tuberal hypothalamus). The zli (compare **A**) shows its *Shh*-positive core, which gives it its anteroposterior signaling capacity as a secondary organizer; the transverse zli spike connects ventrally with the similarly Shh-positive basal plate (different genomic enhancers are implied, so that the zli is not an extension of the basal plate); there is additional separated Shh expression at the preoptic area of the subpallium. On the other hand, *Pax3* signal is characteristic of a dorsal part of the pretectal alar plate and corresponding roof plate (there is also selective

(Continued)

FIGURE 5 | expression at the thalamic roof plate). This pattern gives partial molecular support to the interneuromeric thalamo-pretectal boundary, in lying just caudal to the retroflex tract (but leaves a ventral part of the pretectal alar plate negative). Moreover, extensive Pax3 signal appears likewise at the alar region of the prepontine hindbrain (behind the isthmic constriction; note the Shh signal marks here only the floor plate, and the hindbrain basal plate is unlabeled), and at the alar midbrain. Both the zli, separating p3 and p2, and the thalamo-pretectal border (p2/p1) are transversal limits that are distinctly orthogonal to the longitudinal basal plate and the underlying cephalic flexure. **(C)** Wholemount of a chick embryo reacted for Nkx2.2 *in situ* hybridization (blue signal). This gene marker is upregulated exclusively across the border of *Shh* expression by particularly high levels of diffusing SHH protein. We see accordingly signal as a band that follows the alar-basal border seen in **(B)**, and also climbs up and down the spike of the zli core domain expressing likewise *Shh*. Note this combined *Shh* and *Nkx2.2* expression pattern is continuous through the whole forebrain, from midbrain to hypothalamus, and does not enter into the telencephalon! Moreover, it cuts the hypothalamus into alar and basal moieties (leaving the optic stalk on the alar side), contrary to columnar assumptions. This pair of genes is expressed slightly differently in the hindbrain, namely across the floor-basal boundary, due to the local restriction of Shh to the floor plate. This patterning difference between forebrain and hindbrain corroborates the modern isthmic boundary of the midbrain, as well as the ascription of midbrain to the forebrain. Such patterns as shown here in **(B,C)**, with more gene markers added, is what is meant with the expression "primary molecular definition of a brain boundary": a set of coherent gene or protein expression patterns that demonstrate collectively the reality and precise position of neuroepithelial boundaries before neurogenesis occurs, underpinning differently fated neural wall regions (as corroborated experimentally), and pointing to the implied causal mechanistic correlations. These limits precede neurons in the mantle, though they later overlap with their architectonic boundaries; they accordingly condition by their differential regulatory functions the distinct histogenetic secondary phenomena that occur subsequently at each side of these boundaries; these limits invariably finish as more or less visible adult brain boundaries, and rarely coincide with ventricular sulci (sometimes experimental methods are needed to visualize them at postnatal stages).

extending into the "basal telencephalon" is induced by the prechordal plate, even though the prechordal plate material does not reach beyond the preoptic region. Moreover, lack of prechordal signaling only causes holoprosencephaly (repatterning and cyclopy), but not a loss of the telencephalon and hypothalamus.

Another point hardly discussed in columnar literature is why the VTh, DTh and ETh "columns," supposed to be mutually parallel, seem to end "rostrally" at the diencephalic *roof plate*, the major *dorsal* landmark, rather than having a straightforward telencephalic ending, as one would expect. Theoretically, only the ETh should participate in the roof plate, but it is clear that ETh, DTh and VTh reach that longitudinal zone (see **Figures 1A**, **2C**, **4**, **6**). This conundrum implies that the limiting thalamic "longitudinal" sulci that were used to define these columns somehow are less longitudinal than was assumed, being in fact disposed obliquely, or even *orthogonally,* to the roof plate. The same inconsistent conundrum emerges again in the opposite direction for DTh and VTh. The theoretically "caudal" end of these columns meets *orthogonally* the longitudinal basal plate (**Figures 1A**, **2C**, **4**, **6**). This again should be impossible if DTh and VTh are longitudinal structural entities. It suggests they are in fact transversal domains, as was thought by major contemporaries (Kappers, 1947;

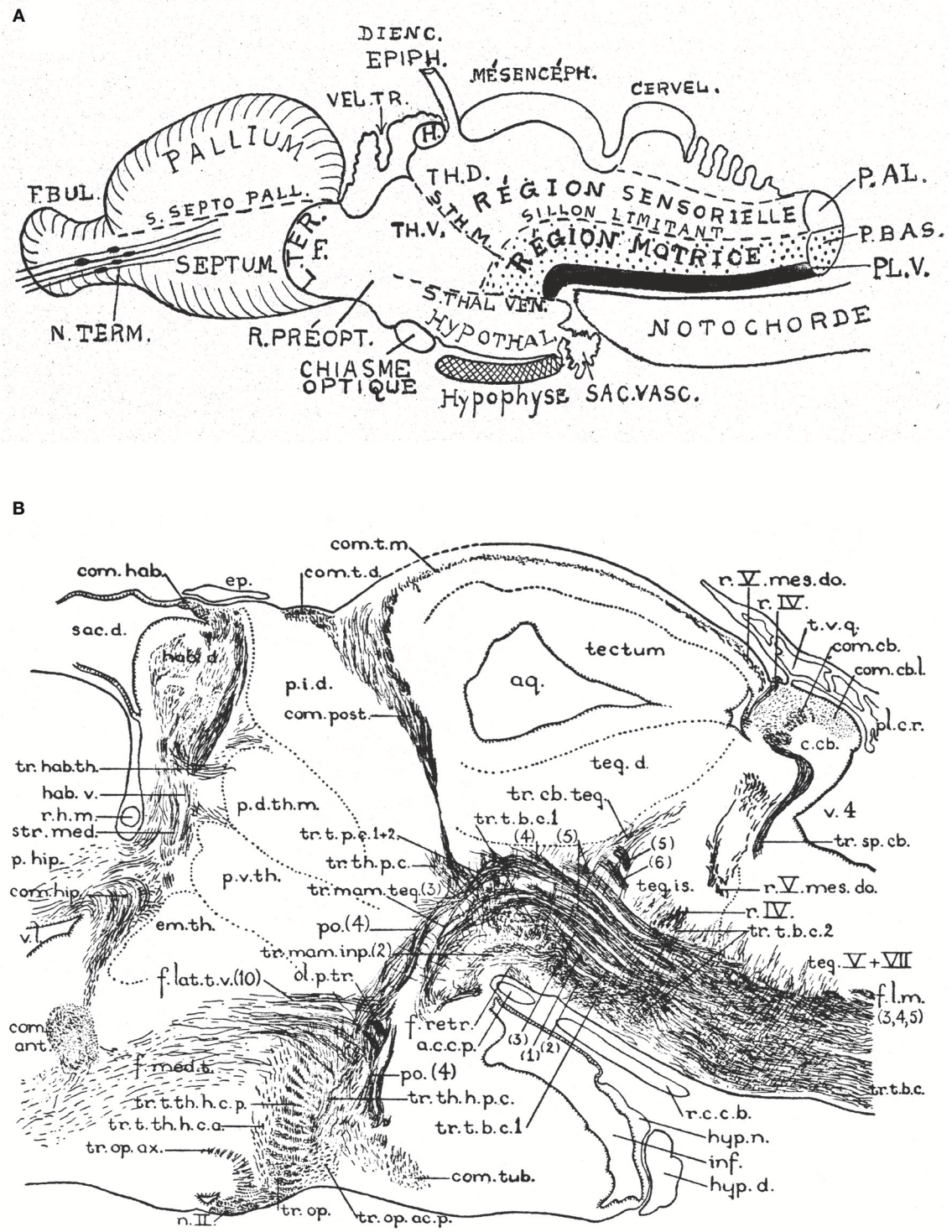

FIGURE 6 | Two classic images showing evidence that supposed longitudinal diencephalic columns actually represent transversal forebrain domains (no copyright permission required). **(A)** Schematic drawing of a primitive anamniote brain by Kappers (1947) that includes on one hand the basic floor, basal, alar and roof longitudinal zones of His (1893) (region sensorielle = alar plate; region motrice = basal plate; sillon limitante = sulcus limitans of His; the floor plate is in dense black; note its rostral end is roughly correlated with the tip of the notochord). Herrick's (1910) thalamic sulci stm and stv that limit the DTh, VTh, and HTh columns are also represented. Kappers here clearly implies that he thinks that these sulci and "columns" are transversal, since he draws them orthogonal to the longitudinal zonation system. **(B)** This drawing is a very realistic rendering by Herrick (1936) of a fiber-stained sagittal section through the brain of *Amblystoma* (an urodele). Note a cephalic

(Continued)

FIGURE 6 | flexure is distinctly present, and longitudinal tracts coursing from the brainstem into the forebrain clearly curve around the flexure, continuing into the hypothalamus and supraoptic commissures. The peduncular tract diverges dorsalward at a right angle [f.lat.t.v.(10)]. The midbrain is clearly separated from the diencephalon by the posterior commissure (com.post.). In front of that Herrick identified a pretectal region tagged as "pars intermedia diencephali (p.i.d.)," not a standard component of his diencephalic system; next come a pars dorsalis thalami, middle part (p.d.th.m; this is probably just a "middle" part because the "p.i.d." was considered a caudal part of the same, and either the "ventral habenula" or the "eminentia thalami" was a rostral part) and a pars ventralis thalami (p.v.th). In the prosomeric model the latter must be complemented with the eminentia thalami (em.th.), which we now know belongs to the dorsal alar VTh. These alar territories converge orthogonally ventralwards onto the basal tegmentum full of longitudinal fibers and the cephalic flexure, and also point in the contrary direction toward the habenular region and the roof plate. The arrangement of all elements agrees perfectly with Kappers' schema in **(A)**.

Figure 6A). According to this morphologic consistency analysis, something seemed to be wrong with the columnar forebrain axis and the conclusion that the diencephalon contains four "longitudinal" columns.

The *prosomeric model* uses as axial reference the molecularly-defined floor plate and alar-basal boundary (primary patterns, as opposed to tertiary phenomena such as ventricular sulci used by Herrick, 1910). The modern alar-basal boundary only differs from the sulcus limitans of His in ending under the optic chiasma rather than above it (**Figures 1B**, **2B**, **3**, **5A–C**, **10**; Puelles L. et al., 2012a; Paxinos and Franklin, 2013; Puelles and Rubenstein, 2015); note it is theoretically advantageous to have the eyes and chiasma as alar structures; otherwise you have a sensory pathway entering the basal plate, as happens undiscussed in the columnar view (e.g., Swanson, 2012, 2018). Our model resolves all the mentioned columnar conundrums, revealing that VTh, DTh and pretectum are alar subregions of straightforward transversal neuromeric units of the diencephalon (p1–p3; **Figures 1B**, **5**, **10**); note particularly how the observed topologic relationships with the roof, basal and floor plates are resolved. The diencephalon accordingly lies altogether caudal to the hypothalamus, and the basal plate does not extend into the telencephalon (**Figures 2B**, **5B,C**, **10**).

The inescapable morphologic problem of the columnar model, which causes a host of secondary problems, is that the forebrain axis was arbitrarily formulated, and turns out to be inconsistent with modernly investigated causal mechanisms, as well as with many molecular and structural patterns of the forebrain wall.

MIDBRAIN TERMINOLOGICAL PROBLEMS

The caudal midbrain limit was traced classically along the "ponto-mesencephalic sulcus" that runs just above the pons (**Figure 7A**). The rostral midbrain limit, or mes-diencephalic border, was given classically by an imaginary plane passing in front of the superior colliculus (normally across the posterior commissure; **Figure 7A**). This limit extended under the medial geniculate body and ended ventrally at the upper end of the interventricular fossa, close to the mamillary bodies (**Figure 7A**). This boundary was proposed by His (1893); **Figure 2A**) who acknowledged it was tentative and arbitrary, due to lack of suitable landmarks (he did not recognize the posterior commissure as the relevant landmark he needed). However, his tentative border became a dogma for over 100 years. Curiously, His (1893) also proposed an essentially correct isthmo-mesencephalic *caudal* boundary of the midbrain in the same work (**Figure 2A**), but this was not accepted by conventional neuroanatomy. As a consequence of these long-standing midbrain limits, the whole interpeduncular fossa and visible *pes pedunculi*, plus the lemniscal trigone and the caudal pretectum, were held to be mesencephalic, and so were both oculomotor and trochlear nerves (**Figures 1A**, **7A**).

This classic concept of the midbrain limits has not stood the test of molecular data. Gene expression patterns and experimental embryology data (fate mapping and repatterning studies; studies on secondary organizers) have concluded decisively that both traditional limits defined above are inexact, and even causally impossible, because of regulatory antagonistic developmental mechanisms that do not allow truly diencephalic or hindbrain domains to *be "mesencephalic"* in molecular profile and fate, or viceversa (e.g., rotation experiments of Marín and Puelles, 1994; a prospective pretectal nucleus cannot develop such fate if placed inside the midbrain field). It has been shown, moreover, that the old "midbrain" (**Figure 7A**) does not represent a developmental unit, because it is too inclusive: it arbitrarily encompasses diencephalic derivatives rostrally and hindbrain derivatives caudally (**Figures 1B**, **7B**, **8**). The new, more restricted concept of the midbrain is consistent with gene patterns, causal mechanisms (e.g., effects of the isthmic organizer), and modern notions about neuromeric structure of the neural tube (the prosomeric model).

The first precise definition of the midbrain (which was consistent with His (1893) pioneering formulation of the isthmo-mesencephalic boundary) was proposed by Palmgren (1921), after comparative developmental studies in several vertebrate species, well before the advent of corroborating genetic evidence. Vaage (1969, 1973) provided additional developmental evidence consistent with Palmgren's model in chick embryos. Puelles and Martínez de la Torre (1987), García-Calero et al. (2002), Hidalgo-Sánchez et al. (2005), and Ferran et al. (2007, 2008, 2009) later built upon these precedents, addressing successively the caudal and rostral midbrain boundaries. Additional gene marker evidence was collected by Puelles E. et al. (2012a) for the adult mouse brain. The most relevant markers are the transcription factors *Otx2* (whose forebrain expression domain permanently ends caudally at the caudal midbrain boundary after neurulation) and *Pax6* which marks early on the alar pretecto-tectal limit in all vertebrates (i.e., the rostral midbrain boundary, passing *behind* the posterior commissure; **Figures 7B**, **8**, **9**, **13A**).

Figure 8 illustrates well-known brain nuclei that were classically thought to be mesencephalic (still so in Swanson, 2012, 2018), which turn out to be either diencephalic or hindbrain

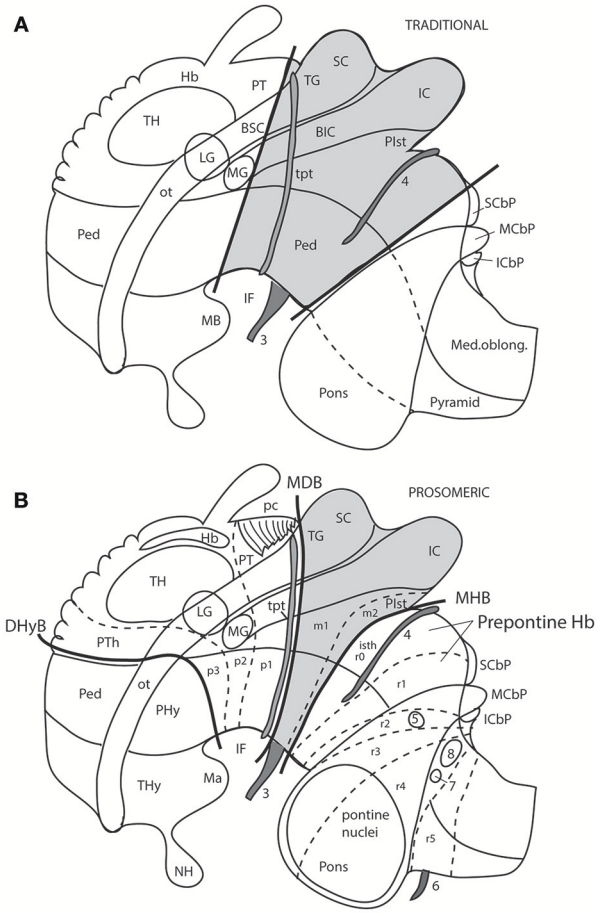

FIGURE 7 | Schemata from Puelles (2016) illustrating the different columnar and prosomeric models of the midbrain, in the context of neighboring diencephalic and hindbrain areas (no copyright permission required). Several superficial tracts were added for anatomic reference: the optic tract (ot), the cerebral peduncle and related medullary pyramid (Ped), the brachia of the superior and inferior colliculi (BSC, BIC), the transverse peduncular tract (tpt, related to the basal optic root), the extraneural oculomotor and trochlear cranial nerve roots (3, 4), and the middle (pontine) cerebellar peduncle (MCbP). **(A)** This drawing illustrates the conventional classic midbrain concept one finds in most textbooks, still abundantly used by clinicians. Thick straight black lines roughly indicate the rostral and caudal midbrain borders (the rostral limit being that suggested tentatively by His, 1893). It passes rostrally to the transverse peduncular tract (tpt; compare the position of this landmark in the caudal pretectum in **B**). It also ascribes most of the interpeduncular fossa (IF) to the midbrain, when in fact this depression is largely diencephalic and rhombencephalic (compare in **B**). The caudal midbrain boundary abuts the upper limit of the MCbP (see also the superior and inferior cerebellar peduncles; SCbP, ICbP; all of them in rhombomere 1, i.e., caudal to the isthmic segment). **(B)** This schema shows the more precise prosomeric concept relative to the same anatomic landmarks. I added with thin dash lines the borders between the diencephalic prosomeres (p1–p3) and the posterior commissure landmark (pc), important for placing the rostral mes-diencephalic boundary (MDB); this landmark jointly with the subcommissural organ characteristically mark the whole dorsal extent of the pretectum, though the crossed fibers converge laterally into a caudal subregion, the "commissural pretectum." The *transverse peduncular tract* carrying retinal fibers of the basal optic root ascends peripherally to the peduncle just in front of the pretecto-mesencephalic border or MDB. This drawing does not depict the tectal gray formation that lies within the midbrain rostrally to the superior

(Continued)

FIGURE 7 | colliculus (compare TG in **Figure 1**). Caudally to the inferior colliculus there is the m2 segment, representing the preisthmus region. Only a small portion of the interpeduncular fossa (IF), coinciding with the oculomotor nerve root, corresponds to the midbrain. The midbrain-hindbrain boundary (MHB) separates m2 from the isthmus (isth = r0). Part of the literature confusingly mixes the isthmus with the r1 proper under the name "r1," using the rationale that the isthmus is not a proper neuromere; the contrary was held by His (1893), Palmgren (1921), and Vaage (1969, 1973), and strong molecular evidence was presented recently by Watson et al. (2017); once the need to separate the isthmus as an additional hindbrain neuromere was heeded, it seemed best to call it r0, rather than change the numbers of all other rhombomeres. The r0 and r1 neuromeres jointly form the prepontine hindbrain (compare with **A**), which lies under the range of effects of the isthmic organizer, thus sharing some features, including dorsal raphe, cerebellar, mesV, and interpeduncular structures, regardless of their respective differential identities. Several hindbrain cranial nerve roots were added to **(B)** in order to see their topography relative to specific rhombomeres (indeed, the nerve roots are valid landmarks to access relative rhombomeric position in all vertebrates): trigeminal root in r2 (5), facial and vestibulo-cochlear nerves in r4 (7, 8), and abducens root in r5 (6). Note the basilar pontine nuclei occupy exclusively the ventral region of r3 and r4. Nevertheless, r2 is also ascribed to the pontine region, because it contains massive fiber bundles of the pontine MCbP coursing into r1 rostrally to the trigeminal root in r2. Since the cerebellum is formed in r0 and r1, all peduncles need to reach these segments in order to find entrance into the cerebellum. This was not appreciated in older times. The thick black line crossing the optic tract in front of the prethalamus (PTh) and behind the peduncular hypothalamus (PHy) is the diencephalo-hypothalamic boundary (DHyB). The thalamus is symbolized by an ovoid mass plus the lateral and medial geniculate bodies (LG, MG). Note the MG represents topologically the ventralmost thalamic mass, actually lying *ventral* to the LG. Both LG and MG lie close to the interthalamic limit (PTh/TH).

derivatives under the modern molecular midbrain definition. The trochlear nucleus and nerve are isthmic (Watson et al., 2010, 2017), while the interpeduncular nucleus complex is isthmic- and r1-derived (Lorente-Cánovas et al., 2012; IP in **Figure 1B**). The dorsal and ventral tegmental nuclei and the locus coeruleus (Aroca and Puelles, 2005; Aroca et al., 2006) clearly are r1-related. Serotonergic raphe cell populations are rhombencephalic in general, including the dorsal raphe nucleus, which was classically thought to be mesencephalic (Alonso et al., 2012); there is only a small rostrally migrated subpopulation of the dorsal raphe nucleus that finally lies in the caudal midbrain (m2 prosomere; identified as "midbrain DR" by Alonso et al., 2012). The mesencephalic trigeminal nucleus of all non-mammals lies exclusively in the midbrain, while in mammals it also extends caudally into the isthmus and rhombomere 1 (mesV in **Figure 8**); this evolutionary difference suggests that the mammalian mesV cells probably have midbrain origins and then migrate tangentially into isthmus and r1. Another modern conclusion is that the decussation of the brachium conjunctivum (superior cerebellar peduncle) lies not in the midbrain, but across the isthmic floor (Paxinos and Franklin, 2013; Watson et al., 2017; Martínez-de-la-Torre et al., 2018).

The midbrain is divided into unequal mesomeres 1 and 2 (m1, m2; **Figures 5A**, **7B**, **8**, **10**; Hidalgo-Sánchez et al., 2005; Puelles, 2013); this division was already affirmed, even if not clearly documented, by Palmgren (1921) and Vaage (1969, 1973). However, these authors thought that m2 was an *atrophic* neuromere that produced no neural derivatives

(a very odd idea, that discredited the notion for a long time). However, Hidalgo-Sánchez et al. (2005) demonstrated both that a particular molecular profile exists in m2 (within the field of midbrain *Otx2* expression, thus corroborating its midbrain neuromeric status distinct from m1) and showed some clearcut alar and basal m2 derivatives (**Figure 9D**; see also Puelles E. et al., 2012a). This development led to the modern concept of a distinct midbrain m2-derived domain, also called *preisthmus*, which lies intercalated between the inferior colliculus and the isthmus proper (**Figures 7B**, **8**, **9**, **10**). The corresponding alar region contains in its intermediate and superficial strata what classically was identified as the cuneiform nucleus or nuclear complex; rodent atlases usually wrongly distribute this complex across both preisthmus and isthmus (Puelles E. et al., 2012a; Puelles, 2016).

The classical "posterior pretectal nucleus" has been modernly recognized to be mesencephalic and renamed "tectal gray," following previous usage in non-mammalian tetrapods (TG in **Figures 1B**, **8**, **9**). The TG is truly mesencephalic, because it lies caudal to the posterior commissure, and it lacks *Pax6* expression typical of neighboring pretectal areas (Ferran et al., 2008).

The midbrain alar plate is thus built by a rostrocaudal sequence of four *major structures*, rather than just the two classic colliculi: *tectal gray, superior colliculus, inferior colliculus* (all three within m1), and *alar preisthmus* within m2 (**Figures 1B**, **7B**, **8**–**10**). As regards the midbrain basal plate, the oculomotor nucleus complex lies within m1, while m2 (preisthmus) is devoid of motoneurons, since the trochlear nucleus is isthmic (**Figure 8**; Watson et al., 2017). The substantia nigra and ventral tegmental area, which are conventionally ascribed only to the midbrain in the old model (**Figure 7A**), actually represent in the new scenario a plurineuromeric isthmo-meso-diencephalic complex that extends from the isthmus to the rostralmost diencephalon (**Figures 7B**, **10**; Medina et al., 1994; Puelles and Medina, 1994; Verney et al., 2001; review in Puelles E. et al., 2012a; Puelles et al., 2012b, 2013; Puelles L. et al., 2012a; Puelles, 2013). Modern experts on the development of this complex already use routinely the expression "mesodiencephalic SN/VTA" (see also a comparative review in tetrapods by Marín et al., 1998). Another typical tegmental midbrain element is the red nucleus. However, only the magnocellular red nucleus is mesencephalic, while the parvocellular red nucleus is pretectal diencephalic (RMC, RPC; **Figure 9D**; Puelles E. et al., 2012a); the classics underlined that the parvocellular red nucleus was limited rostrally by the retroflex tract, and the latter is the transversal landmark that limits thalamus (p2) from pretectum (p1) (see rf in **Figures 1A,B**, **4**).

Other specific points possibly merit detailed examination. For instance, the "midbrain locomotion center" (MLC) is commonly identified anatomically with the cuneiform nucleus, an alar preisthmic derivative which we identify within m2 (Shik and Orlovsky, 1976; Mori et al., 1977; ten Donkelaar, 2011; ten Donkelaar et al., 2018). The literature however tends to conceive the cuneiform nucleus as a tegmental (basal) nucleus, which it is not, if it really is preisthmic (the cuneiform nucleus actually lies just *caudal* to the inferior colliculus, but still in the alar plate). However, the MLC also has been said to lie close to the pedunculopontine tegmental nucleus (PPnTg), which is a well-known cholinergic and NOS positive population which lies within tegmental r1. Therefore, if the MLC is really tegmental in position, then it is incorrectly identified as "cuneiform nucleus," a structure that is distant from the PPnTg (separated by the whole isthmus). Contrarily, if it really is alar preisthmic, then it has been wrongly identified close to the PPnTg in the r1 tegmentum. Considering the alar/basal difference and that these two sites are separated by the whole isthmus, as well as the standard imprecision of atlases on this brain region, it is possible that the identification of the original physiologic electrode recording sites as being at the "cuneiform nucleus" was inexact. The MLC thus perhaps lies instead within the isthmus, where it may well be a tegmental basal structure to be found next (just rostral) to the PPnTg. Unfortunately, if it is isthmic, or belongs to r1, then it does not merit the given name "midbrain locomotion center." I hope that present discussion of the midbrain limits helps in resolving this conundrum.

The diverse points made above on the general subject of "midbrain terms" show that most of the problems are conceptual, and relate to the wrong definitions used classically for the rostral and caudal limits of this brain part, or result from poor knowledge of its basic subdivisions m1 and m2. Once the modern molecularly-based (and experimentally corroborated) definition of the relevant boundaries is seen as the natural one (not man-made, as the old one was), it only remains for us to demand better atlases than we have now (e.g., see the already corrected chick brain atlas; Puelles et al., 2007, 2018).

The main new names that have been proposed for the midbrain include "tectal gray" (for the stratified retinorecipient center found just rostral to the superior colliculus, previously wrongly ascribed to pretectum as "posterior pretectal nucleus"), and "preisthmus" (for the adult derivatives of the alar and basal domains of the m2 prosomere, largely unnoticed by the classics). I proposed that the "superficial cuneiform nucleus" term, whose diversified usage has led to substantial confusion in various atlases and in the literature on the midbrain locomotion center, be substituted by the neologism "subbrachial nucleus", referring to the apparent position of the superficial preisthmus immediately under the brachium of the inferior colliculus [SubB: **Figure 9D**; Puelles, reference atlases issued in 2009 for the public Allen Developing Mouse Brain Atlas, developingmouse.brain-map.org; Puelles E. et al. (2012a)]; this new term already appears used in some rodent atlases (Watson and Paxinos, 2010; Paxinos and Franklin, 2013; Paxinos and Watson, 2014). Finally, a previously unrecognized dorsal paramedian subzone of the collicular plate has been recently identified as producing *outer (dorsal) and inner (ventral) paracommissural tectal nuclei* (TPCD, TPCV; **Figure 9**; Puelles E. et al., 2012a); the TPCV was first reported in mammals as a "tectal longitudinal column" (TLC; Saldaña et al., 2007); it includes a rostral portion that surpasses rostrally the superior colliculus and relates instead to the tectal gray, forming actually a "tectal gray paracommissural nucleus," or TGPC. The related TPCD was mentioned in that publication as a "dorsal column," which was further characterized by Aparicio and Saldaña (2014), who identified now both nuclei as TLCv and TLCd (the

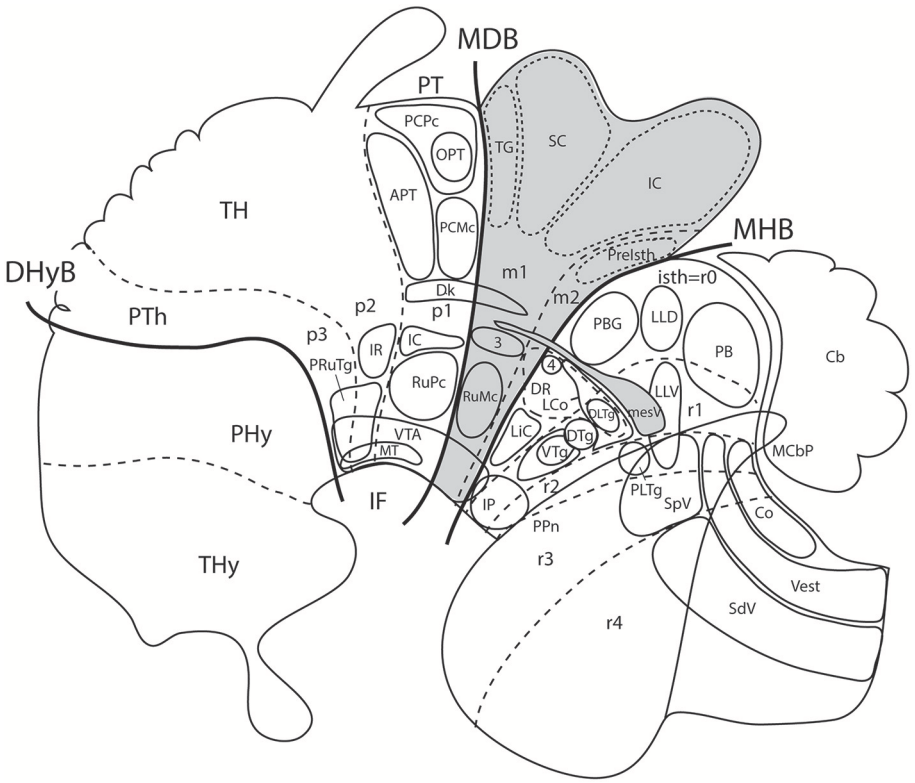

FIGURE 8 | Schema from Puelles (2016) (modified from those in **Figure 7**; no copyright permission required) showing truly mesencephalic centers (gray background) according to the prosomeric model, as opposed to neighboring diencephalic or rhombencephalic (prepontine) formations that have been implicated in erroneous ascription to the midbrain within classic neuroanatomic usage inspired in the columnar model. For specific ascriptions to the isthmic neuromere (r0), see Watson et al. (2017). The trigeminal mesencephalic nucleus is thought to originate in the midbrain and partly migrate into the prepontine hindbrain along the mesV tract. The ventral nucleus of the lateral lemniscus (LLV) has been shown to originate in r4, and migrates subsequently along the tract into its final position (Di Bonito et al., 2013, 2017). The abbreviations correspond to standard ones used in recent rodent atlases. MDB, mes-diencephalic boundary; MHB, midbrain-hindbrain boundary.

TLCd/TPCD was corroborated as a GABAergic population, as had been shown previously by Puelles E. et al., 2012a; their Figures 10.5–10.8; whereas the TLCv/TPCV is glutamatergic; Aparicio and Saldaña, 2014). The "paracommissural" names I propose derive from our previous independent analysis of an apparent homolog of one of these nuclei in the avian brain (Puelles et al., 2007). The descriptor "longitudinal" proposed by Saldaña and colleagues seems less specific than "paracommissural" regarding positional characterization, and I think there is advantage in explicitly referring to their position close to the tectal gray (tgc), tectal (tc), and intercollicular (icol) median commissures (TGPC; TPCD; tgc, tc; **Figure 9A**). The connections of the novel TPCV and TPCD nuclei apparently relate them, respectively to the auditory and visual systems (Saldaña et al., 2007; Aparicio and Saldaña, 2014).

DIENCEPHALON TERMINOLOGICAL PROBLEMS: GENERAL ISSUES

Figures 1B, **5A**, **7A,B**, **10** illustrate how the modern prosomeric model deals with the diencephalic forebrain region in contrast to the conventional columnar tradition (**Figure 1A**). First, the whole pretectum is diencephalic, as redefined by anatomic landmarks (retroflex tract and posterior commissure) and by molecularly stable *Pax6* expression *antagonistic* to the isthmic organizer-controlled midbrain molecular profile (see other pretectal markers in Ferran et al., 2007, 2008). Columnar authors usually ascribed the caudal pretectum to the midbrain and were rather vague about the rest, since in their model it could only enter into the categories of either epithalamus or dorsal thalamus, not being allowed as a distinct diencephalic component because this region was clearly transversal (**Figures 1A**, **2C**, **4**, **6B**). Secondly, the hypothalamus is no longer held to be diencephalic (whereas it represented the columnar diencephalic floor-plus-basal domain; **Figure 1A**), due to the prosomeric definition of the forebrain axis as ending within the acroterminal hypothalamic area (**Figure 1B**; Puelles and Rubenstein, 1993, 2003, 2015; Rubenstein et al., 1994; Puelles L. et al., 2012a; Puelles, 2013; Puelles et al., 2013, 2015; Ferran et al., 2015). The prosomeric hypothalamus is accordingly conceived instead as lying rostral to the diencephalon and forming the rostralmost forebrain region, the *secondary prosencephalon* (basically in agreement with His, 1893, 1895, 1904; **Figures 2A,B**). This

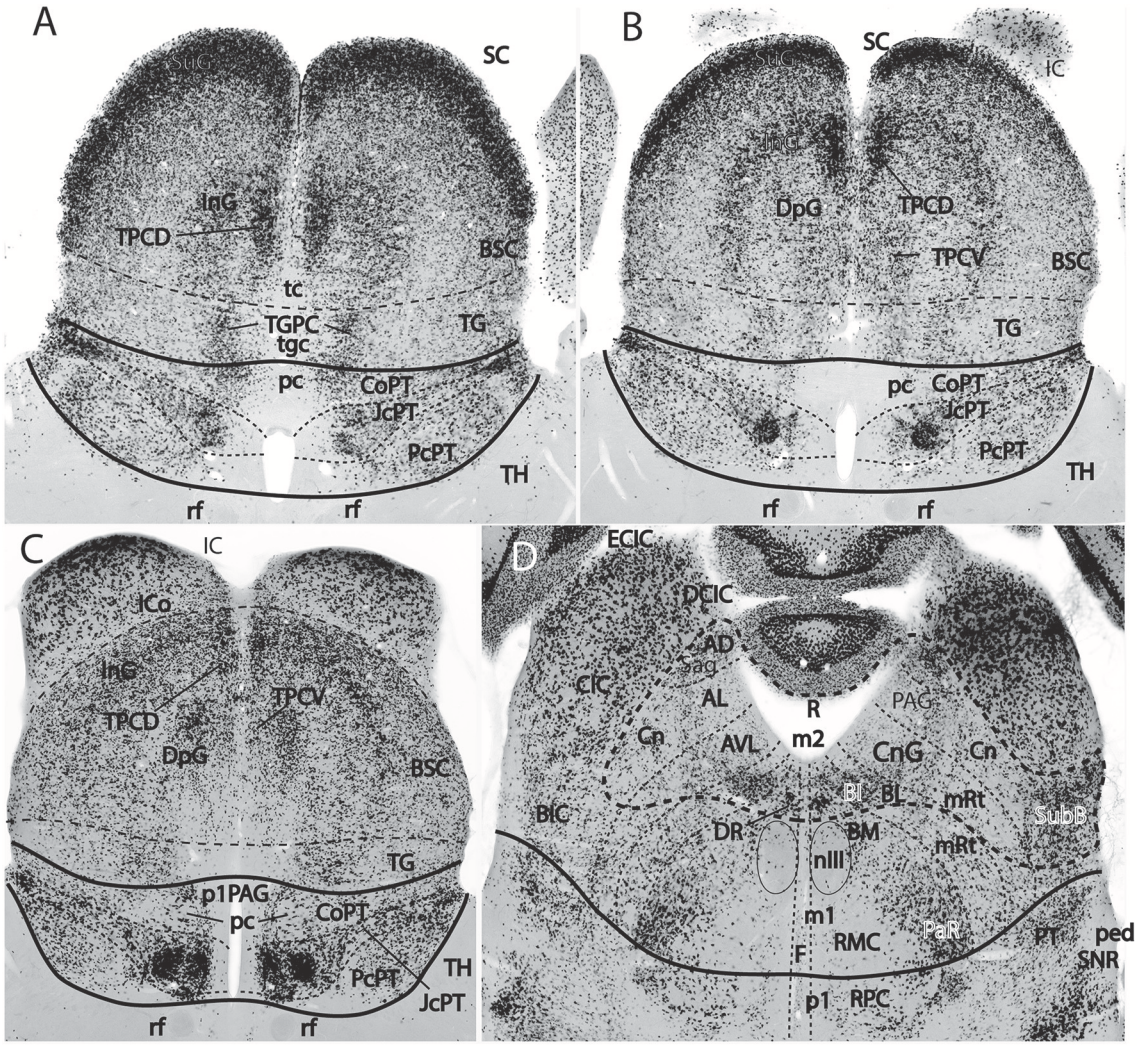

FIGURE 9 | Figure extracted from Puelles E. et al. (2012a) showing fundamental pretectal and midbrain structure in four horizontal sections **(A–D)** in dorsoventral order, illustrating in particular the adult mouse thalamo-pretectal and pretecto-mesencephalic boundaries (thick black lines; no copyright permission required). This material is *in situ* reacted for Gad67, thus showing selectively midbrain alar GABAergic neurons in superficial, intermediate and deep periaqueductal strata (note there are practically none within the neighboring thalamus). The pretecto-mesencephalic border passes just behind the posterior commissure and in front of the distinct superficial, layered and retinorecipient formation identified as tectal gray (pc; TG; **A–C**). The TG differs from the superior colliculus (SC) in the number of superficial GABAergic neurons, as well as in the aspect of its periaqueductal formation. The novel dorsomedial tectal elements termed dorsal and ventral tectal paracommissural (longitudinal) nuclei are shown in position (TPCD, TPCV; **A–C**); there is also a similar tectal gray paracommissural nucleus (TGPC; **A**). The pretectum appears divided into precommissural (PcPT), juxtacommissural (JcPT), and commissural (CoPT) anteroposterior domains with differential structure and molecular profile (**A–C**; Ferran et al., 2008, 2009). The inferior colliculus (IC) starts to appear in **(B**,**C)**, but is shown fully in **(D)**. The section in **(D)** is slightly oblique from left to right, so that the right side passes somewhat under the IC, showing slightly more of the caudally underlying preisthmus or m2-derived midbrain territory (formations enclosed by the thick dash line; note the relevant subpial subbrachial nucleus, SubB, at the right). The small dash lines in **(D)** refer to the limits between different dorsoventral midbrain sectors visible at this level. Neither the oculomotor nucleus (nIII) nor the magnocellular nucleus ruber (RMC) in the basal plate contain GABAergic neurons, but the latter is surrounded laterally by a distinct mass of such cells, forming the pararubral nucleus [PaR; **(D)**; this population derives from the parabasal *Nkx2.2*-positive band illustrated in chicken in **Figure 5C**, and expresses this marker in the adult]. GABAergic cells are also present as a subpopulation in the parvocellular nucleus ruber lying in the pretectal tegmentum, also partly surrounded by the PaR (RPC, **D**).

last region encompasses in vertebrates also the eye vesicles and the telencephalon as alar outgrowths. However, the prechordate *Amphioxus* has a molecularly recognizable rostral hypothalamus that lacks eye or telencephalic evaginations (Albuixech-Crespo et al., 2017); this proves that the ancestral forebrain axis ended in the hypothalamus. The left side hypothalamus (alar and basal) is continuous with the right side hypothalamus across the rostromedian *acroterminal area* (**Figure 10**; neologism introduced by Puelles L. et al., 2012a; Ferran et al., 2015; Puelles and Rubenstein, 2015). The shared alar-basal boundary of the whole forebrain distinctly separates (after use of early molecular markers, neurogenetic

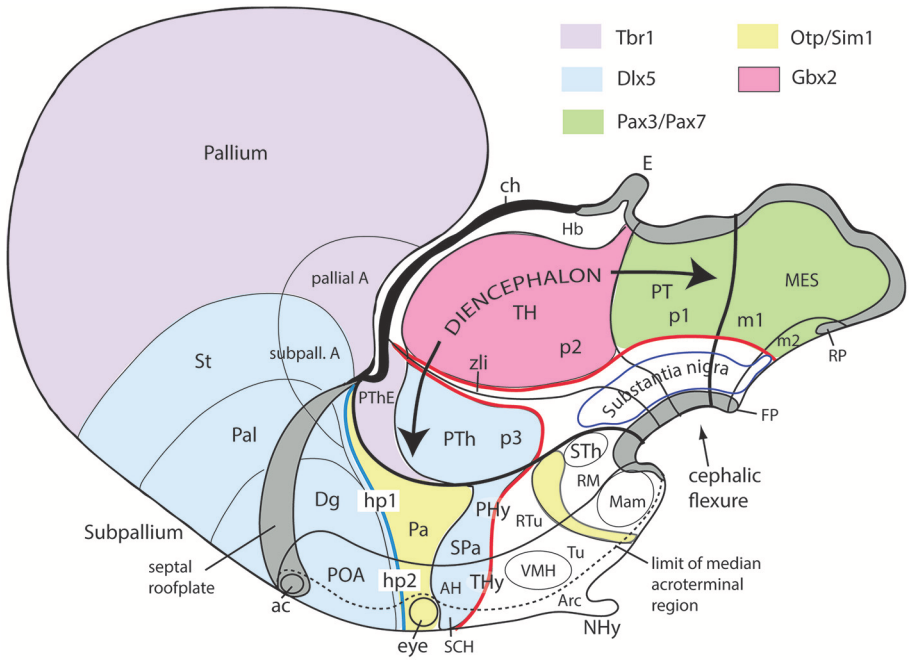

FIGURE 10 | Schematic map copied from Puelles (2015) of various gene expression patterns that agree with prosomeric analysis of the forebrain (largely centered on alar plate domains of the different prosomeres across midbrain, diencephalon and hypothalamus; no copyright permission required); alar-basal limit in red, though the zona limitans transverse spike (zli) is independent from the basal plate, irrespective of its molecular similarity (Shh expression; see **Figure 5B**). The mesodiencephalic extent of the dopaminergic substantia nigra and associated ventral tegmental area is mapped, as well as the distinct perimamillary/periretromamillary basal hypothalamic band, in yellow (see text); the separate alar hypothalamic paraventricular area (Pa; also in yellow)shares these particular markers (but not others). Dlx5 is shared among given prethalamic (PTh), hypothalamic (SPa, AH, SCH) and subpallial (St, Pal, Dg, POA) domains typically producing GABAergic neurons. A thick blue line represents the hypothalamo-telencephalic boundary; note telencephalic subpallial inclusion of the POA due to shared gene expression, and local ending of the roof plate at the anterior commissure (ac). Hypothalamic alar and basal subdivisions and some individual nuclei mentioned in the text are identified.

labeling, or differentiation markers; **Figures 2B**, **5**) continuous alar and basal zones across the midbrain, diencephalon and hypothalamus (roughly as defined by His, 1893, 1895, 1904; **Figure 2A**). In the prosomeric model, the telencephalon and eyes are singular *alar* hypothalamic derivatives that evaginate and show differential growth and patterning (**Figures 1B**, **10**). The "hypothalamus" can be conceived more correctly as a "hypotelencephalon," *sensu topologico stricto*. His (1893) proposed this prefix –"hypo-"= Greek synonim of "under" or "sub"- because he held the hypothalamus (like its antecedent, the subthalamus) to be an exclusively basal domain, whereas the thalamus proper was alar (**Figure 2A**); it thus made sense to name one domain as lying "under" the other, but this sense is different (about 90°) from that used later in the columnar model (**Figure 1A**). It eventually was realized using the genoarchitectonic perspective that both diencephalon and hypothalamus have basal and alar parts, and one lies caudal to the other (**Figures 1B**, **5**, **10**). One minor terminological problem that arises at this point is that the name "third ventricle" was traditionally applied to the old larger diencephalon inclusive of the hypothalamus. We now need to distinguish rostrocaudally distinct *hypothalamic and diencephalic parts of the third ventricle* (it seems not advisable to alter the number of ventricular cavities).

The "*diencephalon proper,*" an expression we have often used remembering the *diencephalo sensu stricto* of His (His, 1893, 1895, 1904), refers colloquially to the smaller prosomeric diencephalon. This lies intercalated anteroposteriorly between the secondary prosencephalon and the redefined midbrain. It represents a sizeable complete tubular sector of the neural tube which possesses bilaterally all four major longitudinal zones: floor, basal, alar and roof plates (**Figure 10**). Note the columnar model defined the hypothalamus as the basal and floor domain of the traditional diencephalon; as a consequence of the different axis used, the true basal and floor diencephalic domains of the prosomeric diencephalon proper are very differently placed—e.g., caudal to the mamillary and retromamillary regions-; these regions were substituted in columnar interpretations by the somewhat interlocked concepts of "prerubral tegmentum" and "posterior hypothalamus," which allowed an *ad hoc* and theoretically inconsistent continuity between basal hypothalamus and basal midbrain (inconsistent because this bridge is visibly orthogonal to the postulated "longitudinal" axis of the columnar model; see **Figures 1A**, **3**). Due to its complete dorsoventral structure, the prosomeric diencephalon proper resolves satisfactorily the observable relationships of its neuromeric subdivisions with the roof and floor domains (**Figures 1B**, **5A**, **10**). Significantly, it limits

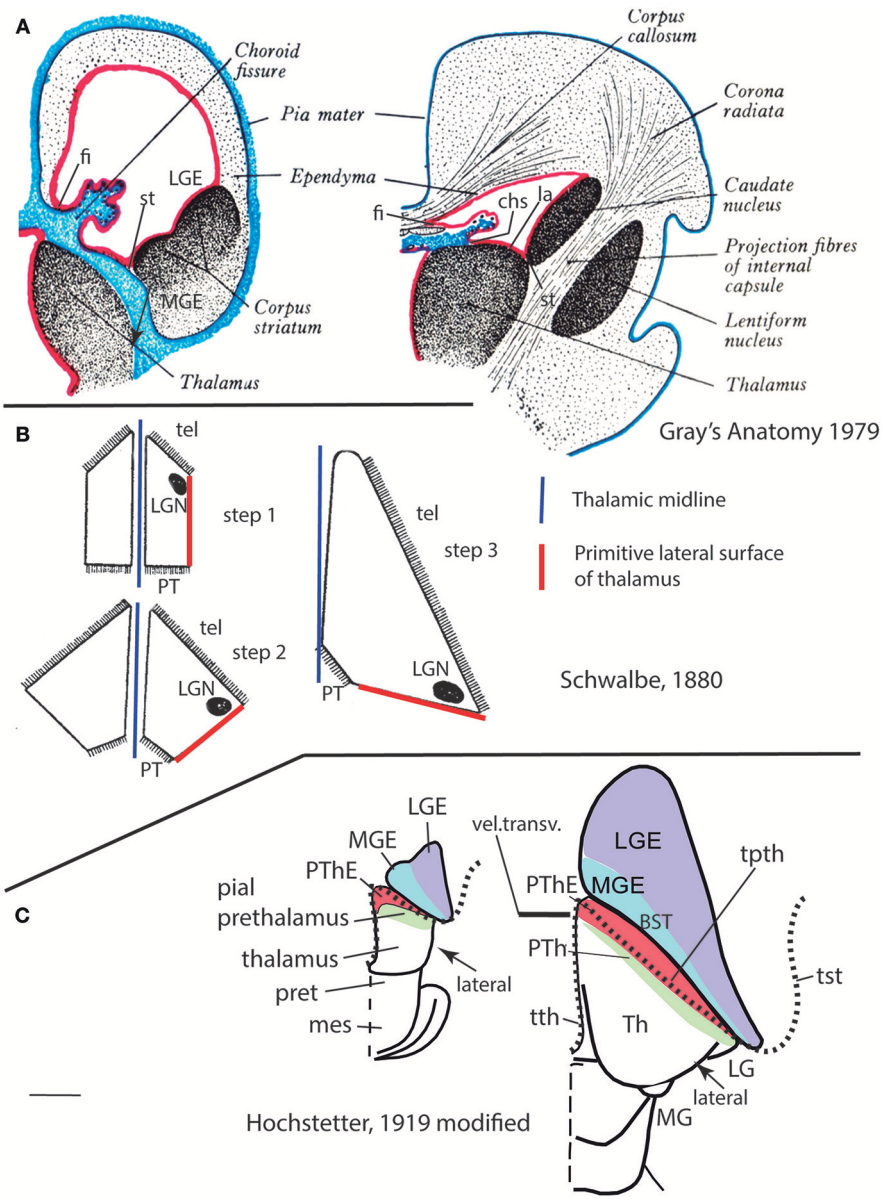

FIGURE 11 | Schematics taken from the literature (all partly modified), to illustrate the classic concept of the lamina affixa **(A)**, the morphogenetic deformation of the thalamus **(B)** and my new emphasis on the associated deformations at the prethalamus and prethalamic eminence, bearing on a new conception of the taenial insertions of the chorioidal fissure **(C)** (no copyright permission required). **(A)** Was extracted from the 1979 British edition of Gray's Anatomy. It illustrates precisely how many classic authors imagined a partial adhesion called "lamina affixa" occurred between overlapping parts of the thalamus and the medial wall of the telencephalon (see an equivalent schema in Dèjerine, 1895). A medial part of the hemispheric wall jumping between the hippocampal fimbria (fi) and the stria terminalis locus (st) was supposed to be primarily chorioidal in texture (leaving unexplained how such tissue derives from the roof plate). Only a dorsal part of it, called "pars libera," was held to contribute to the development of the definitive adult chorioidal fissure (marked as chorioid fissure at left). However, a lower part of the initial chorioid tissue was imagined to adhere to the thalamus, forming the "lamina affixa" (la; at right). The figured classic conception is conjectural, since it holds without demonstration that one half of the primary medial telencephalic wall adheres to upper and lower parts of the thalamic pial surface. The chorioid-thalamus adhesion (la) would obscure the original chorioidal taenia *imagined* as inserted primarily next to the prospective stria terminalis (st), creating an apparently novel "thalamic taenia" of the chorioidal fissure at the so-called chorioidal sulcus of the thalamus (chs; right side; note there is already a thalamic taenia associated to the roof of the 3rd ventricle). The stria terminalis site was originally held to be associated to the "corpus striatum" [meaning the whole mass of basal ganglia; we now know the st is associated specifically to the lateral ganglionic eminence (LGE; left side), whereas the pallidum and diagonal formations, including the periventricular bed nuclei of the stria terminalis, are derivatives of the medial ganglionic eminence (MGE; left side); see Puelles et al., 2013, 2016]. After the conjectured fusion, the part of the upper thalamic surface covered by the chorioid lamina affixa would apparently protrude at the floor of the lateral ventricle, forming with the medial ganglionic eminence the "terminal" or "opto-striatal" sulcus, a.k.a. as "thalamo-striatal" sulcus. Another imagined adhesion process with consequences was that of the primary lateral thalamic pial surface with the "corpus striatum," which would allow the thalamic fibers to reach the internal capsule (right side of **A**; this second conjecture was supported expressly by Dèjerine (1895), but is no longer widely supported presently, since the internal capsule fibers are now known to course first internally through the

(Continued)

FIGURE 11 | prethalamus—crossing the reticular nucleus—and only afterwards access the telencephalic stalk through the alar peduncular hypothalamus—e.g., see Puelles and Rubenstein (2003, 2015); see also **Figure 10**; remarkably, Swanson (2012) still postulates implicitly in his rat flat map that thalamic fibers reach the telencephalon across a pial adhesion, and not through the prethalamus). **(B)** Is a modified reproduction of three drawings by Schwalbe (1880) illustrating how the lateral side of the embryonic thalamus progressively deforms into a caudally oriented direction as a consequence of internal thalamic growth and parallel massive growth of the telencephalon and its stalk by the passage of numerous thalamocortical and corticothalamic fibers. Actually, the deforming (and enlarging) striped rostral thalamic boundary is not with the telencephalon, as imagined by Schwalbe, but with the prethalamus (compare **C**). Lack of understanding of this deformation stands at the basis of the erroneous idea of a *metathalamus* containing the medial and lateral geniculate bodies as derivatives of a neuroepithelial region immediately "posterior' to the main thalamus, which would have to be pretectal (see real topologic position of these primordia in **Figure 7B**, and comments in the text). **(C)** These two schemata were modified from originals in the work of Hochstetter (1919), who aimed to visualize the same thalamic deformation highlighted before by Schwalbe (1880). Hochstetter accepted like his predecessor the simplistic idea that the thalamus can directly contact the striatum (false assumption giving rise to the widely believed lamina affixa theory shown schematically in **A**). Modern prosomeric neuroembryology emphasizes the fact that the prethalamic part of the diencephalon is an intermediate neuromere rostral to the thalamus, which does not disappear (compare **Figures 5**, **10**), and therefore *must* become intercalated at the thalamo-telencephalic transition in the fashion depicted in my changes to these schemata. The prethalamus (green and red areas) becomes deformed (both stretched radially and flattened rostrocaudally) into a rather thin territory placed all along the supposed interface of the thalamus with the telencephalon. The flattened prethalamus is depicted as a thin *green* band representing its dorsal pial surface that remains visible in dorsal perspective, accompanied by the similarly stretched dorsalmost prethalamic area, the red-labeled prethalamic eminence, also in dorsal perspective (PThE). The latter shows in this view both its original pial and ventricular surfaces, evaginated in part through the interventricular foramen into the medial hemispheric wall (what protrudes at the lateral ventricle next to the terminal sulcus, without needing any questionable adhesion, is the eminential prethalamus, and not the thalamus proper). The neighboring telencephalic basal ganglia are reinterpreted as including the lateral and medial ganglionic eminences (LGE in violet, MGE in light blue), and the MGE is further marked as containing periventricularly the BST complex, which contains in this view only the supracapsular stria terminalis. Finally, a line of black dots indicates the non-fimbrial sequential insertions of the forebrain chorioidal tela (see fimbrial insertion—fi- in **A**). The complementary chorioidal insertion begins at thalamic levels (in front of the epiphysis) with the *taenia thalamica* proper (tth; right side), which ends at the velum transversum fold, or thalamo-prethalamic border at the chorioidal roof (vel.transv.; represented by thick transverse black bar). We successively reach next the small *pre-foraminal* and *foraminal* parts of the *taenia prethalamica* (new term introduced here), which extend the chorioidal insertion into the interventricular foramen, now attaching at the eminential prethalamus. From there the dot line proceeds along a *post-foraminal* prethalamic taenial region (tpth; right side) that courses along the stretched red PThE up to its apparent "caudal" end (note this is no real rostrocaudal course, according to Schwalbe and Hochstetter, because it remains within the deformed prethalamus). This post-foraminal prethalamic taenia correlates in topography with the classic "thalamic" chorioidal sulcus (chs; **A**, right side; this was previously held to correspond to an apparent attachment at the border between the pars affixa and the pars libera of the fissural chorioidal tela—compare **A**-, but is reinterpreted here as being prethalamic and relating in depth to the prethalamic reticular nucleus—compare **Figure 12**; it is to be noted that, since chorioidal tissue is essentially roof plate, it is impossible that the thalamus has a second chorioidal roof plate apart of the one that covers the 3rd ventricle). Once the stretched PThE ends above the optic tract, next to the posterolateral pulvinar and the LG (right side), the continuation of the non-fimbrial insertion line of the chorioidal fissure apparently jumps here from the diencephalon (prethalamus) onto the telencephalon. It is only here where we can truly see a taenial attachment at the infracapsular BST (tail portion), or, finally, at the medial amygdala. Here it meets the amygdalar tip of the fimbrial taenia. This *sphenoidal taenia* decorates the sphenoidal horn of the lateral ventricle, participating with the fimbrial taenia in the final part of the chorioidal fissure. This attachment characteristically is no longer associated to the stretched eminential surface that covers the prethalamic reticular nucleus (compare **Figure 12**).

rostrally with the whole secondary prosencephalon, i.e., both with the hypothalamus and the telencephalon (**Figures 1B**, **10**). It should be known that a variable rostrodorsal alar portion of the prethalamic diencephalon evaginates jointly with the telencephalic vesicle, entering into its definitive medial wall, and causing some anatomic peculiarities at this largely hidden area (**Figure 1B**; see below, as well as Lakke et al., 1988, their Figures 4, 5A, which are consistent with our **Figure 4**).

The diencephalon is divided into three diencephalic prosomeres (p1–p3, **Figure 1B**; always numbered in caudo-rostral order). These were first clearly recognized in birds, reptiles and mammals by Rendahl (1924). He identified them as synencephalon (p1), posterior parencephalon (p2), and anterior parencephalon (p3), terms still found occasionally in the literature (e.g., in Puelles and Martínez de la Torre, 1987, or in Lakke et al., 1988, cited above). Rendahl ascribed the hypothalamus to p3, perhaps in partial abeyance to Herrick's (1910) model; this inconsistency was already corrected by Puelles and Martínez de la Torre (1987) (review with schematics in Puelles, 2018). On formulating the prosomeric model (Puelles and Rubenstein, 1993; Rubenstein et al., 1994), we preferred to give terminological protagonism to the much more common terms "pretectum" (p1), "thalamus" (p2), and "prethalamus" (p3), which we redefined in agreement with the novel molecular evidence, but in substantial topologic agreement with a good number of classic observations regardless of the offered non-neuromeric interpretations [e.g., Bailey, 1916; (**Figure 4**); Miura, 1933; Gilbert, 1935; Herrick, 1936 (**Figure 6B**), Coggeshall, 1964; Altman and Bayer, 1988]; indeed, the embryos show transversal ventricular ridges rather than longitudinal ventricular sulci as mutual boundaries of these diencephalic domains (**Figures 5A**, **6A**; see the scanning electron microscopic study of Lakke et al., 1988); the implied necessary error lies in the arbitrary columnar axis.

All true pretectal nuclei are diencephalic, building the molecularly distinct alar plate of the p1 diencephalic prosomere (Ferran et al., 2007, 2008; Puelles E. et al., 2012a; **Figures 1B**, **5A**, **7B**, **8**–**10**); this means that a pretectal molecular character, as explored by Ferran and collaborators, excludes being "thalamic" or "epithalamic," as well as being "mesencephalic." The "thalamus" and "prethalamus" terms substitute for the outdated columnar ones "dorsal thalamus" and "ventral thalamus," respectively, emphasizing with the new prefix that their mutual topologic relationship is strictly *anteroposterior* ("pre-" used in thalamus/prethalamus exactly as we already used before tectum/pretectum; **Figures 1B**, **5**, **7**, **8**). Note also that in the prosomeric model (**Figure 1B**) the epithalamus or habenular region is no longer a fundamental component of the diencephalon, being listed merely as a distinct hyperdorsal

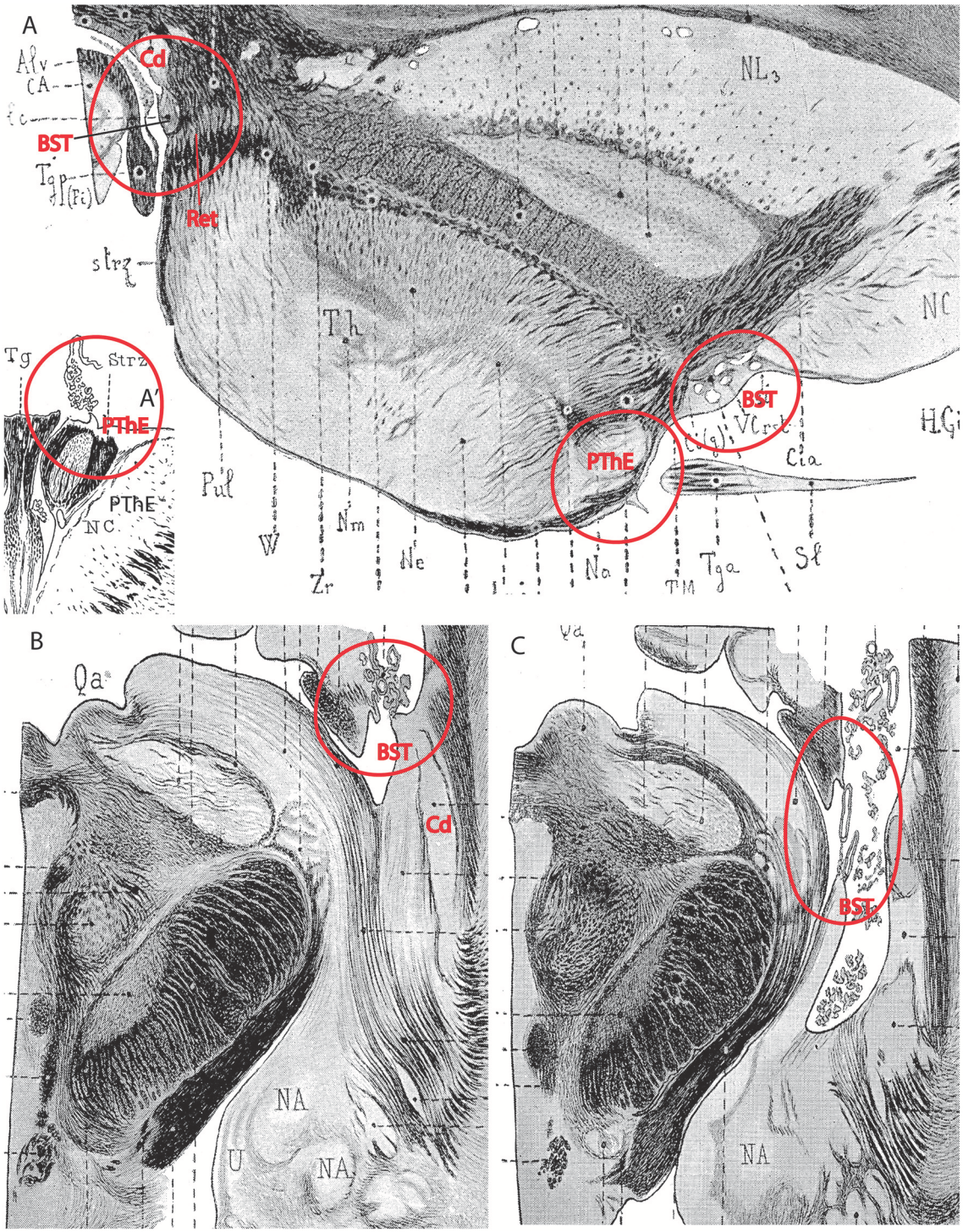

FIGURE 12 | This plate brings together four separate drawings (or drawing details) modified by red annotations, taken from the work of the French neuroanatomist Dèjerine (1895) on the adult human brain (no copyright permission required). They illustrate my new interpretation of the roof-plate-derived chorioidal insertions (taeniae) associated to thalamic, prethalamic and telencephalic structures, as presented in **Figure 11C** (and negating what I call the *lamina affixa* myth). The Dèjerine (1895) work is one of the few places where this issue can be examined objectively in the adult human brain, because it contains very precise drawings of numerous sections in various planes. Other similarly useful material (not shown) is embryonic and can be found, e.g., in the human developing brain atlas of Hochstetter (1919), and other works showing abundant sections of appropriate embryonic material at high magnification. Dèjerine's drawings frequently depict the chorioidal tela insertions without deterioration, probably thanks to the celloidin embedding method used, which preserved the delicate chorioidal tela (normally torn or fragmentary in many published sources where sections from hand-dissected brains are shown). My thesis is that the classic lamina affixa theory (see text of **Figure 11A**)

(Continued)

FIGURE 12 | is a myth that emerged because classic authors confused parts of the prethalamus as being thalamic, and pallido-diagonal parts of the telencephalic subpallium as being part of the "corpus striatum," and as a result misinterpreted the local massive morphogenetic distortions, including the appearance of part of the prethalamic eminence beyond the interventricular foramen. The prediction tested in these images is that the fissural chorioidal insertion classically held to be the transition of the same tela between *pars affixa* and *pars libera* (**Figure 11B**), and found beyond the interventricular foramen along the "thalamic" chorioidal sulcus, actually represents an insertion *along the prethalamic eminence* (which thus substitutes for the mythic thalamic ventricular bulge). This interpretation negates any adherence whatsoever; the surface classically interpreted as the *lamina affixa* covering the top of the thalamus would be a part of the ventricular surface of the prethalamic eminence that evaginates along the interventricular foramen into the lateral ventricle consequently to morphogenetic deformation of the prethalamus in the context of massive telencephalic evagination, growth and rotation. The deformed dorsal eminential prethalamus is systematically associated in depth with the reticular nucleus (also alar prethalamic, and crossed by the thalamo-cortical connections). Wherever the chorioidal taenia is prethalamic, one sees the reticular nucleus directly underneath, and this occurs along the whole chorioidal sulcus. However, once the prethalamus ends beyond the pulvinar, the fissural chorioidal tela apparently extends wholly into the temporal lobe of the hemisphere (as does the hippocampal fimbria), becoming fixed *now* at the subpallial locus of the *temporal* infracapsular bed nucleus of the stria terminalis, medially to the caudate tail (but not before, at the supracapsular BST, next to the caudate body and head, as was classically assumed). This new hemispheric insertion continues all the way to the medial amygdala retro-uncal region, where the fissure ends jointly with the fimbria. In **(A)** we see a detail of a horizontal section passing through the interventricular foramen, in which we can easily identify the pallidal and striatal basal ganglia, the internal capsule and the thalamus, which is surrounded throughout rostrolaterally by the reticular nucleus (prethalamus; marked Zr, zona reticularis, by Dèjerine, 1895). The red circle with the BST tag calls attention to the subventricular bulge of the BST complex next to the caudate head; it can be seen that there is no chorioidal insertion on it, though the stria terminalis tract and typical accompanying optostriate vessels are there (note also that the thalamus proper does not reach the BST, because the prethalamic reticular nucleus intercalates in between). The prosomeric model predicts that the thalamus never contacts any telencephalic component, being necessarily separated (even if tenuously) by some part of the prethalamus. The chorioidal insertion at the foraminal beginning of the chorioidal fissure appears instead at the slightly prominent neighboring locus circled in red and identified as the prethalamic eminence (PThE), some distance away from the BST locus. Classic authors uniformly interpreted the "thalamic eminence" as belonging to dorsal thalamus, namely as the anterior thalamic nucleus (and so did Dèjerine, 1895 as well), but developmental knowledge accrued in the meantime leads us to interprete this mass as prethalamic (the anterior nucleus lies slightly higher, as seen in other Figures of Dèjerine, 1895). Note a number of characteristic gene markers are present at this locus (see calretinin in **Figure 13A** and others in Shimogori et al., 2010). Since the chorioidal fissure is a telencephalic formation, albeit continuous with the diencephalic chorioidal roof, and at some levels the insertion occurs at the BST locus (as we will see below), classic authors speculated that the insertion at this rostral foraminal level also was at the BST bulge irrespective that one could not see it. This led to using the general explanation believed at the time that a section of the predicted chorioidal tela adhered to the neighboring "thalamic surface," forming the so-called *lamina affixa*. However, as we see, proper analysis shows there is no "thalamus," but only *prethalamus*, between the rostral BST and the foraminal chorioidal insertion at the PThE. What was supposed to be thalamus covered by *lamina affixa* is in fact standard ventricular surface of evaginated PThE that protrudes in a diminishing gradient beyond the interventricular foramen, all the way to the area next to the pulvinar (note that the pulvinar belongs jointly with the geniculate nuclei to the true lateral wall of the thalamus; **Figures 11B**,**C**). This rostral PThE protrusion is seen also in a coronal section passing through the same locus in the inset **(A′)** (red circle at left with PThE tag). The fiber packets seen within the PThE in **(A,A′)** probably represent components of the stria medullaris, which courses through the PThE into the more caudal thalamic habenula. In coronal sections placed all along the thalamus between its rostral and caudal poles we would see that the insertion line along the chorioidal sulcus is always precisely associated in depth to the point where the reticular nucleus approaches the brain surface (not shown; see any such section in Dèjerine, 1895). However, in the section shown in **(A)**, we also see behind the caudal pole of the pulvinar another chorioidal insertion (also emphasized by a red circle). This non-fimbrial taenial insertion jumps at the center of the caudal red circle from the hippocampal fimbria marked Tgp (Fi) into a small telencephalic area originally labeled "Ic," that is, "lamina cornea," an old name for the supracapsular BST (BST in red). This new insertion lies just outside the reticular nucleus band surrounding the thalamus [Zr]. The classic lamina cornea is what we now identify as the BST, a derivative of the medial ganglionic eminence which accompanies the striatal tail of the lateral ganglionic eminence (Cd in red; the tail appears as a white mass above the lamina cornea or BST). Here we see a non-fimbrial taenial insertion that no longer occurs directly on top of the reticular nucleus, but lies immediately outside it, associated truly to the telencephalic BST formation, medially to the caudate tail (white round mass seen above it). This image thus practically shows the locus where the prethalamic PThE chorioidal insertion ends and a sphenoidal telencephalic BST insertion begins. **(B)** Shows a somewhat lower horizontal section through the ventral pulvinar (still above the geniculate bodies) and **(C)** passes through the ventral part of the internal capsule and the medial amygdala/uncus area (NA, U in **B**); the red circle indicates that the fissural chorioidal insertion continues attached to the sphenoidal BST portion, next to the caudate tail (Cd). The section in **(C)** is slightly more ventral and the red circled area shows the chorioidal insertion finally reaching the medial amygdala (labeled NA).

subregion of the thalamus (alar p2; ETh; Hb; hab; hb; **Figures 1B**, **7**, **10**, **13B**), found next to the local roof plate, which displays the unique pineal gland (ep/E; **Figures 1**, **5A,B**, **10**). Another distinct hyperdorsal subregion characterizes the prethalamus (p3), and is termed by us the "*prethalamic eminence*" (PThE/pthe). The latter was known in classic works as the "thalamic eminence," because various authors did not distinguish in adults the respective ventral/dorsal thalamic derivatives and perhaps wrongly thought this eminence represented the rostral pole of the whole thalamic mass (however, Gilbert, 1935 used that term knowing the structure was ventral thalamic). However, for molecular and topologic reasons it is now very clear that the hyperdorsal diencephalic subregion that builds an eminence at the back of the interventricular foramen (next to the local roof chorioidal tissue) lies rostral to the thalamo/prethalamic limit, the zona limitans intrathalamica (PThE/pthe; zli; **Figures 4**, **5**, **10**, **13A**); accordingly, it must be ascribed to the prethalamus (PTh; **Figures 1B**, **5**; alar p3), and named accordingly "prethalamic eminence" (as many recent authors are already doing). The stria medullaris tract runs *longitudinally* through the PThE before reaching the habenular region. This was thought to be a *ventrodorsal* course in columnar accounts, but posed another semantic conundrum, because the tract's position parallel to the thalamic chorioidal taenia (**Figure 1A**), an obvious *longitudinal* roof plate landmark, remained unexplained these last 100 years. Similarly, Swanson (2012) has a schema where the whole chorioidal fissure, a straightforward roof plate derivative (**Figures 1A,B**), is figured as a ventrodorsally oriented component of the early embryonic lateral forebrain wall.

Importantly, the p3 or prethalamic prosomere completely separates the thalamic prosomere (p2) from the telencephalon and hypothalamus (**Figures 1B**, **5A**, **10**, **13A**). This is an incontrovertible prosomeric conclusion that needs to be

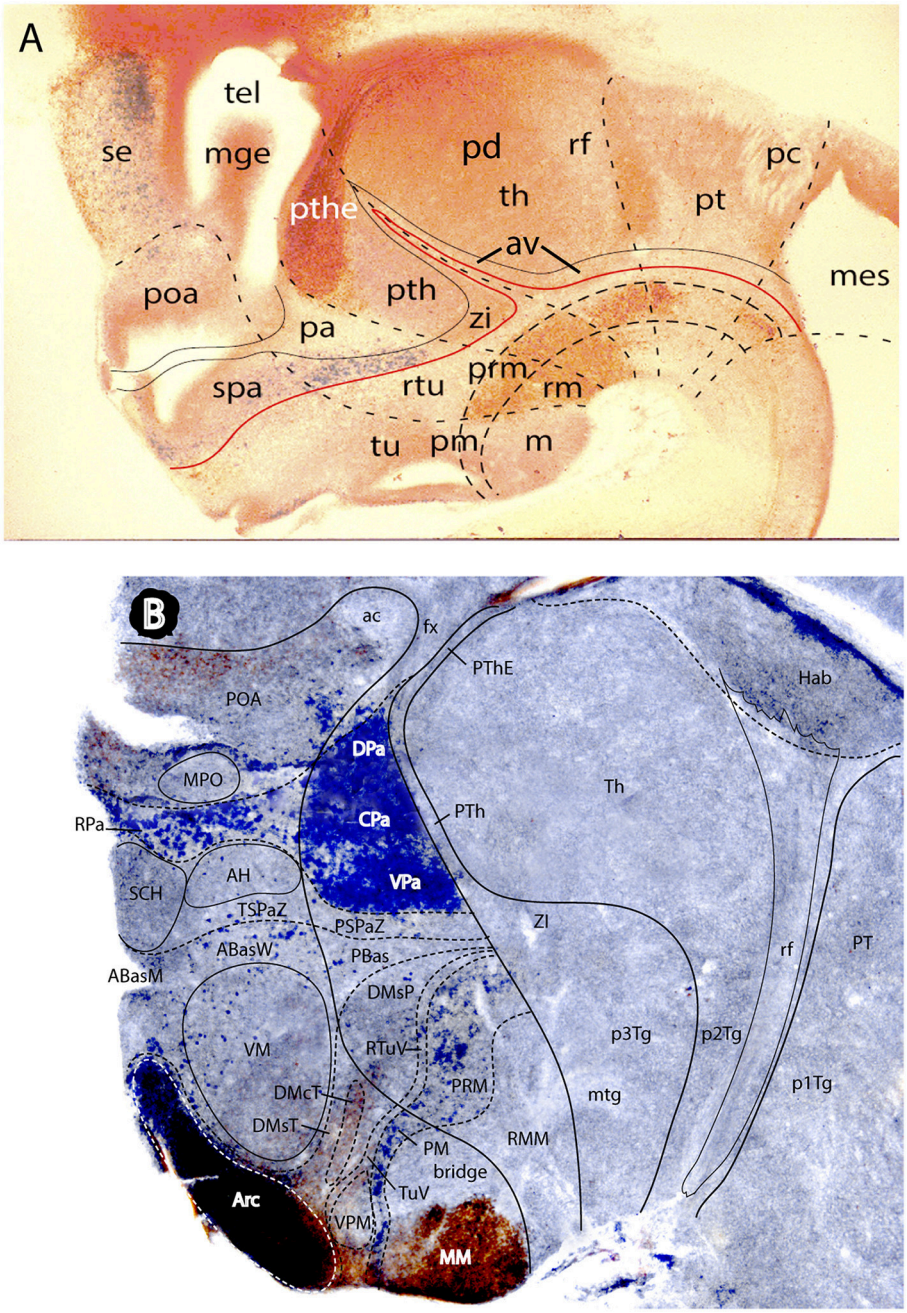

FIGURE 13 | Two mouse brain sagittal sections reacted genoarchitectonically to visualize prethalamic and hypothalamic subdomains in a broader forebrain context (particularly diencephalic). Material extracted and slightly modified from (Puelles L. et al., 2012a) no copyright permission required). **(A)** Is a E16.5 mouse embryo sagittal section showing weak Dlx5/6-LacZ blue reaction at sites of *Dlx* gene expression e.g., the hypothalamic subparaventricular area (spa), continuous caudally with the prethalamic zona incerta area (zi), the latter being also continuous over the *Nkx2.2*-positive shell domains of the zona limitans (compare **Figure 5C**) with further alar areas always next to the basal plate down to the midbrain (this band coincides with sites producing GABAergic neurons). Calretinin immunoreaction was combined in **(A)** (brown reaction), to highlight the prethalamic eminence subregion (pthe) as well as some partial basal plate patterns across hp1, dp3, and dp2. The dash lines mark interprosomeric boundaries running from roof to floor. Note retroflex tract (rf) and posterior commissure (pc) as boundary-related landmarks. The alar prethalamus appears accordingly divided into three dorsoventral subdomains, namely the prethalamic eminence (pthe), the subjacent area occupied by the major prethalamic derivatives (reticular nucleus, and the pregeniculate and subgeniculate visual centers—marked "pth") and the zona incerta area (zi). Note the underlying prethalamic tegmentum (separated by the red alar-basal boundary) is also divided into three dorsoventral subdomains (longitudinal dash lines), which also extend throughout the whole forebrain. The hypothalamic alar plate, in contrast, is divided only into two dorsoventral zones, the paraventricular area (pa) and the subparaventricular area (spa). The pa has a sharp molecular boundary with the alar prethalamus (pth); see also **(B)**. It is larger dorsoventrally within hp1, whereas the spa is larger within hp2 (peduncular vs. terminal hypothalamus; compare **Figure 10**). The basal plate hypothalamic territory is divided dorsoventrally in three

(Continued)

FIGURE 13 | longitudinal zones: tu/rtu (tuberal and retrotuberal; this expands rostralwards into the acroterminal area; check **Figure 10**), pm/prm (perimamillary/periretromamillary), and m/rm (mamillary and retromamillary). The preoptic area (poa) falls inside the telencephalic subpallium, jointly with the ganglionic eminences (here only the mge is seen) and the subpallial septum (se). **(B)** This sagittal section of an adult mouse brain shows hypothalamic molecular domains complementary to those labeled in **(A)**. The blue signal corresponds to Otp-LacZ reaction present in neurons that express the *Otp* gene. This signal is mainly characteristic of the oxytocin/vasopressin neurons of the hypophysiotropic magnocellular paraventricular nucleus. Here we see even more clearly than in the embryo **(A)** that there are quantitative differences between the paraventricular derivatives in PHy (the principal paraventricular nucleus; subdivided by Puelles L. et al. (2012a) into dorsal, central and ventral parts- DPa, CPa, VPa- which show differences with other markers) and THy (dorsal to unstained SCH and AH subparaventricular nuclei); the Pa area of THy contains less important paraventricular populations, but displays preponderant presence of the subpial supraoptic nucleus cells. Another site where islets of Otp-LacZ reaction are found is the basal pm/prm band, here again of larger size in PHy than in THy. Other Otp-expressing cells lie around the ventromedial nucleus (the VM shell), or are mixed with other neurons at the arcuate nucleus (Arc). The latter formation appears strongly counterstained with anti-NKX2.1 immunoreaction (brown), which extends somewhat into the neighboring terminal dorsomedial nucleus subregion (DM-T) and into the medial mamillary body (MM). The diencephalon shows a well-developed habenular complex (Hab), with the descending retroflex tract in characteristic prosomeric position (rf). Note also considerable adult compression of the periventricular stratum of the alar prethalamus (PTh, PThE), always intercalated between thalamus and hypothalamo-telencephalic structures.

assimilated with its corollaries by any attentive modern neuroanatomic mind. Indeed, columnar literature frequently assumed that the thalamus directly contacts striatal telencephalic formations across the so-called "opto-striate, or thalamo-striate sulcus" (see **Figure 11A** taken from the 1979 edition of Gray's Anatomy); however, this classic "thalamus" really was the indistinct sum of alar thalamus and alar prethalamus (**Figure 11C**). The thalamo-striate sulcus, also known as sulcus terminalis, would roughly correspond to a *prethalamo-subpallial boundary*. While the prefix "thalamo" in the cited classic sulcus name is obviously wrong and means "prethalamo," the suffix "striatal" is also wrong as regards the basal ganglion that establishes such "thalamic" contact, given that other subpallial parts of the telencephalon are now known to be nearer to the prethalamic diencephalon than the striatum (the latter is in fact most distant, being a derivative of the lateral ganglionic eminence; LGE; **Figure 11C**). The pallidal and diagonal subpallial areas are the elements derived from the medial ganglionic eminence that are closest to the diencephalon or, more precisely, to the prethalamus (Pal; Dg; **Figure 10**; MGE; **Figure 11C**; see our subpallium model in Puelles et al., 2013, 2016). They are represented at the ventricular surface by the lateral and medial bed nuclei of the stria terminalis, respectively; thus, the only really possible contact is between the *prethalamus* and the *diagonal area plus BSTM*, and certainly not the striatum. Interestingly, the classic authors clearly were not able to distinguish the derivatives of the embryonic medial and lateral ganglionic eminences even in advanced embryos, or perhaps were blocked in their thinking by the idea that all subpallium was striatal (e.g., Hochstetter, 1919, a major embryologist, in whose sections one often can see the darker and smaller pallidum domain); other classics failed at the same task for different reasons, e.g., because they wrongly assumed that the pallidal complex was hypothalamic (e.g., Christ, 1969; Kuhlenbeck, 1973).

As we now know, the transversal thalamic and prethalamic diencephalic wall regions, as well as the hypothalamus, were wrongly interpreted as longitudinal columns in the columnar model, which caused many confusing inconsistencies and conundrums (supposed "longitudinal" items found orthogonal to other longitudinal elements, or postulated "ventrodorsal" items found clearly parallel to longitudinal landmarks). In the prosomeric model, the *names* pretectum, thalamus and prethalamus are easily understood and consistently applicable with reference to all sorts of histologic material, if they are used strictly according to the respective alar domains of the p1–p3 prosomeres. Moreover, we also can apply the same easy terms to the whole segments when we loosely say "pretectal, thalamic or prethalamic segments, prosomeres or neuromeres." In those expressions it is understood that we are adding the tegmental (basal/floor) portions of these units to the main alar components (**Figures 10**, **13A**). We even find it is sometimes useful to employ allusively the expressions "pretectal, thalamic or prethalamic basal plate or tegmentum" (alternative to p1Tg, p2Tg, p3Tg).

SPECIFIC PRETECTAL ISSUES

As regards the nomenclature of pretectal grisea there are no major semantic problems, because the axial references are here comparable in both models. **Figure 8** shows a number of pretectal structures that classic literature tended to ascribe wrongly to the midbrain, notably the terminal nuclei of the basal or accessory optic tract, the classic posterior pretectal nucleus and the parvocellular red nucleus. There are otherwise problems due to our present very poor knowledge of the number of true pretectal nuclei in mammals, due to the region's classical Cinderella status, heightened by the undistinctive Nissl aspect of the mammalian pretectum (but see horizontal images in **Figure 9**; Puelles E. et al., 2012a, as well as recent work by Márquez-Legorreta et al., 2016). We are presently working on the mouse pretectum with genoarchitectonic markers, hoping to redress (partially, at least) this situation (Ferran et al., in preparation). The main semantic problem in the pretectum apparently was the incorrect "posterior pretectal nucleus" name, because this nucleus is instead distinctly mesencephalic, as commented above. The literature on mammalian visual projections mentions a nucleus of the optic tract, which is a term referring in my opinion to the retinorecipient superficial stratum of the classic posterior pretectal nucleus, though it is often used as if it was an independent pretectal entity. In order to erase the consequent confusion in the literature, we have proposed to name "*tectal gray*" the single rostral mesencephalic retinorecipient entity found rostral to the superior colliculus

and caudal to the posterior commissure. This name and topographic ascription already existed in earlier comparative neuroanatomy of non-mammalian tetrapods (TG; **Figure 9**; review in García-Calero et al., 2002; Puelles et al., 2007, 2018).

SPECIFIC THALAMIC ISSUES

As regards the "thalamus" (alar p2), a term whose prosomeric meaning incorporates the habenular region (the columnar "epithalamus") to the old "dorsal thalamus," the modern view merely applies to its morphologic referent an oblique intrinsic dorsoventral dimension which is different from the columnar one (**Figures 1A,B**, **5**, **7**, **8**, **10**, **13A**). This is so because at this point the natural forebrain length axis starts to bend together with the cephalic flexure (**Figure 1B**); usefully, the strictly dorsoventral course of the retroflex tract always marks the caudal thalamic border and the real dorsoventral direction at the back of the thalamus (rf; **Figures 1B**, **13A,B**; Puelles et al., 2012b). This tract is compact and is seen only periventricularly. However, there exists as well a fiber-rich more lateral pretecto-thalamic limiting lamina that delineates the same boundary through most of the mantle layer. This fibrous lamina was first described, as far as I know, by Coggeshall (1964), in a curious non-neuromeric paper dealing with evident neuromeres in the rat, who called "posterior thalamic septum" the transversal fibrous laminar boundary of the thalamus. He clearly related it to the thalamo-pretectal interneuromeric constriction (his "middle thalamic fold"; [p2/p1 limit]). His material also reveals that the zli of Rendahl (1924) and Gilbert (1935) [the p3/p2 limit] represented his "anterior diencephalic fold," while his "posterior diencephalic fold" was the pretecto-mesencephalic interneuromeric border caudal to the posterior commissure –[p1/m1 limit]; check pc in **Figures 1B**, **7B**, **8**, **9A**, **13A**: cp in **Figure 4**. Recently Márquez-Legorreta et al. (2016) have rediscovered this limiting septum in a chemoarchitectonic analysis of this area in the adult rat, calling it "pretecto-thalamic lamina," after discussion of other references to it in the literature. Like the pretectum before, the more massive thalamus is also wedge-shaped, being longer dorsally than ventrally (**Figures 1B**, **10**, **13A,B**). This slight change in the spatial orientation of the dorsoventral thalamic dimension affects somewhat our appreciation of the relative topology of individual thalamic nuclei or nuclear complexes. For instance, columnar interpretation wrongly takes the medial geniculate body to be the "caudalmost" thalamic mass, when in fact it is the *ventralmost* thalamic mass, lying strictly ventral to the lateral geniculate body, as is readily seen in embryonic or any correctly interpreted adult material (LG; MG; **Figures 7A,B**); this is also confirmed by observing the topography of the well-known homologous entity in amphibians, reptiles or birds (Puelles, 2001; Puelles et al., 2007, 2018), a comparison unfortunately made difficult by the ancestral periventricular locus of the MG homolog in these lineages (Puelles, 2001).

The vague conceptual status of the pretectum as a caudal extension of dorsal thalamus, as well as the emphasis given by columnar authors to adult human relationships produced the now obsolete notion of the "metathalamus," which would contain both the lateral and medial geniculate bodies in caudal proximity to (or identity with) the pretectum. Altman and Bayer (1995) unfortunately construed an aberrantly misguiding story about a pretended "methathalamic" (actually false pretectal) origin of both thalamic geniculate nuclei in the rat, which I had the opportunity to review critically in TINS by editorial invitation (Puelles, 1996). My relevant detailed comments did not obtain any contrary argumentative response from the authors. What happens with regard to the apparent "methathalamic" position of geniculate formations in primates is that the disproportionate growth of the thalamic mass in concert with the even more massive telencephalic growth and rotation deforms it unequally, so that its primary lateral surface (which carries the early-born and thus subpial geniculate bodies) is pushed backwards under the pulvinar, thus becoming oriented caudalwards, close to the independent pretectum (**Figure 11B**; this process was clearly illustrated by Gilbert, 1935; see also **Figure 9** in Puelles et al., 2019, this book). This deformation due to differential growth was probably first pointed out by Schwalbe (1880), and was emphasized again by Hochstetter (1895, 1919), and a few other authors (however, none of these authors realized that the ventral thalamus or prethalamus also suffers a congruent deformation, with significant flattening of its mantle layer, due to its intercalation between telencephalon and thalamus; see **Figure 11C**). In the meantime, various other embryologists (e.g., Miura, 1933; Gilbert, 1935; Ströer, 1956; Coggeshall, 1964, and many others until present times), as well as comparative neuroanatomists, have concluded unanimously that the thalamic geniculate nuclei are both formed rostrally, next to the zona limitans intrathalamica. This explains why the thalamic lateral geniculate relates via the small intergeniculate leaflet to the prethalamic pregeniculate nucleus. The medial geniculate lies strictly *ventral* to the lateral geniculate primordium, as can be easily seen in nearly tangential sagittal sections through postnatal brains.

In a review (Puelles, 2001), I explored the possibility to explain the regionalized evolution of the whole thalamic mass into constant complexes or pronuclei out of which variable numbers of individual thalamic nuclei might evolve. The system stood on the basis of three (or perhaps four) dorsoventrally superposed "thalamic tiers" (dorsal, intermediate and ventral), understood as primordial pronuclei. It was held that these units retain evolutionarily some comparable connectivity (and other) properties in the thalamus of all advanced vertebrates. The cited three tiers are easily seen as individual cell masses in reptiles (Díaz et al., 1994; Dávila et al., 2000). Redies et al. (2000) and Martínez-de-la-Torre et al. (2002) examined them with molecular markers in the chick, where the intermediate tier acquires particular significance (review in Puelles et al., 2007, 2018). Indeed, individual tiers develop differentially in each lineage (eventually a tier involutes or grows disproportionately in some species). The dorsal tier (possibly complemented by a novel "associative" fourth tier) expands particularly in mammals correlative to evolutionary differential cortical growth (the potential fourth tier attending predominantly to associative cortex). The reference atlases and particularly the ontology I developed later for the public Allen Developing Mouse Brain

Atlas (developingmouse.brain-map.org; offered since 2009) tried to show how the standard nomenclature for mammalian thalamic nuclei could be subsumed under the dorsoventral tier theory.

A further detail that recent molecular research has discovered relative to the thalamus, not contemplated by columnar schemata, is that the main thalamic mass consists largely of excitatory glutamatergic neurons. In rodents, inhibitory interneurons are visible only in the lateral geniculate nucleus, but other mammalian lineages including primates show them nearly everywhere, mixed with the thalamocortical projection neurons. It turns out that these cell types are produced separately. The thalamic alar domain first results patterned differentially into a thin anteroventral boomerang-shaped progenitor domain placed next to the zli core and the basal plate (av; **Figure 13A**) and a larger posterodorsal progenitor domain representing all the rest (pd; **Figure 13A**). The anteroventral domain is strongly influenced by the proximity of high SHH levels at the underlying basal plate and at the zona limitans (**Figure 5B**), resulting in a correlative *Nkx2.2* expression pattern at the av (and other forebrain areas under a similar influence, as shown in **Figure 5C**; by the way, this *Nkx2.2* band is the modern marker for the forebrain alar-basal boundary; discussion in Puelles E. et al., 2012a and Puelles and Rubenstein, 2015). The *Nkx2.2*-positive av domain has a differential molecular profile and fate compared to the larger posterodorsal *Gbx2*-positive rest of the thalamic progenitor layer (review in Puelles and Martinez, 2013, which also contains an hypothesis of how the zli organizer forms). Only the thin av domain produces inhibitory neurons, and it represents the source of the inhibitory neurons that secondarily invade tangentially the purely excitatory populations of the main posterodorsal thalamic mass, starting with the lateral geniculate nucleus. This tangential invasion is curiously selective with regard to the tiers, since the LG belongs to the dorsal tier, while the MG, which lacks such interneurons in rodents (Puelles et al., 2012b), belongs to the more precociously produced ventral tier (Puelles, 2001). A few inhibitory cells may invade the thalamic posterior periventricular nucleus through the thalamo-pretectal border. This distinction between differential progenitor domains of the thalamus according to functional cell type produced is not yet registered in any way in the standard nomenclature.

SPECIFIC PRETHALAMIC ISSUES

The prethalamus (alar p3) is another Cinderella-like area in the forebrain. Its intrinsic dorsoventral dimension is even more inclined than that of the thalamus relative to the brainstem axis, because of the cephalic flexure (PTh; **Figures 1B**, **5**, **7**, **8**, **10**, **13A**). This diencephalic territory apparently was subliminally deemed less important than the thalamus because its neurons, which largely are of inhibitory nature (Puelles et al., 2012b), do not project into the telencephalon. The better known prethalamic derivative is the "thalamic reticular nucleus," which already represents a semantic error; it manifestly lies within the PTh intermediate stratum (**Figure 13A**); for clarity, this well-known element should preferably be named "prethalamic reticular nucleus," or simply "reticular nucleus." Other prethalamic derivatives are the pregeniculate and subgeniculate retinorecipient nuclei (lying at the subpial stratum under the optic tract) and the zona incerta (across all strata, at the ventral end of the prethalamic alar domain; **Figure 13A**). The problem posed by the "zona incerta" is that many columnar accounts place it in the "subthalamus." The latter concept is a misguided rest of its first introduction by Forel (1877), who referred it to the *basal* forebrain domain lying underneath the "thalamus." His (1893, 1895, 1904) later renamed Forel's tegmental subthalamus as "hypothalamus." As further historic steps led to expansion of the hypothalamus concept by aggregation of added alar plate subregions (review in Puelles L. et al., 2012a), some authors that apparently did not realize that the "subthalamus" term was already outdated tried to visualize a sort of fifth longitudinal column that could be called "subthalamus," and which would lie intercalated between Herrick (1910) ventral thalamus and hypothalamus (this implies a shaky pentacolumnar version of the columnar model). Since such a fifth column strictly does not exist, or it would have been seen before, these attempts to construe a subthalamic column were condemned to compose the subthalamus out of parts taken either from the hypothalamus or from the ventral thalamus, or from both. We thus see literature placing arbitrarily in that virtual subthalamic region the alar prethalamic zona incerta and the alar "dorsal hypothalamic area" ("dorsal" here means in columnar parlance "close to ventral thalamus"). The only structure whose "subthalamic" identification is in some sense (*sensu* His, 1893) not contradictory is the subthalamic nucleus, because it is a migrated derivative of the *basal* hypothalamic retromamillary area (STh; **Figure 10**) and finally lies deep to the peduncle under the local alar plate, or thalamus *sensu lat*o of His (1893) (details in Puelles L. et al., 2012a; another name of this nucleus was for a time "hypothalamic nucleus," showing that at the turn of the twentieth century "subthalamus" and "hypothalamus" were synonyms). Some embryological studies led authors to believe that distinct ventricular zone domains could be visualized for the subthalamus and the hypothalamus, but these turned out to correspond to the two hypothalamic prosomere domains identified by us (Puelles L. et al., 2012a; Puelles and Rubenstein, 2015); both are clearly hypothalamic. For clarity's sake, Puelles L. et al. (2012a) argued that we should eliminate altogether any continued use of the "subthalamus" terminology, excepting the individual *subthalamic and parasubthalamic nuclei*, which cause no problem and must be understood as basal hypothalamic formations (STh originates within basal and retromamillary PHy; **Figure 10**; later it migrates dorsalward, acquiring secondarily a position within the equally basal retrotuberal area; RTu; **Figure 10**). Conversely, the zona incerta must be firmly ascribed to the ventral rim of the prethalamus, or the ventral rim of alar p3 (zi; **Figure 13A**).

Finally, as mentioned above, the hyperdorsal subregion of the prethalamus forms the prethalamic eminence (PThE/pthe; **Figures 10**, **13A**; see also **Figure 6B** for amphibians). A sizeable part of this region bends over through the interventricular foramen into the medial telencephalic wall, carrying with it its attached roof plate chorioidal tela and chorioidal taenia (a

taenia is an insertion of a portion of roofplate chorioidal tela into the dorsal lip of the corresponding alar plate; see **Figure 1B** and thick black roof plate in **Figure 10**; also compare Figures 4, 5A of Lakke et al., 1988; I have decided to use what seems the etymologically correct orthography of this term, if it derives from the Greek *khorion or chorion*—vascularized fetal membrane, and thus leads to "chorioidal," as used by numerous classic authors, but not so much by modern ones; Werner, 1956, p. 156). Accordingly, the prominent ventricular contour which we see delimiting the back side of the interventricular foramen (e.g., the calretinin-positive pthe; **Figure 13A**) is not the true dorsal end of this part of the prethalamus; the evaginated part lies hidden as a flap that extends beyond this eminential bulge within the immediate medial telencephalic wall, in the vicinity of the medial ganglionic eminence (mge; **Figure 13A**), and separated from the latter by the sulcus terminalis. The prethalamic chorioidal tela thus projects into the medial telencephalic wall, contributing to the formation of the supracapsular part of the classic chorioidal fissure. Given that most of the authors along these last 100 years have not been very much aware of the prethalamus (having misinterpreted the prethalamic eminence as a thalamic eminence), nor of its specific transition into the medial wall of the telencephalon via the prethalamic eminence, a general false belief was prevalent that the thalamus directly contacts and attaches to the subpallial (striatal) telencephalon (see **Figures 11A,B**). The neuroanatomists dealing with the chorioidal fissure generally failed to understand the local morphologic configuration (e.g., see Swanson, 2012 concept of the roofplate-derived fissure, by definition a longitudinal item, represented as a transverse structure). As a result of this confusion, a mythical, largely conjectural interpretation developed of what one sees at this obscure corner of the forebrain after dissection or sectioning, particularly in the human brain. This was the theory of the *lamina affixa*, an hypothetic, but really inexistent, piece of chorioidal tela believed to interconnect the telencephalic sulcus terminalis with the supposedly adjacent thalamus (referring in fact to what actually was misinterpreted prethalamus).

This theory states that the chorioidal tela that closes the telencephalic chorioidal fissure was originally wholly free of contact with the diencephalon and jumped from its clearcut fimbrial taenial insertion (border of the hippocampus; no problem with that) to another insertion at the stria terminalis, at the border of the *corpus striatum* (see left part of **Figure 11A**; note this is speculative, not real; nobody has shown a real section like this). Part of the fissural chorioidal tela would then adhere firmly to a neighboring part of thalamic pial surface, up to the so-called chorioidal sulcus (chs; right part of **Figure 11A**). The adhered part of chorioidal tissue would form the so-called *pars affixa of the fissure*, or *lamina affixa*, and, since this lamina is so thin, this supposedly causes a *pial* part of the dorsal thalamus to emerge under its covering at the floor of the lateral ventricle, just medially to the stria terminalis and the thalamo-striatal terminal sulcus (right side of **Figure 11A**); the non-adhered rest of the fissural chorioidal tela would be the *pars libera*, which would go on to form the chorioidal plexus of the lateral ventricle (**Figure 11A**). This theory is a conjecture, because the postulated adhesion process has not been demonstrated histologically in an embryonic series. However, this account is found in most neuroanatomy textbooks.

I proposed years ago in a conference on human brain development held in Rome that consideration of the obligatory presence of prethalamic derivatives in that scene showed the lamina affixa theory to be an unnecessary myth, since the observed morphologies and relationships could be explained alternatively, without recurring to undemonstrated adherence between telencephalic and thalamic pial surfaces. **Figures 11**, **12** (and their legends) collect my position and some evidence supporting it.

I basically suggest that we can distinguish three successive parts of the *prethalamic chorioidal tela,* which derives from the p3 roof plate, and attaches primarily to the hyperdorsal alar PThE (**Figures 1B**, **10**): (1) a small *pre-foraminal* part is found just caudal to the interventricular foramen; it includes the chorioidal tela closing the rostral diencephalic part of the third ventricle, and it jumps from the pre-foraminal prethalamic taenia into its contralateral homonym; this rather small part probably forms the rostral arm of the *velum transversum*, since the zli, the interthalamic p3/p2 boundary, ends dorsally at the velum (a transversal fold in the chorioid roof plate, classically interpreted as tel-diencephalic limit, but corresponding in fact to p3/p2 zli boundary; h.s-t.r.; v.t.; in **Figure 4**; VEL.TR. in **Figure 6**; see also Lakke et al., 1988; their Figure 5A; vel.transv. in **Figure 11C**, right side). This small pre-foraminal prethalamic taenial sector is usually misidentified as part of the "thalamic taenia" (term that should be restricted to p2, that is, to areas caudal to the velum transversum; see tth in **Figure 11C**); (2) a small *foraminal* portion of the prethalamic taenia is next found above the interventricular foramen itself and the major intraventricular bulging portion of the PThE (**Figures 11C**, **12A**,A′); here the taenia relates to the chorioidal roof of the interventricular foramen; the local chorioidal tela probably jumps from the foraminal prethalamic taenia into the taenial insertion at the back of the subfornical organ and the hippocampal commissure; (3) finally, there is a longer *post-foraminal* art of the prethalamic taenia, whose insertion runs along the thalamic "chorioidal sulcus," which really represents the free dorsal lip of the deformed prethalamic eminence (i.e., the "thalamic chorioidal sulcus" is really a stretched *prethalamic* insertion site). The real nature of the morphogenetically stretched PThE is revealed because it correlates systematically with the linear band where the deeper prethalamic reticular nucleus maximally approaches the brain surface (dot line over the red PThE in **Figure 11C**; see legend and images in **Figure 12**; this relationship was never recognized before). This longer post-foraminal portion of the prethalamic chorioidal tela jumps across the fissure from its stretched PThE insertion to the opposed fimbrial supracapsular taenia (and, accordingly, is *not* inserted in the area of the stria terminalis, but in the PThE). The surface classically interpreted as *lamina affix*a covering the "thalamus" extends between the post-foraminal prethalamic taenia and the stria terminalis, next to sulcus terminalis. This surface is ventricular and represents the evaginated trans-foraminal ventricular surface of the PThE participating in the medial wall

of the hemisphere, or the floor of its lateral ventricle, up to the sulcus terminalis.

After the chorioidal sulcus and the prethalamic chorioidal tela both finish close to the caudal thalamic pole, apparently at the lateralmost part of the caudal pulvinar, not far from the underlying lateral geniculate nucleus, and, more precisely, next to the prethalamic pregeniculate nucleus (**Figure 11C**), there continues a purely telencephalic part of the non-fimbrial fissural chorioidal taenia, the final, or *sphenoidal taenia* sector. Here we see the chorioidal fissure tela jumping from the fimbria to an extra-diencephalic taenial attachment at the *sphenoidal (infracapsular) BST* and later at the posterodorsal medial amygdala (isolated dot line marked tst in **Figure 11C**; compare BST; **Figures 12A–C**). In humans the fimbrial taenia ends at the uncus, next to the dentate gyrus; see dissection data obtained by Klingler (1948).

Villiger and Ludwig (1946) and Villiger et al. (1951) are the only authors who considered this prethalamic taenial issue, in context with the known torsional morphogenesis of the hemisphere around its stalk, which brings the primitively posterior temporal pole into a more anterior position, particularly in large-brained mammals. They thought that the prethalamic chorioidal roof plate might be stretched as far as the uncus and medial amygdala, but I doubt this interpretation because an even more stretched PThE and reticular nucleus would be expected then to reach as well the amygdala, which does not happen, apparently.

PROBLEMS WITH THE HYPOTHALAMUS

The hypothalamus is the forebrain site where the columnar-inspired conventional terminology of the last 100 years is most conflictive with the prosomeric concepts, due to the blatant difference in the respective axial references (90° of difference; i.e., the columnar *length* axis corresponds to the prosomeric *dorsoventral* dimension). So far a complete alternative nomenclature with a consistent prosomeric terminology has not been proposed. I worked on it while writing the Puelles L. et al. (2012a) chapter, but finally abandoned this effort, thinking it would require too many changes, and, therefore, also demand too much from the receiving end. It seemed best for clarity to momentarily keep most conventional names (with sparse novelties or adjustments), while we emphasized the topologic and causal interpretation advantages derived from the prosomeric model and its molecular underpinnings, such as a dorsoventral molecular patterning partially shared with more caudal forebrain regions (comments on this in Puelles and Rubenstein, 2015). Along with this idea we postulated two prosomeric units within the redefined hypothalamus (hypothalamic prosomeres 1 and 2, or hp1, hp2; numbered in caudorostral order, like in the diencephalon; see our rationale for this in Puelles and Rubenstein, 2015). The idea was to first try to win over the readership with our theoretic morphologic analysis, and later let the field address gradually, with only occasional help from our side, the problem posed by the incongruent columnar anatomic descriptive terms. The major scientific advantage of the prosomeric model of the hypothalamus is that it allows causal analysis within a framework of patterning mechanisms that is common for the whole forebrain as far back as the isthmo-mesencephalic boundary. This desirable aim absolutely needs correcting the arbitrary and aberrant decision taken by Herrick (1910) on the axial reference. Once this is done, standard anatomic descriptors will have changed meanings and will need to be adapted to the correct axis. The field will find the how, when, and who to do it.

I already covered above the general position of the hypothalamus relative to the diencephalon (and the prethalamus in particular). A second basic point to attend is the hypothalamo-telencephalic border. Columnar convention during the second half of the twentieth century has held that the hypothalamus includes "rostrally" the preoptic region. This was initially not so, particularly when the "hypothalamus" term was first defined by Forel (1877) and His (1893, 1895, 1904), referred exclusively to a basal plate entity (**Figure 2A**). However, other authors later incorporated alar regions to the hypothalamus concept, as it stands at present (historic review in Puelles L. et al., 2012a), and that tendency eventually also led to a tentative joint description of the preoptic area with the hypothalamus (e.g., Le Gros Clark, 1938, p. 9: "Although, strictly speaking, this area is no part of the hypothalamus....., it requires to be described briefly here because the two cannot be separated morphologically"). Later the step was taken to adopt its straightforward ascription to the hypothalamus (McRioch et al., 1940; Christ, 1969). One unifying morphologic principle apparently was the shared third ventricle relationship. Notably, the magnocellular cells of the paraventricular and supraoptic nuclei were first classified as preoptic (i.e., telencephalic), and only later thought to be hypothalamic.

Once the molecular era began, it turned out that the preoptic area shows distinct similarity in gene expression patterns (and causal mechanisms) with the adjoining telencephalic subpallium (moreover, many preoptic neurons migrate tangentially into the telencephalic subpallium and pallium, a feature characteristic of subpallial domains, and none of its derivatives move into the hypothalamus). In parallel, there is a sharp molecular boundary between the preoptic area and the neighboring hypothalamic paraventricular area (Flames et al., 2007; Shimogori et al., 2010; Puelles L. et al., 2012a; Puelles and Rubenstein, 2015). Again in this case, the judgment of pre-columnar experts turned out to be correct in the long run, and the relevant conclusion appears incorporated in the prosomeric model, namely the ascription of the preoptic area to the telencephalic subpallium. Obviously, this boundary is interpreted as a dorsoventral (longitudinal) one within the prosomeric model, insofar as the whole telencephalic field develops within the dorsal part of the hypothalamic alar plate (Puelles and Rubenstein, 2015).

The transition into the telencephalon, however, is double, because we have two hypothalamo-telencephalic prosomeres (hp1 and hp2; *loc.cit.*). The sum of alar and basal hypothalamic domains of these prosomeres were newly named *peduncular hypothalamus* (PHy) and *terminal hypothalamus* (THy), respectively (**Figure 10**; Puelles L. et al., 2012a). I thought that these terms were needed immediately, to provide a

clear prosomeric way to move around in the hypothalamus, pending full terminological corrections. The new terms evaded continuous discussion about the meaning of the descriptors "dorsal, ventral, rostral, caudal." These terms are descriptive and easy to remember. "Peduncular hypothalamus" refers to the selective (dorsoventral) course of the *cerebral peduncle* through the PHy (see **Figure 7B**; also various relevant images in Puelles L. et al., 2012a and Puelles and Rubenstein, 2015). The peduncle only bends caudalwards when it reaches the basal plate of PHy, passing around the subthalamic nucleus (e.g., **Figure 6B**). This peri-subthalamic peduncular bend is readily visible in rodents and other small mammals, but not in the human brain, where massive peduncular growth results in an *apparent* straight course of the hypothalamic peduncle into the pes pedunculi.

On the other hand, "terminal hypothalamus" refers to the topologic *terminal position* of this region at the rostral end of the neural tube. Another related neologism that I introduced in Puelles L. et al. (2012a) was the "*acroterminal area,*" a name needed for the distinct bow-like vertical border of THy at the rostralmost end of the hypothalamus (it extends from the rostromedian mamillary body to the median septopreoptic crossing point of the anterior commissure (**Figure 10**; this latter locus was settled as being preoptic because its ventricular cells selectively express *Shh*, a feature not found outside the preoptic area; Puelles et al., 2016). The acroterminal area is an unpaired *transversal* entity, with floor, basal, alar and roof parts, oddly as it seems, and shows throughout its height (we must fight the psychological tendency to think of this height as a length) unique morphological characteristics, i.e., formations not existing elsewhere in the hypothalamus and the whole brain. These bespeak of a series of singular basal and alar prechordal inductive effects, which give rise to the neurohypophysis and median eminence, the anterobasal and chiasmatic areas, the vascular organ of the lamina terminalis, and the lamina terminalis itself, ending at the anterior commissure median crossing bed itself (see further details on this area in Puelles L. et al., 2012a; Ferran et al., 2015; Puelles and Rubenstein, 2015). There existed no earlier columnar term for this singular neural wall locus.

The terminal hypothalamus thus transits dorsalward into the unevaginated preoptic telencephalon, while the peduncular hypothalamus transits similarly into the evaginated hemisphere. The caudal limit of the subpallial preoptic region with the neighboring diagonal area relates to the end of the strong preoptic ventricular zone expression of *Shh* (Puelles et al., 2016; Puelles, 2017), as well as with the course of the fornix tract (Puelles and Rubenstein, 2015). This implies that the PHy must contact at this border with a different subpallium component, namely the diagonal area, which jointly with the pallidum forms the medial ganglionic eminence (Puelles et al., 2013, 2016).

The major constituents of the alar regions of both THy and PHy are represented by two genoarchitectonically and chemoanatomically quite distinct longitudinal domains (with various shared markers across THy and PHy i.e., across hp1 and hp2; **Figures 10**, **13A,B**; but see differential markers in Ferran et al., 2015). The relatively dorsal subdomain is the already mentioned paraventricular area, where magnocellular and parvocellular cell populations of the paraventricular nucleus and the supraoptic nucleus are produced (**Figure 13B**). These are glutamatergic and peptidergic neurons (probably excitatory neurons throughout; **Figures 14A–C**), and the area can be subdivided dorsoventrally into three subzones showing some differential characteristics (DPa, CPa, VPa; **Figure 13B**; Puelles L. et al., 2012a). The detailed topographic terminology evolved within the columnar interpretation for such supraopto-paraventricular cell populations is quite complex, with the added problem that individual cell groups were conceived along the logic of "potatoes in a potato sack," i.e., without any histogenetic or patterning ordering principle. This is a general problem with columnar hypothalamic schemata, where constituent nuclei are illustrated literally as an elongated heap of variously sized balls devoid of developmental positional rules (e.g., Krieg, 1932; Ströer, 1956; Swanson, 2012). Indeed, columnar theory of the diencephalon did not even use alar and basal subdivisions, and considered the four postulated columns (**Figure 1A**) as homogeneous units at least for functional purposes, if not histologically (Herrick, 1948; Kuhlenbeck, 1973). Columnar authors in general, perhaps because of their emphasis on functions, did not postulate any developmental unit analogous to progenitor areas or histogenetic migration areas extending physically from the ventricle to the pial surface as a step in eventual differential columnar maturation. Indeed, the emergence of a multitude of nuclei in the thalamus or the hypothalamus occurs as if by magic (compare recently Alvarez-Bolado and Swanson, 1995; text p.24); mechanistic partitioning concepts leading to present-day progenitor zones evolved only within neuromeric models (e.g., Palmgren, 1921; Rendahl, 1924; Bergquist and Källén, 1954; Vaage, 1969, 1973; Puelles and Martínez de la Torre, 1987; review in Nieuwenhuys and Puelles, 2016), but were not used until the molecular era corroborated them, because of the columnar dogma that neuromeres supposedly did not exist. The lack of any positional logic for the multiple entities differentiated in 4 strata (see Puelles L. et al., 2012a, their Figures 8.30–8.33) makes any columnar hypothalamus map quite chaotic when examined in detail, a problem which is made worse by the novel evidence of numerous neuronal tangential migrations happening in various directions (review in Díaz et al., 2015; I refer to cells produced strictly at some hypothalamic subdivision which move developmentally into several adult positions; that poses a different sort of terminological problem). In practice, individual columnar supraopto-paraventricular cell groups were described as lying rostral to some preoptic formations, where others were placed caudal to them, but were also partly thought to lie caudal to some tuberal (basal) formations (e.g., as described by Swanson, 1987). Such chaotic positioning allowed by the columnar model (compare the correlative prosomeric mapping in **Figure 13B**) resulted apparently from the vagaries of the section plane employed and the intrinsic morphogenetic deformations of the histogenetic units observed using the prosomeric model (**Figures 5**, **10**, **13–15**). We accordingly proposed our much simpler schema of the paraventricular area with differential

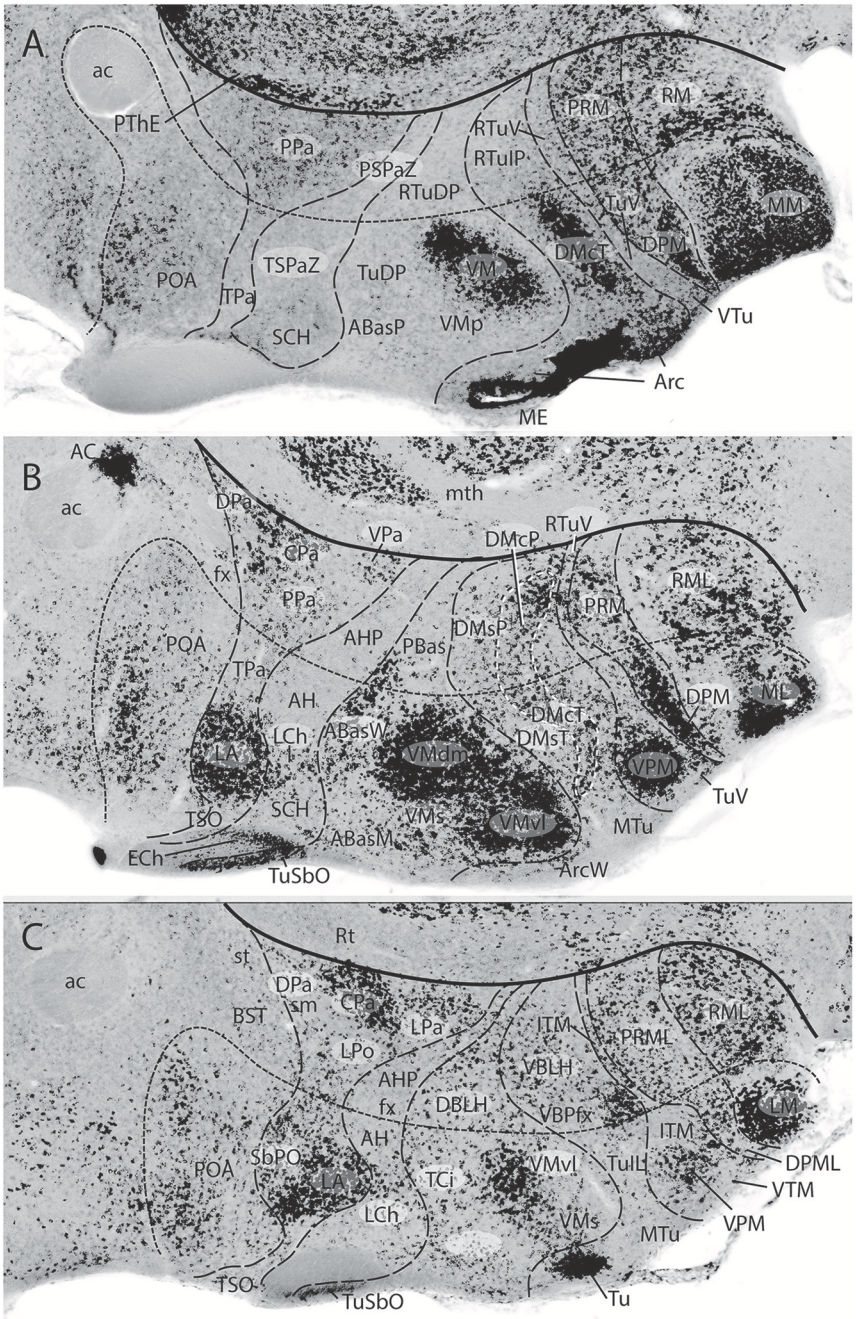

FIGURE 14 | Three sagittal sections through the adult mouse hypothalamus, shown in medio-lateral sequence **(A–C)**, which were *in situ* reacted for *Glu2*, a gene marker of glutamatergic excitatory neurons (from Puelles L. et al., 2012a; no copyright permission required). The thick black line indicates the hypothalamo-diencephalic boundary (dorsal to the left; caudal to the top). The nearly parallel line with minute dashes is the *intrahypothalamic* segmental boundary that separates PHy from THy (or hp1 from hp2). Orthogonal dash lines separate alar and basal longitudinal progenitor domains. The images immediately make clear that the abundance of glutamatergic neurons is substantially higher at THy than at PHy **A–C**; this is part of the evidence why these domains are considered different prosomeres; some columnar authors described similar compartments as "dorsal and ventral" hypothalamus regions, whereas some other columnar authors identified them as dorsoventrally related subthalamus and hypothalamus columns (the PHy contains the subthalamic nucleus in sections lateral to **C**). Within the paraventricular alar area, numerous excitatory neurons appear aggregated at the lateral anterior nucleus (LA) within THy **(B,C)**; there is also a dense patch selectively at the CPa subnucleus in PHy **(C)**. The subparaventricular area is largely devoid of this cell type (SCH, AH, AHP). The massive bipartite glutamatergic population within the VM hypothalamic complex **(A–C)** contrasts with the overall scarcity found at the neighboring DM formation, excepting the latter's periventricular positive core population seen in **(A)** (probably migrated; DMcT, DMcP). The ventral and dorsal premamillary populations (VPM, DPM) also are largely excitatory **(A,B)**, as are the mamillary and retromamillary formations (MM, LM, RM, RML; **A–C**). Note the subpallium found dorsal to the hypothalamus (e.g., POA) is generally poor in glutamatergic neurons, as is the reticular prethalamus (Rt; **B,C**). In contrast, the prethalamic eminence only contains glutamatergic neurons (PThE; **A**).

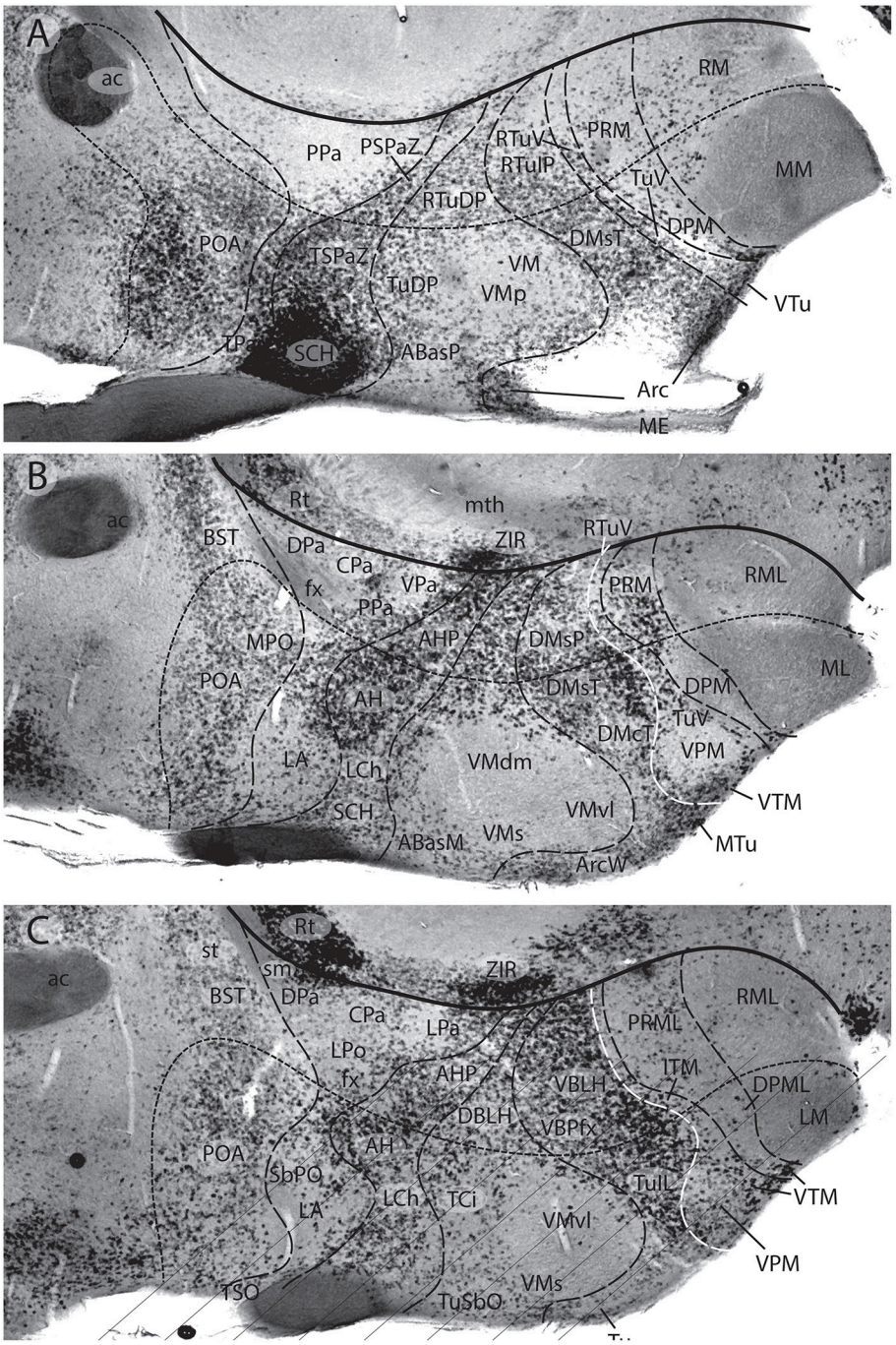

FIGURE 15 | Three sagittal sections adjacent to those in **Figure 14**, through the adult mouse hypothalamus, shown in medio-lateral sequence **(A–C)**. They were *in situ* reacted for *Gad67*, a gene marker of GABAergic inhibitory neurons (from Puelles L. et al., 2012a; no copyright permission required). The thick black line indicates the hypothalamo-diencephalic boundary (same overall orientation as **Figure 14**). The nearly parallel line with minute dashes is the intrahypothalamic segmental boundary separating PHy from THy (or hp1 from hp2). Orthogonal dash lines separate alar and basal longitudinal progenitor domains. The overall image readily shows that the hypothalamic formations with marked numbers of excitatory neurons (**Figure 14**) have few if any GABAergic neurons (e.g., check LA, also most of the principal Pa nucleus, VM, VPM, DPM, MM, ML, LM; RM, RML—**A–C**). The maximal presence of GABAergic neurons appears at the SCH nucleus, and less markedly at the neighboring AH and AHP, all of them subparaventricular derivatives. The full dorsomedial formation across both THy and PHy is also rich in GABAergic neurons. The prethalamus (e.g., Rt; ZIR) also emerges as a GABAergic territory **(B,C)**. There is also a shell of GABA cells around the VM nucleus **(A–C)**. The preoptic area (POA) is also well provided with GABAergic neurons **(A–C)**. Seeing the curved and topographically oblique (deformed) boundary lines that separate paraventricular from subparaventricular alar entities, as well as basal formations, one understands that the habitual atlas coronal sections are not helpful in understanding these alternative distributions highlighted by the selective molecular markers and more appropriate sagittal section planes.

size across THy and PHy (**Figure 13B**), with a minimum of individual name changes, to make sense in our own descriptions (see Puelles L. et al., 2012a). We also distinguished different strata of the same area and derivatives that migrate tangentially away.

The second longitudinal domain of the alar hypothalamus lies immediately dorsal to the alar-basal boundary and underneath the paraventricular area (both across THy and PHy). This territory produces (in contrast to the suprajacent paraventricular area) mainly inhibitory GABA-positive neurons, a point inexplicably not commented by recent columnar authors. There is no theory nor discussion whatsoever about how a column (as defined within the columnar model) might produce separate groups of excitatory and inhibitory neurons (the fact is that if it is a really homogeneous unit, the column should not produce these distinct types of neurons). However, such alternative cell type distributions occur locally at various parts of the hypothalamus (see **Figures 14**, **15**), consistently with differential genetic profiles enabling specific areas defined in the prosomeric model to produce either excitatory or inhibitory neurons, as happens elsewhere in the brain (subsequent tangential migration may intermix partially these separately produced populations). This clearly means that the columnar hypothalamus is not a real histogenetic unit (Puelles L. et al., 2012a; Díaz et al., 2015).

The name that immediately occurred to us for this mainly inhibitory alar hypothalamic band was the "*subparaventricular area*." Luckily, this term had been already introduced precisely at this hypothalamic level, though in a more restricted sense, by the columnar authors Watts et al. (1987). We were happy to absorb it as an exercise in conciliation, and expanded it into its use in our model (SPa; **Figures 10**, **13–15**; Puelles L. et al., 2012a). This area contains rostrally the acroterminal optic chiasma and is continuous caudally with the prethalamic zona incerta (spa; **Figure 13A**). This domain had no previous columnar name, due to the reasons commented above, but some well-known potato-like nuclei belong to it (e.g., the suprachiasmatic nucleus, SCH, and the anterior hypothalamic nucleus, AH/AHP, jointly with some less important elements). The "supra-"prefix in "suprachiasmatic" is inexact, because the nucleus is merely deep to the chiasma (i.e., nearer to the ventricle), not dorsal to it, but the SCH nucleus is so distinct in any case that this semantic difference seems not excessively problematic (this comment applies also to the "supraoptic commissures"). Similarly, the "anterior" descriptor in "anterior hypothalamic nucleus" happens to be acceptable in prosomeric interpretation, because the AH nucleus lies within the subparaventricular THy, which topologically is an *anterior* hypothalamic position also in our model. This term was actually used ambiguously by columnar authors, since they applied it to a nucleus that lies at the middle of the hypothalamus (particularly, if you believe that the preoptic area is an anterior hypothalamus part, as many authors still assume). This occurs because there was an historic time when the columnar hypothalamus ended at the AH, while its supraopto-paraventricular neighbors were still preoptic (i.e., telencephalic). This nucleus thus was for a time the most "anterior" part of the hypothalamus according to the columnar axis. Later, when the columnar model added the preoptic area to the hypothalamus, various authors (some in major atlases) started to identify the "anterior nucleus" partly or wholly inside the preoptic area (reviewed in detail in Puelles L. et al., 2012a), but nobody apparently noticed this error in topographic consistency. This example shows that a morphologically inaccurate descriptor (or an innocent descriptor used within an inaccurate model) tends to have perverse practical consequences, because sooner or later there are users that naively confide in the *apparent meaning* and are led astray into wrong conclusions.

Trying to be conservative, we largely used for the basal hypothalamic region names that already were in use before. We found basically three longitudinal zones stacked dorsoventrally across basal THy and PHy (**Figures 10**, **13**). We distinguished dorsally a revised *tuberal/retrotuberal region* (Tu/RTu) and ventrally a *mamillary/retromamillary region* (M/RM), separated by an intermediate basal band, again distinct molecularly and structurally from Tu/RTu and M/RM, but previously unnamed, or very badly named, which we termed *perimamillary/periretromamillary area* (PM/PRM) (see **Figures 13A,B**).

As regards the change to "retromamillary", it seemed ridiculous to continue describing as "supramamillary" a zone lying adjacent to the floor plate, caudally to the mamillary body (RM; **Figure 10**). Columnar authors always passed lightly over the fact of a *floor* plate present at the pretended *caudal* end of a column, since it could not be explained; it was inconsistent with the model. They would have preferred a direct axial continuity of the mamillary body with the pons (see **Figure 3**), but the cephalic flexure insists in obstaculizing that recourse. We in fact proposed the change to "*retromamillary*" already many years before (Puelles and Martínez de la Torre, 1987), and this version has gained some acceptance in the meantime.

I also have been campaigning for a long time for the "single m" orthography of "mammillary." My rationale is as follows: this word derives from Latin "mamilla," or nipple, rather than from "mamma," or breast; in the latter case we would have to say "mammary body," and nobody does that, irrespective how one subjectively visualizes this brain entity; the problem is that few people nowadays realize that "mamillary" means "nipple-like," whose root "mamilla" has only one "m"; many classic neuroanatomists possibly knew it, and thus agreed on the "mamillary" orthography. It was mainly post-war colleagues possibly unaware of this etymologic subtlety that spread the wrong orthography. There is a notable review of this orthographic issue by Jones (2011), which is well documented and worth perusing. Jones apparently concludes that it is a matter of usage, and he prefers the one "m" solution, but he weakens his own position by assuming that "mamilla" means "small breast," in contradiction with my Concise Oxford Dictionary, which says it means "nipple." I presented the case to the recent FIPAT brain nomenclature committee (ten Donkelaar et al., 2017), but my position was outvoted in favor of conventional usage (search the word under "hypothalamus" in ten Donkelaar et al., 2018). Paraphrasing Kuhlenbeck's citation at the head of this essay, I'll continue spelling "mamillary" with one "m."

These basal longitudinal domains (all three cutting *de facto* across the columnar hypothalamic unity, but providing conceptual pigeonholes for a number of unexplained potatoes and associated patterning thinking; Puelles, 2017) have double names in our terminology because these domains show some differences between THy and PHy, irrespective of their fundamental molecular and cell typological continuity (these partial differences underpin the idea that THy and PHy belong to different prosomeres if the partial boundaries happen to sum up into a single intrahypothalamic boundary; see Ferran et al., 2015). *Mamillary* and *retromamillary* areas clearly refer to differences between THy and PHy at the ventralmost basal subregion; the anatomists of course already knew that the mamillary body is different in various aspects from the retromamillary area (e.g., projections), though both basically contain excitatory neurons. We now have a neuromeric explanation of why this may be so. Moreover, structures of the *tuberal area* proper, such as infundibulum, median eminence, arcuate nucleus, and neurohypophysis, are only found within basal THy lying under the alar-basal boundary, not more ventrally or more caudally. This also happens with the largest tuberal hypothalamic nucleus, the ventromedial hypothalamic nucleus; it clearly does not extend to the caudal end of the hypothalamus (VM; **Figures 10**, **13**–**15**). Some other structural features, such as the dorsomedial nucleus, extend instead uniformly across both THy and PHy (see **Figure 15C**). We thus innovated somewhat by proposing to call *retrotuberal area* the PHy domain placed just behind the THy tuberal area, and dorsal to the periretromamillary area (Tu; RTu; **Figures 10**, **13**–**15**). While the "*ventromedial*" descriptor in VM is barely acceptable in prosomeric coordinates (the nucleus is "ventral" since it is basal, and it lies next to the periventricular stratum, being thus also "medial"), it would be more precise if the name could be changed to "rostroventromedial nucleus," because of its restriction to THy, but this results a bit clumsy. It may be useful to remember that Ramón y Cajal (1911) simply named it the "*principal hypothalamic nucleus*." The topographic name "dorsomedial nucleus" (DM) is instead rather hopeless, since, being partly retrotuberal and partly tuberal, the nucleus lies "*caudal*" to the VM within the PHy and "*ventral*" to the VM within the THy. This occurs because the VM is not born where we see it in the adult; it results from a localized dorsoventral migration stream coming from the dorsalmost tuberal subregion of the THy, which specializes in glutamatergic neurons, as opposed to the underlying DM area, which is rich in GABAergic neurons (**Figures 14**, **15**; some evidence of this migration was shown in Puelles L. et al., 2012a; their Figure 8.26). Without the VM migration, the DM would form a perfectly level longitudinal column through the tuberal/retrotuberal areas, but because of the dorsoventral penetration of the VM it results compressed ventrally (there is no cell mixing at all). The VM also has a peripheral shell of variously migrated cell types, many coming from the alar domains (Díaz et al., 2015).

Further semantic complication emerges when we consider the conventional ventral and dorsal premamillary nuclei (VPM; DPM; **Figures 14**, **15**). The VPM was found to be a migrated blob of excitatory cells stabilizing within the ventralmost terminal part of DM, ventrally to the VM (i.e., within tuberal THy); thanks to various early gene markers, this blob surprisingly was found to originate from the retromamillary area in PHy (see details in Puelles L. et al., 2012a; the migration has been since corroborated experimentally). On the other hand, the DPM, also containing excitatory glutamatergic neurons, belongs to the molecularly distinct perimamillary domain (i.e., restricted to THy; **Figures 14**, **15**) that separates the mamillary/retromamillary regions from the tuberal/retrotuberal region. The main perimamillary derivative represents precisely the population identified as DPM in columnar accounts. It so happens, therefore, that by its retromamillary origin, the VPM is "caudal" to the DPM, but by its adult migrated tuberal position it is "dorsal" to the same. Obviously, this means that in prosomeric coordinates the DPM lies strictly "ventral" to the adult VPM (a terminological disaster). There is no way to save the columnar use of these descriptors, and suggestions for a reasonable solution are invited. I think we should find a nice descriptive term for the migrated "VPM", possibly such as "ovoid nucleus" (Ov), or something like that, and rename the terminal DPM simply as "perimamillary nucleus" (PM). The perimamillary nucleus and its peduncular periretromamillary companion form a longitudinal band that shares some molecular markers [e.g., *Otp* and *Sim1* expression, also present at the alar paraventricular area (**Figure 10**). This poses an interesting patterning problem, since these bands are separate but parallel to each other]. However, they also express each other differential markers and also have differential connections according to their respective ascription to THy or PHy. The PRM nucleus found next to the retromamillary area was initially termed "posterior hypothalamus" in the columnar literature (e.g., Bodian, 1939). Unfortunately, this concept of the posterior hypothalamus was later extended arbitrarily into the diencephalic tegmentum as far back as the retroflex tract (PHTh; **Figure 1A**); this diencephalic tegmental area does not share the hypothalamic *Otp* and *Sim1* markers, implying that this is a case of an inappropriate term, which should be discontinued.

There are many other details that might be discussed on hypothalamic ancient and modern nomenclature and their respective advantages or problems. I think that we have had enough "spice of life" for the present essay. The reader may have gotten a general idea of where we presently are, and knows where he/she may seek further details and explanations, if so desired.

AUTHOR CONTRIBUTIONS

The author confirms being the sole contributor of this work and has approved it for publication.

FUNDING

Supported by Séneca Foundation contract 19904/GERM/15.

REFERENCES

Albuixech-Crespo, B., López-Blanch, L., Burguera, D., Maeso, I., Sánchez-Arrones, L., Moreno-Bravo, J. A., et al. (2017). Molecular regionalization of the developing amphioxus neural tube challenges major partitions of the vertebrate brain. *PLoS Biol.* 15:e2001573. doi: 10.1371/journal.pbio.2001573

Alonso, A., Merchán, P., Sandoval, J. E., Sánchez-Arrones, L., Garcia-Cazorla, A., Artuch, R., et al. (2012). Development of the serotonergic cells in murine raphe nuclei and their relations with rhombomeric domains. *Brain Struct. Funct.* 218, 1229–1277. doi: 10.1007/s00429-012-0456-8

Altman, J., and Bayer, S. A. (1988). Development of the rat thalamus: I. Mosaic organization of the thalamic neuroepithelium. *J. Comp. Neurol.* 275, 346–377. doi: 10.1002/cne.902750304

Altman, J., and Bayer, S. A. (1995). *Atlas of Prenatal Rat Brain Development*. Boca Raton, FL: CRC Press.

Alvarez-Bolado, G., Rosenfeld, M. G., and Swanson, L. W. (1995). Model of forebrain regionalization based on spatiotemporal patterns of POU-III homeobox gene expression, birthdates, and morphological features. *J. Comp. Neurol.* 355, 237–295. doi: 10.1002/cne.903550207

Alvarez-Bolado, G., and Swanson, L. W. (1995). *Developmental Brain Maps: Structure of the Embryonic Rat Brain*. Amsterdam; London: Elsevier.

Aparicio, M. A., and Saldaña, E. (2014). The dorsal tectal longitudinal column [TLCd]: a second longitudinal column in the paramedian region of the midbrain tectum. *Brain Struct. Funct.* 219, 607–630. doi: 10.1007/s00429-013-0522-x

Aroca, P., Lorente-Cánovas, B., Mateos, F. R., and Puelles, L. (2006). Locus coeruleus neurons originate in alar rhombomere 1 and migrate into the basal plate: studies in chick and mouse embryos. *J. Comp. Neurol.* 496, 802–818. doi: 10.1002/cne.20957

Aroca, P., and Puelles, L. (2005). Postulated boundaries and differential fate in the developing rostral hindbrain. *Brain Res. Rev.* 49, 179–190. doi: 10.1016/j.brainresrev.2004.12.031

Bailey, P. (1916). Morphology of the roof plate of the forebrain and the lateral chorioid plexuses in the human embryo. *J. Comp. Neurol.* 26, 79–120. doi: 10.1002/cne.900260104

Bergquist, H., and Källén, B. (1954). Notes on the early histogenesis and morphogenesis of the central nervous system in vertebrates. *J. Comp. Neurol.* 100, 627–659. doi: 10.1002/cne.901000308

Bodian, D. (1939). Studies on the diencephalon of the Virginia opossum. Part I. The nuclear pattern. *J. Comp. Neurol.* 71, 259–323. doi: 10.1002/cne.900710203

Christ, J. F. (1969). "Derivation and boundaries of the hypothalamus, with atlas of hypothalamic grisea," in *The Hypothalamus,* eds W. Haymaker, E. Anderson, and W. J. H. Nauta (Springfield, IL: Charles C. Thomas), 13–60 .

Coggeshall, R. E. (1964). A study of diencephalic development in the albino rat. *J. Comp. Neurol.* 122, 241–270. doi: 10.1002/cne.901220208

Dávila, J. C., Guirado, S., and Puelles, L. (2000). Calcium-binding proteins in the diencephalon of the lizard *Psammodromus algirus*. *J. Comp. Neurol.* 427, 67–92. doi: 10.1002/1096-9861(20001106)427:1<67::AID-CNE5>3.0.CO;2-2

Dèjerine, J. (1895). *Anatomie des Centres Nerveux. Vol. 1*. Paris: Masson.

Di Bonito, M., Narita, Y., Avallone, B., Sequino, L., Mancuso, M., Andolfi, G., et al. (2013). Assembly of the auditory circuitry by a Hox genetic network in the mouse brainstem. *PLoS Genet.* 9:e1003249. doi: 10.1371/journal.pgen.1003249

Di Bonito, M. A., Studer, M., and Puelles, L. (2017). Nuclear derivatives and axonal projections originating from rhombomere 4 in the mouse hindbrain. *Brain Struct. Funct.* 222, 3509–3542. doi: 10.1007/s00429-017-1416-0

Díaz, C., Morales-Delgado, N., and Puelles, L. (2015). Ontogenesis of peptidergic neurons within the genoarchitectonic map of the mouse hypothalamus. *Front. Neuroanat.* 8:162. doi: 10.3389/fnana.2014.00162

Díaz, C., Yanes, C., Trujillo, C. Mª., and Puelles, L. (1994). The lacertidian reticular thalamic nucleus projects topographically upon the dorsal thalamus: experimental study in *Gallotia galloti*. *J. Comp. Neurol.* 343, 193–208. doi: 10.1002/cne.903430202

Ferran, J. L., Dutra de Oliveira, E., Sánchez-Arrones, L., Sandoval, J. E., Martínez-de-la-Torre, M., and Puelles, L. (2009). Genoarchitectonic profile of developing nuclear groups in the chicken pretectum. *J. Comp. Neurol.* 517, 405–451. doi: 10.1002/cne.22115

Ferran, J. L., Puelles, L., and Rubenstein, J. L. R. (2015). Molecular codes defining rostrocaudal domains in the embryonic mouse hypothalamus. *Front. Neuroanat.* 9:46. doi: 10.3389/fnana.2015.00046

Ferran, J. L., Sánchez-Arrones, L., Bardet, S. M., Sandoval, J., Martínez-de-la-Torre, M., and Puelles, L. (2008). Early pretectal gene expression pattern shows a conserved anteroposterior tripartition in mouse and chicken. *Brain Res. Bull.* 75, 295–298. doi: 10.1016/j.brainresbull.2007.10.039

Ferran, J. L., Sánchez-Arrones, L., Sandoval, J. E., and Puelles, L. (2007). A model of early molecular regionalization in the chicken embryonic pretectum. *J. Comp. Neurol.* 505, 379–403. doi: 10.1002/cne.21493

Flames, N., Pla, R., Gelman, D. M., Rubenstein, J. L. R., Puelles, L., and Marín, O. (2007). Delineation of multiple subpallial progenitor domains by the combinatorial expression of transcriptional codes. *J. Neurosci.* 27, 9682–9695. doi: 10.1523/JNEUROSCI.2750-07.2007

Forel, A. (1877). Untersuchungen über die Haubenregion und ihre oberen Verknüpfungen im Gehirn des Menschen und einiger Säugethiere, mit Beiträgen zu den Methoden der Gehirnuntersuchung. *Arch. Psychiat.* 7, 393–495. doi: 10.1007/BF02041873

García-Calero, E., Martínez-de-la-Torre, M., and Puelles, L. (2002). The avian griseum tectale: cytoarchitecture, NOS expression and neurogenesis. *Brain Res. Bull.* 57, 353–358. doi: 10.1016/S0361-9230(01)00723-7

Gilbert, M. S. (1935). The early development of the human diencephalon. *J. Comp. Neurol.* 62, 81–115. doi: 10.1002/cne.900620105

Herrick, C. J. (1910). The morphology of the forebrain in amphibia and reptilia. *J. Comp. Neurol.* 20, 413–547. doi: 10.1002/cne.920200502

Herrick, C. J. (1936). Conduction pathways in the cerebral peduncle of *Amblystoma*. *J. Comp. Neurol.* 63, 293–352. doi: 10.1002/cne.900630207

Herrick, C. J. (1948). *The Brain of the Tiger Salamander, Amblystoma tigrinum*. Chicago: The University Chicago Press.

Hidalgo-Sánchez, M., Martínez-de-la-Torre, M., Alvarado-Mallart, R. M., and Puelles, L. (2005). Distinct pre-isthmic domain, defined by overlap of *Otx2* and *Pax2* expression domains in the chicken caudal midbrain. *J. Comp. Neurol.* 483, 17–29. doi: 10.1002/cne.20402

His, W. (1893). Vorschläge zur Eintheilung des Gehirns. *Arch. Anat. Entwickelungsges* 3, 173–179.

His, W. (1895). Die anatomische Nomenclatur. Nomina anatomica. *Neurol. Suppl. Bd. Arch. Anat. EntwGesch.* 1895(Suppl.), 155–177.

His, W. (1904). *Die Entwicklung des menschlichen Gehirns während der ersten Monate*. Leipzig: Hirzel Verlag.

Hochstetter, F. (1895). Über die Beziehung des Thalamus opticus zum Seitenventrikel der Grosshirnhemispheren. *Anat. Anz.* 10, 295–302.

Hochstetter, F. (1919). *Beiträge zur Entwicklungsgeschichte des menschlichen Gehirns, I.Teil*. Vienna; Leipzig: Franz Deuticke.

Johnston, J. B. (1906). *The Nervous System of Vertebrates*. Philadelphia, PA: Blakiston.

Johnston, J. B. (1909). The morphology of the forebrain vesicles in vertebrates. *J. Comp. Neurol.* 19, 457–539. doi: 10.1002/cne.920190502

Jones, E. G. (2011). Mamillary or mammillary? What's in an "m"? *J. Hist. Neurosci.* 20, 152–159. doi: 10.1080/0964704X.2010.533089

Kappers, C. U. A. (1947). *Anatomíe Comparée du Systeme Nerveux*. Haarlem: De Erven F. Bohn.

Klingler, J. (1948). Die makroskopische Anatomie der Ammonsformation. *Denkschr Schweizer Naturforschend Gesellsch* 78, 1–82.

Krieg, W. J. S. (1932). The hypothalamus of the albino rat. *J. Comp. Neurol.* 55, 18–89. doi: 10.1002/cne.900550104

Kuhlenbeck, H. (1973). *The Central Nervous System of Vertebrates,* Vol. 3, *Part II: Overall Morphologic Pattern*. Basel: S. Karger.

Lakke, E. A. J. F., van der Veeken, J. G. P. M., Mentink, M. M. T., and Marani, E. (1988). A SEM study on the development of the ventricular surface morphology in the diencephalon of the rat. *Anat.Embryol.* 179, 73–80. doi: 10.1007/BF00305101

Le Gros Clark, W. E. (1938). "Morphological aspects of the hypothalamus," in *The Hypothalamus. Morphological, Functional, Clinical and Surgical Aspects,* ed W. E. Le Gros Clark (Edinburgh: The William Ramsay Henderson Trust and Oliver & Boyd), 1–68.

Locy, W. A. (1895). *Contribution to the Structure and Development of the Vertebrate Head*. Boston, MA: Ginn &Co.

Lorente-Cánovas, B., Marín, F., Corral-San-Miguel, R., Hidalgo-Sánchez, M., Ferrán, J. L., Puelles, L., et al. (2012). Multiple origins, migratory paths and molecular profiles of cells populating the avian interpeduncular nucleus. *Dev. Biol.* 361, 12–26. doi: 10.1016/j.ydbio.2011.09.032

Marín, F., and Puelles, L. (1994). Patterning of the embryonic avian midbrain after experimental inversions: a polarizing activity from the isthmus. *Dev. Biol.* 163, 19–37. doi: 10.1006/dbio.1994.1120

Marín, O., Smeets, J. A. J., and González, A. (1998). Evolution of the basal ganglia in tetrapods: a new perspective based on recent studies in amphibians. *TINS* 21, 487–494. doi: 10.1016/S0166-2236(98)01297-1

Márquez-Legorreta, E., Horta, J. A., junior, Berrebi, A. S., and Saldaña, E. (2016). Organization of the zone of transition between the pretectum and the thalamus, with emphasis on the pretectothalamic lamina. *Front. Neuroanat.* 10:82. doi: 10.3389/fnana.2016.00082

Martínez, S., Puelles, E., Puelles, L., and Echevarria, D. (2012). "Molecular regionalization of developing neural tube," in *The Mouse Nervous System,* eds C. Watson, G. Paxinos, and L. Puelles (San Diego, CA: Academic Press; Elsevier), 2–18.

Martínez-de-la-Torre, M., Garda, A.-L., Puelles, E., and Puelles, L. (2002). *Gbx2* expression in the late embryonic chick dorsal thalamus. *Brain Res. Bull.* 57, 435–438. doi: 10.1016/S0361-9230(01)00721-3

Martínez-de-la-Torre, M., Lambertos, A., Peñafiel, R., and Puelles, L. (2018). An exercise in brain genoarchitectonics: Analysis of AZIN2-Lacz expressing neuronal populations in the mouse hindbrain. *J. Neurosci. Res.* 96, 1490–1517. doi: 10.1002/jnr.24053

McClure, C. (1890). The segmentation of the primitive vertebrate brain. *J. Morphol.* 4, 35–56. doi: 10.1002/jmor.1050040104

McRioch, D. K., Wislocki, G. B., and O'Leary, J. L. (1940). "A précis of preoptic, hypothalamic and hypophysial terminology with atlas" in *The Hypothalamus and Central Levels of Autonomic Function,* eds J. F. Fulton, S. W. Ranson, and A. M. Frantz (Baltimore, MD: Williams and Wilkins), 3–30.

Medina, L., Puelles, L., and Smeets, W. A. J. (1994). Development of catecholamine systems in the brain of the lizard *Gallotia galloti*. *J. Comp. Neurol.* 350, 41–62. doi: 10.1002/cne.903500104

Miura, R. (1933). Über die Differenzierung der Grundbestandteile im Zwischenhirn des Kaninchen. *Anat. Anz.* 77, 1–65.

Mori, S., Shik, M. L., and Yagodnitsyn, A. S. (1977). Role of pontine tegmentum for locomotor control in mesencephalic cat. *J. Neurophysiol.* 40, 284–295. doi: 10.1152/jn.1977.40.2.284

Nieuwenhuys, R., and Puelles, L. (2016). *Towards a New Neuromorphology*. Berlin, Springer Verlag. doi: 10.1007/978-3-319-25693-1

Orr, H. J. (1887). Contribution to the embryology of the lizard. *J. Morphol.* 1, 311–372. doi: 10.1002/jmor.1050010204

Palmgren, A. (1921). Embryological and morphological studies on the midbrain and cerebellum of vertebrates. *Acta Zool.* 2, 1–94. doi: 10.1111/j.1463-6395.1921.tb00464.x

Paxinos, G., and Franklin, B. J. (2013). *The Mouse Brain in Stereotaxic Coordinates*, *4th Edn*. San Diego, CA: Academic Press.

Paxinos, G., and Watson, C. (2014). *The Rat Brain in Stereotaxic Coordinates*, *7th Edn.* San Diego, CA: Academic Press.

Puelles, E., Martinez-de-la-Torre, M., Watson, C., and Puelles, L. (2012a). "Midbrain," in *The Mouse Nervous System*, eds C. Watson, G. Paxinos, and L. Puelles (San Diego, CA:Academic Press; Elsevier), 337–359.

Puelles, L. (1996). Review of: atlas of prenatal rat brain development (Bayer and Altman, 1995). *TINS* 19, 116–117.

Puelles, L. (2001). Thoughts on the development, structure and evolution of the mammalian and avian telencephalic pallium. *Phil. Trans. Roy. Soc. Ser.B Biol. Sci.* 356, 1583–1598. doi: 10.1098/rstb.2001.0973

Puelles, L. (2013). "Plan of the developing vertebrate nervous system, relating embryology to the adult nervous system (prosomere model,overview of Brain organization)." in *Comprehensive Developmental Neuroscience: Patterning and Cell Type Specification in the Developing CNS and PNS,* eds J. L. R. Rubenstein and P. Rakic (Amsterdam: Academic Press), 187–209.

Puelles, L. (2015). "Genoarchitectonic brain maps," in *Brain Mapping: An Encyclopedic Reference,* Vol. 1. *Anatomy and Physiology*, ed A. W. Toga, (San Diego, CA; Oxford: Academic Press; Elsevier), 210–215.

Puelles, L. (2016). Comments on the limits and internal structure of the mammalian midbrain. *Anatomy* 10, 60–70. doi: 10.2399/ana.15.045

Puelles, L. (2017). "Role of secondary organizers in the evolution of forebrain development in vertebrates," in *Handbook of Evolutionary Neuroscience,* ed S. V. Shepherd (Chichester: Wiley-Blackwell), 350–387.

Puelles, L. (2018). Developmental studies of avian brain organization. *Int. J. Dev. Biol.* 62, 207–224. doi: 10.1387/ijdb.170279LP

Puelles, L., Harrison, M., Paxinos, G., and Watson, C. (2013). A developmental ontology for the mammalian brain based on the prosomeric model. *TINS* 36, 570–578. doi: 10.1016/j.tins.2013.06.004

Puelles, L., and Martínez de la Torre, M. (1987). Autoradiographic and Golgi study on the early development of n. isthmi principalis and adjacent grisea in the chick embryo: a tridimensional viewpoint. *Anat. Embryol.* 176, 19–34. doi: 10.1007/BF00309748

Puelles, L., and Martinez, S. (2013). "Patterning of the diencephalon," in *Comprehensive Developmental Neuroscience: Patterning and Cell Type Specification in the Developing CNS and PNS,* eds J. L. R. Rubenstein and P. Rakic (Amsterdam: Academic Press), 151–172.

Puelles, L., Martínez, S., Martínez-de-la-Torre, M., and Rubenstein, J. L. R. (2015). "Gene maps and related histogenetic domains in the forebrain and midbrain,"in *The Rat Nervous System, 4th Edn*, ed G. Paxinos (New York, NY: Academic Press/Elsevier), 3–24.

Puelles, L., Martinez-de-la-Torre, M., Bardet, S., and Rubenstein, J. L. R. (2012a). "Hypothalamus," in *The Mouse Nervous System,* eds C. Watson, G. Paxinos, and L. Puelles (San Diego, CA:Academic Press; Elsevier), 221–312.

Puelles, L., Martínez-de-la-Torre, M., Martínez, S., Watson, C., and Paxinos, G. (2018). *The Chick Brain in Stereotaxic Coordinates: an Atlas featuring Neuromeric Subdivisions and Mammalian Homologies. 2nd Edn*. San Diego, CA: Elsevier; Academic Press.

Puelles, L., Martínez-de-la-Torre, M., Paxinos, G., Watson, C., and Martínez, S. (2007). *The Chick Brain in Stereotaxic Coordinates: An Atlas Featuring Neuromeric Subdivisions and Mammalian Homologies*. San Diego, Ca: Elsevier; Academic Press.

Puelles, L., Martínez-Marin, R., Melgarejo-Otalora, P., Ayad, A., Valavanis, A., and Ferrán, J. L. (2019). "Patterned vascularization of embryonic mouse forebrain and neuromeric topology of major human subarachnoidal arterial branches: Prosomeric mapping," in *Recent Developments in Neuroanatomical Terminology,* eds H. ten Donkelaar and L. Puelles (Lausanne: Frontiers in Neuroanatomy Special Topics).

Puelles, L., and Medina, L. (1994). "Development of neurons expressing tyrosine hydroxylase and dopamine in the chicken brain: a comparative segmental analysis," in *Phylogeny and Development of Catecholamine Systems in the CNS of Vertebrates,* eds A. Reiner and W. J. A. J. Smeets (Cambridge: Cambridge University Press), 381–406.

Puelles, L., Merchán, P., Morales-Delgado, N., Castro, B., Díaz, C., and Ferrán, J. L. (2016). Radial and tangential migration of telencephalic somatostatin neurons originated from the mouse diagonal area. *Brain Struct. Funct.* 221, 3027–3065. doi: 10.1007/s00429-015-1086-8

Puelles, L., and Rubenstein, J. L. R. (1993). Expression patterns of homeobox and other putative regulatory genes in the embryonic mouse forebrain suggest a neuromeric organization. *TINS* 16, 472–479. doi: 10.1016/0166-2236(93)90080-6

Puelles, L., and Rubenstein, J. L. R. (2003). Forebrain gene expression domains and the evolving prosomeric model. *TINS* 26, 469–476. doi: 10.1016/S0166-2236(03)00234-0

Puelles, L., and Rubenstein, J. L. R. (2015). A new scenario of hypothalamic organization: rationale of new hypotheses introduced in the updated

prosomeric model. *Front. Neuroanat.* 9:27. doi: 10.3389/fnana.2015.00027

Puelles, L., Watson, C., Martinez-de-la-Torre, M., and Ferrán, J. L. (2012b). "Diencephalon," in *The Mouse Nervous System,* eds C. Watson, G. Paxinos, and L. Puelles (SanDiego, CA: Academic Press; Elsevier), 313–336.

Ramón y Cajal, S. (1911). *Histologie du Systeme Nerveux de l'Homme et des Vertebrés*, Vol.2. Transl. by L. Azoulay. Madrid: CSIC.

Ranson, S. W. (1928). *The Anatomy of the Nervous System*. Philadelphia, PA: Saunders.

Redies, C., Ast, M., Nakagawa, S., Takeichi, M., Martínez-de-la-Torre, M., and Puelles, L. (2000). Morphologic fate of diencephalic prosomeres and their subdivisions revealed by mapping cadherin expression. *J. Comp. Neurol.* 421, 481–514. doi: 10.1002/(SICI)1096-9861(20000612)421:4<481::AID-CNE3>3.0.CO;2-H

Rendahl, H. (1924). Embryologische und morphologische Studien über das Zwischenhirn beim Huhn. *Acta Zool.* 5, 241–344. doi: 10.1111/j.1463-6395.1924.tb00169.x

Rubenstein, J. L. R., Martínez, S., Shimamura, K., and Puelles, L. (1994). The embryonic vertebrate forebrain: the prosomeric model. *Science* 266, 578–580. doi: 10.1126/science.7939711

Saldaña, E., Viñuela, A., Marshall, A. F., Fitzpatrick, D. C., and Aparicio, M. A. (2007). The TLC: a novel auditory nucleus of the mammalian brain. *J. Neurosci.* 27, 13108–13116. doi: 10.1523/JNEUROSCI.1892-07.2007

Schwalbe, G. (1880). Beiträge zur Entwicklungsgeschichte des Zwischenhirns. *Sitz. Ber. Gen. Ges. Med. Naturwiss* 20, 2–7.

Shik, M. L., and Orlovsky, G. N. (1976). Neurophysiology of locomotor automatism. *Physiol. Rev.* 56, 465–501. doi: 10.1152/physrev.1976.56.3.465

Shimogori, T., Lee, D. A., Miranda-Angulo, A., Yang, Y., Wang, H., Jiang, L., et al. (2010). A genomic atlas of mouse hypothalamic development. *Nat. Neurosci.* 13, 767–775. doi: 10.1038/nn.2545

Ströer, W. F. H. (1956). Studies on the diencephalon. I. The embryology of the diencephalon of the rat. *J. Comp. Neurol.* 105, 1–24. doi: 10.1002/cne.901050102

Swanson, L. W. (1987). "The hypothalamus," in *Hypothalamus, Hippocampus, Amygdala, Retina*, (*Series Handbook of Chemical Neuroanatomy,* Vol. 5), eds A. Björklund and T. Hökfelt , eds A. Björklund, T. Hökfelt and L. W. Swanson (New York, NY: Elsevier), 1–124.

Swanson, L. W. (2012). *Brain Architecture*, *2nd edn*. London: Oxford.

Swanson, L. W. (2018). Brain maps 4.0 – structure of the rat brain: an open access atlas with global nervous system nomenclature ontology and flatmaps. *J. Comp. Neurol.* 526, 935–943. doi: 10.1002/cne.24381

ten Donkelaar, H. J. (2011). *Clinical Neuroanatomy: Brain Circuitry and Disorders*. Berlin: Springer. doi: 10.1007/978-3-642-19134-3

ten Donkelaar, H. J., Broman, J., Neumann, P. E., Puelles, L., Riva, A., Tubbs, R. S., et al. (2017). Towards a terminologia neuroanatomica. *Clin. Anat.* 30, 145–155. doi: 10.1002/ca.22809

ten Donkelaar, H. J., Kachlik, D., and Tubbs, R. S. (2018). *An Illustrated Terminologia Neuroanatomica, A Concise Encyclopedia of Human Neuroanatomy*. Berlin: Springer.

Vaage, S. (1969). The segmentation of the primitive neural tube in chick embryos (*Gallus domesticus*). A morphological, histochemical and autoradiographical investigation. *Ergebn. Anat. Entwicklungs. Gesch.* 41, 3–87.

Vaage, S. (1973). The histogenesis of the isthmic nuclei in chick embryos (*Gallus domesticus*). I. A morphological study. *Z. Anat. Entwickl. Gesch.* 142, 283–314. doi: 10.1007/BF00519134

Verney, C., Zecevic, N., and Puelles, L. (2001). Structure of longitudinal brain zones that provide the origin for the substantia nigra and ventral tegmental area in human embryos, as revealed by cytoarchitecture and tyrosine hydroxylase, calretinin, calbindin, and GABA immunoreactions. *J. Comp. Neurol.* 429, 22–44. doi: 10.1002/1096-9861(20000101)429:13.0.CO;2-X

Villiger, E., and Ludwig, E. (1946). *Gehirn und Rückenmark, Leitfaden für das Studium der Morphologie und des Faserverlaufes.* Basel: Benno Schwabe & Co.

Villiger, E., Ludwig, E., and Rasmussen, A. T. (1951). *Atlas of Cross Section Anatomy of the Brain, Guide to the Study of the Morphology and Fiber Tracts of the Human Brain.* New York, NY: McGraw-Hill.

von Kupffer, C. (1906). "Die Morphogenie des Zentralnervensystems," in *Handbuch der Vergleichenden und Experimentellen Entwicklungslehre der Wirbeltiere*, Vol. 2, *Part 3*, ed O. Hertwig (Jena: Fischer Verlag), 1–272.

Watson, C., Kirkaldie, M., and Paxinos, G. (2010). *The Brain. An Introduction to Functional Neuroanatomy*. San Diego, CA: Academic Press.

Watson, C., and Paxinos, G. (2010). *Chemoarchitectonic Atlas of the Mouse Brain.* San Diego, CA: Academic Press.

Watson, C., Shimogori, T., and Puelles, L. (2017). Mouse FGF8-Cre lineage analysis defines the territory of the postnatal mammalian isthmus. *J. Comp. Neurol.* 525, 2782–2799. doi: 10.1002/cne.24242

Watts, A. G., Swanson, L. W., and Sanchez-Watts, G. (1987). Efferent projections of the suprachiasmatic nucleus. I. Studies using anterograde transport of *Phaseolus vulgaris* leucoagglutinin in the rat. *J. Comp. Neurol.* 258, 204–229. doi: 10.1002/cne.902580204

Werner, C. F. (1956). *Wortelemente Lateinisch-Griechischer Fachausdrücke in der Biologie, Zoologie und Vergleichenden Anatomie*. Leipzig, Akademische Verlagsgesellschaft Geest & Portig K.-G.

Xie, Y., and Dorsky, R. I. (2017). Development of the hypothalamus: conservation, modification and innovation. *Development* 144, 1588–1599. doi: 10.1242/dev.139055

Ziehen, T. (1906). "Die Morphogenie des Zentralnervensystems der Säugetiere," in *Handbuch der Vergleichenden und Experimentellen Entwicklungslehre der Wirbeltiere*, Vol.2, *Part 3.* ed O. Hertwig (Jena: Fischer Verlag), 273–351.

Conflict of Interest Statement: The author declares that the research was conducted in the absence of any commercial or financial relationships that could be construed as a potential conflict of interest.

Copyright © 2019 Puelles. This is an open-access article distributed under the terms of the Creative Commons Attribution License (CC BY). The use, distribution or reproduction in other forums is permitted, provided the original author(s) and the copyright owner(s) are credited and that the original publication in this journal is cited, in accordance with accepted academic practice. No use, distribution or reproduction is permitted which does not comply with these terms.

frontiers in Neuroanatomy

HYPOTHESIS AND THEORY
published: 12 February 2019
doi: 10.3389/fnana.2019.00010

Time for Radical Changes in Brain Stem Nomenclature—Applying the Lessons From Developmental Gene Patterns

Charles Watson[1,2]*, *Caitlin Bartholomaeus*[1] and *Luis Puelles*[3]

[1] School of Biological Sciences, University of Western Australia, Perth, WA, Australia, [2] Neuroscience Research Australia, The University of New South Wales, Sydney, NSW, Australia, [3] Department of Human Anatomy and IMIB-Arrixaca Institute, School of Medicine, University of Murcia, Murcia, Spain

The traditional subdivision of the brain stem into midbrain, pons, and medulla oblongata is based purely on the external appearance of the human brain stem. There is an urgent need to update the names of brain stem structures to be consistent with the discovery of rhombomeric segmentation based on gene expression. The most important mistakes are the belief that the pons occupies the upper half of the hindbrain, the failure to recognize the isthmus as the first segment of the hindbrain, and the mistaken inclusion of diencephalic structures in the midbrain. The new nomenclature will apply to all mammals. This essay recommends a new brain stem nomenclature based on developmental gene expression, progeny analysis, and fate mapping. In addition, we have made comment on the names given to a number of internal brain stem structures and have offered alternatives where necessary.

Keywords: brain stem, hindbrain, midbrain, isthmus, rhombomeres

OPEN ACCESS

Edited by:
Paul Manger,
University of the Witwatersrand, South Africa

Reviewed by:
Marten P. Smidt,
University of Amsterdam, Netherlands
Adhil Bhagwandin,
University of Cape Town, South Africa
Nina Patzke,
Hokkaido University, Japan

***Correspondence:**
Charles Watson
c.watson@curtin.edu.au

Received: *25 October 2018*
Accepted: *22 January 2019*
Published: *12 February 2019*

Citation:
Watson C, Bartholomaeus C and Puelles L (2019) Time for Radical Changes in Brain Stem Nomenclature—Applying the Lessons From Developmental Gene Patterns. Front. Neuroanat. 13:10. doi: 10.3389/fnana.2019.00010

INTRODUCTION

For over a century, teachers and scientists have described the mammalian brain stem as having three parts—the midbrain, the pons, and the medulla oblongata—and the names of numerous structures inside the brain stem are consistent with this subdivision. This subdivision was based purely on the external appearance of the human brain stem and there is an urgent need to update the names of brain stem structures to be consistent with modern research findings relative to molecularly defined brain stem developmental units. Studies of developmental gene expression show that the current use of the term "pons" is in most cases very misleading (Puelles et al., 2013; Watson et al., 2017a). In addition, gross misinterpretations of brain stem organization have led to the mistaken inclusion of diencephalic structures in the midbrain, and the failure to recognize the isthmus as the first segment of the hindbrain. This essay will summarize the problems that have arisen from the conventional use of the traditional brain stem nomenclature, and will suggest alternatives based on developmental gene expression, progeny analysis, and fate mapping. In addition, we will comment on the names given to a number of internal brain stem structures and offer alternatives where we think it necessary.

The key to understanding the "natural" (i.e., gene-modulated) anatomy of the brain stem lies in an appreciation of its segmental rostrocaudal organization, without forgetting its parallel dorsoventral differentiation. A complete picture of the segmental organization has been revealed by a number of studies of gene expression during development, which have been summarized by Puelles et al. (2013) and Tomás-Roca et al. (2016).

GENE EXPRESSION REVEALS THE SEGMENTAL ORGANIZATION OF THE BRAIN STEM

The segmental organization of the brain stem was first observed by embryologists in the late nineteenth century, who described a series of outpouchings in the developing vertebrate brain stem (von Baer, 1828; Orr, 1887). The significance of this finding was lost in the subsequent period dominated by the columnar organization theories of Herrick (1910, 1948). But over about the past 25 years, the outpouchings have been recognized as evidence for the fundamental segmental organization of the brain stem. The change came about through the advent of studies on developmental gene expression (e.g., Gaunt et al., 1986; Murphy et al., 1989; Wilkinson et al., 1989a,b; Sundin and Eichele, 1990; Krumlauf et al., 1993), the creation of molecularly-defined regional progeny, and clonal restriction (Lumsden and Keynes, 1989; Fraser et al., 1990; Lumsden, 1990, 1991). These gene-based progeny studies were enabled by the invention of gene targeting in mice (Capecchi, 1989). It is now clear that the brain stem of all vertebrates is made up of a rostro-caudal series of segments that arise in early development and impose an anatomical and functional organization that persists in the adult brain. An additional point of significance is that the midbrain has in recent years been ascribed to the forebrain, taking it out of the brain stem. The midbrain has been found to share a number of gene expression patterns with diencephalon and hypothalamus and lacks true continuity with the hindbrain (Puelles, 2013). The midbrain contains two segments, called mesomeres (Puelles et al., 2012a; Puelles, 2013), whereas the hindbrain is divided into 12 neuromeres—the isthmus and 11 rhombomeres (Puelles et al., 2013; Tomás-Roca et al., 2016; Watson et al., 2017a). Unfortunately, some authors (notably those led by Lumsden and Krumlauf) have consistently ignored the significance of the isthmus and have not accepted the existence of the four caudal rhombomeres (r8 to r11), based on the fact that they lack overt constrictions between them (e.g., Lumsden and Krumlauf, 1996; Tümpel et al., 2009). However, the gene expression evidence for the isthmic segment (Watson et al., 2017c) and the presence of four "hidden" rhombomeres, known as cryptorhombomeres, is now very strong (Marín et al., 2008; Puelles, 2013; Puelles et al., 2013; Tomás-Roca et al., 2016). One surprising finding in relation to the caudal rhombomeres is that the pyramidal decussation is located in the spinal cord, and not in the caudal hindbrain as has been traditionally assumed (Tomás-Roca et al., 2016). The pyramidal tract fibers decussate after they cross the medullo-spinal boundary and so the pyramidal decussation in no longer a component of the hindbrain.

The first comprehensive attempt to illustrate the boundaries and contents of the segmental elements of the brain stem (two mesomeres, isthmus, and 11 rhombomeres) in different planes of section was presented in the chick brain atlas of Puelles et al. (2007). Many of the segments in the brain stem in birds and mammals can be confidently identified by the presence of one or more signature nuclei; examples are the trochlear nucleus in the isthmus and the abducens nucleus in r5. A diagram summarizing mammalian segmental components can be found in Tomás-Roca et al. (2016), and a modified version of this figure is shown in our **Figure 4**. **Table 1** shows the segmental position of selected structures in the mammalian brain stem and adjacent diencephalon and spinal cord.

A relatively small set of genes is involved in establishing the rostrocaudal segmental plan of the central nervous system. Those vital to brain stem development include *Pax* family genes, *Otx2*, *Wnt1*, *Gbx2*, *Fgf8*, *Shh genes*, and *Hox* family genes. Their role in the segmentation of the brain stem is summarized in **Figure 1**, which shows that expression of *Pax 6* in the alar diencephalon ends sharply at the junction between the pretectal area and the midbrain (Schwarz et al., 1999; see images in Puelles et al., 2012a; Duan et al., 2013), *Otx2* is expressed in forebrain and midbrain (Puelles et al., 2012a,b); *Gbx2* is expressed in the rostral hindbrain (isthmus and r1) but not in the midbrain (Puelles et al., 2012a); *Fgf8* is selectively expressed in the isthmus (Watson et al., 2017c); and the *Hox* genes are expressed from r2 to the caudal end of the spinal cord (Puelles et al., 2013). The expression of the *Hox*-related gene *Egr2* reveals the anatomy of rhombomeres 3, 4, and 5 in a convincing way (**Figure 2**).

There is a question as to whether the gene expression data acquired from mice can be confidently applied to other mammals, and perhaps to other vertebrates. We are confident such extrapolations can be made, because the anatomy and development of the brain stem is highly conserved (for a general discussion of this issue see Nieuwenhuys et al., 1998; Gilland and Baker, 2005). For example, the pattern of gene expression in the development of the brain stem in chicks mirrors that described in the mouse in almost every respect, even though the species are separated by around 300 million years of evolution. A few exceptions do exist (such as the translocation of the facial motor nucleus from r4 to r6 in mammals), but the point to point similarities are extraordinary (Cambronero and Puelles, 2000; Puelles et al., 2007; Tomás-Roca et al., 2016). However, the evolutionary history of brain stem development is a much bigger subject than we have attempted to address in the present paper.

PROBLEMS WITH TRADITIONAL BRAIN STEM NOMENCLATURE

When the traditional nomenclature of the brain stem is tested against the new understanding of brain stem organization based on developmental gene expression, five major areas of misinterpretation become apparent. These are the true identity of the pons, the existence of the isthmus, the true definition of the midbrain without diencephalic and hindbrain additions, the location of the substantia nigra and VTA (though this is rather a diencephalon problem), and the segmental origin of the cerebellum.

The True Identity of the Pons

The primary problem with the use of the word "pons" is that its historical meaning attaches to the voluminous formation seen on the ventral surface of the human brain. The basilar pontine formation is exceptionally large in humans

TABLE 1 | Segmental components of the mammalian caudal diencephalon, midbrain, and hindbrain and position of major structures within these segments.

DIENCEPHALON		
Diencephalic prosomere 1 (dp1)		
	Posterior commissure	pc
	Pretectal nuclei	PT
	Darkschewitsch nucleus	Dk
	Interstitial nucleus of Cajal	InC
	Red nucleus, parvocellular part	RPC
MIDBRAIN		
Mesomere 1 (m1)	Superior colliculus	SC
	Inferior colliculus	IC
	Oculomotor nucleus	3N
	Emerging oculomotor nerve	3n
	Red nucleus, magnocellular part	RMC
Mesomere 2 (m2)	Sagulum nucleus	Sag
	Retrorubral field (DA8)	RRF
	Subbrachial nucleus	SubB
HINDBRAIN		
Isthmocerebellar (prepontine)		
Isthmus (is)	Trochlear nucleus	4N
	Emerging trochlear nerve	4n
	Parabigeminal nucleus	PBG
	Microcellular tegmental nucleus	MiTg
	Prodomal interpeduncular nucleus	IPpro
Rhombomere 1 (r1)	Locus coeruleus	LC
	Rostral interpeduncular nucleus	IPR
	Caudal interpeduncular nucleus	IPC
	Parabrachial nuclei	MPB/LPB
PONTINE REGION		
Rhombomere 2 (r2)	Rostral motor trigeminal nucleus	5N
	Emerging motor trigeminal nerve	5n
Rhombomere 3 (r3)	Caudal motor trigeminal nucleus	5N
	Rostral pontine nuclei	Pn
Rhombomere 4 (r4)	Emerging facial nerve	7n
	Caudal pontine nuclei	Pn
RETROPONTINE		
Rhombomere 5 (r5)	Abducens nucleus	6N
	Emerging abducens nucleus	6n
	Superior olive and trapezoid body	SOl/tz
Rhombomere 6 (r6)	Facial nucleus (migrated)	7N
	Emerging glossopharyngeal nerve	9n
MEDULLA OBLONGATA		
Rhombomere 7 (r7)	Compact ambiguus nucleus	AmbC
Rhombomere 8 (r8)	Compact ambiguus nucleus	AmbC
	Rostral inferior olive	IO
Rhombomere 9 (r9)	Semicompact ambiguus nucleus	AmbSC
	Middle inferior olive	IO
Rhombomere 10 (r10)	Loose ambiguus nucleus	AmbL
	Caudal inferior olive	IO
	Area postrema	AP
Rhombomere 11 (r11)	Retroambiguus nucleus	RAmb
ROSTRAL SPINAL CORD		
C1 segment	Pyramidal decussation	pyx

(correlative with expansion of the cerebral cortex), and this has led to misinterpretation over its true topological position. In many mammals, the basilar pontine nuclei (Pn) and the reticulotegmental nucleus (RtTg) aggregate at the ventral part of rhombomeres 3 and 4, and the pontine bulge is restricted to the ventral surface of these two rhombomeres. An interesting developmental feature of the basilar pons is that the neurons that form the pontine nuclei develop in the rhombic lip of rhombomeres 6 and 7 and then migrate tangentially under the pia to their final location in rhombomeres 3 and 4 (**Figure 2**).

On the other hand, human anatomy textbooks uniformly state that the pons extends from the *caudal end* of the midbrain to the *beginning* of the medulla oblongata just rostral to the exit of the vestibulocochlear and abducens nerves. The differential growth of the basilar pons in humans hides much of the rostral prepontine hindbrain (from isthmus to part of rhombomere 2), on one side, and the part of the retropontine hindbrain containing the abducens nucleus, superior olive, and facial nucleus, on the other (**Figures 3**, **4**).

One result of the superimposition of the human version of pontine topography and nomenclature to those mammals with a small basilar pons is that many structures far away from the basilar pons are called "pontine" because in the human brain they are overlaid by the enlarged "pontine" region. The solution to this problem is relatively simple: discontinue the use of the word "pons" as a topographical descriptor in all mammals, and restrict the use of the term pons to the basilar pontine formation in r3-r4. Note the variable pontine "expansion" into r1 and r2 in primate brains lacks any basilar pontine nuclei (Pn) in its interior, and contains exclusively crossed fibers of the middle cerebellar peduncle (mcp) that surround the trigeminal root in alar r2 (see **Figure 6**). The modern segmented hindbrain model emphasizes the need to distinguish prepontine, pontine, retropontine and medullary territories, each of which appears subdivided into transversal rhombomeric domains. This provides a new level of precision to support modern anatomical and functional analysis.

The Existence of the Isthmus

The isthmus, understood as a distinct hindbrain segment separating the midbrain from the other hindbrain rhombomeres, was already identified morphologically by His (1893, 1895), but was later arbitrarily ascribed to the midbrain in conventional neuroanatomical texts. In contemporary works, the isthmic territory is defined early in development by the selective expression of *Fgf8* (coding for the diffusible morphogen FGF8, which serves as the signal of the isthmic organizer—signal needed for the formation of the cerebellum and the caudal midbrain). The mature progeny of the isthmus have been demonstrated in a recent Cre *Fgf8* lineage study (Watson et al., 2017c). Within the isthmic territory so defined, lie the trochlear nucleus (and its emerging nerve), the parabigeminal nucleus, the microcellular tegmental nucleus, and the decussation of the superior cerebellar peduncle (Watson et al., 2017c). The isthmus therefore lies between the caudal midbrain and rhombomere 1 (r1).

Most neuroanatomical texts used by health science students do not comment on the presence of the isthmus at all (e.g.,

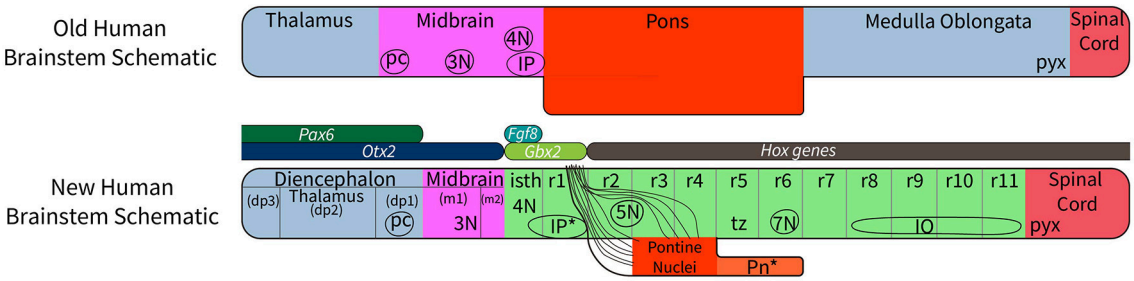

FIGURE 1 | A diagram to compare the traditional view of subdivisions of the human brain stem with the new system of segmentation revealed by developmental gene expression. At the top, the subdivisions of the "old" human brain stem (the traditional version) are based on the assumption that the midbrain extends from the thalamus to the rostral margin of the pons; this concept wrongly holds that the pretectum (dp1) and the isthmus (isth) belong to the midbrain (Puelles et al., 2012a). Comparing the traditional version of the human brain stem with the new segmental schema (bottom schema) we see that the "old" pons was held to extend between levels r1 to r6. In reality, r5 and r6 represent a hidden rostral retropontine part of the "medulla oblongata," whereas the migrated basilar pons is located only within r3 and r4. Part of the confusion relating to the extent of the pons is due to a mushroom-like rostral expansion of the pons created by rostral pontine cerebellopetal fibers that surround the trigeminal root in r2 as they approach the cerebellum in r1(see **Figure 6**), thus adding part of r2 to the apparent pontine bulge in humans. On the other hand, mammals with less massive pontine development than humans show a simpler, less deformed general arrangement, which leaves the ventral surface of r5 and r6 exposed. In addition, the "old" version of the human brain stem places the pyramidal decussation (pyx) at the caudal end of the medullary brain stem, whereas the decussation actually lies in the rostral spinal cord. The most important difference between the "new" human brain stem and the generic mammalian brain stem is that the basilar pons in the human bulges rostrally into r2, where only crossed fibers of the middle cerebellar peduncle are found, and caudally, where the overhanging part of the basilar pontine nuclei partly hides the underlying rhombomeres r5 to r6 (Pn*). The positions of the oculomotor (3N), trochlear (4N), and facial (7N) nerve nuclei, the interpeduncular nuclei (the prodromal, caudal and rostral IP parts are collectively labeled as IP*); the posterior commissure (pc), and the inferior olive are shown for reference. The rostrocaudal extent of key developmental genes is shown in the middle of the diagram. Note *Fgf8* codes for the morphogen signal of the isthmic organizer, whose hindbrain gradient ends at the r1/r2 boundary. This image is loosely based on a figure presented by Watson et al. (2017a).

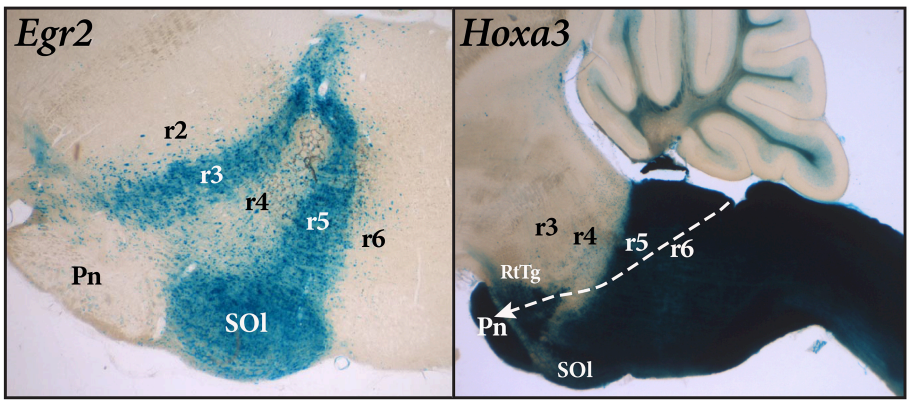

FIGURE 2 | Sagittal sections of mouse brain stem with *Egr2*-Cre and *Hoxa3*-Cre fate mapping. The blue *Egr2* label is seen in the cells of rhombomere 3 (r3) and rhombomere 5 (r5). Rhombomere 5 contains the labeled cells of the superior olive (SOl), but the pontine nuclei within r4 (Pn), which migrate from r6-r7, remain largely unlabeled. The section on the right, showing expression of *Hoxa3,* reveals a sharp delineation between rhombomere 4 (r4) and rhombomere 5 (r5). However, the pontine nuclei within r3 and r4, as well as the RtTg nucleus, are labeled in this case because they have migrated from the rhomic lip of rhombomeres 6 and 7 (r6-r7) as indicated by the path of the white arrow.

Hendelman and Walter, 2005; Haines, 2012; Jacobson et al., 2017; Mtui et al., 2017). A few make note of the organizing role of the isthmic region in the development of the midbrain/hindbrain junction, but do not acknowledge its presence in the mature brain (e.g., Martin, 2003; Nieuwenhuys et al., 2008; Barker et al., 2017). A small number of textbooks recognize the presence of the isthmus in both the developing and developed brain but mistakenly describe it as forming the caudal part of the midbrain (e.g., Butler and Hodos, 2005; Kiernan and Rajakumar, 2013). The modern concept of the isthmus concept establishes a new caudal boundary for the midbrain region, which coincides with the caudal expression limit of the gene *Otx2* in all vertebrates (Puelles, 2013; Puelles et al., 2013).

The Mistaken Inclusion of Diencephalic Structures in the Rostral Midbrain and the Modern Rostral Midbrain Boundary

The diencephalon consists of three segments (diencephalic prosomeres 1, 2, and 3, labeled dp1–3 in **Figure 1**) defined by gene expression (Puelles et al., 2012a; Puelles, 2013). The caudal diencephalic prosomere (dp1—the pretectal region) is sharply

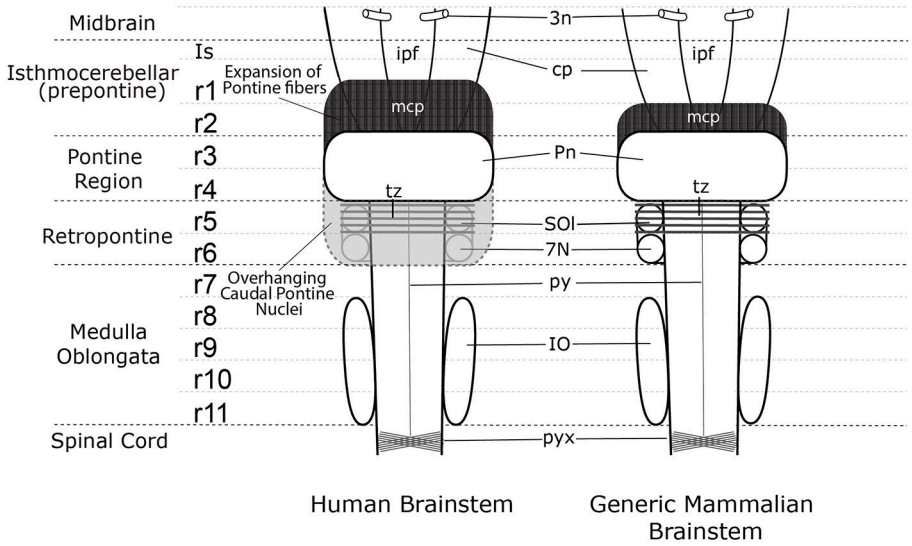

FIGURE 3 | A comparison of the external view of the human brain stem (left) and generic mammalian brain stem (right). In the midbrain the emerging oculomotor nerve (3n) is shown. Note the interpeduncular fossa extends into the prepontine hindbrain (ipf), where the interpeduncular nuclear complex is found (not shown). The surfaces of the cerebral peduncles (cp) and the interpeduncular fossa (ipf) visible in the human brain stem are reduced by the rostral expansion of the cerebellopetal pontine fibers coursing through r2 into the cerebellum in r1(middle cerebellar peduncle—mcp). The trapezoid body (tz) and superior olive (SOl) identify rhombomere 5 (r5), but these structures are not visible on the ventral surface of the human brain stem as they are covered by the overhanging caudal pons. The migrated facial nucleus (7N) is found in rhombomere 6 (r6) (Di Bonito et al., 2013; Puelles et al., 2018), but it is also covered by the overhanging caudal expansion of pontine nuclei in the human brain stem. The inferior olive extends from rhombomere 8 (r8) to rhombomere 11 (r11). The spinal cord begins at the start of the pyramidal decussation (pyx).

separated from the rostral border of the midbrain by a plane passing just behind the posterior commissure and in front of the oculomotor nerve root (**Figures 3**, **4**; Puelles et al., 2012a). Diverse developmental genoarchitectonic studies reveal that a number of caudal diencephalic structures have been mistakenly placed within the boundaries of the midbrain, while experimental analysis has shown that a midbrain fate is incompatible with some genes expressed in the diencephalic pretectum, such as *Pax6* (Puelles, 2013, 2016).

These misplaced structures include the nucleus of Darkeschewitz (dp1), the interstitial nucleus of Cajal (dp1), the rostral (parvicellular) red nucleus (dp1), the pre-Edinger-Westphal nucleus (dp1), the subcommissural organ, the posterior commissure and its related nuclei (dp1), and the medial terminal nucleus of the accessory optic tract (dp1, dp2, and dp3). Moreover, the classical "posterior pretectal nucleus" is now ascribed to the rostral midbrain (m1), since it lies in the rostral part of the superior colliculus, but caudal to the posterior commissure. This nucleus is now named the "tectal gray" (TG, see **Figure 4**) which is consistent with comparative usage in tetrapods (Puelles et al., 2012a).

A partial explanation for the confusion relating to the rostral and caudal boundaries of the midbrain is lack of appreciation of the impact of the cephalic flexure on giving a marked wedge shape to the midbrain. The cephalic flexure is a sharp bend of almost 180 degrees in the neural axis at the rostral end of the brain stem, so that the ventral surface of the midbrain is compressed into a very small area between the diencephalon and the isthmus, coinciding with the region containing the emerging root of the oculomotor nerve. In a sagittal section, this results in the midbrain forming a wedge shaped profile. In fact, the emerging rootlets of the oculomotor nerve provide the only reliable guide to the identification of the ventral surface of the midbrain (**Figure 4**; see also Puelles et al., 2012a). Traditional representations of the midbrain have arbitrarily attempted to endow it with a ventral surface of about the same extent as the dorsal (tectal) surface. Based on this error, both textbooks and journal articles placed many structures within the midbrain that actually belong to the isthmus (caudally) or diencephalon (rostrally). The correct location of many of these structures is seen in **Figure 4**, which shows the boundaries of the midbrain on a diagram of a sagittal section of a rodent brain.

The Location of the Substantia Nigra and the VTA

A further complication resulting from the severe cephalic flexion of the neuraxis at the level of the midbrain is a misunderstanding of the segmental location of the substantia nigra and the VTA. It is widely assumed that both of these structures lie *within the midbrain*, but in fact only a caudal portion of both the substantia nigra and the VTA can be found in the compressed true ventral midbrain (**Figure 4**), and the rostral parts of the substantia nigra and VTA lie in the diencephalon, across its prosomeres 1, 2, and 3. The caudalmost parts of these dopaminergic populations lie in the isthmus (Puelles et al., 2012a,b). The overall result is that only about one quarter of the substantia nigra and VTA can be said to belong to the midbrain, and modern literature refers to a "mesodiencephalic SN/VTA complex." Some differential gene expression has been observed along these four parts of the SN/VTA, suggesting that each segmental module possibly

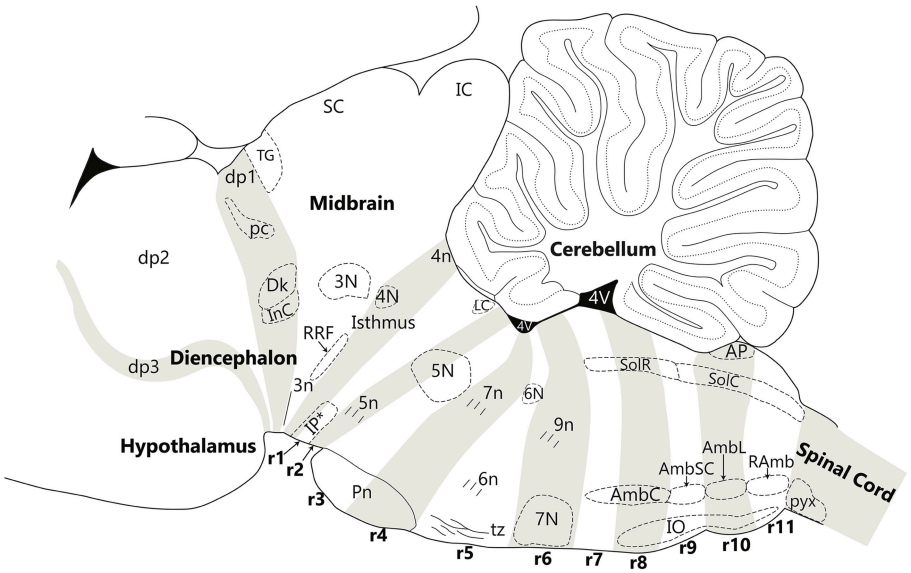

FIGURE 4 | Nuclear and fiber landmarks that identify the segments of the hindbrain, midbrain and diencephalon. In this Figure, the cerebellum, fourth ventricle and hypothalamus are labeled for orientation. Note that fate-mapping data have shown that the cerebellum is a tectal structure restricted to the isthmus and r1, irrespective that in the adult it overhangs far backwards over the dorsal choroidal surface of the pontine, retropontine and medullary regions. The diencephalic prosomere 1 (dp1), which contains the pretectal posterior commissure (pc), Darkschewitsch nucleus (Dk) and the interstitial nucleus of Cajal (InC), is delimited anteroposteriorly by the extent of the posterior commissure (pc). The midbrain contains the oculomotor nucleus (3N) and emerging oculomotor nerve (3n) in mesomere 1 and the retrorubral field (RRF) in mesomere 2. Mesomere 2 is a thin wedge of the midbrain, caudal to 3N, the red nucleus and the inferior colliculus. The hindbrain is comprised of twelve segments—the isthmus (r0) and rhombomeres 1–11 (r1 to r11). The isthmus contains the trochlear nucleus (4N), the emerging trochlear nerve (4n) and the prodromal part of the interpeduncular nucleus (IP*). Rhombomere 1 (r1) contains the rostral and caudal parts of the interpeduncular nucleus (IP*), the dorsal and ventral tegmental nuclei, and the locus coeruleus (LC). Rhombomere 2 (r2) contains the rostral part of the motor trigeminal nucleus (5N) and the emerging motor trigeminal nerve. Rhombomere 3 (r3) contains the caudal part of the motor trigeminal nucleus (5N) and the rostral pontine nuclei (Pn). Rhombomere 4 (r4) contains the caudal pontine nuclei (Pn) and the emerging facial nerve (7n). Rhombomere 5 (r5) contains the abducens nucleus (6N), the emerging abducens nerve (6n), and the decussation of the trapezoid body (tz), along with the superior olivary complex. Rhombomere 6 (r6) contains the migrated facial nucleus (7N) and the emerging glossopharyngeal nerve (9n). Rhombomere 7 (r7) and 8 (r8) contain the compact ambiguus nucleus (AmbC) and the rostral end of the solitary nucleus (gustatory nucleus—SolR). Rhombomere 8 also contains the rostral tip of the inferior olive (IO). Rhombomere 9 (r9) contains the semicompact ambiguus nucleus (AmbSC) and the middle region of the inferior olive (IO). Rhombomere 10 (r10) contains the loose ambiguus nucleus (AmbL), the area postrema (AP), and the caudal region of the inferior olive (IO). Rhombomere 11 (r11) contains the retroambiguus nucleus (RAmb) and the caudal tip of the inferior olive. The spinal cord begins at the start of the pyramidal decussation (pyx).

manifests subtle differential properties (e.g., in projection targets or afferent sources, or in sensitivity to degenerative changes in Parkinson's disease).

The Segmental Origin of the Cerebellum

The cerebellum is an outgrowth of the dorsalmost alar plate of the caudal isthmus and the first rhombomere (Alvarez-Otero et al., 1993; Aroca and Puelles, 2006). It is therefore an integral part of the prepontine hindbrain, contradicting the old assumption that it forms a developmental unit with the pons. The vermis of the cerebellum is mainly derived from the rhombic lip of the isthmic alar plate, and the hemisphere of the cerebellum is mainly derived from the rhombic lip of the r1 alar plate, as demonstrated by experimental fate mapping and recent progeny analysis (Alvarez-Otero et al., 1993; Wingate, 2001; Aroca and Puelles, 2006; Watson et al., 2017a,b).

OPTIONS FOR RENAMING PARTS OF THE BRAIN STEM

The study of developmental gene expression makes it clear that the hindbrain is composed of 12 segments—the isthmus (which can be counted as r0) and the other 11 rhombomeres. The reason referring to the isthmus as r0 is that the isthmus territory was long thought to develop inside r1. And once it was realized it was an independent rhombomere [in fact the first one in the series the r0 convention was adopted to avoid changing all other rhombomere numbers; (Puelles, 2013)]. Embryologists have long considered the isthmus to be a part of the hindbrain, starting from the work of His (1893, 1895), and later complemented by Palmgren (1921), Vaage (1969, 1973) and Puelles and Martinez-de-la-Torre (1987), so the concern as to whether the traditional term "rhombencephalon" includes or not the isthmus seems a moot one.

The solution is to acknowledge the existence of 12 hindbrain rhombomeres (r0 to r11) sharing a number of gene determinants and cell fates not present in the midbrain (which should now be considered to form the caudal part of the forebrain). For example, the genes which lead to the specification of serotonergic neurons are found only in rhombomeres 0 to 1 (r0 to r11), and are not generated in the midbrain. Note that the newly named r0 element is synonymous with the classic name "isthmus," since this term consistently refers to the rostralmost part of the hindbrain or rhombencephalon. It is important to note again here that the

cerebellum is a developmental dorsal alar derivative of the r0 and r1 units, and so it is also an intrinsic part of the hindbrain. Some previous uses of the term rhombencephalon apparently excluded the cerebellum. The close developmental relationship between the cerebellum and the rostral or, modernly, prepontine hindbrain is not widely appreciated, and the cerebellum is often wrongly treated as if it were an entity separate from the remainder of the brain stem.

There have been various attempts to harmonize or conciliate the parts of the neuromeric hindbrain with the older subdivision into pons and medulla (see Watson et al., 2017a). We suggest dividing the hindbrain into isthmocerebellar or prepontine (r0, r1), pontine (r2, r3, and r4), retropontine (r5 and r6) and medullary (r7 to r11) levels (see **Figures 5**, **6**). These divisions provide a logical approach to naming the areas of the hindbrain associated with the pontine regions. This approach retains largely unchanged the use of the term medulla oblongata, which is common to all current textbooks. There may subsist, however, also a need for a larger scale subdivision of the hindbrain for some clinical purposes. We therefore suggest that the region from isthmus (r0) to rhombomere 6 can be referred to as "rostral hindbrain" and the region from rhombomeres 7 to 11 can be referred to as "caudal hindbrain" (or medulla oblongata) (**Figure 5**). This definition of the rostral hindbrain includes the isthmocerebellar, pontine and retropontine regions described above. However, we realize that in order to make embryological and physiological rhombomere-related scientific progress accessible to clinical topographic analysis of pathology and surgery within the conventional "pons" region (e.g., modern segmental understanding of motor, reticular, vestibular, auditory, trigeminal, respiratory or cardiocirculatory functional subregions) it may take decades to extinguish its indiscriminative use as a regional descriptor for the whole rostral hindbrain.

Recommended Brain Stem Nomenclature for Different Levels of Learning (High School, Undergraduate University/Medical School)

The clinical usage of pons and medulla oblongata is primarily based upon the external view of the human hindbrain and is commonly represented in medical student textbooks (see for example Barr's The Human Nervous System 10th edition, Kiernan and Rajakumar, 2013). **Figure 5** proposes different levels of nomenclature for the hindbrain required at different levels of education. It is structured such that the lowest level of the nomenclatural understanding (high school human biology) is compatible with the more complex picture allowing a student to build on their initial simpler but already partly updated understanding of the brain stem as they progress into medical school and beyond.

BRAIN STEM NOMENCLATURE IN THE TERMINOLOGICA NEUROANATOMICA

The 2017 update of Terminologica Neuroanatomica (FIPAT. Terminologica Neuroanatomica. FIPAT.library.dal.ca. Federative International Program for Anatomical Terminology. February 2017) has attempted to resolve some of the many conflicts in brain stem nomenclature. Overall, the authors have done a fine job of producing a modern nomenclature plan. However, the thickets of nomenclature are dense and challenging and there are many historical hangovers to be dealt with. From the point of view of this paper the best news is that the trochlear nucleus has been moved from the midbrain to the hindbrain. However, a number of rostral hindbrain (isthmic) structures have been unfortunately left in the midbrain. They include the cuneiform nucleus, the parabigeminal nucleus, the caudal linear nucleus, pedunculopontine tegmental nucleus (now properly called peduncular tegmental nucleus because it is nowhere near the pons), and the dorsal raphe nucleus. The latter needs explanation because a small rostral part does invade the midbrain, while the main nucleus stays in the isthmus. The interpeduncular nucleus is also included in the midbrain even though it belongs to r1.

On the rostral side of the midbrain there are some nuclei which should have been moved to the caudal diencephalon, such as the parvocellular red nucleus.

FURTHER POSSIBLE CHANGES TO TRADITIONAL NAMES OF BRAIN STEM NUCLEI

In addition to the major nomenclatural issues described above, contemporary research points to the need for recognition of previously unrecognized features of a number of other groups of brain stem nuclei. These nuclei belong to the interpeduncular group, the precerebellar nuclei, the reticular and tegmental nuclei, and the monoaminergic nuclei of the hindbrain.

The Location of Parts of the Interpeduncular Nucleus

The interpeduncular nucleus (IP) occupies a subpial ventral median position associated to the hindbrain part of the interpeduncular fossa (ipf; see **Figure 3** and note the classic literature often wrongly ascribed the interpeduncular fossa to the midbrain or even to the diencephalon). The IP is a bilaterally symmetrical complex of diverse subnuclei arranged anteroposteriorly and mediolaterally. The IP receives bilateral forebrain input via the habenulo-interpeduncular tract (facsiculus retroflexus) of both sides. A small rostral part of the interpeduncular nuclear complex has been experimentally demonstrated to originate from the isthmus (Lorente-Cánovas et al., 2012). This represents the prodromal (rostralmost) interpeduncular subnucleus. Caudal to this unit the interpeduncular nucleus has two main parts known as rostral IP (IPR) and caudal IP (IPC). These are located in, and originate from, rhombomere 1 (IPR, IPC; see **Figure 6**; Lorente-Cánovas et al., 2012).

Precerebellar Nuclei

The precerebellar nuclei are a set of neuronal populations that generally originate from the hindbrain rhombic lip, variously migrate tangentially to diverse dorsoventral sites within a variety of hindbrain rhombomeres, and project excitatory mossy

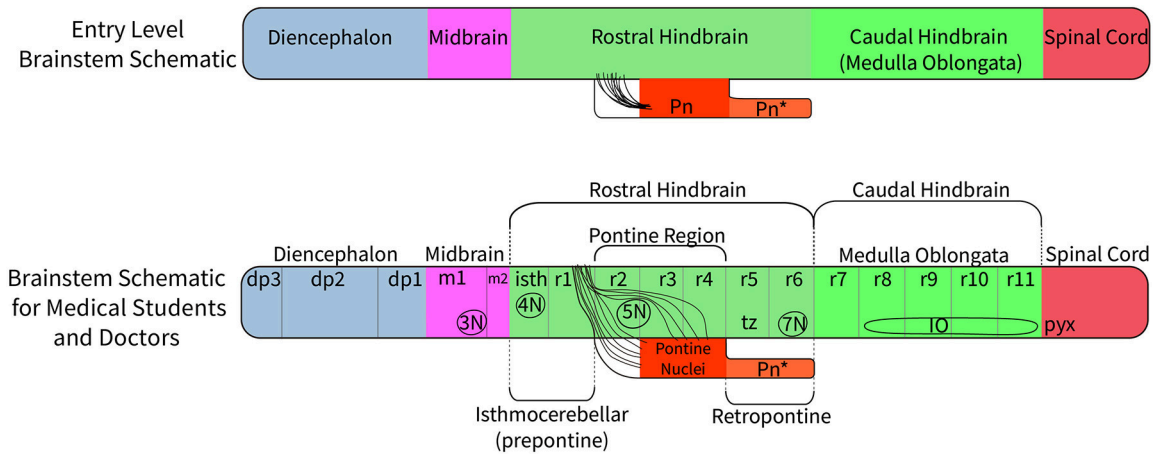

FIGURE 5 | A suggested approach to represent the nomenclature for the diencephalon, midbrain and hindbrain for students at different levels of education. At an entry level (such as a high school level) a student would merely need to understand that on the basis of molecular regionalization there are rostral and caudal parts of the hindbrain. They should know that cerebellar evolutionary enlargement causes the pons (Pn) in primates to form a ventral bulge starting roughly at the middle of the rostral hindbrain, but forming a mushroom-like expansion with pontocerebellar fibers stretching forwards within neighboring rostral hindbrain areas to reach the cerebellum. In humans there is an additional pontine deformation overhanging the ventral surface of the caudalmost rostral hindbrain (Pn*). At a medical student and health professional level, the structures which need to be recognized include the three segments of the diencephalon (dp3, dp2, and dp1), the signature contents of the midbrain (oculomotor nucleus, 3N, and the emerging oculomotor nerve, not pictured) and the full set of hindbrain rhombomeres (isth/r0–r11). The intermediate hindbrain position of the pontine bulge at r2-r4, defines the boundaries of the prepontine (r0,r1 or isthmocerebellar) and retropontine (r5, r6) subregions. The pontine nuclei in r3 to r4 give rise to the crossed middle cerebellar peduncle which reaches forward in front and behind the trigeminal root (5n) in r2 to enter the cerebellum through r1. In humans, the caudal part of the basilar pontine nuclei overhang, and therefore hide, the most of the ventral surface of rhombomeres 5 and 6; thus r5 and r6 actually represent a distinct retropontine subregion, as a transition into the medullary region (r7 to r11).

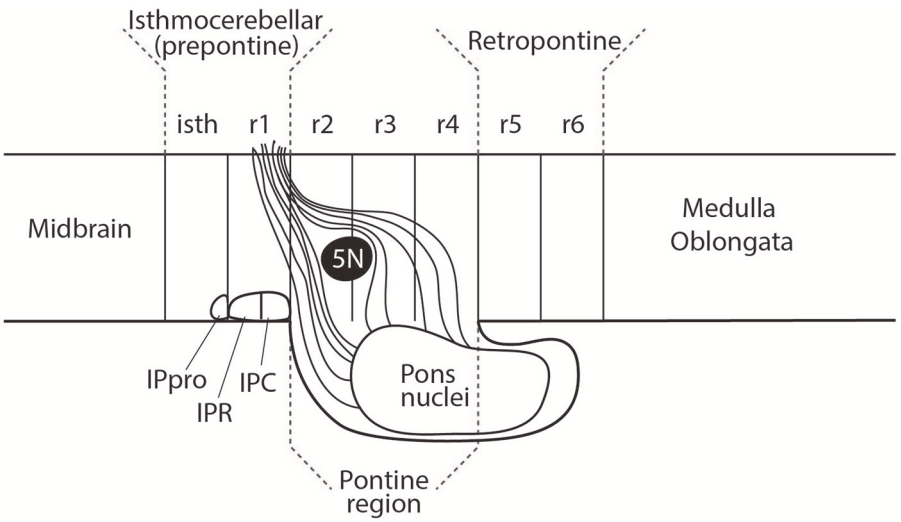

FIGURE 6 | The rostral part of the interpeduncular nucleus (IPR) is often mistakenly placed in the isthmus. This diagram shows the fate-mapped true location of the prodromal interpeduncular subnucleus (IPpro) in the isthmus (isth) and the location of both the IPR and IPC subnuclei in rhombomere 1 (r1). This relates to an apparent subdivision of r1 into distinct rostral and caudal parts, a concept which has received inadequate attention (see Vaage, 1973; Alonso et al., 2012; Puelles, 2013).

fiber input into the cerebellum, mostly contralaterally. The list of such populations includes the basilar pontine nuclei and the reticulotegmental nucleus within r3 to r4, the lateral reticular nuclei, some reticular, trigeminal and vestibular cells, and the external cuneate nucleus. The prepositus hypoglossi nucleus, the intercalated nucleus, and the nucleus of Roller (both medullary) might extend this list. The inferior olive also may be regarded as precerebellar in that sense, but it differs in that its projection ends as climbing fibers within the cerebellum, whereas the others end as mossy fibers. Finally, two previously overlooked hindbrain cell groups have been recently shown to project to the cerebellum. They

are the linear nucleus and the interfascicular trigeminal nucleus.

The Linear Nucleus—An Extension of the Lateral Reticular Nucleus

In 2009, Fu et al., showed that a dorsal extension of the lateral reticular nucleus, which they named the linear nucleus, projects to the cerebellum. This nucleus appears to be a constant feature of mammalian brains. However, it should be recognized that the first description of the nucleus, and the original application of the name linear, must be credited to Cajal (Ramon y Cajal, 1904/1995), who described it as forming a part of the lateral reticular nucleus. A segmental analysis of this nucleus in the mouse has recently been completed by Martinez-de-la-Torre et al. (2018).

The Interfascicular Trigeminal Nucleus

This nucleus had previously been named the tensor tympani part of the motor trigeminal nucleus in rodent brain atlases (Franklin and Paxinos, 2005; Paxinos and Watson, 2007), because it was thought to be a subset of small motor neurons of the motor trigeminal nucleus innervating the tensor tympani muscle. However, the neurons forming the interfascicular trigeminal nucleus were labeled following injection of retrograde tracer in the cerebellum, and the labeled neurons were found to be choline acetyltransferase (ChAT) negative, proving that they are not motor neurons (Fu et al., 2012). In addition, the cells of the interfascicular trigeminal nucleus are strongly labeled in mice via *Wnt1Cre* and *Atoh1CreER* lineage fate mapping—a feature common to the major precerebellar nuclei that arise from the rhombic lip and that issue mossy fibers (Fu et al., 2011, 2012).

Reticular and Tegmental Nuclei of the Brain Stem

Many nuclei in the brain stem that are not directly associated with the cranial nerves or the cerebellum have been labeled as reticular or tegmental nuclei. In the past the reticular nuclei were considered to form a heterogeneous functional group which was divided mainly into pontine and medullary reticular formation domains. This simplistic concept has been abandoned now in favor of a separate consideration of individually named reticular nuclei or cell groups, ascribed if possible to specific rhombomeres, or to rhombencephalic subregions (prepontine, pontine, retropontine, medullary). Unfortunately, some nuclei that have retained the name "reticular" belong to entirely different molecular and functional entities. These include the reticulotegmental and lateral reticular nuclei, which are both precerebellar nuclei. An associated problem is the widespread use of the imprecise term 'ascending reticular activating system.' This usage derives from the work of Moruzzi and Magoun (1949) who famously showed that ascending pathways from the brain stem caused the cerebrum to become alert; they assumed that the brain stem nuclei that gave rise to the ascending activating pathways must reside in the so-called reticular core of the brain stem. This proved to be incorrect, since the hindbrain cell groups that promote wakefulness do not belong to the group of identified reticular nuclei: a series of elegant studies by the Saper group (see Saper et al., 2001) have shown that the hindbrain nuclei that promote wakefulness are the locus coeruleus, the raphe nuclei, and the major forebrain and hindbrain cholinergic nuclei—none of which should be considered to belong to the reticular nuclei of the brain stem. Because of this, the term "ascending reticular activating system" should be replaced by the newer term "ascending arousal system."

We wish to draw attention to significant nomenclatural issues relating to some nuclei in the reticular/tegmental group; these are the intermediate reticular zone, the retrorubral (now the retroisthmic nucleus), the pedunculotegmental nucleus, and the nucleus incertus.

The Intermediate Reticular Zone

In the hindbrain the large cell (gigantocellular) reticular nuclei are medially placed and the small celled (parvicellular) reticular nuclei are laterally placed. The narrow region between these two large groups can be called the intermediate reticular nucleus (IRt).The intermediate reticular (IRt) nucleus of the rat was first recognized by Paxinos and Watson (1986) as a radial zone between the gigantocellular and parvicellular reticular nuclei which is slightly more reactive for AChE than the adjacent zones. Many peptidergic neurons tend to concentrate there (review in Puelles, 2013). This zone seems to lie next (just lateral) to the plane separating the derivatives of the alar and basal plates, which roughly extends radially from the sulcus limitans in the floor of the fourth ventricle to the pial surface of the brain stem where the vagal and glossopharyngeal rootlets emerge (Martinez-de-la-Torre et al., 2018; Puelles et al., 2018). Within the caudal part of the IRt are located the ambiguus and retroambiguus nuclei, the Botzinger (respiratory) nuclei, and the NA1 noradrenaline cell group.

Retrorubral Nucleus

Two structures in the brain stem have been given the name "retrorubral"—the retrorubral dopaminergic field (A8 dopamine cell group) which lies selectively in m2 (Puelles et al., 2012a) and the retrorubral tegmental or reticular nucleus, which is located r1. Unfortunately, many papers confuse these two structures and the hindbrain retrorubral nucleus sometimes is described as containing dopamine neurons (probably this error relates to the observed existence of such neurons in the *isthmic* tegmentum; Puelles et al., 2012a). To avoid this confusion, Paxinos and Watson (2014) renamed the retrorubral nucleus as the "retroisthmic nucleus" since it lies immediately caudal to the caudal boundary of the isthmus. The retroisthmic nucleus is therefore defined as an area in rhombomere 1 between the pedunculotegmental nucleus medially, and the lateral lemniscus and its nuclei laterally. Rostrodorsal to it appears the microcellular tegmental nucleus of the isthmus, and rostral to it is the caudal (isthmic) pole of the substantia nigra.

Pedunculotegmental Nucleus

The pedunculotegmental nucleus (PTg) is a prominent cholinergic (and NOS positive) cell group in r1, within the rostral hindbrain of the human, monkey, rat, and mouse. Paxinos and Watson (2006) and Puelles et al. (2007) renamed the

pedunculopontine tegmental nucleus as the pedunculotegmental nucleus (PTg), because it is not a pontine structure and clearly, lying in r1, it has no close topographical relationship to the pontine nuclei in r3 and r4. It is one of many prepontine nuclei given a 'pontine' suffix simply because they lie in the area covered by the rostrally expanded pons in the human brain.

In the human and in the rhesus monkey, the PTg has been described as having a compact cholinergic part (pars compacta) and a diffuse non-cholinergic part (pars dissipata). In rodents, however, Swanson (1992) and Paxinos and Watson (2006) named the non-cholinergic area found lateral to PTg as the retrorubral nucleus. The retrorubral nucleus has never been recognized in primates. Paxinos and Watson (2006) concluded that the retrorubral nucleus of the rodent is, in fact, the homolog of the PTg pars dissipata of primates. A study of AChE sections of human, monkey and rat brains confirms that the PTg in all three species is strongly AChE positive in cells and neuropil. Furthermore, the area immediately lateral to PTg (the primate pars dissipata and the rodent retrorubral nucleus) in all three species is only lightly stained for AChE.

The Incertus Nucleus

The identity of the incertus nucleus has been questioned since it was originally named by Streeter (1903). The area named by Streeter was quite extensive and includes areas not currently thought to relate to the true incertus nucleus. The current view is that the incertus nucleus lies close to the ependyma of the fourth ventricle, medial and ventral to the posterodorsal tegmental nucleus (PDTg, which lies within basal r2), close to the locus coeruleus in the rat (which lies in lateral basal r1), and consists of a medial compact part and a lateral diffuse part. The two parts of the incertus nucleus were given different names in the influential rabbit brain atlas of Meessen and Olszewski (1949). Meessen and Olzewski named the compact part as 'nucleus O of the central gray,' and called the diffuse part 'the alpha part of the central gray.' In a series of editions of the widely cited rat brain atlas (Paxinos and Watson, 1986, 1997, 1998, 2005, 2006, 2014), the authors continued to use the Meessen and Olzewski terminology. However, because the extensive recent experimental literature on the incertus nucleus has not adopted the Meessen and Olzewski nomenclature (e.g., Goto et al., 2001; Olucha-Bordonau et al., 2003; Ma et al., 2009), we feel it is time to abandon the Meessen and Olzewski terms (nucleus O and alpha parts of the central gray) in favor of the accepted modern names for the compact and diffuse parts of the incertus nucleus.

Monoaminergic Nuclei in the Brain Stem

Monoamine groups in the brain stem were first demonstrated by Dahlström and Fuxe (1964) using the method of formalin vapor-induced fluorescence. The original description of the anatomy of these groups was further developed by Fuxe et al. (1970) and Hökfelt et al. (1974) and many subsequent publications by this group. The fluorescent cell groups were originally given arbitrary names (A1, A2 etc. and B1, B2 etc.), and these alphanumeric titles do not provide information concerning the function of the different groups. Because of this, we recommend following the nomenclature adopted by Paxinos et al. (2012) in their atlas of the marmoset brain, and subsequently adopted in atlases of the rat brain (Paxinos and Watson, 2014) and mouse brain (Paxinos and Franklin, 2013). Paxinos et al. (2012) named dopamine groups with the prefix DA, noradrenalin groups with the prefix NA, and adrenaline groups with the prefix Ad. However, we have retained the name of locus coeruleus for the previously named A6 group, and the name supralemniscal nucleus for the B9 serotonin group. Similarly, we have retained the names retrorubral field (RRF), substantia nigra compact part (SNC), and ventral tegmental area (VTA) for the dopamine groups previously defined as A8, A9, and A10 (Paxinos et al., 2012).

Many Previously Unrecognized Brain Stem Nuclei Have Appeared in Atlases Since 1982

The various editions of the Paxinos and Watson rat brain atlas since 1982 have identified and named many brain stem nuclei that had not been defined in previous atlases. Many of these newly identified nuclei have since been identified in atlases of the brains of the mouse (Paxinos and Franklin, 2013), marmoset (Paxinos et al., 2012), rhesus monkey (Paxinos et al., 2009), and human (Paxinos et al., 2018). These newly identified nuclei include the rhabdoid nucleus, the interstitial nucleus of the superior cerebellar peduncle, and the trigeminosolitary transition zone.

THE USE OF EPONYMS

Over the last 50 years there has been a sensible push to reduce the number of eponyms used in describing neuroanatomical features, and there is a logical argument to remove them all. However, we agree with Paxinos and Watson (2014) that there is no real prospect of expunging a small number of famous and popular eponyms in relation to the brain stem, and we should simply accept their existence. We would therefore retain Barrington's nucleus, the nucleus of Darkschewitsch, the nucleus of Roller, the interstitial nucleus of Cajal, the Edinger-Westphal nucleus, and the cap of Kooy (inferior olive). We observe that in recent years we have also been forced to accept one new eponym—that of Botzinger.

RECOMMENDATIONS

1. Abandon the subdivision of the hindbrain into "pons" and "medulla."
2. Restrict the use of the term 'pons' to refer to the nuclei and fiber bundles of the basilar pontine formation.
3. Recognize the isthmus (rhombomere 0) as the first segment of the hindbrain.
4. Recognize that the cerebellum is a derivative of the rostral prepontine hindbrain.
5. Recognize that the posterior commissure and associated nuclei, the nucleus of Darkshewitsch, the interstitial nucleus of Cajal, and the rostral part of the red nucleus

belong to the caudal diencephalon and not to the midbrain.
6. Consider the evidence for including the midbrain in the forebrain on genoarchitectural grounds, which would have the effect of making the old term "brain stem" synonymous with the hindbrain.
7. Adopt a modern functional and segmental nomenclature for the classification of the monoamine cell groups of the brain stem (see Alonso et al., 2012 for serotonergic cell groups of the hindbrain raphe).

AUTHOR CONTRIBUTIONS

LP was primarily responsible for the direction of this research. CW was responsible for the design of the paper. All three authors contributed equally to the writing of this paper.

FUNDING

The work of LP was supported by funding from the SENECA Foundation (Murcia) 19904/GERM/15.

REFERENCES

Alonso, A., Merchán, P., Sandoval, J. E., Sánchez-Arrones, L., Garcia-Cazorla, A., Artuch, R., et al. (2012). Development of the serotonergic cells in murine raphe nuclei and their relations with rhombomeric domains. *Brain Struct. Funct*. 218, 1229–1277. doi: 10.1007/s00429-012-0456-8

Alvarez-Otero, R., Sotelo, C., and Alvarado-Mallart, R. M. (1993). Chick/quail chimeras with partial cerebellar grafts: an analysis of the origin and migration of cerebellar cells. *J. Comp. Neurol.* 333, 597–615.

Aroca, P., and Puelles, L. (2006). Postulated boundaries and differential fate in the developing rostral hindbrain. *Brain Res. Rev*. 49, 179–190. doi: 10.1016/j.brainresrev.2004.12.031

Barker, R. A., Cicchetti, F., and Robinson, E. S. J. (2017). *Neuroanatomy and Neuroscience at a Glance*. Newark. NJ: John Wiley & Sons.

Butler, A. B., and Hodos, W. (2005). *Comparative Vertebrate Neuroanatomy: Evolution and Adaptation*. Hoboken, NJ: John Wiley & Sons.

Cambronero, F., and Puelles, L. (2000). Rostrocaudal nuclear relationships in the avian medulla oblongata: a fate map with quail chick chimeras. *J. Comp. Neurol.* 427, 522–545. doi: 10.1002/1096-9861(20001127)427:43.0.CO;2-Y

Capecchi, M. R. (1989). The new mouse genetics: altering the genome by gene targeting. *Trends Genet.* 5, 70–76.

Dahlström, A., and Fuxe, K. (1964). Evidence for the existence of monoamine containing neurons in the central nervous system. 1. Demonstration of monoamines in the cell bodies of brain stem neurons. *Acta Physiol. Scand.* 62(Suppl. 232), 3–55.

Di Bonito, M., Narita, Y., Avallone, B., Sequino, L., Mancuso, M., Andolfi, G., et al. (2013). Assembly of the auditory circuitry by a Hox genetic network in the mouse brainstem. *PLoS Genet.* 9:e1003249. doi: 10.1371/journal.pgen.1003249

Duan, D., Fu, Y., Paxinos, G., and Watson, C. (2013). Spatiotemporal expression patterns of Pax6 in the brain of embryonic, newborn, and adult mice. *Brain Struct. Funct*. 218, 353–372. doi: 10.1007/s00429-012-0397-2

Franklin, K., and Paxinos, G. (2005). *The Mouse Brain in Stereotaxic Coordinates. 3rd Edn*. San Diego, CA: Elsevier Academic Press.

Fraser, S., Keynes, R., Lumsden, A. (1990). Segmentation in the chick embryo hindbrain is defined by cell lineage restrictions. *Nature* 344, 431–435.

Fu, Y., Tvrdik, P., Makki, N., Machold, R., Paxinos, G., and Watson, C. (2012). The interfascicular trigeminal nucleus – a precerebellar nucleus in the mouse defined by retrograde tracing and gene expression. *J. Comp. Neurol*. 521, 697–708. doi: 10.1002/cne.23200

Fu, Y., Tvrdik, P., Makki, N., Paxinos, G., and Watson, C. (2011). Precerebellar cell groups in the hindbrain of the mouse defined by retrograde tracing and correlated with cumulative *Wnt1*-cre genetic labeling. *Cerebellum* 10, 570–584. doi: 10.1007/s12311-011-0266-1

Fuxe, K., Hökfelt, T., and Ungerstedt, U. (1970). Morphological and functional aspects of central monoamine neurons. *Int. Rev. Neurobiol.* 13, 93–126.

Gaunt, S. J., Miller, J. R., Powell, D. J., and Duboule, D. (1986). Homoeobox gene expression in mouse embryos varies with position by the primitive streak stage. *Nature* 324, 662–664.

Gilland, E., and Baker, R. (2005). Evolutionary patterns of cranial nerve efferent nuclei in vertebrates. *Brain Behav. Evol.* 66, 234–254. doi: 10.1159/000088128

Goto, M., Swanson, L. W., and Canteras, N. S. (2001). Connections of the nucleus incertus. *J. Comp. Neurol.* 438, 86–122. doi: 10.1002/cne.1303

Haines, D. E. (2012). *Neuroanatomy: An Atlas of Structures, Section, and Systems. 8th Edn*. Philadelphia, PA: Lippincott William & Wilkins.

Hendelman, M. D., and Walter, J. (2005). *Atlas of Functional Neuroanatomy. 2nd Edn*. Baton Rouge, LA: CRC Press.

Herrick, C. J. (1910). The morphology of the forebrain in amphibia and reptilia. J. Comp. *Neurol.* 20, 413–547.

Herrick, C. J. (1948). *The Brain of the Tiger Salamander, Ambystoma Tigrinum*. Chicago, IL: University of Chicago Press.

His, W. (1893). Vorschläge zur Eintheilung des Gehirns. *Arch. Anat. Entwickl Gesch. Jahrg.* 1893, 173–179.

His, W. (1895). Die anatomische nomenclatur, nomina anatomica. *Neurol. Suppl. Bd. Arch. Anat. Entwickl Gesch. Jahrg.* 1895, 155–177.

Hökfelt, T., Fuxe, K., and Johansson, O. (1974). Immunochemical evidence for the existence of adrenaline containing neurons in the rat brain. *Brain Res*. 66, 235–2551.

Jacobson, S., Marcus, E. M., and Pugsley, S. (2017). *Neuroanatomy for the Neuroscientist*. Cham: Springer

Kiernan, J., and Rajakumar, R. (2013). *Barr's The Human Nervous System: An Anatomical Viewpoint*. Philadephia, PA: Lippincott Williams & Wilkins.

Krumlauf, R., Marshall, H., Studer, M., Nonchev, S., Sham, M. H., and Lumsden, A. (1993). Hox homeobox genes and regionalisation of the nervous system. *J. Neurobiol.* 24, 1328–1340.

Lorente-Cánovas, B., Marín, F., Corral-San-Miguel, R., Hidalgo-Sánchez, M., Ferrán, J. L., Puelles, L., et al. (2012). Multiple origins, migratory paths and molecular profiles of cells populating the avian interpeduncular nucleus. *Dev. Biol.* 361, 12–26. doi: 10.1016/j.ydbio.2011.09.032

Lumsden, A. (1990). The cellular basis of segmentation in the developing hindbrain. *Trends Neurosci.* 13, 329–335.

Lumsden, A. (1991). Cell lineage restrictions in the chick embryo hindbrain. *Philos. Trans. R. Soc. Lond. B Biol. Sci*. 331, 281–286.

Lumsden, A., and Keynes, R. (1989). Segmental patterns of neuronal development in the chick hindbrain. *Nature* 337, 424–428.

Lumsden, A., and Krumlauf, R. (1996). Patterning the vertebrate neuraxis. *Science* 274, 1109–1115

Ma, S., Olucha-Bordonau, F. E., Hossain, M. A., Lin, F., Kuei, C., Liu, C., et al. (2009). Modulation of hippocampal theta oscillations and spatial memory by relaxin-3 neurons of the nucleus incertus. *Learn. Mem*. 16, 730–742. doi: 10.1101/lm.1438109

Marín, F., Aroca, P., and Puelles, L. (2008). Hox gene colinear expression in the avian medulla oblongata is correlated with pseudorhombomeric domains. Devel. *Biol.* 323, 230–247. doi: 10.1016/j.ydbio.2008.08.017

Martin, J. H. (2003). *Neuroanatomy: Text and Atlas. 3rd Edn*. New York, NY: McGraw-Hill.

Martinez-de-la-Torre, M., Lambertos, A., Peñafiel, R., and Puelles, L. (2018). An exercise in brain genoarchitectonics: Analysis of AZIN2-Lacz expressing neuronal populations in the mouse hindbrain. *J Neurosci. Res*. 96:1490–1517. doi: 10.1002/jnr.24053

Meessen, H., and Olszewski, J. (1949). *A Cytoarchitectonic Atlas of the Rhombencephalon of the Rabbit*. Basel: S Karger.

Moruzzi, G., and Magoun, H. W. (1949). Brain stem reticular formation and activation of the EEG. *Electroenceph. Clin. Neurophysiol.* 1, 455–473

Mtui, E., Gruener, G., Dockery, P., and Fitzgerald, M. J. T. (2017). *Fitzgerald's Clinical Neuroanatomy and Neuroscience. 7th Edn.* Philadelphia, PA: Elsevier

Murphy,. P., Davidson, D. R., and Hill, R. E. (1989). Segment-specific expression of a homoeobox-containing gene in the mouse hindbrain. *Nature* 341, 156–159.

Nieuwenhuys, R., ten Donkelaar, H. J., and Nicholson, C. (1998). *The Central Nervous System of Vertebrates*. Berlin: Springer.

Nieuwenhuys, R., Voogd, J., and Huijzen, C., van (2008). *The Human Central Nervous System, 4th Edn*. New York, NY: Springer.

Olucha-Bordonau, F. E., Teruel, V., Barcia-González, J., Ruiz-Torner, A., Valverde-Navarro, A. A., and Martínez-Soriano, F. (2003). Cytoarchitecture and efferent projections of the nucleus incertus of the rat. *J. Comp. Neurol.* 464, 62–97. doi: 10.1002/cne.10774

Orr, H. (1887). Contribution to the embryology of the lizard; With especial reference to the central nervous system and some organs of the head; together with observations on the origin of the vertebrates. *J. Morph.* 1, 311–372.

Palmgren, A. (1921). Embryological and morphological studies on the midbrain and cerebellum of vertebrates. *Acta Zool.* 2, 1–94.

Paxinos, G., and Franklin, K. (2013). *Paxinos and Franklin's The Mouse Brain in Stereotaxic Coordinates, 4th Edn*. San Diego, CA: Elsevier Academic Press.

Paxinos, G., Furlong, T., and Watson, C. (2018). *Human Brain stem – Cytoarchitecture, Chemoarchitecture, Myeloarchitecture*. San Diego, CA: Elsevier Academic Press.

Paxinos, G., Huang, X.-F., and Toga, A. W. (2009). *The Rhesus Monkey Brain in Stereotaxic Coordinates, 2nd Edn*. San Diego, CA: Elsevier Academic Press.

Paxinos, G., and Watson, C. (1986). *The Rat Brain in Stereotaxic Coordinates, 2nd Edn*. San Diego: Academic Press.

Paxinos, G., and Watson, C. (1997). *The Rat Brain in Stereotaxic Coordinates, Compact 3rd Edn*. San Diego, CA: Academic Press.

Paxinos, G., and Watson, C. (1998). *The Rat Brain in Stereotaxic Coordinates, 4th Edn*. San Diego, CA: Academic Press.

Paxinos, G., and Watson, C. (2005). *The Rat Brain in Stereotaxic Coordinates, 5th Edn*. San Diego, CA: Elsevier Academic Press.

Paxinos, G., and Watson, C. (2006). *The Rat Brain in Stereotaxic Coordinates, 6th Edn*. San Diego, CA: Elsevier Academic Press.

Paxinos, G., and Watson, C. (2007). *The Rat Brain in Stereotaxic Coordinates*. Sydney, NSW: Academic Press.

Paxinos, G., and Watson, C. (2014). *Paxinos and Watson's The Rat Brain in Stereotaxic Coordinates, 7th Edn*. San Diego, CA: Elsevier Academic Press.

Paxinos, G., Watson, C., Petrides, M., Rosa, M., and Tokuno, H. (2012). *The Marmoset Brain in Stereotaxic Coordinates*. San Diego, CA: Elsevier Academic Press.

Puelles, E., Martínez-de-la-Torre, M., Watson, C., and Puelles, L. (2012a). "Midbrain," in *The Mouse Nervous System,* eds C. Watson, G. Paxinos, and L. Puelles (San Diego, CA: Elsevier Academic Press), 337–359.

Puelles, L. (2013). "Plan of the developing vertebrate nervous system relating embryology to the adult nervous system (prosomere model,overview of brain organization)," in *Comprehensive Developmental Neuroscience: Patterning and Cell Type Specification in the Developing CNS and PNS,* eds J. L. R. Rubenstein and P. Rakic (Amsterdam: Academic Press), 187–209.

Puelles, L. (2016). Comments on the limits and internal structure of the mammalian midbrain. *Anatomy* 10, 60–70. doi: 10.2399/ana.15.045

Puelles, L., Harrison, M., Paxinos, G., and Watson, C. (2013). A developmental ontology for the mammalian brain based on the prosomeric model. *Trends Neurosci.* 36, 570–578. doi: 10.1016/j.tins.2013.06.004

Puelles, L., and Martinez-de-la-Torre, M. (1987). Autoradiographic and Golgi study on the early development of n. isthmi principalis and adjacent grisea in the chick embryo: a tridimensional viewpoint *Anat. Embryol.* 176, 19–34. doi: 10.1007/BF00309748

Puelles, L., Martínez-de-la-Torre, M., Ferran, J.-L., and Watson, C. (2012b). "Diencephalon," in *The Mouse Nervous System,* eds C. Watson, G. Paxinos, and L. Puelles (San Diego, CA: Elsevier Academic Press), 313–336.

Puelles, L., Martínez-de-la-Torre, M., Paxinos, G., Watson, C., and Martínez, S. (2007). *The Chick Brain in Stereotaxic Coordinates: an Atlas Featuring Neuromeric Subdivisions and Mammalian Homologies*. San Deigo, CA: Elsevier Academic Press.

Puelles, L., Tvrdik, P., and Martínez-de-la-Torre, M. (2018). The postmigratory alar topography of visceral cranial nerve efferents challenges the classical model of hindbrain columns. *Anat. Rec. Apr.* 16, 2018. doi: 10.1002/ar.23830

Ramon y Cajal, S. (1904/1995). *Histology of the Nervous System of Man and Vertebrates, Vol 2.* New York, NY: Oxford University Press, 771–773.

Saper, C. B., Chou, T. C., and Scammell, T. E. (2001). The sleep switch: hypothalamic control of sleep and wakefulness. *Trends Neurosci* 24, 726–731. doi: 10.1016/S0166-2236(00)02002-6

Schwarz, M., Alvarez-Bolado, G., Dressler, G., Urbánek, P., Busslinger, M., and Gruss, P. (1999). Pax2/5 and Pax6 subdivide the early neural tube into three domains. *Mech. Devel.* 82, 29–39.

Streeter, G. L. (1903). Anatomy of the floor of the fourth ventricle. The relations between the surface markings and the underlying structures. *Am. J. Anat.* 2, 299–313.

Sundin, O. H., and Eichele, G. (1990). A homeo domain protein reveals the metameric nature of the developing chick hindbrain. *Genes Dev.* 4, 1267–1276.

Swanson, L. W. (1992). *Brain Maps: Structure of the Brain*. Amsterdam: Elsevier

Tomás-Roca, L., Corral-San-Miguel, R., Aroca, P., Puelles, L., and Marín, F. (2016). Crypto-rhombomeres of the mouse medulla oblongata, defined by molecular and morphological features. *Brain Struct. Funct.* 221, 815–838. doi: 10.1007/s00429-014-0938-y

Tümpel, S., Weidemann, L. M., and Krumlauf, R. (2009). "Hox genes and the segmentation of the vertebrate hindbrain," in *Hox Genes,* ed R. Pourquié (San Diego, CA, Elsevier Academic Press), 103–138.

Vaage, S. (1969). The segmentation of the primitive neural tube in chick embryos (*Gallus domesticus*). *Ergeb. Anat. Entwicklungsgesch.* 41, 1–88.

Vaage, S. (1973). The histogenesis of the isthmic nuclei in chick embryos (Gallus domesticus).I. A morphological study. *Z. Anat. Entwicklungsgesch* 142, 283–314.

von Baer, K. E. (1828). *Über Entwickelungsgeschichte der Thiere: Beobachtung und Reflexion*. Königsberg: Bornträger.

Watson, C., Kirkcaldie, M., and Puelles, L. (2017a). "Developmental gene expression redefines the Mammalian brain stem," in *Evolution of Nervous Systems, 2nd Edn*, ed J. Kaas (Oxford: Elsevier), 467–475.

Watson, C., Mitchelle, A., and Puelles, L. (2017b). "A new mammalian brain ontology based on developmental gene expression," in *Evolution of Nervous Systems, 2nd Edn*, ed J. Kaas (Oxford: Elsevier), 53–75.

Watson, C., Shimogori, T., and Puelles, L. (2017c). Mouse Fgf8-Cre-LacZ lineage analysis defines the territory of the postnatal mammalian isthmus. *J. Comp. Neurol.* 525, 2782–2799. doi: 10.1002/cne.24242

Wilkinson, D. G., Bhatt, S., Chavrier, P., Bravo, R., and Charnay, P. (1989a). Segment-specific expression of a zinc-finger gene in the developing nervous system of the mouse. *Nature* 337, 461–464.

Wilkinson, D. G., Bhatt, S., Cook, M., Boncinelli, E., and Krumlauf, R. (1989b). Segmental expression of Hox-2 homeobox-containing genes in the developing mouse hindbrain. *Nature* 341, 405–409.

Wingate, R. J. (2001). The rhombic lip and early cerebellar development. *Curr. Opin. Neurobiol.* 11, 82–88. doi: 10.1016/S0959-4388(00)00177-X

Conflict of Interest Statement: The authors declare that the research was conducted in the absence of any commercial or financial relationships that could be construed as a potential conflict of interest.

Copyright © 2019 Watson, Bartholomaeus and Puelles. This is an open-access article distributed under the terms of the Creative Commons Attribution License (CC BY). The use, distribution or reproduction in other forums is permitted, provided the original author(s) and the copyright owner(s) are credited and that the original publication in this journal is cited, in accordance with accepted academic practice. No use, distribution or reproduction is permitted which does not comply with these terms.

frontiers in Neuroanatomy

ORIGINAL RESEARCH
published: 19 June 2019
doi: 10.3389/fnana.2019.00059

Patterned Vascularization of Embryonic Mouse Forebrain, and Neuromeric Topology of Major Human Subarachnoidal Arterial Branches: A Prosomeric Mapping

Luis Puelles[1†], Rafael Martínez-Marin[1†], Pedro Melgarejo-Otalora[1†], Abdelmalik Ayad[1], Antonios Valavanis[2] and José Luis Ferran[1]*

[1]Department of Human Anatomy, School of Medicine, University of Murcia and IMIB-Arrixaca Institute, Murcia, Spain, [2]Department of Neuroradiology, University Hospital of Zurich, Zurich, Switzerland

The prosomeric brain model contemplates progressive regionalization of the central nervous system (CNS) from a molecular and morphological ontogenetic perspective. It defines the forebrain axis relative to the notochord, and contemplates intersecting longitudinal (zonal, columnar) and transversal (neuromeric) patterning mechanisms. A checkboard pattern of histogenetic units of the neural wall results, where each unit is differentially fated by an unique profile of active genes. These natural neural units later expand their radial dimension during neurogenesis, histogenesis, and correlative differential morphogenesis. This fundamental topologic framework is shared by all vertebrates, as a Bauplan, each lineage varying in some subtle aspects. So far the prosomeric model has been applied only to neural structures, but we attempt here a prosomeric analysis of the hypothesis that major vessels invade the brain wall in patterns that are congruent with its intrinsic natural developmental units, as postulated in the prosomeric model. Anatomic and embryologic studies of brain blood vessels have classically recorded a conserved pattern of branches (thus the conventional terminology), and clinical experience has discovered a standard topography of many brain arterial terminal fields. Such results were described under assumptions of the columnar model of the forebrain, prevalent during the last century, but this is found insufficient in depth and explanatory power in the modern molecular scenario. We have thus explored the possibility that brain vascularization in rodents and humans may relate systematically to genoarchitectonic forebrain subdivisions contemplated in the prosomeric model. Specifically, we examined first whether early vascular invasion of some molecularly characterized prosomeric domains shows heterochrony. We indeed found a heterochronic pattern of vascular invasion that distinguishes between adjacent brain areas with differential molecular profiles. We next mapped topologically on the prosomeric model the major arterial branches serving the human brain. The results of this approach bear on the possibility of a developmentally-based modern arterial terminology.

Keywords: brain arteries, penetrating vessels, arterial topology, arterial branching, terminal fields, molecular profile

OPEN ACCESS

Edited by:
Paul Manger, University of the Witwatersrand, South Africa

Reviewed by:
Manuel A. Pombal, University of Vigo, Spain
Ayhan Cömert, Ankara University, Turkey

***Correspondence:**
José Luis Ferran
jlferran@um.es

[†]These authors have contributed equally to this work

Received: *17 January 2019*
Accepted: *22 May 2019*
Published: *19 June 2019*

Citation:
Puelles L, Martínez-Marin R, Melgarejo-Otalora P, Ayad A, Valavanis A and Ferran JL (2019) Patterned Vascularization of Embryonic Mouse Forebrain, and Neuromeric Topology of Major Human Subarachnoidal Arterial Branches: A Prosomeric Mapping. Front. Neuroanat. 13:59. doi: 10.3389/fnana.2019.00059

INTRODUCTION

Once development of the closed neural tube progresses beyond patterning, regionalization and initial surface growth, the processes of neurogenesis and differentiation commence in an heterochronic pattern, showing gradual construction of a heterogeneous mantle layer. According to its state of differential histogenetic specification, each progenitor domain is programmed to produce characteristic neuronal populations, whose identity is now largely known by molecular maps and fate mapping experiments (Puelles et al., 1987, 2000; Cobos et al., 2001; García-López et al., 2004, 2009; Pombero and Martínez, 2009; Puelles and Ferran, 2012). Generation of immature mantle strata (pronuclei) and definitive nuclei or layers of each cerebral region is closely correlated with the acquisition of a network of penetrating and internally ramifying blood vessels which supply the metabolites demanded by the growing tissue (James and Mukouyama, 2011).

The development of the central nervous system (CNS) wall is a stereotyped regionalization process, orchestrated by diverse signaling molecules spreading gradientally from primary and secondary organizers. Intersecting anteroposterior (AP) and dorsoventral (DV) patterning effects taking place during early brain regionalization specify primary cerebral compartments, as well as secondary subdivisions. These display a checkboard pattern of orthogonal boundaries (AP patterning produces transverse segments or neuromeres, separated by interneuromeric boundaries, whereas DV patterning produces longitudinal zones). This establishes already at early neuroepithelial stages a checkered fundamental plan of construction of the neural tube wall (a brain Bauplan), which is apparently shared among all vertebrates (Nieuwenhuys and Puelles, 2016). The basic details of this neuromeric and longitudinal Bauplan have been recently encapsulated by the *prosomeric model* (**Figure 1A**; Puelles and Rubenstein, 1993, 2003, 2015; Puelles et al., 2013; Puelles, 2013). Note the historically earlier *columnar model* (Herrick, 1910; Kuhlenbeck, 1973; Swanson, 2012) attended essentially to longitudinal subdivisions—e.g., "brain columns,"—but disregarded transversal units other than the major brain vesicles. This feature, jointly with an arbitrarily-defined forebrain axis, eventually caused its present insufficiency as a brain model.

According to the prosomeric model, the transverse neuromeric regions constitute natural AP brain developmental units shared by all vertebrates, each characterized by a distinctive *molecular profile* (a combination of active and inactive developmental genes—mostly transcription factors—which jointly control the activation at each distinct unit of particular cascades of downstream genes. Consequently, this entails differential sequential histogenetic phenomena all the way to adult fate. Individual genes may be shared in the profiles of adjacent or distant units, but each local combination is unique (sharing of some genes may lead to similarities in the final structure, as, e.g., presence of motoneurons as a local property). However, all these neuromeric histogenetic units soon become subdivided dorsoventrally (by parallel, orthogonally oriented DV molecular signaling, and consequent variations in the molecular profile) into a primary pattern of DV longitudinal zones, classically known as "*floor, basal, alar and roof plates*" (His, 1904). The resulting, subtly modified molecular profile of these zonal longitudinal domains within each neuromere diversifies the local histogenetic fates (e.g., types and number of neurons that can be produced). Some properties are shared along the whole length of these zones, that is, in all neuromeres (in some cases only in particular spans of such units). Both the neuromeres and their primary DV zones often register subsequently more advanced partial AP or DV regionalization. This generates (e.g., within the primary basal and alar plates) a number of smaller neuroepithelial subregions known as *microzones*, whose differential molecular profile becomes finally stable and homogeneous among an entire well-delimited neuroepithelial cell population. The microzones are also known as *progenitor areas* and have typologically quite specific neuronal derivatives, which may aggregate together at the local mantle layer, or disperse variously into neighboring or distant regions, mixing with other cell types. In the wall of the spinal cord myelomeres there appear in general five basal microzones and six alar ones; this number is roughly maintained along the hindbrain, with occasional variation in some of its neuromeres (Puelles, 2013); the final microzonal pattern is less well understood in the forebrain (but see Puelles et al., 2012a). It is well possible that microzonal alar and basal divisions basically continue showing a similar number in the forebrain, with changes mainly in their relative dimensions (larger DV dimension). In this respect, the behavior of the extraordinarily enlarged telencephalic field is exceptional, since it displays numerous further microzonal and areal subdivisions, particularly in the pallium; in contrast, the neural retina field also enlarges considerably in surface, but essentially remains a single microzone, unless we distinguish as such central, pericentral and peripheral retinal subregions. At the end of the regionalization process, the fully specified neuroepithelial microzones thus represent a definitive set of neural progenitor domains, which are each differentially specified molecularly in a way that confers to them quite distinct neural potencies and fates.

As a background for the present study, we need to give a brief introduction to forebrain neuromeric units. Neuromeres, in general, may be classified into three large tagmatic regions: 7 *prosomeres* in the recently expanded forebrain (the latter now includes the secondary prosencephalon, the diencephalon and the midbrain), 12 *rhombomeres* in the hindbrain, and over 30 *myelomeres* in the spinal cord (**Figure 1A**). These three initial tagmatic domains first divide into proneuromeric regions, which subsequently subdivide into the final neuromeric units. The forebrain is AP-regionalized into three proneuromeres called *secondary prosencephalon*, *diencephalon* and *mesencephalon* (**Figure 1A**; Puelles, 2013, 2018). The secondary prosencephalon (rostralmost forebrain component) will develop two hypothalamo-telencephalic prosomeres (hp1, hp2; **Figure 1A**), which will generate hypothalamic and telencephalic derivatives (the telencephalon is an expansive *alar* hypothalamic outgrowth, as are the eye cups and stalks). The diencephalon develops three diencephalic prosomeres (p1, p2, p3; **Figure 1A**). These units will be the

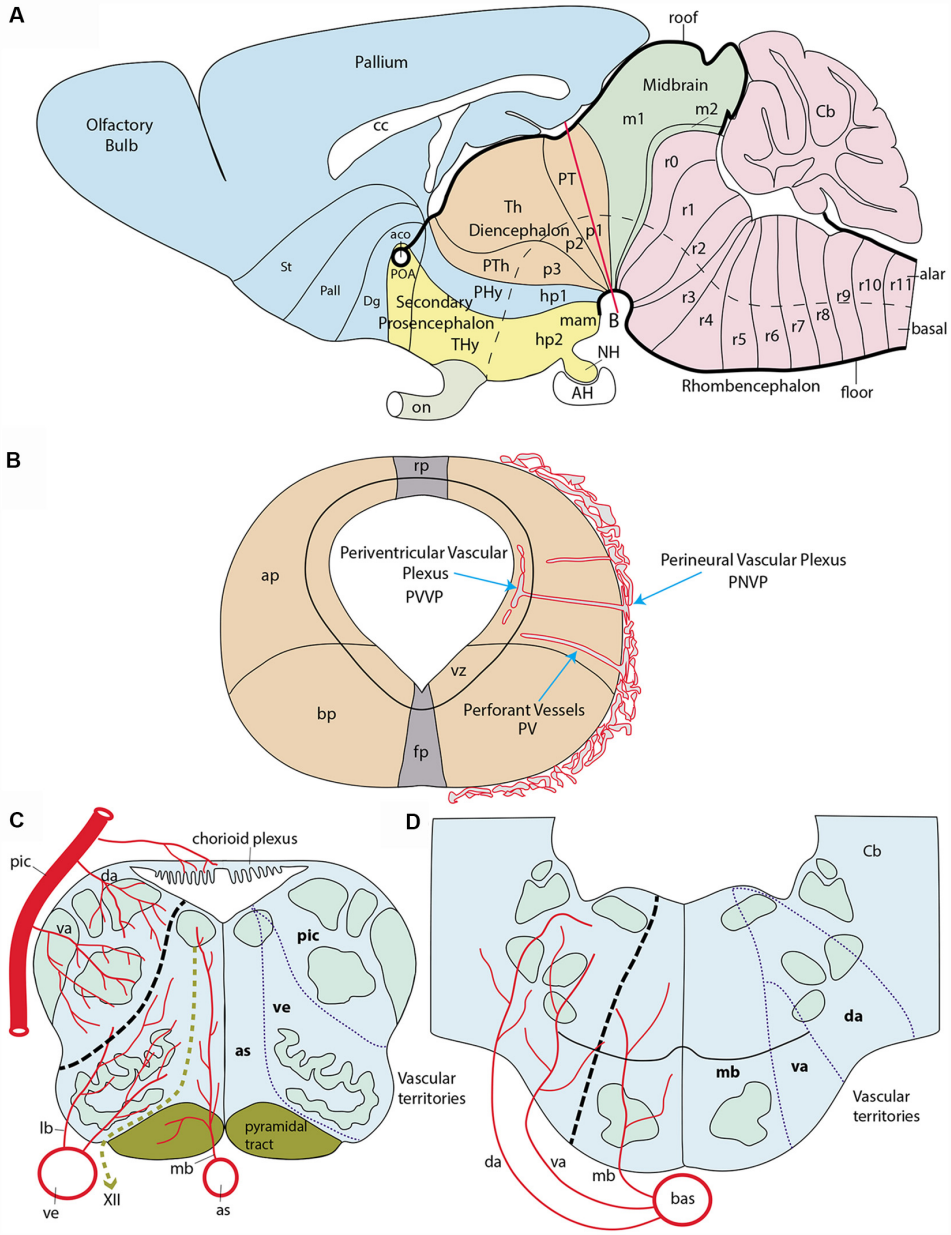

FIGURE 1 | Schematic introduction to topologic mapping of brain arteries, based on the rodent brain. **(A)** Lateral view of updated prosomeric model showing color-coded forebrain and hindbrain regions, subdivided into neuromeric units (pink = hindbrain, r0-r11; green = midbrain, m1, m2; cream = diencephalon, p1-p3; blue = first hypothalamo-telencephalic prosomere, hp1, contains peduncular hypothalamus, PHy, and evaginated telencephalon, with pallium and subpallial subdivisions St, Pall, Dg; yellow = second hypothalamo-telencephalic prosomere, hp2, contains terminal hypothalamus, THy, and unevaginated subpallial preoptic area, POA). The roof and floor plates are marked with thick black lines. Note convergence of transverse interneuromeric boundaries at the cephalic flexure, due to axial bending of the forebrain. The red line finishing near the big letter **(B)** represents a transversal plane of section through the p1 neuromere. **(B)** Schematic cross-section at the level marked by red line in **(A)**. It illustrates the main vascularization steps. The fundamental longitudinal zones, floor, basal, alar and roof plates (fp, bp, ap, rp) are displayed jointly with the alar-basal boundary. Early brain-invading blood vessels form a perineural vascular plexus (PNVP), perforant vessels (PV) and a deep periventricular vascular plexus (PVVP; note the PVVP actually lies within the proliferative ventricular zone, rather than periventricularly). **(C)** Schema of main basal and alar arterial vessels in the human hindbrain medulla. The black dash line at left marks the alar-basal boundary, while the green dash line identifies the hypoglossal nerve root. Direct penetrating mediobasal and laterobasal branches (mb, lb) originate respectively from the longitudinal anterior spinal (as) or vertebral (ve) arteries, while arteries serving the alar plate, representing so-called short or long circumferential vessels, distinguish ventral and dorsal levels of this domain. We identify them as ventroalar (va) and dorsoalar (da) arteries. At this particular level the va and da branches originate from the postero-inferior cerebellar artery (pic), but otherwise, they each originate directly from the basilar artery. The respective as, ve (basal) and pic (alar) dependent fields are delimited at right. **(D)** Schema of main basal and alar arterial vessels in the human hindbrain pons. The black dash line at left marks the alar-basal boundary. Mediobasal (mb) as well as ventrolar and dorsoalar (va, da) arteries arise as lateral branches of the basilar artery (bas) and penetrate radially their respective basal and alar terminal fields, delineated at the right side.

source within the alar plate of the well-known pretectal (p1), thalamic (p2) and prethalamic (p3) regions. The midbrain represents the caudal-most forebrain region and contributes two midbrain prosomeres of unequal size (m1, large, and m2, small; **Figure 1A**). We do not need to detail the 12 neuromeric subdivisions which develop in the hindbrain (rhombomeres r0-r11; **Figure 1A**) or spinal cord (myelomeres; not shown; Puelles, 2013; Puelles and Rubenstein, 2015; Albuixech-Crespo et al., 2017).

As mentioned above, fate mapping studies in several vertebrates (teleosts, amphibia, birds and mammals), as well as longitudinal ontogenetic descriptive analysis of differential gene expression, have allowed to correlate at least partially the early transverse neuromeric and longitudinal zonal units and their respective ulterior microzonal subdivisions with the derived, anatomically characteristic, parts of the adult brain. The relevant conclusions on these fates have been abundantly corroborated with other approaches such as, e.g., experimental embryology and transgenic phenotypes (patterning analysis), chemoarchitecture, and genoarchitecture. This implies that it is possible to extrapolate early embryonic data on regionally discrete vascular invasion patterns with adult patterns of vascularization, using available fate maps.

Blood vessels do not yet invade the neural primordia at neural plate and early neural tube stages. The vascularization of the CNS begins shortly after the early stages of molecular regionalization of the tubular neuroepithelium take place. This process appears to be closely related with increased demands of oxygen and nutrients by neural progenitors when they initiate neurogenesis (Fish and Wythe, 2015; Tata et al., 2015). There are two distinct phases in CNS early vessel formation. During the first phase, known as *phase of external vascularization* (or *vasculogenesis*), angioblasts from the lateral plate and paraxial mesoderm produce endothelial cells that coalesce and differentiate into a primitive vascular network that covers superficially the entire neural tube; this network is identified as the *perineural vascular plexus* (PNVP; **Figure 1B**). This process occurs between E8.5 and E10 in the mouse and days 2–4 *in ovo* in the chicken; the human PNVP is observed at six gestation weeks (Marín-Padilla, 2012). During the following *phase* of *internal vascularization*, individual vessels sprouting from the PNVP perforate the piamater and penetrate the parenchyma of the brain tissue (*angiogenesis*). These initial *perforating vessels* seem to follow a straight radial course between the external limiting membrane and the ventricular surface (PV; **Figure 1B**). Once they are *inside* the ventricular zone, close to the ventricular lumen, they tend to produce circumferential branches at right angles (i.e., parallel to the ependym), which fuse with similar branches from other penetrating radial vessels, giving rise to a *periventricular vascular plexus* (PVVP; **Figure 1B**; Evans, 1909; Craigie, 1955; Stewart, 1955; Bär and Wolff, 1972; Bagnall et al., 1989; Couly et al., 1995; Kurz et al., 1996; Ruhrberg and Bautch, 2013; Fish and Wythe, 2015).

At later stages, after histogenetic growth of the mantle layer progresses, new radial vessels penetrate and additional collateral circumferential branches are produced within the mantle, which fuse or ramify as needed to cover the local vascular needs. Many of the added penetrating radial vessels remain restricted to given strata of the mantle layer. Marín-Padilla (2012) states that after 12 gestation weeks in human embryos, there is a constant distance of some 400 μm between each pair of penetrating vessels, from which it is deduced that a new PV is presumably intercalated wherever neural surface growth causes this spatial threshold to be surpassed. Indeed, the mean intervascular distance does not change between 12 gestation weeks and birth, with a hundredfold change in total brain weight (from 4 to 410 grams). Marín-Padilla (personal communication) thinks this threshold is due to a mean diffusion range of oxygen, which is efficient only within a radius of some 200 μm around the perforating vessel.

However, the precise temporospatial pattern obtained during brain vascularization is controversial, insofar as no attention has been given to such regional elements as proneuromeric regions and/or their neuromeric subdivisions, or to possible angiogenetic differences between the precociously differentiated basal plate and the more retarded, but more extensive alar plate. This analytic neglect obeys to the prominence during the relevant historic period of the columnar brain model, which considered transverse subdivisions unimportant (or inexistent). Early authors mapping vessel penetration in the forebrain and hindbrain regions (e.g., those cited above) generally considered this a sequential wave-like propagated process that starts in the caudal medullary rhombencephalon close to the spinal cord and then progressively extends rostralward and caudalward, until covering the whole brain. Any heterochronic vascular observation due to advanced vs. retarded neuromeres within the diverse brain regions was necessarily interpreted as an irrelevant variation within the simplistic columnar paradigm. Interestingly, an expanding general wave starting at the lower medulla was also the spatiotemporal pattern described in the same historic period for *precocious neurogenesis*. This view on wave-like neurogenesis was later corrected once it was discovered that paired rhombomeres (r2, r4, r6) develop in advance of unpaired ones (thus becoming the ones that carry the cranial nerve roots). This alternation generates subtle heterochronic aspects that had gone undetected before neuromeric models started to be contemplated (see, e.g., Puelles et al., 1987; Puelles, 2018). Marín-Padilla (2012) still described vascular invasion as starting at the caudal medullary rhombencephalon and progressing wave-like rostralwards through the rostral rhombencephalon, midbrain, and diencephalon, to finally reach the telencephalic region, thought to be located most "rostrally and dorsally." Consciously or not, this description assumes the columnar model, which wrongly defines the telencephalon as the rostralmost forebrain portion. The prosomeric model instead visualizes the rostralmost forebrain as represented by the whole secondary prosencephalon (hypothalamus, eyes and telencephalon), where the telencephalon is conceived as a dorsal hypothalamic outgrowth (**Figure 1A**).

Other authors (Vasudevan et al., 2008) analyzing specifically telencephalic angiogenesis in mouse embryos observed precocious perforating vessels sprouting from the PNVP into

the presumptive ganglionic eminences at E9.5, with subsequent "gradiental progress" of the invasion from subpallial into pallial regions (i.e., microzonal subdivisions of the telencephalic field). The telencephalic PVVP reportedly appears completed at E11 (Vasudevan et al., 2008). On the other hand, mouse hindbrain studies described the most precocious perforating vessels at E9.5 and earliest PVVP formation at E10.25 (Fantin et al., 2010). According to Daneman et al. (2009), sprouting of PVs from the PNVP begins uniformly at E10.5 in mouse. A shared stage of initial penetration at the telencephalon and hindbrain apparently weighs against the conventionally assumed overall caudorostral gradient.

The neuroepithelium is held to produce signals that stimulate external (PNVP) and internal (perforant vessels and PVVP) vascularization. The *vascular endothelial growth factor A* (VEGF A) produced by neural progenitors under hypoxic conditions is possibly the main stimulus for early neural vasculogenesis and angiogenesis. Apparently, this factor also seems the vehicle of positional information for heterochronic vessel formation (Hogan et al., 2004; Coultas et al., 2005; Santhosh and Huang, 2015). VEGF binds to tyrosine kinase receptors (VEGFR) present on the PNVP endothelial cells, as well as on the perforating vessels and their PVVP branches (Tata et al., 2015). VEGF-A/VEGFR2 (*Flk1*, *Kdr*) is the most important signaling pathway for early angiogenesis, and its genetic deletion is known to be lethal (Koch et al., 2011). The entrance of blood vessels into the brain is also strongly modulated by VEGF isoforms (Tata et al., 2015). In addition, canonical Wnt signaling from radial glia cells is another key element for vasculogenesis and angiogenesis in the neural tube. Wnt7a/7b ligands activate the canonical GSK/β-catenin pathway in endothelial cells, apparently aiding them significantly in their penetration (migratory) activity at early steps of vessel formation (Stenman et al., 2008; Daneman et al., 2009). Later in embryogenesis radial glia cells turn off the *Wnt* canonical pathway, thus contributing to vessel stabilization (Ma et al., 2013).

Regardless of evidence that arterial and venous vessels may show characteristic molecular differences from early developmental stages (e.g., *neuropilin* 1 and 2; Herzog et al., 2001), use of *Vegfr2* expression as a panendothelial vascular marker is convenient for the analysis of overall temporo-spatial patterns in early forebrain vascularization of mouse embryos. We compared at various early stages by *in situ* hybridization this vascular marker with some well-known regional markers of molecularly-defined neuroepithelial domains, consistently with our own earlier prosomeric studies (e.g., Dlx5, Pax3, Pax6, Shh, and Tcf7l2; Puelles and Rubenstein, 2003, 2015; Ferran et al., 2007, 2008, 2015a,b,c). We found that the PNVP is still incomplete at stage E8.5, but appears best developed next to the alar plate region of the forebrain. Some precocious perforating vessels (PVs) are seen from E8.5 onwards at various unrelated sites (heterotopy), leading subsequently also to independent incipient formation of the PVVP at specific neural domains. Vascular perforation thus follows in the space of the brain wall a heterochronic pattern that disagrees with any overall caudorostral or ventrodorsal gradients but is consistent with neuromeric and zonal brain wall subdivisions. We discuss whether these data, taken jointly with existing knowledge on general neural production of VEGF-A, are on the whole consistent with the existing theoretic notion that the heterochronic order of vascular invasion may reflect underlying *neurogenetic heterochrony* characteristic of differentially fated neural domains (e.g., predicting basal plate earlier than alar plate). The results seem partially contradictory with this interpretation, insofar as the early PNVP formation at alar levels coincides with a retarded local neurogenetic pattern, whereas neurogenesis advances precociously in an initially non-vascularized basal plate domain. We thus hypothesize that vascular penetration may obey different attracting mechanisms (signaling pathways) for PNVP and PVs formation, as well as for alar vs. basal brain territories. The expanded forebrain (including midbrain) may also follow different rules than the hindbrain and spinal cord. A partial causal connection of vascular penetration with local neurogenesis may obtain independently at some loci within these separate fields.

This analysis opens a new scenario in which to study the topology and local trajectory of major vascular entities relative to fate-mapped derivatives of the different developmental histogenetic units represented in the mature brain, naturally keeping in mind the accompanying anatomic deformations due to differential expansion/compression and morphogenesis of adjacent developmental units. This novel sort of analysis is attempted here in a tentative way, using the more detailed adult human data from the literature. The resulting prosomeric vascular map shows remarkably salient features. We envisage that one possible end result may be a complementary developmental nomenclature of brain vessels. In principle, this might be useful for some clinical applications (e.g., in interventional radiological analysis of arterio-venous malformations, or in selective chirurgical obturation of some vascular pedicles).

MATERIALS AND METHODS

Mouse Embryos

All experimental procedures were conducted according to the legislation from the European Community (86/609/EEC) and Spanish Government (Royal Decree, 1201/2005; Law 32/2007). All mouse experiments were approved by the ethical committee from the University of Murcia. *Swiss albino* mouse embryos staged according to Theiler criteria (TS; Theiler, 1989) were collected at different embryonic days (E) after fertilization (see text and Figures). At least 10 embryos were analyzed at each selected stage and three or four series of sections were obtained from each brain to analyze different markers (see below). Some additional expression patterns of *Vegfr2*, *Eng* and *Ctgf* were obtained from *in situ* hybridization images downloaded from the Allen Developing Mouse Brain Atlas.

Tissue Processing

All the experimental procedures related with extraction and processing of brain samples in embryos were performed as

previously described (Ferran et al., 2015a). Brains were fixed in phosphate-buffered 4% paraformaldehyde (0.1 M PB; pH 7.4) at 4°C for 24 h. Afterward, embryonic brains were transferred to 30% sucrose in 0.1 M PBS (phosphate-buffered saline solution) and then embedded in 15% gelatin/20% sucrose. Serial 20 μm-thick sections were obtained using a cryostat (Leica CM3500 S), collected as parallel series on SuperFrost Plus slides (Menzel-Gläser, Braunschweig, Germany), and stored at −20°C.

RT-PCR

Pax3, Pax6, Tcf7l2 and *Vegfr2* cDNA fragments were obtained by reverse transcription (RT). RNA was extracted with Trizol reagent (Invitrogen, Carlsbad, CA, USA) from fresh dissected brains of *Mus musculus* embryos. The RNA was treated with DNase I (Invitrogen, Carlsbad, CA, USA). RNA samples were then retro-transcribed into single-stranded cDNA with Superscript III reverse transcriptase and oligo dT anchored primers (Invitrogen, Carlsbad, CA, USA, SuperScript First-Strand Synthesis System for RT-PCR). The cDNA was used as a template for PCR with *Taq* polymerase (Promega, Madison, WI, USA) and specific primers. The PCR products were cloned into pGEM-T Easy Vectors (Promega, Cat. A1360) and sequenced (SAI, University of Murcia, Murcia, Spain). Primers:

- MPax3F: 5′ TACCAGCCCACGTCTATTC 3′
- MPax3R: 5′ AGGTCATGCTGGGACAATTC 3′
- MPax6F: 5′ GGCCAGCAACACTCCTAGTC 3′
- MPax6R: 5′ TGTGTGTTGTCCCAGGTTCA 3′
- MTcf7l2F: 5′ AAAATGCCGCAGCTGAACG 3′
- MTcf7l2R: 5′CCATATGGGGAGGGAACC 3′
- MVegfr2F: 5′ AGCGTTGTACAAATGTGAAG 3′
- MVegfr2R: 5′ CTGGCATCATAAGGCAAGCG 3′

In situ Hybridization

All the steps followed during the entire procedure are detailed in Ferran et al. (2015a,b). Sense and antisense digoxigenin-UTP-labeled riboprobes for mouse *Dlx5*, *Pax3, Pax6, Shh*, *Tcf7l2* and *Vegfr2* were synthesized according the manufacturer's suggestions (Roche Diagnostics S.L., Applied Science, Barcelona, Spain) and using specific polymerases (Fermentas, Madrid, Spain). Probe sequence information is provided in **Table 1**. Hybridizations were carried out overnight at 72°C. RNA-labeled probes were detected by an alkaline phosphatase-coupled anti-digoxigenin antibody (diluted 1:3.500; Roche Diagnostics, Manheim, Germany), and the compound nitroblue tetrazolium/5-bromo-4-chloro-3-indolyl phosphate (NBT/BCIP; Roche Diagnostics, Manheim, Germany) was used as a chromogenic substrate for the alkaline phosphatase reaction.

Imaging

Digital images were obtained with a ScanScope CS digital slide scanner (Aperio Technologies, Vista, CA, USA). Contrast and focus were adjusted by applying Adobe Photoshop CS3 software (Adobe Systems Inc., San Jose, CA, USA).

RESULTS

During the determination of artery or vein identity, several molecules are involved in the differential specification of their endothelial cells. According to a number of studies, genes involved in the promotion of an arterial identity include *EphrinB2a, Shh, Ihh, Notch1/4, Jag1/2, Dll4*, and *Np1*; a venous identity obeys instead to the activity of *COUP-TFII, Np2, EphB4* and *Vegfr3 (Flt4)*. However, most of these determinants are not exclusive arterial or vein markers (they appear active also in other developing systems), and not all of them are expressed at early stages in the whole arterial or venous network of the brain (Swift and Weinstein, 2009; Fish and Wythe, 2015). Having in mind the difficulty to find selective markers for the whole brain arterial or venous network from early stages of development onwards, we opted for one of the well-known panendothelial markers (*Vegfr*1 or *rFlt1*, *Vegfr2* or *Flk1/Kdr*, *Cdh5* or *Eng*; Swift and Weinstein, 2009). We elected *Vegfr2* (*Flk1/Kdr*) for our study because it is highly expressed from the beginning of vascularization of the CNS and during early stages of development in the entire vascular network of the brain.

The Perineural Vascular Plexus (PNVP) and First Perforant Vessels (PV) at E8.5 Stage

The analysis of *Vegfr2* expression at E8.5 shows that external vascularization is highly developed, but a dense perineural vascular plexus (PNVP) does not yet cover the entire brain surface, relating preferentially to alar portions of the neural tube. A horizontal section through dorsal alar territories of diencephalon (*Pax6*-positive) and midbrain (*Pax6*-negative) shows abundant PNVP next to the alar pial surface, but no PNVP at the respective roof plate sites (rp; **Figures 2A,B**; section level marked in the inset drawing). We can see also that there appear incipient perforating vessels inside the caudal-most diencephalon and rostral alar midbrain (red arrowheads; Mb; **Figures 2A,B**; note none more caudally in the midbrain). The DMB tag marks the di-mesencephalic boundary, which is underlined molecularly by selective

TABLE 1 | Probes.

Gene symbol	NCBI accession no.	Size (bp)	Positions	Publication/Laboratory
Dlx5	NM_010056.2	1,180	106–1,285	Morales-Delgado et al. (2011)
Pax3	NM_008781.4	953	1,321–2,273	Present results
Pax6	NM_001244198.2	928	1,158–2,085	Present results
Shh	NM_009170.2	643	442–1,084	McMahon A. lab
Tcf7l2	NM_001142918.1	826	530–1,355	Present results
Vegfr2	NM_01612.2	900	1,829–2,728	Present results

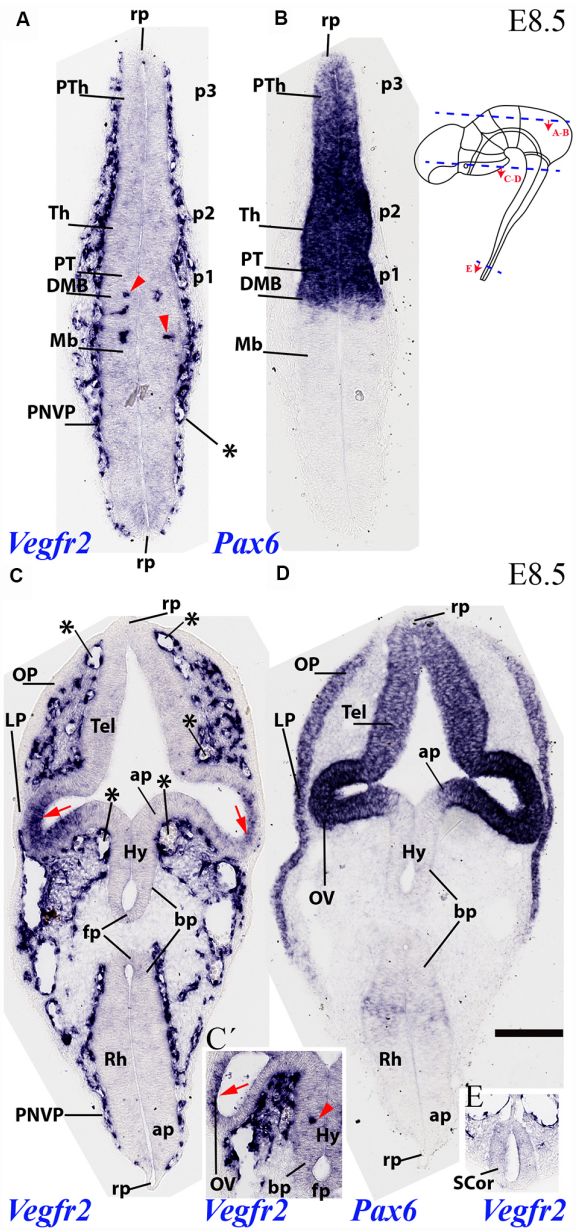

FIGURE 2 | Two horizontal sections through mouse secondary prosencephalon, diencephalon and mesencephalon at E8.5 showing varying degrees of external vascularization by the PNVP (labeled with endothelium-selective Vegfr2 riboprobe; **A**,**C**), compared in consecutive sections with Pax6, an alar plate marker for the diencephalic neuromeres p1-p3 **(B)** and the secondary prosencephalon (telencephalon and optic vesicle in **D**). Inset to **(B)**: semi-schematic representation of the plane of section of the horizontal sections **(A,B)** and **(C,D)**. Note the PNVP-nude roof plate area rostrally and caudally (rp; **A**). The earliest Vegfr2-positive perforant vessels are marked with red arrowheads in **(A)** and inset (**C'**; detail of alar hypothalamus, Hy). The red arrows in **(C)** point to areas of non-vascular Vegfr2 expression at the neural retina primordia. Note also in **(C)** the remarkable lack of PNVP at the forebrain and hindbrain floorplate (FP) and neighboring basal plate (bp). The median and paramedian perichordal mesoderm also lacks vascularization, in contrast with lateral mesoderm areas next to the neural alar plate (unlabeled). Inset **(E)** shows the very retarded state of vascularization at the spinal cord (SCor). Asterisks: developing venous seins. Scale bar: 150 μm.

diencephalic expression of *Pax6* as a progressive site for vascular penetration (compare **Figures 2A,B**), irrespective that the corresponding roof, basal and floor plates are devoid of PNVP.

Another section level from the same E8.5 specimen intersected transversally the secondary prosencephalon and obliquely the hindbrain (level in the inset drawing), showing in both cases the vascular pattern of both alar and basal plates, as well as the roof and floor plates (**Figures 2C,D**). *Pax6* mRNA is present at this stage in an upper part of the alar plate of the secondary prosencephalon, including the eye stalk and eye vesicle (strong *Pax6* expression) and the neighboring telencephalic stalk and pallium (weaker expression). The *Vegfr2* signal shows some large or medium size vessels (probably venous sinuses) associated to the pallial telencephalic surface, but there is no continuous PNVP yet at this site (asterisks mark these large vessels; Tel; **Figure 2C**); moreover, the telencephalic roof plate is wholly devoid of PNVP (rp; **Figure 2C**). The eye stalk area is already surrounded by a thick PNVP, but not so the peripheral part of the optic vesicle (OV) whose prospective neural retina field shows itself marked neuroepithelial *Vegfr2* expression, possibly responding to signals emanating from the lens placode (OV; red arrows; LP; **Figures 2C,D**).

There appear at this level three particularly large venous blood vessels, in a dorsoventral pattern (next to roof plate, and above and under the eye stalk; asterisks; **Figure 2C**). The associated hypothalamic PNVP seems to cover exclusively the *Pax6*-negative/*Dlx*-positive alar (*Dlx* pattern not shown) hypothalamus (ap), contrasting with a nude hypothalamic basal plate (bp) and an associated clearcut lineal boundary between ventral avascular and dorsal vascularized paramedian mesoderm. The hypothalamic floor plate (fp) is also nude of PNVP (Hy; ap; bp; fp; **Figure 2C**). The inset **Figure 2C′** shows a more intensely reacted detail of an adjacent section, showing an isolated perforating vessel observed within the alar hypothalamus at this stage (Hy; red arrowhead; the red arrow points to *Vegfr2*-positive prospective neural retina, as in **Figure 2C**). In contrast with these precocious forebrain areas, the hindbrain (Rh; fp; bp; ap; rp; **Figure 2C**) and spinal cord (SC or; **Figure 2E**) are still devoid of PVs, and the spinal cord also lacks a PNVP.

PNVP, Penetrating Vessels (PV) and First Periventricular Vascular Plexus (PVVP) at E9.5

At E9.5, the neuromeres start to grow in surface, limited by their non-growing transverse interneuromeric boundaries, as best visualized in horizontal and sagittal sections. The major DV subdomains become molecularly identifiable. We accordingly compared at this stage *Vegfr2*-expressing vessels with *Dlx5*, *Pax3*, *Pax6*, *Shh* and *Tcf7l2* mRNA areal neuroepithelial or mantle (neuronal) expression in consecutive horizontal sections (**Figure 3**). The same section plane (illustrated in **Figure 3H**) cuts transversally the secondary prosencephalon (**Figures 4**, **5**), due to the

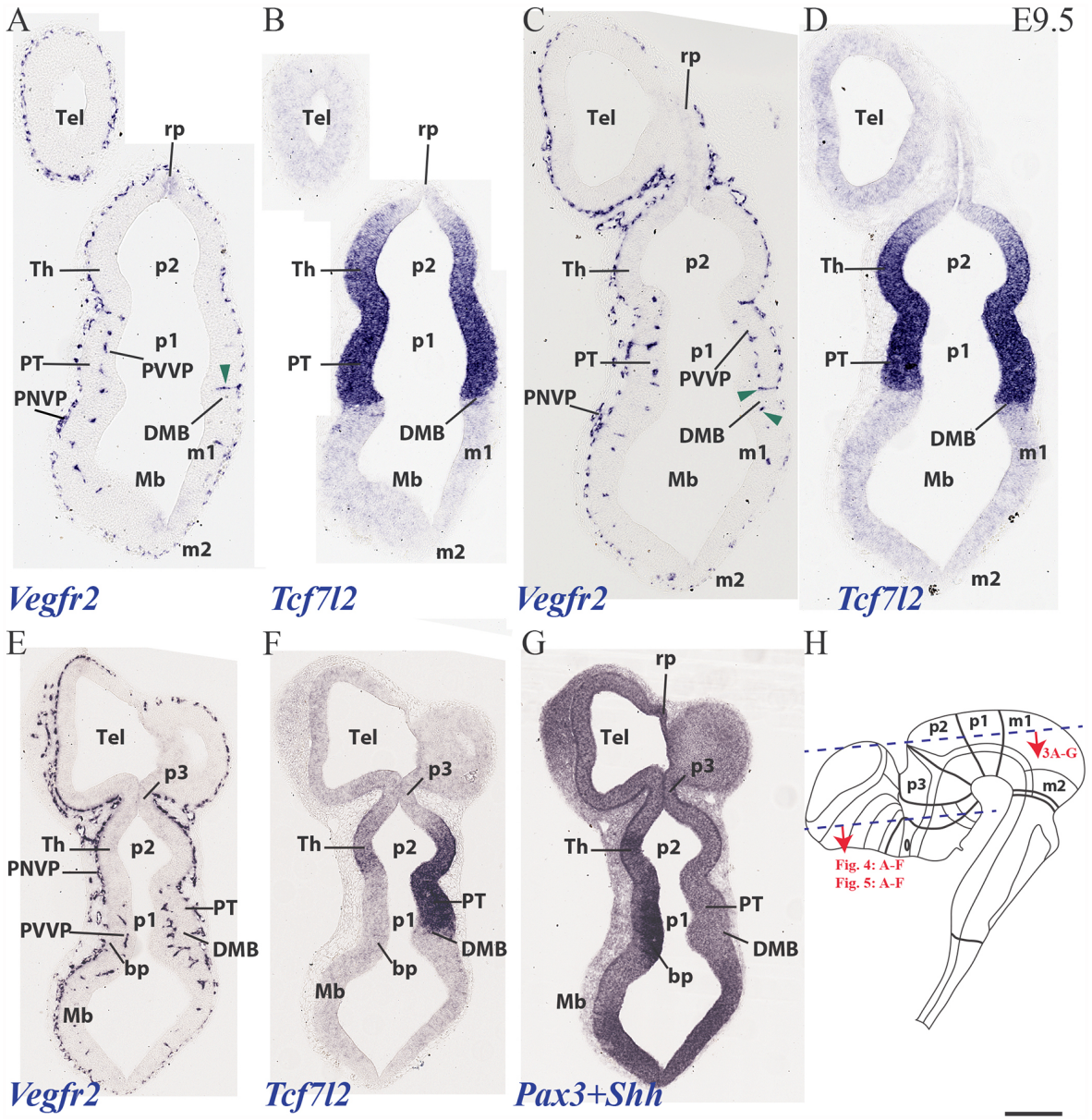

FIGURE 3 | Horizontal sections through a mouse telencephalon, diencephalon and mesencephalon at E9.5 showing the vascularization by the PNVP and early perforant and periventricular (PVVP) vessels (Vegfr2; **A,C,E**), compared in consecutive sections with markers of diencephalic alar plate (Tcf7l2 and Pax3; **B,D,F,G**) and basal plate (Shh; **G**). See description in the text. Green arrowheads: perforant vessels. **(H)** Semi-schematic representation of the plane of section corresponding to the horizontal sections shown in **Figures 3–5**. Scale bar: 250 μm.

cephalic flexure. With the cited genoarchitectonic markers it is possible to recognize subpallial vs. pallial telencephalic subdomains, and some alar and basal hypothalamic and diencephalic domains. The PNVP covers at E9.5 practically the entire alar and basal plates of the prosencephalon, with the exception of the rostralmost basal plate at the median tuberal acroterminal region and possibly a paramedian basal band next to the floor plate, where a PNVP is still absent. Some scattered vessels appear over the midbrain and hindbrain roof plate (**Figures 3–5**).

The PNVP covering alar diencephalon and midbrain seems complete but somewhat stretched out (less thick than at E8.5), possibly due to the intervening surface expansion of these brain units. The horizontal sections through the forebrain shown in **Figures 3A–H**, where *Tcfl2* expression labels selectively the p1 and p2 alar plate domains (pretectum or PT in p1, thalamus or Th in p2; **Figures 3B,D,F**), show an increasing number of PVs contributing to an incipient PVVP formation across the three dorsoventral section levels shown (**Figures 3A,C,E**). This pattern is nevertheless restricted to PT and rostral

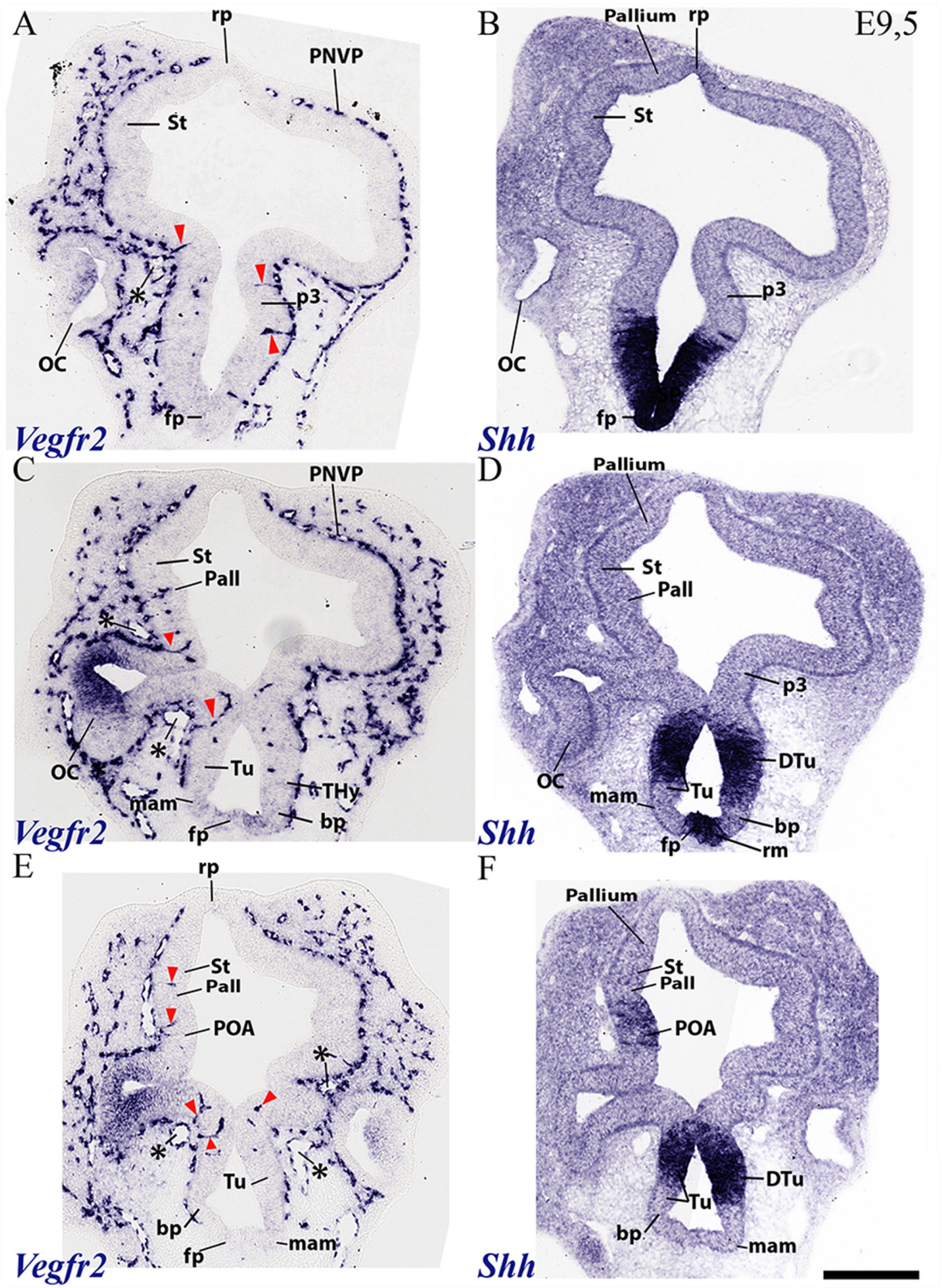

FIGURE 4 | Horizontal sections through a mouse secondary prosencephalon and diencephalon at E9.5 showing PNVP vascularization and first perforant vessels (Vegfr2; **A,C,E**), compared in consecutive sections with a marker of hypothalamic and diencephalic basal plate (Shh; **B,D,F**). See schematic representation of plane of section in **Figure 3H**. See description in the text. Red arrow heads: perforant vessels. Asterisks: presumed venous sinuses. Scale bar: 250 μm.

midbrain (Mb). A detailed analysis of the radial course of the pretectal perforant vessels (PVs) strongly suggests that these vessels never cross interprosomeric boundaries [e.g., green arrowhead pointing to a pretectal PV entering just in front of the di-mesencephalic boundary (DMB) **Figure 3C**].The incipient PVVP seems clearly most advanced at the ventralmost level (PVVP; **Figure 3E**), in a section that lies close to the alar-basal boundary (note transition from alar *Tcf7l2* expression in **Figure 3F**, right side, into basal *Shh* expression in **Figure 3G**, left side). The alar midbrain shows on the whole fewer PVs than the PT, and they are now markedly scattered caudalwards, possibly due to differential interstitial growth (Mb; m1; **Figures 3A,C,E**); no significant midbrain alar PVVP is apparent, except close to the basal plate (Mb; bp; **Figure 3E**). In contrast, the thalamus in p2 (p2; Th; PNVP; **Figures 3A,C,E**) and the prethalamus in p3 (p3; **Figures 3E,F**) appear covered by a full alar PNVP since E8.5, but show no PVs yet at E9.5. The earliest prethalamic PVs are found at the rostral end of this neuromeric domain (red arrowheads; p3; **Figures 4A,C**, **5B**).

The dorsocaudal parts of the telencephalic vesicle sectioned in the **Figure 3** series (see drawing in **Figure 3H**) are the most immature ones in terms of proliferation and neurogenesis. There is here a rather uniform PNVP cover, possibly weaker next to the median roof plate, but no PVs are present (Tel; **Figures 3A,C,E**). In contrast, the telencephalic sections illustrated in **Figures 4**, **5** are topological transverse sections through the secondary prosencephalon (see drawing in **Figure 3H**; in both cases, the levels proceed caudorostrally). **Figure 4** compares *Vegfr2* with the floor and basal marker *Shh* (noting there is a tuberal and mamillary basal patch in the hypothalamus that secondarily downregulates its primary *Shh* expression; compare *Shh*-negative basal plate areas in **Figures 4D,E** with the sagittal section at E10 in **Figure 6F**). The upper boundary of the *Shh* signal marks the alar-basal limit throughout (**Figures 4B,D,F**, **6F**).

The overall cover of PNVP at the section levels shown in **Figure 4** has expanded more fully towards the roof plate, and also extends now more ventralwards in the hypothalamus, where PNVP and PVs are found now both in its alar and upper basal regions, though respecting still the ventralmost region next to the floor plate, where the mamillary pouch lies (red arrowheads; fp; bp; Tu; mam; rm; **Figures 4A–F**). The alar hypothalamic areas around the optic stalk show the best developed PVs (red arrowheads; **Figures 4A,C,E**). The optic stalk and prospective pigmented retina are provided already by a PNVP, but are devoid of PVs, while the neural retina itself continues to express *Vegfr2* (**Figures 4A,C,E**, **5B,E**). We still see large venous blood vessels below and above the optic stalks (asterisks; **Figures 4C,E**). The hypothalamic floor plate and ventral part of the basal plate continue nude of PNVP, in parallel with its neighboring mesoderm.

As regards the telencephalon, we observed at E9.5 the earliest PVs within the subpallium, particularly at its incipiently defined preoptic area subdomain, recognized by its characteristic selective expression of *Shh* (within the alar plate; red arrowheads; POA; **Figure 4F**), but possibly also within *Shh*-negative pallidum (red arrowheads; Pall; **Figure 4C**). The striatum seems still devoid of PVs (St; **Figures 4A,C,E**).

Figure 5 shows similar section levels as **Figure 4**, but it compares *Vegfr2* (**Figures 5B,E**) with *Pax6*, characteristic of the alar plate in the telencephalic pallium and diencephalon (**Figures 5A,D**, **6B,E**) and *Dlx5* expression, present in the subpallium (**Figure 7F**) and the alar prethalamus (PTh; **Figures 5C,F**). The telencephalic subpallium shows weak *Pax6* signal at its prospective striatal subdomain but is *Pax6*-negative in its pallidal, diagonal and preoptic subdomains (**Figure 7H**; check also Puelles et al., 2000, 2013, 2016). As seen before in **Figure 4**, many PVs can be observed in subpallial and hypothalamic alar and upper basal domains, but PVs are still absent in the striatum as well as in pallial telencephalic regions (red arrowheads; **Figures 5B,E**). The subpallial region displays the largest number of PVs in the preoptic domain and fewer of them in the diagonal and pallidal neighboring domains. A comparison of *Vegfr2*, *Pax6* and *Dlx5* expression indicates that the hypothalamic PVs are localized at the E9.5 stage either at the dorsal tuberal area (upper basal plate) or at the subparaventricular/paraventricular areas (alar plate). Such PVs are still absent in the most basal (mamillary and perimamillary) domains next to the floor (mam; **Figures 4C,E**, **5B,E**).

PNVP, PVs and PVVP Vascular Pattern in the Prosencephalon of Mice at E10

We compared in an E10 sagittal section series *Vegfr2* signal (**Figures 6C,D,G**) with *Pax3* (a marker of midbrain and pretectal alar plate; **Figure 6A**), *Pax6* (marker of diencephalic and secondary prosencephalic alar plate, with exception of the *Dlx*-positive ventral subdomain of the hypothalamic alar plate; **Figures 6B,E**; Puelles et al., 2012a) and *Shh* (a floor and basal plate marker in the whole forebrain, except in a tubero-mamillary band within basal hypothalamus; *Shh* only labels floor plate in the hindbrain; **Figure 6F**). The series proceeds lateromedially. Lateral sections in **Figures 6A–D** first pass tangentially through the lateral alar wall of p1 and p2, plus the midbrain, and subsequent sections finally show the corresponding ventricular cavities. It can be observed that Th in p2 continues largely devoid of PVs, whereas PT in p1 displays them regularly, as well as the neighboring midbrain. The alar prethalamus also shows now a significant number of PVs (p3; PTh; **Figures 6D,G**), more or less in continuity with those in the alar hypothalamus (Hy; **Figure 6G**), and starts to build a local PVVP. The alar thalamic p2 field thus represents a non-invaded discontinuity (retarded heterochrony) within the central neuromeric unit of the diencephalon. As the sections approach the alar-basal boundary found underneath these alar regions (**Figures 6E,F**), we observe already in **Figure 6D** a significant number of PVs disposed uniformly along the Mb, PT, Th and PTh basal plate (tegmentum), even starting to form a PVVP. This basal PV pattern is reproduced less markedly in the hypothalamus (e.g., within the *Shh*-positive retromamillary area; Hy; **Figure 6D**, and the similarly *Shh*-positive dorsal tuberal area; red arrowhead; Hy; **Figure 6G**). Some PVs are found as well at the acroterminal (rostralmost) basal tuberal domain (Atd; **Figure 6G**).

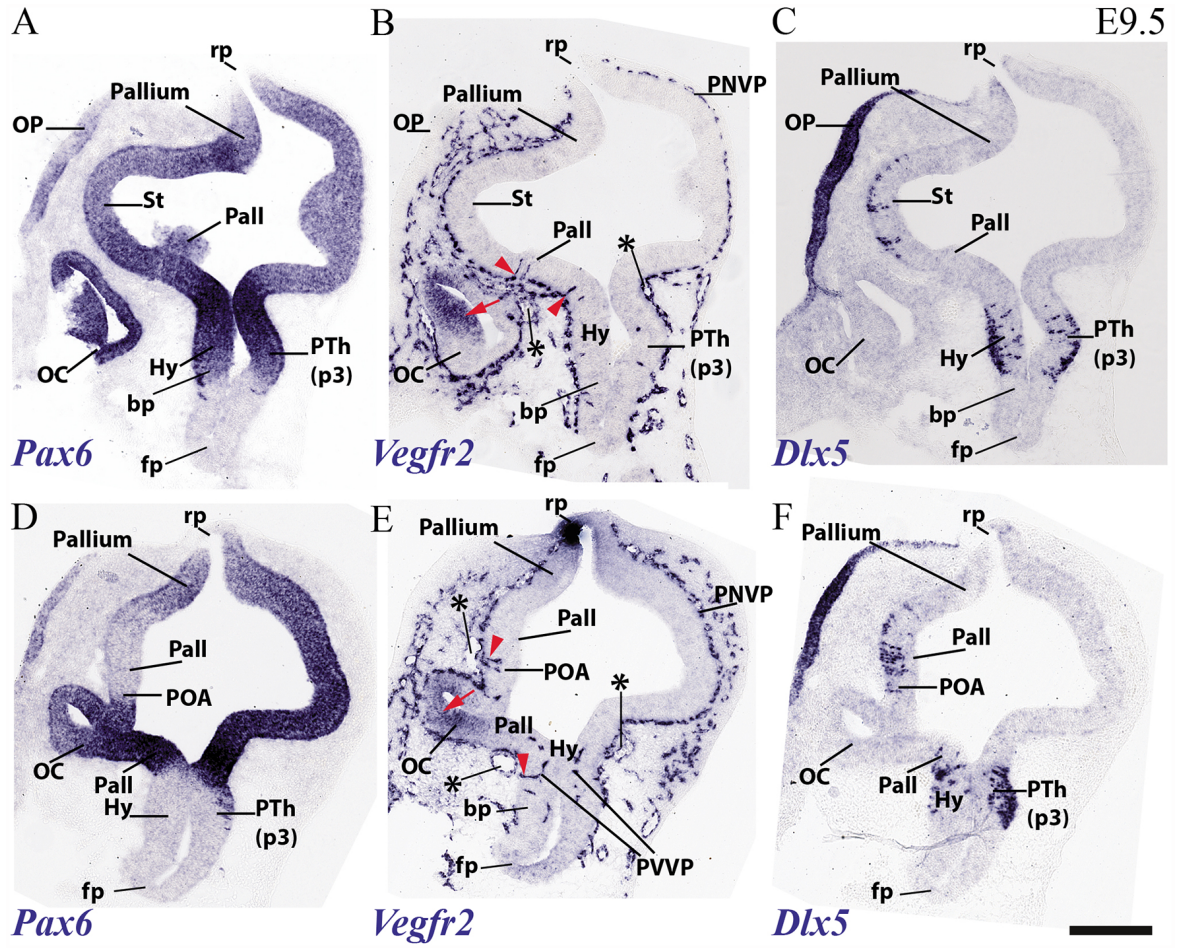

FIGURE 5 | Transversal sections through a mouse secondary prosencephalon and diencephalon at E9.5 showing PNVP vascularization and first perforant vessels (Vegfr2; **B,E**), compared in consecutive sections with markers of telencephalic pallium and striatum (Pax6; **A,D**) and telencephalic subpallium and part of alar hypothalamus (Dlx5; **C,F**). Red arrowheads: perforant vessels, red arrow: non-vascular expression of Vegfr2 at the retinal primordium of the optic vesicle. Asterisks: presumed venous sinuses. See schematic representation of plane of section in **Figure 3H**. Scale bar: 200 μm.

Pax6 and *Shh* labeling are useful to demarcate the different St, Pall, Dg and POA subdomains of the telencephalic subpallium (**Figures 6E,F**). This allowed us to corroborate at E10 our impression gained on E9.5 material that PVs are still selectively absent from the developmentally more retarded striatal subdomain, some PVs are present in the pallidum, and the largest number of PVs characterizes the diagonal and preoptic areas (St, Pall, Dg, POA; **Figures 6C,D,G**). No PVs are observed at the *Pax6*-positive pallial region. Note as well in **Figure 6G** that the cerebellar plate (Cb) shows a distinct PNVP, but no PVs, as occurs as well at the neighboring caudal midbrain.

PNVP, PVs and PVVP Vascular Pattern in the Prosencephalon of Mice at E11.5

During this stage further neuromeric and telencephalic growth occurs, and the molecular diversity is increased by new inner partitions; moreover, the mantle layer increases considerably in thickness, but without reaching a final status yet (**Figures 7A–H**). This increases the radial complexity of the neural wall with particularities at each developmental unit. Axonal navigation has started as well, though identifiable fiber strata may be detected only at few places (e.g., the posterior commissure in **Figure 7C**). In the secondary prosencephalon, a notable change is represented by a large increase in thickness of the whole subpallial region, where a lateral intraventricular bulge known as the lateral ganglionic eminence (striatal domain), and a smaller medial intraventricular bulge defined as the medial ganglionic eminence (pallidal plus diagonal domains) are observed, next to the non-evaginated preoptic area (LGE, MGE, POA; **Figures 7F–H**). Hypothalamic dorsoventral microzonal subdivisions, and pretectal anteroposterior partitions become molecularly defined at E11.5.

At around this stage, the outer limiting membrane of the entire neural tube is covered by the PNVP; this includes hypothalamic basal acroterminal domains, as well as the previously uncovered floor and roof plates (**Figures 6G**, **7B,D,G**).

The perforant vessels (PVs) in the alar diencephalon and midbrain are still most abundant, and are particularly visible at

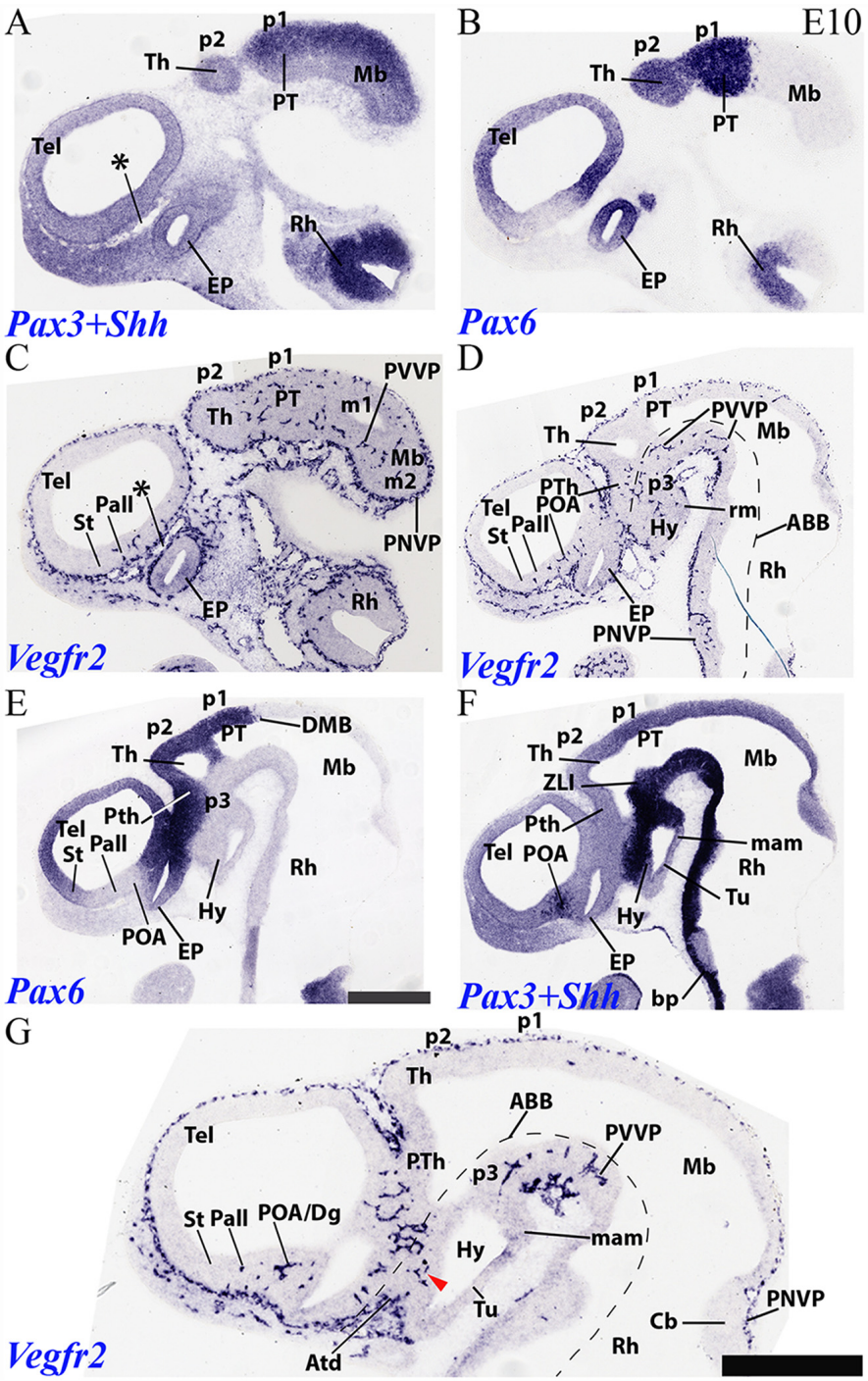

FIGURE 6 | Sagittal sections through a mouse forebrain and hindbrain at E10 (in lateral to medial order) showing PNVP vascularization, perforant vessels and PVVP formation (Vegfr2; **C,D,G**), compared in consecutive sections with markers of alar forebrain (Pax6; **B,E**) and alar and basal forebrain/hindbrain (Pax3+Shh; **A,F**). Red arrow heads: earliest PVs at the dorsal part of the hypothalamic basal plate; note more advanced local alar plate. Asterisks: presumed venous sinuses. See further description in the text. Scale bar: 400 μm.

the pretectum (PT; p1; **Figures 7A–C**), where an anteroposterior alar regionalization into precommissural, juxtacommissural and commissural subdomains can be appreciated and distinguished molecularly (PcP, JcP, CoP; **Figure 7C**; Ferran et al., 2008). The CoP coincides with the aggregated transversally coursing fibers of the posterior commissure. The alar midbrain shows less PVs than the pretectum, but already displays a PVVP that reaches the *Vegfr2*-positive roof plate (**Figures 7B,D**; compare **Figure 7E**,

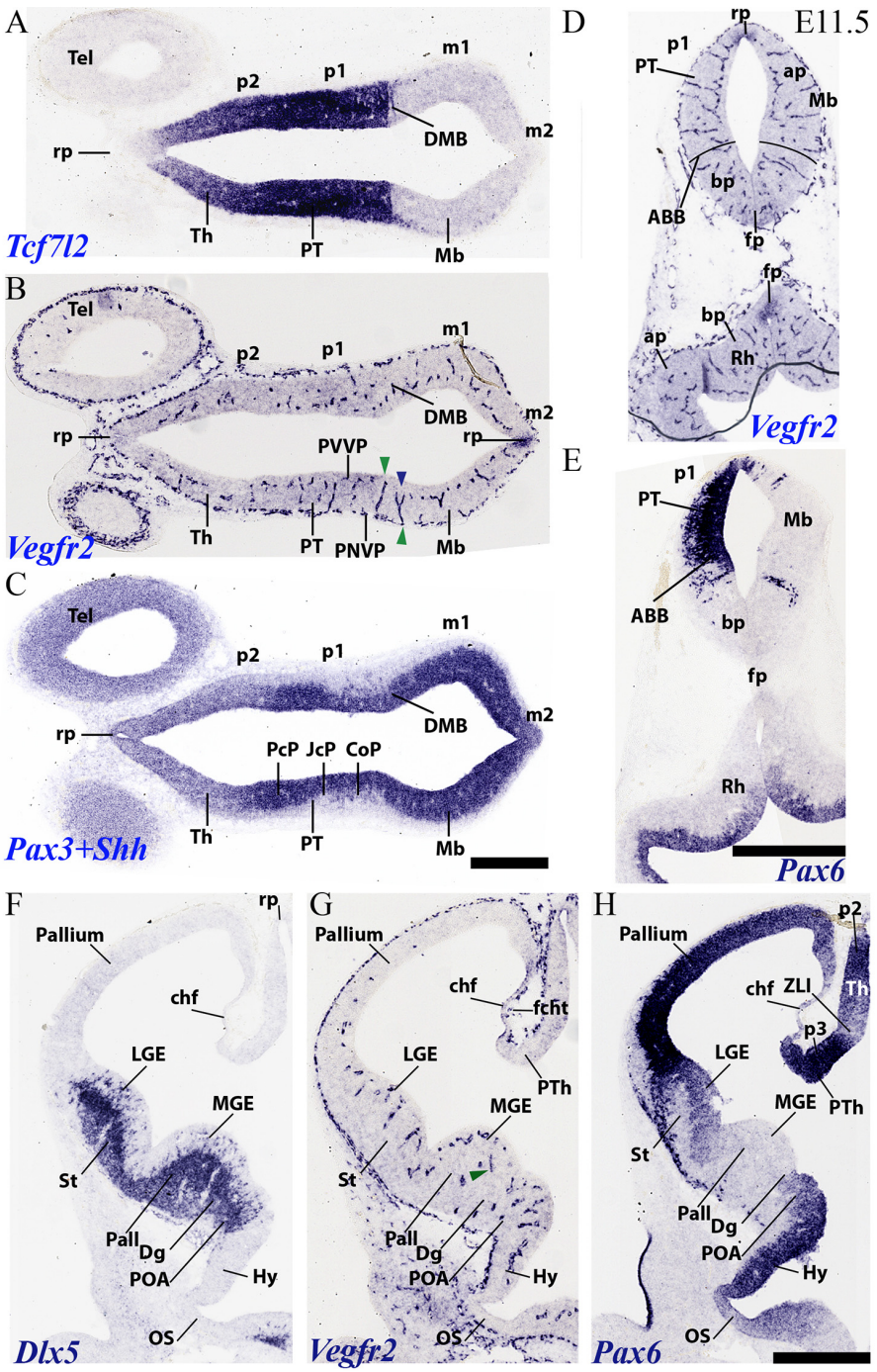

FIGURE 7 | Horizontal **(A–C)** and transversal **(D–H)** sections through embryonic mouse alar forebrain at E11.5 showing PNVP vascularization, perforant vessels and PVVP formation (Vegfr2; **B,D,G**), compared in consecutive sections with various markers of the alar forebrain (Tcf7l2: **A**; Pax3+Shh: **C**; Pax6: **E,H**, and Dlx5: **F**). **(A–C)** Horizontal sections displaying diencephalic neuromeres p2 (Th) and p1 (PT) and midbrain (Mb), jointly with dorsal part of telencephalic vesicle (Tel), in order to observe segmental differences in degree of alar vascularization. **(D,E)** Consecutive transversal sections passing through the midbrain-diencephalic border (left side = PT; right side = Mb), and showing also a hindbrain cross-section underneath (Rh). The alar-basal boundary is indicated (ABB), as delineated by Pax6 alar signal in **(E)**. Green arrowheads: perforant vessels restricted radially to a specific neural histogenetic domain; blue arrowhead: a perforant vessel ramifies into PVVP within Mb, but does not invade adjacent PT. **(F–H)** Three consecutive cross-sections through the secondary prosencephalon (hypothalamus plus telencephalon), midways through the telencephalic vesicle, illustrating vascularization patterns (Vegfr2; **G**) in the subpallium (medial and lateral ganglionic eminences, MGE, LGE; marked by Dlx5 expression in **F**) and the pallium (marked by Pax6 expression in **H**; Pax6 signal also appears in the preoptic area, POA). See description in the text. Scale bars: 400 μm.

a section roughly across the DMB, and showing as well the *Pax6*- expression limit at the alar-basal border; ABB). On the other hand, the alar thalamus domain shows now already an incipient PVVP, but PVs are rarely found (p2; Th; **Figures 7B,G**). This raises the possibility that this thalamic PVVP is largely an extension of the PVVP from the underlying p2 basal plate, rather than an independently formed alar one (see "Discussion" section below in connection with singular basal penetrating thalamic arteries). A characteristic basal plate pattern is observed in **Figure 7D**, which displays the Mb on the right side and the PT on the left side; the basal PVVP seems less developed than the alar PVVP. The midbrain and hindbrain floor plate expresses weakly *Vegfr2* (fp; **Figure 7D**), as does the midbrain and diencephalic roof plate (rp; **Figures 7B,D**).

The alar hypothalamus near the optic stalk shows PVs and an incipient PVVP (Hy; **Figure 7G**; not so the optic stalk itself, restricted to a PNVP). Proceeding from alar hypothalamus into subpallial telencephalon (the cited sizeable ganglionic eminences), we still observe a step-like change in the number of PVs across the POA, Dg, Pall and St subdomains. The striatal primordium now displays for the first time PVs and incipient PVVP (**Figure 7G**; compare limits in **Figures 7F,H**). Moreover, we also first see at E11.5 some PVs and an incipient PVVP at the pallial region adjoining the subpallium; the density of pallial vessels decreases gradientally towards the convexity of the hemisphere. The pallial area lying immediately next to the striatum is the ventral pallium, where the olfactory cortex is produced. This is followed by the claustro-insular complex, or lateral pallium, the neocortical primordium or dorsal pallium, the cingulate mesocortex and the hippocampal allocortex, or medial pallium, which would map on the medial wall of the hemisphere (Puelles et al., 2000, 2019; Puelles, 2014; Watson and Puelles, 2017). This medial wall also displays the thinner neuroepithelial tela of the chorioidal fissure (chf; **Figures 7F–H**), which interconnects the prospective hippocampal fimbrial taenia with a prethalamic taenia at the roof plate end of the prethalamic eminence (PTh; **Figures 7G,H**). The invasion of the future chorioidal plexus of the lateral ventricle through the chorioidal fissure has not yet begun at E11.5. In fact, there is only a tenuous PNVP at the outer or pial surface of the fissural chorioidal tela (fcht; **Figure 7G**).

Topologic Positioning of Major Brain Vessels on the Prosomeric Model

The external vascularization by the perineural vascular plexus (PNVP) covers during early development the entire neural tube and will derive in the adult in a complex extracerebral compartment. This compartment is represented in adult animals by an external venous system (outer dural), a middle compartment of main arterial and venous vessels (arachnoidal layer), and an inner compartment represented by a pial anastomotic plexus. The blood supplied by the main arterial vessels reaches the arachnoidal layer, from where smaller branches connect variously with the capillary plexus covering the outer limiting membrane. Terminal vessels from this plexus penetrate the neural tissue and connect therein with capillaries (Marín-Padilla, 1987, 2012; Scremin and Holschneider, 2012; Scremin, 2015). Perforant vessels (PVs) sprout progressively from the PNVP, intercalating apparently at a standard mean distance of 400 μm (Marín-Padilla, 2012) as they penetrate the brain parenchyma along a more or less radial path that initially reaches the ventricular zone of the neuroepithelium, where final circumferential branches are given to build the PVVP (**Figure 1B**). At later stages, other lateral branches sprout from the PVs at several levels through the mantle layer. Numerous accounts and mappings exist about the main brain vascularization fields that correspond to branches of the vertebral, basilar, and internal carotid arteries.

While these facts are well known, our results on differential positional timing of PV entrance in relation to molecular compartments of the brain wall led us to become interested in an issue that apparently has never been considered before, namely the question whether the arachnoid vessels course and produce secondary branches in a specific topologic relationship with the brain's subdivisions according to the prosomeric model (these are understood as *natural* developmental units of the brain, as opposed to other sorts of arbitrarily defined anatomic partitions; Nieuwenhuys and Puelles, 2016). Previous impulse towards exploring this issue came from the reported experience of interventional neuroradiologists with arteriovenous malformations; this pathology apparently often reveals peculiar positional restrictions (boundaries) of the abnormal vessels, which have been conjectured by Valavanis (2003) to be associated to molecular compartments of the brain wall. Assuming that the position of the main forebrain arterial branches is relatively well conserved in mammals and even in tetrapods (see however about rodent variations in Scremin, 2015), we opted in our analysis for the best known human arterial pattern.

Using for simplicity semi-realistic lateral-, medial- and dorsal-view schemata based on a rodent brain (**Figures 8**, **9**), it is feasible to produce a systematic semi-topological classification of the known arterial vessels relative to the prosomerically subdivided surface of the brain. Surface regions represent so many radial histogenetic units reaching in depth the ventricle (presumed mantle layer course of radially penetrating vessels; **Figures 1C,D**). We left aside for the moment the venous vessels, which are nevertheless susceptible of the same approach (e.g., Padget, 1948, 1957). Some points posed technical difficulties, because some brain portions are grossly deformed morphogenetically in rodents and humans, and may show vascular positions in the adult that do not seem similar to the original embryonic ones. Some extrapolation had to be applied. We also attempted a less realistic, more topological schema (**Figure 10**), and checked at the Allen Developing Mouse Brain Atlas[1] the predicted vascular branch trajectories detected by various vascular gene markers (**Figure 11**). The present results are just a first approximation to this new mapping approach.

Theoretically, the approximation courses through the arachnoid layer are expected to be either longitudinal (i.e., parallel to the brain length axis, which we must remember is sharply bent ventralward at the cephalic flexure; **Figure 1A**),

[1] developingmouse.brain-map.org

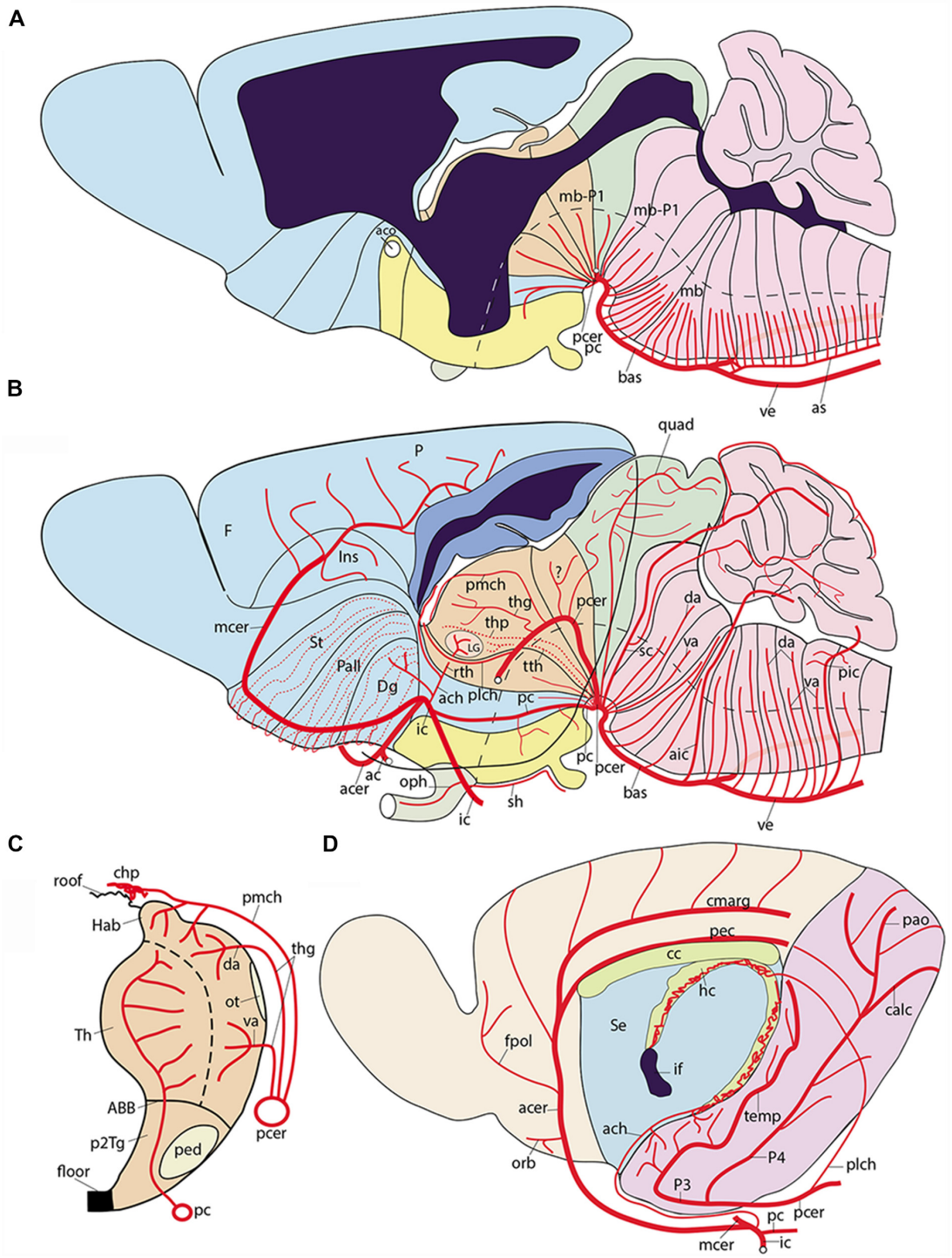

FIGURE 8 | Semi-realistic schemata based on the updated prosomeric model shown in **Figure 1A**, illustrating the forebrain and hindbrain regions **(A,B)**, a thalamus cross-section **(C)**, and the isolated telencephalon **(D)**, cut in various ways to visualize vascular patterns relative to brain histogenetic units contemplated in the model (transversal neuromeres and dorsoventral alar/basal longitudinal zones). Note the color code of the different brain regions in **(A,B)** coincides with that in **Figure 1A**. **(A)** Schematic paramedian sagittal section (ventricular cavity in black), showing the origins, penetration sites and intraneural topologically transverse course of a continuous set of medial vessels serving the paramedian basal plate all the way into the hypothalamus; these fan out in the forebrain due to the axial incurvation at the cephalic flexure (note similarly bent alar-basal boundary drawn in as a longitudinal black dash line). The basal plate arteries sprout sequentially from the anterior spinal and vertebral arteries (as, ve), the basilar artery (bas), the stem of the posterior cerebral artery (pcer), and the posterior communicating artery (pc); this last artery is not shown, since it lies lateral to this nearly median plane of section). **(B)** Schema aiming to depict typical courses of arteries serving

(*Continued*)

FIGURE 8 | Continued
the alar plate domains of the brain (alar-basal boundary again as bent longitudinal black dash line). The alar plate vessels mainly derive from the ve, bas, pcer, mcer and pc arteries. In the hindbrain they first circumvent the basal plate domain with an initial ventrodorsal course in the subarachnoidal space, adapted topologically to the diverse neuromeric regions, and then they penetrate either ventral or dorsal parts of the corresponding alar plate sector (va, da); special cases are represented by the postero-inferior, postero-superior and superior cerebellar arteries, which produce va and da branches as well as chorioidal branches for their neuromere, and then jump into the overlying cerebellum. At the midbrain, the quadrigeminal artery behaves somewhat like a va + da artery, but the dorsalmost part of the colliculi are served by a hyperdorsal supracollicular network of da-like vessels (not shown). The diencephalon shows a contrasting pattern, insofar as alar arteries arise either as perforating arteries (from the pcer P1 segment, or the posterior communicating artery, pc; pcer; see cross-section in **C**), which first penetrate the basal plate and then continue internally dorsalward until reaching periventricular alar centers, or as dorsally coursing va, da or chorioidal branches of the posterior cerebral artery, which follows a longitudinal topologically rostralward course along the diencephalic ventral alar plate domain (pcer; its P2 segment), before it bends lateralwards into the posterior telencephalic cortex (P3 and P4 segments). In **(B)** the pcer diencephalic branches are visualized after graphically removing the caudal part of the hemisphere than normally hides them (the floating caudal contour of the eliminated part of the hemisphere was drawn in as a curved line extending from the occipital pole to the temporal pole, for reference; a deeper blue distinguishes the cut surface at the telencephalic pallium; the section across the lateral ventricle appears in black); the diencephalon thus liberated is shown undeformed according to the prosomeric model in **Figure 1A**, so that its PT, Th and PTh regions are seen in their original relationships. The pcer can be seen first contouring the basal peduncle dorsalward in front of the midbrain, and then bending rostralwards along the ventral part of the diencephalic alar plate; it appears cut off at the point where it would enter lateralwards and caudalwards its telencephalic P3 segment (seen in **D**). Two thalamic perforating arteries are represented (tth, thp), jointly with examples of non-perforating va/da thalamic branches of the P2 pcer (thg, pmch). It is not yet known whether there exist also pretectal and prethalamic perforating arteries. In addition, postulated pretectal and prethalamic va/da arteries which may have been misidentified as "thalamic" are also drawn in (see text). The posterolateral chorioidal artery (plch) is a pcer branch that courses dorsally next to the interthalamic zona limitans boundary (passing rostral to the thalamic lateral geniculate primordium; LG) and reaches the chorioidal roofplate of the prethalamus. The latter is continuous caudally with the thalamic one (served by the pmch) and rostrally with the telencephalic counterpart (served by the ach). Compare the thalamus pattern in **(B)** with the schematic cross-section in **(C)**. **(C)** Schematic section transversal to the thalamic neuromere, visualizing its floor, basal, alar and roof plates, jointly with its main arteries. The thalamus lies in the alar domain, capped by the habenula (Th, Hab); the basal domain represents the p2Tg field. Perforant vessels such as tth (from pc) or thp (directly from pcer P1 segment) penetrate the p2Tg (tth rostrally to thp) and then course periventricularly into the alar thalamus, where they serve different polar or paramedian deep populations. The superficial thalamic nuclei are served instead by direct va/da (thg) branches of the rostrally oriented pcer, as well as by collaterals of the pmch artery (pcer) reaching the habenula and the chorioidal plexus of the 3rd ventricle. The LG also receives irrigation from the ach artery, *via* its recurrent thalamic branch (rth, ach, LG; in **B**). **(D)** Schema of the interhemispheric telencephalic face after removing graphically the diencephalon and hypothalamus (interventricular foramen in black; if), showing the main arterial vessels covering this area. The cortex appears color-coded as depending either on the acer (pale yellow territory) or on the pcer (pink territory). The acer gives out orbital (orb), frontopolar (fpol) branches, as well as the terminal pericallosal (pec) and callosomarginal (cmarg) arteries, which produce other frontal and parietal ramifications at the convexity. The pcer gives out its temporo-hippocampal branch (temp) and calcarine (calc) and parieto-occipital (pao) branches. We also see represented the dual irrigation of the chorioidal plexus of the lateral ventricle. This occurs *via* two vessels entering the chorioidal fissure, which stretches from the roof of the interventricular foramen until the uncal pole of the sphenoidal ventricular horn. The ach arises directly from the internal carotid (ic) and enters the uncal tip of the fissure, distributing to the sphenoidal or telencephalic portion of the lateral plexus, which ends roughly under the callosal splenium. In contrast, the plch arises from the pcer, and contours the whole surface of the prethalamus (removed graphically) until reaching the prethalamic supracapsular part of the lateral plexus, which extends from the foramen to the area under the splenium, where it may anastomose with the ach plexus portion. Each of these arterial chorioidal territories has its own venous outflow.

or transversal (orthogonal to the brain axis and parallel to the changing DV dimension of the neuromeres; **Figure 1A**). Significant contradiction of our expectations would emerge if oblique vascular courses are found. Some vascular arbors are quite complex, as exemplified by the posterior cerebral artery, which ends in the temporo-occipital telencephalic cortex, but also gives branches to chorioidal roof specializations, as well as to ample alar and basal diencephalic and midbrain areas. The issue will be also touched below whether some vessels on occasion jump from one brain subdivision to another (e.g., from the hindbrain medulla to the cerebellum, implying mixed coverage of different neuromeres).

The Vertebral and Median Basilar System

The vertebral arteries (ve) converge into the basilar trunk (bas) approximately at r5 level [producing there also the median descending anterior spinal artery (as)]. The median basilar artery thereafter courses longitudinally along the pontine (r4-r2) and prepontine (r1-r0; r0 = isthmus) hindbrain levels (bas; **Figure 8A**) up to its final bifurcation into the right and left posterior cerebral arteries (pcer) just beyond the midbrain m1 prosomere (marked by the oculomotor nerve root). Along this median course, numerous *paramedian radial arteries* are produced which penetrate transversally the medial basal plate of the pontine and prepontine rhombomeres all the way to the ventricle (paramedian or mediobasal pontine arteries; mb; **Figures 1D**, **8A**; note much conventional anatomy wrongly ascribes prepontine hindbrain structures to the midbrain; Puelles, 2016; see also Puelles, 2019 [this book] on neuroanatomic terminology). Paramedian or mediobasal penetrating branches of the anterior spinal artery (as) also show the same basal plate related course for the medullary rhombomeres (r5-r11; *mediobasal medullary arteries*; mb; **Figures 1C**, **8A**). At medullary levels, we see also *lateral paramedian or laterobasal* branches of the vertebral arteries, which penetrate lateral parts of the medullary basal plate (e.g., passing through the migrated inferior olives; see lb; **Figure 1C**). Similar transversal neuromeric medial branches arise from the rostral end of the basilar artery (bas), the origin of the posterior cerebral artery (pcer), or the posterior communicating artery (pc), and penetrate in essentially the same radial way the interpeduncular surface of the prepontine hindbrain (e.g., level of interpeduncular nucleus), the midbrain and the posterior perforated space rostral to the oculomotor nerve roots (diencephalic in nature). There are specific isthmic basal branches of the basilar artery, which we found labeled with the *Ctfg* and *Eng* markers in the mouse (mb; Isth; **Figures 11B,D**). The more rostral medial branches reach directly

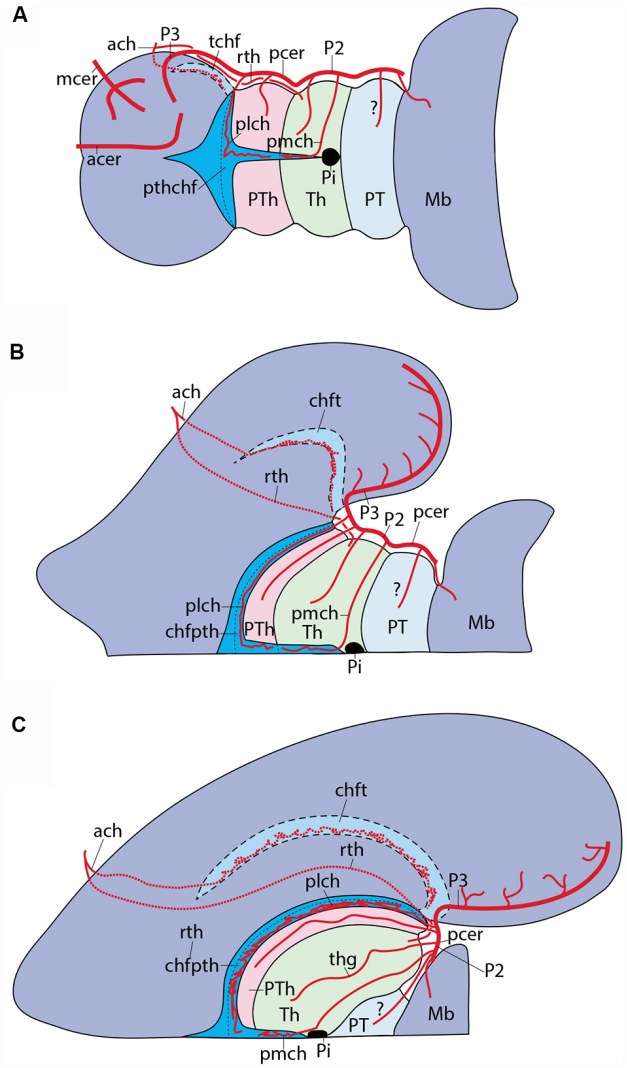

FIGURE 9 | **(A–C)** Schemata of dorsal views of the forebrain, representing three arbitrary developmental stages in which the diencephalo-telencephalic transition evolves dramatically due to the massive growth of the telencephalon, accompanied by disproportionate growth of the thalamus (Th) with respect to pretectum (PT) and prethalamus (PTh) in the diencephalon. **(A)** Initial stage, shortly after telencephalic evagination begins. A color code was applied to the three diencephalic alar territories, and the visible chorioidal roof mainly associated to the prethalamus was represented in brilliant blue, while the final telencephalic portion extends out of our view in all three schemata (seen by transparency in pale blue) into the primitive posterior pole of the hemisphere (the uncus). The pcer artery is disposed longitudinally along the whole alar diencephalon and finally reaches its telencephalic terminal region. We see also the acer and the mcer reaching independently their respective fields. Pretectal, thalamic and prethalamic alar branches arise sequentially from the pcer, as it contours each neuromere, and we see also the pmch reaching the thalamic roof and the plch reaching the prethalamic roof. Separately, the ach reaches the caudal tip of the telencephalic chorioidal fissure (by transparency). **(B)** At this stage, the hemisphere starts to bulge caudalwards and the thalamic mass grows jointly with the internal capsule as it bridges the hemispheric stalk in front of the prethalamus. This development start to cause a stretching of the prethalamus and its associated chorioidal formation (pink plus bright blue). All the vessels are absolutely passive in this process and simply adapt to the emerging new increasingly compressed

(*Continued*)

FIGURE 9 | Continued

position of the lateral face of the diencephalon and the stretching consequent to the growth of a larger telencephalic mass. **(C)** At this nearly final stage, the deforming process has brought the lateral diencephalic surface to a transversal topography (90° from its primitive position in **A**). The pink and bright blue prethalamic region is enormously stretched and thinned out, but it still occupies the interface between the telencephalon and the thalamus. The pretectum results partly hidden, but also remains in its original caudal position. The prethalamic chorioidal plexus served by the plch participates in the upper supracapsular part of the fissure (bright blue), having reduced its preforaminal portion and increased in length (by stretching its postforaminal portion); the telencephalic chorioidal plexus served by the ach appears stretched out (pale blue; still by transparency), but essentially in the same position as before. The pmch serves the small thalamic chorioidal plexus in front of the pineal (Pi). As a consequence of such morphogenesis, the pcer seems to have lost its longitudinal P2 course, but topologically this course continues to be present.

the basal plate domains of the diencephalic neuromeres and even the retromamillary hypothalamic area, which corresponds to the peduncular basal hypothalamus (hp1; **Figure 1A**; compare **Figure 8A**, and vessel marked with red asterisk in **Figure 11D**). It is not clear so far whether similar medial branches penetrate the mamillary region of the terminal hypothalamus, which is postulated in the prosomeric model as the rostralmost basal plate territory (mam; **Figure 1A**). This area borders the acroterminal hypothalamic region, which represents the rostral median end of the forebrain, and extends between the mamillary body and the anterior commissure, including unique basal formations such as the tubero-mamillary area, median eminence, infundibulum and neurohypophysis, and unique alar formations such as the optic chiasma, the preoptic lamina terminalis and the anterior commissure (Puelles et al., 2012a; Ferran et al., 2015c; Puelles and Rubenstein, 2015). This somewhat "special" rostromedian territory seems to receive direct branches from the internal carotid (e.g., the superior hypophysial artery, and the ophthalmic artery), or branches from the anterior communicating artery (sh; oph; ac; **Figures 8A,B**). In this domain the vessels usually penetrate along radial lines approaching the ventricle in curves best observed in horizontal sections (e.g., Puelles et al., 2012a, their Figure 8.12).

Apart of these clearly transversal and segmental medial paramedian or mediobasal arteries, lateral branches of the basilar and vertebral arteries follow analogous but longer parallel courses relative to the DV dimension of all rhombomeres in order to serve their alar plate territories through alar entrance points (e.g., pic; **Figure 1C**; bas branches in **Figure 1D**). To this end, they contour superficially the hindbrain basal plate domain and then penetrate either ventrally or more dorsally the alar plate domain. One of these lateral alar arteries is the *postero-inferior cerebellar artery*, which we judge to parallel r9 in its transversal dorsalward approach to the medullary sensory centers and its subsequent jump into the caudal cerebellum, giving other branches to the posterior spinal artery, and the IV ventricle chorioidal plexus (pic; **Figures 1C**, **8B**). There are also several so-called *lateral medullary arteries* related to r6-r8, which we classify as ventral and dorsal alar vessels (va, da; **Figure 8B**). The human *antero-inferior cerebellar artery*, seems to run dorsalward transversally along the r4/r5 boundary, or

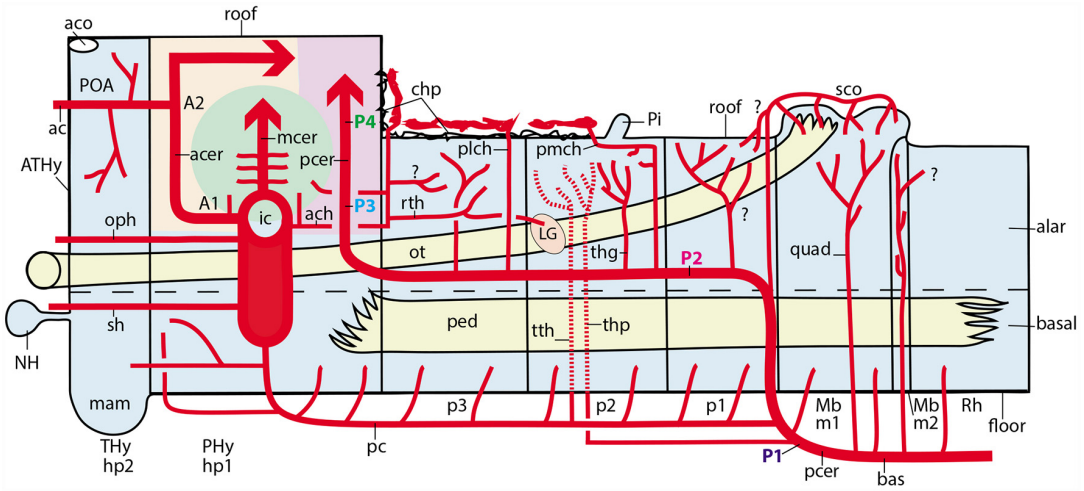

FIGURE 10 | Schematic topologic representation of known or newly postulated forebrain arterial vessels mapped upon the prosomeric model. As regards the topologic forebrain map, which essentially reproduces the semi-realistic version of **Figure 1A**, its axial dimension has been straightened [elimination of the cephalic flexure, straight floor, straight alar-basal boundary (dash line), nearly straight roof (this has a step as the evaginated telencephalon is reached, for clarity, but even this might be straightened out), and, accordingly, the basal and alar plates also are straight]. Reference structures such as the cerebral peduncle (ped) and the optic tract (ot) are straight or nearly straight. All neuromeres and interneuromeric borders are orthogonally transversal to the axial dimension. In these conditions, it is possible to represent faithfully spatially oriented structures such as the arteries. Dorsal is the direction into the roof, while ventral directs into the brain floor; rostral lies to the left, and caudal to the right. The main subarachnoidal vessels serving this territory derive from the ic, pc, pcer, and bas arteries. One should first examine these fundamental vessels. The ic courses transversally in ventrodorsal direction next to the PHy (crossing the ot); it is thus parallel to the peduncular hypothalamic sector–not shown- tagged as PHy). Its major terminal branches entering transversally into the telencephalon overhead are the acer and mcer vessels, positioned in the map as corresponds after flattening the hemisphere (there is a yellow/green color code for the acer and mcer fields). The posterior telencephalic field is covered by the final, similarly transversal, segment of the pcer (pale violet code). The thick arrows in each case represent simplified pallial arborizations, whereas central branches to the subpallium appear as thin collaterals. The acer also gives out the ac artery which importantly serves the preoptic (POA) and septal regions (the septum lies near the telencephalic roof, paradoxically, and surrounds the anterior commissure, aco, which fate-maps as the rostral end of the roof). The median front of the forebrain is given by the acroterminal preopto-hypothalamic domain (ATHy). Note the optic chiasma (unlabeled) and the neurohypophysis (NH) lie at alar and basal levels of this acroterminal area, respectively. The sh and oph branches of the ic are thus longitudinal arteries. The pc vessel arises from the ic and then topologically descends first along the PHy and then bends caudalwards into a longitudinal para-tegmental course until it meets the pcer near its origin from the bas. Our topologic straightening of the normally bent length dimension has caused the pc to appear as long as it topologically is, though this is not seen in the unstraightened brain, where we mostly see its short transversal hypothalamic course. The pcer continues bilaterally the median bas artery but changes its relative position by contouring dorsalward the peduncle (in front of the midbrain) into a ventral alar level, which it then uses to extend rostralward (longitudinally) until it enters into the telencephalon. This is the basic layout. The midbrain thus appears as a transitional caudal forebrain domain where the vascular patterns gradually change from typical hindbrain features to typical diencephalic characteristics. This again apparently changes when we arrive at the secondary prosencephalon, where our analysis was handicapped by scarce and confusing data (this is the less detailed part of our vascular map, but it can be developed in the future). One fundamental pattern that is pretty clear is that the brain basal plate is irrigated separately from the larger alar plate. A multiplicity of basal (mediobasal or laterobasal) arteries enter the basal tegmentum at all neuromeric levels, as predicted originally by His (1895, 1904) and as expected by the prosomeric model (not so the columnar model, which predicts that basal arteries should extend through the acroterminal dimension into the subpallial telencephalon; there is no sign of that). These basal plate vessels arise sequentially from the as, ve, bas, pcer (P1) and pc arteries. With exception of the thalamic perforant arteries (tth, thp; seen by transparency), which first behave as basal vessels, but then extend intraneurally into the alar domain, a separate set of arteries address the hindbrain, midbrain and diencephalic alar plate. In the hindbrain a pattern of ventroalar and dorsoalar arteries arising from the bas or ve vessels (commonly known as short and long circumferential branches) is clearly repeated, even when some segmental vessels add a jump into the overhanging cerebellum, a morphogenetic deformation (pic, aic, sc). Most dorsoalar hindbrain arteries may give out chorioidal branches. The midbrain also has dedicated alar arteries, such as the quad at the m1 mesomere, possibly duplicated at the m2 companion segment; they arise from the bas or pcer P1. The map next shows that the diencephalic alar plate is covered by successive neuromeric alar branches of the pcer, some of which (in p2 and p3) are chorioidal branches. The pattern thus has changed by moving the bas-like pcer bilaterally to a longitudinal course which is displaced to an alar topology (compare **Figure 8C**). Apart the midbrain basal branches of the pcer P1, diencephalic basal branches largely originate from the pc artery. The map also places the route and ending sites of the pmch and plch arteries, in contrast with the ach artery, which oddly also produces a recurrent thalamic branch (rth) which targets the lateral geniculate body by extending longitudinally, but backward, into at least the prethalamus and the thalamus.

next to it (aic; **Figure 8B**); indeed, it reportedly passes rostral to the abducens nerve root in r5 and caudal to the facial and stato-acoustic nerve roots in r4, giving alar plate branches complementary to those of the pic. A similar antero-inferior cerebellar artery with identical neuromeric topography exists in the mouse, which serves a large part of the IVth ventricle chorioidal plexus and then jumps into the caudal cerebellum (r1; Scremin and Holschneider, 2012). The *lateral short and long circumferential pontine arteries* are also ventral and dorsal alar branches of the basilar artery at pontine levels, corresponding at least to r3 and r4 (va, da; **Figures 1D**, **8B**), but possibly also to r2 and r1 (since the pontine formation partly covers these domains as well; see Watson et al., 2019, this book). We did not find useful human data specifically on r2 and r1 vascularization (apparently, these domains were not recognized as distinct regions in conventional columnar neuroanatomy), but we expect

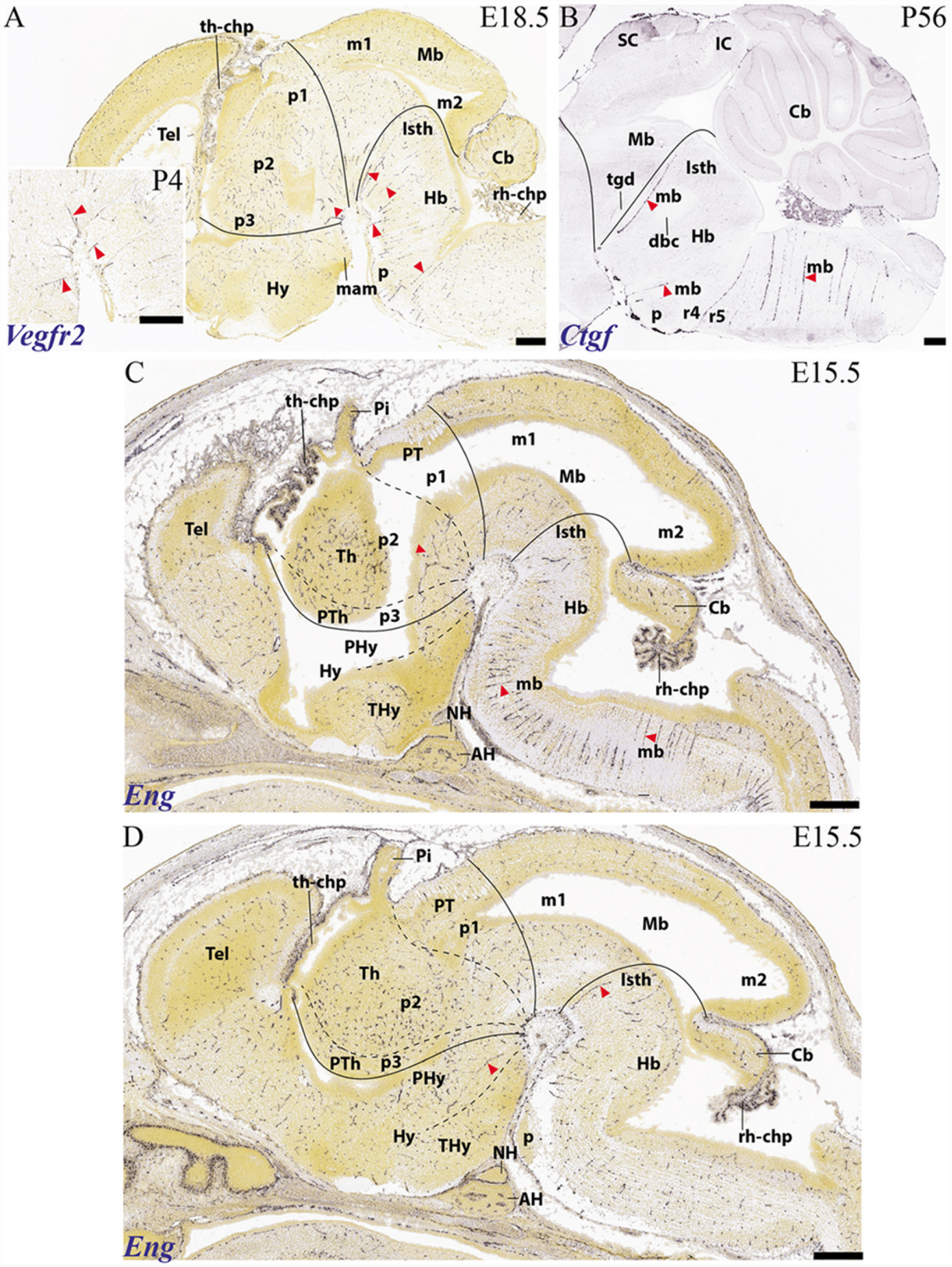

FIGURE 11 | Examples of basal arteries labeled with different gene markers in paramedian sagittal sections (material downloaded from the Allen Developing Mouse Brain Atlas). The illustrated vessels distribute along topologically transversal courses into different neuromeric units of the hindbrain and/or forebrain (major limits indicated by black lines; diencephalic and secondary prosencephalic interneuromeric limits marked by dash lines). **(A)** E18.5 mouse embryo, *Vegfr2* labeled arteries (red arrowheads; inset shows higher magnification detail of cephalic flexure). **(B)** Adult mouse, *Ctfg* label, some radial hindbrain mediobasal arteries (red arrowheads caudal to the isthmo-mesencephalic boundary; black trace; check Mb; Isth). **(C)** E15.5 mouse embryo, *Eng* label, red arrowheads pointing out mediobasal vessels in the thalamic and hindbrain basal plate. Note also chorioidal plexi (th-chp; rh-chp). **(D)** E15.5 mouse embryo, *Eng* label, red arrowheads pointing out mediobasal vessels in the peduncular hypothalamus and the isthmic rhombomere.

that these neuromeric units (important because they hold most of the principal sensory and motor trigeminal nuclei, apart of vestibulocochlear centers; Puelles, 2013) are also served in their alar domains by segment-specific *lateral (ventral and dorsal alar) circumferential prepontine arteries* that probably have been observed, but were misclassified as "pontine" (va, da; **Figure 8B**). The isthmus or r0 level is characterized by the well-known *superior cerebellar artery*, an alar plate targetted vessel which approaches the cerebellum through its rostral end, topologically associated to the isthmus-derived vermis, but possibly also crossing into the r1-related paramedian hemisphere (sc; **Figure 8B**; this description agrees with the medial and lateral branches of the mouse superior cerebellar artery; Scremin and Holschneider, 2012).

The Posterior Cerebral Artery System

The pcer artery diverges sharply from the bas course, since it follows a topographically transversal course lounging ventrodorsally the pes pedunculi in front of the midbrain, reaching the local alar plate (it thus behaves as a circumferential vessel with regard to the peduncle). The initial pcer is conventionally divided into segments P1 and P2 by the confluence or origin of the posterior communicating artery; the latter is often interpreted developmentally as a longitudinal descending branch of the internal carotid (Padget, 1948). The pcer extends beyond the midbrain and ends serving temporal and occipital cortical territories (segments P3 and P4). The P1 segment of the pcer gives rise to some medial (interpeduncular) *midbrain* and *diencephalic basal branches* (mb-P1; **Figure 8A**), plus the *quadrigeminal* and *thalamo-perforant arteries* which target parts of the alar plate (in human; see Scremin and Holschneider, 2012). The large alar collicular plate of the midbrain is partly served by the quadrigeminal artery, also a "lateral or ventral alar artery" targeting alar domains (**Figure 8B**), and partly by a dorsal alar, supracollicular network of unclear origin (Scremin, 2015). In contrast to most other alar plate-irrigating vessels treated here, the thalamo-perforant or inferior thalamic artery apparently enters the brain through the posterior perforated space (presumably through the basal plate of the thalamic p2 prosomere; thp; **Figure 8B**), and then follows a deep ventrodorsal penetrant course next to the ventricular lining until it reaches the medial thalamic region in the alar plate (this deep course is similar to that of other perforating thalamic branches issued by the posterior communicating artery; see pc; **Figure 8C**; Salamon, 1971, 1973; Lazorthes et al., 1976; Percheron, 1976a,b; Haines, 1997; Duvernoy, 1999; Naidich et al., 2009; Ten Donkelaar, 2011).

As mentioned above, the posterior communicating artery may be understood either as a descending branch of the internal carotid or as a bilateral rostral basal extension of the pcer. It contributes distinct mediobasal branches for the diencephalic and hypothalamic prosomeres and provides also perforating thalamic arteries at p2 level (see "Discussion" section). Otherwise, the pc does not seem to produce alar plate branches (**Figure 10**).

The P2 segment of the pcer reportedly produces various posterolateral alar thalamic branches (the *thalamo-geniculate arteries*) which invade the anterolateral part of the thalamus and contribute to parts of the pulvinar and the geniculate bodies (thg; **Figures 8B,C**, **10**; Lazorthes et al., 1976; Percheron, 1976a,b; Ten Donkelaar, 2011). Other less evident pcer branches possibly penetrate similarly the pretectum and caudolateral parts of the prethalamus (Salamon, 1971, 1973). Neither the general nor the specialized literature mentions the pretectum nor the prethalamus as regards vascularization, but we know they are differentially vascularized, as we saw in the first part of this report. According to Puelles and Rubenstein (2003), we call "prethalamus" the classic "ventral thalamus."

As a consequence of differentially massive thalamic and telencephalic growth, the prethalamus, lying intercalated between telencephalon and thalamus (PTh, Th; **Figure 1A**), becomes flattened between them. The classics referred systematically to a so-called "thalamo-striatal" interface (also to the thalamo-striate sulcus, a.k.a. sulcus terminalis) as representing the tel-diencephalic border. According to present embryological knowledge, this boundary is neither thalamic nor striatal, since the *prethalamus* prosomere takes the thalamus's position on the diencephalic side, and the *medial ganglionic eminence*—MGE- takes the striatum's—LGE- position on the telencephalic side). Moreover, the MGE has been subdivided recently into parallel pallidal and diagonal area components (Puelles et al., 2013, 2016; see also Flames et al., 2007). The latter component, the *diagonal area*, seems to be the subpallial element that contacts with the prethalamus across the sulcus terminalis (the diagonal area is a full radial histogenetic domain that comprises the diagonal band nuclei at the surface, the substantia innominata, basal nucleus of Meynert and the internal pallidum at intermediate mantle levels, and the medial part of the supracapsular bed nuclei of the stria terminalis at periventricular level). The main prethalamic cell masses are the superficial pregeniculate and subgeniculate visual nuclei (lying next to the thalamic lateral geniculate nucleus), the reticular nucleus and the zona incerta complex, plus the prethalamic eminence (classically misnamed "thalamic eminence"). Increasing the confusion, the literature sometimes wrongly ascribes some of these entities to an outdated category, the subthalamus (review in Puelles et al., 2012a).

The existence of at least one alar prethalamic artery branching out from the pcer at the end of its P2 segment is thus a distinct possibility (**Figure 10**), though it might originate alternatively from the posterior communicating artery, or from the tubero-mamillary artery (see "Discussion" section on this vessel) that serves the anterior thalamic pole; the *posterolateral chorioidal artery*, branch of the pcer, possibly represents a good candidate for the missing alar prethalamic branch (see below). A further possibility is that the alar prethalamus is partly served by the anterior chorioidal artery, since this is described to reach with its branches the lateral geniculate body, implying that it would have to cross first the prethalamus (ach; plch; LG; **Figures 8B**, **10**; see "Discussion" section).

The pcer also emits within its P2 (diencephalic) segment branches for the diencephalic dorsal alar and roof neighborhoods, including the *posteromedial chorioidal artery* serving the pulvinar, geniculate bodies, habenula and the

thalamic chorioidal plexus of the 3rd ventricle, and the mentioned *posterolateral chorioidal artery* for the prethalamic eminence and the prethalamic participation in the supracapsular part of the chorioidal fissure and corresponding lateral ventricle chorioidal plexus. The plch was reported by Stewart (1955) to ascend transversally along the zona limitans intrathalamica (the prethalamo-thalamic boundary; see plch; **Figure 8B**). It serves selectively the part of the lateral ventricle chorioidal plexus that extends caudolaterally from the interventricular foramen, along the thalamic chorioidal sulcus, and ends at the begin of the sphenoidal ventricular horn, roughly alevel with the lateral adult geniculate body (see plch; pmch; ach; **Figures 8C**, **9A–D**).

The topology of all the P2 pcer branches is difficult to visualize in human material even after careful dissections, due to their apparently indiscriminate collection within the deep and narrow arachnoid pocket that separates the medial aspect of the temporal lobe from the backwards-oriented (originally lateral) diencephalic surface and the midbrain (see progressive diencephalic deformation affecting thalamus and prethalamus, as well as the corresponding chorioidal telae, in **Figures 9A,B,D**). We deduce that after coursing topologically *rostralwards* along the whole primitive lateral aspect of the diencephalon, producing relevant segmental alar branches for the three diencephalic segments (**Figures 9A,B,D**), the pcer starts its P3 segment as the artery reaches the temporal lobe of the telencephalon close to its uncal pole (Haines, 1991, 1997). There it produces its anterior and posterior temporal branches, including secondary uncus, amygdala and hippocampal branches. The final P4 segment gives rise to parieto-occipital and calcarine terminal branches (**Figure 8D**).

The Internal Carotid System and the Middle Cerebral Artery

We estimated the topological position of the internal carotid artery syphon relative to the brain surface as ascending from basal into alar regions along the peduncular hypothalamus (the artery passes early on in development behind the eye vesicle and stalk, both derivatives from the terminal hypothalamus, and its major terminal branches serve the evaginated telencephalon). Accordingly, it crosses orthogonally the longitudinal optic tract (ic; ot; PHy; THy; **Figure 10**). In contrast to the visualization problems posed by the pcer, the internal carotid and its main collateral and terminal branches seem rather straightforward, since both the telencephalic subpallium (except POA) and pallium are dorsal derivatives of the same prosomere (hp1, ic; **Figure 10**). However, as we will see, the ic also gives collateral branches into the THy, as well as recurrent collateral branches into the diencephalon. We think that the *superior hypophysial artery* (sh) is given out as a rostrally directed longitudinal branch while the ic is passing next to the hypothalamic basal plate region; this branch would have to grow strictly lengthwise from PHy into the THy region to reach the neurohypophysis (sh; **Figures 8A,B**, **10**). This agrees with the basal position of the neurohypophysis (Puelles et al., 2012a; Puelles and Rubenstein, 2015). On the other hand, the *ophthalmic artery* (oph) is also a rostrally directed longitudinal branch that arises instead from the ic at alar plate level of PHy, and it invades longitudinally the eye, a THy derivative (oph; **Figures 8A,B**, **10**). The ic also gives out two caudally directed or recurrent longitudinal branches.

One of them is the *posterior communicating artery* (pc), which clearly arises from the ic at alar levels of the forebrain (topologically dorsal to the optic tract; embryonic analysis—e.g., Padget, 1948—confirms that it is a descending or recurrent branch of the ic, not a branch of the pcer). The pc first courses ventralwards (crossing the optic tract) along the dorsoventral dimension of the peduncular hypothalamus. Here several basal or tegmental branches are given for both PHy and THy. After it reaches the cephalic flexure, it arches longitudinally backwards under basal p3 and p2 until it meets the pcer at roughly p1 level (see Stewart, 1955). Along this longitudinal segment the pc gives out sequentially 7–8 tegmental branches for the hypothalamus and the three diencephalic neuromeres, a pattern that corroborates its local longitudinal nature (pc; **Figure 10**; these branches are confusingly known as *posterolateral central arteries*, which complement the analogous *posteromedial central arteries* originated from the pcer; Ten Donkelaar, 2011; his Figure 2.10). It would be clearer terminologically to call them *hypothalamic basal* and *diencephalic basal* arteries, since the prefix "postero-" used for both pc- and pcer- basal branches is ambiguous as to their specific origins, and the "central" descriptor appears in a different usage for deep branches of the cerebral arteries entering the telencephalic subpallium, a property not shared by these selective forebrain basal plate vessels. In the human brain the implicitly bipartite bent course of the pc (first transversally dorsoventral across the optic tract and then longitudinal under the diencephalic tegmentum) results secondarily straightened out due to massive growth of the peduncle, so that in the usual basal images of the polygon of Willis the pc seems to course in a straight line orthogonally to the optic tract.

The literature mentions among the "pc central branches" a distinct "tubero-thalamic" perforating artery (tth; Lazorthes et al., 1962, 1976; Plets et al., 1970; Percheron, 1976a), which is contradictorily represented by Ten Donkelaar (2011; his Figure 2.20) as a branch of the pc arising midways along its longitudinal trajectory. We think, consistently with this drawing, that it probably penetrates ventrally the p2 tegmentum and takes internally a deep perforating dorsalward course into the anteromedian pole of the (alar) thalamus (tth, pc; **Figures 8B,C**, **10**; it serves there the anterior thalamic nucleus and the polar part of the ventral anterior thalamic nucleus). However, the description of this artery in the Ten Donkelaar's (2011) text is confusing, since it is defined as a "*premamillary* (anterior thalamoperforating or tubero-thalamic) artery," whose territory includes the *posterior part of the optic chiasm, the optic tract, the posterior part of the hypothalamus with the mamillary body*, *and the reticular nucleus of the thalamus*, apart the terminal thalamic arborization (data attributed to Plets et al., 1970; Percheron, 1976a). A premamillary-thalamic or tuberal-thalamic course might allow the collateral vascularization of the chiasma and mamillary region, but does not agree at all with the perforating tegmental course *depicted* by Ten

Donkelaar (2011; his Figure 2.20a,b), which clearly implies a penetration caudal to the retromamillary area (remember the ic correlates topologically with the retromamillary PHy; **Figure 10**). Our analysis suggests that this perforating artery probably relates primarily to the p2 (thalamic) diencephalic neuromere, which contains the thalamus in its alar domain. Once the pc branch has entered the thalamic tegmentum, it might give out rostrally coursing hypothalamic branches that reach the mamillary body and even the more distant optic chiasma *after crossing the prethalamic, retrotuberal and tuberal tegmentum*. Additional dorsally perforating branches for the *alar prethalamic* reticular nucleus might arise as well. However, we do not have any positive evidence corroborating such hypothalamic or prethalamic branches of the tth, as illustrated in the literature. The "tubero-" root in the name of this thalamic artery apparently refers explicitly to a penetration through the *tuberal region*, or perhaps the *tubero-mamillary area* (the tubero-mamillary area lies between NH and mam in **Figure 10**), but it does not seem plausible that a branch of the pc enters so far rostrally into the forebrain basal plate to finally reach the thalamus. A possibly satisfactory resolution of this semantic conundrum is that the "tubero-" root in the name possibly refers instead to the "posterior tuberculum," an old anatomic term used for what we now conceive as the thalamic (p2) tegmental region (e.g., see such use in Puelles et al., 1987). The course of the tth depicted by Ten Donkelaar (2011) would agree with the alternative name we propose—"*tuberculo-thalamic perforant artery*"—which would describe perfectly this vessel. We suggest that, unless strong evidence for a straightforward tuberal entrance of this vessel into basal terminal (premamillary) hypothalamus is available, or is newly found, its name should be changed to "*tuberculo-thalamic perforant artery*." Whether it is true (and not a myth based on a semantic error confusing "tubercular" with "tuberal") that parts of the tuberal and chiasmatic hypothalamus and of the prethalamus are served by the tth will need renewed research. We would not be surprised if the alar prethalamus is found to receive an analogous "tuberculo-prethalamic perforant artery," branching off directly from the pc or from the root of the tth.

The ic next produces another recurrent collateral branch, the *anterior chorioidal artery* (ach), normally originated shortly above the pc. The ach arises within the telencephalic region, since immediately it gives out "central" collaterals to pallidal and diagonal (i.e., innominate area) subpallial regions, and then follows in the subarachnoidal space the hemispheric sulcus (the classic tel-diencephalic border) until it reaches the roof-plate-related tip of the chorioidal fissure, where it dips into the telencephalic part of the lateral ventricle chorioid plexus (ach; chp; **Figures 8C**, **9**, **10**). Before the embryonic ach reaches its chorioid target, it produces a longitudinally descending (recurrent) diencephalic collateral that eventually reaches beyond the prethalamus (alar p3) the neighborhood of the lateral geniculate primordium in the thalamic (alar p2) lateral wall (ach; LG; p3, p2; **Figure 10**; Stewart, 1955). This implies that this recurrent branch of the ach enters the alar diencephalon following longitudinally the optic tract across the lateral surface of the prethalamus, in order to reach the lateral geniculate nucleus (LG) present at the primitive lateral surface of the thalamus proper (ach; p3; p2; LG; **Figure 10**; we showed in **Figure 9** the subsequent deformation of this lateral diencephalic wall carrying the LG). Various authors have affirmed that the ach participates at least partially in the vascularization of the LG and other neighboring superficial nuclei (e.g., Stewart, 1955; Salamon, 1971, 1973; Tatu et al., 1998, 2001; Tatu's relevant mappings are reproduced as Figures 2.7b, 2.8a,b, and 2.9a in Ten Donkelaar, 2011). Unfortunately, these sources do not mention whether the same recurrent branch of the ach also vascularizes *en passant* the neighboring prethalamic (ventral thalamic) retinorecipient centers (pregeniculate and subgeniculate nuclei), and/or more deeply the reticular nucleus, which lies next to the substantia innominata, as would be possible (see "Discussion" section). Additionally, Salamon (1971) states that the ach artery (actually its recurrent diencephalic branch) also serves part of the pes pedunculi, including the substantia nigra. Importantly for our topologic mapping, these two entities reside in the basal plate (**Figure 10**). Since the peduncle extends all the way from the hypothalamus into the pons (ped; **Figure 10**), and the substantia nigra is mes-diencephalic (Puelles et al., 2012b; Puelles, 2016), we interpret that Salamon (1971) probably referred to prethalamic and thalamic parts of the diencephalic tegmentum and associated parts of the substantia nigra (rather than more caudal pretectal and midbrain parts). These basal loci may be served by transverse collateral tegmental branches arising from the recurrent ach diencephalic branch as it courses caudalwards along the alar p3 and p2 territories. However, the objective evidence for these details is poor so far.

As represented in **Figure 10**, the *anterior chorioidal artery* is thus basically a telencephalic roofplate-targeting, dorsalward growing branch of the ic that courses dorsalward (transversally) along the interneuromeric hemispheric sulcus (hp1/p3 boundary). It finally participates in the temporal (telencephalic) part of the lateral ventricle chorioidal plexus. Somewhat surprisingly, it also turns out to give out a longitudinal recurrent diencephalic branch apparently serving superficial retinorecipient parts of prethalamus and thalamus (this branch has been illustrated by Padget, 1948 and Stewart, 1955). This strictly collateral vessel which advances in a wholly different direction (**Figure 10**) is routinely referred to also as the "anterior chorioidal artery," though its specific thalamic (and tegmental) target is not chorioidal at all, producing confusion in the reader (see "Discussion" section). It would be convenient to give this longitudinal vessel a distinctive name—perhaps "*recurrent thalamic artery*"—understanding it as a branch of the ach.

In the human brain the ach proper enters the uncal end of the chorioidal fissure found at the temporal (sphenoidal) tip of the lateral ventricle, and it serves the sphenoidal part of the lateral chorioidal plexus along its parafimbrial course (irrigating also adjoining subpallial elements such as the tail of the caudate nucleus and the amygdalar parts of the bed nucleus stria terminalis formation) until the telencephalic plexus meets close to the pulvinar the prethalamic part of the lateral chorioid plexus, served by the posterolateral chorioid artery (from the pcer system). These rather difficult chorioidal relationships are

repeatedly schematized in our **Figures 8C**, **9**, **10** as we presently understand them. The literature normally gives a simpler but less satisfying view of these details, because it disregards wholly the existence of the prethalamus, a diencephalic neuromere which unavoidably separates the telencephalon from the thalamus. The prethalamus has its own chorioidal roof plate domain, ampler than that of the thalamus/epithalamus, and this *must* enter into the picture (**Figures 8C**, **9**, **10**). As is variously illustrated in these schemata, we hold that the post-foraminal portion of the classical chorioidal fissure which seems attached to the thalamic chorioidal sulcus (next to the mythic lamina affixa) represents actually most of the prethalamic roof plate. Only the terminal portion of the fissural chorioid plexus found along the sphenoidal horn of the lateral ventricle is properly telencephalic (see also, Puelles, 2019; this book). This concept of a double prethalamo-telencephalic nature of the fissural roof plate tela is consistent with the existence of the repeatedly described separate plch and ach arterial peduncles of the two moieties of the chorioidal plexus of the lateral ventricle. Interestingly, Padget (1957) observed likewise two separate chorioidal veins collecting the respective efflux of these two chorioidal capillary plexus domains.

The internal carotid resolves in its two terminal branches, the anterior and middle cerebral arteries (mcer, acer; **Figures 8B**, **10**). These only need to ascend ventrodorsally in a strictly transversal topologic course within the evaginated telencephalic part of the hp1 neuromere (acer; mcer; hp1; **Figures 1**, **10**) into their respective central and superficial target areas. We applied a color code in **Figure 10** to delimit schematically the main flattened cortical arterial regions. We think it merits commenting that the mcer seems at first glance to cover only central parts of the hemisphere, but this region actually corresponds to the whole topologic anteroposterior extent, since once the human hemisphere adopts its characteristic inverted C-shape, the mcer field ranges from the frontal lobe at the front, passing through the insula and parietal lobe, to the retrocommissural upper temporal gyri, reaching also the temporal pole, the topological caudal end of the hemisphere (compare Ten Donkelaar, 2011; his Figure 2.5). The cortical areas at the convexity and those occupying the interhemispheric cortex, that is, the cortex lying closer to the septocommissural *roof plate*, are ascribed to the acer and the pcer, with the parieto-occipital fissure as approximate mutual boundary in the human brain. In their initial ascending course, both acer and mcer produce first deep "central branches" for the subpallium, where the recurrent artery of Heubner (acer) and numerous lenticulo-striate arteries (mcer) penetrate the anterior perforated space to serve *via* straightforward radial courses the striato-pallidal basal ganglia within. The schema suggests that the tail of the caudate and the temporal-lobe-related part of the bed nucleus striae terminalis, jointly with the centromedial (subpallial) amygdala, are served by the ach, as commented above, though a contribution from amygdalar branches of the pcer is not impossible.

The acer gives out the *anterior communicating artery* (ac; a rostrally oriented longitudinal vessel extending from a hp1 neighborhood into a hp2-related preoptic zone; ac; POA; **Figure 10**), as well as its orbital and frontopolar branches, and then immediately proceeds into a cingulate course (pericallosal and callosomarginal branches providing irrigation to the interhemispheric limbic, frontal and parietal lobes and the correlative convexity areas; acer; fpol; pcall; cmarg; **Figure 8C**). This main course lies parallel to the septocommissural plate (particularly the pericallosal branch), and this implies topologically a final *longitudinal* anteroposterior course inside the cortex, and next to the commissural roof plate, approaching final potential retrosplenial anastomoses with the parieto-occipital pcer branches (acer; pcer; **Figures 8B,C**, **10**).

DISCUSSION

The two parts of this report will be discussed in the following sections. The comments center on the spatiotemporal and topologic patterns observed, rather than on potential mechanisms, since we have not studied these. We'll limit speculative comments to a minimum.

Early Vascular Penetration Patterns in Mouse Embryos

Heterochronic Formation of the PNVP

Our data about the timing of PNVP formation in the mouse are roughly consistent with earlier literature cited in the Introduction, as well as with the human studies of Padget (1948) and Stewart (1955). A sizeable PNVP network was present as early as E8.5, and related selectively to alar plate territories of the whole forebrain (albeit only with partial covering of the telencephalic and eye vesicles). In the hindbrain, the PNVP covered the alar plate and a lateral part of the basal plate. The floor plate and the roof plate were distinctly devoid of this formation at this stage. The PNVP ventral boundary related to the molecularly-defined alar-basal border in the forebrain was quite distinct, and could be followed also into the paraneural mesoderm. The vascularly nude ventral neural and mesoderm domains relate topographically to the perichordal environment, which is reportedly rich in chorda-produced and diffused SHH morphogen. The notochord ends rostrally under the mamillary pouch (Puelles et al., 2012a; Puelles and Rubenstein, 2015). Midline SHH concentrations are sufficient to induce homeotically the *Shh* gene at the *floor and basal plate* of all forebrain regions (midbrain, diencephalon, hypothalamus; Martínez et al., 2012; Puelles, 2013), but only at the *floor plate* of the hindbrain. The similarity in the differential forebrain vs. hindbrain spatial SHH and vascularization pattern tempts us to conjecture that the observed early lack of ventral PNVP may be directly or indirectly related to local SHH effects inhibiting vascular sprouting in a given spatial range around the notochord.

It is known as well that the basal plate is the region that most precociously initiates neurogenesis, curtailing early its proliferative growth, whereas the alar plate is retarded in neurogenesis and shows protracted proliferative expansion (Puelles et al., 1987; review in Puelles, 2018). The predominant initial alar distribution of the PNVP thus suggests a relationship with actively proliferating zones of the brain wall with

scarce differentiation phenomena. Whether caused by a local notochordal blocking effect, or by a slowed proliferation (or both), the basal retardation is gradually resolved during the following days of gestation, apparently by reduction and physical separation of the notochord from the floor plate, and by parallel circumferential expansion of the primordial alar PNVP into the pial surface of the basal plate (and, ultimately, of the floor plate). In contrast, the paramedian mesoderm continues scarcely vascularized; at E10 and E11.5 the local cellularity has sharply decreased (cell death?), and ample spaces appear fluid-filled; this suggests incipient formation of the basal subarachnoid cisterns (see the cephalic flexure in **Figure 6D**, and similar images in **Figure 7**).

Heterochronic Formation of Penetrating Vessels (PVs)

The earliest forebrain PVs were already found at E8.5, that is, roughly as reported in the literature, but distantly from the lower medulla, which appears devoid of PVs at this stage. These E8.5 forebrain PVs were found at both sides of the dorsal di-mesencephalic border (DMB), identified by selective alar diencephalic *Pax6* expression (**Figures 2A,B**). Independently of the initial parallelism of PVs in the pretectum and in the neighboring rostralmost tectal plate, subsequent stages examined showed that PVs in this area rapidly proceeded to cover homogeneously the whole alar pretectum (in an apparent dorso-ventral gradient), but progressed less quickly at the dorsal midbrain. The dorsal tectal plate always showed a marked rostrocaudal decreasing gradient in the number of PVs. We think that this difference in pattern between alar pretectum and alar midbrain is due to the marked proliferative gradient known to occur rostrocaudally across the midbrain, due to reported mitogenic signaling from the isthmic organizer and caudal midbrain *Wnt1* expression (Puelles, 2013).

Why forebrain PVs should first form at the dorsal-most pretectal area and adjoining midbrain is difficult to explain without speculation. There is some amount of proliferative and neurogenetic precociousness associated to this site (the pretectum is the most precocious part of the diencephalon, i.e., is the first neuromere visualized in this area), but neurogenesis seems to start 1–2 days later, which seems to exclude this differentiative process as a causal determinant of the local PVs. This neural tube locus is also particular in developing at the local roof plate both a major commissure (the posterior commissure, which emerges quite early) and a secretory organ (the subcommissural organ), which secretes material into the ventricular fluid that forms the mysterious fiber of Reissner. It may be conjectured that the barely known molecular idiosyncrasy of this environment somehow triggers early sprouting of PVs.

In contrast with the precociously invaded alar pretectum, the alar thalamus remains nude of PVs until E11.5 (3 days later!), while the alar prethalamus displays earliest PVs at E9.5 and soon is profusely penetrated (similar to pretectum, but slightly later). There is accordingly a rostrocaudal gradient in the midbrain and no gradient at all in the diencephalon, whose three neuromeric units display independent heterochronic timetables, all of them apparently unrelated to neurogenetic patterns, since neurogenesis is delayed throughout the whole alar diencephalon (Puelles et al., 1987; Puelles, 2018).

Agreeing with earlier observations, hypothalamic PVs were first observed in the alar hypothalamus at E9.5, rostrally to those in the prethalamus, while the PNVP has not yet covered the hypothalamic basal plate. This alar site lies ventral to the optic stalk area. This points to the prospective subparaventricular area, where the anterior hypothalamic and suprachiasmatic nuclei develop (Puelles et al., 2012a). Separated by the non-vascularized optic stalk and eye vesicle (which only start to be invaded by PVs at E11.5), other more dorsal E9.5 PVs appeared at the preoptic region (telencephalic subpallium). POA is marked selectively by its ventricular expression of *Shh* (Bardet et al., 2010; Puelles et al., 2016), from where tangentially migrating neurons ulteriorly extend into adjacent diagonal and pallidal areas, but not into prospective striatum. Earlier work (e.g., Vasudevan et al., 2008) also identified earlier vascularization of the subpallium compared to the pallium but did not notice that the striatal anlage is relatively retarded within the subpallium. The pallium starts to be invaded by PVs at E11.5, 2 days later.

Our observations indicated a rapid appearance of PVs in the forebrain basal plate between E9.5 and E10. The m1 mesomere shows both basal and alar PVs at E10, as well as an incipient basal PVVP. In contrast, the thalamus still remains vascularly nude at E10. Incipient PVs were also observed at the dorsal part of the hypothalamic basal plate at E10. Dorsally to this locus, the alar hypothalamic areas, and the preoptic, diagonal and pallidal subpallial subdomains were already abundantly served by PVs at this stage, while the more dorsal pallial and striatal regions remained free of PVs in the telencephalon. A subpallial telencephalic PNVP network starts to be developed at about the same stage.

Insofar as there is already precocious *neurogenesis* in the forebrain basal plate at E10, it may be considered that the maturational change in the basal mantle layer may be causally related to the rather sudden retarded appearance of PVs throughout this forebrain longitudinal zone. This pattern also shows spatial correlation with the basal forebrain expression of *Shh* (**Figures 6D,F**), and no doubt with various other molecular markers typical of this longitudinal zone. Since we previously correlated high perichordal SHH levels (in the mesoderm) with *retardation* of initial basal PNVP formation, but now it seems that the SHH-rich area of the basal forebrain *abruptly develops* PVs, differential effects would be implied. An early *blocking* SHH effect on mesodermal *PNVP formation* may be functionally distinguishable from a *permissive* SHH effect 1.5 days later on intraneural *PV sprouting*. The tubero-mamillary basal hypothalamic area that secondarily downregulates by E10 its early *Shh* expression remarkably remains devoid of PVs (Tu; mam; Hy; **Figures 6F,G**).

The results obtained at E11.5 reveal a much more homogeneously advanced state of forebrain vascularization as regards the presence of both PVs and PVVP networks practically everywhere, with the exception of the most immature parts of the cortex. The thalamus nevertheless still maintains a relatively peculiar aspect, in displaying mainly PVVP formation, with scarce PVs. This suggests that perhaps PVs penetration

is barely starting at this stage, irrespective that a PVVP started earlier elsewhere may have started to expand tangentially into the thalamus (Th; **Figure 7B**). Such an extrinsic PVVP source of thalamic irrigation probably implies the underlying basal plate, given the correlative unique existence of a *tuberculo-thalamic perforant artery* (a pc branch; formerly probably misnamed as "tubero-thalamic"; see "Results" section) and an *inferior paramedian perforant thalamic artery* (a pcer branch). These singular vessels both penetrate vertically the thalamic basal plate (at the interpeduncular fossa) and then ascend through the periventricular stratum to irrigate alar plate periventricular thalamic derivatives (see **Figure 8C**). This basal + alar pattern is not seen anywhere else in the brain, with the possible exception of the prethalamic reticular nucleus (see above). A major periventricular part of the thalamus would thus be served directly *across the PVVP via* perforant arteries, while the topologically superficial rest of the thalamus would be covered by the thalamo-geniculate arteries and branches of the posteromedial chorioidal artery (pcer system) or the recurrent thalamic branch of the anterior chorioidal artery (ic system). The latter directly penetrate through superficial points the alar thalamus proper.

Observations on the telencephalon at E11.5 show a very significant change. The whole subpallium is now in the midst of massive neurogenesis, as shown particularly by the *Dlx5*-labeled lateral and medial ganglionic eminences (**Figure 7F**). PVs are now present also in the striatal subdomain (LGE), but in less number than at the Pall-Dg-POA subdomains (MGE), where the PVVP is also better developed (LGE; MGE; **Figure 7G**). A few PVs are also starting to invade the neighboring pallium, apparently independently from those entering the striatum. The pallial PVs appear dispersed spatially in a ventrodorsal gradient, probably influenced by the larger surface expansion rate of the more immature upper parts of the pallium. *Pax6*-reacted adjacent sections reveal a sharp gradient in the retarded development of the pallial mantle layer (pallium vs. LGE; **Figure 7H**). Blood vessels have not yet begun to invaginate the thin tela closing the local prethalamic chorioidal fissure to form an incipient chorioidal plexus (chf; **Figure 7G**).

Analysis of these forebrain results suggests that there is perhaps no simple explanation of the overall vascularization pattern. Alar plate vs. basal plate differences are clearcut and are shared with minor variations by all forebrain segments. This indicates that each one of these longitudinal zones obeys to particular rules as regards both PNVP and PVs formation. The most precocious *alar* PVs do not seem related topographically to sites characterized later by early neurogenesis. We already conjectured that basal PNVP and PV formation may be transiently blocked at early stages, due to direct or indirect chordal effects, or to local absence of VEGF-A. It may be further speculated that the primary cause of a heterochronic pattern of alar vascularization might reside in the emergence of unique regional (neuromeric) alar molecular profiles which modulate differentially not only the timing of intrinsic histogenetic progress within the alar neural wall (e.g., proliferation, neurogenesis and axonal navigation), but possibly also the type of vascular-attractive signal (or mixture of signals) being released. This primarily heterochronic and possibly chemically heterogeneous regional pattern would be diversely translated into different local amounts of VEGF-A or other signals at specific places and time-points, with eventual supra-threshold spiking that might elicit selective punctiform vascular responses (PVs) simultaneously at different places. Early molecular regionalization of the neural wall, plus additional modulating factors operating discretely at given ranges in the paraneural mesoderm (blocking early effect of SHH or other chordal signals), thus probably jointly impede a general wave of vascular penetration. Contrarily, molecular differential compartmentalization may restrict the highest capacity to trigger vascularization to discrete, spatially separated domains, which (each for different reasons) turn out to be relatively more favorable for vascular interactions, whereas other domains require more time to reach an equivalent status.

Another relevant factor causing heterogeneous vascular patterns may be represented at given sites by temporally heterogeneous formation of multiple disjoint PVVP fields, rather than a single all-encompassing PVVP wave, which was not observed in our material. The "outskirts" of these fields eventually may "violate" under appropriate circumstances some areal/zonal molecular boundaries, thus invading adjacent theoretically independent vascular domains. This might generate occasionally locally fused flux gradients between two or more neighboring histogenetic areas, allowing eventual formation of perforant periventricular arterial routes, as discussed above for the perforant thalamic vessels coursing periventricularly (*via* PVVPs; **Figure 8C**). In contrast, the short and long circumferential neuromeric arteries branching of from the basilar artery and reaching directly ventral and dorsal neuromeric parts of the hindbrain alar plate probably result from alternative condensation of blood flux *via* the perineural network (*via* PNVPs). Our data suggest anti-intuitively that the short mediobasal branches start to develop *later* than the correlative ventral and dorsal alar branches.

Topology of Adult Human Arteries Relative to the Prosomeric Map

In the three aspects discussed above (PNVP, PVs, PVVP), we corroborated the initial hypothesis that embryonic brain vascularization progresses spatially and temporally in heterochronic and non-gradiental coordination with the spatially patterned molecular regionalization (and consequent differential histogenesis) of the brain wall. Notably, this occurs consistently with the prosomeric model, and not with the columnar model. Discrimination was found both along the DV axis (e.g., roof/alar/basal/floor differences) and the AP axis (e.g., neuromeric differences within the alar plate; absence of intraneural longitudinal vessels). Earlier columnar descriptions and interpretations of this complex pattern turned out to be less discriminative and did not reach similar conclusions. This difference was expected, since the columnar model does not accept neuromeres, and misinterprets diencephalic and hypothalamic neuromeres as longitudinal columns, due to its arbitrary forebrain axis definition (see Puelles, 2018, 2019, this book). The only subdivision principle available to Herrick,

Kuhlenbeck and their followers was the column (theoretically thought to be *functionally* homogeneous—i.e., a column was held to subserve the same function along the whole brain, and therefore was not expected to show differential structural aspects along its length). The simplistic description by many columnar authors of a general wave of vascular invasion, thought to spread uniformly caudo-rostrally from a starting point at the lower medulla, probably was due to the poor capacity of their morphological paradigm to subdivide the hindbrain columns into smaller components (e.g., neuromeric units). As mentioned in the "Introduction" section, this unreal vascular wave propagation concept was paralleled by an equally simplistic propagation wave of neurogenesis postulated by other columnar authors up to the late 70s.

Subsequent neuromeric analysis, first without gene markers (e.g., Bergquist and Källén, 1954; Vaage, 1969; Puelles et al., 1987; review in Puelles, 2018), and later with them (e.g., Puelles and Rubenstein, 1993, 2003, 2015), demonstrated that overall proliferation or differentiation waves do not exist in the brain, due to the numerous interposed boundaries and the independent heterochronic behavior of small areal domains of the neural wall. We now know this is due to early transversal and longitudinal molecular patterning, which differentiates the neural wall into a checkboard pattern of well-delimited and molecularly diverse areas. Such compartments were first crudely recognized as "migration areas" by major neuromeric authors such as Bergquist and Källén (1954) or as "radial histogenetic units" (Puelles et al., 1987). These "fundamental morphogenetic units," as they are called modernly (Nieuwenhuys and Puelles, 2016), autonomously regulate in a heterochronic manner their ulterior histogenesis according to their own unique gene activation profiles. A number of ulterior developmental processes possibly including vascularization (but also tangential cell migration and axonal navigation) proceed by appropriate reactions of moving cells or cell processes to molecular signals written out differentially at individual histogenetic units, either in the epitopic decoration of the cell membrane of radial glia and ventricular cells, or with a variety of molecules attached to neuronal membranes and to the intercellular matrix, or, alternatively, as molecules diffused gradientally within the local intercellular fluid. Such direct or indirect cell-cell interactions frequently generate polarization of the growing elements in longitudinal or transverse directions, when the interacting elements follow chemical traces shared particularly by longitudinal rather than neuromeric (transverse) developmental units, or vice versa. Since the histogenetic processes that construct the brain largely occur in its lateral walls (the floor and roof plates being rather quiescent regions), the distinction within these walls of transverse neuromeres and longitudinal basal and alar zones is particularly relevant (**Figure 1A**). Of course, finer subdivisions are also distinguishable as development advances (e.g., microzones or progenitor domains; see Puelles, 2013), but we have not found necessary to examine them at our present preliminary level of topologic analysis of the vascular pattern.

In the second part of this report, we accordingly addressed adult vascular patterns, knowing well that adult blood vessels not always reflect in their topography the early embryonic relationships they originally had relative to the invaded organ. However, the detailed mapping studies reported by Padget (1948, 1957) and Stewart (1955) for arteries and veins in the human brain offer considerable help, even though these authors hardly commented in this context on developmental units in the brain primordium. Since we know the deformed prosomeric regionalization pattern of adult rodent brains, we found it was possible to attempt tentative ascription of well described adult blood vessels to specific alar or basal penetration points and inner distribution fields within given unitary developmental blocks (neuromeres) of the forebrain and hindbrain Bauplan, or to particular courses of the subarachnoid arteries relative to the chessboard-like pattern of primary transverse and longitudinal boundaries deduced to exist intrinsically in the neural wall. The literature on brain vascular supply readily suggests that the pattern of human subarachnoid arteries is reproducible and not chaotic (and the same applies to other vertebrates studied). Leaving apart statistically minor variations, a number of constant features can be detected, which can be mapped with a degree of certainty with regard to the relative invariant position (topology) within our prosomeric model.

Our expectation was to find evidence that vessels named conventionally "anterior, middle, or posterior this or that" in adult neuroanatomy actually relate significantly in their subarachnoid and intraneural course with the underlying longitudinal and transversal partitions of the brain wall (**Figure 1A**). There is, of course, a before and an after to consider as the artery first approaches along a particular route and then penetrates the wall at a given neuromeric basal or alar area (e.g., collateral branches need to be considered as separate problems). In our present first approximation, we did not represent in high detail the vascular distribution within particular superficial or deep terminal fields, but terminal branches were expected *a priori* to remain largely within a given neuromeric and alar or basal areal unit of the brain wall. Two sorts of exceptions were observed in this regard, perforating thalamic vessels, and some rhombomeric arteries jumping into the cerebellum; the thalamic recurrent branch of the ach also may be inconsistent with the general model.

Given the tridimensional complexity of the object of study, we elaborated various sorts of schemata ranging from more realistic to more abstract ones, expecting them to jointly clarify our interpretation. The semi-realistic ones visualize the *human* brain arteries as represented upon a prosomeric brain map adapted from the simpler but homologous mouse brain morphology (we selected the human arteries, which in some aspects differ from the mouse ones, because of their higher practical interest for clinical readers; the mouse or rat pattern also would have served our general purpose but would have been less interesting). A prosomeric schema adapted to the shape of the human brain also is possible, but posed difficulties at the present stage due to the extensive deformations of the human brain and our poorer experimental knowledge of the corresponding developmental fate maps. In the next two sections, we will comment on our mappings of basal and alar plate arteries, which in many cases can be readily distinguished, with some exceptions. Along these

sections, it will become apparent that restriction of most arteries to specific neuromeric territories is readily observable, with minimal exceptions to this rule.

Basal Plate Arteries

Throughout the brain, there is a numerous set of paramedian segmentally-restricted arteries that selectively supply the basal plate longitudinal zone, as defined by the prosomeric model (largely based on the old concept of His). We represented such basal plate arteries in our **Figure 8A**, consistently with the excellent sagittal injected photographic examples provided by Scremin and Holschneider (2012) and Scremin (2015) for rodents. Multiple paramedian basal branches are given out sequentially from the as, bas, pcer and pc vessels. These penetrate radially the basal zone in the topological transversal plane of the individual neuromeres (several branches per neuromere), as expected according to the observable incurvations of the brain axis, particularly at the cephalic flexure (see also mb; **Figures 1C,D**, **11**). According to the literature, at medullary levels these radially penetrating basal vessels can be subdivided into "paramedian" and "lateromedial" arteries arising at the as and ve arteries (Salamon, 1971, 1973; Lazorthes et al., 1976; Ten Donkelaar, 2011). The alternative terms "mediobasal" and "laterobasal" arteries would be more explicit about the appropriate embryological and topologic ascription (mb, lb; **Figure 1C**). This duplication probably owes to the existence in the medullary area of two options, so that the as and ve basal branches "share" the basal plate distribution field. Note that alar populations tangentially migrated into the basal plate apparently get supplied by the local vessels. Similarly, basal neurons migrated tangentially into the alar plate are likewise served by the local alar branches. This suggests that their respective spatial selectivity refers to the neuromeric unit and to its basal/alar subdivision, but does not involve specific chemical contact-mediated recognition of basal or alar neurons.

Analogous medial vessels serving the segmental units of the forebrain basal plate sort out of the rostral end of the basilar artery or the initial course of the posterior cerebral artery, as *posteromedial central arteries*, as well as from the posterior communicating artery, *posterolateral central arteries* (Ten Donkelaar, 2011; his Figure 2.10). These arteries penetrate through the posterior perforated space, which, according to the prosomeric model, is diencephalic and in part hypothalamic—retromamillary—rostrally to the oculomotor root. The standard (columnar) neuroanatomy textbook version wrongly ascribes this space entirely to the midbrain. These forebrain mediobasal arteries irrigate topologically equivalent basal or medial portions of the midbrain, diencephalon and hypothalamic neuromeric territories (m1, m2; p1-p3; hp1-hp2). The longitudinal continuity of such basal plate vessels through the midbrain and diencephalic tegmentum into at least the retromamillary basal hypothalamus (**Figure 11D**), and not beyond, represents a pattern that corroborates the original basal plate concept of His (1895, 1904), which is maintained in the prosomeric model. In contrast, this pattern contradicts the columnar conception of the basal plate, which threats the whole hypothalamus including the preoptic area as the basal plate of the overlying diencephalon, and conceives likewise a telencephalic basal plate (Swanson, 2012). There clearly are no further basal plate medial arteries beyond the mamillary area (see also Scremin, 2015; his **Figure 7**).

This basal plate region is always strongly bent ventrally at the cephalic flexure, which causes these topologically radial arterial branches entering successive neuromeres to fan out in the sagittal plane (**Figure 8A**; neuromeric color code as in **Figure 1A**). As commented above, exceptionally some of these medial basal arteries—like the tuberculo-thalamic perforant artery from the pc, and inferior thalamic perforant artery from the pcer—spread their terminal branches beyond the basal plate proper into the suprajacent alar neuromeric domains (p2; alar thalamus domain). It is unclear in the literature whether this perforant pattern, which we related above to a possible pathway created *via* the PVVP networks, is a local peculiarity of p2, or something non-exceptional for the forebrain. We need specific analysis of this point.

Alar Plate Arteries

Hindbrain

Individual or double alar plate arterial branches for each of the hindbrain neuromeres are given out by the vertebral and basilar arteries. These alar arteries are usually designated "short or long circumferential arteries," particularly when originating from the basilar artery. This name refers to their external dorsal course circumventing the basilar pontine gray or the olivary bulges of the basal medulla, before entering their alar targets. An alternative terminology sensitive to the alar topography of their penetration sites and terminal fields might be "ventral alar" and "dorsal alar" arteries. Some of the alar segmental branches are short and penetrate the ventral or liminar sector of the alar plate (close to the alar-basal border), whereas others are longer and invade more extensive dorsal parts of the hindbrain alar plate, eventually supplying as well chorioidal roof plate branches (mainly described for the cerebellar arteries). It should be noted that fate-mapping studies have shown that each rhombomere possesses its own band of chorioidal roof (e.g., Marín and Puelles, 1995); it might be expected, thus, that all segmental dorsal alar arteries give out a chorioidal branch at their end.

The sc, aic and pic cerebellar arteries are special cases of such alar branches, since, *after* having performed their alar segmental role, they invade the cerebellum, escaping the neuromeric rule [they originate at isthmic (or r0), r5 and r9 levels and jump from there into r1, the main cerebellar site]; it is unclear why a major cerebellar artery does not arise directly at r1 level. Apparently, no pic artery reaches the cerebellum in the mouse, where the corresponding r9 branch of the vertebral artery remains a standard dorsal alar branch (Scremin and Holschneider, 2012).

A collateral point that merits passing comment is that the ventral *alar* hindbrain domain that is served by the short circumferential "*ventral alar*" neuromeric arteries singularly includes in its mantle layer, apart the somatosensory/viscerosensory columns and associated lateral reticular formation, the *branchiomotor and visceromotor cranial*

nerve nuclei, as can be readily observed in the detailed schemata shown by Ten Donkelaar (2011) as his Figures 2.26c (motor trigeminal nucleus) and 2.27a–c (facial, ambiguus, dorsal vagus nuclei). This fact probably confused previous authors about the real position of the alar-basal boundary, and deterred them from realizing that these short circumferential arteries are selective *alar plate arteries*, similarly as anteromedian (mediobasal) and anterolateral (laterobasal) basilar segmental branches are typically *basal plate arteries*. In general, it can be noticed that neuroanatomic terminology for arteries does not use the concepts *alar* and *basal*, nor the descriptors *transversal* vs. *longitudinal*, which figure so prominently as objective patterns consistent with molecular genoarchitecture in our topologic prosomeric analysis of early steps in PNVP, PV and PVVP formation. The explanation for the cited mixing of basal visceromotor and branchiomotor brainstem nuclei with alar locations is known since the work of Ju et al. (2004). These originally basal-derived motor populations translocate their somata tangentially into the ventral part of the alar plate at intermediate developmental stages. This migratory process had already been visualized by various authors in the seventies and eighties (e.g., Windle, 1970), but had not been recognized as finishing inside the ventral or liminar alar plate. Ju et al. (2004) benefitted from a molecular delimitation of the alar-basal border to reach the correct conclusion. This result was recently corroborated in the mouse, using transgenic specific labeling of all alar-derived hindbrain neurons (Puelles et al., 2018; see this reference for a full review of this topic). There are comparative grounds to believe this is a general process in vertebrates, with few species variants (Nieuwenhuys and Puelles, 2016). Accordingly, the migratory interpretation can be extrapolated as well to the human brainstem. This represents a clearcut case where alar arterial branches serve basal neuronal populations that migrate into their alar plate territory.

Midbrain

There are also distinct arteries that penetrate directly the midbrain alar plate, though these data invariably refer to m1 (the rostral midbrain prosomere or mesomere), and we have no data at all about the recently recognized mesomere 2, whose alar domain is now known as "preisthmus" (an inconspicuous area lying caudal to the inferior colliculus, but rostral to the isthmic hindbrain; see reviews in Puelles et al., 2012; and Puelles, 2013, 2016). Some authors merely mention "mesencephalic" arteries, without further precisions about alar vs. basal distribution (e.g., Padget, 1948). The "quadrigeminal artery" described by Haines (1991, 1997) in the human brain clearly is an alar midbrain vessel (quad; **Figure 10**). It is probably identical with the "transverse collicular" artery cited as an early branch of the rodent pcer by Scremin (2015). This author mentions that its distribution ends at the brachium of the inferior colliculus and neighboring part of the inferior colliculus, which possibly indicates a *ventral alar* nature. On the other hand, multiple *dorsal alar* arteries penetrate radially both colliculi, originating in rodents from a "supracollicular plexus," probably derived also from the pcer, which apparently anastomoses with overlying cortical vascularization (Scremin, 2015). This would represent another violation of the rule restricting neuromeric branches to specific neuromeres. Some sources also mention collicular branches stemming from the superior cerebellar artery, which is topologically isthmic in its initial course (sc; **Figure 8B**); this also would violate the said rule.

Diencephalon

Irrespective of confusing aspects due to poor resolution in the literature of the diencephalic vascular complexity, comparison of the pcer system of vessels with the prosomeric model has led us to realize that, interpreted topologically, the pcer course after it emerges from the basilar artery cannot be really "posterior," as it seems at first glance. After passing rostral to the oculomotor nerve, the artery first moves transversally out of the floor plate-related median position of the basilar artery, to a position lateral to the pes pedunculi, roughly at the level of the pretectum (the mes-pretectal border lies just in front of the oculomotor nerve root; pcer; **Figure 8B**). This is possibly equivalent to a dorsoventral locus just above the alar-basal boundary, i.e., in a ventral part of the alar plate. This locus manifestly lies at the caudal part of the diencephalon, and from there the pcer necessarily must approach *longitudinally and rostralwards* the telencephalon (pcer; **Figures 1A**, **8B**, **9A–C**). To be able to approach the telencephalon, it must course successively along the lateral wall of the neuromeric pretectal, thalamic and prethalamic alar diencephalic regions, which undoubtedly lie rostral to the midbrain, and caudal to the telencephalic pallium (**Figures 1A**, **8B**). In its P2 segment, the pcer is thus essentially a longitudinally coursing alar forebrain vessel giving rise successively to alar branches to midbrain, pretectum, thalamus and prethalamus (**Figures 1A**, **8B**, **9A**). The existence in humans of multiple transverse alar diencephalic branches of the pcer is well documented (e.g., Salamon, 1971, 1973). The pcer also contributes doubly to the diencephalic chorioidal roof plate domain in its thalamic and prethalamic sectors (posteromedial and posterolateral choroid branches, respectively), but not to the telencephalic chorioidal sector, served by the anterior chorioidal artery (**Figures 8B,C**, **9A–D**, **10**).

We have thus realized that diencephalic alar vascularization relates importantly to the longitudinal diencephalic courses of: (1) the pcer, rostralward along its P2 segment; (2) the *recurrent thalamic artery* or rth (we propose this new term), caudalward from the ach (the rth is conventionally named also "ach," though this particular recurrent branch does not relate at all with chorioidal plexi); and (3) partly, to the pc and its perforant thalamic branches (**Figures 8B**, **9**, **10**). All three of these sources are in principle able to produce sequentially branches that enter separately the three diencephalic prosomeres (p1-p3; pretectum, thalamus, prethalamus). The pcer P2 segment and the rth branch of the ach course along the diencephalic alar plate, while the pc lies under the basal plate (pcer; rth; pc; **Figure 10**); the latter only reaches the thalamus and potentially other alar diencephalic domains—prethalamus, pretectum?—*via* perforant branches ingressed *via* the basal plate. Surprisingly, the longitudinal topology of these three sources of diencephalic branches had not been emphasized before in the relevant literature. Our **Figure 9** schemata aim to explain in

particular why the longitudinal pcer segment does not seem to be longitudinal in the adult.

Padget (1948, 1957) and Stewart (1955) mentioned "diencephalic" arteries and veins, but did not attend to possible neuromeres, and did not recognize either that these vessels were selective alar or perforant alar branches. This probably occurred because the columnar paradigm prevalent at the time understood the thalamus as a floating egg intercalated between striatum and midbrain, lacking any basal/tegmental correlate. The true diencephalic tegmentum (see **Figures 1A**, **8A**) was instead given over to the midbrain/hypothalamus pair, thought to be mutually continuous, thus causing long-standing erroneous beliefs about the midbrain nature of the whole interpeduncular fossa and of the whole substantia nigra and ventral tegmental area, both of which are plurisegmental and mesodiencephalic (Puelles et al., 2012b; Puelles, 2013, 2016, 2019 this book). Actually, the columnar thalamus initially contained dorsal and ventral moieties (Herrick, 1910; Kuhlenbeck, 1973), but many authors using the columnar paradigm thought it to be simpler to refer to the whole egg-shaped mass as an unit. This distorting view still emerges in modern sources such as the Allen Mouse Brain Atlas (adult version). The simplified egg-shaped mass compounding thalamic and prethalamic elements is the terrain whose vascularization has been actively investigated, to the exclusion of any other diencephalic portion (e.g., the work of Tatu et al., 1998, 2001 and others reproduced in Ten Donkelaar, 2011 includes the prethalamic reticular nucleus as a thalamic component). Thus, diencephalic vascularization became largely simplified to just "thalamic" vessels, with some weakly connected hypothalamic asides (because the columnar model expects the hypothalamus to be a basal and floor part of the diencephalon, a point that we already have shown the basal plate vessels do not corroborate). In conclusion, the subject of alar diencephalic vascularization merits a thorough reexamination consistent with the modern prosomeric approach, to clarify relevant details pertaining to its individualized pretectal, thalamic and prethalamic neuromeric territories, and clearly distinguish from them the separate and relatively more rostral alar hypothalamic territory, which needs an analysis connected instead with *telencephalic* vascularization (only very modestly attempted in our **Figure 10**, due to lack of precise data).

The alar vascularization of the pretectum is wholly undescribed so far. This is no doubt due to the Cinderella-like character it gained as a consequence of the columnar tradition to *not recognize* this territory as a straightforward neuromere distinct from the thalamus in front and the midbrain at the back (see contrary prosomeric evidence and discussion in Ferran et al., 2008; Puelles, 2013, 2016, 2018; Nieuwenhuys and Puelles, 2016). Columnar authors figuratively swept the pretectum under the carpet by arbitrarily dividing pretectal derivatives into caudal ones ascribed to the midbrain and rostral ones ascribed either to the epithalamus or to the dorsal thalamus. We have shown in the first part of our "Results" section that the mouse alar pretectum has a characteristically precocious early vascularization pattern that is independent from thalamus and midbrain. It seems thus reasonable to predict that some of the alar "thalamic" branches of the pcer actually are alar "pretectal" branches (symbolically represented by branches with a question sign in p1; **Figures 8B**, **9**, **10**). It is hoped that future research will cover this weak spot in vascular neuroanatomy. It would be of particular interest to know whether some of the pretectal basal plate arteries extend as "pretectal perforant" arteries into the overlying alar domain. Moreover, it may be expected that specific arterial branches so far undescribed serve the secretory subcommissural organ at the pretectal roof plate.

Recorded description of thalamic vascularization is in contrast quite advanced, having been systematized into five arterial pedicles worked out by several authors (Lazorthes et al., 1962, 1976; Plets et al., 1970; Percheron, 1976a,b, 1977; Tatu et al., 1998, 2001): (1) tubero-thalamic perforant artery from the pc; (2) inferior thalamic perforant from the pcer; (3) inferolateral thalamo-geniculate vessels from the pcer; (4) pulvinar branches from the plch artery of the pcer; and (5) geniculate branches from the ach (internal carotid). Of these, numbers 1 and 2 are perforant vessels that reach the alar thalamus *via* the underlying basal plate, presumably entering selectively through the p2 tegmentum (e.g., Salamon, 1971, his Figure 33; Haines, 1997; his Figure 14.14). We already advanced above the hypothesis that such extraordinary perforant courses (**Figure 8C**) may perhaps be explained by the observed peculiar retardation of PVs appearance in the thalamic alar field (practically none found still at E11.5), and the possible emergence of alternative PVVP pathways spreading into the thalamus from more precociously-formed basal plate PVVP in the same neuromere. We also reached the conclusion that the habitual descriptions of the tubero-thalamic artery as being related at its entry point to optic chiasma and tuberal or tubero-mamillary (or premamillary/mamillary) areas, and supposedly serving the mamillothalamic tract and the prethalamic reticular nucleus, seem inconsistent with all the drawings published of this artery, which consistently show it arising from the pc midway along its "diencephalic tegmental" course between the ic and the pcer. There is no inner logic, nor any actual evidence, as far as we can tell, for derivation of branches from this perforant artery under the thalamus into distant rostral hypothalamic areas (three neuromeres away; **Figure 10**). We think we may have here a semantic error due to faulty ascription of the "tubero-" root instead of the proper "tuberculo-" root to the name of this artery. As accepted by tradition, the "tubero-thalamic perforant" concept implies the assumption of a false premamillary general position and a false tuberal terminal field. It is on the other hand possible that analysis of the historic sources of this term may yet reveal that the original expression (perhaps in Latin?) was "tuberculo-thalamic perforant artery," referring to a different tuberosity. Indeed, in classic comparative neuroanatomic works what we now identify as thalamic and prethalamic tegmentum was referred to as "posterior tuberculum," meaning that it produced a bulge into the ventricular surface at the posterior end of the third ventricle. Our analysis therefore proposes a credible "*tuberculo-thalamic perforant artery*" in place of the doubtful "tubero-thalamic" notion. Other branches of the pc possibly

may supply the tuberal and tubero-mamillary basal plate regions, and a separate (and so far undescribed) perforant pc branch given at p3 level may serve the reticular nucleus and other alar prethalamic derivatives.

Numbers 3 and 4 among the thalamic pedicles cited above are direct alar arteries derived from the pcer P2 segment along its longitudinal course lounging the primitive alar diencephalic lateral surface. The thalamo-geniculate arteries may divide into external pretectal, thalamic and prethalamic branches, unless there exist completely separate pcer arteries for each of these alar diencephalic territories (**Figure 9**). Given that the posteromedial and posterolateral chorioidal arteries of the pcer finish at the roof plate and nearby hyperdorsal alar thalamic sites, such as the habenula and the associative thalamic nuclei (laterodorsal, lateral posterior, pulvinar), they may perhaps be considered to represent dorsal alar thalamic arteries, whereas the thalamo-geniculate arteries may represent ventral alar thalamic vessels, particularly if they also serve the topologically more ventral thalamic nuclei. The ventralmost thalamic nucleus is the medial geniculate body (Puelles, 2001). However, this division into ventral and dorsal alar vessels may be an unnecessary extrapolation into the diencephalon of brainstem patterns.

The issue of prethalamic vascularization is hardly covered at all by the literature so far (but Stewart, 1955 maps the "thalamic" chorioidal vessels relative to the well characterized ventral thalamus, zona limitans and dorsal thalamus, wrongly understanding them as columnar elements rather than as neuromeric ones). A distinct prethalamic part of the diencephalic wall placed *rostral* to the presumptive mammalian thalamus was already depicted by Ziehen (1906) and Bailey (1916), before Rendahl (1924) first defined the zona limitans boundary (see reviews in Puelles, 2018; and also Puelles, 2019; this book). The unfortunate prevalence of Herrick (1910) columnar model already in this period somehow dispersed any interest in that objective topologic relationship, which made diencephalic "columns" impossible (compare Swanson, 2012 "columnar" persistence in the negation of the zona limitans, against substantial recent molecular and experimental evidence). Present analysis is expected to stimulate researchers disposing of relevant material to re-examine it with the compressed and tridimensionally deformed prethalamic region in mind (**Figure 9**). Our present analysis of the marked morphogenetic deformation of the prethalamus (covered also in Puelles, 2019, this book) follows, corroborates and expands earlier classic examples, notably those of Schwalbe (1880) and Hochstetter (1895, 1898, 1919).

The present dearth of data on the prethalamic vascularization pattern may result clarified by pointing out that the posterolateral chorioidal artery (pcer system) seems essentially a prethalamic dorsal alar artery (consistently with data of Padget, 1948, 1957 and Stewart, 1955). Indeed, it targets the dorsalmost alar prethalamus (the prethalamic eminence) and the associated chorioidal plexus (the post-foraminal part of the lateral ventricle chorioidal formation; see Puelles, 2019, this book). Other prethalamic arteries may come from the inferolateral or thalamo-geniculate arteries (pcer system), as was suggested above, and/or from the anterior chorioidal artery (either *via* its *recurrent thalamic* branch, as it approaches the lateral geniculate body, or *via* its *subpallial collateral branches* to the internal pallidum and innominate area, which lie quite close to the reticular nucleus; Puelles, 2019, this book). Note in this latter regard that if we interpret at face value the dotted *central* territory of the ach in Figures 2.8, 2.9 of Ten Donkelaar (2011; extracted from Tatu et al., 1998, 2001; see also Lazorthes et al., 1962, 1976), this territory abuts directly the ovoid thalamus mass, precisely along its limit with the prethalamic reticular nucleus, which is thus implied to fall within the ach territory (perhaps unwittingly). At more dorsal section levels (such as Ten Donkelaar's correlative Figure 2.7) it is the mcer central distribution field in the *striatum* which abuts directly the thalamic ovoid (note it was wrongly believed in older times that the thalamus contacts the striate body), implying that the corresponding adjacent upper part of the prethalamic reticular nucleus might be served by the mcer *via* its lateral striate or pallidal branches. However, if we examine the relative positions of the mcer territory and the prethalamus in our **Figure 10**, it seems doubtful that a striatal mcer branch can reach the reticular nucleus, or the immediate vicinity of the thalamus. Such branches would have to cross the interposed pallidal and diagonal subpallial domains. It is more probable that Lazorthes et al. (1962, 1976), Percheron (1977), Tatu et al. (1998, 2001) and Ten Donkelaar (2011) may have unwittingly forgotten the intercalated prethalamic (i.e., ventral thalamic) position of the reticular nucleus (plus some other grisea), and been led astray by the old assumption that the striatum contacts directly the thalamus at the opto-striate sulcus, a postulate that is untenable nowadays (see Puelles, 2019, this book). In that case, we need a better informed corroboration of the exact relationship of the branches of the ach or mcer arteries with the prethalamic reticular nucleus and other prethalamic derivatives.

In addition, the literature stating that our *tuberculo-thalamic perforant artery* (the conventional tubero-thalamic artery; tth; **Figure 8D**) serves also the reticular nucleus (Tatu et al., 1998, 2001) suggests either collateral thalamo-prethalamic branches crossing the interthalamic zona limitans, or a parallel prethalamic perforant artery either from the posterior communicating artery, or from the root of the tth.

The plch artery and its corresponding fissural plexus portion (**Figures 8D**, **9**, **10**; see below) clearly seems related to the prethalamic taenia, which normally is not described in the adult brain (though embryos clearly show it; see Bailey, 1916; Puelles, 2019, this book). On the other hand, the anterior chorioidal artery, a direct and early developing branch of the internal carotid artery (Padget, 1948), serves the sphenoidal part of the same chorioidal plexus, irrigating also the tail of the caudate nucleus and the tail of the bed nucleus striae terminalis, among other targets (see below). Padget (1957) identifies separate veins for these two chorioidal masses of the lateral ventricle. This gives added weight to the argument affirming that the supracapsular fissural chorioidal sector whose apparent taenia lies along the thalamic chorioidal sulcus is actually prethalamic, while only the sphenoidal sector is fully telencephalic (according to the prosomeric model, there *must*

be a prethalamic chorioidal sector intercalated between the thalamic and telencephalic chorioidal formations; **Figure 10**). **Figures 9**, **10** further explain and complement our conclusions on these chorioidal arteries, together with the widely admitted notion that the posteromedial chorioidal artery, also a branch of the pcer, serves selectively the thalamic median chorioidal plexus of the third ventricle.

Secondary Prosencephalon

The present topologic analysis of the vascular pattern at the secondary prosencephalon is also mapped in **Figure 10**. The terminal branches of the ic—acer, mcer—are not problematic. We see the anterior communicating artery as a longitudinal alar vessel that contributes to serving the preoptic and overlying septal regions. The oph and sh arteries are also longitudinal vessels (alar and basal, respectively). The pc artery apparently contributes significantly to the basal hypothalamic field (Ten Donkelaar, 2011; Scremin, 2015), though this is somewhat at odds with Salamon (1973) thesis that the rostral part of the diencephalic tegmentum (substantia nigra and peduncle), lying caudal to the basal hypothalamus, is served by the ach (from the internal carotid). In general, one may conclude that the vascularization of the hypothalamus requires additional research within our present model.

ETHICS STATEMENT

All mouse experiments were approved by the ethical committee from the University of Murcia.

AUTHOR CONTRIBUTIONS

The work was planned by JF and LP. RM-M and PM-O carried out the experiments, with technical help from AA. All authors analyzed and discussed the data. LP, AV, and JF wrote the manuscript.

FUNDING

This work was funded by the Spanish Ministry of Economy and Competitiveness (Ministerio de Economía y Competitividad) grant BFU2014-57516P to LP and JF, PGC2018-098229-B-100 to JF, and the Séneca Foundation (Fundación Séneca) contract 19904/GERM/15 to LP.

ACKNOWLEDGMENTS

Infrastructure support provided by IMIB and the University of Murcia is also acknowledged.

REFERENCES

Albuixech-Crespo, B., López-Blanch, L., Burguera, D., Maeso, I., Sánchez-Arrones, L., Moreno-Bravo, J. A., et al. (2017). Molecular regionalization of the developing amphioxus neural tube challenges major partitions of the vertebrate brain. *PLoS Biol.* 15:e2001573. doi: 10.1371/journal.pbio.2001573

Bagnall, K., Higgins, S., and Sanders, E. (1989). The contribution made by cells from a single somite to tissues within a body segment and assessment of their integration with similar cells from adjacent segments. *Development* 107, 931–943.

Bailey, P. (1916). Morphology of the roof plate of the forebrain and the lateral choroid plexuses in the human embryo. *J. Comp. Neurol.* 26, 79–120. doi: 10.1002/cne.900260104

Bär, T., and Wolff, J. (1972). The formation of capillary basement membranes during internal vascularization of the rat's cerebral cortex. *Z. Zellforsch. Mikrosk. Anat.* 133, 231–248. doi: 10.1007/bf00307145

Bardet, S. M., Ferran, J. L., Sanchez-Arrones, L., and Puelles, L. (2010). Ontogenetic expression of sonic hedgehog in the chicken subpallium. *Front. Neuroanat.* 4:28. doi: 10.3389/fnana.2010.00028

Bergquist, H., and Källén, B. (1954). Notes on the early histogenesis and morphogenesis of the Central Nervous System in vertebrates. *J. Comp. Neurol.* 100, 627–659. doi: 10.1002/cne.901000308

Cobos, I., Shimamura, K., Rubenstein, J. L. R., Martínez, S., and Puelles, L. (2001). Fate map of the avian anterior forebrain at the four-somite stage, based on the analysis of quail-chick chimeras. *Dev. Biol.* 239, 46–67. doi: 10.1006/dbio.2001.0423

Coultas, L., Chawengsaksophak, K., and Rossant, J. (2005). Endothelial cells and VEGF in vascular development. *Nature* 438, 937–945. doi: 10.1038/nature04479

Couly, G., Coltey, P., Eichmann, A., and Le Douarin, N. M. (1995). The angiogenic potentials of the cephalic mesoderm and the origin of brain and head blood vessels. *Mech. Dev.* 53, 97–112. doi: 10.1016/0925-4773(95)00428-9

Craigie, E. H. (1955). "Vascular patterns of the developing nervous system," in *Biochemistry of the Developing Nervous System*, ed. H. Waelsch (New York, NY: Academic Press), 28–49.

Daneman, R., Agalliu, D., Zhou, L., Kuhnert, F., Kuo, C. J., and Barres, B. A. (2009). Wnt/β-catenin signaling is required for CNS, but not non-CNS, angiogenesis. *Proc. Nat. Acad. Sci. U S A* 106, 641–646. doi: 10.1073/pnas.08051 65106

Duvernoy, H. M. (1999). *Human Brain Stem Vessels.* 2nd Edn. Berlin, Heidelberg, New York: Springer.

Evans, H. M. (1909). On the development of the aortae, cardinal and umbilical veins and the other blood vessels of vertebrate embryos from capillaries. *Anat. Rec.* 3, 498–518. doi: 10.1002/ar.1090030903

Fantin, A., Vieira, J. M., Gestri, G., Denti, L., Schwarz, Q., Prykhozhij, S., et al. (2010). Tissue macrophages act as cellular chaperones for vascular anastomosis downstream of VEGF-mediated endothelial tip cell induction. *Blood* 116, 829–840. doi: 10.1182/blood-2009-12-257832

Ferran, J. L., Ayad, A., Merchan, P., Morales-Delgado, N., Sánchez-Arrones, L., Alonso, A., et al. (2015a). "Exploring brain genoarchitecture by single and double chromogenic in situ hybridization (ISH) and immunohistochemistry (IHC) in whole-mount embryos," in *in situ Hybridization Methods, Neuromethods*, (Vol. 99) ed. G. Hauptmann (New York, NY: Springer Science), 61–82.

Ferran, J. L., Ayad, A., Merchan, P., Morales-Delgado, N., Sánchez-Arrones, L., Alonso, A., et al. (2015b). "Exploring brain genoarchitecture by single and double chromogenic in situ hybridization (ISH) and immunohistochemistry (IHC) on cryostat, paraffin, or floating sections," in *in situ Hybridization Methods, Neuromethods*, (Vol 99) ed. G. Hauptmann (New York, NY: Springer Science), 83–107.

Ferran, J. L., Puelles, L., and Rubenstein, J. L. R. (2015c). Molecular codes defining rostrocaudal domains in the embryonic mouse hypothalamus. *Front. Neuroanat.* 9:46. doi: 10.3389/fnana.2015.00046

Ferran, J. L., Sánchez-Arrones, L., Bardet, S. M., Sandoval, J. E., Martínez-de-la-Torre, M., and Puelles, L. (2008). Early pretectal gene expression pattern shows a conserved anteroposterior tripartition in mouse and chicken. *Brain Res. Bull.* 75, 295–298. doi: 10.1016/j.brainresbull.2007.10.039

Ferran, J. L., Sánchez-Arrones, L., Sandoval, J. E., and Puelles, L. (2007). A model of early molecular regionalization in the chicken embryonic pretectum. *J. Comp. Neurol.* 505, 379–403. doi: 10.1002/cne.21493

Fish, J. E., and Wythe, J. D. (2015). The molecular regulation of arteriovenous specification and maintenance. *Dev. Dynam.* 244, 391–409. doi: 10.1002/dvdy.24252

Flames, N., Pla, R., Gelman, D. M., Rubenstein, J. L. R., Puelles, L., and Marín, O. (2007). Delineation of multiple subpallial progenitor domains by the combinatorial expression of transcriptional codes. *J. Neurosci.* 27, 9682–9695. doi: 10.1523/JNEUROSCI.2750-07.2007

García-López, R., Pombero, A., and Martínez, S. (2009). Fate map of the chick embryo neural tube. *Dev. Growth. Differ.* 51, 145–165. doi: 10.1111/j.1440-169x.2009.01096.x

García-López, R., Vieira, C., Echevarria, D., and Martínez, S. (2004). Fate map of the diencephalon and the zona limitans at the 10-somites stage in chick embryos. *Dev. Biol.* 268, 514–530. doi: 10.1016/j.ydbio.2003.12.038

Haines, D. E. (1991). *Neuroanatomy. An Atlas of Structures, Sections and Systems.* 3rd edn. Baltimore, Munich: Urban and Schwarzenberg.

Haines, D. E. (1997). "A survey of the cerebrovascular system," in *Fundamental Neuroscience*, ed. D. E. Haines (New York, NY: Churchill-Livingstone), 113–128.

Herrick, C. J. (1910). The morphology of the forebrain in amphibia and reptilia. *J. Comp. Neurol.* 20, 413–547. doi: 10.1002/cne.920200502

Herzog, Y., Kalcheim, C., Kahane, N., Reshef, R., and Neufeld, G. (2001). Differential expression of neuropilin-1 and neuropilin-2 in arteries and veins. *Mech. Dev.* 109, 115–119. doi: 10.1016/s0925-4773(01)00518-4

His, W. (1895). Die anatomische nomenclatur. *Nomina Anatomica. Arch. Anat. Entwicklungsges.* 1895, 1–180.

His, W. (1904). *Die Entwicklung des Menschlichen Gehirns Während der Ersten Monate.* Leipzig: Hirzel.

Hochstetter, F. (1895). Über die Beziehung des Thalamus opticus zum Seitenventrikel der Grosshirnhemispheren. *Anat. Anz.* 10, 295–302.

Hochstetter, F. (1898). "Beiträge zur Entwicklungsgeschichte des Gehirns," in *Bibliotheca Medica. Abtheilung Anatomie*, (Vol. 2) eds G. Born and A. Heft (Stuttgart: Erwin Nägele), 1–26.

Hochstetter, F. (1919). *Beiträge zur Entwicklungsgeschichte des Menschlichen Gehirns. I. Teil.* Wien/Leipzig: Franz Deuticke.

Hogan, K. A., Ambler, C. A., Chapman, D. L., and Bautch, V. L. (2004). The neural tube patterns vessels developmentally using the VEGF signaling pathway. *Development* 131, 1503–1513. doi: 10.1242/dev.01039

James, J. M., and Mukouyama, Y. (2011). Neuronal action on the developing blood vessel pattern. *Semin. Cell Dev. Biol.* 22, 1019–1027. doi: 10.1016/j.semcdb.2011.09.010

Ju, M. J., Aroca, P., Luo, J., Puelles, L., and Redies, C. (2004). Molecular profiling indicates avian branchiomotor nuclei invade the hindbrain alar plate. *Neuroscience* 128, 785–796. doi: 10.1016/j.neuroscience.2004.06.063

Koch, S., Tugues, S., Li, X., Gualandi, L., and Claesson-Welsh, L. (2011). Signal transduction by vascular endothelial growth factor receptors. *Biochem. J.* 437, 169–183. doi: 10.1042/BJ20110301

Kuhlenbeck, H. (1973). *The Central Nervous System of Vertebrates. 3, Part II: Overall Morphological Pattern.* Basel: Karger.

Kurz, H., Gärtner, T., Eggli, P. S., and Christ, B. (1996). First blood vessels in the avian neural tube are formed by a combination of dorsal angioblast immigration and ventral sprouting of endothelial cells. *Dev. Biol.* 173, 133–147. doi: 10.1006/dbio.1996.0012

Lazorthes, G., Gouazé, A., and Salamon, G. (1976). *Vascularisation et Circulation de L'Encéphale.* Paris: Masson.

Lazorthes, G., Poulhes, J., Bastide, G., Gaubert, J., Roulleau, J., and Amaral-Gomes, F. (1962). Les territoires artériels du névraxe. l'angio-architectonie artérielle de l'écorce cérébrale. *Bull. Assoc. Anat.* 158, 1–27.

Ma, S., Kwon, H. J., Johng, H., Zang, K., and Huang, Z. (2013). Radial glial neural progenitors regulate nascent brain vascular network stabilization via inhibition of Wnt signaling. *PLoS Biol.* 11:e1001469. doi: 10.1371/journal.pbio.1001469

Marín, F., and Puelles, L. (1995). Morphological fate of rhombomeres in quail/chick chimeras: a segmental analysis of hindbrain nuclei. *Eur. J. Neurosci.* 7, 1714–1738. doi: 10.1111/j.1460-9568.1995.tb00693.x

Marín-Padilla, M. (1987). "Embryology," in *Microneurosurgery Vol IIIA: AVM of the Brain—History, Embryology, Pathological Considerations, Hemodynamics, Diagnostic Studies, Microsurgical Anatomy*, ed. M. G. Yasargil (Stuttgart: Georg Thieme), 23–45.

Marín-Padilla, M. (2012). The human brain intracerebral microvascular system: development and structure. *Front. Neuroanat.* 6:38. doi: 10.3389/fnana.2012.00038

Martínez, S., Puelles, E., Puelles, L., and Echevarria, D. (2012). "Molecular regionalization of the developing neural tube," in *The Mouse Nervous System*, eds C. Watson, G. Paxinos and L. Puelles (London: Academic Press), 2–18.

Morales-Delgado, N., Merchan, P., Bardet, S. M., Ferrán, J. L., Puelles, L., and Díaz, C. (2011). Topography of somatostatin gene expression relative to molecular progenitor domains during ontogeny of the mouse hypothalamus. *Front. Neuroanat.* 5:10. doi: 10.3389/fnana.2011.00010

Naidich, T. P., Duvernoy, H. M., Delman, B. N., Sorensen, A. G., Kollias, S. S., and Haacke, E. M. (2009). *Radiology.* Wien, New York, NY: Springer.

Nieuwenhuys, R., and Puelles, L. (2016). *Towards A New Neuromorphology.* Berlin: Springer.

Padget, D. H. (1948). The development of the cranial arteries in the human embryo. Carnegie Inst. Wash. Pub. 575. *Contrib. Embryol.* 32, 205–261.

Padget, D. H. (1957). The development of the cranial venous system in man, from the viewpoint of comparative anatomy. Carnegie Inst. Wash. Pub. 611. *Contrib. Embryol.* 36, 79–140.

Percheron, G. (1976a). Les artères du thalamus humain I. Artères et territoires thalamiques polaires de l'artère communicante postérieure. *Rev. Neurol.* 132, 297–307.

Percheron, G. (1976b). Les artères du thalamus humain II. Artères et territoires thalamiques paramédians de l'artère basilaire communicante. *Rev. Neurol.* 132, 309–324.

Percheron, G. (1977). Les artères du thalamus humain. Les artères choroïdiennes. *Rev. Neurol.* 133, 533–545, 547–558.

Plets, C., De Reuck, J., Vander Eecken, H., and Van den Bergh, R. (1970). The vascularization of the human thalamus. *Acta Neurol. Belg.* 70, 687–770.

Pombero, A., and Martínez, S. (2009). Telencephalic morphogenesis during the process of neurulation: an experimental study using quail-chick chimeras. *J. Comp. Neurol.* 512, 784–797. doi: 10.1002/cne.21933

Puelles, L. (2001). Thoughts on the development, structure and evolution of the mammalian and avian telencephalic pallium. *Philos. Trans. R. Soc. Lond. B Biol. Sci.* 356, 1583–1598. doi: 10.1098/rstb.2001.0973

Puelles, L. (2013). "Plan of the developing vertebrate nervous system (prosomere model, overview of brain organization)," in *Comprehensive Developmental Neuroscience*, (Vol. 3), eds J. L. R. Rubenstein and P. Rakic (Amsterdam: Academic Press), 187–209.

Puelles, L. (2014). "Development and evolution of the claustrum, Chapter 5," in *Functional Neuroanatomy of the Claustrum*, eds J. Smythies, V. S. Ramachandran and L. Edelstein (New York, NY: Academic Press), 119–176.

Puelles, L. (2016). Comments on the limits and internal structure of the mammalian midbrain. *Anatomy* 10, 60–70. doi: 10.2399/ana.15.045

Puelles, L. (2018). Developmental studies of avian brain organization. *Int. J. Devel. Biol.* 62, 207–224. doi: 10.1387/ijdb.170279LP

Puelles, L. (2019). Survey of midbrain, diencephalon and hypothalamus neuroanatomic terms whose prosomeric definition conflicts with columnar tradition. *Front. Neuroanat.* 13:20. doi: 10.3389/fnana.2019.00020

Puelles, L., Amat, J. A., and Martínez-de-la-Torre, M. (1987). Segment-related, mosaic neurogenetic pattern in the forebrain and mesencephalon of early chick embryos: I. Topography of AChE-positive neuroblasts up to stage HH18. *J. Comp. Neurol.* 266, 247–268. doi: 10.1002/cne.902660210

Puelles, L., and Ferran, J. L. (2012). Concept of neural genoarchitecture and its genomic fundament. *Front. Neuroanat.* 6:47. doi: 10.3389/fnana.2012.00047

Puelles, L., Harrison, M., Paxinos, G., and Watson, C. (2013). A developmental ontology for the mammalian brain based on the prosomeric model. *Trends Neurosci.* 36, 570–578. doi: 10.1016/j.tins.2013.06.004

Puelles, L., Kuwana, E., Puelles, E., Bulfone, A., Shimamura, K., Keleher, J., et al. (2000). Pallial and subpallial derivatives in the embryonic chick and mouse telencephalon traced by the expression of the genes Dlx-2, Emx-1, Nkx-2.1, Pax-6, and Tbr-1. *J. Comp. Neurol.* 424, 409–438. doi: 10.1002/1096-9861(20000828)424:3<409::AID-CNE3>3.0.CO;2-7

Puelles, E., Martinez-de-la-Torre, M., Watson, C., and Puelles, L. (2012). "Midbrain," in *The Mouse Nervous System*, eds C. Watson, G. Paxinos and L. Puelles (London; San Diego, CA: Academic Press/Elsevier), 337–359.

Puelles, L., Martínez-de-la-Torre, M., Bardet, S., and Rubenstein, J. L. R. (2012a). "Hypothalamus," in *The Mouse Nervous System*, eds C. Watson, G. Paxinos and L. Puelles (London; San Diego, CA: Academic Press/Elsevier), 221–312.

Puelles, L., Watson, C., Martínez-de-la-Torre, M., and Ferran, J. L. (2012b). "Diencephalon," in *The Mouse Nervous System*, eds C. Watson, G. Paxinos, and L. Puelles (London; San Diego, CA: Academic Press/Elsevier), 313–336.

Puelles, L., Morales-Delgado, N., Merchan, P., Castro-Robles, B., Martínez-de-la-Torre, M., Díaz, C., et al. (2016). Radial and tangential migration of telencephalic somatostatin neurons originated from the mouse diagonal area. *Brain Struct. Funct.* 221, 3027–3065. doi: 10.1007/s00429-015-1086-8

Puelles, L., Alonso, A., García-Calero, E., and Martínez-de-la-Torre, M. (2019). Concentric ring topology of mammalian cortical sectors and relevance for patterning studies. *J. Comp. Neurol.* 527, 1731–1752. doi: 10.1002/cne.24650

Puelles, L., and Rubenstein, J. L. R. (1993). Expression patterns of homeobox and other putative regulatory genes in the embryonic mouse forebrain suggest a neuromeric organization. *Trends Neurosci.* 16, 472–479. doi: 10.1016/0166-2236(93)90080-6

Puelles, L., and Rubenstein, J. L. R. (2003). Forebrain gene expression domains and the evolving prosomeric model. *Trends Neurosci.* 26, 469–476. doi: 10.1016/S0166-2236(03)00234-0

Puelles, L., and Rubenstein, J. L. R. (2015). A new scenario of hypothalamic organization: rationale of new hypotheses introduced in the updated prosomeric model. *Front. Neuroanat.* 9:27. doi: 10.3389/fnana.2015.00027

Puelles, L., Tvrdik, P., and Martínez-de-la-Torre, M. (2018). The postmigratory alar topography of visceral cranial nerve efferents challenges the classical model of hindbrain columns. *Anat. Rec.* 302, 485–504. doi: 10.1002/ar.23830

Rendahl, H. (1924). Embryologische und morphologische Studien über das Zwischenhirn beim Huhn. *Acta. Zool.* 5, 241–344. doi: 10.1111/j.1463-6395.1924.tb00169.x

Ruhrberg, C., and Bautch, V. L. (2013). Neurovascular development and links to disease. *Cell. Mol. Life Sci.* 70, 1675–1684. doi: 10.1007/s00018-013-1277-5

Salamon, G. (1971). *Atlas de la Vascularization Arterielle du Cerveau chez l'Homme.* Paris: Sandoz Editions.

Salamon, G. (1973). *Atlas of the Arteries of the Human Brain.* 2nd edn. Paris: Asclepios.

Santhosh, D., and Huang, Z. (2015). Regulation of the nascent brain vascular network by neural progenitors. *Mech. Dev.* 138, 37–42. doi: 10.1016/j.mod.2015.06.005

Schwalbe, G. (1880). Beiträge zur Entwicklungsgeschichte des Zwischenhirns, Sitz. *Ber. Gen. Ges. Med. Naturwiss* 20, 2–7.

Scremin, O. U. (2015). "Cerebral vascular system," in *e Rat Nervous System*, 4th Edn. ed. G. Paxinos (New York, NY: Academic Press), 985–1011.

Scremin, O. U., and Holschneider, D. P. (2012). "Vascular supply," in *The Mouse Nervous System*, eds C. Watson, G. Paxinos and L. Puelles (London: Elsevier), 459–472.

Stenman, J. M., Rajagopal, J., Carroll, T. J., Ishibashi, M., McMahon, J., and McMahon, A. P. (2008). Canonical Wnt signaling regulates organ-specific assembly and differentiation of CNS vasculature. *Science* 322, 1247–1250. doi: 10.1126/science.1164594

Stewart, G. G. (1955). *The Development of the Blood Supply to the Human Embryo Basal Ganglia.* Canada: University of Alberta. Doctoral Thesis.

Swanson, L. W. (2012). *Brain Architecture.* 2nd Edn. Oxford; New York, NY: Oxford University Press.

Swift, M. R., and Weinstein, B. M. (2009). Arterial-venous specification during development. *Circ. Res.* 104, 576–588. doi: 10.1161/CIRCRESAHA.108.188805

Tata, M., Ruhrberg, C., and Fantin, A. (2015). Vascularisation of the central nervous system. *Mech. Dev.* 138, 26–36. doi: 10.1016/j.mod.2015.07.001

Tatu, L., Moulin, T., Bogousslavsky, J., and Duvernoy, H. (1998). Arterial territories of the human brain: cerebral hemispheres. *Neurology* 50, 1699–1708. doi: 10.1212/wnl.50.6.1699

Tatu, L., Moulin, T., Bogousslavsky, J., and Duvernoy, H. (2001). "Arterial territories of human brain," in *Stroke Syndromes*, eds J. Bogousslavsky and L. R. Caplan (Cambridge, MA: Cambridge University Press), 375–404.

Ten Donkelaar, H. J. (2011). *Clinical Neuroanatomy. Brain Circuitry and Its Disorders.* Berlin: Springer.

Theiler, K. (1989). *The House Mouse. Atlas of Embryonic Development.* 2nd Edn. New York, NY, Berlin, Heidelberg: Springer.

Vaage, S. (1969). The segmentation of the primitive neural tube in chick embryos (Gallus domesticus). A morphological, histochemical and autoradiographical investigation. *Ergeb. Anat. Entwicklungsgesch.* 41, 3–87.

Valavanis, A. (2003). "New techniques and results in treatment of vascular malformations," in *ASNR 97–99. Presented at the 41st Annual Meeting of the American Society of Neuroradiology*, Washington, DC.

Vasudevan, A., Long, J. E., Crandall, J. E., Rubenstein, J. L. R., and Bhide, P. G. (2008). Compartment-specific transcription factors orchestrate angiogenesis gradients in the embryonic brain. *Nat. Neurosci.* 11, 429–439. doi: 10.1038/nn2074

Watson, C., and Puelles, L. (2017). Developmental gene expression in the mouse clarifies the organization of the claustrum and related endopiriform nuclei. *J. Comp. Neurol.* 525, 1499–1508. doi: 10.1002/cne.24034

Watson, C., Bartholomaeus, C., and Puelles, L. (2019). Time for radical changes in brain stem nomenclature – applying the lessons from developmental gene patterns. *Front. Neuroanat.* 13:10. doi: 10.3389/fnana.2019.00010

Windle, W. F. (1970). Development of neural elements in human embryos of four to seven weeks gestation. *Exp. Neurol.* 5, 44–83.

Ziehen, T. (1906). "Die morphogenie des zentralnervensystems der säugetiere," in *Handbuch der Vergleichenden und Experimentellen Entwicklungslehre der Wirbeltiere*, (Vol. 2, Part 4) ed. O. Hertwig (Jena: Fischer), 273–368.

Conflict of Interest Statement: The authors declare that the research was conducted in the absence of any commercial or financial relationships that could be construed as a potential conflict of interest.

Copyright © 2019 Puelles, Martínez-Marin, Melgarejo-Otalora, Ayad, Valavanis and Ferran. This is an open-access article distributed under the terms of the Creative Commons Attribution License (CC BY). The use, distribution or reproduction in other forums is permitted, provided the original author(s) and the copyright owner(s) are credited and that the original publication in this journal is cited, in accordance with accepted academic practice. No use, distribution or reproduction is permitted which does not comply with these terms.

GLOSSARY

A	amygdala
A1	anterior cerebral artery segment 1
A2	anterior cerebral artery segment 2
ABB	alar-basal boundary
ac	anterior communicating artery
acer	anterior cerebral artery
ach	anterior chorioidal artery
aco	anterior commissure
AH	adenohypophysis
aic	anteroinferior cerebellar artery
AP	anteroposterior axis or dimension
ap	alar plate
ATHy	acroterminal hypothalamus
Atd	acroterminal domain
as	anterior spinal artery
bas	basilar artery
calc	calcarine artery
Cb	cerebellum
cc	corpus callosum
chp	chorioidal plexus
chf	chorioidal fissure
cmarg	callosomarginal artery
CoP	commissural pretectum
bp	basal plate
da	dorsoalar artery
dbc	decussation of brachium conjunctivum
Dg	diagonal domain
DMB	diencephalo-mesencephalic boundary
DTu	dorsal tuberal region
DV	dorsoventral axis or dimension
EP	eye primordium
F	frontal lobe
fcht	fissural chorioidal tela
fp	floor plate
fpol	frontopolar artery
Hb	Hindbrain
hc	hippocampal commissure
Hy	hypothalamus
hp1	hypothalamo-telencephalic prosomere 1
hp2	hypothalamo-telencephalic prosomere 2
ic	internal carotid artery
if	interventricular foramen
Isth	Isthmus
IC	inferior colliculus
Ins	insular lobe
JcP	juxtacommissural pretectum
lb	laterobasal artery
LG	lateral geniculate body
LGE	lateral ganglionic eminence
LP	lens placode
m1	mesomere 1
m2	mesomere 2
mam	mamillary body
mb	mediobasal artery
mb	mediobasal branches P1 segment posterior cerebral artery
Mb	midbrain
mcer	medial cerebral artery
MGE	medial ganglionic eminence
NH	neurohypophysis
OC	optic cup
on	optic nerve
OP	olfactory placode
oph	ophthalmic artery
orb	orbitofrontal artery
OS	optic stalk
ot	optic tract
OV	optic vesicle
P	parietal lobe
p	pons
p1	prosomere 1
p2	prosomere 2
p3	prosomere 3
P1	posterior cerebral artery segment 1
P2	posterior cerebral artery segment 2
P3	posterior cerebral artery segment 3
P4	posterior cerebral artery segment 4
Pall	pallidum
pao	parieto-occipital artery
pc	posterior communicating artery
pcer	posterior cerebral artery
PcP	precommissural pretectum
pec	pericallosal artery
ped	peduncle
PHy	peduncular hypothalamus
Pi	pineal gland
pic	posterior inferior cerebellar artery
plch	posterolateral chorioidal artery
pmch	posteromedial chorioidal artery
POA	preoptic area
PT	pretectum
PTh	prethalamus
pthchf	prethalamic chorioidal fissure
PNVP	perineural vascular plexus
PV	perforant vessels
PVVP	periventricular vascular plexus
quad	quadrigeminal artery
r0	rhombomere 0
r1	rhombomere 1
r2	rhombomere 2
r3	rhombomere 3
r4	rhombomere 4
r5	rhombomere 5
r6	rhombomere 6
r7	rhombomere 7
r8	rhombomere 8
r9	rhombomere 9
r10	rhombomere 10
r11	rhombomere 11
Rh	rhombencephalon
rh-chp	rhombencephalic chorioidal plexus
rm	retromamillary region
rp	roof plate
rth	recurrent thalamic artery
SC	superior colliculus
sc	superior cerebellar artery
sco	supracollicular arterial network
SCor	spinal cord
Se	septum
sh	superior hypophyseal artery
SP	subpallium
St	striatum
tchf	telencephalic chorioidal fissure
Tel	telencephalon
temp	temporal artery
tgd	midbrain dorsal tegmental decussation
Th	thalamus
th-chp	thalamic chorioidal plexus
thg	thalamo-geniculate artery
Tu	tuberal region
va	ventroalar artery
ve	vertebral artery
ZLI	zona limitans intrathalamica
THy	terminal hypothalamus
thp	thalamo-perforant artery
tth	tuberculo-thalamic artery (commonly misnamed “tubero-thalamic”)

frontiers in Neuroanatomy

REVIEW
published: 19 November 2018
doi: 10.3389/fnana.2018.00093

Toward a Common Terminology for the Gyri and Sulci of the Human Cerebral Cortex

Hans J. ten Donkelaar[1*†], *Nathalie Tzourio-Mazoyer*[2†] *and Jürgen K. Mai*[3†]

[1] Department of Neurology, Donders Center for Medical Neuroscience, Radboud University Medical Center, Nijmegen, Netherlands, [2] IMN Institut des Maladies Neurodégénératives UMR 5293, Université de Bordeaux, Bordeaux, France, [3] Institute for Anatomy, Heinrich Heine University, Düsseldorf, Germany

The gyri and sulci of the human brain were defined by pioneers such as Louis-Pierre Gratiolet and Alexander Ecker, and extensified by, among others, Dejerine (1895) and von Economo and Koskinas (1925). Extensive discussions of the cerebral sulci and their variations were presented by Ono et al. (1990), Duvernoy (1992), Tamraz and Comair (2000), and Rhoton (2007). An anatomical parcellation of the spatially normalized single high resolution T1 volume provided by the Montreal Neurological Institute (MNI; Collins, 1994; Collins et al., 1998) was used for the macroscopical labeling of functional studies (Tzourio-Mazoyer et al., 2002; Rolls et al., 2015). In the standard atlas of the human brain by Mai et al. (2016), the terminology from Mai and Paxinos (2012) is used. It contains an extensively analyzed individual brain hemisphere in the MNI-space. A recent revision of the terminology on the central nervous system in the *Terminologia Anatomica* (TA, 1998) was made by the Working Group Neuroanatomy of the Federative International Programme for Anatomical Terminology (FIPAT) of the International Federation of Associations of Anatomists (IFAA), and posted online as the *Terminologia Neuroanatomica* (TNA, 2017: http://FIPAT.library.dal.ca) as the official FIPAT terminology. This review deals with the various terminologies for the cerebral gyri and sulci, aiming for a common terminology.

Keywords: terminology, gyri, sulci, cerebral cortex, human brain

OPEN ACCESS

Edited by:
Marcello Rosa,
Monash University, Australia

Reviewed by:
Muhammad A. Spocter,
Des Moines University, United States
Charles R. Watson,
Curtin University, Australia

***Correspondence:**
Hans J. ten Donkelaar
hans.tendonkelaar@radboudumc.nl;
hjtendonkelaar@gmail.com

† These authors have contributed equally to this work

Received: *08 September 2018*
Accepted: *16 October 2018*
Published: *19 November 2018*

Citation:
ten Donkelaar HJ, Tzourio-Mazoyer N and Mai JK (2018) Toward a Common Terminology for the Gyri and Sulci of the Human Cerebral Cortex. Front. Neuroanat. 12:93. doi: 10.3389/fnana.2018.00093

INTRODUCTION

Although the gyri and sulci of the human brain were already beautifully illustrated by Vicq d'Azyr (1786) and von Soemmerring (1791), they were named and defined by Gratiolet (1854), Huschke (1854), Ecker (1869), Pansch (1868, 1879), Jensen (1871), Wernicke (1876), Eberstaller (1884, 1890), and Brissaud (1893), and extensified by, among others, Dejerine (1895), Retzius (1896), von Economo and Koskinas (1925), and Rose (1935). More recently, extensive discussions of the cerebral sulci and their variations were presented by Ono et al. (1990), Duvernoy (1992), Tamraz and Comair (2000), and Rhoton (2007). An anatomical parcellation of the spatially normalized single high resolution T1 volume provided by the Montreal Neurological Institute (MNI) was used for the macroscopical labeling of functional studies (Tzourio-Mazoyer et al., 2002; Rolls et al., 2015), using largely the Dejerine terminology. The previously much used Talairach atlas (Talairach and Tournoux, 1988) proved to be rather inaccurate for the cytoarchitectonic allocation of functional activations (Tzourio-Mazoyer et al., 2002; Eickhoff et al., 2005). In the standard atlas of the human

brain by Mai et al. (2016), the terminology from Mai and Paxinos (2012) is used. It contains an individual brain hemisphere in the MNI-space. In a recent pocket atlas (Mai and Majtanik, 2017), a probabilistic neuroanatomy of 152 individuals was presented to which the main atlas is registered. Mai and colleagues used the Brodmann (1909) and von Economo and Koskinas (1925) subdivisions of the cerebral cortex. A comprehensive cellular-resolution atlas of the adult human brain (Ding et al., 2016) presents the first digital human brain atlas across a complete adult female brain. The terminology used largely follows Brodmann terminology.

Recently, a revision of the terminology on the central nervous system in the *Terminologia Anatomica* (TA, 1998) was made by the Working Group Neuroanatomy of the Federative International Programme for Anatomical Terminology (FIPAT) of the International Federation of Associations of Anatomists (IFAA), and posted online as the *Terminologia Neuroanatomica* (TNA, 2017: http://FIPAT.library.dal.ca; for an introductory paper, see ten Donkelaar et al., 2017) as the official FIPAT terminology. This review deals with the various terminologies for the cerebral gyri and sulci on the superolateral, inferomedial, and basal surfaces of the cerebrum, aiming for a common terminology. It combines the data from the TNA (2017), an illustrated version (ten Donkelaar et al., 2018) and additional terms found in preparing this review.

BRIEF REVIEW OF THE LITERATURE

In **Figure 1**, the wealth of gyri and sulci of the human cerebral cortex as distinguished by von Economo and Koskinas (1925) is shown. The gyri of the cerebral lobes are indicated by the classical numbering such as F1-F3, T1-T4, and the sulci without capitals (f1, f2, etc). Clearly visible are the first and second intermediate parietal sulci of Jensen and Eberstaller (s.imdI and s.imdII, respectively) as well as the frontomarginal sulcus of Wernicke with various components. Many of the smaller or infrequent sulci were forgotten, several of which were reintroduced in the recent human brain mapping era and in the TNA. The **Supplementary Table 1** contains a list of synonyms and eponyms for the cerebral gyri and the **Supplementary Table 2** those of the main sulci.

Terminological differences used in Tzourio-Mazoyer's approach (Tzourio-Mazoyer et al., 2002; Rolls et al., 2015; **Figure 2**) vs. the *Terminologia Anatomica* (TA, 1998) concern the use of eponyms such as Rolandic operculum, Sylvian fissure and Heschl's gyrus, and the use of gyrus instead of lobule for the superior and inferior parietal lobules.

In the atlas of Mai et al. (2016) and the recent pocket atlas by Mai and Majtanik (2017), the use of the term fissure is advocated for the lateral, parietooccipital and hippocampal sulci. In the BNA (1895), the terms fissurae cerebri lateralis, collateralis, parietooccipitalis, calcarina, and hippocampi were used. In the JNA (1936), only the lateral, Sylvian fissure remained as fissure. This was corrected in the PNA (1955) and later editions, and for the cerebrum, the term fissure is in use only for the interhemispheric fissure. Therefore, the term fissure should not have been advocated anymore.

Minor differences in Mai et al. (2016) are the use of the terms central operculum for the subcentral gyrus, anterior intermediate parietal sulcus for the first intermediate parietal sulcus of Jensen (see also Zlatkina and Petrides, 2014), medial occipitotemporal gyrus as a common term for the lingual gyrus and the parahippocampal gyrus, periinsular sulcus for the circular sulcus of the insula, and a rather extensive terminology for the opercula, including frontal, frontoparietal, and temporal opercula (**Figure 3**). Their frontoparietal operculum includes the anterior central (precentral) operculum, the subcentral gyrus, the posterior central (postcentral) operculum, and the parietal operculum. The first three collectively may belong to the subcentral gyrus.

In their atlas of the human brain in MNI space, Mai et al. (2016) presented photographs of cell-stained sections of the right hemisphere of a 24-year-old male from the Vogt-collection in Düsseldorf (Vogt and Vogt, 1919). Schematic drawings show delineations of the cortex, which are based on the original maps of Brodmann (1909). The surface-based maps by Van Essen (2005); Van Essen et al. (2012) were modified by manually estimating areal boundaries on the atlas drawing and transforming them on the surface of the 3D reconstruction. Nieuwenhuys et al. (2015) adapted the standard brain, generated from the colin27 brain (http://www.bic.mni.mcgill.ca/ServicesAtlases/Colin27). In **Figures 4**, **5**, gyri and sulci are shown for the lateral and medial aspects, respectively. The colin27 image is the result of averaging 27 linearly registered high-resolution T1-weighted scans of the same individual (Collins, 1994; Collins et al., 1998; Holmes et al., 1998), matched to the MNI305-space (Mazziota et al., 2001). Several neuroimaging software systems adopted the colin27 template as the standard reference. Nieuwenhuys et al. (2015) noted a few peculiarities of the colin27 template brain: (1) the Broca area of the inferior frontal gyrus is very large, but the middle frontal gyrus is relatively narrow; (2) the superior temporal sulcus is not continuous with the groove marking the cortex of the angular gyrus; (3) both the collateral and cingulate sulci are interrupted, and the posterior part of the cingulate sulcus shows an unusual zigzag course; and (4) the upper surface of the splenium of the corpus callosum has a remarkable bump. It may be added that no attempt was made to subdivide the lateral aspect of the occipital lobe, and that the fairly constant frontomarginal sulcus is absent.

In this review, the terminology of the recent TNA (2017) is presented along with short descriptions and currently used synonyms, and summarized in **Tables 1**–**3**. Both English and Latin official terms from the TNA are used. The sulci of the cerebral cortex can be divided into **interlobar sulci**, separating the cerebral lobes, and **lobar sulci** present in a lobe.

SUPEROLATERAL SURFACE OF THE CEREBRAL HEMISPHERE

The lateral aspect of the cerebrum (**Figure 6**; and **Table 1**) shows two **interlobar sulci**: the lateral and central sulci. The *lateral sulcus* (*sulcus lateralis* of Sylvius), known for a long time as the *Sylvian fissure*, between the frontal and temporal lobes, has three branches: the *anterior* (*ramus anterior*) or *horizontal*

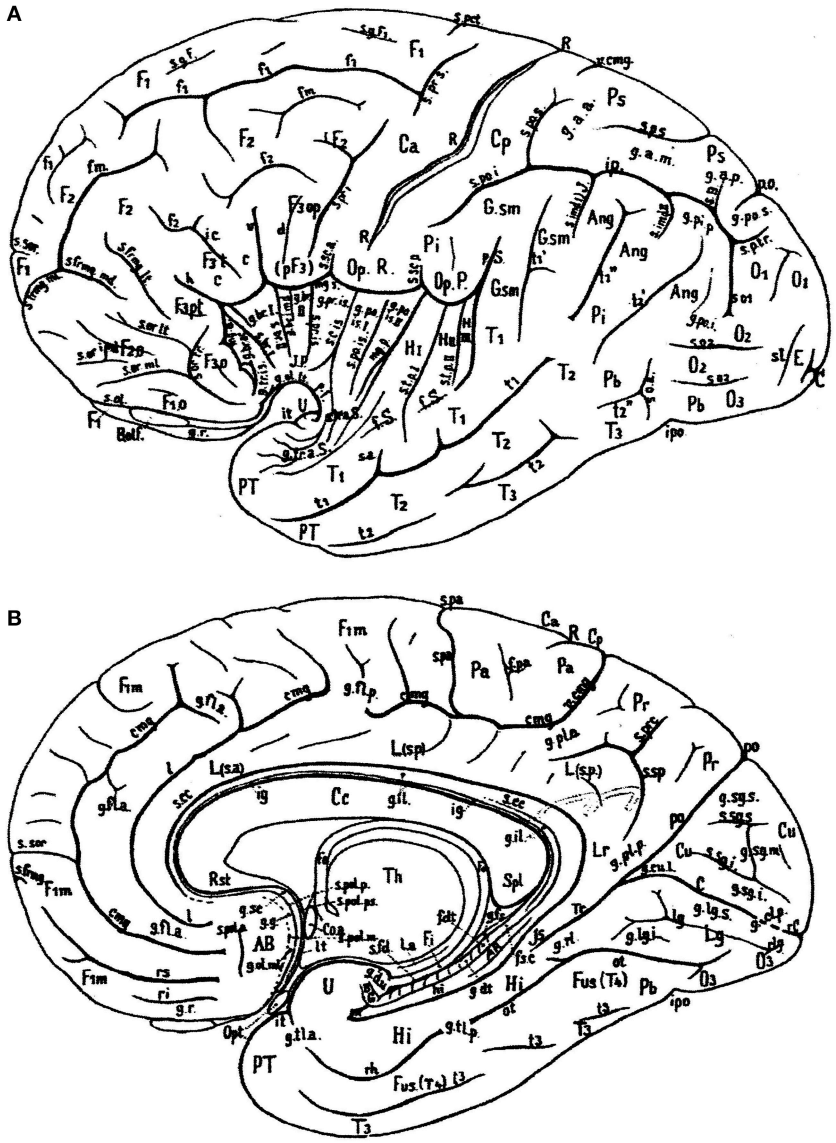

FIGURE 1 | Sulcal pattern in the human cerebral cortex: **(A)** Lateral aspect; **(B)** medial aspect (after von Economo and Koskinas, 1925). *AB,* area parolfactoria of Broca; *Ang,* angular lobule; *AR,* gyri of Andreas Retzius; *BB,* band of Broca; *BG,* bandelette of Giacomini; *B.olf,* olfactory bulb; *C,* calcarine fissure; *Ca*, *Cp,* anterior and posterior central gyri; *Cc,* corpus callosum; *Coa,* anterior commissure; *Cu,* cuneus; *cmg,* callosomarginal sulcus; *d,* diagonal sulcus of Eberstaller; *E,* descending occipital gyrus of Ecker; *F1, F2, F3,* first, second and third frontal gyri; *F3o*, *F3op*, *F3pt*, *F3t,* orbital, opercular, pretriangular, and triangular parts of F3; *f1, f2*, superior and inferior frontal sulci; *f.dt,* fascia dentata; *f.m,* middle frontal sulcus; *fo,* fornix; *f.pa,* paracentral fossa; *fs.c,* fasciola cinerea; *f.Sy,* Sylvian fissure; *Fus (T4),* fusiform gyrus; *g.ant.a, g.ant.d, g.ant.prc,* anticentral, antidiagonal and antiprecentral gyrus of operculum; *Gsm,* supramarginal lobule; *g.a.a., g.a.m., g.a.p.,* arcuate gyri of anterior, middle and posterior superior parietal lobule; *g.amb,* gyrus ambiens; *g.br.a., g.br.l, ll, lll, g.br.imd,* accessory short, first, second and third short and intermediate short gyri of insula; *g.cl.p.,* posterior cuneolingual gyrus; *g.dt,* dentate gyrus; *g.d.u.,* digital gyri of uncus; *g.fl.a., g.fl.p.,* anterior and posterior frontolimbic gyri; *g.fs,* fasciolar gyrus; *g.g,* geniculate gyrus; *g.il,* intralimbic gyrus; *g.lg.i, g.lg.s,* inferior and superior lingual gyri; *g.ol.lt, g.ol.ml,* lateral and medial olfactory gyri; *g.pip,* posterior inferior parietal gyrus; *g.pl.a, g.pl.p,* anterior and posterior parietolimbic gyrus; *g.po.i, g.po.s,* inferior and superior parieto-occipital gyrus; *g.po.is.l, g.po.is.ll, first* and second postcentral gyrus of insula; *g.pr.is,* precentral gyrus of isthmus; *g.r,* straight gyrus; *g.rl,* retrolimbic gyrus; *g.sc,* subcallosal gyrus; *g.sg.i, g.sg.m, g.sg.s,* inferior, middle, and superior sagittal gyrus of cuneus; *g.sml,* semilunar gyrus; *g.str,* subtriangular gyrus of operculum; *g.tl.a, g.tl.p,* anterior and posterior temporolimbic gyrus; *g.tr.a.S,* anterior transverse temporal gyri of Schwalbe; *g.tr.is,* transverse gyrus of insula; *g.tr.op.l, g.tr.op.ll, g.tr.op.lll,* first, second and third transverse gyrus of parietal operculum; *H.l, H.ll, first* and second gyrus of Heschl; *Hi,* hippocampal gyrus; *h,* horizontal branch of Sylvian fissure; *hi,* hippocampal fissure; *Is,* isthmus; *ic,* incisura capiti; *ig,* indusium griseum; *ip,* interparietal sulcus; *ipo,* preoccipital incisure; *it,* temporal incisure; *Lg,* lingula; *L.s.a, L.s.p,* anterior and posterior part of superior limbic gyrus; *Lr,* retrosplenial part of limbic gyri; *l,* intralimbic sulcus; *l.a,* lamina affixa; *l.g,* lingual sulcus; *lt,* lamina terminalis; *mg.a, mg.p,* anterior and posterior margin of circular sulcus of insula; *O1, O2, O3,* first, second and third occipital gyrus; *Op.P,* parietal operculum; *Op.R,* frontal operculum of Rolando; *Opt,* optic nerve; *ot,* occipitotemporal (collateral) fissure; *Pa,* paracentral lobule; *Pb,* basal parietal region; *Pi,* inferior parietal lobule; *Pr,* precuneus; *Ps,* superior parietal lobule; *PT,* temporopolar gyrus; *p.f,* falciform incisure; *po,* parieto-occipital fissure; *p.Sy,* posterior branch of Sylvian fissure; *R,* sulcus of Rolando;

(Continued)

FIGURE 1 | *Rst,* rostrum of corpus callosum; *rC,* retrocalcarine fissure; *rh,* rhinal fissure; *ri, rs,* inferior and superior rostral sulcus; *rl,* retrolingual sulcus; *Spl,* splenium of corpus callosum; *s.a,* acoustic sulcus; *s.B,* sulcus of Brissaud; *s.br.l, s.br.ll, first* and second short sulcus of insula; *s.cc,* sulcus of corpus callosum; *s.c.is,* central sulcus of insula; *s.fd,* fimbriodentate sulcus; *s.frmg.ml, s.frmg.md, s.frmg.lt,* medial, middle, and lateral frontomarginal sulcus; *s.g.F1,* sulcus of first frontal gyrus; *s.imdl, s.imdll, first* (of Jensen) and second (of Eberstaller) intermediate sulcus; *s.l,* lunate sulcus; *so1, so2, first* and second occipital sulcus; *s.ol* olfactory sulcus; *s.or.imd, s.or.lt, s.or.ml, s.or.tr,* intermediate, lateral, medial, and transverse orbital sulcus; *s.pa,* paracentral sulcus; *s.po.i, s.po.s,* inferior and posterior postcentral sulcus; *s.po.is* postcentral sulcus of isthmus; *s.pol.a, s.pol.m, s.pol.p, s.pol.ps,* anterior, middle, posterior, and postremal paraolfactory sulcus; *s.prc,* precuneate sulcus; *s.prd,* prediagonal sulcus; *s.pr.i, s.pr.s,* inferior and superior precentral sulcus; *s.pr.is,* precentral sulcus of insula; *s.p.s, s.p.tr,* superior and transverse parietal sulcus; *s.rh.i,* internal rhinal sulcus; *s.san,* semianular sulcus; *s.sc.a, s.sc.p,* anterior and posterior subcentral sulcus; *s.sg.i, s.gs.s,* inferior and superior sagittal sulcus of cuneus; *s.so,* suboccipital sulcus; *s.sor,* supraorbital sulcus; *s.sp,* subparietal sulcus; *s.tp.l, s.tp.ll, first* and second deep temporal sulcus; *s.tr.a.S,* anterior transverse temporal sulci of Schwalbe; *s.tr.op.l, s.tr.op.ll, first* and second transverse sulcus of parietal operculum; *T1, T2, T3,* first, second and third temporal sulcus; *Th,* thalamus; *Tr,* trunk of the parieto-occipital and calcarine fissures; *Tr.o,* olfactory trigonum; *Tu.o,* olfactory tubercle; *t1, t2, t3,* first, second and third temporal sulci; *U,* uncus; *v,* ventral branch of the Sylvian fissure; *v.cmg,* vertical branch of callosomarginal sulcus.

ramus, the *ascending* (*ramus ascendens*) or *vertical ramus* and the *posterior ramus* (*ramus posterior*), separating the parietal and temporal lobes. The *central sulcus* (*sulcus centralis* of Rolando) separates the frontal and parietal lobes. It is not a straight line but forms two arches from the superior margin of the hemisphere downwards to the lateral sulcus, the genu superior and the genu inferior (Broca, 1878a). The upper arch borders a "knob," which protrudes posteriorly, and contains the hand area of the somatosensory cortex (Rumeau et al., 1994; Yousry et al., 1997). The *parietooccipital sulcus* (*sulcus parietooccipitalis* of Gratiolet) indicates the border between the parietal and occipital lobes superiorly, and the *preoccipital notch* (*incisura preoccipitalis* of Meynert) marks that border inferiorly.

The **frontal lobe** (**lobus frontalis**) shows the following **gyri**: the *superior*, *middle* and *inferior frontal gyri* (*gyrus frontalis superior*, *-medius,* and *-inferior*), classically numbered F1, F2, and F3, separated by *superior* and *inferior frontal sulci* (*sulcus frontalis superior* and-*inferior*, classically numbered f1 and f2, see **Figure 1**), and the *precentral gyrus* (*gyrus precentralis*). The central sulcus usually does not reach the lateral sulcus, and is separated from it by a short gyrus, the *subcentral gyrus* (*gyrus subcentralis*), delimited in front and behind by the *anterior* and *posterior subcentral sulci* (*sulcus subcentralis anterior* and-*posterior*), respectively, as distinguished by Dejerine (1895); Testut and Latarjet (1948). The subcentral gyrus is also known as the central or Rolandic operculum. The inferior frontal gyrus comprises three parts, *orbital*, *triangular* and *opercular* (*pars orbitalis*, *pars triangularis* and *pars opercularis*). The opercular part forms the frontal operculum. Occasionally, the *diagonal sulcus* (*sulcus diagonalis* of Eberstaller) can divide the opercular part of the inferior frontal gyrus into two parts. The triangular part may also be indented from above by a *radiate sulcus* (*sulcus radiatus* of Eberstaller). The orbital part is continuous with the basal surface of the frontal lobe, where it merges with the lateral orbital gyrus. The triangular and opercular parts form together the *motor language area* of Broca (1863); Amunts et al. (1999); Amunts and Zilles (2012). Recent mapping approaches based on cytoarchitecture, transmitter receptor distribution and connectivity revealed a highly differentiated segregation of this region (Amunts and Zilles, 2012). The *frontomarginal sulcus* (*sulcus frontomarginalis* of Wernicke) is fairly constant, found at the frontal pole, and connected posteriorly with the middle frontal sulcus. It has two branches, one deep medial branch that borders the frontopolar gyri, and a shallow lateral branch that separates the frontomarginal sulcus from the medial frontal gyrus and the orbital part of the inferior frontal gyrus, respectively. The *frontopolar area* (*area frontopolaris*) at the *frontal pole* (*polus frontalis*) shows three frontopolar gyri, superior, middle, and inferior, that are clearly separated by limiting sulci, interposed between the superior frontal gyrus and the frontomarginal gyrus. Bludau et al. (2014) distinguished two cytoarchitectonically and functionally distinct areas: the lateral frontopolar area 1 (Fp1) and the medial frontopolar area 2 (Fp2).

The **temporal lobe** (**lobus temporalis**) is formed by the *superior*, *middle* and *inferior temporal gyri* (*gyrus temporalis superior*, *-medius,* and - *inferior*), classically numbered T1, T2, and T3, separated by the *superior* and *inferior temporal sulci* (*sulcus temporalis superior* and - *inferior*, classically numbered t1 and t2). The *temporopolar cortex* (*cortex temporopolaris*) at the *temporal pole* (*polus temporalis*) is a heterogenous region, situated between isocortex laterally, proisocortex in caudorostral continuation and paleocortex caudodorsally (Ding et al., 2009; Blaizot et al., 2010).

On the upper surface of the superior temporal gyrus (**Figure 7**), forming the temporal operculum, the *planum polare*, the *anterior* and *posterior transverse gyri* (*gyrus temporalis transversus anterior* and - *posterior* of Heschl) and the *planum temporale* can be distinguished, separated by sulci. The *anterior transverse temporal sulcus* (*sulcus temporalis transversus anterior*) separates the planum polare from the transverse temporal gyri of Heschl, the two transverse temporal gyri are subdivided by the *intermediate transverse temporal sulcus* (*sulcus temporalis transversus intermedius*), and the *posterior transverse temporal sulcus* (*sulcus temporalis transversus posterior*) separates the posterior transverse temporal gyrus from the planum temporale. There is usually one transverse gyrus of Heschl on the left and two on the right (Heschl, 1878; Marie et al., 2015; Tzourio-Mazoyer and Mazoyer, 2017). These transverse gyri contain the primary auditory cortex. The *planum temporale* is on the left usually larger than on the right (von Economo and Horn, 1930; Geschwind and Levitsky, 1968; Galaburda et al., 1978; Ide et al., 1999; Tzourio-Mazoyer and Mazoyer, 2017). The posterior part of the superior temporal gyrus forms the *sensory* or *receptive language area* of Wernicke (1874).

The temporal lobe is the location of strong asymmetries of its surface with a strong leftward asymmetry of the planum temporale (von Economo and Horn, 1930; Geschwind and

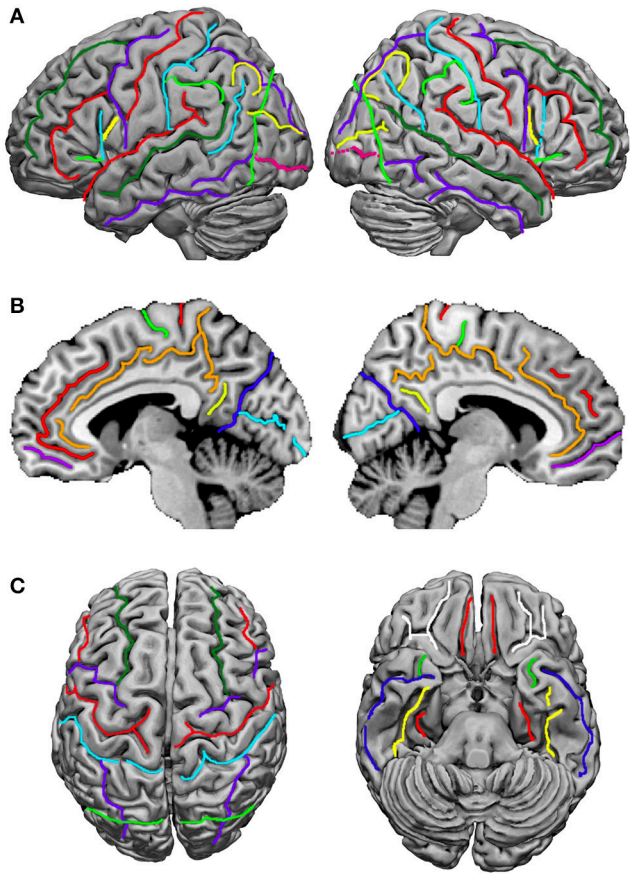

FIGURE 2 | Sulci definition on the 3-D renderings of the T1 MNI single subject brain: **(A)** Lateral view; left hemisphere on the left. From the frontal pole to the occipital pole, the following sulci are indicated: the superior frontal sulcus (*dark green*), the inferior frontal sulcus (*red*), the anterior, horizontal ramus of the lateral, Sylvian sulcus (*light green*), the ascending, vertical ramus of the lateral sulcus (*cyan*), the diagonal sulcus (*yellow*), the precentral sulcus (*purple*), the central, Rolandic sulcus (*red*), the postcentral sulcus (*cyan*), the intraparietal and intraoccipital sulci (*purple*), the anterior limit of the occipital lobe, corresponding in its inferior part to the anterior occipital sulcus (*light green*), the transverse occipital sulcus (*yellow*), and the inferior occipital sulcus (*pink*). **(B)** medial view; from the frontal to the occipital pole: the paracingulate sulcus (*red*), the cingulate sulcus (*orange*), the anterior rostral sulcus (*purple*), the paracentral sulcus (*light green*), the central, Rolandic sulcus (*red*), the marginal ramus (*orange*), the subparietal sulcus (*yellow*), the parieto-occipital sulcus (*blue*), and the calcarine sulcus (*cyan*). **(C)** At the left, superior view: the superior frontal sulcus (*dark green*) runs in the same direction and is symmetric in an horizontal plane with the intraoccipital sulcus (*purple*); the central, Rolandic sulcus (*red*), the precentral sulcus (*purple*), and the postcentral sulcus (*cyan*) run parallel. At the right, basal view: in the frontal lobe the orbital (*white*) and olfactory (*red*) sulci are depicted, and in the temporal lobe, the rhinal sulcus (*light green*), the inferior temporal sulcus (*dark blue*), the occipitotemporal sulcus (*yellow*) and the collateral sulcus (*red*). Adapted from Tzourio-Mazoyer et al. (2002).

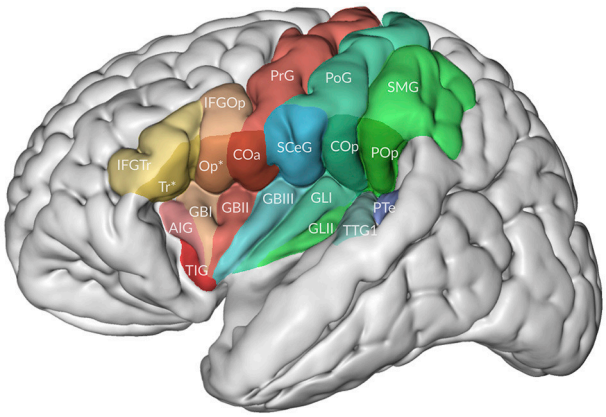

FIGURE 3 | The relation of the opercula to the insula. Adapted from Mai and Majtanek (2017; kindly provided by Milan Majtanik, Düsseldorf). *AIG,* accessory insular gyrus; *COa*, *Cop,* anterior (precentral) and posterior (postcentral) opercula; *GBI-III,* short insular gyri; *GLI-II,* long insular gyri; *IFGOp,* with *Op**, *IFGTr,* with *Tr** opercular and triangular parts of inferior frontal gyrus with opercular and triangular parts of frontal operculum, *PoG,* postcentral gyrus; *POp,* parietal operculum; *PrG,* postcentral gyrus; *PTe,* planum temporale; *SCeG,* subcentral gyrus; *SMG,* supramarginal gyrus; *TIG,* transverse insular gyrus; *TTG1,* anterior transverse temporal gyrus.

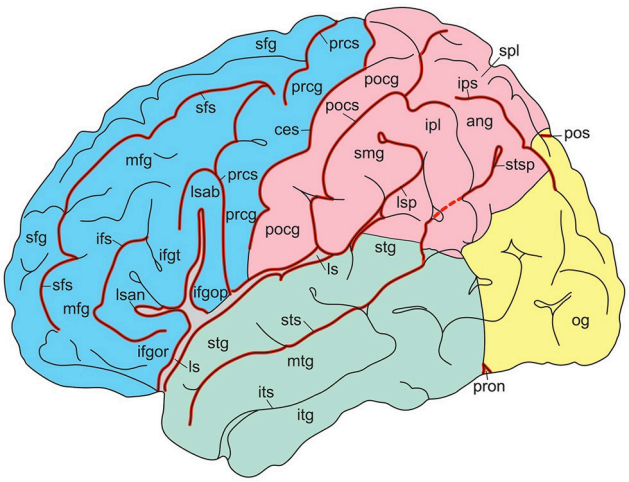

FIGURE 4 | Gyri and sulci of the lateral aspect of the standard brain (from Nieuwenhuys et al., 2015; with permission from Springer Nature). *ang,* angular gyrus; *ces,* central sulcus; *ifgop, ifgor, ifgt,* inferior frontal gyrus, orbital, opercular, and triangular parts; *ifs,* inferior frontal sulcus; *ipl,* inferior parietal lobule; *ips,* intraparietal sulcus; *itg,* inferior temporal gyrus; *its,* inferior temporal sulcus; *ls, lsab, lsan, lsp,* lateral sulcus with ascending, anterior, and posterior branches; *mfg,* middle temporal gyrus; *mtg,* middle temporal sulcus; *og,* occipital gyri; *pocg,* postcentral gyrus; *pocs,* postcentral sulcus; *pos,* parietooccipital sulcus; *prcg,* precentral gyrus; *prcs,* precentral sulcus; *pron,* preoccipital notch; *sfg,* superior frontal gyrus; *sfs,* superior frontal sulcus; *smg,* supramarginal gyrus; *spl,* superior parietal lobule; *stg,* superior temporal gyrus; *sts*, *stsp,* superior temporal sulcus with posterior part.

Levitsky, 1968; Galaburda et al., 1978; Ide et al., 1999; Toga and Thompson, 2003; Tzourio-Mazoyer and Mazoyer, 2017), the Heschl gyrus and of its sulci depth. A leftward asymmetry of the lateral sulcus is already present at birth (Hill et al., 2010).

The triangular **insula** of Reil lies in the depths of the lateral sulcus and is covered by the frontal, frontoparietal, parietal, and temporal opercula (Türe et al., 1999; Naidich et al., 2004; Morel

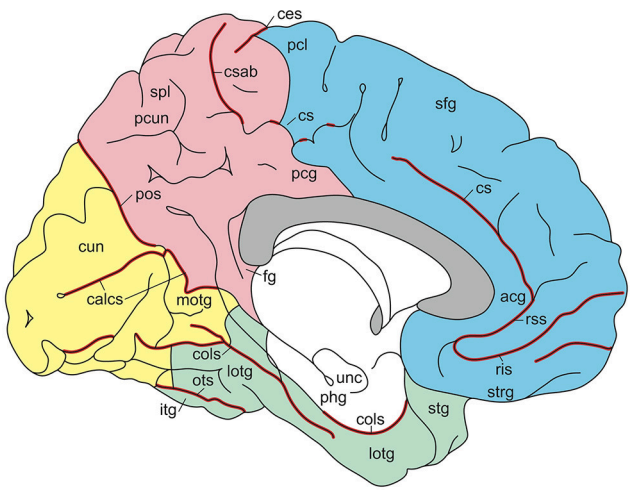

FIGURE 5 | Gyri and sulci of the medial aspect of the standard brain (from Nieuwenhuys et al., 2015; with permission from Springer Nature). *acg,* anterior cingulate gyrus; *calcs,* calcarine sulcus; *ces,* central sulcus; *cols,* collateral sulcus; *cs, csab,* cingulate sulcus with ascending branch; *cun* cuneus; *fg,* fasciolar gyrus; *itg,* inferior temporal gyrus; *lotg,* lateral occipitotemporal gyrus (fusiform gyrus); *motg,* medial occipitotemporal gyrus (lingual gyrus); *ots,* occipitotemporal sulcus; *pcg,* posterior cingulate gyrus; *pcl,* paracentral lobule; *pcun,* precuneus; *phg,* parahippocampal gyrus; *pos,* parietooccipital sulcus; *ris, rss,* rostral inferior and rostral superior sulcus; *sfg,* superior frontal gyrus; *spl,* superior parietal lobule; *stg,* superior temporal gyrus; *strg,* straight gyrus; *unc,* uncus.

et al., 2013; **Figure 8**). The *limen insulae*, the insular threshold or frontotemporal junction, forms the transition from the anterior perforated substance on the basal aspect of the frontal lobe to the insula. The insula is surrounded by the *circular sulcus of the insula* (*sulcus circularis insulae* of Reil) or *periinsular sulcus*, and contains several vertically directed gyri, usually three *short gyri* (*gyri breves insulae*), anterior, middle and posterior, and one or two *long gyri* (*gyri longi insulae*), anterior and posterior, separated by the *central sulcus of the insula* (*sulcus centralis insulae*) or *transverse insular sulcus* of Eberstaller. The three short gyri converge to the apex of the insula, and are joined to the orbital part of the inferior frontal gyrus by a short annectant gyrus, the *transverse insular gyrus* (*gyrus transversus insulae* of Eberstaller).

The lateral aspect of the **parietal lobe** (**lobus parietalis**) shows the *postcentral gyrus (gyrus postcentralis)*, the *postcentral sulcus (sulcus postcentralis)*, and the *superior* and *inferior parietal lobules (lobulus parietalis superior* and - *inferior)*, numbered P1 and P2, respectively, and separated by the *intraparietal sulcus (sulcus intraparietalis)*. Dorsally, the parietal lobe is connected with the occipital lobe by the *parietooccipital arc (arcus parietooccipitalis)* of Gratiolet. Another "pli de passage" connects the posterior part of the angular gyrus with the superior occipital gyrus. In monkeys, the intraparietal sulcus contains numerous **intraparietal areas** (AIP, LIP, MIP, PIP, and VIP; Rizzolatti et al., 1998; ten Donkelaar, 2011; Zilles and Amunts, 2012). In an fMRI study, Seitz and Binkofski (2003) identified AIP and VIP in the human brain. Two cytoarchitectonic areas were identified and termed hIP (human IntraParietal) 1 and hIP2 in the anterior part of the intraparietal sulcus (Choi et al., 2006), which may be the anatomical correlates of VIP and AIP, respectively (see also Zlatkina and Petrides, 2014). A third intraparietal area, hIP3, was delineated in the anterior medial wall of the intraparietal sulcus, directly across hIP1 and hIP2 (Scheperjans et al., 2008a,b).

The **inferior parietal lobule** (**IPL**) consists of the *supramarginal* and *angular gyri* (*gyrus supramarginalis* and - *angularis*), both of which can be further subdivided (see Caspers et al., 2012). The *supramarginal gyrus* surrounds the posterior ascending ramus of the lateral sulcus and can be subdivided into five areas. The *angular gyrus* lies around the caudal end of the superior temporal gyrus and is composed of two areas. The *first intermediate sulcus* (*sulcus intermedius primus* of Jensen) may subdivide the inferior parietal lobule into the supramarginal and angular gyri, and the *second intermediate sulcus* (*sulcus intermedius secundus* of Eberstaller) may be found posterior to the Jensen sulcus, dividing the angular gyrus into anterior and posterior parts.

The *transverse parietal sulcus* (*sulcus parietalis transversus* of Brissaud) may subdivide the **superior parietal lobule** (**SPL**) into anterior and posterior portions, when it extends on the superolateral aspect of the cerebrum. The SPL includes the preparietal area, the superior parietal area, each with subdivisions (see Scheperjans et al., 2008a,b). The *parietal operculum* (*operculum parietale*) contains four cytoarchitectonic areas (OP1-OP4), corresponding to the secondary somatosensory cortex (Eickhoff et al., 2006a,b).

Most of the **occipital lobe** (**lobus occipitalis**) is found on the medial aspect of the cerebrum. An imaginary line between the parietooccipital sulcus superiorly and the preoccipital notch inferiorly indicates the border between the occipital lobe and the parietal and temporal lobes. On the superolateral aspect, the following occipital gyri and sulci can be found: the *superior occipital gyrus* (O1 or *gyrus occipitalis superior*), the *middle occipital gyrus* (O2 or *gyrus occipitalis medius*), the upper and lower parts of which are separated by the *lunate sulcus* (*sulcus lunatus*), the *inferior occipital gyrus* (O3 or *gyrus occipitalis inferior*) and the *descending occipital gyrus* (*gyrus occipitalis descendens* of Ecker). An *inferior occipital sulcus* (*sulcus occipitalis inferior*) may divide the lower part of O2 from O3. For variations of the gyri and sulci on the occipital lobe convexity, see Ono et al. (1990), Alves et al. (2012) and Malikovic et al. (2012).

INFEROMEDIAL SURFACE OF THE CEREBRAL HEMISPHERE

On the inferomedial surface of the cerebral hemisphere, **interlobar sulci** include the continuation of the central sulcus, the cingulate sulcus, the sulcus of the corpus callosum, the parietooccipital sulcus, the subparietal sulcus and the collateral sulcus (**Figure 9**; and **Table 2**). The *cingulate sulcus* (*sulcus cinguli* or "scissure limbique" of Broca, 1878b) runs parallel to the corpus callosum and ascends above the posterior part (the splenium) of the corpus callosum toward the superior

TABLE 1 | Sulci and on the superolateral surface of the cerebral hemisphere (based on TNA, 2017; ten Donkelaar et al., 2018).

English official terms and synonyms	Latin official terms and synonyms	Abbreviations and acronyms	Eponyms
Superolateral interlobar sulci	**Sulci interlobares superolaterales**		
central sulcus	sulcus centralis	ces	sulcus of Rolando
lateral sulcus	sulcus lateralis	ls	sulcus of Sylvius
posterior ramus	ramus posterior	lsp	
ascending ramus	ramus ascendens	lsas	
anterior ramus	ramus anterior	lsan	
parietooccipital sulcus	sulcus parietooccipitalis	pos	sulcus of Gratiolet
preoccipital notch	incisura preoccipitalis	pn	incisure of Meynert
Frontal lobe	**Lobus frontalis**		
frontomarginal sulcus	sulcus frontomarginalis	fmgs	sulcus of Wernicke
frontal pole	polus frontalis	FP	
frontopolar area	area frontopolaris	FPA	
superior frontopolar gyrus	gyrus frontopolaris superior	SFPG	
middle frontopolar gyrus	gyrus frontopolaris medius	MFPG	
inferior frontopolar gurus	gyrus frontopolaris inferior	IFPG	
frontomarginal gyrus	gyrus frontomarginalis	FMG	
frontal operculum	operculum frontale	FOp	
inferior frontal gyrus	gyrus frontalis inferior	IFG; F3	
orbital part	pars orbitalis	IFGOr	
triangular part	pars triangularis	IFGTr	area of Broca
radiate sulcus	sulcus radiatus	ras	sulcus of Eberstaller
opercular part	pars opercularis	IFGOp	area of Broca
diagonal sulcus	sulcus diagonalis	dis	sulcus of Eberstaller
inferior frontal sulcus	sulcus frontalis inferior	ifs; f2	
middle frontal gyrus	gyrus frontalis medius	MFG; F2	
precentral gyrus	gyrus precentralis	PRG	
precentral sulcus	sulcus precentralis	prs	
anterior subcentral sulcus	sulcus subcentralis anterior	ascs	
subcentral gyrus	gyrus subcentralis	SCeG	central or Rolandic operculum
posterior subcentral sulcus	sulcus subcentralis posterior	pscs	
superolateral superior frontal gyrus	gyrus frontalis superior superolateralis	SFGL; F1	
superior frontal sulcus	sulcus frontalis superior	sfs; f1	
Parietal lobe	**Lobus parietalis**		
postcentral gyrus	gyrus postcentralis	POG	
postcentral sulcus	sulcus postcentralis	pcs	
superior parietal lobule	lobulus parietalis superior	SPL; P1	
parietooccipital arc	arcus parietooccipitalis	POcA	first parietooccipital passage of Gratiolet
intraparietal sulcus	sulcus intraparietalis	ips	
first intermediate sulcus; anterior intermediate sulcus	sulcus intermedius primus; sulcus intermedius anterior	fis	sulcus of Jensen
second intermediate sulcus; posterior intermediate sulcus	sulcus intermedius secundus; sulcus intermedius posterior	sis	sulcus of Eberstaller
transverse parietal sulcus	sulcus parietalis transversus	tps	sulcus of Brissaud
inferior parietal lobule	lobulus parietalis inferior	IPL; P2	
angular gyrus	gyrus angularis	AG	
parietal operculum	operculum parietale	POp	
supramarginal gyrus	gyrus supramarginalis	SMG	

(Continued)

TABLE 1 | Continued

English official terms and synonyms	Latin official terms and synonyms	Abbreviations and acronyms	Eponyms
Occipital lobe	**Lobus occipitalis**		
occipital pole	polus occipitalis	OP	
lunate sulcus	sulcus lunatus	lus	
transverse occipital sulcus	sulcus occipitalis transversus	tos	
superior occipital gyrus	gyrus occipitalis superior	SOG; O1	
middle occipital gyrus	gyrus occipitalis medius	MOG; O2	
inferior occipital gyrus	gyrus occipitalis inferior	IOG; O3	
descending occipital gyrus	gyrus occipitalis descendens	DOG	gyrus of Ecker
Temporal lobe	**Lobus temporalis**		
temporal pole	polus temporalis	TP	
temporopolar cortex	cortex temporopolaris	TPC	
superior temporal gyrus	gyrus temporalis superior	STG; T1	
anterior part	pars anterior	STGa	
posterior part	pars posterior	STGp	area of Wernicke
temporal operculum	operculum temporale	TOp	
polar plane	planum polare	PPo	
transverse temporal gyri	gyri temporales transversi		gyri of Heschl
anterior transverse temporal gyrus	gyrus temporalis transversus anterior	TTGa	
posterior transverse temporal gyrus	gyrus temporalis transversus posterior	TTGp	
temporal plane	planum temporale	PTe	
transverse temporal sulci	sulci temporales transversi		
anterior transverse temporal sulcus	sulcus temporalis transversus anterior	atts	
intermediate transverse temporal sulcus	sulcus temporalis transversus intermedius	itts	
posterior transverse temporal sulcus	sulcus temporalis transversus posterior	ptts	
superior temporal sulcus	sulcus temporalis superior	sts; t1	
middle temporal gyrus	gyrus temporalis medius	MTG; T2	
inferior temporal sulcus	sulcus temporalis inferior	its; t2	
superolateral inferior temporal gyrus	gyrus temporalis inferior superolateralis	ITGL; T3	
Insula; insular lobe	**Insula; lobus insularis**	Ins	
insular gyri	gyri insulae		
long gyrus of insula	gyrus longus insulae	LGI	
short gyri of insula	gyri breves insulae	SGI	
transverse insular gyrus	gyrus transversus insulae	TIG	
central sulcus of insula	sulcus centralis insulae	csi	
circular sulcus of insula; periinsular sulcus	sulcus circularis insulae	cas	sulcus of Reil
limen insulae; insular threshold; frontotemporal junction	limen insulae; junctio frontotemporalis	LI	

*For a summarizing figure, see **Figure 6**.*

margin of the hemisphere. It gives off a *marginal branch* or *sulcus* (*ramus marginalis* or *sulcus marginalis*). The cingulate sulcus continues around the rostrum of the corpus callosum, where it is also known as the *superior rostral sulcus* (*sulcus rostralis superior*). This sulcus may continue as the *inferior rostral sulcus* (*sulcus rostralis inferior*), which separates the straight gyrus from the medial surface of the frontal lobe (see **Figure 5**). Immediately rostral to the ascending part of the cingulate sulcus courses the medial end of the central sulcus. The cingulate sulcus divides the medial aspect of the cerebral cortex into an outer and an inner zone. The **outer zone** is composed of the medial part of the *superior frontal gyrus* (F1 or *gyrus frontalis superior*) and the *paracentral lobule* (*lobulus paracentralis*), which surrounds the medial end of the central sulcus, and has frontal and parietal components. Frequently, a series of furrows delineates the *paracingulate sulcus* (*sulcus paracinguli*), which separates the medial division of the superior frontal gyrus from the *paracingulate gyrus* (*gyrus paracinguli*; see **Figure 2B**), also known as the external cingulate gyrus (Ono et al., 1990). This gyrus is separated ventrally by the cingulate sulcus from the cingulate gyrus (Ono et al., 1990; Paus et al., 1996; Ide et al., 1999). Such a double-parallel pattern, where the paracingulate sulcus surrounds the cingulate sulcus, was found in 24% of either hemisphere in Ono's cases. Ide et al.

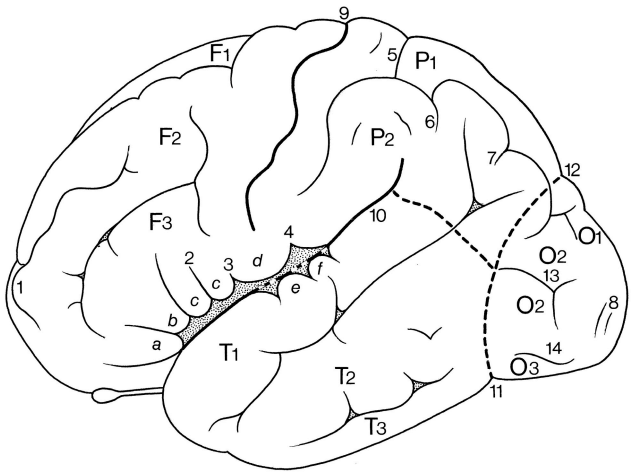

FIGURE 6 | Gyri and sulci on the superolateral surface of the cerebral hemisphere (after Duvernoy, 1992; ten Donkelaar et al., 2018). *a*, *b*, *c,* orbital, triangular, and opercular (divided into two parts by *2*) parts of the inferior frontal gyrus; *d,* subcentral gyrus; *e*, *f,* transverse temporal gyri of Heschl; *F1*, *F2*, *F3,* superior, middle, and inferior frontal gyri; *O1*, *O2*, *O3,* superior, middle, and inferior occipital gyri; *P1*, *P2,* superior and inferior parietal lobules; *T1*, *T2*, *T3,* superior, middle, and inferior temporal gyri; *1,* frontomarginal sulcus of Wernicke; *2,* diagonal sulcus of Eberstaller; *3,* anterior subcentral sulcus; *4,* posterior subcentral sulcus; *5,* transverse parietal sulcus of Brissaud; *6,* first intermediate sulcus of Jensen; *7,* second intermediate sulcus of Eberstaller; *8,* descending occipital gyrus of Ecker; *9,* central sulcus; *10,* lateral sulcus; *11,* preoccipital notch of Meynert; *12,* parietooccipital sulcus; *13,* lunate sulcus; *14,* inferior occipital sulcus.

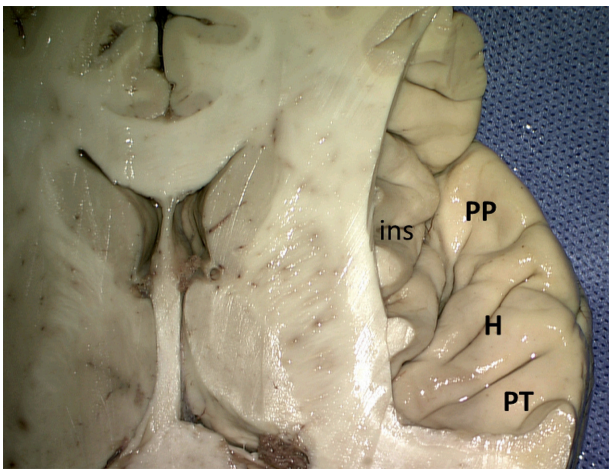

FIGURE 7 | Superior view of the right superior temporal sulcus (kindly provided by Robert Bartoš, Ústí nad Labem, Czech Republic). *ins,* insula; *H,* Heschl gyri; *PP,* planum polare; *PT,* planum temporale.

(1999) found a single sulcus more frequently on the right (69%) than on the left (31%) hemispheres, whereas the double pattern was more frequent on the left (68%) than right (32%) hemispheres.

Caudal to the paracentral lobule lies the large *precuneus* (P1), bordered by the *marginal branch of the cingulate sulcus (ramus marginalis sulci cinguli)* rostrally, the *parietooccipital sulcus (sulcus parietooccipitalis* of Gratiolet) caudally, and the *subparietal sulcus (sulcus subparietalis)* ventrally.

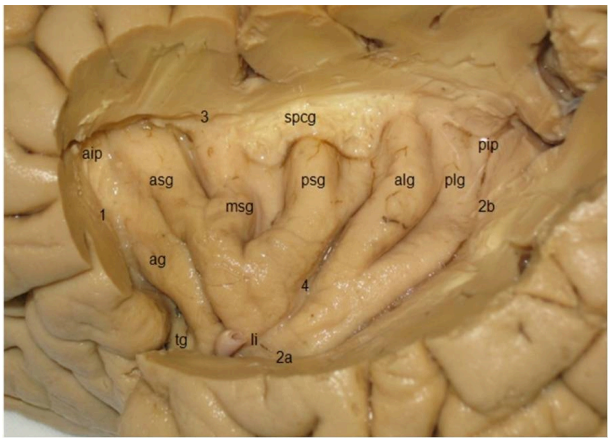

FIGURE 8 | Lateral view of the insula, showing three short gyri, an accessory gyrus and two long gyri (kindly provided by Robert Bartoš, Ústí nad Labem, Czech Republic). *ag,* accessory gyrus; *aip,* anterior insular point; *alg,* anterior long gyrus; *asg,* anterior short gyrus, li limen insulae; *msg,* middle short gyrus; *pip,* posterior insular point; *plg,* posterior long gyrus; *psg,* posterior short gyrus; *spcg,* gyrus supracentralis; *tg,* transverse insular gyrus; *1–3,* circular insular sulcus (*1* anterior periinsular sulcus, *2a*, *2b,* inferior insular sulcus, horizontal, and posterior parts; *3,* superior periinsular sulcus); *4,* central insular sulcus.

The **inner zone**, separated from the corpus callosum by the *sulcus of the corpus callosum* (*sulcus corporis callosi*), and earlier known as the *fornicate gyrus* (*gyrus fornicatus* of Meynert), is formed by the *cingulate gyrus* (*gyrus cinguli*). The cingulate gyrus can be divided into four parts: an anterior part, a midcingulate cortex, a posterior part and a retrosplenial part (Vogt and Palomero-Gallagher, 2012). The cingulate gyrus is continuous through a narrowing (*isthmus gyri cinguli*) with the *parahippocampal gyrus* (*gyrus parahippocampalis* or T5) in the temporal lobe. The *collateral sulcus* (*sulcus collateralis*, also known as the medial occipitotemporal sulcus) separates T5 from T4, the temporal part of the *fusiform gyrus* (*gyrus fusiformis*, also known as the lateral occipitotemporal gyrus). Areas of the fusiform gyrus within the inferotemporal cortex are part of the ventral visual stream area (see Rosenke et al., 2018), and they process higher-order visual information associated with faces, limbs, words, and places. Caspers et al. (2013) identified two areas, FG1 and FG2, medial and lateral in the posterior part of the fusiform gyrus, respectively. Lorenz et al. (2017) identified two new areas, FG3 and FG4, medial and lateral in the midfusiform gyrus, respectively, separated by the *midfusiform sulcus* (*sulcus fusiformis medius*). The *occipitotemporal sulcus* (*sulcus occipitotemporalis*, also known as the lateral occipitotemporal sulcus) separates the medial part of the *inferior temporal gyrus* (T3 or *gyrus temporalis inferior*) from T4. Various classifications for the temporal sulci and gyri have been published (Ono et al., 1990; Duvernoy, 1992; Hanke, 1997;

TABLE 2 | Sulci and gyri on the inferomedial surface of the cerebral hemisphere (based on TNA, 2017; ten Donkelaar et al., 2018).

English official terms and synonyms	Latin official terms and synonyms	Abbreviations and acronyms	Eponyms
Inferomedial interlobar sulci	**Sulci Interlobares inferomediales**		
sulcus of corpus callosum	sulcus corporis callosi	scc	
cingulate sulcus	sulcus cinguli	cgs	
marginal branch; marginal sulcus	ramus marginalis; sulcus marginalis	cgsmb	
parietooccipital sulcus	sulcus parietooccipitalis	pos	sulcus of Gratiolet
subparietal sulcus	sulcus subparietalis	sps	
collateral sulcus	sulcus collateralis	cos	
central sulcus	sulcus centralis	ces	
Frontal lobe	**Lobus frontalis**		
inferomedial superior frontal gyrus	gyrus frontalis superior inferomedialis	SFGM; F1	
paracingulate sulcus	sulcus paracinguli	pcgs	
paracingulate gyrus	gyrus paracinguli	PCG	
paracentral sulcus	sulcus paracentralis	pacs	
paracentral lobule	lobulus paracentralis	PCL	
anterior paracentral gyrus	gyrus paracentralis anterior	APaG	
subcallosal area; subcallosal gyrus	area subcallosa; gyrus subcallosus	SCA	
paraterminal gyrus	gyrus paraterminalis	PTG	
paraolfactory area	area paraolfactoria	PaOA	
paraolfactory gyrus	gyrus paraolfactorius	PaOG	
paraolfactory sulci	sulci paraolfactorii		
anterior paraolfactory sulcus	sulcus paraolfactorius anterius	apaos	
posterior paraolfactory sulcus	sulcus paraolfactorius posterius	ppaos	
orbital gyri	gyri orbitales		
medial orbital gyrus	gyrus orbitalis medialis	MOrG	
anterior orbital gyrus	gyrus orbitalis anterior	AOrG	
posterior orbital gyrus	gyrus orbitalis posterior	POrG	
lateral orbital gyrus	gyrus orbitalis lateralis	LOrG	
posteromedial orbital lobule	lobulus orbitalis posteromedialis	PMOL	
Posterolateral orbital region	regio orbitalis posterolateralis	PLOR	
orbital sulci	sulci orbitales		
lateral orbital sulcus	sulcus orbitalis lateralis	lors	
transverse orbital sulcus	sulcus orbitalis transversus	tors	
medial orbital sulcus	sulcus orbitalis medialis	mors	
superior rostral sulcus	sulcus rostralis superior	srs	
inferior rostral sulcus	sulcus rostralis inferior	irs	
straight gyrus	gyrus rectus	SG	
olfactory sulcus	sulcus olfactorius	ols	
anterior perforated substance; rostral perforated substance	substantia perforata anterior; substantia perforata rostralis	APS	
Olfactory structures	**Structurae olfactoriae**		
olfactory bulb	bulbus olfactorius	OB	
olfactory peduncle	pedunculus olfactorius	op	
olfactory tract	tractus olfactorius	ot	
olfactory trigone	trigonum olfactorium	OT	
olfactory tubercle	tuberculum olfactorium	Tu	
olfactory striae	striae olfactoriae		
medial olfactory stria	stria olfactoria medialis	mos	
lateral olfactory stria	stria olfactoria lateralis	los	
retrobulbar region	regio retrobulbaris	RBR	
piriform cortex	cortex piriformis; cortex olfactorius primarius	Pir	

(Continued)

TABLE 2 | Continued

English official terms and synonyms	Latin official terms and synonyms	Abbreviations and acronyms	Eponyms
frontal part	pars frontalis	PirF	
temporal part	pars temporalis	PirT	
Parietal lobe	**Lobus parietalis**		
paracentral lobule	lobulus paracentralis	PCL	
posterior paracentral gyrus	gyrus paracentralis posterior	PPaG	
transverse parietal sulcus	sulcus parietalis transversus	tps	sulcus of Brissaud
precuneus	precuneus	PCun; P1	
subparietal sulcus	sulcus subparietalis	sps	
Occipital lobe	**Lobus occipitalis**		
cuneus	cuneus	Cun; O6	
calcarine sulcus	sulcus calcarinus	cas	
lingual gyrus; medial occipitotemporal gyrus	gyrus lingualis; gyrus occipitotrmporalis medialis	LG; O5	
fusiform gyrus; lateral occipitotemporal gyrus	gyrus fusiformis; gyrus occipitotemporalis lateralis	FG; O4	
occipitotemporal sulcus; lateral occipitotemporal sulcus	sulcus occipitotemporalis; sulcus occipitotemporalis lateralis	ots	
Temporal lobe	**Lobus temporalis**		
inferomedial inferior temporal gyrus	gyrus temporalis inferior inferomedialis	ITGM; T3	
occipitotemporal sulcus; lateral occipitotemporal sulcus	sulcus occipitotemporalis; sulcus occipitotemporalis lateralis	ots	
fusiform gyrus; lateral occipitotemporal gyrus	gyrus fusiformis; gyrus occipitotemporalis lateralis	FG; T4	
medial part	pars medialis	FGM	
lateral part	pars lateralis	FGL	
ectorhinal cortex	cortex ectorhinalis	EcC	
midfusiform sulcus	sulcus fusiformis medius	mfs	
collateral sulcus; medial occipitotemporal sulcus	sulcus collateralis; sulcus occipitotemporalis medialis	cos	
parahippocampal gyrus	gyrus parahippocampalis	PHG; T5	

*For summarizing figures, see **Figures 9**, **10**.*

Huntgeburth and Petrides, 2012; Chau et al., 2014; Cikla et al., 2016) with different relations between the collateral and rhinal sulci and patterns of the various sulci.

The posterior part of the medial cerebral cortex has two deep sulci, which converge toward the splenium. The interlobar *parietooccipital sulcus* (*sulcus parietooccipitalis* of Gratiolet) separates the parietal and occipital lobes, and the lobar *calcarine sulcus* (*sulcus calcarinus*) divides the **occipital lobe** into a dorsal part, the *cuneus* (O6) and a ventral part, the *lingual* or *medial occipitotemporal gyrus* (O5; *gyrus lingualis* or *gyrus occipitotemporalis medialis*). The lingual gyrus may be divided into two parts by the *lingual sulcus* (*sulcus lingualis*). The primary visual cortex is mainly found on both sides of the calcarine sulcus. Below the lingual gyrus, separated by the *occipitotemporal sulcus* (*sulcus occipitotemporalis*), lies the occipital part of the *fusiform* or *lateral occipitotemporal gyrus* (O4; *gyrus fusiformis* or *gyrus occipitotemporalis lateralis*). The visual areas outside the *striate area* (*area striata*) are grouped together as the *extrastriate areas* (*areae extrastriatae*; for current views and further discussion, see Wang et al., 2015).

BASAL SURFACE OF THE CEREBRAL HEMISPHERE

On the basal surface of the cerebral hemisphere, the occipital lobes are largely covered by the cerebellum, so only the frontal and temporal lobes are visible (**Figure 10**; and **Table 2**). On the orbital surface of the frontal lobe, the *olfactory sulcus* (*sulcus olfactorius*) with the **olfactory bulb** and **tract** separates the *straight gyrus* (*gyrus rectus*) from the *orbital gyri*. The olfactory tract divides into the **medial** and **lateral olfactory striae**, of which only the lateral olfactory tract contains secondary olfactory fibers. Between these striae lies the **anterior perforated substance** of Vicq d'Azyr, a region studded with small openings through which the anteromedial central arteries and the recurrent artery of Heubner from the anterior cerebral artery and the lenticulostriate arteries from the middle cerebral artery pass to the basal ganglia and the internal capsule. The medial part of the temporal lobe is formed by the *parahippocampal gyrus* (T5; *gyrus parahippocampalis* or *medial occipitotemporal gyrus*), the continuation of the cingulate gyrus. The most rostral part of the

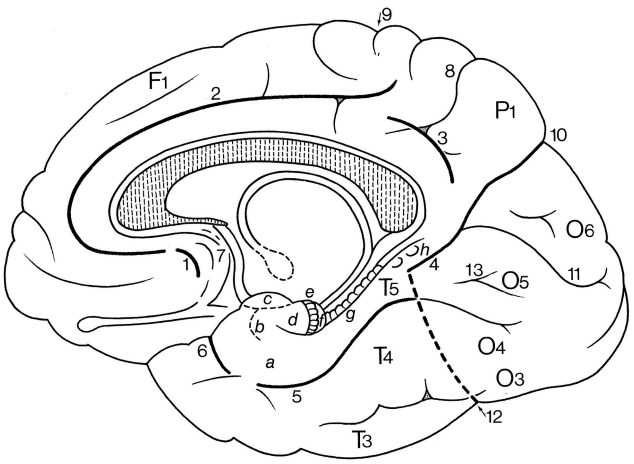

FIGURE 9 | Gyri and sulci on the inferomedial surface of the cerebral hemisphere (after Duvernoy, 1992; ten Donkelaar et al., 2018). (1) below F1, the paracingulate sulcus; and (2) below the subcallosal part of 2, the rostral sulcus. *a,* entorhinal cortex; *b,* ambient gyrus; *c,* semilunar gyrus; *d,* uncinate gyrus; *e,* band of the dentate gyrus of Giacomini; *f,* intralimbic gyrus or uncal apex; *g,* dentate gyrus; *h,* gyri of Andreas Retzius or subsplenial gyri; *F1,* superior frontal gyrus; *P1,* precuneus; *O3,* inferior occipital gyrus; *O4,* fusiform gyrus (occipital part); *O5,* lingual gyrus; *O6,* cuneus; *T3,* inferior temporal gyrus; *T4,* fusiform gyrus (temporal part); *T5,* parahippocampal gyrus; *1–6,* parts of the "limbic sulcus" or "scissure limbique": *1,* anterior paraolfactory sulcus; *2,* cingulate sulcus; *3,* subparietal sulcus; *4,* anterior part of parietooccipital sulcus; *5,* collateral sulcus; *6,* rhinal sulcus; *7,* posterior paraolfactory sulcus; *8,* transverse parietal sulcus of Brissaud; *9,* central sulcus; *10,* parietooccipital sulcus; *11,* calcarine sulcus; *12,* preoccipital notch of Meynert; *13,* lingual sulcus.

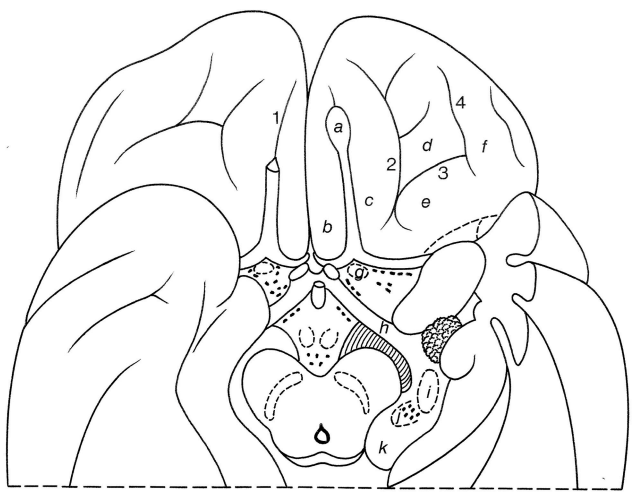

FIGURE 10 | Gyri and sulci on the orbital part of the frontal lobe, shown for the basal surface of the cerebral hemisphere (after Duvernoy, 1992; ten Donkelaar et al., 2018). *a,* olfactory bulb; *b,* straight gyrus; *c*, *d*, *e*, *f,* medial, anterior, posterior, and lateral olfactory gyri; *g,* olfactory tubercle; *h,* optic tract; *i,* lateral geniculate body; *j,* medial geniculate body; *k,* pulvinar; *1,* olfactory sulcus; *2,* medial orbital sulcus; *3,* transverse orbital sulcus; *4,* lateral orbital sulcus.

parahippocampal gyrus protrudes medially as the **uncus**. Below the uncus lies the **amygdala**. Lateral to the parahippocampal gyrus, the following structures can successively be observed: the *collateral sulcus* (*sulcus collateralis*), the *fusiform gyrus* (T4; *gyrus fusiformis*) or *lateral occipitotemporal gyrus*, the *occipitotemporal sulcus* (*sulcus occipitotemporalis*), and the *inferior temporal gyrus* (T3; *gyrus temporalis inferior*).

The naming of two "olfactory gyri" in the TA (1998) suggested that there were clearly identifiable gyral structures; this is not true. These terms persisted from the old description of the "rhinencephalon" (see Gastaut and Lammers, 1961; Stephan, 1975) and have been deleted in the TNA (2017). The real olfactory cortex is the *piriform* or *primary olfactory cortex* (*cortex piriformis* or *cortex olfactorius primarius*), which can be divided into frontal and temporal parts (Allison, 1954; Heimer et al., 1977, 1999; Zilles, 2004; Zilles and Amunts, 2012; ten Donkelaar et al., 2018).

In the TNA (2017), the TA names for the sulci and gyri in the orbitofrontal cortex have been corrected. Lateral to the olfactory sulcus, there are two longitudinally directed sulci, the *medial orbital sulcus* (*sulcus orbitalis medialis*) and the *lateral orbital sulcus* (*sulcus orbitalis lateralis*), which are joined by the *transverse orbital sulcus* (*sulcus orbitalis transversus*) to form an H or a K pattern (Duvernoy, 1992; Chiavaras and Petrides, 2000; Öngur et al., 2003; Petrides and Pandya, 2012; Rolls et al., 2015; ten Donkelaar et al., 2018). The following orbital gyri can be found: the *medial orbital gyrus* (*gyrus orbitalis medialis*) between the olfactory sulcus and the medial orbital sulcus, the *anterior orbital gyrus* (*gyrus orbitalis anterior*), the cortex rostral to the transverse orbital sulcus, the *posterior orbital gyrus* (*gyrus orbitalis posterior*), the cortex caudal to the transverse orbital sulcus, and the *lateral orbital gyrus* (*gyrus orbitalis lateralis*) lateral to the lateral orbital sulcus. The caudal parts of the medial and posterior orbital gyri merge to form the *posteromedial orbital lobule* (*lobulus orbitalis posteromedialis*) as described by Türe et al. (1999) and Naidich et al. (2004). The posteromedial orbital lobule gives rise to the *transverse insular gyrus* (*gyrus transversus insulae*). Mai and Majtanik (2017) also distinguished a *posterolateral orbital region* (*regio orbitalis posterolateralis*) between the posterior orbital gyrus and the orbital part of the inferior frontal gyrus.

THE LIMBIC LOBE

The cingulate gyrus and the parahippocampal gyrus form a border (limbus) around the corpus callosum and the brain stem (Broca, 1878b). Broca subdivided his *grand lobe limbique* into inner (the hippocampal formation) and outer (the cingulate and parahippocampal) rings for which now the general descriptive term **limbic lobe** is used (Heimer et al., 2008; Nieuwenhuys et al., 2008). The **"scissure limbique"** separates the limbic lobe from the rest of the cerebral cortex and can be seen as an **interlobar sulcus** (Duvernoy, 1992; ten Donkelaar et al., 2018). It consists of (**Figure 11**; and **Table 3**): the *anterior paraolfactory sulcus* (*sulcus paraolfactorius anterior*) in the subcallosal area, the *cingulate sulcus* (*sulcus cinguli*), part of the subparietal sulcus, the rostral part of the parietooccipital sulcus, the *collateral sulcus* (*sulcus collateralis*), and the *rhinal sulcus* (*sulcus rhinalis*).

The limbic lobe consists of an inner ring (known as the intralimbic gyrus in the French literature; Testut and Latarjet,

TABLE 3 | Structures of the limbic lobe (based on TNA, 2017; ten Donkelaar et al., 2018).

English official terms and synonyms	Latin official terms and synonyms	Abbreviations and acronyms	Eponyms
Limbic gyrus; outer ring of limbic lobe	**Gyrus limbicus**		
subcallosal area; subcallosal gyrus	area subcallosa; gyrus subcallosus	SCA	
cingulate gyrus	gyrus cinguli	CG	
anterior cingulate cortex	gyrus cinguli, pars anterior	ACC	
midcingulate cortex	gyrus cinguli, pars media	MCC	
posterior cingulate cortex	gyrus cinguli, pars posterior	PCC	
retrosplenial cortex	cortex retrosplenialis	RSC	
isthmus of cingulate gyrus	isthmus gyri cinguli	ICG	
parahippocampal gyrus	gyrus parahippocampalis	PHG; T5	
entorhinal cortex	cortex entorhinalis	EC	
white reticular substance	substantia reticularis alba		substance of Arnold
hippocampal warts	verrucae hippocampi		
perirhinal cortex	cortex perirhinalis	PRC	
uncus	uncus	Un	
ambient gyrus	gyrus ambiens	AmG	
semianular sulcus	sulcus semianularis	sas	
semilunar gyrus	gyrus semilunaris	SLG	
uncinate gyrus	gyrus uncinatus	UG	
band of dentate gyrus	limbus fasciae dentatae	BDG	band of Giacomini
intralimbic gyrus; uncal apex	gyrus intralimbicus	ILG	
collateral sulcus	sulcus collateralis	cos	
rhinal sulcus	sulcus rhinalis	rhs	
intrarhinal sulcus	sulcus intrarhinalis	irhs	
Hippocampal formation; inner ring of limbic lobe	**Formatio hippocampi**		
precommissural part of hippocampus	pars precommissuralis hippocampi	HiP	
supracommissural part of hippocampus	pars supracommissuralis hippocampi	HiS	
lateral longitudinal stria	stria longitudinalis lateralis	lls	taenia tecta; stria of Lancisi
indusium griseum	indusium griseum	IGr	
medial longitudinal stria	stria longitudinalis medialis	mls	taenia libera; stria of Lancisi
retrocommissural part of hippocampus; hippocampus proper	pars retrocommissuralis hippocampi; hippocampus proprius	HiR	
pes hippocampi; pes of hippocampus	pes hippocampi	PHip	
head; anterior segment	caput; pars anterior	HiH	
body; middle sement	corpus; pars media	HiB	
tail; posterior segment	cauda; pars posterior	HiT	
hippocampal sulcus	sulcus hippocampalis	his	
dentate gyrus	gyrus dentatus	DG	
fimbriodentate sulcus	sulcus fimbriodentatus	fds	
fimbria of hippocampus	fimbria hippocampi	FiH	
gyri of andreas retzius; subsplenial gyri	dentes subiculi; gyri subspleniales	GAR; SG	
fasciolar gyrus	gyrus fasciolaris	FG	
fasciola cinerea	fasciola cinerea	FC	
subiculum	subiculum	S	
presubiculum	presubiculum	PrS	
parasubiculum	parasubiculum	PaS	

*For summarizing figures, see **Figures 9**, **11**.*

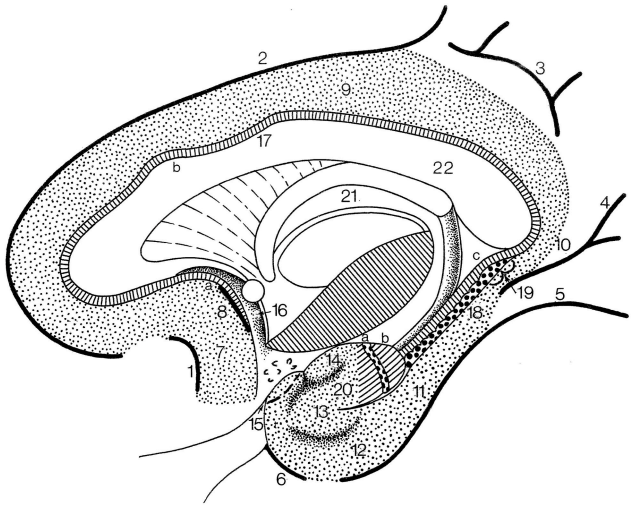

FIGURE 11 | The limbic lobe (after Duvernoy, 1998; ten Donkelaar et al., 2018). *1,* anterior paraolfactory sulcus; *2,* cingulate sulcus; *3,* subparietal sulcus; *4,* rostral part of calcarine sulcus; *5,* collateral sulcus; *6,* rhinal sulcus; *7,* subcallosal gyrus; *8,* posterior paraolfactory sulcus; *9,* cingulate gyrus; *10,* isthmus; *11,* parahippocampal gyrus; *12,* entorhinal cortex; *13,* ambient gyrus; *14,* semilunar gyrus; *15,* piriform cortex; *16,* paraterminal gyrus; *17,* indusium griseum; *18,* dentate gyrus; *19,* gyri of Andreas Retzius; *20,* uncinate gyrus; *21,* fornix; *22,* corpus callosum; *a,* bandelette of Giacomini; *b,* apex of uncus.

1948), the hippocampal formation (see below), and an outer ring, the limbic gyrus. The **limbic gyrus** (*gyrus limbicus*) includes: (1) the *subcallosal area* (*area subcallosa* or *gyrus subcallosus*), which includes the *paraolfactory gyrus* (*gyrus paraolfactorius*) between the anterior and posterior paraolfactory sulci, and the *paraterminal gyrus* (*gyrus paraterminalis*) just rostral to the lamina terminalis; (2) the *cingulate gyrus* (*gyrus cinguli*); (3) the *isthmus of the cingulate gyrus* (*isthmus gyri cinguli*); (4) the *parahippocampal gyrus* (*gyrus parahippocampalis*); (5) the *entorhinal cortex* (*cortex entorhinalis*); and (6) the *uncus*. In the TNA (2017), the uncus is treated as a structure separate from the parahippocampal gyrus, following Insausti and Amaral (2012). The *entorhinal cortex* (cortex entorhinalis; Braak and Braak, 1992; Insausti et al., 1995, 2017) is located at the rostral part of the parahippocampal gyrus, which includes the *uncus* (*uncus*) and small gyri called the the *uncinate gyrus* (*gyrus uncinatus*), the *ambient gyrus* (*gyrus ambiens*) and the *semilunar gyrus* (*gyrus semilunaris*). The entorhinal cortex corresponds to BA28 and has been subdivided into eight different subfields (Insausti et al., 1995). Adjacent is the perirhinal (Anglo-Saxon terminology) or transentorhinal (German terminology) cortex. The entorhinal cortex can be defined macroscopically by the white reticular matter (*substantia reticularis alba* of Arnold) and the hippocampal warts (*verrucae hippocampi*) described by Retzius (1896) and Klingler (1948). The entorhinal cortex is characterized by a dissecting layer (*lamina dissecans*), separating the external and internal layers, for which Rose (1926) introduced the term schizocortex.

The **uncus** *(uncus)* includes a number of bulges: (1) the *uncinate gyrus (gyrus uncinatus),* its most rostral part, corresponding to the *amygdalohippocampal transition area (area transitionis amygdalohippocampalis)*; (2) the *band of the dentate gyrus (limbus fasciae dentatae* of Giacomini), the middle part, corresponding to the dentate gyrus; and (3) the *intralimbic gyrus* or *uncal apex (gyrus intralimbicus)*, the most caudal part of the uncal bulge and corresponding to the CA3 field. The dorsal limit of the uncus is rather inconspicuous, but its ventral limit is marked by the *hippocampal sulcus (sulcus hippocampalis)*. The hippocampal sulcus continues rostralwards as the *intrarhinal sulcus (sulcus intrarhinalis)*, forming the ventral limit of the *ambient gyrus (gyrus ambiens)*. The *semianular sulcus (sulcus semianularis)* separates the ambient gyrus from the *semilunar gyrus (gyrus semilunaris)*, which forms the periamygdaloid cortex.

The *perirhinal cortex* (*cortex perirhinalis*) is a periarchicortical structure (Suzuki and Amaral, 1994; Augustinack et al., 2013) around the *perirhinal sulcus* (*sulcus perirhinalis*) and corresponds to the *transentorhinal region* (*regio transentorhinalis*) of Braak and Braak (1992). Its laminar structure is comparable to that of the entorhinal cortex. Adjacent to the perirhinal cortex is the *ectorhinal cortex* (*cortex ectorhinalis*), an isocortical part of the inferior temporal surface, but sometimes included in the perirhinal cortex (Ding and Van Hoesen, 2010).

Classically, the **hippocampal formation** (*formatio hippocampi*) is divided into three, originally adjacent, allocortical areas (Stephan, 1975; Duvernoy, 1998; ten Donkelaar, 2011): (1) the *dentate gyrus* (*gyrus dentatus*); (2) the *hippocampus proper* or *Ammon's horn* (*hippocampus proprius* or *cornu ammonis*); and (3) the *subiculum* (*subiculum*). These three structures are known as the **archicortex**. A small indentation between the fimbria and the molecular layer of the dentate gyrus has been termed the *fimbriodentate sulcus* (*sulcus fimbriodentatus*) by Gastaut and Lammers (1961). Several periallocortical structures, including the entorhinal cortex, the presubiculum and the parasubiculum, all parts of the parahippocampal gyrus, have also been included within the term "hippocampal formation," since they are closely related and share a common pattern of projections (Insausti and Amaral, 2012). The TNA (2017), however, follows the classic view.

The hippocampal formation develops from the medial pallium, and during the outgrowth of the cerebral hemispheres, first caudalwards and subsequently ventralwards and rostralwards, the *retrocommissural part* of the hippocampus (*pars retrocommissuralis hippocampi*) becomes situated in the temporal lobe (see ten Donkelaar et al., 2014). Rudiments of the *supracommissural part* of the hippocampus (*pars supracommissuralis hippocampi*) can be found above the corpus callosum as the *indusium griseum* (*indusium griseum*), a thin cell layer, flanked by the *lateral longitudinal stria* of Lancisi (*stria longitudinalis lateralis*), also known as the taenia tecti, and the *medial longitudinal stria* of Lancisi (*stria longitudinalis medialis*), also known as the taenia libera. The *precommissural part* of the hippocampus (*pars precommissuralis hippocampi*) disappears.

Macroscopically, the following parts of the hippocampus can be distinguished (Duvernoy, 1998; Insausti and Amaral, 2012; ten Donkelaar et al., 2018): (1) the *pes hippocampi* or *pes of the hippocampus* (*pes hippocampi*) showing the *hippocampal*

digitations (*digitationes hippocampi*); (2) the *head* or *anterior segment* (*caput* or *pars anterior*); (3) the *body* or *middle segment* (*corpus* or *pars media*); (4) the *tail* or *posterior segment* (*cauda* or *pars posterior*); and (5) the *gyri of Andreas Retzius* or *subsplenial gyri* (*dentes subiculi* or *gyri subspleniales*) described by Gustav Retzius (Retzius, 1896) in honor of his father Anders Adolf, a series of small bumps marking the caudal limit of the CA1 field. Here, the parahippocampal gyrus meets the retrosplenial region caudally. Two obliquely oriented small gyri are located deep to the gyri of Andreas Retzius. The medial one is the *fasciola cinerea* (*fasciola cinerea*), the visible caudal end of the dentate gyrus as described by Giacomini (1884) and Klingler (1948). The lateral gyrus, corresponding to the caudal end of the CA3 field, is the *fasciolar gyrus* (*gyrus fasciolaris*).

CONCLUSIONS

In this review, an attempt for a common terminology for the cerebral gyri and sulci is presented, largely following the recently published Terminologia Neuroanatomica (TNA, 2017). The differences found in the modern literature mainly concern:

1. The use of the term fissure for certain deep sulci; here, it is advocated to restrict the term fissure to the interhemispheric fissure, and to use the term sulcus for all other grooves;
2. The use of the topographical terms lateral and medial occipitotemporal gyri for the fusiform gyrus and the lingual gyrus, respectively.
3. These terms and some other frequently used terms are placed as synonyms, both in English and Latin in the TNA, and are summarized in **Tables 1**–**3**.
4. We suggest a simple system of abbreviations with capitals for gyri and small letters for sulci.
5. In the near future, several new subdivisions will have to be included. The TNA database at the FIPAT websites (www.unifr.ch/ifaa; http://FIPAT.library.dal.ca) will be regularly updated.

AUTHOR CONTRIBUTIONS

All authors listed have made a substantial, direct and intellectual contribution to the work, and approved it for publication.

SUPPLEMENTARY MATERIAL

The Supplementary Material for this article can be found online at: https://www.frontiersin.org/articles/10.3389/fnana.2018.00093/full#supplementary-material

REFERENCES

Allison, A. C. (1954). The secondary olfactory areas in the human brain. *J. Anat.* 88, 481–488.

Alves, R. V., Ribas, G. C., Párraga, R. G., and de Oliveira, E. (2012). The occipital lobe convexity sulci and gyri. *J. Neurosurg.* 116, 1014–1023. doi: 10.3171/2012.1.JNS11978

Amunts, K., Schleicher, A., Bürgel, U., Mohlberg, U., Uylings, H. B., and Zilles, K. (1999). Broca's region revisited: cytoarchitecture and intersubject variability. *J. Comp. Neurol.* 412, 319–341.

Amunts, K., and Zilles, K. (2012). Architecture and organizational principles of Broca's region. *Trends Cogn. Sci.* 16, 418–426. doi: 10.1016/j.tics.2012.06.005

Augustinack, J. C., Huber, K. E., Stevens, A. A., Roy, M., Frosch, M. P., van der Kouwe, A. J. W., et al. (2013). Predicting the location of human perirhinal cortex, Brodmann's area 35, from MRI. *Neuroimage* 64, 32–42. doi: 10.1016/j.neuroimage.2012.08.071

Blaizot, X., Mansilla, F., Insausti, A. M., Constans, J. M., Salinas-Alamán, A., Prõ-Sistiaga, P., et al. (2010). The human parahippocampal region: I. temporal pole cytoarchitectonics and MRI correlation. *Cereb. Cortex* 20, 2198–2222. doi: 10.1093/cercor/bhp289

Bludau, S., Eickhoff, S. B., Mohlberg, H., Caspers, S., Laird, A. R., Fox, P. T., et al. (2014). Cytoarchitecture, probability maps and functions of the human frontal pole. *Neuroimage* 93, 260–275. doi: 10.1016/j.neuroimage.2013.05.052

BNA, Basle Nomina Anatomica (1895). Published by W. *His: Die anatomische Nomenclatur. Nomina anatomica. Verzeichnis der von der Anatomischen Gesellschaft auf ihrer IX. Versammlung in Basel angenommenen Namen. Arch. Anat. Physiol., Anat. Abth., Suppl.-Bd. Leipzig: Veit*, 1–180.

Braak, H., and Braak, E. (1992). The human entorhinal cortex: normal morphology and lamina-specific pathology in various diseases. *Neurosci. Res.* 15, 6–31. doi: 10.1016/0168-0102(92)90014-4

Brissaud, E. (1893). *Anatomie du Cerveau de L'homme: Morphologie des Hémisphères Cérébraux, ou Cerveau Proprement Dit*. Paris: Masson.

Broca, P. (1863). Localisation des fonctions cérébrales. Siège de la faculté du langage articulé. *Bull. Soc. Anthropol. Paris* 4, 200–208.

Broca, P. (1878a). Nomenclature cérébrale: Dénomination et subdivision des hémisphères et des anfractuosités de la surface. *Rev. Anthropol.* 2, 193–236.

Broca, P. (1878b). Anatomie comparée des circonvolutions cérébrales. Le grand lobe limbique et la scissure limbique dans la série des mammifères. *Rev. Anthropol.* 2, 385–498.

Brodmann, K. (1909). *Vergleichende Lokalisationslehre der Grosshirnrinde in ihren Prinzipien dargestellt auf Grund des Zellenbaues*. Transl. by L.J. Garey in English (1999) Brodmann's Localisation in the Cerebral Cortex. Leipzig, Barth, London: Imperial College Press.

Caspers, J., Amunts, K., and Zilles, K. (2012). "Posterior parietal cortex", in *The Human Nervous System, 3rd ed.*, eds J. K. Mai and G. Paxinos (Amsterdam: Elsevier), 1036–1053.

Caspers, S., Zilles, K., Eickhoff, S. B., Schleicher, A., Mohlberg, H., and Amunts, K. (2013). Cytoarchitectonical analysis and probabilistic mapping of two extrastriate areas of the human fusiform gyrus. *Brain Struct. Funct.* 218, 511–526. doi: 10.1007/s00429-012-0411-8

Chau, A. M., Stewart, F., and Gragnaniello, C. (2014). Sulcal and gyral anatomy of the basal occipito-temporal lobe. *Surg. Radiol. Anat.* 36, 959–965. doi: 10.1007/s00276-014-1294-6

Chiavaras, M. M., and Petrides, M. (2000). Orbitofrontal sulci of the human and macaque monkey. *J. Comp. Neurol.* 422, 35–54. doi: 10.1002/(SICI)1096-9861(20000619)422:1<35::AID-CNE3>3.0.CO;2-E

Choi, H. J., Zilles, K., Mohlberg, H., Schleicher, A., Fink, G. R., Armstrong, E., et al. (2006). Cytoarchitectonic identification and probabilistic mapping of two distinct areas within the anterior ventral bank of the human intraparietal sulcus. *J. Comp. Neurol.* 495, 53–69. doi: 10.1002/cne.20849

Cikla, U., Menekse, G., Quraishi, A., Neves, G., Keles, A., Liu, C., et al. (2016). The sulci of the inferior surface of the temporal lobe: An anatomical study. *Clin. Anat.* 29, 932–942. doi: 10.1002/ca.22767

Collins, D. L. (1994). *3D Model-Based Segmentation of Individual Brain Structures From Magnetic Resonance Imaging Data*. PhD thesis, McGill University.

Collins, D. L., Zijdenbos, A. P., Kollokian, V., Sled, J. G., Kabani, N. J., Holmes, C. J., et al. (1998). Design and construction of a realistic digital brain phantom. *IEEE Trans. Med. Imag.* 17, 463–468. doi: 10.1109/42.712135

Dejerine, J. (1895). *Anatomie des Centres Nerveux, Vol 1*. Paris: Rueff.

Ding, S.-L., Royall, J.,l., Sunkin, S. M., Ng, L., Facer, B. A. C., Lesnar, P., et al. (2016). Comprehensive cellular-resolution atlas of the adult human brain. *J. Comp. Neurol.* 524, 3127–3481. doi: 10.1002/cne.24080

Ding, S.-L., and Van Hoesen, G. W. (2010). Borders, extent, and topography of human perirhinal cortex as revealed using multiple modern neuroanatomical and pathological markers. *Hum. Brain Mapp.* 31, 1359–1379. doi: 10.1002/hbm.20940

Ding, S.-L., Van Hoesen, G. W., Cassell, M. D., and Poremba, A. (2009). Parcellation of human temporal polar cortex: a combined analysis of multiple cytoarchitectonic, chemoarchitectonic, and pathological markers. *J. Comp. Neurol.* 514, 595–623. doi: 10.1002/cne.22053

Duvernoy, H. (1992). *Le Cerveau Humain. Surface, Coupes Sériée Tridimensionelles et IRM*. Berlin; New York, NY: Springer.

Duvernoy, H. (1998). *The Human Hippocampus. Functional Anatomy, Vascularization and Serial Sections With MRI, 2nd ed*. Berlin; New York, NY: Springer.

Eberstaller, O. (1884). Zur Oberflächenanatomie der Grosshirnhemisphären. *Wien. Med. Bl.* 7, 479–482, 542–582, 644–646.

Eberstaller, O. (1890). *Das Stirnhirn. Ein Beitrag zur Anatomie der Oberfläche des Grosshirns*. Wien: Urban & Schwarzenberg.

Ecker, A. (1869). *Die Hirnwindungen des Menschen*. Braunschweig: Vieweg.

Eickhoff, S. B., Amunts, K., Mohlberg, H., and Zilles, K. (2006b). The human parietal operculum. II. Stereotaxic maps and correlation with functional imaging. *Cereb. Cortex* 16, 268–279. doi: 10.1093/cercor/bhi106

Eickhoff, S. B., Schleicher, A., Zilles, K., and Amunts, K. (2006a). The human parietal operculum. I. cytoarchitectonic mapping of subdivisions. *Cereb. Cortex* 16, 254–267. doi: 10.1093/cercor/bhi105

Eickhoff, S. B., Stephan, K. E., Mohlberg, H., Grefkes, C., Fink, G. R., Amunts, K., et al. (2005). A new SPM toolbox for combining probabilistic cytoarchitectonic maps and functional imaging data. *Neuroimage* 25, 1325–1335. doi: 10.1016/j.neuroimage.2004.12.034

Galaburda, A. M., Sanides, F., and Geschwind, N. (1978). Human brain: cytoarchitectonic left-right asymmetries in the temporal speech region. *Arch. Neurol.* 35, 812–817. doi: 10.1001/archneur.1978.00500360036007

Gastaut, H., and Lammers, H. J. (1961). *Anatomie du Rhinencéphale*. Paris: Masson.

Geschwind, N., and Levitsky, W. (1968). Human brain: left-right asymmetries in temporal speech region. *Science* 161, 186–187. doi: 10.1126/science.161.3837.186

Giacomini, C. H. (1884). Fascia dentata du grand hippocampe dans le cerveau de l'homme. *Arch. Ital. Biol.* 5, 1–16, 205–209, 396–417.

Gratiolet, L. P. (1854). *Mémoire Sur Les Plis Cérébraux de L'homme et Des Primates*. Paris: Bertrand.

Hanke, J. (1997). Sulcal pattern of the anterior parahippocampal gyrus in the human adult. *Ann. Anat.* 179, 335–339. doi: 10.1016/S0940-9602(97)80071-4

Heimer, L., de Olmos, J., Alheid, G. F., Pearson, J., Sakamoto, N., Marksteiner, J., et al. (1999). The human basal forebrain, Part 2. *Handb. Chem. Neuroanat.* 15, 57–226. doi: 10.1016/S0924-8196(99)80024-4

Heimer, L., Van Hoesen, G. W., and Rosene, D. L. (1977). The olfactory pathways and the anterior perforated substance in the primate brain. *Int. J. Neurosci.* 12, 42–52.

Heimer, L., Van Hoesen, G. W., Trimble, M., and Zahm, D. S. (2008). *Anatomy of Neuropsychiatry*. Amsterdam: Elsevier.

Heschl, R. L. (1878). *Über Die Vordere Quere Schläfenwindung des Menschlichen Grosshirns*. Wien: Braumüller.

Hill, J., Dierker, D., Neil, J., Inder, T., Knutsen, A., Harwell, J., et al. (2010). A surface-based analysis of hemispheric asymmetries and folding of cerebral cortex in term-born human infants. J. *Neurosci.* 30:2268–2276. doi: 10.1523/JNEUROSCI.4682-09.2010

Holmes, C. J., Hoge, R., Collins, L., Woods, R., Toga, A. W., and Evans, A. C. (1998). Enhancement of MR images using registration for signal averaging. *J. Comput. Assist. Tomogr.* 22, 324–333. doi: 10.1097/00004728-199803000-00032

Huntgeburth, S. C., and Petrides, M. (2012). Morphological patterns of the collateral sulcus in the human brain. *Eur. J. Neurosci.* 35, 1295–1311. doi: 10.1111/j.1460-9568.2012.08031.x

Huschke, E. (1854). *Schädel, Hirn und Seele des Menschen und der Thiere nach Alter, Geschlecht und Race*. Jena: Mauke.

Ide, A., Dolezal, C., Fernández, M., Labb,é, E., Mandujano, R., Montes, S., et al. (1999). Hemispheric differences in variability of fissural patterns in parasylvian and cingulate regions of human brains. *J. Comp. Neurol.* 410, 235–242. doi: 10.1002/(SICI)1096-9861(19990726)410:2<235::AID-CNE5>3.3.CO;2-7

Insausti, R., and Amaral, D. G. (2012). "Hippocampal formation", in *The Human Nervous System, 3rd ed*, eds J. K. Mai and G. Paxinos (Amsterdam: Elsevier), 896–942.

Insausti, R., Muñoz-López, M., Insausti, A. M., and Artachon-Pérula, E. (2017). The human periallocortex: Layer pattern in presubiculum, parasubiculum and entorhinal cortex. A review. *Front. Neuroanat.* 11:84. doi: 10.3389/fnana.2017.00084

Insausti, R., Tuñón, T., Sobreviela, T., and Insausti, A. M. (1995). The human entorhinal cortex: a cytoarchitectonic analysis. *J. Comp. Neurol.* 355, 171–198. doi: 10.1002/cne.903550203

Jensen, J. (1871). Abhandlung über die Furchen und Windungen der menschlichen Grosshirnhemisphären. *Allg. Z. Psychiatr.* 27, 473–516.

JNA, Jenaer Nomina Anatomica (1936). *Approved June 1935 by the Anatomische Gesellschaft in Jena, Published Early 1936 by H. Stieve*. Jena: Fischer.

Klingler, J. (1948). *Die Makroskopische Anatomie der Ammonsformation. Denkschr. Schweiz. Naturforsch. Ges., Vol 78*. Zürich: Fretz.

Lorenz, S., Weiner, K. S., Caspers, J., Mohlberg, H., Schleicher, A., Bludau, S., et al. (2017). Two new cytoarchitectonic areas on the human mid-fusiform gyrus. *Cereb. Cortex* 27, 373–385. doi: 10.1093/cercor/bhv225

Mai, J. K., and Majtanik, M. (2017). *Human Brain in Standard MNI Space. A Comprehensive Pocket Atlas*. London, San Diego, CA: Academic Press/Elsevier.

Mai, J. K., Majtanik, M., and Paxinos, G. (2016). *Atlas of the Human Brain, 4th Edn*. San Diego, CA: Academic Press/Elsevier.

Mai, J. K., and Paxinos, G. eds. (2012). *The Human Nervous System, 3rd ed*. Amsterdam: Elsevier.

Malikovic, A., Vucetic, B., Milisavljevic, M., Tosevski, J., Sazdanovic, P., Milojevic, B., et al. (2012). Occipital sulci of the human brain: variability and morphometry. *Anat. Sci. Int.* 87,61–70. doi: 10.1007/s12565-011-0118-6

Marie, D., Jobard, G., Crivello, F., Perchey, G., Petit, L., Mellet, E., et al. (2015). Descriptive anatomy of Heschl's gyri in 430 healthy volunteers, including 198 left-handers. *Brain Struct. Funct.* 220, 729–743. doi: 10.1007/s00429-013-0680-x

Mazziota, J., Toga, A., Evans, A., Fox, P., Lancaster, J., Zilles, K., et al. (2001). A probabilistic atlas and reference system for the human brain: international consortium for brain mapping (icbm). *Philos. Trans. R. Soc. Lond. B. Biol. Sci.* 356, 1293–1322. doi: 10.1098/rstb.2001.0915

Morel, A., Gallay, M. N., Baechler, A., Wyss, M., and Gallay, D. S. (2013). The human insula: architectonic organization and postmortem MRI registration. *Neuroscience* 236, 117–135. doi: 10.1016/j.neuroscience.2012.12.076

Naidich, T. P., Kang, E., Fatterpekar, G. M., Delman, B. N., Gultekin, S. H., Wolfe, D., et al. (2004). The insula: anatomic study and MR imaging display at 1.5 T. *AJNR Am. J. Neuroradiol.* 25, 222–232.

Nieuwenhuys, R., Broere, C. A. J., and Cerliani, L. (2015). A new myeloarchitectonic map of the human neocortex based on data from the Vogt-Vogt school. *Brain Struct. Funct.* 220, 2551–2573. doi: 10.1007/s00429-014-0806-9

Nieuwenhuys, R., Voogd, J., and van Huyzen, C. (2008). *The Human Central Nervous System, 4th Edn*. Heidelberg: Springer.

Öngur, D., Ferry, A. T., and Price, J.L. (2003). Architectonic subdivision of the human prefrontal cortex. *J. Comp. Neurol.* 460, 425–449. doi: 10.1002/cne.10609

Ono, M., Kubik, S., and Abernathey, C. D. (1990). *Atlas of the Cerebral Sulci*. Stuttgart; New York, NY: Thieme.

Pansch, A. G. (1868). Über die typische Anordnung der Furchen und Windungen auf den Grosshirnhemisphären des Menschen und der Affen. *Arch. Anthropol.* 3, 227–257.

Pansch, A. G. (1879). *Die Furchen und Wülste am Grosshirn des Menschen*. Berlin: Oppenheim.

Paus, T., Tomaiuolo, F., Otaky, N., MacDonald, D., Petrides, M., Atlas, J., et al. (1996). Human cingulate and paracingulate sulci: pattern, variability, asymmetry, and probabilistic map. *Cereb. Cortex* 6, 207–214. doi: 10.1093/cercor/6.2.207

Petrides, M., and Pandya, D. N. (2012). "The frontal cortex," in *The Human Nervous System, 3rd Edn.*, eds J. K. Mai and G. Paxinos (Amsterdam: Elsevier), 988–1011.

PNA, Parisiensia Nomina Anatomica (1955). *Approved by the Sixth International Congress of Anatomists held at Paris 1955, privately circulated; PNA printed by Spottiswoode, Ballantine & Co, London; revised editions appeared as Nomina*

Anatomica (2nd ed 1961, 3rd 1966, 4th 1977, published by Excerpta Medica, Amsterdam, a 5th ed 1983 and a 6th ed 1989, published by Williams & Wilkins, Baltimore, and Churchill Livingstone, Edinburgh, respectively).

Retzius, G. (1896). *Das Menschenhirn: Studien in der Makroskopischen Morphologie*. Stockholm: Norstedt.

Rhoton, A. L. Jr. (2007). The cerebrum. *Neurosurgery* 61 (SHC Suppl 1), SHC37–SHC119. doi: 10.1227/01.NEU.0000255490.88321.CE

Rizzolatti, G., Luppino, G., and Matelli, M. (1998). The organization of the cortical motor system: new concepts. *Electroencephalogr. Clin. Neurophysiol.* 106, 283–296. doi: 10.1016/S0013-4694(98)00022-4

Rolls, E. T., Joliot, M., and Tzourio-Mazoyer, N. (2015). Implementation of a new parcellation of the orbitofrontal cortex in the automated anatomical labeling atlas. *Neuroimage* 122, 1–5. doi: 10.1016/j.neuroimage.2015.07.075

Rose, M. (1926). Über das histogenetische Prinzip der Einteilung der Grosshirnrinde. *J. Psychol. Neurol.* 32, 97–160.

Rose, M. (1935). "Cytoarchitektonik und myeloarchitektonik der Groβhirnrinde," in *Handbuch der Neurologie*, *Bd. 1*, eds O. Bumke and O. Förster (Berlin: Springer), 588–778.

Rosenke, M., Weiner, K. S., Barrett, M. A., Zilles, K., Amunts, K., Goebel, R., et al. (2018). A cross-validated cytoarchitectonic atlas of the human ventral visual stream. *Neuroimage* 170, 257–270. doi: 10.1016/j.neuroimage.2017.02.040

Rumeau, C., Tzourio, N., Murayama, N., Peretti-Viton, P., Levrier, O., Joliot, M., et al. (1994). Location of hand function in the sensorimotor cortex: MR and functional correlation. *AJNR Am. J. Neuroradiol.* 15, 567–572.

Scheperjans, F., Eickhoff, S. B., Hömke, L., Mohlberg, H., Hermann, K., Amunts, K., et al. (2008a). Probabilistic maps, cytoarchitectonic morphology, and variability of areas in human superior parietal cortex. *Cereb. Cortex* 18, 2141–2157. doi: 10.1093/cercor/bhm241

Scheperjans, F., Hermann, K., Eickhoff, S. B., Amunts, K., Schleicher, A., and Zilles, K. (2008b). Observer-independent cytoarchitectonic mapping of the human superior parietal cortex. *Cereb. Cortex* 18, 846–867. doi: 10.1093/cercor/bhm116

Seitz, R. J., and Binkofski, F. (2003). Modular organization of parietal lobe functions revealed by functional activation studies. *Adv. Neurol.* 93, 281–292.

Stephan, H. (1975). *Allocortex. Handbuch der mikroskopischen Anatomie des Menschen, Vol 4, Teil 9*. Heidelberg: Springer.

Suzuki, W. A., and Amaral, D. G. (1994). The perirhinal and parahippocampal cortices of the macaque monkey: cortical afferents. *J. Comp. Neurol.* 350, 497–533. doi: 10.1002/cne.903500402

TA, Terminologia Anatomica (1998). *International Anatomical Terminology*. Stuttgart; New York, NY: FCAT, Thieme.

Talairach, J., and Tournoux, P. (1988). *Co-planar Stereotaxic Atlas of the Human Brain 3-Dimensional Proportional System: An approach to cerebral imaging*. Stuttgart; New York, NY: Thieme.

Tamraz, J. C., and Comair, Y. G. (2000). *Atlas of Regional Anatomy of the Brain Using MRI*. Berlin; New York, NY: Springer.

ten Donkelaar, H. J. (2011). *Clinical Neuroanatomy: Brain Circuitry and its Disorders*. Heidelberg; Dordrecht; London; New York, NY: Springer.

ten Donkelaar, H. J., Broman, J., Neumann, P. E., Puelles, L., Riva, A., Tubbs, R. S., et al. (2017). Towards a Terminologia Neuroanatomica. *Clin. Anat.* 30, 145–155. doi: 10.1002/ca.22809

ten Donkelaar, H. J., Kachlík, D., and Tubbs, S. T. (2018). *An Illustrated Terminologia Neuroanatomica. A Concise Encyclopedia of Human Neuroanatomy*. Heidelberg; New York, NY: Springer.

ten Donkelaar, H. J., Lammens, M., and Hori, A. (2014). *Clinical Neuroembryology: Development and Developmental Disorders of the Human Central Nervous System, 2nd ed*. Heidelberg; New York, NY; Dordrecht; London: Springer.

Testut, L., and Latarjet, A. (1948). *Traité d'anatomie Humaine*, *Vol. 2*. Paris: Doin.

TNA, Terminologia Neuroanatomica (2017). *FIPAT.library.dal.ca*. Dalhousie: Federative International Programme for Anatomical Terminology.

Toga, A. W., and Thompson, P. M. (2003). Mapping brain asymmetry. *Nat. Rev. Neurosci.* 4:37–48. doi: 10.1038/nrn1009

Türe, U., Yaşargil, D. C. H., Al-Mefti, O., and Yaşargil, M. C. (1999). Topographic anatomy of the insular region. *J. Neurosurg.* 90, 720–733. doi: 10.3171/jns.1999.90.4.0720

Tzourio-Mazoyer, N., Landeau, B., Papathanassiou, D., Crivello, F., Etard, O., Delcroix, N., et al. (2002). Automated anatomical labeling of activations in SPM using a maroscopic anatomical parcellation of the MNI MRI single-subject brain. *Neuroimage* 15, 273–289. doi: 10.1006/nimg.2001.0978

Tzourio-Mazoyer, N., and Mazoyer, B. (2017). Variations of planum temporale asymmetries with Heschl's gyri duplications and association with cognitive abilities: MRI investigation of 428 healthy volunteers. *Brain Struct. Funct.* 222, 2711–2726. doi: 10.1007/s00429-017-1367-5

Van Essen, D. C. (2005). A population-average, landmark- and surface-based (pals) atlas of the human cerebral cortex. *Neuroimage* 28, 635–662. doi: 10.1016/j.neuroimage.2005.06.058

Van Essen, D. C., Glasser, M. F., Dierker, D. L., Harwell, J., and Coalson, T. (2012). Parcellation and hemispheric asymmetries of human cerebral cortex analysed on surface-based atlases. *Cereb. Cortex* 22, 2241–2262. doi: 10.1093/cercor/bhr291

Vicq d'Azyr, F. (1786). *Traité D'anatomie et de Physiologie, Avec des Planches Coloriées Réprésentant au Naturel les Divers Organes de L'homme et des Animaux, Tome I*. Paris: Didot.

Vogt, B. A., and Palomero-Gallagher, N. (2012). "Cingulate cortex," in *The Human Nervous System*, *3rd ed*, eds J. K. Mai and G. Paxinos (Amsterdam: Elsevier), 943–987.

Vogt, C., and Vogt, O. (1919). Allgemeinere ergebnisse unserer Hirnforschung. *J. Psychol. Neurol.* 25, 279–461.

von Economo, C., and Horn, L. (1930). Über Windingsrelief, Maβe und Rindenarchitektonik der Supratemporalfläche. *Z. Ges. Neurol. Psychiatr.* 130, 678–757.

von Economo, C., and Koskinas, G. N. (1925). *Die Cytoarchitektonik der Hirnrinde des erwachsenen Menschen*. In English transl. by L.C. Triarhou (2008). *Atlas of Cytoarchitectonics of the Adult Human Cerebral Cortex*. Berlin; Heidelberg; New York, NY; Basel: Karger, Springer.

von Soemmerring, S. T. (1791). *Vom Baue des Menschlichen Körpers, Vol 5: Hirnlehre und Nervenlehre*. Frankfurt am Main: Varrentrap & Wenner.

Wang, L., Mruczek, R. E., Arcaro, M. J., and Kastner, S. (2015). Probabilistic maps of visual topography in human cortex. *Cereb. Cortex* 25, 3911–3931. doi: 10.1093/cercor/bhu277

Wernicke, C. (1874). *Der aphasische Symptomenkomplex. Eine Psychologische Studie Auf Anatomischer Basis*. Breslau: Cohn & Weigert.

Wernicke, C. (1876). Das Urwindungssystem des menschlichen Gehirns. *Arch. Psychiatr. Nervenkr.* 6, 298–326. doi: 10.1007/BF02230815

Yousry, T. A., Schmid, U. D., Alkadhi, H., Schmidt, D., Peraud, A., Buettner, A., et al. (1997). Localization of the hand motor area to a knob on the precentral gyrus. a new landmark. *Brain* 120, 141–157.

Zilles, K. (2004). "Architecture of the human cerebral cortex. regional variation and laminar organization," in *The Human Nervous System*, *2nd ed*, eds G. Paxinos and J.K. Mai (Amsterdam: Elsevier), 997–1055.

Zilles, K., and Amunts, K. (2012). "Architecture of the human cerebral cortex," in *The Human Nervous System*, *3rd ed*, eds J. K. Mai and G. Paxinos (Amsterdam: Elsevier), 836–895.

Zlatkina, V., and Petrides, M. (2014). Morphological patterns of the intraparietal sulcus and the anterior intermediate parietal sulcus of Jensen in the human brain. *Proc. Roy. Soc. B* 281:20141493. doi: 10.1098/rspb.2014.1493

Conflict of Interest Statement: The authors declare that the research was conducted in the absence of any commercial or financial relationships that could be construed as a potential conflict of interest.

Copyright © 2018 ten Donkelaar, Tzourio-Mazoyer and Mai. This is an open-access article distributed under the terms of the Creative Commons Attribution License (CC BY). The use, distribution or reproduction in other forums is permitted, provided the original author(s) and the copyright owner(s) are credited and that the original publication in this journal is cited, in accordance with accepted academic practice. No use, distribution or reproduction is permitted which does not comply with these terms.

frontiers in Neuroanatomy

ORIGINAL RESEARCH
published: 21 February 2019
doi: 10.3389/fnana.2019.00021

Cytoarchitectonic Areas of the *Gyrus ambiens* in the Human Brain

Ricardo Insausti[1]†, Marta Córcoles-Parada[1†], Mar Maria Ubero[2], Adriana Rodado[1], Ana Maria Insausti[3] and Mónica Muñoz-López[1]*

[1] Human Neuroanatomy Laboratory, School of Medicine, University of Castilla–La Mancha, Albacete, Spain, [2] Departamento de Anatomía, Universidad Católica San Antonio de Murcia, Murcia, Spain, [3] Faculty of Health Sciences, University Public of Navarra, Pamplona, Spain

The *Gyrus ambiens* is a gross anatomical prominence in the medial temporal lobe (MTL), associated closely with Brodmann area 34 (BA34). It is formed largely by the medial intermediate subfield of the entorhinal cortex (EC) [Brodmann area 28 (BA28)]. Although the MTL has been widely studied due to its well-known role on memory and spatial information, the anatomical relationship between *G. ambiens*, BA34, and medial intermediate EC subfield has not been completely defined, in particular whether BA34 is part of the EC or a different type of cortex. In order to clarify this issue, we carried out a detailed analysis of 37 human MTLs, determining the exact location of medial intermediate EC subfield and its extent within the *G. ambiens*, its cortical thickness, and the histological–MRI correspondence of the *G. ambiens* with the medial intermediate EC subfield in 10 *ex vivo* MRI. Our results show that the *G. ambiens* is limited between two small sulci in the medial aspect of the MTL, which correspond almost perfectly to the extent of the medial intermediate EC subfield, although the rostral and caudal extensions of the *G. ambiens* may extend to the olfactory (rostrally) and intermediate (caudally) entorhinal subfields. Moreover, the cortical thickness averaged 2.5 mm (1.3 mm for layers I–III and 1 mm for layers V–VI). Moreover, distance among different landmarks visible in the MRI scans which are relevant to the identification of the *G. ambiens* in MRI are provided. These results suggest that BA34 is a part of the EC that fits best with the medial intermediate subfield. The histological data, together with the *ex vivo* MRI identification and thickness of these structures may be of use when assessing changes in MRI scans in clinical settings, such as Alzheimer disease.

Keywords: human, entorhinal cortex, subfield EMI, ambient gyrus, cytoarchitectonics, BA34

OPEN ACCESS

Edited by:
Hans J. ten Donkelaar, Radboud University Nijmegen, Netherlands

Reviewed by:
Menno P. Witter, Norwegian University of Science and Technology, Norway
Loreta Medina, Universitat de Lleida, Spain

****Correspondence:***
Ricardo Insausti
ricardo.insausti@uclm.es

† These authors have contributed equally to this work

Received: *23 September 2018*
Accepted: *05 February 2019*
Published: *21 February 2019*

Citation:
Insausti R, Córcoles-Parada M, Ubero MM, Rodado A, Insausti AM and Muñoz-López M (2019) Cytoarchitectonic Areas of the Gyrus ambiens in the Human Brain. Front. Neuroanat. 13:21. doi: 10.3389/fnana.2019.00021

Abbreviations: BA, Brodmann area; BA35, Brodmann area 35 or perirhinal cortex; BA36, Brodmann area 36 or entorhinal cortex; EC, entorhinal cortex; E_C, caudal subfield of the entorhinal cortex; E_{CL}, caudal limiting subfield of the entorhinal cortex; E_I, intermediate subfield of the entorhinal cortex; E_{LC}, lateral caudal subfield of the entorhinal cortex; E_{LR}, lateral rostral subfield of the entorhinal cortex; E_{MI}, medial intermediate subfield of the entorhinal cortex; E_O, olfactory subfield of the entorhinal cortex; E_R, rostral subfield of the entorhinal cortex; GA, *Gyrus ambiens*; GS, *Gyrus semilunaris*; GU, *Gyrus uncinatus*; MTL, medial temporal lobe; PHG, parahippocampal gyrus.

INTRODUCTION

The entorhinal cortex (EC) or *Cortex Entorhinalis*[1] is a component of the hippocampal formation (HF), which is formed by different archicortical (dentate gyrus, CA fields, subiculum) and periarchicortical areas (presubiculum, parasubiculum, EC). In humans, the EC forms part of the parahippocampal gyrus (PHG) or *Gyrus parahippocampalis*. The PHG is located in the ventromedial surface of the temporal lobe, which, with the adjacent cortex lining the collateral sulcus *or sulcus collateralis*, forms the medial temporal lobe (MTL).

The MTL has been associated to functions such as memory and processing of spatial information (Aggleton and Mishkin, 1985; Maguire et al., 2000; Squire et al., 2004). The vast majority of the information entering the nonhuman primate EC comes exclusively from polysensory association areas (for review, see Insausti et al., 2017). The majority of the cortical input reaches the upper layers of EC subfields over the rostro-caudal and medio-lateral extents of the EC (Suzuki and Amaral, 1994; Insausti and Amaral, 2008; Mohedano-Moriano et al., 2008). The cortical output leaves the EC through the deep layers (V and VI) and sends information back to polysensory areas that send input to EC (Muñoz and Insausti, 2005). Pathological processes in the EC are considered as one of the hallmarks of Alzheimer disease (Braak and Braak, 1992) with a decrease in neuron number occurs, not only in upper layers (Gómez-Isla et al., 1996), but also in deep layers as well (Arnold et al., 1991).

Along the years, the study of the MTL, and in particular in the field of Alzheimer disease, has also incorporated neuroimaging techniques which can determine both the location of the EC in MRI images (Insausti et al., 1998a), as well as its structural and volumetric changes (Juottonen et al., 1998; Khan et al., 2014).

The EC laminar structure is known since Hammarberg (1895) and can be found in classical neuroanatomical work (Cajal, 1901; Lorente de Nó, 1933), although it was not topographically described until Brodmann (1909). He divided the MTL into area 28 (EC), located in the anterior portion of the PHG, and area 34, which lies medial to area 28. BA34 corresponds approximately to the macroscopically visible ambient gyrus or *Gyrus ambiens (GA)*. The GA forms in the human brain a visible protuberance situated in the medialmost portion of the anterior temporal lobe. This parcellation of the cerebral cortex is not completely accepted by contemporary authors who challenge the correspondence of Brodmann's cortical areas as defined by functional studies (Nieuwenhuys et al., 2015).

The GA as an anatomical structure is known since Solly (1836), who described it in relation to the *limen insulae* (Swanson, 2015). The GA was assigned first to the olfactory system and later included as part of the piriform area by Smith in 1919 (Swanson, 2015). Williams and Warwick (1980) include the GA as part of the prepiriform area, which continues caudally into the entorhinal area.

The GA (**Figures 1A,B**) is the largest and most outstanding gross macroscopic prominence of the PHG. Other bulge in the most anterior part of the MTL is the semilunar gyrus (GS), separated from the GA by the semianular sulcus or *sulcus semianularis*[2]. Cytoarchitectonically, the GS corresponds to periamygdaloid cortex (Insausti and Amaral, 2012). Another bulge close to the GA is uncinate gyrus (GU), which lies caudal to the GA and GS, at the transition between the caudalmost portion of the amygdala and the hippocampus (**Figure 1B**). Therefore, the GA can be considered as a medial extension of the PHG in the MTL.

As mentioned above, the cortex situated in the anterior part of the PHG is the EC, a phylogenetically conserved brain region present in all mammals (Stephan, 1975). The cytoarchitecture of the EC has been subject of study since the middle of the nineteenth century, and it has been subdivided into different subfields (Amaral et al., 1987; Insausti et al., 1995, and references therein). The best-known synonym of EC is BA28, and both are used in an interchangeable way. Somewhat less clear is the type of cortex present in BA34. Brodmann describes it as: "*Area 34 – the dorsal entorhinal area. It lies mainly to the inferior rhinencephalic sulcus* (*Retzius, 1896*), *so that this sulcus forms the approximate border between both types*" (Brodmann, 1909, translation of Garey, 1994). The other area alluded to is BA28 or EC. It is obvious that Brodmann only gives an account of the location of his dorsal entorhinal area, without any further elaboration on cytoarchitectonic characteristics.

Brodmann's gross anatomical drawing of the human cortical area shows that area 34 is largely coincident with the macroscopic GA. Moreover, Brodmann indicates the "inferior rhinencephalic sulcus" (Retzius, 1896) as the boundary between areas 28 and 34 and refers to the cortex of the "lunate gyrus" of Retzius (equivalent to GS) on the medial side of area 34 (**Figure 1A**). Therefore, Brodmann makes a clear distinction of two separate areas, area 28 or EC, and area 34 in the anterior part of the PHG. Area 34 is still in use by some authors (Krimer et al., 1997; Ding, 2013).

The gross anatomical organization of the MTL has been dealt with in several reports (Amaral and Insausti, 1990; Duvernoy, 2005; Insausti and Amaral, 2012), and they all agree with the commonly accepted pattern of the series of bulges present in the medialmost aspect of the MTL. However, the pattern of sulci present in the PHG is more controversial, and reports in the literature show a disparity of names (Heckers et al., 1990; Ono et al., 1990; Heinsen et al., 1996; Hanke, 1997; Duvernoy, 2005; Huntgeburth and Petrides, 2012). Finally, although the cytoarchitectonic segmentation of the human EC has been studied along the last century, some differences still persist (Insausti et al., 1995; Krimer et al., 1997).

Modern MRI techniques reveal the anatomy of the MTL in detail and great accuracy (Yushkevich et al., 2015; Iglesias et al., 2016), so that the shape and extension of the medial temporal bulges (GA, GS, and GU) can be readily assessed. Thereby, the anatomical identification of the medial temporal

[1]Latin nomenclature, from Terminología Neuroanatómica (2017) FIPAT.library.dal.ca. Federative International Programme for Anatomical Terminology is mentioned in *italics* in the text, alongside the common English terms used in neuroanatomical literature (illustrated version in ten Donkelaar et al., 2018).

[2]Usually cited in its Latin form, thereby we will continue using this form in the manuscript.

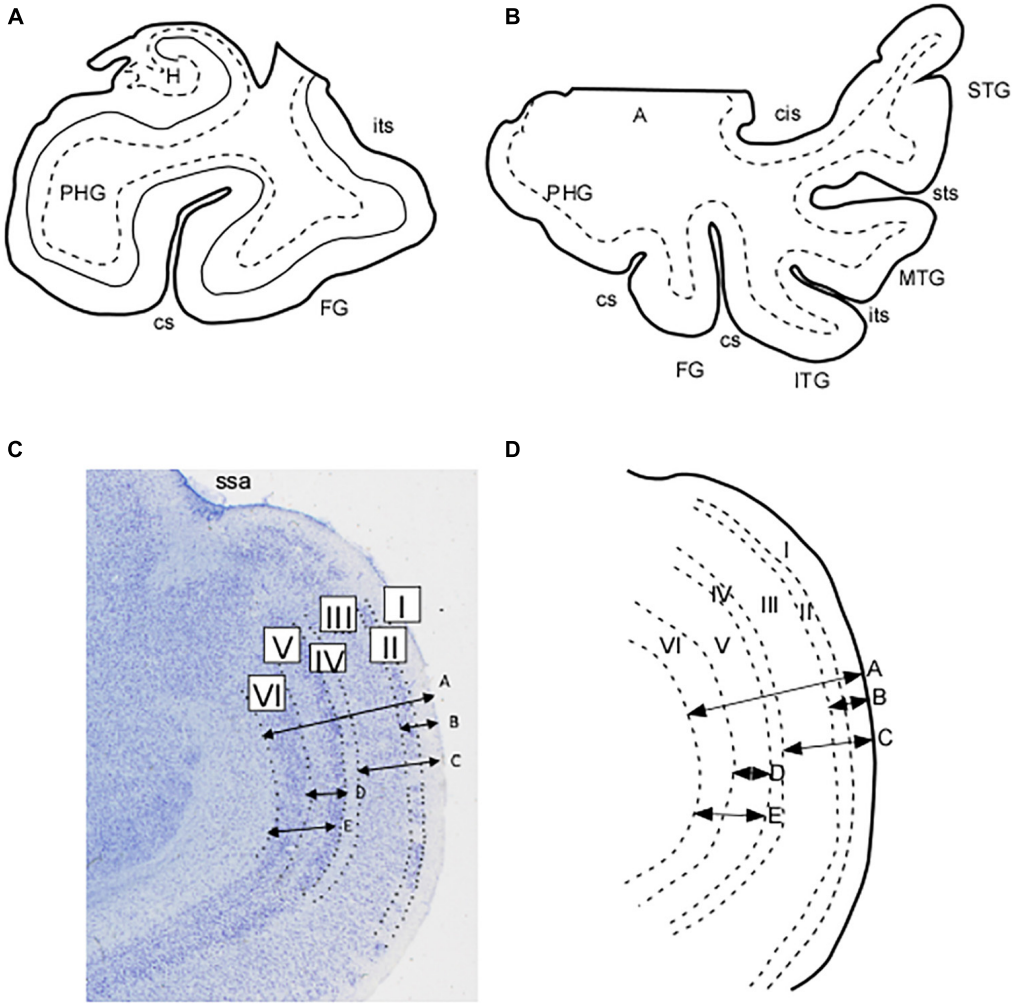

FIGURE 1 | Schematic representation of the extent of the blocks employed in this study. **(A)** Block limited to the parahippocampal and fusiform gyri. **(B)** Blocks of the whole temporal lobe as far as the circular sulcus of the insula. **(C)** Microphotograph in which the layers of the EC subfield E_{MI} can be appreciated. Arrows represent the measurements made of the total and partial thicknesses of the cortex in E_{MI}. These are represented schematically in **(D)** as indicated: A, total thickness of subfield E_{MI}; B, thickness of layers I and II; C, thickness of layers I–III; D, thickness of layer V; E, thickness of layers V and VI. Abbreviations: A, amygdala; cs, collateral sulcus; FG, fusiform gyrus; H, hippocampus; ITG, inferior temporal gyrus; its, inferior temporal sulcus; MTG, middle temporal gyrus; PHG, parahippocampal gyrus; ssa, *sulcus semianularis*; STG, superior temporal gyrus; sts, superior temporal sulcus.

prominences (Stephan, 1975; Amaral and Insausti, 1990; Duvernoy, 2005; Insausti and Amaral, 2012; Ding and Van Hoesen, 2015) makes it possible to use its morphometry in studies on neurodegenerative diseases, such as in Alzheimer disease.

The aim of this descriptive study is twofold. First, we sought to explore the detailed macroscopic anatomy of the GA, and its relationship with other bulges and sulci at the upper MTL, in order to check the feasibility of MRI identification of the GA in relation to other medial temporal landmarks. Second, we wanted to determine the cytoarchitectonic fields that conform the GA, both at the mediolateral and rostrocaudal extents, as our previous cytoarchitectonic parcellation of the human EC suggest that the GA may contain more than one EC subfield (Insausti et al., 1995).

MATERIALS AND METHODS

The study was performed according to the Declaration of Helsinki and approved by the Ethical Committee on Clinical Research of the University Hospital of Albacete (meeting of January 2015).

The results presented are based on observations of 37 MTLs of control cases, ranging between 12 and 110 years, from the Human Neuroanatomy Laboratory archive at the University of Navarra (1985–1998) and the University of Castilla–La Mancha (1999–present). Most of them were fixed by immersion in 10% buffered formalin for at least 4 weeks. Brains were photographed and blocked in 1 cm thick slabs (coronal plane), either perpendicular to the line traced along the anterior and posterior commissures as previously used in other studies (Insausti et al., 1995),

or taking the posterior end of both mammillary bodies as references.

The anterior and posterior surfaces of the slabs were individually photographed and the MTL was dissected through a medial cut along the entorhinal sulcus (Gloor, 1997) or posterior to the end of the *Gyrus intralimbicus*, at the most caudal level of the uncus, also known as the uncal apex by Duvernoy (2005), along the choroidal fissure (*fissura choroidea*). The block of tissue encompassed either the lateral occipitotemporal sulcus (*sulcus occipitotemporalis lateralis*) as presented in **Figure 2A**, or the most complete temporal lobe by the circular sulcus of the insula (*sulcus circularis insulae*) at the level of the insular cortex (**Figure 2B**). The dissected temporal lobe blocks included from the temporal pole and anterior PHG to the end of the hippocampus and associated cortices at the beginning of the lingual gyrus (*Gyrus lingualis*).

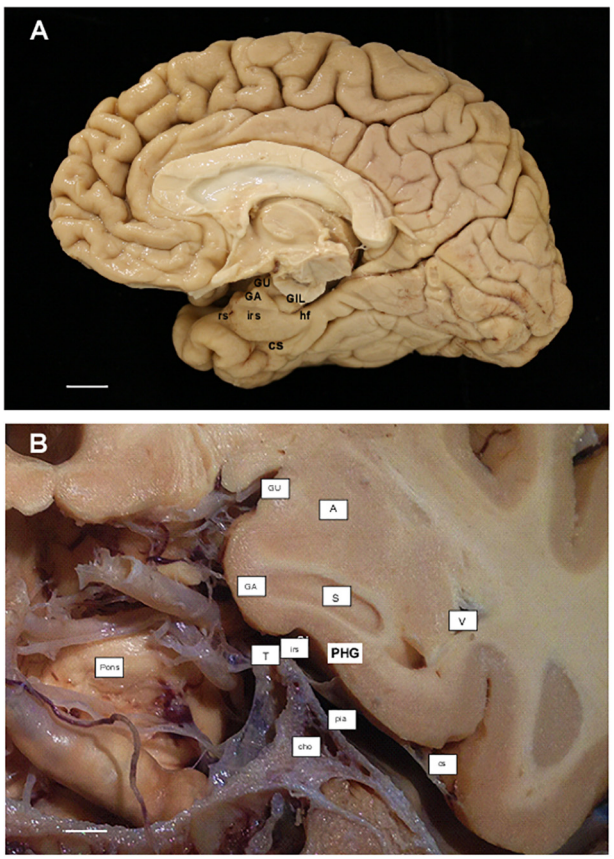

FIGURE 2 | (A) Photograph of the medial aspect of a cerebral hemisphere showing the main gross anatomical structures in relation to the remainder of cerebral structures. Scale bar equals 1 cm. **(B)** Photograph of a cadaveric preparation of a coronal section of the head at the level of the Subiculum (start of the hippocampus). Notice the ventral limit of the intrarhinal sulcus in relation to the *G. ambiens* (GA). The free edge of the tentorium (T) can be appreciated in close proximity to the intrarhinal sulcus. Scale bar equals 5 mm. Abbreviations as in previous Figure 1: cho, anterior choroidal artery; GA, *Gyrus ambiens*; GIL, *Gyrus intralimbicus*; GU, *Gyrus uncinatus*; hf, hippocampal fissure; irs, intrarhinal sulcus; pia, pia mater; Pons, anterior aspect of the pons; rs, rhinal sulcus; S, subiculum; T, tentorium; V, lateral ventricle, temporal horn.

The dissected blocks were placed in 4% paraformaldehyde in 0.1 M phosphate buffer for a period of 2–4 weeks. Serial 50 μm thickness sections were obtained with the use of a sliding microtome coupled to a freezing unit as described previously (Insausti et al., 1995; Blaizot et al., 2010). One-in-ten sections were Nissl stained with 0.25% thionin for cytoarchitectonic evaluation (500 μm interval between adjacent sections).

Annotation of boundaries was made by means of a *camera lucida* attached to a Nikon SMZ or a Leica MZ6 stereomicroscope. In all cases, a thorough analysis of the cytoarchitectonic features was made on the basis of previously reported criteria for the EC (Insausti et al., 1995), perirhinal cortex[3] (Salinas, 1995), and posterior parahippocampal cortex[4] (Insausti, 1992). Sections throughout the GA were selected for estimation of total thickness, as well as that of its layers (**Figure 2**).

In each case the linear distance between the pia mater and the boundary with the white matter was measured, along with different combinations of layers and cell free spaces up to five length determinations: (1) total thickness of EC subfield E_{MI} taken at the most convex point of the GA; (2) thickness of layer I plus layer II, which estimates the value of the layer origin of the projection to the molecular layer of the dentate gyrus; (3) thickness of the sum of layers I, II, and III as an estimate of the layers that project both to the CA fields of the hippocampus and to the dentate gyrus; (4) layer V thickness as an account of the main output layer of the EC; (5) combined thickness of layers V and VI as a more complete EC output. **Figures 1C,D** show a microphotograph of the GA with representation of the distances, as well as its schematic representation. The results for the distances are presented in **Table 1**.

[3]The name perirhinal cortex is employed as the combination of BA perirhinalis (BA35) and area ectorhinalis (BA36).

[4]The name posterior parahippocampal cortex refers to the posterior part of the PHG, caudal to both entorhinal and perirhinal cortices. This cortical strip was included as part of perirhinal cortex by Brodmann, although it was identified as areas TH and TF by von Economo and Koskinas (1925), as well as in Bailey and von Bonin (1951).

TABLE 1 | Values of the thickness of the EC subfield E_{MI}.

Cases	Age	Layers				
		I–VI	I–II	I–III	V	V–VI
Case 1	71	2.8	0.7	1.5	0.3	1.2
Case 2	58	2.3	0.5	1.2	0.4	0.8
Case 3	78	3.2	0.4	1.3	0.3	1.2
Case 4	82	2.0	0.6	0.8	0.3	0.8
Case 5	83	3.0	0.5	1.5	0.4	0.9
Case 6	59	2.6	0.5	1.2	0.5	1.1
Case 7	90	3.0	0.6	1.5	0.5	1.2
Case 8	61	2.5	0.6	1.3	0.5	1.0
Case 9	83	2.3	0.5	1.3	0.4	0.9
Case 10	75	2.2	0.4	1.2	0.3	0.8
	Mean	2.59	0.52	1.30	0.40	1.00
	SD	0.39	0.87	0.30	0.09	0.15

In order to complete the measurement of the GA, two-dimensional maps were constructed and measured with a planimetric program as described previously (Insausti et al., 1998b). In this study, the unfolding corresponds to the middle of the EC, either through *lamina dissecans* or the interval between layers III and V when the *lamina dissecans* is absent.

Finally, a total of 10 control subjects MRI from the Radiology Service of the Albacete University Hospital were assessed. Distances from the temporal pole to the *limen insulae*, the beginning of the hippocampus (subiculum), and the distance between the intrarhinal sulcus and the *Gyrus intralimbicus* was also calculated as an indirect estimation of the GA extent, calculated from the difference of the two distances alluded to above. The radiological parameters have been reported previously (Delgado-Gonzalez et al., 2015).

RESULTS

Extent and Limits of the *Gyrus ambiens*

The term GA may be derived from its positions facing the ambient cistern (*cisterna ambiens*), as a descriptive term (latin, *ambiens*, something that surrounds) that is one of the cerebrospinal fluid spaces in the brain, surrounding the upper part of the mesencephalon, vessels, and nerves (**Figures 1A,B**).

In our series, the GA is present in all cases medial to the PHG. Two sulci, one dorsal and one ventral, demarcate the GA in the upper, medial part of the MTL. The sulcus located more dorsally is the *sulcus semianularis* (**Figures 1A,B**). This sulcus is located at the rostromedial part of the external surface of the amygdaloid complex [cortical part, which is considered as peripaleocortex (Stephan and Andy, 1970)]. Dorsal to the *sulcus semianularis* lies the periamygdaloid cortex and other medial amygdaloid nuclei; ventral to it lies the GA, so that it can be considered as the boundary between the GA and periamygdaloid cortex. This was a constant feature in our series, although in some cases the periamygdaloid cortex straddled over the *sulcus semianularis* for a few hundred microns.

The GA is limited ventrally by the intrarhinal sulcus in all our cases (**Figure 1B**), although in some cases it was very shallow and inconspicuous. This small sulcus runs approximately in the most medial one-third of the distance between the *sulcus semianularis* and the collateral sulcus. The GA is coincident with the point at which, in a series of coronal sections, the PHG reaches its maximal breadth. At this midpoint of the PHG, the medial shoulder of the collateral sulcus forms the ventral limit of the PHG, while its lateral bank and shoulder belongs to the fusiform gyrus (*Gyrus fusiformis*), also known as lateral occipitotemporal gyrus (*Gyrus occipitotemporalis lateralis*) (Nieuwenhuys et al., 2008).

In our series of temporal lobes, the intrarhinal sulcus starts at approximately 9 mm behind the frontotemporal junction (*limen insulae*). At this point, the GA begins to be visible on the anterior part of the PHG. The intrarhinal sulcus extends longitudinally for several millimeters (7–10 mm), although we have observed its shape to vary from a small dimple to a marked depression. Sometimes, a secondary additional sulcus could be appreciated on the surface of the PHG. Moreover, in our series of coronal sections, the end of the intrarhinal sulcus coincided with the start of the hippocampal fissure (*fissura hippocampalis*) (Amaral and Insausti, 1990; Insausti and Amaral, 2012). In most cases, the intrarhinal sulcus extends as far back as the GA, which corresponds to the level of the hippocampal head. A great symmetry in length of the intrarhinal sulcus between left and right hemispheres was found in our sample of MRI cases (n = 10)[5]. Dorsal to the GA, the GS continues with the GU, which corresponds to the amygdalo-hippocampal area and ends as the hippocampal amygdaloid transitional area (HATA of Rosene and Van Hoesen, 1987; Ding and Van Hoesen, 2015).

The pattern of appearance of the intrarhinal sulcus and the GA above described is the most common in our series of brains, regardless of age. Other variations in the morphology of the GA depend on the presence of other smaller indentations at the surface of the PHG.

Cytoarchitectonics of the *Gyrus ambiens* Cortex

We present the topological and cytoarchitectonic features of the cortex of the GA, and its relationship with the cortex of the remainder of the PHG at this level.

Most of the PHG cortex is occupied by an intervening type of cortex, the periallocortex, located between the allocortical fields of the hippocampus, subiculum (three layers), and proisocortex (six layers); the latter also known as mesocortex in the current neuroanatomical nomenclature (cortex of five or six layers, with incomplete lamination scheme). It is the EC, along with the presubiculum and parasubiculum, that form the periallocortex of the PHG (Braak, 1980; Insausti et al., 2017). The basic laminar structure of the EC is of six layers and, although they are also named as layers I–VI, they do not correspond to the layers found in the isocortex (neocortex). The EC presents gradual variation along the anterior–posterior and medial–lateral axes, which justifies the separation of up to eight subfields, in which the transition of one EC subfield to another is gradual rather than sharp (Insausti et al., 1995).

According to the lamination scheme in terms of number and organization of the cortical layers, we determined in our series that the GA, like the EC, is made up of periallocortex. Besides, the continuation between the GA cortex and the remainder of EC is very noticeable (**Figures 3**, **4**). Rostromedially, the GS cortex can be considered as peripaleocortex; it occupies the extensive region that borders the boundary between the periallocortex of the GA and the peripaleocortex of the GS. In a caudal direction, and once the hippocampal fissure is present, the GA comes to an end, and its location is now taken by the GU, which corresponds to the amygdalo hippocampal area, and further caudally by the hippocampus amygdaloid transitional area (Rosene and Van Hoesen, 1987). Therefore, the GA is limited dorsally by the

[5]Measurements of the intrarhinal sulcus were taken from MRI series of images in the coronal plane of both sexes. Distances encompassed from the first slice in which the intrarhinal sulcus appears, as far as the first slice where the hippocampal fissure could be noticed.

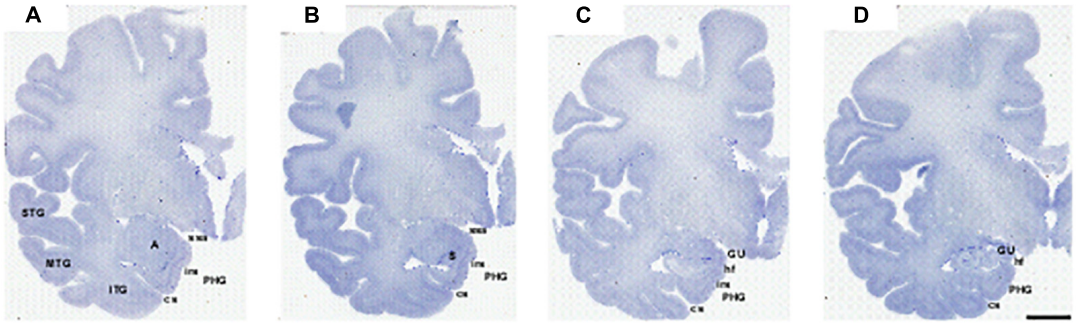

FIGURE 3 | Series of photomicrographs of a whole cerebral hemisphere in coronal sections from rostral **(A)** to caudal **(D)**, in which the relationship of the GA with the hemisphere and the intrarhinal sulcus are displayed. In panel **(A)**, the rostral level of GA is at the level of the mid amygdala. Panel **(B)** shows that the maximal extent of the GA is at the level of the commencement of the Subiculum (S). Panel **(C)** is at the end of the intrarhinal sulcus at the transition with the GU, near the opening of the hippocampal fissure. Note the *sulcus semianularis* is still evident in panels **(A–C)**. Panel **(D)** shows the GU past the intrarhinal sulcus at the level of the hippocampus–amygdaloid transitional area (HATA). Abbreviations as in previous figures. Scale bar equals 1 cm.

GS, ventrally by the periallocortex of the EC, rostrally by the anterior portion of the EC, and caudally by the GU. Two of the boundaries (ventral and rostral) correspond to EC while the other two (dorsal and caudal) correspond to parts of the amygdaloid complex.

Our observations indicate that the GA consists of periallocortex, similar to the EC in number and organization of the layers. The main topological features of EC subfields rostrally adjacent to the GA are as follows, according to the nomenclature of Insausti et al. (1995). The anterior pole of the EC shows subfields Entorhinal Olfactory subfield (E_O) and Entorhinal Lateral Rostral subfield (E_{LR}), which are the most rostrally located subfields. E_O resembles the periamygdaloid cortex in terms of appearance (both present a conspicuous layer II organized in clumps) although subfield E_O shows six layers, as the remainder of the EC, in contrast to the three layers of periamygdaloid cortex. Subfield E_O abuts laterally subfield E_{LR} (for details, see Insausti et al., 1995). Immediately caudal to E_O subfield is Entorhinal Rostral subfield (E_R), which also borders the GA anteriorly. Subfield E_R presents six layers completely developed, although it lacks *lamina dissecans*. In a caudal direction the dorsomedial aspect of the EC corresponds to Entorhinal Medial Intermediate subfield (E_{MI}), which is the periallocortex that, along with the incipient angular bundle, makes up the GA.

E_{MI} is very noticeable because of specific features. First, E_{MI} shows clearly the typical and complete set of layers that characterize the EC. Interestingly, this subfield resembles closely the appearance of the monkey EC, especially at midlevel. Second, it can be accurately distinguished in coronal sections as the medial prominence formed by the GA. In this way, subfield E_{MI} covers the majority of the macroscopically GA (**Figures 3**, **4**). In most cases, it is separated from the most ventral part of the periamygdaloid cortex by a conspicuous cell-free space in the medial border of E_{MI}, which lies slightly ventral to the *sulcus semianularis* (**Figure 4D**). The remainder of the EC is in the macroscopically visible PHG. The common features of EC layering are present in all fields, but it is subfield E_{MI} that displays them more clearly. **Figure 1** shows plainly the stack of layers that characterizes subfield E_{MI}. Although the cytoarchitectural features of subfield E_{MI} have been reported previously (Insausti et al., 1995), briefly, layer I is made up of fibers in continuation with the layers in the periamygdaloid cortex. The pial surface looks smoother relative to other portions of the EC, and, although subfield E_{MI} also presents *verrucae hippocampi*[6] their appearance is somewhat flatter. Layer II is narrow and more akin to layer II of subfield E_O. A thin cell-poor stratum interposes between layers II and III. Layer III is made up of small pyramids, orderly arranged in unicellular columns. A drop in the density in the deep portion of layer III announces *lamina dissecans*. Layer IV is *lamina dissecans*, one of the most outstanding features of the human periallocortical regions (Insausti et al., 2017). *Lamina dissecans* presents a cell-free space, which extends from the border with layer III to the big pyramids that populate the upper portion of layer V. Layer V is made up of three sublayers: Va, which contains densely packed big and dark pyramids; Vb, which displays lower density of pyramids, otherwise similar to those in sublayer Va; and Vc, a cell-poor stratum which runs parallel to *lamina dissecans*. Layer VI is also multilayered, although not as clearly as layer V. For this reason, this is the only subfield that displays clearly two cell-free bands, *lamina dissecans* and sublayer Vc, on either side of the dark, big pyramids of layer V, parallel to the convex surface of the GA. While subfield E_I also presents *lamina dissecans* and sublayer Vc, it displays a less distinct appearance relative to E_{MI}. Likewise, subfields E_C and E_{CL}, located caudally to E_I, also show a prominent sublayer Vc, although they do not display *lamina dissecans* (Insausti et al., 1995).

For all of the above, periallocortex of the GA is the same as the cytoarchitectonic type of subfield E_{MI}, and thence, EC as one of its subfields (Insausti et al., 1995). There is no other periallocortical field between the GA and the amygdaloid complex, and thereby

[6]The term *verrucae hippocampi* is used as in Klingler (1948) and Simic et al. (2005) to indicate the elevations in the pial surface of otherwise smooth surface of the cortex.

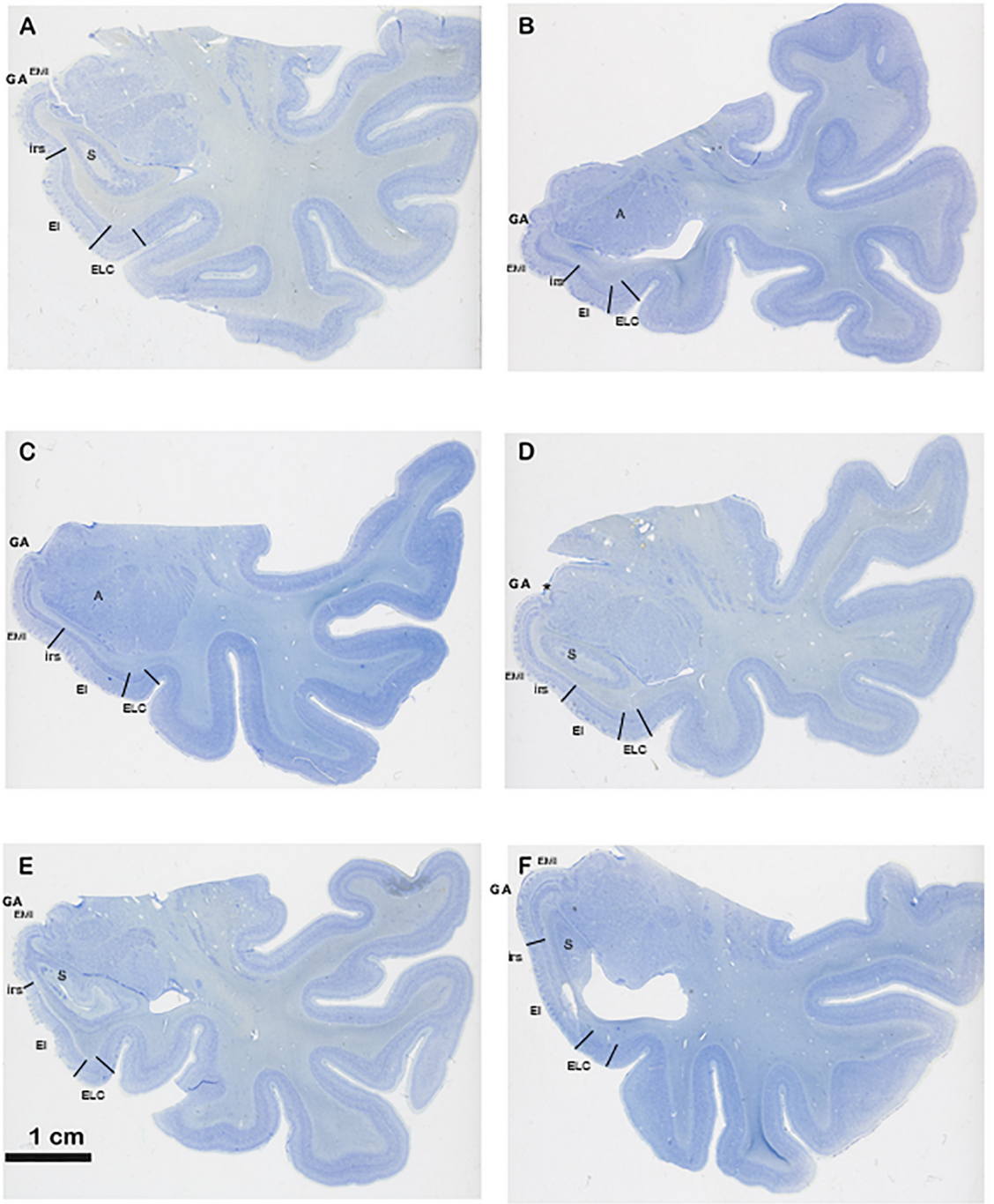

FIGURE 4 | Series of six different cases at the level of the commencement of the Subiculum. The series show different shapes and morphological variability of the GA, in particular differences in depth of the intrarhinal sulcus. Note the sequence from deeper intrarhinal sulcus **(A–C)** to shallower **(D,E)**, to very shallow **(F)**. Abbreviations as in previous figures: EMI, medial intermediate subfield of the EC; EI, intermediate subfield of the EC; ELC, lateral caudal subfield of the EC. Scala bar equals 1 cm.

we must conclude that BA34 is the same as EC subfield E_{MI} as defined here, and therefore, a part of BA28, not a different one.

In conclusion, the continuity of the EC along the extent of the GA is given by (a) the ventral continuation of E_{MI} cytoarchitectonic layers with the subfield E_I in continuation of the EC; (b) the structural difference with the medially adjacent periamygdaloid cortex (peripaleocortex). The rostral part of E_{MI} may encroach upon E_O and E_R, and that completes the GA area. The GA extension is completed by the rostral part of E_O and E_R, as shown in **Figure 5**.

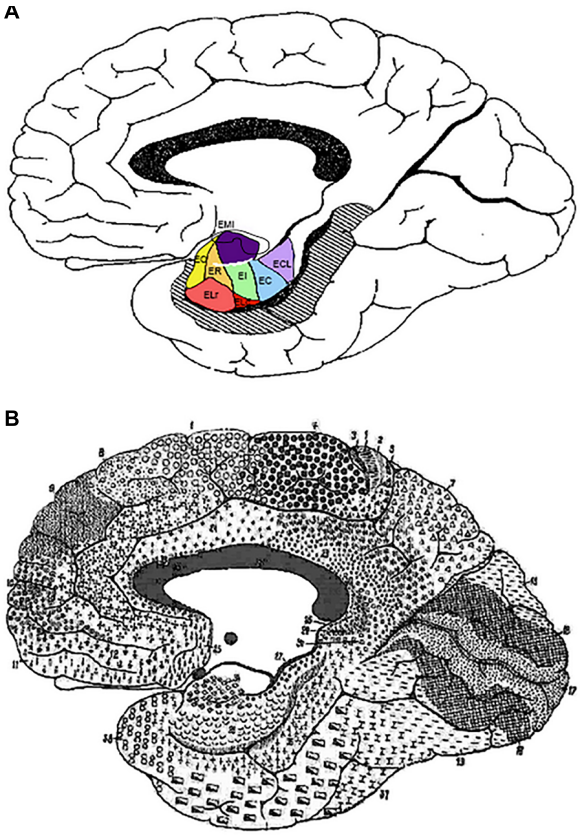

FIGURE 5 | (A) Depiction of the outline of Brodmann's map of the medial surface of the brain. It shows the approximate transformation of EC subfields according to the parcellation of Insausti et al. (1995) into Brodmann's scheme. **(B)** Brodmann (1909) cytoarchitectonic map. Note the overall correspondence of EC subfield E_{MI} with BA34. Abbreviations as in previous figures: EC, caudal subfield of the EC; ECL, caudal limiting subfield of the EC; ELr, lateral rostral subfield of the EC; EO, olfactory subfield of the EC; ER, rostral subfield of the EC.

Morphometric Parameters of Entorhinal Cortex Subfield E_{MI}

Cortical Thickness of GA/E_{MI}

In an anterior to posterior direction, the longitudinal extent of the EC is about 2.5 cm. The GA lies at the middle of the EC (**Figures 2**, **5**). We completed this longitudinal distance with the measurement of the EC subfield E_{MI} in **Table 1**, corresponding to 10 control cases (Age range, 58–90).

The total thickness of EC subfield EMI ranged between 2 and 3.2 mm [mean 2.59; standard deviation (SD) ± 0.39], and it is relatively constant regardless of the age of the subject. Values for layers I–II of the subfield EMI range from 0.4 to 0.7 mm (mean 0.52; *SD*±0.87). Layers I–III (EMI upper layers) resulted in values that ranged between 0.8 and 1.5 mm (mean 1.30; *SD* ±0.30). Layer V thickness was the smallest value, as it corresponds to a single layer; values ranged between 0.3 and 0.5 mm (mean 0.40; *SD* ±0.09). The addition of layers V and VI varied between 0.8 and 1.2 mm (mean 1.00; *SD* ±0.15). Data are presented in **Table 1**, and show that the range of variability is low, probably due to the sharpness of the limits among layers in this EC subfield.

Two-Dimensional Reconstruction Measurements of E_{MI}

Two-dimensional reconstructions allow the measurement of the extent of any cortical area. EC has been unfolded taking the middle of the EC thickness as the unfolding line. Subfield E_{MI} extent was unfolded, and the values expressed as percentage of the total EC unfolded surface. Data from a representative number of cases are shown in **Table 2**. Age ranged from 15 to 110 years to offer a glimpse of the complete lifespan, excluding childhood. All measurements are expressed in mm^2 as absolute value, also the value of E_{MI} extent, which is also shown as a percentage of the total EC surface.

The EC total surface ranged from 350 to 197 mm^2. Values under 200 mm^2 corresponded to the two oldest representative cases, 91 and 110 years, respectively (197.3 and 196.0 mm^2). Interestingly, in those two old cases, the values of E_{MI} were in the normal range. Values of E_{MI} extent ranged from 15.0 to 5.0 mm^2. Therefore, the percentage of the EC total surface ranged between 1.5 and 6.3%. It is noteworthy to point that the oldest case in our

TABLE 2 | Values of the areal extent of subfield E_{MI}.

Cases	Age	EC (mm^2)	E_{MI} (mm^2)	%
Case 1	15	244.7	14.5	5.9
Case 2	22	213.5	12.0	5.6
Case 3	32	312.8	13.0	4.2
Case 4	54	297.5	5.0	1.7
Case 5	54	350.7	15.0	4.3
Case 6	54	345.8	9.5	2.7
Case 7	58	331.9	8.0	2.4
Case 8	61	340.5	6.5	1.9
Case 9	62	207.2	8.5	4.1
Case 10	63	260.0	12.5	4.8
Case 11	64	315.8	7.0	2.2
Case 12	64	302.6	6.0	2.0
Case 13	66	336.7	12.5	3.7
Case 14	70	341.9	5.0	1.5
Case 15	71	254.2	13.5	5.3
Case 16	77	268.6	6.5	2.4
Case 17	77	256.4	8.0	3.1
Case 18	78	351.1	7.5	2.1
Case 19	83	197.6	12.5	6.3
Case 20	84	335.8	6.0	1.8
Case 21	84	217.2	5.0	2.3
Case 22	84	309.6	9.5	3.1
Case 23	85	211.9	5.5	2.6
Case 24	85	269.2	8.0	3.0
Case 25	87	211.3	5.5	2.6
Case 26	91	197.3	7.0	3.5
Case 27	110	196.0	8.0	4.1
	Mean	277.0	8.8	3.3
	SD	56.0	3.2	

series showed a percentage of 4.1%, which is in the high range in percentage of all series.

MRI Appearance of the *Gyrus ambiens*

The location and extent of the GA in the MTL was established, and the rostrocaudal dimension determined, as well as reference distances with different landmarks used on former MRI studies (Insausti et al., 1998b; Franko et al., 2014).

The series of coronal sections in MRI included levels at which the GA can be recognized. The main landmark for identification of the GA is at the level where the temporal horn of the lateral ventricle starts, or at the level of the start of the subiculum, slightly caudal to the lateral ventricle starting point. Very often, the *sulcus semianularis* separating the GA and the GS is visible, signaling the dorsal boundary of the GA. The intrarhinal sulcus is also visible in the PHG, although its depth may be somewhat variable. An example of the radiological appearance of the GA is shown in **Figure 6**.

We determined various parameters in relation to distance from the temporal pole, *limen insulae* (frontotemporal junction), start of the subiculum, and the end of the uncus (*Gyrus intralimbicus*), aiming at establishing the location and rostrocaudal extent of the GA in MRI images of 10 human control cases. **Table 3** presents the distances among those landmarks. The distance from the beginning of the temporal pole and the *limen insulae* was fairly constant, 2.5 cm as an average. The EC starts about 2 mm behind the *limen insulae*. The bulge indicating the GA was considered the start of the intrarhinal sulcus. From that point, the distance to the start of the subiculum gave values between 7.2 and 14.4 mm (mean 9.36 mm; *SD* ±2.39 for the left hemisphere and 9.12 mm; *SD* ±2.48 for the right hemisphere). The length between the start of the hippocampal fissure and the end of the hippocampal head in the rostrocaudal axis varied between 21 and 14 mm (left hemisphere, mean 18.96 mm; *SD* ±2.39; right hemisphere, mean 18.48 mm; *SD* ±3.59).

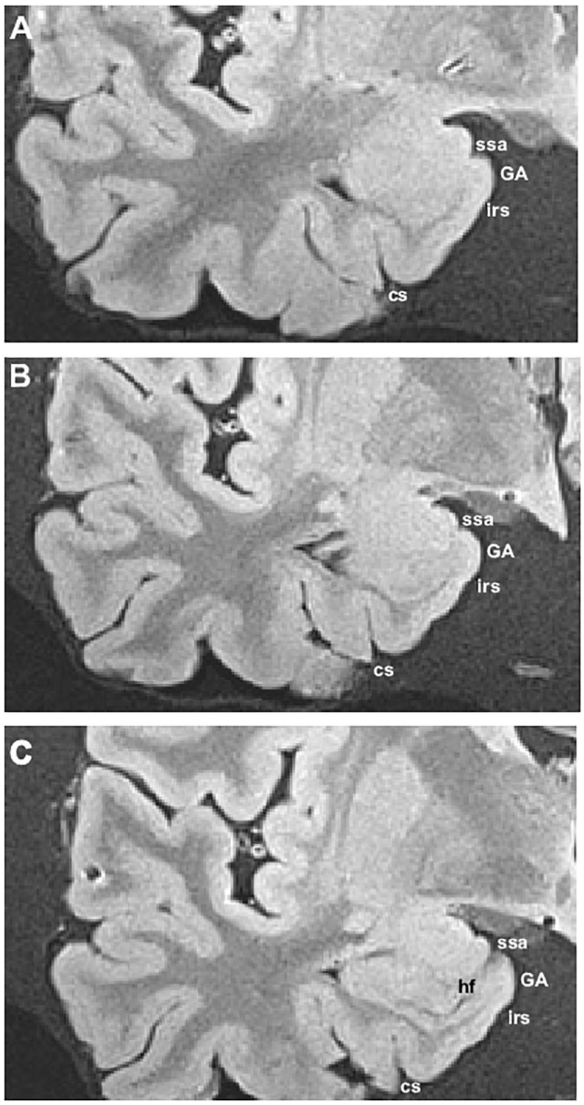

FIGURE 6 | *Ex vivo* MRI appearance of the GA in coronal sections of three different cases. The boundary of the GA (subfield E_{MI}) was determined by histological examination. Abbreviations as in previous figures.

DISCUSSION

Intrarhinal Sulcus and the GA

In the present report we show that the ventral limit of EC subfield E_{MI} (and therefore of the GA) corresponds topographically to the intrarhinal sulcus. The existence of a sulcus that delineates the ventral limit of the GA is well accepted in the literature, although the terminology employed varies among authors.

The sulci of the MTL surface have been examined by different authors, who have shown the variability of the sulci present in the EC. A detailed study of those EC sulci is reported by Hanke (1997), where he refers as "intrarhinal nick" to the sulcus ventral to the GA. Specifically, he states that "the intrarhinal nick forming the lateral border of the ambient gyrus, corresponds to the impression of the of the anterior petroclinoideal plica of the cerebellar tent, and was lacking in 30.4% of the cases." This suggests that, at the gross morphological level, the intrarhinal sulcus is present in more than two-thirds of the population, thus making it a rather constant feature of the EC. We noticed in our series the constant presence of the intrarhinal sulcus, albeit it was sometimes shallow and not clearly noticeable unless one is aware of the ventral limit of the GA. The presence or absence equally on both sides of the brain suggests that there is no interhemispheric asymmetry (Hanke, 1997). We also found a great hemispheric symmetry of the intrarhinal sulcus in our series of cases. The depth of the intrarhinal sulcus has been associated with the degree of "brain swelling" (Heinsen et al., 1996). While we do not have specific data about brain swelling in the neuropathological report of our cases, it seems unlikely that this condition of the brain is responsible for the appearance of the intrarhinal sulcus.

Other interpretations of the EC sulci in the literature have been proposed (Duvernoy, 2005; Ding and Van Hoesen, 2015),

TABLE 3 | Length values among MTL landmarks in relation to the GA.

Cases	Temporal pole – *limen insulae*		irs-subiculum		irs-*Gyrus intralimbicus*	
	Left hemisphere	Right hemisphere	Left hemisphere	Right hemisphere	Left hemisphere	Right hemisphere
Case 1	24.0	24.0	9.6	7.2	19.2	19.2
Case 2	26.4	24.0	9.6	9.6	19.2	16.8
Case 3	21.6	24.0	12.0	12.0	21.6	19.2
Case 4	21.6	21.6	7.2	7.2	16.8	14.4
Case 5	24.0	21.6	7.2	9.6	16.8	21.6
Case 6	26.4	26.4	7.2	7.2	16.8	16.8
Case 7	26.4	24.0	9.6	9.6	19.2	19.2
Case 8	24.0	21.6	7.2	7.2	16.8	16.8
Case 9	24.0	24.0	9.6	7.2	19.2	14.4
Case 10	38.4	36.0	14.4	14.4	24.0	26.4
Mean	25.68	24.72	9.36	9.12	18.96	18.48
SD	4.81	4.24	2.39	2.48	2.39	3.59

irs, intrarhinal sulcus.

in particular as an imprint of the free edge of the cerebellar tentorium. However, such imprint would probably interfere with the vascular supply of the EC. This fact, plus the almost constant presence of the intrarhinal sulcus, lead us to conclude that it is a sulcus that forms the ventral boundary of the GA, and thence of the EC subfield E_{MI}, rather than an imprint of the cerebellar tentorium on the EC surface. The name of intrarhinal sulcus is justified as it lies entirely within the extent of the EC.

The GA Is Cytoarchitectonically EC Subfield E_{MI}

Our study shows that the GA is an EC subfield (E_{MI}) which, very likely, coincides with BA34 (Brodmann, 1909). Brodmann named area 34 as "dorsal EC," thus acknowledging that the EC and area 34 share common features. Although Brodmann does not provide a full cytoarchitectonic description of neither area 34 nor area 28 in his 1909 book, he depicts both area 34 and area 28 in great topographical detail, and specifically he states that both areas are separated by the "inferior rhinal sulcus of Retzius," which corresponds to the intrarhinal sulcus. It is unclear why Brodmann separates area 34 as distinct of area 28, at the same time that he calls it "dorsal EC," instead simply EC. It could be speculated that, taking into consideration a similar lamination between subfield E_{MI} and the nonhuman primate EC, Brodmann identified area 34 as a distinct area bases on the similitude with the nonhuman primate EC[7].

MRI Identification of the Rostromedial Part of the EC

The MRI scans used for clinical or experimental studies do not allow the segmentation of specific subfields of the EC. For example, subfield E_O is very difficult to identify in common MRI images (Insausti et al., 1998b; Pruessner et al., 2002; Wolk et al., 2017). However, given that the GA can be identified in MRI examinations, and the very good (almost perfect) match between subfield E_{MI} and the GA, E_{MI} could be the first EC subfield identifiable in MRI scans.

Anatomical and Functional Significance

Subfield E_{MI} presents histo- and immunohistochemical peculiarities, that singles it out of other EC subfields. The distribution of parvalbumin-stained neurons is reduced relative to more lateral parts at similar rostro-caudal levels (Braak et al., 1991; Tuñon et al., 1992; Schmidt et al., 1993; Solodkin and Van Hoesen, 1996; Mikkonen et al., 1997). Calbindin and calretinin immunoreactivity stains more heavily the medial part of the EC (Tuñon et al., 1992; Mikkonen et al., 1997), and therefore, it is largely complementary to that of parvalbumin.

Other neurochemical substances in the EC also distinguish rostromedial EC subfields E_{MI} and E_O. E_{MI} and adjacent parts of E_O present a paucity of tyrosine hydroxylase-immunoreactive fibers relative to more lateral parts of the EC (Akil and Lewis, 1994). The increasingly and gradual decrease of tyrosine hydroxylase fiber density make subfield E_{MI} distinguishable from the adjacent E_I, although the seamless continuation of the layers with subfield E_{MI} support the contention of its being a subfield of EC. The study of the distribution of choline acetyltransferase in the HF shows that E_{MI} displays low density of choline acetyltransferase fibers, density that increases in E_I with perfect continuation of the EC layers. Significantly, the boundary seems to be coincident with the intrarhinal sulcus (De Lacalle et al., 1994).

Experimental studies in nonhuman primates reveal that the organization of the projections between the EC and the dentate gyrus of the hippocampus share a similar pattern in the nonhuman primate (Witter et al., 1989) and rodent HF (Ruth et al., 1982). The anterior portion of the hippocampus (ventral part in the rodent), which in humans corresponds to

[7]Brodmann studied first the cortical parcellation in the nonhuman primate brain, and thereafter in the human brain (Lorente de Nó, personal communication), therefore he was familiarized with the nonhuman primate EC.

the hippocampal head, receives innervation from rostromedial portions of the EC. The body and tail of the hippocampus (septal or dorsal part in the rodent) are innervated from progressively more lateral and caudal levels of the EC. Cytoarchitectonic studies of the EC in humans show that rostromedial portions of the EC belong to the E_O and E_{MI} subfields of the EC. The likely homology between EC subfield E_O and the nonhuman primate EC subfield E_O (Amaral et al., 1987; Insausti et al., 2002) strongly suggests that this subfield would innervate the head of the hippocampus. Likewise, EC subfield E_{MI}, which is not present in the nonhuman primate (it is the only EC cytoarchitectonic subfield that is present exclusively in humans), would also likely innervate the head of the hippocampus (Insausti, 1993).

Up to date, *ex vivo* MRI scans and histology offer the best existing correlation between MRI and the extent of the EC (Adler et al., 2018). The correlation between *ex-vivo* MRI scans of the MTL with the subsequent histological confirmation are useful for localization of MTL structures (Insausti et al., 1998b; Franko et al., 2014; Delgado-Gonzalez et al., 2015; Adler et al., 2018). However, no specific studies on the GA are available. Our results in a small set of cases suggest that the identification of E_{MI} is feasible, and it may be of use in MRI volumetric determinations.

The MRI identification of the GA has functional implications, as topographical differences in the longitudinal axis of the hippocampus are associated with different functional properties (Maguire et al., 2000; Fanselow and Dong, 2010). The identification of an outstanding GA in most subjects would be useful in the determination of EC subfield E_{MI} and partially of E_O, with the subsequent implications in the volumetric measurements and cortical thickness studies, as, for instance, in Alzheimer disease (Wolk et al., 2017).

Summary of Findings and Conclusions

The present study characterizes the location of GA and the type of cortex that overlies it. It thus seems to be justified to conclude that the cortex lining the GA is the EC subfield E_{MI}, and therefore part of EC. Likewise, BA34 would be identical to EC subfield E_{MI}. The topographical situation of the GA in the MTL, plus the coincidence with the EC subfield E_{MI} brings the opportunity of its accurate determination in MRI explorations.

ETHICS STATEMENT

Ethical Committee on Clinical Research of the University Hospital of Albacete, on its meeting of January 2015. Brains obtained before 2002 did not require written consent of next to kin. Brains obtained after this date were obtained under the body and brain donor program of the School of Medicine of the University of Castilla–La Mancha.

AUTHOR CONTRIBUTIONS

RI designed the study and wrote the manuscript. MC-P and RI contributed equally to the manuscript. MU and AR carried out the measurements. AI and MM-L performed the cytoarchitectonic analysis of the cases.

FUNDING

This research was partially funded by UCLM funds to the Human Neuroanatomy Laboratory, and the National Institutes of Mental Health 1-R01-AG-056014-01.

REFERENCES

Adler, D. H., Wisse, L. E. M., Ittyerah, R., Pluta, J. B., Ding, S. L., Xie, L., et al. (2018). Characterizing the human hippocampus in aging and Alzheimer's disease using a computational atlas derived from ex vivo MRI and histology. *Proc. Natl. Acad. Sci. U.S.A.* 115, 4252–4257. doi: 10.1073/pnas.1801093115

Aggleton, J. P., and Mishkin, M. (1985). Mamillary-body lesions and visual recognition in monkeys. *Exp. Brain Res.* 58, 190–197. doi: 10.1007/BF00238967

Akil, M., and Lewis, D. A. (1994). The distribution of tyrosine hydroxylase-immunoreactive fibers in the human entorhinal cortex. *Neuroscience* 60, 857–874. doi: 10.1016/0306-4522(94)90268-2

Amaral, D. G., and Insausti, R. (1990). "Hippocampal formation," in *The Human Nervous System*, ed. G. Paxinos (San Diego, CA: Academic Press), 711–755. doi: 10.1016/B978-0-12-547625-6.50026-X

Amaral, D. G., Insausti, R., and Cowan, W. M. (1987). The entorhinal cortex of the monkey: I. Cytoarchitectonic organization. *J. Comp. Neurol.* 264, 326–355. doi: 10.1002/cne.902640305

Arnold, S. E., Hyman, B. T., Flory, J., Damasio, A. R., and Van Hoesen, G. W. (1991). The topographical and neuroanatomical distribution of neurofibrillary tangles and neuritic plaques in the cerebral cortex of patients with Alzheimer's disease. *Cereb. Cortex* 1, 103–116. doi: 10.1093/cercor/1.1.103

Bailey, P., and von Bonin, G. (1951). *The Isocortex of Man*. Champaign, IL: University of Illinois Press.

Blaizot, X., Mansilla, F., Insausti, A. M., Constans, J. M., Salinas-Alaman, A., Pro-Sistiaga, P., et al. (2010). The human parahippocampal region: I. Temporal pole cytoarchitectonic and MRI correlation. *Cereb. Cortex* 20, 2198–2212. doi: 10.1093/cercor/bhp289

Braak, E., Strotkamp, B., and Braak, H. (1991). Parvalbumin-immunoreactive structures in the hippocampus of the human adult. *Cell Tissue Res.* 264, 33–48. doi: 10.1007/BF00305720

Braak, H. (1980). *Architectonics of the Human Telencephalic Cortex*. Berlin: Springer. doi: 10.1007/978-3-642-81522-5

Braak, H., and Braak, E. (1992). The human entorhinal cortex: normal morphology and lamina-specific pathology in various diseases. *Neurosci. Res.* 15, 6–31. doi: 10.1016/0168-0102(92)90014-4

Brodmann, K. (1909). *Vergleichende Lokalisationslehe der Grosshirnrinde*. Leipzig: Verlag von Johann Ambrosius Barth.

Cajal, S. R. Y. (1901). Estructura de la corteza olfativa del hombre y mamíferos. *Trab. Lab. Invest. Biol. Univ. Madrid* 1, 1–132.

Delgado-Gonzalez, J. C., Mansilla-Legorburo, F., Florensa-Vila, J., Insausti, A. M., Vinuela, A., Tunon-Alvarez, T., et al. (2015). Quantitative measurements in the human hippocampus and related areas: correspondence between Ex-Vivo MRI and histological preparations. *PLoS One* 10:e0130314. doi: 10.1371/journal.pone.0130314

De Lacalle, S., Lim, C., Sobreviela, T., Mufson, E. J., Hersh, L. B., and Saper, C. B. (1994). Cholinergic innervation in the human hippocampal formation including the entorhinal cortex. *J. Comp. Neurol.* 345, 321–344. doi: 10.1002/cne.903450302

Ding, S. L. (2013). Comparative anatomy of the prosubiculum, subiculum, presubiculum, postsubiculum, and parasubiculum in human, monkey, and rodent. *J. Comp. Neurol.* 521, 4145–4162. doi: 10.1002/cne.23416

Ding, S. L., and Van Hoesen, G. W. (2015). Organization and detailed parcellation of human hippocampal head and body regions based on a combined analysis of cyto- and chemoarchitecture. *J. Comp. Neurol.* 523, 2233–2253. doi: 10.1002/cne.23786

Duvernoy, H. M. (2005). *The Human Hippocampus*, 3rd Edn. Berlin: Springer-Verlag.

Fanselow, M. S., and Dong, H. W. (2010). Are the dorsal and ventral hippocampus functionally distinct structures? *Neuron* 65, 7–19. doi: 10.1016/j.neuron.2009.11.031

Franko, E., Insausti, A. M., Artacho-Perula, E., Insausti, R., and Chavoix, C. (2014). Identification of the human medial temporal lobe regions on magnetic resonance images. *Hum. Brain Mapp.* 35, 248–256. doi: 10.1002/hbm.22170

Garey, L. J. (1994). *Brodmann's 'Localisation in the Cerebral Cortex'*. Smith-Gordon: London.

Gloor, P. (1997). *The Temporal Lobe and Limbic System*. New York, NY: Oxford University Press.

Gómez-Isla, T., Price, J. L., McKeel, D. W. Jr., Morris, J. C., Growdon, J. H., and Hyman, B. T. (1996). Profound loss of layer II entorhinal cortex neurons occurs in very mild Alzheimer's disease. *J. Neurosci.* 16, 4491–4500. doi: 10.1523/JNEUROSCI.16-14-04491.1996

Hammarberg, C. (1895). *Studien uber Klinic und Pathologie der Idiotie nebst Untersuchungen über die normale Aatomie der Hirnrinde*. Berling: Akademische Buchdruckerie.

Hanke, J. (1997). Sulcal pattern of the anterior parahippocampal gyrus in the human adult. *Ann. Anat.* 179, 335–339. doi: 10.1016/S0940-9602(97)80071-4

Heckers, S., Heinsen, H., Heinsen, Y., and Beckmann, H. (1990). Morphometry of the parahippocampal gyrus in schizophrenics and controls. Some anatomical considerations. *J. Neural Transm. Gen. Sect.* 80, 151–155. doi: 10.1007/BF01257080

Heinsen, H., Gossmann, E., Rub, U., Eisenmenger, W., Bauer, M., Ulmar, G., et al. (1996). Variability in the human entorhinal region may confound neuropsychiatric diagnoses. *Acta Anat.* 157, 226–237. doi: 10.1159/000147885

Huntgeburth, S. C., and Petrides, M. (2012). Morphological patterns of the collateral sulcus in the human brain. *Eur. J. Neurosci.* 35, 1295–1311. doi: 10.1111/j.1460-9568.2012.08031.x

Iglesias, J. E., Van Leemput, K., Augustinack, J., Insausti, R., Fischl, B., Reuter, M., et al. (2016). Bayesian longitudinal segmentation of hippocampal substructures in brain MRI using subject-specific atlases. *Neuroimage* 141, 542–555. doi: 10.1016/j.neuroimage.2016.07.020

Insausti, A. M. (1992). *Estudio Cito y Mieloarquitectónico de la Circunvolución Parahipocámpica Posterior del Hombre y sus Cambios en la Senescencia Normal y en la Enfermedad de Alzheimer*. Ph.D. thesis, Universidad de Navarra, Pamplona.

Insausti, R. (1993). Comparative anatomy of the entorhinal cortex and hippocampus in mammals. *Hippocampus* 3 Spec No, 19–26.

Insausti, R., and Amaral, D. G. (2008). Entorhinal cortex of the monkey: IV. Topographical and laminar organization of cortical afferents. *J. Comp. Neurol.* 509, 608–641. doi: 10.1002/cne.21753

Insausti, R., and Amaral, D. G. (2012). "Hippocampal formation," in *The Human Nervous System*, 3rd Edn, eds J. K. Mai and G. Paxinos (Amsterdam: Elsevier), 896–942. doi: 10.1016/B978-0-12-374236-0.10024-0

Insausti, R., Insausti, A. M., Sobreviela, M. T., Salinas, A., and Martinez-Penuela, J. M. (1998a). Human medial temporal lobe in aging: anatomical basis of memory preservation. *Microsc. Res. Tech.* 43, 8–15.

Insausti, R., Juottonen, K., Soininen, H., Insausti, A. M., Partanen, K., Vainio, P., et al. (1998b). MR volumetric analysis of the human entorhinal, perirhinal, and temporopolar cortices. *AJNR Am. J. Neuroradiol.* 19, 659–671.

Insausti, R., Marcos, P., Arroyo-Jimenez, M. M., Blaizot, X., and Martinez-Marcos, A. (2002). Comparative aspects of the olfactory portion of the entorhinal cortex and its projection to the hippocampus in rodents, nonhuman primates, and the human brain. *Brain Res. Bull.* 57, 557–560. doi: 10.1016/S0361-9230(01)00684-0

Insausti, R., Munoz-Lopez, M., Insausti, A. M., and Artacho-Perula, E. (2017). The human periallocortex: layer pattern in presubiculum, parasubiculum and entorhinal cortex. A Review. *Front. Neuroanat.* 11:84. doi: 10.3389/fnana.2017.00084

Insausti, R., Tunon, T., Sobreviela, T., Insausti, A. M., and Gonzalo, L. M. (1995). The human entorhinal cortex: a cytoarchitectonic analysis. *J. Comp. Neurol.* 355, 171–198. doi: 10.1002/cne.903550203

Juottonen, K., Laakso, M. P., Insausti, R., Lehtovirta, M., Pitkanen, A., Partanen, K., et al. (1998). Volumes of the entorhinal and perirhinal cortices in Alzheimer's disease. *Neurobiol. Aging* 19, 15–22. doi: 10.1016/S0197-4580(98)00007-4

Khan, U. A., Liu, L., Provenzano, F. A., Bereman, D. E., Profaci, C. P., Sloan, R., et al. (2014). Molecular drivers and cortical spread of lateral entorhinal cortex dysfunction in preclinical Alzheimer's disease. *Nat. Neurosci.* 17, 304–311. doi: 10.1038/nn.3606

Klingler, J. (1948). Die makroskopische anatomie der ammonsformation. *Denkschr. Schweiz. Naturforsch. Ges.* 78, 1–80.

Krimer, L. S., Hyde, T. M., Herman, M. M., and Saunders, R. C. (1997). The entorhinal cortex: an examination of cyto- and myeloarchitectonic organization in humans. *Cereb. Cortex* 7, 722–731. doi: 10.1093/cercor/7.8.722

Lorente de Nó, R. (1933). Studies on the structure of the cerebral cortex. I. The area ofentorhinalis. *J. Psychol. Neurol.* 45, 381–438.

Maguire, E. A., Gadian, D. G., Johnsrude, I. S., Good, C. D., Ashburner, J., Frackowiak, R. S., et al. (2000). Navigation-related structural change in the hippocampi of taxi drivers. *Proc. Natl. Acad. Sci. U.S.A.* 97, 4398–4403. doi: 10.1073/pnas.070039597

Mikkonen, M., Soininen, H., and Pitkanen, A. (1997). Distribution of parvalbumin-, calretinin-, and calbindin-D28k-immunoreactive neurons and fibers in the human entorhinal cortex. *J. Comp. Neurol.* 388, 64–88. doi: 10.1002/(SICI)1096-9861(19971110)388:1<64::AID-CNE5>3.0.CO;2-M

Mohedano-Moriano, A., Martinez-Marcos, A., Pro-Sistiaga, P., Blaizot, X., Arroyo-Jimenez, M. M., Marcos, P., et al. (2008). Convergence of unimodal and polymodal sensory input to the entorhinal cortex in the fascicularis monkey. *Neuroscience* 151, 255–271. doi: 10.1016/j.neuroscience.2007.09.074

Muñoz, M., and Insausti, R. (2005). Cortical efferents of the entorhinal cortex and the adjacent parahippocampal region in the monkey (*Macaca fascicularis*). *Eur. J. Neurosci.* 22, 1368–1388. doi: 10.1111/j.1460-9568.2005.04299.x

Nieuwenhuys, R., Broere, C. A., and Cerliani, L. (2015). A new myeloarchitectonic map of the human neocortex based on data from the Vogt-Vogt school. *Brain Struct. Funct.* 220, 2551–2573. doi: 10.1007/s00429-014-0806-9

Nieuwenhuys, R., Voogd, J., and Van Huijzen, C. (2008). *The Human Central Nervous System*. Berlin: Springer-Verlag. doi: 10.1007/978-3-540-34686-9

Ono, M., Kubik, S., and Abernathey, C. D. (1990). *Atlas of the Cerebral Sulci*. Stuttgart: Georg Thieme Verlag.

Pruessner, J. C., Kohler, S., Crane, J., Pruessner, M., Lord, C., Byrne, A., et al. (2002). Volumetry of temporopolar, perirhinal, entorhinal and parahippocampal cortex from high-resolution MR images: considering the variability of the collateral sulcus. *Cereb. Cortex* 12, 1342–1353. doi: 10.1093/cercor/12.12.1342

Retzius, G. (1896). *Das Menschenhirn*. Stockholm, PA: Norstedt & Söner.

Rosene, D. L., and Van Hoesen, G. W. (1987). "The hippocampal formation of the primate brain: a review of some comparative aspects of cytoarchitecture and connections," in *Cerebral Cortex*, eds E. G. Jones and A. Peters (New York, NY: Plenum), 345–456. doi: 10.1007/978-1-4615-6616-8_9

Ruth, R. E., Collier, T. J., and Routtenberg, A. (1982). Topography between the entorhinal cortex and the dentate septotemporal axis in rats: I. Medial and intermediate entorhinal projecting cells. *J. Comp. Neurol.* 209, 69–78. doi: 10.1002/cne.902090107

Salinas, A. (1995). *Estructura de la Corteza Perirrinal Humana. Modificaciones con el Envejecimiento y la Enfermedad de Alzheimer*. Ph.D. thesis, Universidad de Navarra, Pamplona.

Schmidt, S., Braak, E., and Braak, H. (1993). Parvalbumin-immunoreactive structures of the adult human entorhinal and transentorhinal region. *Hippocampus* 3, 459–470. doi: 10.1002/hipo.450030407

Simic, G., Bexheti, S., Kelovic, Z., Kos, M., Grbic, K., Hof, P. R., et al. (2005). Hemispheric asymmetry, modular variability and age-related changes in the human entorhinal cortex. *Neuroscience* 130, 911–925. doi: 10.1016/j.neuroscience.2004.09.040

Solly, S. (1836). *The Human Brain, Its Configuration, Structure, Development, and Physiology*. London: Longman.

Solodkin, A., and Van Hoesen, G. W. (1996). Entorhinal cortex modules of the human brain. *J. Comp. Neurol.* 365, 610–617. doi: 10.1002/(SICI)1096-9861(19960219)365:4<610::AID-CNE8>3.0.CO;2-7

Squire, L. R., Stark, C. E. L., and Clark, R. E. (2004). The medial temporal lobe. *Annu. Rev. Neurosci.* 27, 279–306. doi: 10.1146/annurev.neuro.27.070203.144130

Stephan, H. (1975). *Allocortex*. Berlin: Springer-Verlag. doi: 10.1007/978-3-642-80890-6

Stephan, H., and Andy, O. J. (1970). "The allocortex in primates," in *The Primate Brain*, eds C. R. Noback and W. Montagna (New York, NY: Appleton-Century-Crofts).

Suzuki, W. A., and Amaral, D. G. (1994). Topographic organization of the reciprocal connections between the monkey entorhinal cortex and the perirhinal and parahippocampal cortices. *J. Neurosci.* 14(3 Pt 2), 1856–1877. doi: 10.1523/JNEUROSCI.14-03-01856.1994

Swanson, L. W. (2015). *Neuroanatomical Terminology*. Oxford: Oxford University Press.

ten Donkelaar, H. J., Kachlik, D., and Tubbs, R. S. (2018). *An Illustrated Terminologia Neuroanatomica*. Cham: Springer. doi: 10.1007/978-3-319-64789-0

Tuñon, T., Insausti, R., Ferrer, I., Sobreviela, T., and Soriano, E. (1992). Parvalbumin and calbindin D-28k in the human entorhinal cortex. An inmunohistochemical study. *Brain Res.* 589, 24–32. doi: 10.1016/0006-8993(92)91157-A

von Economo, C., and Koskinas, G. N. (1925). *Die Cytoarchitektonik der Hirnrinde des Erwachsenen Menschen: Textband und Atlas mit 112 Mikrophotographischen Tafeln*. Vienna: Julius Springer.

Williams, P. L., and Warwick, R. (1980). *Gray's Anatomy*, 36th Edn. Edinburgh: Churchill Livingston.

Witter, M. P., Van Hoesen, G. W., and Amaral, D. G. (1989). Topographical organization of the entorhinal projection to the dentate gyrus of the monkey. *J. Neurosci.* 9, 216–228. doi: 10.1523/JNEUROSCI.09-01-00216.1989

Wolk, D. A., Das, S. R., Mueller, S. G., Weiner, M. W., Yushkevich, P. A., and Alzheimer's Disease Neuroimaging Initiative (2017). Medial temporal lobe subregional morphometry using high resolution MRI in Alzheimer's disease. *Neurobiol. Aging* 49, 204–213. doi: 10.1016/j.neurobiolaging.2016.09.011

Yushkevich, P. A., Pluta, J. B., Wang, H., Xie, L., Ding, S. L., Gertje, E. C., et al. (2015). Automated volumetry and regional thickness analysis of hippocampal subfields and medial temporal cortical structures in mild cognitive impairment. *Hum. Brain Mapp.* 36, 258–287. doi: 10.1002/hbm.22627

Conflict of Interest Statement: The authors declare that the research was conducted in the absence of any commercial or financial relationships that could be construed as a potential conflict of interest.

Copyright © 2019 Insausti, Córcoles-Parada, Ubero, Rodado, Insausti and Muñoz-López. This is an open-access article distributed under the terms of the Creative Commons Attribution License (CC BY). The use, distribution or reproduction in other forums is permitted, provided the original author(s) and the copyright owner(s) are credited and that the original publication in this journal is cited, in accordance with accepted academic practice. No use, distribution or reproduction is permitted which does not comply with these terms.

frontiers in Neuroanatomy

REVIEW
published: 11 January 2019
doi: 10.3389/fnana.2018.00114

Toward a Common Terminology for the Thalamus

Jürgen K. Mai[1]* *and Milan Majtanik*[2]

[1] Institute for Anatomy, Heinrich-Heine-University, Duesseldorf, Germany, [2] Institute of Informatics, Heinrich-Heine-University, Duesseldorf, Germany

The wealth of competing parcellations with limited cross-correspondence between atlases of the human thalamus raises problems in a time when the usefulness of neuroanatomical methods is increasingly appreciated for modern computational analyses of the brain. An unequivocal nomenclature is, however, compulsory for the understanding of the organization of the thalamus. This situation cannot be improved by renewed discussion but with implementation of neuroinformatics tools. We adopted a new volumetric approach to characterize the significant subdivisions and determined the relationships between the parcellation schemes of nine most influential atlases of the human thalamus. The volumes of each atlas were 3d-reconstructed and spatially registered to the standard MNI/ICBM2009b reference volume of the Human Brain Atlas in the MNI (Montreal Neurological Institute) space (Mai and Majtanik, 2017). This normalization of the individual thalamus shapes allowed for the comparison of the nuclear regions delineated by the different authors. Quantitative cross-comparisons revealed the extent of predictability of territorial borders for 11 area clusters. In case of discordant parcellations we re-analyzed the underlying histological features and the original descriptions. The final scheme of the spatial organization provided the frame for the selected terms for the subdivisions of the human thalamus using on the (modified) terminology of the Federative International Programme for Anatomical Terminology (FIPAT). Waiving of exact individual definition of regional boundaries in favor of the statistical representation within the open MNI platform provides the common and objective (standardized) ground to achieve concordance between results from different sources (microscopy, imaging etc.).

Keywords: thalamus, parcellation, nomenclature, terminology, MNI standard space, concordance analysis, human

OPEN ACCESS

Edited by:
Javier DeFelipe,
Cajal Institute (CSIC), Spain

Reviewed by:
Mihail Bota,
University of Southern California, United States
Hans J. ten Donkelaar,
Radboud University Nijmegen, Netherlands

***Correspondence:**
Jürgen K. Mai
mai@uni-duesseldorf.de

Received: *04 August 2018*
Accepted: *27 November 2018*
Published: *11 January 2019*

Citation:
Mai JK and Majtanik M (2019) Toward a Common Terminology for the Thalamus. Front. Neuroanat. 12:114. doi: 10.3389/fnana.2018.00114

INTRODUCTION

Modern neuroimaging research requires consistent, internally complete and systematic nomenclature (Swanson, 2015). Particularly for the new generation of discovery tools a solid thalamus parcellation and nomenclature is essential. Traditional textbooks, however, are not helpful as they normally mediate a stereotypical picture of the human thalamus with a spheroid structure in the center of an established standardization grid (standard space) with nuclei that are named according their topographic positions (anterior, central etc.) and show an orderly arrangement of in- and output relations.

In clear contrast to such idealized representations is the complexity of the internal organization and the nomenclature of the human thalamus when it comes to a detailed interpretation. The reader

is confronted with multiple parcellation schemes with often bewildering terms. Comparing the different competing delineations and deciphering the innumerable and often non-matching terms is coping with frustration.

The three most important reasons for the disparate and demotivating situation are first, the great individual variations in topographic relationships of human thalamic nuclei, second, the impact of age and disease and, third, the different concepts of researchers from different "schools."

The extent to which these three aspects influence the representation of the thalamus is illustrated in the following figures. The **Figure 1** shows the profile of 12 coronal sections through the thalamus of different brains cut at the level of the posterior commissure. The substantial differences of the profile and the discrepancies of the internal parcellation of the main divisions are obvious, irrespective the different naming of subareas and the different authorships. Similar results are obvious if sections are compared which were cut at any other orientation. The interindividual differences and the great topographic variations hinder to define measures and variables like those advanced for the rodent brain (Swanson and Bota, 2010).

The second important reason for differing segmentations of the human thalamus is the influence of age and disease. Global changes in volume, shape and neural connectivity across the adult lifespan are well-studied (Hughes et al., 2012; Hess et al., 2014). Changes of the detailed topographic organization that occur in the course of aging and disease have not been systematically determined with respect to thalamus maps. **Figure 2** shows a comparison of the delineations of the thalamus in a "normal" individual and in a case of Parkinson's disease. The delineations by the same author (Hassler, 1977; Hassler et al., 1979) ensure that the same criteria were applied without observer bias. Even under these ideal conditions the maps show clear differences at the corresponding section level. The variance is even more impressive if the delineations are compared on cross sections through the thalamus in the standard space.

The most aggravating hindrance for a harmonizing nomenclature is due to different concepts of researchers from different "schools." **Figure 3** gives an example of the interpretation by specialists that were asked to analyze the very same serial thalamus sections. Their maps reveal appreciable differences with respect to architectonic interpretation and terminology. Neither the segmentation nor the terms used for the lateral nuclei show any concordance. The area delineated by Hopf as Ncl. ventro- and *zentro*intermedius (V.im and Z.im.e) that is characterized by well-known cellular features and identified as target for the cerebellar afferents, has almost no areal and conceptual counterpart in the other diagrams. This outcome illustrates that the interpretation of the same cyto- and myeloarchitecture is driven by diverging criteria. This includes the incorporation of certain types of bias and possibly prejudgement depending from experience with animal or human brains, tradition or "schools."

The regions distinguished in the human thalamus were described with variant terms. They are associative to historical aspects and show linguistic differences (Latin vs. English terminology), were adopted to harmonize the naming system between species and reflect the influence from human pathology. Walker (1966) has properly noted that "… anatomists have attempted to designate thalamic components, delineated morphologically, by topographic or descriptive adjectives, numbers or letters, both Greek and Arabic. Since the compartments so defined have no common point of reference, thalamic nuclei of different schools are not comparable, so the disciples of each creed have adhered rigidly to their own dogma and rejected all others."

The need of a comprehensible thalamic nomenclature, readable with immediate meaning, has been addressed early. Already 75 years ago Vogt and Vogt (1941/1942) noted in their studies on the human thalamus ("*Thalamusstudien*") the commitment to rely on areas distinguished by biologically significant features and on the use of an intelligible nomenclature. Their quest for a consistent, derivable naming scheme was also driving the work of many other authors, many of them adding additional parameters from developmental, functional, molecular or comparative studies (Grünthal, 1934; Dekaban, 1953, 1954; Hassler, 1959; Riley, 1960; Andrew and Watkins, 1969; Mehler, 1971; Van Buren and Borke, 1972; Emmers and Tasker, 1975; Hirai and Jones, 1989; Macchi and Jones, 1997; Morel et al., 1997; Jones, 2007; Ding et al., 2016).

In order to keep the varied information manageable and to make it usable for research many tables of synonyms for the human thalamus have been created. Those tables involving studies from authors of different "schools" pretend a suitable comparison but indeed offer a poor basis for the harmonization of the thalamic nomenclature. As can be deduced from **Figure 3** they just provide lists of closest matching terms for compartments with limited topographic and semantic congruency.

Another approach to reach "a general agreement … and to establish and to adopt a standardized nomenclature" included the analysis of the very same set of sections through the thalamus by several authorities representing different Anglo-American and German "schools" (Dewulf, 1971). This attempt did likewise not result in a concordant and harmonized nomenclature (**Figure 3**). The huge discrepancies between the delineations prevented the adoption of the recommended parcellation scheme and the proposed nomenclature.

Instead of deriving at an exemplary or unitary and generally accepted terminology for the human thalamus one faces the emergence of even new parcellations and new terms evoked by the modern imaging and informatics technologies. Explorations of the human thalamus by magnetic resonance imaging (MRI) have provided feature maps that may not match to the anatomically specified nuclei or formations (Keifer et al., 2015; Chien et al., 2017; Kumar et al., 2017). In a time when the usefulness of neuroanatomical methods is increasingly appreciated for modern computational analysis of the brain (Devlin and Poldrack, 2007; Bohland et al., 2009; Mitra, 2014) the limited cross-correspondence between recent anatomical atlases creates fundamental problems.

Considering the strong influences of individual anatomy, the appreciable age- and disease-related changes, the impact of

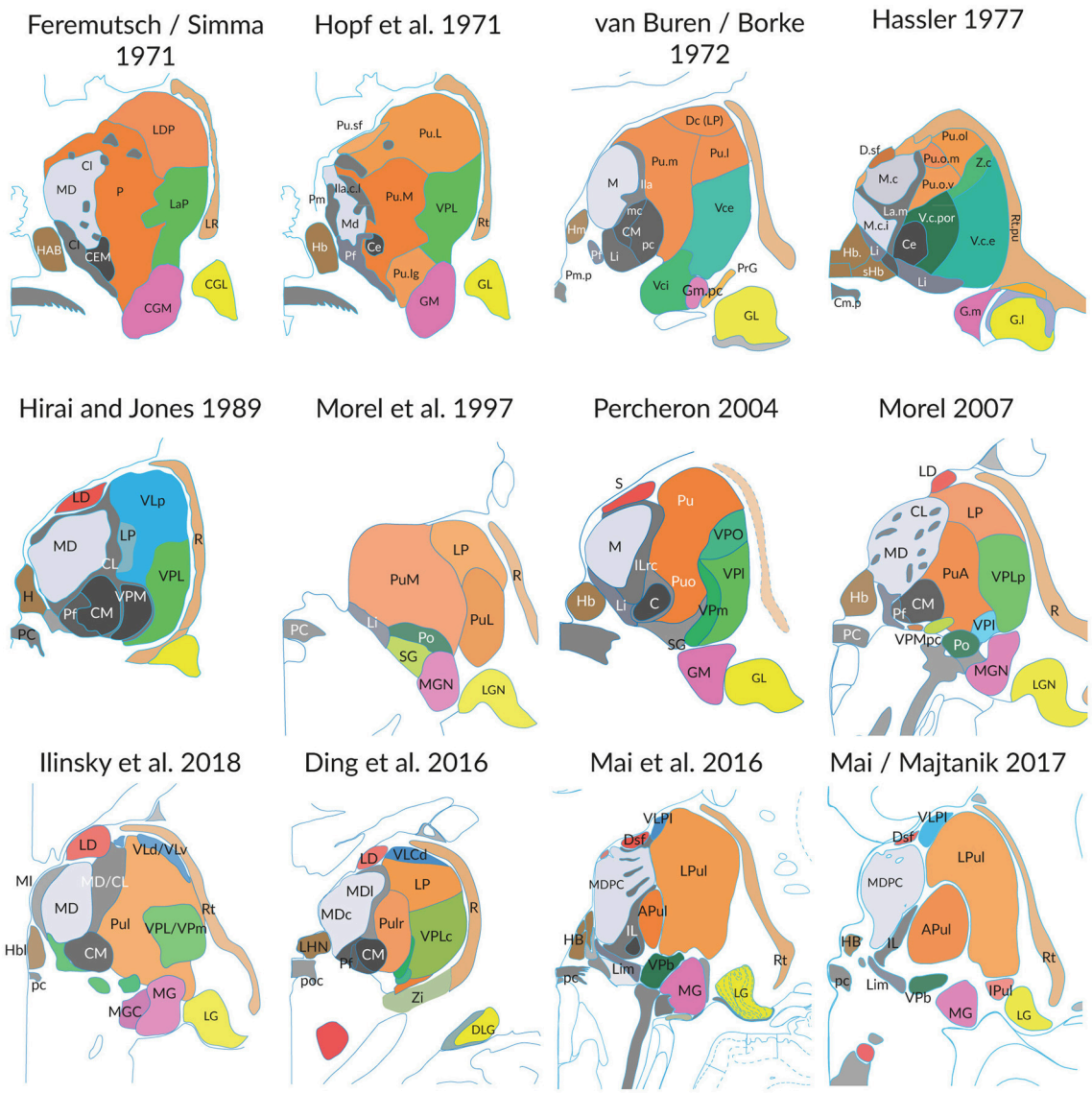

FIGURE 1 | Individual differences of the thalamus in post-mortem brains (medial is to the left). Each figure shows the cross-section areas and topographies of individual thalamic nuclei in coronal sections at the level of the posterior commissure as presented in the original work of the authors. The section planes are close to perpendicular to the intercommisural line (ICL), the reference line connecting the anterior and posterior commissure, except the slices from Hopf, Feremutsch and Simma, Hirai and Jones, Ding. These are tilted up to 22° to the intercommissural plane. The diagrams were redrawn and color was added. The color in each section designates comparable nuclei or territories (blue: cerebellar territory; green: somatosensory complex; orange: pulvinar; light gray: mediodorsal nucleus; dark gray and black: intralaminar nuclei). For abbreviations see **Supplementary Table 5**.

different concepts for the interpretation of thalamic anatomy and the impact of imaging technologies we envision the need for a different approach to resolve some of the inconsistencies in terminology. This approach uses the possibilities offered by computer science and stresses the representation of the variant thalamic areas in a common space. The coordinates in this space represent the communality of any features related to the human thalamus. As a common space we selected the standard MNI/ICBM2009b symmetric template (Fonov et al., 2009). This selection ensures that the coordinates act as unifying concept for the naming of thalamic structures. The objective goal is the negligence of terms in favor of topographic precision. In the end, the terminology which reflects different concepts shall become converted in coordinates which define space.

MATERIALS AND METHODS

Synoptic Representation of Nine Anatomic Atlases of the Human Thalamus

We used nine thalamus atlases (**Table 1**) represented in two different spaces: the original space and the standard MNI space. The original space refers to the representation of the atlas as in

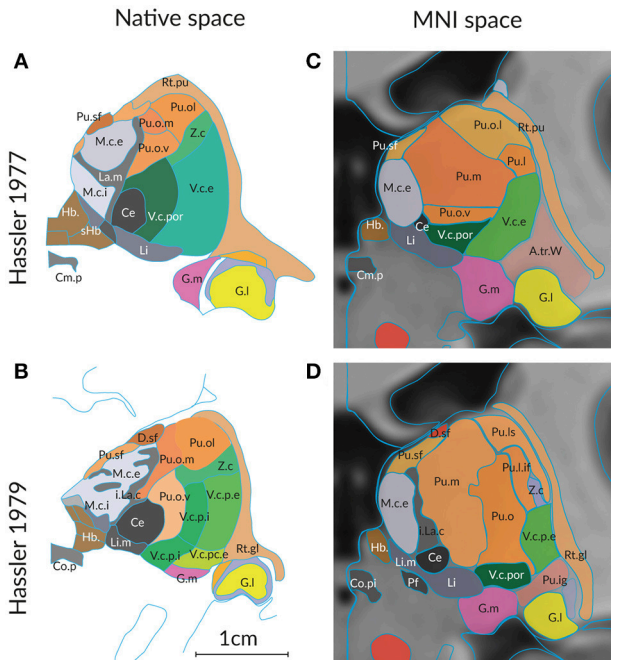

FIGURE 2 | Differences in the structural organization of the thalamus of a "normal" **(A,C)** and a compromised thalamus **(B,D)** analyzed by the same author. Parcellation of the thalamus of a 57 year old male without pathologic change in the brain (Hassler, 1977) and of a person with the diagnosis of Parkinson's disease (Hassler et al., 1979). **(A,B)** Representation of a coronal section through the posterior commissure as originally published (cf. **Figure 1**). The scale bar was taken from the original figures; color was added. **(C,D)** Display of the profiles generated from the 3D reconstruction of the serial sections from both cases. The individual 3D volume was registered into the standard space (using the MNI/ICBM co-registered 3D-AHB model) and a coronal section is presented that passes through the posterior commissure. Color code as in **Figure 1**. For abbreviations see **Supplementary Table 5**.

the original publication. The standard MNI space relates to the thalamus space of the MNI/ICBM2009b template.

In the original space only sections or drawings from the publications were used. For the representation of the atlases in the standard space the atlases were 3D reconstructed with our geometric shape constrained 3D reconstruction techniques for serial sections (Mai et al., 2016). Briefly, first a raw model is 3D reconstructed from delineations of one or more histological slice series by simultaneous slice to slice registration procedure. From this model a 3D surface representation is created such that the surfaces are smooth, the surface nodes are distributed according to the inter-slice section distances and the surface area optimally represents the volume of the area. This 3D surface model and its volume representation is then diffeomorphically registered to the MNI space with our procedure (Mai and Majtanik, 2017). The contours of the atlas areas in the MNI space for **Figures 2** and **4** were then re-sampled as sections of the 3D surfaces with planes at given locations. Eight of the nine atlases were 3D reconstructed as described and registered to the MNI/ICBM2009b standard space (Fonov et al., 2009). The Ilinsky et al. atlas (Ilinsky et al., 2018) was obtained from the http://www.lead-dbs.org website and registered to the symmetrical MNI/ICBM2009b template.

The "new" atlases representing individual anatomy in the standard space provide a database of parcellation concepts of the human thalamus and of the variant terminology. We have compared the terminology used by the different experts and have listed corresponding regions (**Supplementary Table 2**). These regions provided the definitions of clusters which were used for the mathematical evaluation of discriminated areas and computation of equivalence of the parcellation concepts. We estimate the equivalence of the concepts by concordance between the areas. We assume that areas with high concordance correspond to equivalent concepts.

Alltogether we have analyzed the following 11 regions: anterior intralaminar region (ILA), central intralaminar region (ILCe), anterodorsal region (A), medial region (M), medial ventroanterior region (VAM), lateral ventroanterior region (VAL), ventrolateral region (VL), ventroposterior complex (VP), posterior region (P), and geniculate region (LGB/MGB). For each cluster we computed concordance of the contained areas across nine thalamic parcellations (**Supplementary Tables 1**, **2**). Not included within the concordance study were the periventricular and midline regions due to the small width of these regions and the inconsistencies in the delineation of the nuclei in the different atlases.

Concordance Analysis

The degree of conformity of the topography of segmented thalamic regions was assessed by means of concordance analysis. For the concordance analysis an atlas refers to a parcellation of the thalamus in the standard MNI space. The concordance problem can be defined as a quantitative analysis of spatial relationships between parcellations of underlying thalamus space (Bohland et al., 2009). A high concordance of two thalamic parcellations results from high pair-wise spatial overlap between their areas. This analysis provides a valid base for the identification of major conflicts with regard to the characterization and extent of thalamic areas, for comparing the actually used terminology and for defining the most appropriate terms (TNA, 2017). It is understood that we broaden the understanding of "terminology" to include also the anatomic position and neighborhood relations of thalamic structures.

Hierarchical Analysis Levels

In view of the large quantity of nuclei distinguished by some authors it is appropriate to use a hierarchic scale for the thalamic nuclei. We distinguished between three levels of granularity for the concordance analysis, namely "areas," "clusters" and "global thalamus." They denote topographically circumscribed "areas" or groups of structurally and functionally related neighboring areas or "formations" and the sum of all distinguished clusters.

We performed the concordance analysis for these three levels of granularity. The finest, *area (local)–level* concordance analysis, compares local pairwise relationship between areas. The middle, *cluster (group)–level* concordance analysis, contrasts 11 clusters and the coarsest, *global (thalamus)–level* concordance analysis, computes concordances between whole thalamus atlases.

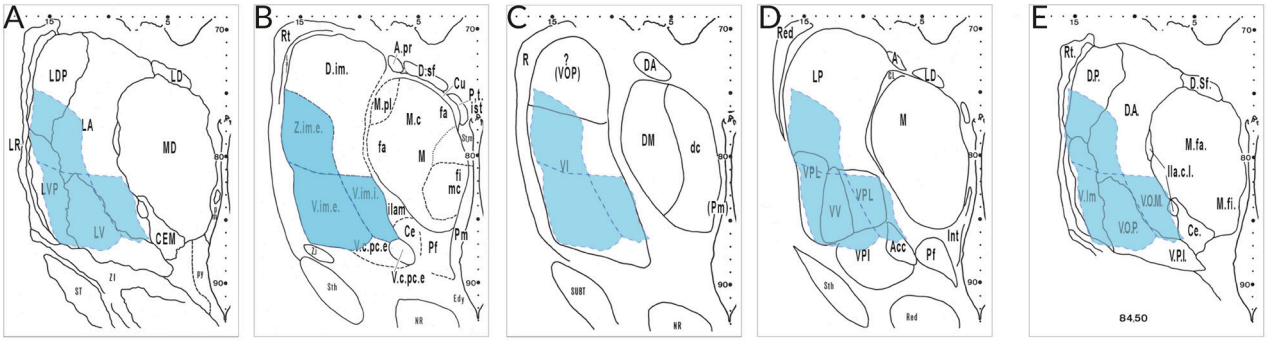

FIGURE 3 | Delineations of the same cell- and fiber-stained sections at mid-thalamic level presented by different specialists. The diagrams were taken from the atlas edited by Dewulf after the Louvain Conference 1963 (publ. 1971) from the following authors: **(A)**, Feremutsch and Simma; **(B)**, Hopf; **(C)**, Macchi; **(D)**, Krieg; **(E)**, Feremutsch and Simma ("standardized nomenclature"). Since all five delineations refer to the same section the V.im region demarcated by Hopf (blue color) was superimposed over the remaining diagrams. The V.im region defined by Hopf (V.im.e, V.im.i, and Z.im.e) is overlapping parts of LDP, LA, LV, and LVP in the diagram of Feremutsch and Simma; it corresponds to the major part of VI but also reaches VOP (Macchi); it is designated as VPL and VV but encroaches also LP, VPI, and Acc (Krieg) and is designated in the "standarized nomenclature" as Vim, VOP and VOM but also includes parts of DP and DA, respectively. Acc, not specified (N. arcuatus); DA, not specified (N. dorsalis anterior); DP, not specified (N. dorsalis posterior); LA, N. lateralis thalami, pars principalis; LDP, N. lateralis thalami, pars dorsalis posterior; LP, N. lateralis posterior; LV, N. lateralis thalami, pars ventralis; LVP, N. lateralis thalami, pars ventralis posterior, V.im.e/i; Ncl. intermedius, pars externa/interna; VI, Ncl. ventralis intermedius; VOM, not specified (Ncl. ventrolateralis, pars medialis); VOP, Ncl. ventrolateralis, pars posterior; VPI, Ncl. ventralis posterior inferior; VPL, Ncl. ventralis posterior lateralis; VV, N. ventralis ventralis; Z.im,e, Ncl. zentrolateralis intermedius, pars externa.

TABLE 1 | Thalamus atlases used in this study.

Atlas	Nr. of cardinal planes used	Nr. of areas used	Abbreviation
Hassler, 1977	3	103	HSL
Ilinsky et al., 2018	1	42	ILI
Hassler et al., 1979	1	73	HPD
Van Buren and Borke, 1972	3	53	VBB
Feremutsch and Simma, 1971	1	32	FRM
Percheron, 2004	2	29	PER
Morel, 2007	3	47	MRL
Ding et al., 2016	1	79	DNG
Mai and Majtanik, 2017	1	54	AHB

For the *area (local)-level concordance analysis*, we analyzed the pair-wise spatial correspondences between anatomical areas defined in the nine different atlases transformed to the ICBM/MNI152_2009b space. For any pair of areas, two conditional probability values were calculated based on the spatial overlap between the areas. Following Bohland et al. (2009) we express the pair-wise spatial relationship as a *conditional probability* $P(a_1|b_1)$ of a voxel being in area $\mathbf{a_1}$ according to the atlas **A** if it is in area $\mathbf{b_1}$ according to the atlas B. We use a shortened notation for the conditional probability $P(a|b) = P_{ab}$. The results of local area-level concordance analysis show complex correspondences between areas. It is, however, rather difficult to recognize the correspondence between the atlases for specific areas belonging to traditionally defined thalamic subdivisions. To improve understanding and facilitate visualization of the inter-atlases concordance we analyze correspondences between selected groups of areas at the cluster-level.

A *cluster (group)–level concordance measure* should be one if two area clusters from different atlases are perfectly mutually predictable and zero if there is no predictability between the area clusters. Such cluster-level correspondence measure properties are satisfied by adjusted Wallace index (Wallace, 1983; Pinto et al., 2008). The Wallace index $W_{A\to B}$ quantifies directional correspondence between two clusters of areas. Given two area groups A and B, Wallace index $W_{A\to B}$ between the group A and the group B is the probability that two voxels are classified together in one area in group B knowing that they were classified together in one area in group A. The Wallace coefficient (W) directly indicates the agreement between partitions and therefore can be easily interpreted. As an example, $W_{A\to B} = 0.832$ and $W_{B\to A} = 0.546$ indicate that if two voxel are in the same area in the group A they have about 83% probability of being together in an area in the cluster B, while conversely, this is about 55% probability. This reflects the fact that the group A is more discriminatory than group B and the areas of A subdivide the areas of B.

From the two directional Wallace values we derive the adjusted maximal Wallace index $W_{max} = \max(W_{B\to A}, W_{A\to B})$ and adjusted asymmetry Wallace index $W_{asym} = \mathrm{abs}(W_{B\to A} - W_{A\to B})$, where max(x) denotes the maximum and abs(x) the absolute value of x.

The scalar-valued maximal Wallace index W_{max} for two parcellations has values between 0 and 1 and emphasizes the highest mutual predictability of two area groups, with one denoting perfect mutual predictability of one area group from the other group. The Wallace asymmetry index W_{asym} takes values between zero and W_{max} and estimates the degree of asymmetry in the mutual predictability of the area groups. A large W_{asym} indicates a strong subset configuration between the two groups. In the above example $W_{max} = 0.832$ and $W_{asym} = 0.286$. A *subset* or *subdivision configuration* between areas refers to a spatial

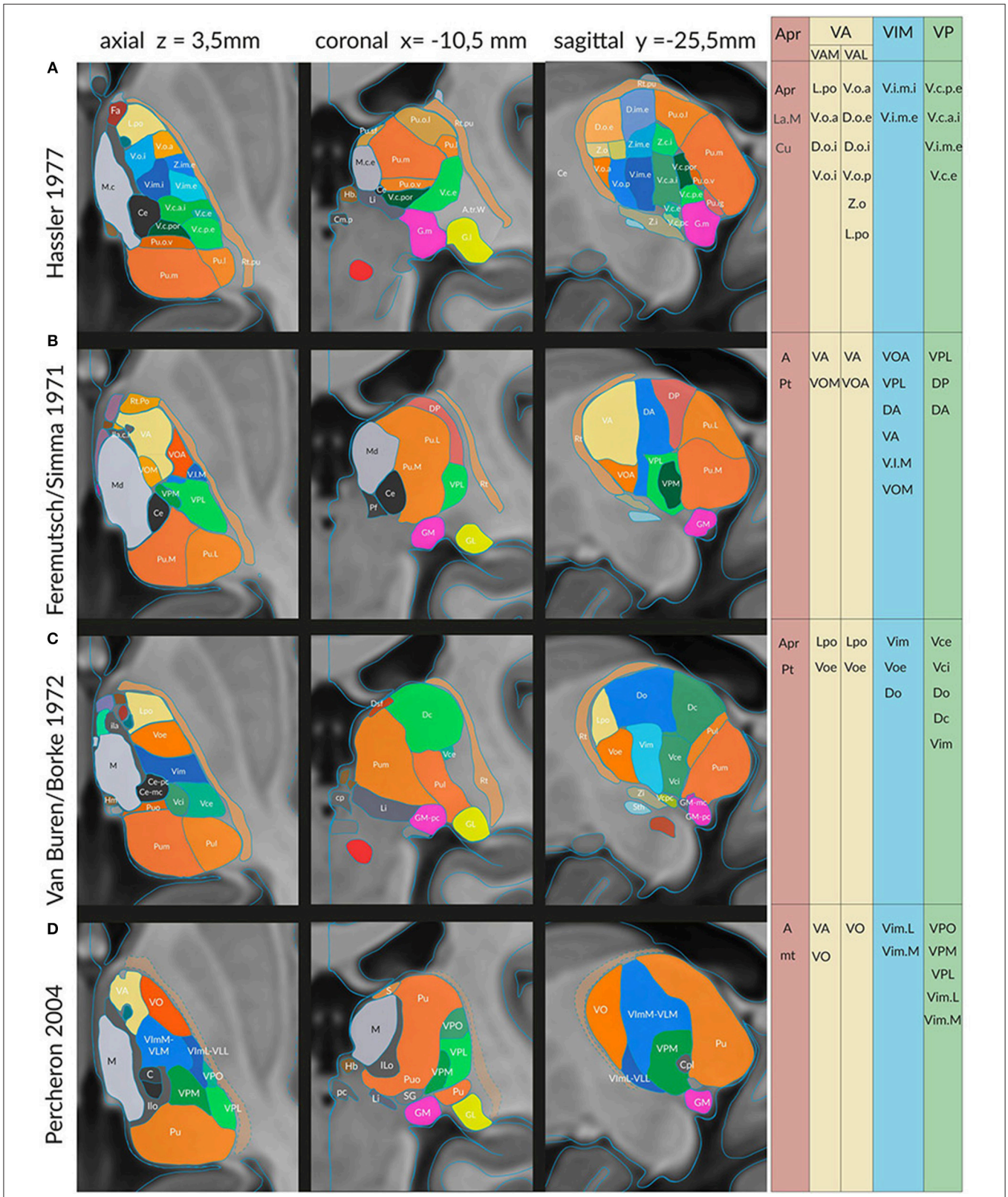

FIGURE 4 | Continued.

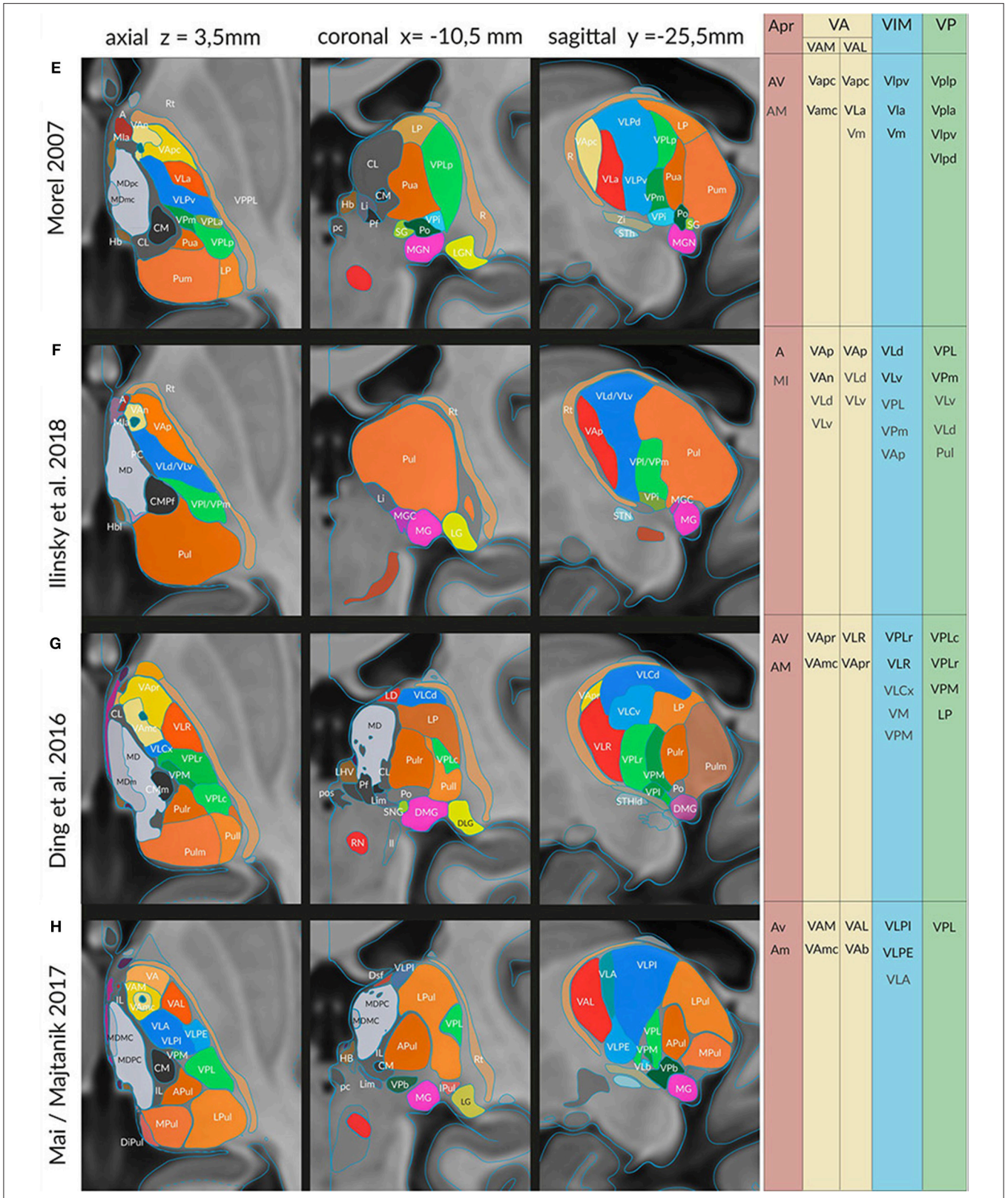

FIGURE 4 | Sections in three cardinal planes from eight different authors indicating segmentations of the thalamus in the common standard (MNI) space: **(A)** Hassler (1977), **(B)** Feremutsch and Simma (1971), **(C)** Van Buren and Borke (1972), **(D)** Percheron (2004), **(E)** Morel (2007), **(F)** Ilinsky et al. (2018), **(G)** Ding et al. (2016) and **(I)** Mai and Majtanik (2017). The exact positions of the three cardinal planes are indicated in the upper line. The color code is the same as in the preceding figures. Right side: areas or nuclei that have been selected for the clusters representing the nigral, pallidal (yellow), cerebellar (blue), sensory (green) territories, and the anterior thalamic nucleus. For abbreviations see **Supplementary Table 2**.

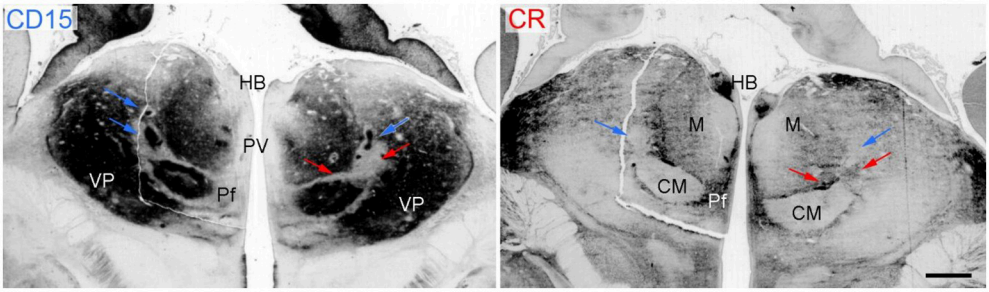

FIGURE 5 | Coronal sections through the thalamus of a fetal human brain at 17 weeks of pregnancy. The immunoreactivity against the cell-surface epitope CD15 (left) and calbindin (right) shows the main thalamic nuclei separated by the intralaminar formation that is CD15 negativ (red arrows) except the associated nuclei (Ncl. centrum medianum CM and Ncl. centralis lateralis, blue arrows) but calbindin positive. Scale bar 1 mm. HB, habenula; Pf, parafascicular nucleus; PV, periventricular region; VP, ventroposterior complex.

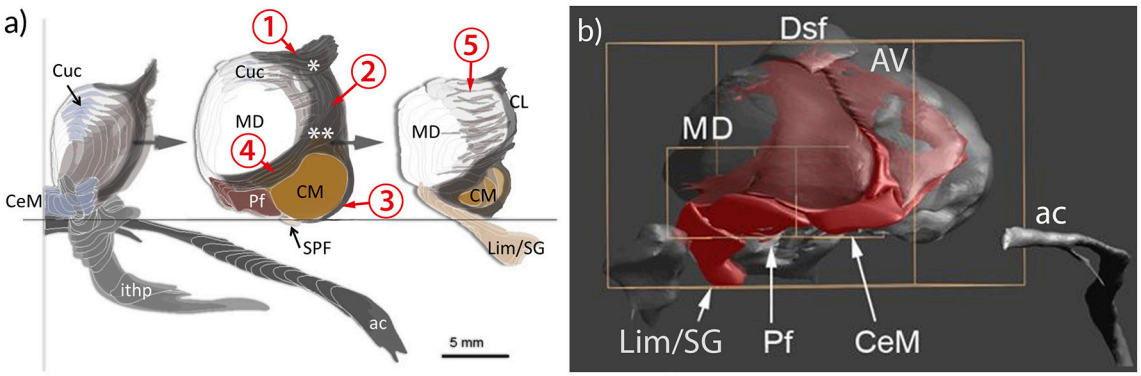

FIGURE 6 | Representation of the intralaminar formation (IL) in relation to the mediodorsal nucleus (MD) and the anterior commissure (ac) and the inferior thalamic peduncle (ithp) as orientation marks. **(a)** MD is sliced to show the anterior, middle and posterior divisions of IL separately. The core of the formation is represented by the portion nestling around the lateral perimeter of the MD and separating the medial from the lateral region of the thalamus. This central portion bifurcates anterodorsally (asterisk) to form the shell below the anterodorsal region. Ventrally the internal lamina also bifurcates (double asterisk) to form a cap that bounds the centromedian nucleus (CM) and then continues around the anterior pole of MD. Cells within the branching areas are the central lateral nucleus (asterisk) and the paracentral nucleus (double asterisk). At the anterior and posterior pole of the MD the internal medullary lamina enlarges and differentiates as central medial nucleus (CeM) anteriorly and as suprageniculate and limitans nuclei (Lim/SG), respectively. **(b)** Medial view of a reconstruction of the IL (red). The IL extends along the ventral surface of MD, represented by the central medial nucleus (CeM), parafascicular nucleus (Pf) and Lim/SG. 1–5: divisions of the IL; 1, superior part; 2. central (lateral) part; 3, circumcentral part (lamella intermedia, Schnopfhagen, 1877; lamella praesemilunaris; Hassler, 1982); 4, anterior part; 5, posterior part (retrocentral part); Cuc, cucullar nucleus.

relationship where an area from one atlas is divided into multiple smaller areas in other atlas.

Global (thalamus)–level concordance analysis estimates correspondences between thalamic parcellations. As a global concordance index we extended the above defined Wallace indices W_{max} and W_{asym} to the whole thalamus parcellations.

Generally three concordance characteristics can be captured by combinations of W_{max} and W_{asym}. The first parameter combination with large W_{max} and low W_{asym} indicates high concordance between atlases with predominantly *one to one* relationship of the areas. The second parameter combination with large W_{max} and large W_{asym} points at high concordance of atlases with *one to multiple* area relationships (subset configuration). Finally the third combination with low W_{max} indicates *lack of concordance* between the atlases.

In order to facilitate the interpretation of the Wallace coefficients as being strongly different from the concordance values under chance we estimated concordance distributions for random parcellations of the thalamus volume. We created random partitions of the thalamus volume consisting of N regions with a random label filling algorithm. For each atlas we generated fifty random parcellations with N equal to the number of areas in that atlas. For each pair of atlases the Wallace indices were computed for 1,000 pairs of size-matched random parcellations. The procedure resulted in estimates of the W_{max} and W_{asym} chance distributions specific to each pair-wise atlas comparison. The distributions for cluster concordances were computed analogously. The 95th percentile values (**Supplementary Table 4**) of these distributions are used to assess whether a given concordance value has <5 percent

chance of originating from comparison of random thalamic parcellations.

RESULTS

Proposal of a Consolidated Nomenclature: The Base Layer

The discussion of the nomenclature of the human thalamus concentrates on regions or nuclei which have substantial topographic and functional importance and are suited for the concordance analysis. We begin with the internal medullary lamina and associated nuclei because this extended compartment provides as "great defining landmark" (Jones, 1998) the key for the parcellation and regional analysis of the human thalamus. The relevance for the organization of the thalamus is obvious during prenatal development when it is readily identifiable separating the differentiating neuronal populations of prospective subdivisions (**Figure 5**; Forutan et al., 2001). Delineation of this formation provides therefore a valuable means for the definition of the topography and the neighborhood relations of thalamic regions.

Intralaminar Formation–Formatio Intralaminaris

The intralaminar formation (IL) is represented by a rather dense feltwork of fibers, the internal medullary lamina (Burdach, 1822) or lamella medullaris (Vogt, 1909), that divides the thalamus into medial, lateral and anterior nuclear regions. Embedded within this feltwork are diverse groups of cells that in some locations form circumscribed nuclei (intralaminar nuclei). These cell ensembles have a common developmental history, a characteristic cell type and similar projections to the striatum (see Mai and Forutan, 2012). Two populations are identified histochemically either by calbindin and CD15 or calretinin immunoreactivity.

The extent and the arrangement of cells and fibers of the internal medullary lamina have been characterized differently. The nuclei associated with this lamina were allocated by most authors to an anterior and posterior division. The anterior portion (Ncll. intralaminares anteriores) is represented by the central medial, paracentral, central lateral, and the cucullar nuclei (Hassler, 1959); the posterior portion consists of the Ncl. centrum medianum (centre médian) and parafascicular nuclei (CM/PF) and the subparafascicular nucleus (SPF). However, many authors also agree that the internal medullary lamina continues beyond CM/PF to the pretectal area (Grünthal, 1934; Feremutsch and Simma, 1954a,b; Hassler, 1959; Percheron, 2004; Jones, 2007; Lenz et al., 2010). This posterior division (Ncll. intralaminares posteriores) shows no clear border and the cell ensembles therein seem to interlock with the mediodorsal nucleus (MD). The associated nuclei are notably the limitans, suprageniculate and posterior nuclei (the posterior nuclear complex) and possibly also the pregeniculate nucleus and the magnocellular division of the medial geniculate body (Lenz et al., 2010). The three components of the IL were integrated within the intralaminar-limitans-retrocentral formation (Percheron, 2004) or involucrum (Hassler, 1959) and are now distinguished as the anterior, central and posterior group of the human intralaminar nuclei (Mai and Forutan, 2012; TNA, 2017; **Figure 6**).

We have applied the group-level concordance analysis separately for the anterior and central division of the intralaminar nuclei. The maximal Wallace index for the anterior division is $W_{max} = 0.54$ and the asymmetry Wallace index is $W_{asym} = 0.16$ and for the central division $W_{max} = 0.68$ and $W_{asym} = 0.27$ (**Table 2A**). These values indicate very low concordance with undetermined subdivision relationships between these areas from different atlases. The very low concordance for IL derives from the highly variable representation of IL in the different atlases. For example, Feremutsch and Simma (1971) did not delineate a continuous IL but isolated segments. In contrast, Morel (2007) defined the posterior portion of the IL five times thicker than Mai et al. (2016) or Ding et al. (2016). Such great differences make a re-evaluation of the IL mandatory.

Periventricular and Midline Region

The region between the ependyma of the third ventricle and the MD is relatively thin in the human thalamus if compared with the corresponding region in subhuman thalami. We distinguish two components: First, the thin sheet of small neurons along the third ventricle below the ependyma which is a component of the ventricular gray substance (Nuclei para- or subependymales thalami, Riley, 1960; substantia grisea centralis thalamica, Hassler, 1982). The second and main portion is constituted by clusters of cells located laterally from the subependymal gray layer. They are collectively termed as midline nuclei knowing that they are defined differently in the literature. We distinguish the paratenial and paraventricular nuclei as the dorsal component, and the reuniens, submedius, and fasciculosus nuclei as the ventral component. The midline nuclei are architectonically strikingly distinct and have different connections. This has let to variant interpretations of their functional relations (Benarroch, 2008).

We address this region because of the considerable differences between the human and subhuman organization and the dissenting opinions about the relation between the cell groups of this region with those of the intralaminar formation. It has been described under several names: midline nuclei (Altman and Bayer, 1988; Krauth et al., 2010), "mediane Kerngruppe" (Niimi, 1949), subependymal formation or paraventricular formation (in Dewulf, 1971; Dom, 1976), midline and epithalamic region (Van Buren and Borke, 1972), paramedian formation (Percheron, 2004). None of these terms refers only to the subependymal or periventricular site of the third ventricle but includes also adjacent areas (Rose, 1942; Van Buren and Borke, 1972; Morel et al., 1997; Krauth et al., 2010; Ding et al., 2016).

Anterodorsal Region

The anterodorsal region forms an oblong rostrocaudally oriented structure that extends from the anterior pole to the dorsal (upper) surface of the thalamus. The entire region is separated from the lateral ventricle by a prominent fibrous layer, stratum zonale, and underlaid by the lamina medullaris superior, the superior bifurcation of the internal medullary lamina (**Figure 6**). It consists of the anterior nuclei and the dorsal superficial

nucleus. The latter nucleus is included due to architectonic and hodologic commonalities.

The *anterior nuclei* consist of the "principal" anteroventral nucleus (AV), underneath the anterior tubercle and of the anteromedial (AM), and anterodorsal (AD) nuclei. The dorsal component of the anterodorsal region is represented by the dorsal superficial (or laterodorsal) nucleus. It appears as flat elongation of the anteroventral nucleus approximately up to the middle of the rostrocaudal dimension of the thalamus. Both parts can be distinguished thanks to the fragmentation of the surrounding medullary fibers.

The AV (Sheps, 1945) is named in analogy to subhumans; anterior principal nucleus (Ncl. anteroprincipalis, Vogt and Vogt, 1941/1942) would be a more appropriate term matching its dominant size in humans. The remaining anterior nuclei were often regarded as accessory, aberrant or even as non-existent. They are, however, distinguished by their individual neurochemical characteristics (see Forutan and Mai, 2012). AM appears as extension of AV toward the frontal pole of the thalamus and bends medially to come close to the midline at the interthalamic adhesion. The distinction of one or even multiple interanteroinferior nuclei (Ncl. anteroinferior, Ncl. anteroreuniens, Hassler, 1982, or Ncl. interanteromedialis, Rioch, 1929) for the most medial division next to the ventricular surface is not justified since the anterior nuclei are not merged at the midline in humans. AD is reduced to a small slot-like ensemble of cells between AV and paratenial nucleus. The distinction between the nuclei of the anterodorsal region is relevant because of the structural and functional segregation of the entrant pathways from the extended hippocampal formation and different projections to the cingulate cortex (see Bubb et al., 2017).

The group-level concordance analysis resulted in the maximal Wallace index being $W_{max} = 0.71$ and the asymmetry $W_{asym} = 0.24$ (**Table 2A**). The values indicate relatively good concordance in this cluster with frequent subdivision relationship between the areas from different atlases. The evaluation shows good overlap at the core area of AV-region but rather variations in the DSf region. The high W_{asym} stresses that some authors did not distinguish the various subdivisions of the anterior nuclei. A more detailed interpretation of the subdivisional relationships between these nuclei is illustrated in **Figure 9B**. The atlases MRL, DNG, HSL and AHB subdivide the anterior ventral nuclei into two or more areas, whereas the remaining atlases delineate only one area.

Medial Region (Mediodorsal Nucleus)

The medial region comprises the field encircled by the IL and midline nuclei. It extends from the interthalamic adhesion to the level of the posterior commissure (and thus covers about 2/3 of the total length of the thalamus). In humans this region coincides with mediodorsal nucleus. This definition stresses the distinctiveness against the IL and the midline nuclei which both show relevant developmental, cytological and chemical differences (Forutan et al., 2001). MD is not a homogeneous nucleus as described by Andrew and Watkins (1969). Even less justified is the fragmentation into six or more subnuclei (Namba, 1958; Hassler, 1959; Gihr, 1964; Niimi and Kuwahara, 1973; Ding et al., 2016). It is common to distinguish three major internal divisions: medial, central and paralaminar (TNA, 2017). Other designations used are determined by either the preference for cyto-, myeloarchitectonic or pure topographic criteria. Based on myeloarchitectonic criteria these are pars fibrosa, fasciculosa and paralamellaris (Hassler, 1959); the largely congruent cytoarchitectonic divisions are the magno-, parvo- and densocellular (or multiform) divisions (Olszewski, 1952; Ding et al., 2016). The terms magno- and parvocellularis for the medial and central divisions may be questioned because morphometry does not support the distinction by cell size in humans (Dewulf, 1971; Van Buren and Borke, 1972). A medial subregion, clearly identified by neurofilament-, CART (cocaine- and amphetamine-regulated transcript)- and also CD15-immunoreactivity, may correspond to the territory of amygdaloid afferents (Forutan et al., 2001). The lateral and posterior periphery of the MD along the laminar border is poorly determined. This creates a wide transitional area that extends over this lamina into the pulvinar. The corrugated pattern affiliates this area to either MD or IL which results in either an extended definition of the MD (Mai et al., 2016) or of the IL (Morel et al., 1997). Gihr (1964) described "giant cells" as specific for this paralaminar or transitory division in humans.

The designation "mediodorsal" nucleus is maintained albeit the homolog, the medioventral nucleus, of humans is not part of the medial region but corresponds to a component of the anterior division of IL: the reuniens nucleus and possibly the submedial nucleus.

The term dorsomedial nucleus is inappropriate; it does not describe the topographically correct location within the thalamus and its counterpart would then be consequently described as ventromedial nucleus, a name reserved for the lateral thalamic region.

The maximal Wallace index is $W_{max} = 0.85$ and the asymmetry Wallace index is $W_{asym} = 0.35$. These values indicate the highest concordance between the atlases with very strong subdivision relationships between the areas delineated in different atlases. This subdivision configuration of the M cluster is reflected in the conditional probability values in the **Supplementary Table 3**. The M cluster data show a consistent dominant overlapping of one area accompanied by one or two areas with minor overlap (MRL, ILI, DNG). The spatial distribution of the high concordance coincides with the extend of the MD areas (**Figure 11**, upper row). Similarly, the strong asymmetry W_{asym} is bounded to the extension of the MD area.

Lateral Region

The lateral region is defined as the area between the internal medullary lamina medially, the external medullary lamina (lamella perithalamica), reticular nucleus and internal capsule laterally and the posterior region (pulvinar) posteriorly. The territory is well outlined especially on axial sections at midlevel of the thalamus. Functionally, the nuclei of the lateral region are identified and characterized by the target/source of their afferent/efferent projections. The *motor* thalamus receives predominatly (indirect) striatal (nigral and pallidal)

TABLE 2A | Cluster-level concordance.

	Clusters									
	IL	**AN**	**CM/PF**	**MD**	**VAM**	**VAL**	**VL**	**VP**	**P**	**LGB/MGB**
Concordance Index W_{max}	0.55	0.71	0.69	0.85	0.79	0.61	0.71	0.71	0.80	0.84
Asymmetry Index W_{asym}	(0.16)	0.24	0.27	0.35	0.27	(0.22)	0.25	0.29	0.27	0.32

The table displays the results using the maximal Wallace index W_{max} and asymmetry Wallace index W_{asym} computed for nine clusters as a measure for inter-atlas group concordances and subset relations of the areas within the groups.

TABLE 2B | Global concordance between atlases.

AHB	0.8166	0.6977	0.8398	0.596	0.6656	0.7302	0.7631	0.7203
	MRL	0.8126	0.7908	0.7269	0.7698	0.7503	0.8266	0.8231
		HSL	0.8547	0.6896	0.6768	0.7473	0.8891	0.7055
			FRM	0.7972	0.8172	0.7984	0.8320	0.8553
				ILI	0.6595	0.6753	**0.8659**	0.6631
					VBB	0.7062	0.8567	0.6968
						HPD	0.8285	0.7783
							PER	0.7304
								DNG

*Quantification of inter-atlas concordance using the adjusted Wallace index W_{max}. The index W_{max} is computed between pairs of whole atlas parcellations and indicates the mean maximal concordance between all pairs of atlas areas. In each cell the values in the upper diagonal entries are the concordance indices for particular pairs of the atlases. The maximal W_{max} value (red) is observed between PER and ILI atlases. The minimal W_{max} is observed between AHB and ILI atlases (blue). For the atlas labels on the diagonal see **Table 1**.*

TABLE 2C | Global asymmetry of concordance between pairs of atlases.

AHB	0.2118	0.1433	0.384	(0.0203)	(0.057)	(0.078)	0.5302	(0.049)
	MRL	0.3555	0.1714	0.2306	0.2053	0.1332	(0.315)	0.2612
		HSL	0.5295	(0.122)	0.1484	0.2213	0.6783	(0.095)
			FRM	0.4041	0.378	0.3053	(0.141)	0.4340
				ILI	(0.026)	(0.098)	0.5513	(0.029)
					VBB	(0.072)	0.5244	(0.055)
						HPD	0.4508	0.1277
							PER	0.581
								DNG

Each cell of the table displays the asymmetry Wallace index W_{asym} for the selected pair of the atlases. The index W_{asym} is computed between pairs of whole atlas parcellations and indicates the mean maximal asymmetry between all pairs of atlas areas. High values of W_{asym} reveal frequent subdivision configuration between atlaes. The maximal W_{asym} value (red) is observed between PER and HSL atlases. The minimal W_{asym} is between AHB and ILI atlases (blue). The values below chance threshold (the 95th percentile of the chance distribution of random parcellations) are in brakets and colored gray.

TABLE 2D | Anatomical characterization of the stimulation sites for tremor patients in the studies of Fiechter et al. (2017) and Hamel et al. (2007).

	AHB	**MRL**	**HSL**	**FRM**	**ILI**	**VBB**	**HPD**	**PER**	**DNG**
Fiechter et al., 2017	VLb (VPl)	VLpv	V.im.e, Ra.prl.	VPL, VPM	VPi, VPlVPm	Vim	Vci,Vcpce	VImM-VLM, VPM	VPLr
Hamel et al., 2007	VMb (VPPC)	VPi	V.c.pc	VPl	VPi	Vcpc	Vcpci, Zic.Rpl	VPM	VPl

*The labels for the nine atlases are provided in the **Supplementary Table 5**. The coordinates of the VIM targets in MNI space for Fiechter et al.: x = 14.3 mm, y = −17.40 mm, z = −2.17 mm and Hamel et al.: x = 12.7 mm, y = −19.6 mm, z = −4.38 mm.*

and cerebellar (and vestibular) input whereas the *sensory* thalamus receives somesthetic and visceral input (Vogt, 1909; see Percheron, 2004). The exact definition of the territories, the afferent fibers and their relation to the projection neurons in humans awaits still clarification (Jones, 2007; Kaas, 2012). **Figure 4** illustrates that the parcellation, based mainly on

histological and histochemical methods, is still very controversial and renders this region a very problematic place in terms of nomenclature.

The main divisions were already specified in the cercopithecan brain by C. Vogt (1909). She distinguished between lenticular (pallidal), prelemniscal (cerebellar) and lemniscal radiations terminating in the ventral oral, intermediate (intermédiaire) and caudal division, respectively. These targets correspond to the ventroanterior (VA), ventrolateral (VL or ventral intermediate, V.im) and ventroposterior (VP) nuclei of later authors (Walker, 1938). With the definition of the territory for the afferents from the substantia nigra (SNR) in the rostralmost part of the lateral thalamus (see Ilinsky et al., 2018) this clear terminology became complicated (**Supplementary Table 2**). The documentation of additional afferents to the lateral region (amygdaloid, kinesthetic, and other fibers) has further impaired the development of a unified terminology.

Other important challenges which influence the segmentation and the terminology of the nuclei of the lateral region were reviewed by Percheron (2004). Most important are geometrical particularities due to the strongly curved main axis and the obliquely arranged nuclei along this axis. The geometric deformation displays the lateral nuclei in cardinal sections as if overlaying each other. If, for example, coronal sections are made, the adjacent nuclei may be cut obliquely depicting alternating volumes. The partial volume effect provokes the questionable distinction between ventral and dorsal partitions of the lateral region. That distinction dates back to Meynert (1872) and had functional impact. It should signify the difference between ventral (V) nuclei that receive "fibers of extrathalamic construction, while symbol D signifies that the nucleus receives no afferent extrathalamic fibers" (Hassler, 1971). Such differentiation between relay and associative nuclei in the lateral thalamus has fundamentally influenced the terminology of the nuclei of the lateral region (Sheps, 1945; Hassler, 1959, 1977; Hopf et al., 1971; Mehler, 1971; Van Buren and Borke, 1972; Niimi and Kuwahara, 1973; Ding et al., 2016). The separation of ventral, dorsal and even central sections of the motor thalamus is unjustified "because the three territories and the individual axons extend over the entire ventrodorsal extent" (Percheron, 2004). Hassler has dropped the "*zentralis*" divisions (Hassler, 1971) but these areas remained delineated in later versions of his atlas diagrams (Hassler, 1977; Hassler et al., 1979). Because the distinction between ventral and dorsal divisions is no longer relevant it would be consequent to label the nuclei within the region lateral to the internal medullary lamina as "lateral nuclei of the thalamus" (Grünthal, 1934; Feremutsch, 1963; Percheron, 1997; TNA). This is, however, unlikely because it has no connection to experimental studies and recent history (Jones, 1997a).

Disagreements also exist with regard to the extent to which the territories from different afferent fiber systems overlap. This issue is important because it determines how accurate the borders between the various motor and sensory territories can be drawn. Earlier investigations, including post-mortem studies, indicated that both striatal (nigral and pallidal) fiber systems have well-defined areas of convergence with the cerebellar territory (Mehler, 1971). Recent anatomical studies employing tracing techniques as well as electrophysiological evidence have indicated segregated but interdigitating territories in subhuman primates (see Hintzen et al., 2018). That this organizational principle may also be valid for the VA-VL-VP limits in the human brain is indicated by the clear cytoarchitectonic borders (see Jones, 1998, Figure 9A and Lenz et al., 2010, Figure 2.23a), by interdigitation of fringes described by Percheron (2004) and by the clear contrast between the calbindin-positive VA and the very moderate intensity level in VL (**Figure 7**).

Another hindrance is posed by discrepancy between Anglo-American authors that are rather "lumpers" while German authors are the so-called "splitters" (Dom, 1976) referring to which extent the lateral nuclei are segmented into subnuclei. Hassler (1977) distinguished excessively high numbers of subdivisions (19 divisions in the motor nuclei of the lateral region) whereas other researchers identified only few divisions in the same area. The correspondence between those multiple areas is rather ambiguous and even questionable if there is no difference in their connectivity and functions, making "some rationalization" (Jones, 1985, p. 378) worthwile.

In our analysis the "splitters" and "lumpers" can be identified by a combination of the Wallace based indices W_{max} and W_{asym}. One can observe high W_{max} and low W_{asym} within the both groups and high W_{max} and high W_{asym} between the groups. For example, the comparison of "splitters" (HSL, Hassler, 1977) and (DNG, Ding et al., 2016) shows high concordance $W_{max} = 0.71$ and very low asymmetry $W_{asym} = 0.01$. On the other hand, the comparison between "splitters" and "lumpers" (HSL and PER, Percheron, 2004) shows high concordance $W_{max} = 0.83$ and high asymmetry $W_{asym} = 0.69$ values. This difference can also be seen in the **Supplementary Table 3** for cluster conditional probabilities. The atlases of "splitters" (HSL,HPD) overlap with the clusters in more areas compared to the atlases of "lumpers" (PER).

Motor thalamus

The interpretation of the organization and delineation of the areas related to the motor thalamus were a matter of intense

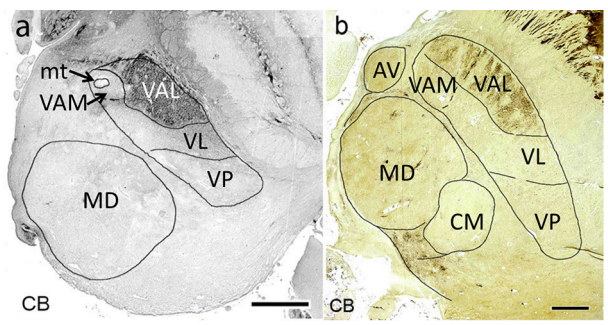

FIGURE 7 | Horizontal calbindin-stained sections through the middle of the mediodorsal nucleus at 19 weeks of gestation **(a)** and at adulthood **(b)**. Within the lateral nuclei calbindin-immunoreactivity is observed exclusively in the pallidal territory (VAL).

dispute (see Percheron et al., 1993). Hassler, Hirai and Jones and Morel et al. divided the pallidal projection field into an anterior and posterior division. These areas were described as V.o.a and V.o.p by Hassler (1977) and as VApr and VLa by Hirai and Jones (1989) and Morel et al. (1997) (see **Supplementary Table 2**). This may be an unnecessary complication because there are presently no obvious cytological, hodological or histochemical differences between both divisions (Ohye, 1990; Münkle et al., 2000; Forutan et al., 2001). Even more questionable is the partitioning by Hassler (1959) who subdivided the territory which now appears to correspond to the target fields of the nigral and pallidal afferents into more than 10 subnuclei: Ncl. latero-polaris with five subdivisions, Ncl. fasciculosus and Nuclei ventro-orales, Ncl. *zentro*lateralis and Ncll. dorso-orales (see Percheron et al., 1996). He regarded the anterior part of the ventro-oral nucleus (V.o.a) as a terminal area of pallidal, the posterior part (V.o.p) as a terminal area of cerebellar fibers.

Given the limited knowledge about the organization of the motor thalamus in humans it appears reasonable to subdivide it into only three territories which serve as targets for the nigral, pallidal and cerebellar afferents. These are the ventral anterior nucleus with medial and lateral divisions and the ventral lateral nucleus or complex (TNA, 2017).

The *ventral anterior nucleus* (VA; TNA) provides the target for basal ganglia afferents (from the internal pallidum and substantia nigra pars reticulata, respectively) (Ilinsky and Kultas-Ilinsky, 2001). They occupy the anterior pole of the lateral nuclei. The fibers from both sources have been described to branch in rather separate medial and lateral areas.

Afferents from the substantia nigra pars reticulata terminate in the medial part of VA in an area around the mammillothalamic tract, named according to its position in the lateral region as medial ventroanterior nucleus (VAM). This part contains large neurons, a characteristic feature which led to the alternative designation as magnocellular ventroanterior nucleus (TNA). The remaining largely lateral region is the territory for the fibers from the internal pallidum. It is named the principal division (TNA) or in correspondence to the mediolateral arrangement of both striatal territories the lateral ventral anterior nucleus (VAL, Mai et al., 2016). Ilinsky et al. (2018) used the main sources of the afferent fibers to designate both regions of VA (VAn–nigral region; VAp–pallidal region). This might be too restrictive as the medial region also receives afferents from the amygdala and limbic cortex. The attribution of a common name (VA) for the (at least) two target areas (VAM and VAL) appears justified because the afferents derive from the GPi/SNR-complex which was split during development by the fibers of the internal capsule. Both projections use GABA as transmitter. Their territories can, however, be separated by their different developmental timeline with respect to synaptogenesis (Kultas-Ilinsky et al., 2003), their different projection to cortical areas without overlap (Percheron, 2004) and their chemoarchitecture because the nigral (medial) VAM (VAmc) area is calbindin negative (sometimes weakly positive) whereas the pallidal (lateral) area VAL is calbindin positive (Morel et al., 1997; Forutan et al., 2001; Calzavara et al., 2005) (**Figure 7**).

The *entry zone* of the nigral afferents is poorly defined. The loosely arranged fibers enter VAM (VAmc) above the anterior field of Forel. This area corresponds to the Ncl. lateropolaris basalis (L.po.b) of Hassler and probably to the principal medial nucleus (Jones, 1985, p. 384). The pallidal afferents invade the thalamus as a compact fiber bundle, the thalamic fascicle (h1). Their entrance zone was described by histological evidence in the human brain as the anterior part of the ventromedial nucleus (VM) Gallay et al. (2008). Mai and Forutan (2012) who mapped the succession of prethalamic fibers from the substantia nigra, the internal pallidum, the cerebellum, the spinal cord and the brain stem on histological sections described the entrance zones for the fibers as basal subnuclei of the respective territories. They were accordingly named as basal ventral anterior nucleus (VAb, with VAMb and VALb subnuclei), as basal ventral lateral nucleus (VLb) and the basal ventral posterior nucleus (VPb) (Mai and Forutan, 2012, Figure 19.24).

The maximal Wallace index for VAM (nigral region) reads $W_{max} = 0.80$ and the asymmetry Wallace index is $W_{asym} = 0.27$. These values indicate *strong concordance* between the atlases with frequent subdivision relationships between the areas from different atlases. The indices for the VAL (pallidal region) $W_{max} = 0.61$ and $W_{asym} = 0.22$ suggest *high variability* between the atlases (unrelated to the terminology).

The *ventral lateral nucleus* (or complex; VL, TNA) provides the target for fibers from the deep cerebellar nuclei but also from the vestibular system and possibly from some kinesthetic neurons. It occupies the area between VA and VP and corresponds to the ventral intermediate nucleus (V.im, Ncl. ventralis intermedius in the terminology of C. Vogt, 1909, as the target of the prelemniscal radiation). V.im was also used by Crouch (1934), Hassler (1959), and Percheron (2004) whereas Jones (2007) and Morel et al. (1997) followed the terminology of Walker (1938) with ventral lateral posterior nucleus (VLp). VLp, however, appears as an inappropriate term because two anatomically, histochemically and functionally different components, one (VLa) receiving pallidal, the other (VLp) cerebellar afferents, are regarded as components of the same VL-region. Nieuwenhuys et al. (2008) described a third component (VLm) receiving nigral afferents.

With the acetylcholesterase (AChE) reaction the VL region is weakly labeled (Hirai and Jones, 1989; Lenz et al., 2010). This contrasts with the very high intensity of VAL (VLa, Lenz et al., 2010, p. 116). Parvalbumin-immunoreactivity also specifies the cerebellar area (Percheron, 2004, p. 627).

VL is divided for topographic reasons in anterior and posterior subdivisions (VLa and VLp; TNA, 2017) which correspond to areas described by Hassler (1959, 1977) and Percheron (2004) as medial and lateral subdivisions. The posterior ventrolateral subdivision (VLp) is clinically relevant because this corresponds to the so-called ventrointermediate or "VIM area" where "tremoro-synchronous" neurons were localized (Albe-Fessard et al., 1966; Ohye and Narabayashi, 1979). Their location coincides with the target selected for the management of some motor symptoms in movement disorders (Ohye, 1990). Mapping the coordinates of contacts accountable for clinical improvement to the standard atlas Mai and Majtanik

(2017) shows the location distal to V.im either in the area of the cerebello-rubro-thalamic fibers shortly before entering the thalamus (close to the posterior subthalamic area) or within the entry zone of the fibers which corresponds to the basal ventrolateral nucleus (VLb) (Fiechter et al., 2017; **Figure 12**; see discussion).

The cerebellar afferents take a position parallel to the ventral thalamic lamina, just ventral to the subparafascicular nucleus and anterolaterally to the parvocellular part of the ventral posterior medial nucleus (VPPC / VPMpc) before they enter the thalamus. This *entry zone* has been variously called Ncl. ventralis caudalis parvocellularis externus (V.c.pc.e, Hassler, 1959), ventral medial nucleus (VM, Gallay et al., 2008) or ventral posterior inferior nucleus (VPI, Jones, 1985). The upper portion of VPI has also been described as relay for vestibular input that projects to the vestibular cortex (Deeke et al., 1974). Forutan and Mai (2012) have referred to the area where cerebellar fibers enter thalamus, as Ncl. ventrolateralis basalis (VLb) in order to emphasize the relationship with the entrance of the adjacent pallidal fibers in the Ncl. ventroanterior basalis (VALb) and the sensory fibers in the Ncl. ventroposterior basalis (VPb).

The ventrolateral region displays rather good concordance $W_{max} = 0.71$ with strong subdivision realtionship $W_{asym} = 0.26$.

Sensory thalamus

The sensory thalamus represents the main relay of the thalamus for somatosensory and viscerosensory afferents. It is described as *ventroposterior complex* (VP, TNA) because of the multiple well-delimited and characterized nuclei. We include also the special sensory nuclei for vision and audition.

VP is histologically separated into the *lateral ventroposterior nucleus* (ventral posterolateral nucleus, VPL, TNA), the *medial ventroposterior nucleus* (ventral posteromedial nucleus, VPM, TNA) and two smaller parvocellular divisions that were termed the external and the internal divisions of the ventrocaudal nucleus (V.c.pc) equivalent to the *ventral posterior inferior nucleus* (VPI, TNA) and the *medial ventroposterior nucleus, parvocellular part* (*ventral posteromedial nucleus, parvocellular part,* VPMpc, TNA) (Welker, 1973; Kaas et al., 1984; Jones, 2007; see Lenz et al., 2010), respective VPMpc and VLb (Mai and Forutan, 2012). These nuclei provide the receptive area for the spinal, lemniscal and trigeminal fibers.

VPL has been divided into several subdivisions (anterior, posterior, medial, lateral) on the basis of size, density, molecular properties and distribution of cells as well as by their responses to cutaneous stimuli (Jones, 2007). The distinction between the cerebellar territory (VL) and the anterior part of VPL can be made by the transition from the large neurons in VL (Lenz et al., 2010) to the mixed large and small-sized neurons in VPL. Histochemically, there is a difference in the AChE-reaction: low in VLp, very intense in VPL.

VPM receives the ascending secondary trigeminal afferents via the trigeminal lemniscus from the head, face, and intraoral structures.

VPL and VPM are separated by a narrow cell-poor septum (lamella arcuata) that is well seen only during fetal development as distinct (CD15-negative) lamina. Against the centromedian nucleus VPM is delimited by a branch of IL (lamella intermedia, Schnopfhagen, 1877, **Figure 6a**). Medially and ventrally VPM abuts on VPMpc. Located dorsally is the anterior pulvinar (APul). VPM shows an intense immunoreactivity against parvalbumin but is calbindin-negative (Morel et al., 1997; Münkle et al., 2000).

Superior ventroposterior nucleus (VPS). Proprioceptive or kinestetic fibers mediating depth sensitivity project to an area anterior and dorsal to VPM and VPL (at the border with the lateral VL). These fibers are joined by those from the vestibular nuclei. The field where neurons are localized that respond to cutaneous and kinesthetic stimulation can be registered to the superior, anterior or oral part of VP. This part has been termed V.c.e.a, VPS, VPO (oral part) or "shell" region (Hassler, 1959; Jones and Friedman, 1982; Kaas et al., 1984; Jones and Macchi, 1997; Jones, 2007). A precise anatomic delineation of this "deep receptor zone" has not yet performed.

The parvocellular extension of the ventral posteromedial nucleus (VPMpc) is located below CM between the VPM laterally and the subparafascicular nucleus (SPF) medially. It receives general and special visceral afferents and is regarded to serve as thalamic taste area (Pritchard, 2012). From the SPF it is distinguished by its synaptophysin immunoreactivity, whereas SPF is positive for substance P and tachykinin (Mai et al., 1986; Hirai and Jones, 1989).

The spinal, lemniscal and trigeminal afferents to the sensory thalamus are difficult to separate in humans. The different components were therefore lumped together and their portal of entry is described under various names (ventrobasal complex, ventrocaudal complex, posterior nucleus, Burton and Jones, 1976; Basalis complex, Percheron, 2004; ventromedial posterior nucleus, VMpo, Craig et al., 1994; Blomqvist et al., 2000; TNA, 2017). We propose the term basal ventroposterior nucleus (VPb, Mai and Forutan, 2012). For detailed discussion see (Lenz et al., 2010).

The maximal Wallace index for the VP region reads $W_{max} = 0.71$ and the asymmetry Wallace index is $W_{asym} = 0.30$. These values indicate strong concordance between the atlases with frequent subdivision relationships between the areas from different atlases.

Metathalamus or geniculate region

The term metathalamus denotes two highly differentiated regions related to the lateral thalamus: the lateral and the medial geniculate bodies. The correctness of both terms has been questioned since they may imply that both regions are no ordinary or integral parts of the lateral thalamus (Kuhlenbeck, 1935; Hassler, 1959; Anthoney, 1994). The term "geniculate bodies" is used because they comprise not only the respective nuclei but also derivatives of the dorsal and the ventral thalamus.

The lateral geniculate body (LGB) forms a landmark structure at the ventrolateral and posterior surface of the diencephalon. LGB is composed almost exclusively by the lateral geniculate nucleus (LGN; more precisely the dorsal lateral geniculate nucleus, LGD). The ventral lateral geniculate nucleus (LGV) which is obvious in most mammals is presented in the human

brain as pregeniculate nucleus (PG). LGD is triangular in shape and appears in coronal sections as a layered structure that is bent on itself.

The LGD can be divided into six visibly distinct layers (laminae), labeled 1 to 6 from ventral to dorsal. Crossed and uncrossed retinal fibers enter a hilum on its ventromedial surface and terminate in different laminae of the LGN: layers 1, 4, and 6 receive axons from the contralateral eye and layers 2, 3, and 5 receive axons from the ipsilateral eye. The two ventral layers contain relatively large neurons and are termed magnocellular layers (M1, M2). The dorsal layers consist of small cells and are denominated as parvocellular layers (P3 to P6). Intercalated between each magnocellular and the parvocellular layers are the koniocellular layers K1-K6 (Hendry and Reid, 2000).

The *pregeniculate nucleus (PG)* lies as a small and narrow band of cells at the dorsolateral margin of the LGD. It is composed of two parts that were described by Balado and Franke (1937) as loose and dense components, and by Hassler (1959) as Ncl. geniculatus griseus and fibrosus. As a remnant of the rodent ventral lateral geniculate nucleus (LGV) it may possibly also represent the primate equivalent of the intergeniculate leaflet (Lima et al., 2012). The location dorsally to the LGD is the result of the rotation of the LGN during development. It is not part of the (dorsal) thalamus like the LGN but a derivative of the ventral thalamus described in murine brain on a developmental basis as prethalamus (Puelles and Rubenstein, 2003).

The *medial geniculate body (MGB)* is the last stage of the ascending auditory pathway. It is recognized as a prominence of the ventrolateral surface of the brain medial to the (intergeniculate) pulvinar. It is demarcated against the lateral geniculate body by myelinated fibers which also surround it at the pial surface but the border against the latero-caudal part of the sensory thalamus is indistinct (**Figure 8**).

The MGB is ovoid-shaped with an intricate internal organization. Its subdivisions have been described mostly by their topographic position, fiber connections and cell morphology (Le Gros Clark, 1933; Winer, 1984). The human MGB is commonly divided into three major divisions which are denoted as parvocellular or principal (lateral) division with major ventral and dorsal components (MGV, MGD) and a magnocellular (medial) division (MGM). Most authors add the suprageniculate-limitans nucleus as the fourth division, the Ncl. geniculatus medialis limitans of Hassler (1959). Alternative terms for the dorsal and ventral divisions of the principal nucleus were the fibrosus and fasciculosus nucleus, respectively (Hassler, 1959).

Cytoarchitectonic analysis results in a much more elaborate organization with additional parcellations especially within the principal division (Morest, 1964; see Harrison and Howe, 1974; Winer, 1984). MGD is very complex with up to 10 subdivisions distinguished (Malmierca and Hackett, 2010). Its main afferents stem from the inferior colliculus; its main target is the auditory association cortex, AII. MGV is the target of fibers of the core ascending, tonotopic information-bearing, auditory pathway from the central nucleus of the inferior colliculus which end within rows of tonotopically organized fibrodendritic laminae. These laminae can be visualized by means of CD15 immunoreactivity (**Figure 8**). The target of the efferents is the primary auditory cortex, AI.

The representation of the MGB in the atlases shows many variations with respect to parcellation. Of the authors who participated in the analysis of a single brain (Dewulf, 1971) only Hopf and Macchi distinguished subdivisions of MGB. Interestingly, however, were the differing locations of subareas within the MGB complex: whereas Hopf depicted the magnocellular division along the lateral margin next to the LGB, Macchi delineated this division on the medial margin, an area marked by Hopf as limitans division. Hassler (1959); Hassler et al. (1979) and Van Buren and Borke (1972) illustrated the magnocellular division (antero) dorsomedially, adjacent to the ventrocaudal nucleus which contrasts Morel (2007) and Amunts et al. (2012) who depicted this division ventrolaterally along the pial surface of the MGB. Most authors describe the magnocellular division as situated medioventrally (Winer, 1992). The imprecision of the topographic definition of subnuclei is

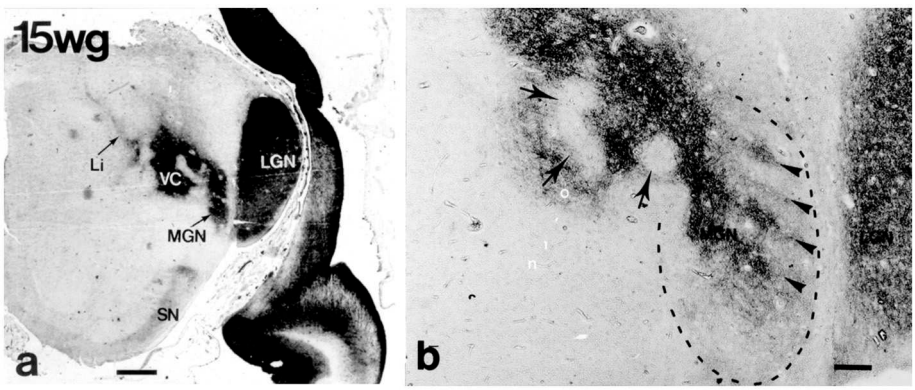

FIGURE 8 | Lateral (LGN) and medial (MGN) geniculate nuclei at 15 weeks of gestation (CD15 immunoreactivity) (from Mai et al., 1999; with permission). **(a)** The continuity of the future MGN with the ventroposterior complex (VC) is apparent. **(b)** Higher magnification shows that the curled, wavy or band like disposition of CD15 immunoreactivity in the ventral parvosellular subnucleus (arrowheads in area surrounded by dashed line) which might correspond to the tonotopically organized fibrodendritic laminae. Arrows indicate regions extending into VC. Scale bars 5 mm in a and 100 μm in **(b)**.

noteworthy in view of the substantial results regarding the development and immunohistochemical properties of the human MGB (Mai et al., 1999; Jones, 2003).

The maximal Wallace index for the metathalamus is $W_{max} = 0.84$ and the asymmetry Wallace index is $W_{asym} = 0.32$. These values show the highest concordance between the atlases and strong subdivision relationships between the areas from different atlases, reflecting multiple numbers of subdivisions for LGB and MGB areas.

Posterior Region

The *pulvinar nuclei* (Pu) form a large, heterogeneous group of nuclei in the posterior region without clear distinction between subregions. The segmentation of the posterior region is normally based on topographic parameters. TNA distinguishes between the pulvinar (with *medial, lateral, anterior,* and *inferior* nuclei) and the lateral posterior nucleus (LP).

The medial and lateral pulvinar nuclei representing the most extensive nuclei are separated by their fiber density. The anterior pulvinar nucleus corresponds to the Ncl. pulvinaris oralis of Hassler (1959); however, he also designated the corresponding location as Ncl. ventro-caudalis portae (Hassler, 1977; **Figure 2**). The inferior pulvinar nucleus (Olszewski, 1952; Jones, 1985; Morel et al., 1997) occupies the ventrolateral portion of the pulvinar, positioned close to the brachium of the superior colliculus. The rostral part, intercalated between the medial and lateral geniculate bodies, is described as *intergeniculate* pulvinar.

The human lateral posterior nucleus (TNA, Hirai and Jones, 1989; Morel et al., 1997; Jones, 2007) is regarded as part of the pulvinar and was therefore designated as oral or anterodorsal pulvinar nucleus (Percheron, 1997, 2004; Mai and Forutan, 2012). It corresponds to the Ncl. dorsalis caudalis (Hassler, 1959; Feremutsch and Simma, 1971; Hopf et al., 1971; Van Buren and Borke, 1972). Morel et al. (1997) integrate within the posterior group besides the pulvinar and the lateral posterior nucleus also the posterior complex (Li, Sg, Po) and the geniculate nuclei.

The maximal Wallace index for the P region is $W_{max} = 0.80$ and the asymmetry Wallace index is $W_{asym} = 0.27$. These values stand for strong concordance between the atlases and moderately frequent subdivision relationships between the areas from different atlases.

Concordance Analysis

Area (Local)-Level Concordance Analysis

The overall results of the area-level analysis across the nine thalamic parcellations are depicted in the **Figure 9A**. The conditional probabilities P_{ij} for all areas are represented as a matrix and visualized as colored image. Each pixel in the image specifies the Pij value by its color. The Pij value estimates local concordance between two areas. It expresses the probability of a voxel for being in area ***i*** in one atlas given that it is in area ***j*** in other atlas. Each row and column represent one specific area in an atlas. Areas belonging to an atlas are grouped together and the borders between the atlases are denoted by white lines inducing the appearance of the rectangular blocks in the image. The number of rows and columns in the image belonging to one

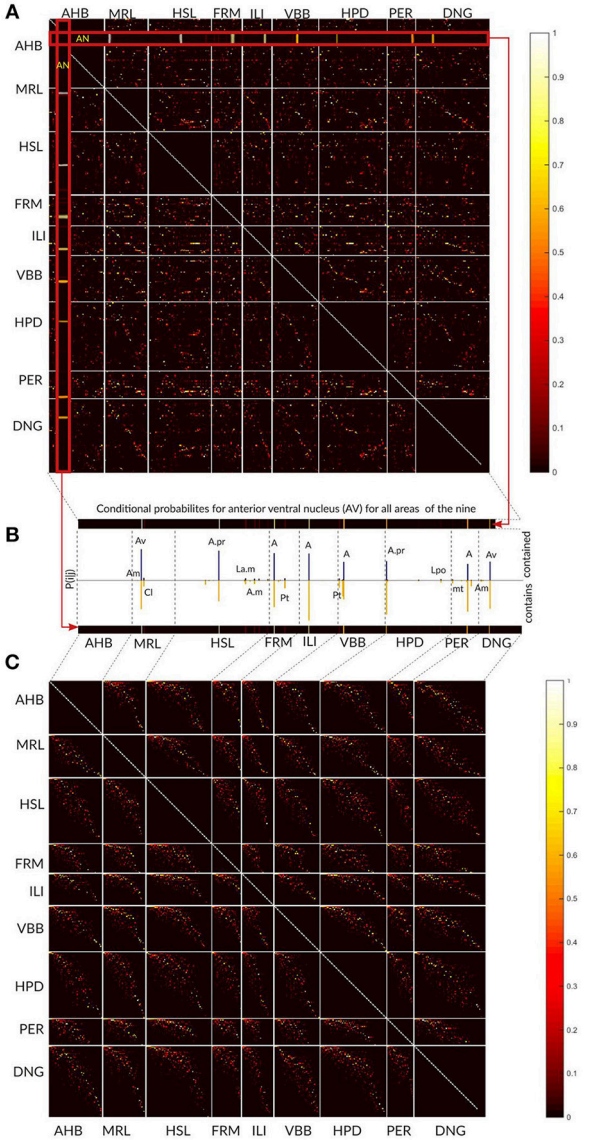

FIGURE 9 | Local area level concordance analysis of the nine atlases shown as image representing the non-symmetric concordance matrix P. **(A)** Each pixel in the image specifies the Pij value by its color. The Pij value expresses the probability of a voxel for being in area ***i*** in one atlas given that it is in area ***j*** in other atlas. Each row and column represent one specific area in an atlas. Areas belonging to an atlas are grouped together and the borders between the atlases are denoted by white lines inducing the appearance of the rectangular blocks in the image. **(B)** Here we show for the anterior ventral nucleus (AV) area from Atlas of the Human Brain how the values in the matrix should be interpreted. The row and column in the matrix that correspond to the AV values (red zoomed rectangles) are displayed as the bars. The color of the pixels in the row and the column (from yellow to red) determines the height of the bars in the plot (see the color bar on the right). The blue bars specify the proportion of AV comprised in other regions, and the yellow bars (below) indicate the proportion of other regions comprised in the AV region. The labels above the bars correspond to the significantly overlapping regions from the other atlases. **(C)** The matrix is shown after modifying the order of the areas independently within each block. The non-zero P_{ij} values form a pixel cloud centered around the diagonal of the block. The brightness of this cloud shows the level of correspondence between the atlases and the width of the cloud approximates the frequency of the subdivision configurations between the atlases.

atlas reflects the number of areas in this atlas. Colored (non-black) pixels point to areas displaying some degree of spatial overlap. The color variations indicate frequent existence of partial overlap between the areas.

In **Figure 9B** we used the anteroventral nucleus (AV) of the Atlas of the Human Brain as an example how the entries in the matrix should be interpreted. The row and column in the matrix that corresponds to AV values (red zoomed rectangles) are displayed as the bars. The color of the pixels in the row and the column (from yellow to red) determines the height of the bars in the plot (compare to the colorbar on the right).

The ordering of areas as shown in **Figure 9A** is rather haphazard, and thus direct visual estimation of the extent of correspondence between two atlases is difficult. Re-arrangement of the rows and columns, i.e., modifying the order of the areas in the atlases, provides a straight-forward interpretation of the image structure as correspondences between the atlases.

We used a singular value decomposition based heuristic from Bohland et al. (2009) to re-order the rows and columns of each rectangular block. This transformation forces the areas with high concordances toward the diagonal and we minimize the overall distance of non-black pixels from the diagonal of that block (**Figure 9C**).

Cluster (Group)-Level Concordance Analysis

To make the concordance analysis more visually tractable we have extended the local area level analysis by the group-level concordance analysis. This analysis was performed separately for 11 groups of regions (see in Material and Methods). The composition of the groups follows the **Supplementary Table 1**. For each group we determined Wallace maximal index W_{max} and Wallace asymmetry index W_{asym} (**Table 2A**).

The highest W_{max} values are observed for the MD (0.85), GM/GL (0.84), VAM (0.79), and P (0.80). These values indicate very high concordance, i.e., predictability of the atlases within these regions (**Table 2A**). We also observe above the chance high W_{asym} values for the following areas: MD (0.35), VAM (0.28), and P (0.26) indicating that many areas in this groups display multiple subset configurations, i.e., an area in one atlas contains multiple areas from another atlas. For example, four atlases divide the area MD into two or more subareas. These subdivisions are responsible for the high W_{asym} value of the M cluster. The asymmetry values for the IL and VAL are below the 95th cut-off threshold indicating that the subdivision configuration in the clusters cannot be distinguished from random thalamus parcellations.

Global (Thalamus)-Level Concordance Analysis

The global concordance analysis estimates the inter-atlas correspondences. The results of the global concordance analysis are presented in the **Table 2B** for W_{max} and the **Table 2C** for W_{asym}. The values in the **Tables 2B,C** are reported with respect to the chance distribution of random parcellations. Values that exceed 5 percent chance to originate from random parcellations are reported in gray color and in brackets. All inter-atlas concordances W_{max} are above the 5 percent cut-off value for chance distributions of random parcellations. Twelve W_{max} values are not clearly distinct from asymmetries of random parcellations and are reported in gray color.

The high number of values makes it difficult to see any characteristic pattern between the atlases. To facilitate the detection of such characteristic patterns we use multi-dimensional scaling (MDS). The MDS transforms the concordance values W_{max} and W_{asym} between the atlases into positions of a 2D space such that more similar atlases occupy nearby points in this two-dimensional space while less similar atlases become more distant. In this approach the atlas similarities expressed as closeness of W_{max} and W_{asym} values are translated into nearby positions in the 2D space.

The results after applying MDS using the global concordances W_{max} and asymmetries W_{asym} from the **Tables 2B,C** are shown in **Figure 10**. Two distinct clusters of atlases are marked by red and blue dashed ellipses, surrounded by dissimilar atlases. The red cluster contains the FRM and PER atlases and the blue cluster includes AHB, DNG, and MRL atlases.

In addition to the inter-atlas predictability from **Tables 2B,C** and to the two clusters discriminated by MDS we are interested in the spatial distribution of the atlas concordances across the thalamus volume. To this end we computed the average global atlas concordance and asymmetry for each voxel of the thalamus. The spatial distributions of W_{max} and W_{asym} exemplify the results of the cluster concordance analysis (**Figure 11**). Clusters of high (M, VAM) and low (VAL) concordances are easily distinguishable in the three planes. Similarly the asymmetry values mirror the results of the cluster concordance analysis. For example the high W_{max} and W_{asym} values of the M cluster follow the expected borders of the MD region. What the cluster concordance analysis does not show are the remarkable gradients

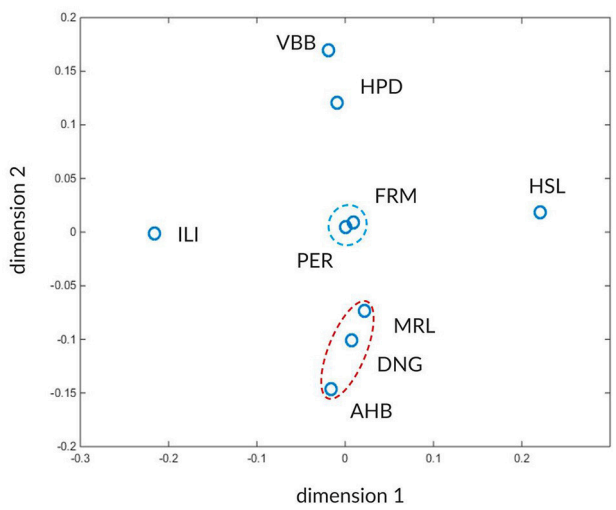

FIGURE 10 | Visualization of inter-atlas relationships using multi-dimensional scaling. The atlases are shown in a 2-D landscape computed from distances derived from the W_{max} and W_{asym} values (**Tables 2B,C**). Atlases that can mutually be better predicted from each other and share similar asymmetry values reside closer in this space. The two recognizable clusters are indicated by red and blue dashed ellipsoids. The arbitrary dimensions one and two give coordinates for the projected atlas similarity values in the 2D space.

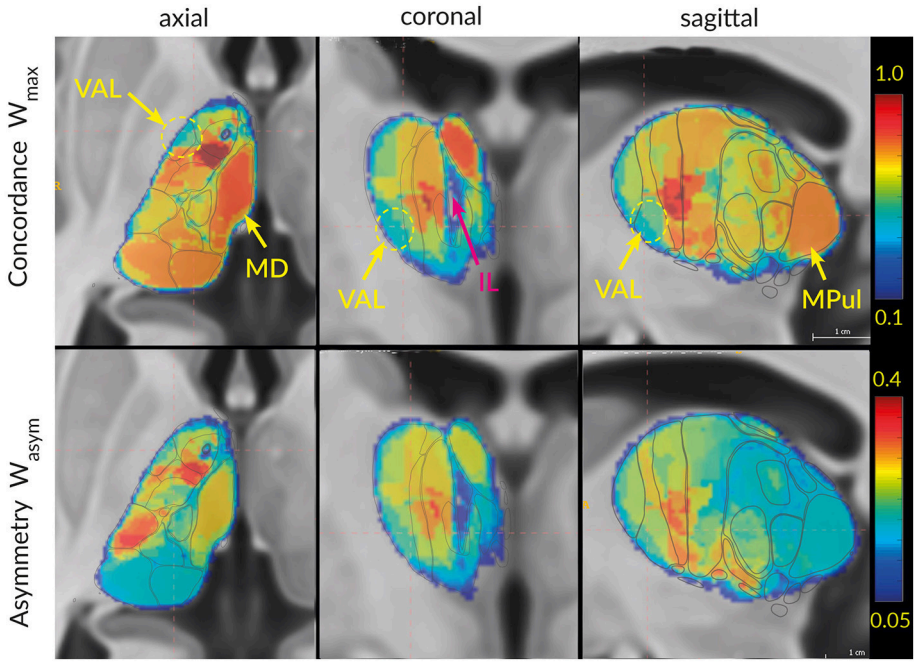

FIGURE 11 | Visualization of W_{max} (top row) and W_{asym} (bottom row) in 3D space. The regions with high concordances and asymmetry (MD, AV) can directly be identified in the slices as areas with strong red color. The ellipsoid and arrows point to the region with the lowest concordances: lateral ventroanterior nucleus (VAL) and intralaminar formation (IL).

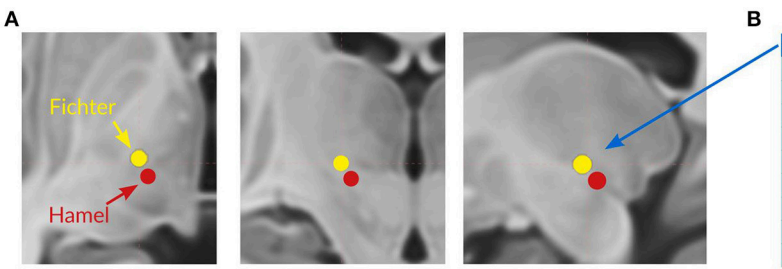

B

CRA-Tool	Fichter et al. 2017	Hamel et al. 2008
AHB	VLb (VPI)	VMb (VPPC)
MRL	VLpv	VPi
HSL	V.im.e, Ra.prl.	V.c.pc
FRM	VPL, VPM	VPI
ILI	VPi, VPlVPm	VPi
VBB	Vim	Vcpc
HPD	Vci,Vcpce	Vci,Vcpce
PER	VImM-VLM,VPM	VPM
DNG	VPLr	VPI

FIGURE 12 | Active deep brain stimulation (DBS) sites in tremor patients from two studies (Hamel et al., 2007; Fiechter et al., 2017) attributed to the VIM region. **(A)** Positions of the DBS stimulation sites in the MNI space. The coordinates of the DBS target in MNI space for Fiechter et al. (yellow) x = 14.3 mm, y = −17.40 mm, z = −2.17 mm and for Hammel et al. (red) y = 12.7 mm, y = −19.6 mm, z = −4.38 mm. **(B)** Anatomical characterization of the targets (**Table 2D**) presented in an analysis tool. Such anatomical characterization is available for each voxel in thalamus.

in the concordance and asymmetry distributions within the clusters. Particularly the strong concordance and asymmetry focus in the VAM subregion dominates the figure.

DISCUSSION

Consistencies and Differences of Thalamus Delineations May be Resolved by Multi-Layered Nomenclature Definition

The description of the thalamus in humans rested in the past on the analysis of individual brains. Our representation of the maps published by various authorities illustrates their enormous discrepancies. These arise in part from the inherent variability of the object but are above all the result of personal interpretation of the findings. As a consequence, the wording used for the description of thalamic features is inconsistent and, in addition, compromised by historic trends influenced by different "schools" (Anthoney, 1994). Same terms may have well-accepted but conflicting meanings and similar features may have diverse interpretations. This makes the correlation and thus the topographic comparison of the results from different research difficult and the application of the diverse tables of synonyms questionable. The differing understanding of the topographic organization of the human thalamus and the dissenting terminological concepts makes it highly unlikely that a harmonized and generally accepted agreement is achieved by renewed discussion of disagreements regarding the meaning or appropriate usage of terms.

Nevertheless, all studies reside on thorough analysis and comprehensible concepts. It is therefore demanded to look for ways to discuss terms and the labeled structure together. To arrive at a more consistent interpretation of histological and radiological features and of their topographic definition a new approach is suggested. We argue that the greatest hindrance for a commonly accepted interpretation of the human thalamus, the variation of neighborhood relations in the individual space, can be overcome by their registration into a common space.

For our approach we exploited the delineations of thalamic nuclei from serial sections that were published from well-reputed researchers. The three-dimensional reconstructions from their maps were registered into a standard ICBM/MNI152_2009b space because it is openly accessible and has been used for the registration of our individual "Atlas of the Human Brain" (AHB, Mai et al., 2016) and our average atlas of the human brain (Mai and Majtanik, 2017).

The registration of the different atlases into the same space allowed us to evaluate consistencies and differences of delineations and neighborhood relations in the same (standard) frame but in relation to the original published materials. It is a matter of course that the three-dimensional reconstruction of this heterogeneous material introduces problems regarding the accuracy and consistency of our result. The registration of the atlases in the standard space does not mean the perfect match of the spatial relationship between the atlases.

Given this limitation we were able to estimate the relative spatial overlaps between the nine atlases within the standard MRI volume. We parcellated this volume into "clusters" (**Supplementary Table 1**) that were developed on the basis of the interpretation of correlating terms, i.e., territories. This process renders susceptibility to personal bias effects. This effect must also be accounted for because the comparison between the atlases–as described here–is in relationship to the AHB or, in the case of the lateral region, to the delineation provided by Hassler (**Figure 4**).

Based on this material we have performed systematic quantitative analysis of the relationships between different anatomical atlases of the thalamus. We claim that not the disagreements in terminology are the major cause of the brain atlas concordance problem but the definition of underlying partition volumes of the brain anatomy (e.g., atlases).

A possible solution of this concordance problem is a multi-layered nomenclature definition. For regions of high concordance only one nomenclature base layer is required. This base nomenclature layer may possibly be generated by some concordance optimization algorithms and be further curated by experts. For the regions of low concordance multiple nomenclature layers should be created to account for the heterogeneity of defining partition concepts.

We aimed to follow the recommendations of the revised terminology in the Terminologia Anatomica (TNA, 2017) made by the Working Group Neuroanatomy of the Federative International Programme for Anatomical Terminology (FIPAT) of the International Federation of Associations of Anatomists (IFAA). As consquence of the screening of the final scheme of nine atlases and the results from the quantitative computational analysis we amended some of those recommendation. In **Supplementary Table 1** we have summarized the selected terms for the subdivisions of the human thalamus and have included references which show the emergence of the listed terms together with some equivalent designations. We understand this recommendation as a base layer terminology that has to be extended by additional layers.

Concordance Analysis

Area (local)-level analysis evaluated pairwise spatial overlap between two areas by conditional probabilities and revealed that the one-to-one relationship between the areas is rarely observed in the data. The voxels within an area in one atlas mostly map to multiple areas of another atlas (**Figure 9**). To visualize this relationship we developed a meaningful visualization of the multiple area mapping by re-ordering columns and rows of blocks in matrix P (**Figure 9C**). For each block we can observe an elongated diagonal cloud of nonzero voxels. The brightness of the cloud indicates the level of correspondence between the areas and the width of the cloud indicates the frequency of the subdivision configurations between the atlases. Bright diagonal clouds indicate high correspondence and high W_{max} values. Broad diagonal clouds hint to frequent one-to-multiple subdivision configurations and is reflected in high W_{asym} values.

The *cluster* (group)-level analysis focuses on the correspondences between multiple areas belonging to a region with common anatomical characteristics. The concordance analysis of such clusters imposes a spatially constrained view on the parcellation equivalence and stability between various atlases. To explore the cluster correspondences we developed the W_{max} and W_{asym} indices. The W_{max} and W_{asym} capture similarity between several areas while allowing for area refinement in one atlas relative to another. The W_{max} captures similar correspondence properties as the S-index defined by Bohland et al. (2009) and does not penalize the subdivision configurations in clusters. Our W_{asym} index directly quantifies the one-to-many subdivisions between the areas in a cluster. A cluster with low concordance values W_{max} points to the fact, that the underlying characteristics of the constituent areas are highly variable between the atlases. A large W_{asym} value for a cluster indicates very strong one-to-many relationships between areas from different atlases. For example, four atlases divide the area MD into two or more subareas. These subdivisions are responsible for the high W_{asym} value of the MD group. The lowest W_{max} values are displayed by the IL (0.55) and VAL (0.61) group (**Table 2A** and **Figure 11**). The low predictability of the IL and VAL cluster points to highly heterogeneous concepts for these areas in the nine atlases.

For direct comparison of the different cluster parcellations we extended the cluster analysis with detailed estimation of the conditional probabilities between the clusters of the "Atlas of the Human Brain" and clusters of the other atlases. **Supplementary Table 3** lists the conditional probabilities and corresponding areas for all eleven groups. We observed that clusters with high W_{max} values in **Table 2A** also show high conditional probabilities in **Supplementary Table 3**. The

high W_{asym} values of the clusters in the **Table 2C** are reflected by the increased numbers of overlapping areas in the **Supplementary Table 3**.

The *global* (thalamus)-level concordance analysis provided quantitative estimates of the inter-atlas correspondences and asymmetries. The large number of pair-wise atlas comparisons shown in **Table 2B** for W_{max} and **Table 2C** for W_{asym} makes it difficult to directly identify more complex patterns of equivalences. To facilitate the recognition of complex correspondence patterns we mapped the atlases into a two-dimensional space using multi-dimensional scaling (**Figure 10**), such that atlases with more similar regions (more overlapping, less asymmetric) appear in closer proximity with one another compared to atlases with less overlapping regions. This intuitive graphical representation allows to capture similarity in concordance and asymmetry between atlases. The MDS revealed two clear clusters (**Figure 10**). The blue cluster contains the FRM and PER atlases and the red cluster includes AHB, DNG, and MRL atlases. The characteristic pattern for the blue cluster originates in very high W_{max} and W_{asym} values of the FRM and PER atlases as compared with the other atlases except for single low asymmetry value of $W_{asym} = 0.14$ between the FRM and PER atlases. The characteristic pattern for the red cluster derives from high values of W_{max} and low values W_{asym} within of the cluster combined with very high values of W_{asym} to the atlases of the red cluster. Atlases outside of the two clusters do not consistently show these patterns.

We interpret these two characteristic patterns in the following way: The atlases combined within the red cluster contain high and those within the blue cluster contain low number of areas. Hence the areas of the red cluster are predominantly small and those within the blue cluster are large. High W_{max} values indicate good concordance between the atlases within of the clusters with low frequency of subdivision configurations. In contrast, the high W_{asym} values between the clusters indicate multiple subdivisions of the blue cluster atlases by the red cluster atlases.

We can also derive the high W_{max} and the low W_{asym} properties of the clusters from the **Figure 4**. The extension, the configuration and the edge orientation of the areas of the blue MDS cluster atlases (FRM, PER) show broad agreement (**Figures 4B,D**, $W_{max} = 0.83$). The number of delineations in the cross-sections is more similar between FRM (32 areas) and PER (29 areas) atlases compared to the other atlases (more than 42 areas). Analogous observation holds for the red MDS cluster (AHB, MRL, DNG) in **Figures 4E,G,H**. In this cluster the number of areas is two times the number of areas of the blue cluster. The overall configuration of the colored regions does not display extreme differences between the three atlases. Noteworthy is the high similarity of the colored region configurations and extensions between the HSL atlas and the blue MDS cluster. The concordance $W_{max} = 0.89$ between the HSL and the PER atlases is the highest observed W_{max} value in the **Table 2B**. The W_{max} of 0.85 between HSL and FRM support this observation. Three times more areas of the HSL atlas cause strong subdivision configurations with the blue cluster and result in high $W_{asym} = 0.67$ for the PER atlas and $W_{asym} = 0.53$ for the FRM atlas. This dissimilarity places the HSL atlas outside of the blue MDS cluster.

Consequences of the Concordance Analysis Approach for the Terminology of the Thalamus

Our classification of substructures into clusters reflects the compromise between the diverging views between our own interpretation and preceding delineations and terms, which often changed over the years. The results of our concordance analysis provide values that request renewed and focused analysis of the parcellation of the human thalamus. The areas with low concordance values W_{max} derive from non-equivalent parcellation concepts resulting in questionable or even diverging labeling. To come closer to unequivocal definitions of the thalamic nomenclature we have to focus on these low concordant areas and must analyze the underlying parcellation concepts to select the most appropriate one with its corresponding name. We suggest including additional parameters which support the registration process. As pointed out, the intralaminar formation presents a key for the parcellation of the human thalamus. The formation is in part identified in the ICBM/MNI152_2009b template. Distance measures to other discriminated structures could constrain the registration process and provide improved inter-space probability.

Provided that the relative position of delineated areas or points of interest remain preserved after the registration process and that their topography matches with the reference cases we can claim first, the neglect or even absence of an individualized anatomy and of anatomic variables and second, the possibility to statistically estimate the degree of concordance between structures.

As final goal of our approach we emphasize that the spatial extension of an area becomes the prime representative of underlying defining concepts and that the anatomical labels forfeit their dominance.

Today there is increased need to translate anatomical information from classical neuroanatomical fields to new use cases. The use of single names to characterize regions of interest is problematic and may lead to obvious discrepancies between anatomical nomenclature reference and anatomical characterization of areas. As example we have analyzed the topography of the so-called "VIM area." This area is defined in correspondence to the area mapped in the atlas from Hassler (1959, 1977). It is often selected as target for deep brain stimulation (DBS) in cases of movement disorders. The outcome of the stimulation is highly correlated with the precision of the electrode targeting. The clinically "effective" area does, however, seldom match the area defined in the anatomical atlas of Hassler. Analysis of the "VIM" target coordinates with best therapeutic effects render coordinates mostly outside the original definition (**Figure 12**). The effective target suggested by Fiechter et al. (2017) coincides with VIM only in three out of nine atlases. This example illustrates, that characterization based on traditionally ascribed names, must not reflect the real position in the standard

space. The difference between the reported label (VIM) and real position is space is striking (**Table 2D**).

With our approach we do not assign "true" labels to the stimulation site but an array of labels along with corresponding concordance for these areas. Such arrays can better inform the researcher about the structure of concept equivalence and facilitates more appropriate interpretation of data and results. Further, the concept of the stimulation site can be extended by aggregation of efficiency outcomes into probabilistic spaces.

This example illustrates the possibility to improve the criteria for the definition of thalamic volumes or subareas by non-morphologic descriptors, e.g., aspects of molecular, connectional or functional organization respecting maximum probability feature maps.

Horn et al. (2017) proposed a tool for characterization of the spatial location of DBS targets by various MNI atlases based on histology, functional or diffusion-weighted MRI and connectome data (Behrens et al., 2003). An estimation of the extent of correspondence with the different atlases may improve the targeting process. We think that a concordance-based measure will provide indicators to reliably assess the quality of specification of areas of interest.

The concordance analysis framework may be extended to the whole brain profiting from developments in the neuroimaging field. The region discriminating concepts, as we already developed for reporting of different views of cortex partitioning (Mai et al., 2016), will be not specific for an area, but defined as multidimensional feature fields within the brain thereby allowing analysis and discrimination of areas by automatic detection algorithms (Glasser et al., 2016). Using such tools spatially defined multi-modal-atlases may be developed that allow mapping of regions defined by a multitude of protocols.

AUTHOR CONTRIBUTIONS

All authors listed have made a substantial, direct and intellectual contribution to the work, and approved it for publication.

ACKNOWLEDGMENTS

The authors are grateful to F. Forutan for his assistance in the segmentation of the thalamus.

SUPPLEMENTARY MATERIAL

The Supplementary Material for this article can be found online at: https://www.frontiersin.org/articles/10.3389/fnana.2018.00114/full#supplementary-material

REFERENCES

Albe-Fessard, D., Guiot, G., Lamarre, Y., and Arfel, G. (1966). "Activation of thalamocortical projections related to tremorogenic processes," in *The Thalamus,* eds D. P. Purpura and M. D. Yahr (New York, NY: Columbia University Press), 237–253.

Altman, J., and Bayer, S. A. (1988). Development of the rat thalamus: I. Mosaic organization of the thalamic neuroepithelium. *J. Comp. Neurol.* 275, 346–377. doi: 10.1002/cne.902750304

Amunts, K., Morosan, P., Hilbig, H., and Zilles, K. (2012). "Auditory system," in *The Human Nervous System, 3rd Edn,* eds J. K. Mai and G. Paxinos (San Diego, CA: Academic Press/Elsevier), 1270–1300. doi: 10.1016/B978-0-12-374236-0.10036-7

Andrew, J., and Watkins, E. S. (1969). *A Stereotaxic Atlas of the Human Thalamus and Adjacent Structures: A Variability Study.* Philadelphia, PA: Lippincott Williams & Wilkins.

Anthoney, T. R. (1994). *Neuroanatomy and the Neurologic Exam: A Thesaurus of Synonyms, Similar Sounding Non-Synonyms and Terms of Variable Meaning.* Boca Raton, FL: CRC Press.

Balado, M., and Franke, E. (1937). Das Corpus geniculatum externum. *Monogr. Ges. Neurol. Psychiat.* 62, 1–116.

Behrens, T. E., Johansen-Berg, H., Woolrich, M. W., Smith, S. M., Wheeler-Kingshott, C. A. M., Boulby, P. A., et al. (2003). Non-invasive mapping of connections between human thalamus and cortex using diffusion imaging. *Nat. Neurosci.* 6, 750–757. doi: 10.1038/nn1075

Benarroch, E. E. (2008). The midline and intralaminar thalamic nuclei. *Neurology* 71, 944–949. doi: 10.1212/01.wnl.0000326066.57313.13

Blomqvist, A., Zhang, E.-T., and Craig, A. D. (2000). Cytoarchitecture and immunohistochemical characterization of a specific pain and temperature relay, the posterior portion of the ventral medial nucleus, in the human thalamus. *Brain* 123, 601–619. doi: 10.1093/brain/123.3.601

Bohland, J. W., Bokil, H., Allen, C. B., and Mitra, P. P. (2009). The brain atlas concordance problem: quantitative comparison of anatomical parcellations. *PLoS ONE* 4:e7200. doi: 10.1371/journal.pone.0007200

Bubb, E. J., Kinnavane, L., and Aggleton, J. P. (2017). Hippocampal–diencephalic–cingulate networks for memory and emotion: an anatomical guide. *Brain Neurosci. Adv.* 1:2398212817723443. doi: 10.1177/2398212817723443

Burdach, K. F. (1822). *Vom Baue und Leben des Gehirns, Vol 2.* Leipzig, Dyk'sche Buchhandlung.

Burton, H., and Jones, E. G. (1976). The posterior thalamic region and its cortical projection in New World and Old World monkeys. *J. Comp. Neurol.* 168, 249–301. doi: 10.1002/cne.901680204

Calzavara, R., Zappalà, A., Rozzi, S., Matelli, M., and Luppino, G. (2005). Neurochemical characterization of the cerebellar-recipient motor thalamic territory in the macaque monkey. *Eur. J. Neurosci.* 21, 1869–1894. doi: 10.1111/j.1460-9568.2005.04020.x

Chien, J. H., Korzeniewska, A., Colloca, L., Campbell, C., Dougherty, P., and Lenz, F. (2017). Human thalamic Somatosensory Nucleus. (Ventral Caudal, Vc) as a Locus for Stimulation by INPUTS from tactile, noxious and thermal sensors on an aactive prosthesis. *Sensors* 17:1197. doi: 10.3390/s17061197

Craig, A. D., Bushnell, M. C., Zhang, E. T., and Blomqvist, A. (1994). A thalamic nucleus specific for pain and temperature sensation. *Nature* 372, 770–773. doi: 10.1038/372770a0

Crouch, R. L. (1934). The nuclear configuration of the thalamus of Macacus rhesus. *J. Comp. Neurol.* 59, 451–485. doi: 10.1002/cne.900590305

Deeke, L., Schwarz, D. W. F., and Fredrickson, J. M. (1974). Nucleus ventroposterior inferior. (VPI). as the vestibular thalamic relay in the rhesus monkey I. Field potential investigation. *Exp. Brain Res.* 20, 88–100. doi: 10.1007/BF00239019

Dekaban, A. (1953). Human thalamus; an anatomical, developmental and pathological study. *I.* Division of the human adult thalamus into nuclei by use of the cyto-myelo-architectonic method. *J. Comp. Neurol.* 99, 639–683. doi: 10.1002/cne.900990309

Dekaban, A. (1954). Human thalamus. An anatomical, developmental and pathological study. II. Development of the human thalamic nuclei. *J. Comp. Neurol.* 100, 69–97. doi: 10.1002/cne.901000105

Devlin, J. T., and Poldrack, R. A. (2007). In praise of tedious anatomy. *NeuroImage* 7, 1033–1058. doi: 10.1016/j.neuroimage.2006.09.055

Dewulf, A. (1971). *Anatomy of the Normal Human Thalamus.* Amsterdam, Elsevier.

Ding, S. L., Royall, J. J., Sunkin, S. M., Ng, L., Facer, B. A., Lesnar, P., et al. (2016). Comprehensive cellular-resolution atlas of the adult human brain. *J. Comp. Neurol. Res. Syst. Neurosci.* 524, 3127–3481. doi: 10.1002/cne.24080

Dom, R. (1976). *Neostriatal and Thalamic Interneurons. Their role in the pathophysiology of Huntington's chorea, Parkinson's disease and catatonic schizophrenia [thesis]*. Catholic University of Leuven. Available online at: http://www.thehumanbrain.info/brain/db_literature/DomRene.pdf

Emmers, R., and Tasker, R. (1975). *The Human Somesthetic Thalamus with Maps for Physiological Target Localization during Stereotactic Neurosurgery*. New York, NY: Raven Press.

Feremutsch, K. (1963). "Thalamus," in *Thalamus Primatologia Handbuch der Primatenkunde, Vol 2, part 2, fasc 6*, eds H. Hofer, A. H. Schültz, and D. Stark (Basel, Karger), 1–226.

Feremutsch, K., and Simma, K. (1954a). Structural analysis of the human thalamus. *Monatsschr. Psychiatr. Neurol.* 127, 88–102. doi: 10.1159/000140100

Feremutsch, K., and Simma, K. (1954b). Structural analysis of the human thalamus. *Monatsschr. Psychiatr. Neurol.* 128, 365–396. doi: 10.1159/000139800

Feremutsch, K., and Simma, K. (1971). "Anatomy of the normal human thalamus," in *Anatomy of the Normal Human Thalamus*, ed A. Dewulf (Amsterdam: Elsevier), 159–168.

Fiechter, M., Nowacki, A., Oertel, M., Fichtner, J., Debove, I., Lachenmayer, M., et al. (2017). Deep brain stimulation for tremor: is there a common structure? *Stereotact. Funct. Neurosurg.* 95, 243–250. doi: 10.1159/000478270

Fonov, V. S., Evans, A. C., McKinstry, R. C., Almli, C. R., and Collins, D. L. (2009). Unbiased nonlinear average age-appropriate brain templates from birth to adulthood. *NeuroImage* 47, (Suppl. 1):S102. doi: 10.1016/S1053-8119(09)70884-5

Forutan, F., and Mai, J. (2012). "Thalamus," in *The Human Nervous System, 3rd Edn.*, eds J. K. Mai and G. Paxinos (San Diego, CA: Academic Press; Elsevier), 618–677.

Forutan, F., Mai, J. K., Ashwell, K. W. S., Lensing-Höhn, S., Nohr, D., Voss, T., et al. (2001). Organisation and maturation of the human thalamus as revealed by CD15. *J. Comp. Neurol.* 437, 476–495. doi: 10.1002/cne.1296

Gallay, M. N., Jeanmonod, D., Liu, J., and Morel, A. (2008). Human pallidothalamic and cerebellothalamic tracts: anatomical basis for functional stereotactic neurosurgery. *Brain Struct. Funct.* 212, 443–463. doi: 10.1007/s00429-007-0170-0

Gihr, M. (1964). Die Zellformen des Nucleus medialis dorsalis thalami des Menschen, Prog. *Brain Res.* 5, 74–87. doi: 10.1016/S0079-6123(08)61368-0

Glasser, M. F., Coalson, T. S., Robinson, E. C., Hacker, C. D., Harwell, J., Yacoub, E., et al. (2016). A multi-modal parcellation of human cerebral cortex. *Nature* 536, 171–178. doi: 10.1038/nature18933

Grünthal, E. (1934). Der Zellbau im Thalamus der Säuger und dem Menschen. Eine beschreibend und vergleichend anatomische Untersuchung. *J. Psychol. Neurol.* 46, 41–112.

Hamel, W., Herzog, J., Kopper, F., Pinsker, M., Weinert, D., Müller, D., et al. (2007). Deep brain stimulation in the subthalamic area is more effective than nucleus ventralis intermedius stimulation for bilateral intention tremor. *Acta Neurochir.* 149, 749–758. doi: 10.1007/s00701-007-1230-1

Harrison, J. M., and Howe, M. E. (1974). "Anatomy of the afferent auditory system of mammals," *in Handbook of Sensory Physiology.* vol. 5:Auditory system. part I. eds Autrum, H., Jung, R., Loewenstein, W. R., Mackay, D. W., Teuber, H. L. (New York, Berlin:Heidelberg: Springer) pp. 283–336. doi: 10.1007/978-3-642-65829-7_9

Hassler, R. (1959). "Anatomy of the Thalamus," in *Introduction to Stereotaxic Operations With an Atlas of the Human Brain*, eds G. Schaltenbrand and P. Bailey (Stuttgart; New York, NY: Georg Thieme Verlag), 230–290.

Hassler, R. (1971). "Attempt at standardization of nomenclature," in *Anatomy of the Normal Human Thalamus*, eds A. Hopf, W. J. S. Krieg, K. Feremutsch, K. Simma, G. Macchi, and A. Dewulf (Amsterdam, Elsevier), 121–138.

Hassler, R. (1977). "Architectonic organization of the thalamic nuclei," in *Atlas for Stereotaxy of the Human Brain: With an Accompanying Guide, 2nd Edn.*, eds G. Schaltenbrand and W. Wahren (Stuttgart: Thieme).

Hassler, R. (1982). "Architectonic organization of the thalamic nuclei," in *Stereotaxy of the Human Brain*, eds G. Schaltenbrand and A. E. Walker (Stuttgart; New York, NY: Georg Thieme Verlag), 140–180.

Hassler, R., Mundinger, F., and Riechert, T. (1979). *Stereotaxis in Parkinson syndrome: clinical-anatomical contributions to its pathophysiology; with an atlas of the basal ganglia in Parkinsonism.* Heidelberg: Springer-Verlag Berlin Heidelberg.

Hendry, S. H., and Reid, R. C. (2000). The koniocellular pathway in primate vision. *Annu. Rev. Neurosci.* 23, 127–153. doi: 10.1146/annurev.neuro.23.1.127

Hess, C. P., Christine, C. W., Apple, A. C., Dillon, W. P., and Aminoff, M. J. (2014). Changes in the thalamus in atypical parkinsonism detected using shape analysis and diffusion tensor imaging. *Am. J. Neuroradiol.* 35, 897–903. doi: 10.3174/ajnr.A3832

Hintzen, A., Pelzer, E. A., and Tittgemeyer, M. (2018). Thalamic interactions of cerebellum and basal ganglia. *Brain Struct. Funct.* 223, 569–587. doi: 10.1007/s00429-017-1584-y

Hirai, T., and Jones, E. G. (1989). A new parcellation of the human thalamus on the basis of histochemical staining. *Brain Res. Rev.* 14, 1–34. doi: 10.1016/0165-0173(89)90007-6

Hopf, A., Krieg, W. J. S., Feremutsch, K., Simma, K., and Macchi, G. (1971). "Attempt at standardization of nomenclature," in *Anatomy of the Normal Human Thalamus*, eds A. Dewulf (Amsterdam, Elsevier), 121–138.

Horn, A., Kühn, A. A., Merkl, A., Shih, L., Alterman, R., and Fox, M. (2017). Probabilistic conversion of neurosurgical DBS electrode coordinates into MNI space. *NeuroImage* 150, 395–404. doi: 10.1016/j.neuroimage.2017.02.004

Hughes, E. J., Bond, J., Svrckova, P., Makropoulos, A., Ball, G., Sharp, D. J., et al. (2012). Regional changes in thalamic shape and volume with increasing age. *Neuroimage* 63, 1134–1142. doi: 10.1016/j.neuroimage.2012.07.043

Ilinsky, I., Horn, A., Paul-Gilloteaux, P., Gressens, P., Verney, C., and Kultas-Ilinsky, K. (2018). Human motor thalamus reconstructed in 3D from continuous sagittal sections with identified subcortical afferent territories. *eNeuro* 5:ENEURO.0060-18.2018. doi: 10.1523/ENEURO.0060-18.2018

Ilinsky, I. A., and Kultas-Ilinsky, K. (2001). "Neuroanatomical organization and connections of the motor thalamus in primates," in Basal Ganglia and Thalamus in Health and Movement Disorders, eds K. Kultas-Ilinsky and I. A. Ilinsky (New York,NY: Plenum Publishers), 77–91. doi: 10.1007/978-1-4615-1235-6_7

Jones, E. G. (1985). *The Thalamus*. New York, NY: Plenum Press.

Jones, E. G. (1997a). Neurosurgical forum: the motor thalamus. *J. Neurosurg.* 87:982.

Jones, E. G. (1998). "The thalamus of primates," in *Handbook of Chemical Neuroanatomy, Vol. 14, The Primate Nervous System, Part II*. eds F. E. Bloom, A. Björklund, and T. Hökfelt (Amsterdam: Elsevier), 1–298. doi: 10.1016/S0924-8196(98)80003-1

Jones, E. G. (2003). Chemically defined parallel pathways in the monkey auditory system. *Ann. N Y Acad. Sci.* 999, 218–233. doi: 10.1196/annals.1284.033

Jones, E. G. (2007). *The Thalamus*, *2nd Edn*. New York, NY: Cambridge University Press.

Jones, E. G., and Friedman, D. P. (1982). Projection pattern of functional components of thalamic ventrobasal complex on monkey somatosensory cortex. *J. Neurophysiol.* 48, 521–544. doi: 10.1152/jn.1982.48.2.521

Jones, E. G., and Macchi, G. (1997). Terminology of the motor thalamus. *J. Neurosurg.* 87, 981–982.

Jones, E. G. (1997b). "A description of the human thalamus," in *Thalamus,* Vol. 2, eds M. Steriade, E. G. Jones and D.A. McCormick (Amsterdam, Elsevier), 425–500.

Kaas, J. H. (2012). "Somatosensory system," in *The Human Nervous System, 3rd Edn,* eds J. K. Mai and G. Paxinos (San Diego, CA: Academic Press/Elsevier), 1074–1109. doi: 10.1016/B978-0-12-374236-0.10030-6

Kaas, J. H., Nelson, R. J., Sur, M., Dyke, R. W., and Merzenich, M. M. (1984). The somatotopic organization of the ventroposterior thalamus of the squirrel monkey, *Saimiri sciureus*. *J. Comp. Neurol.* 226, 111–140. doi: 10.1002/cne.902260109

Keifer, O. P., Gutman, D., Hecht, E., Keilholz, S., and Ressler, K. J. (2015). A comparative analysis of mouse and human medial geniculate nucleus connectivity: A DTI and anterograde tracing study. *NeuroImage* 105, 53–66. doi: 10.1016/j.neuroimage.2014.10.047

Krauth, A., Blanc, R., Poveda, A., Jeanmonod, D., Morel, A., and Székely, G. (2010). A mean three-dimensional atlas of the human thalamus: generation from multiple histological data. *Neuroimage* 49, 2053–2062. doi: 10.1016/j.neuroimage.2009.10.042

Kuhlenbeck, H. (1935). Über die morphologische Stellung des Corpus geniculatum mediale. *Anat Anz* 81, 28–37.

Kultas-Ilinsky, K., Sivan-Loukianova, E., and Ilinsky, I. A. (2003). Reevaluation of the primary motor cortex connections with the thalamus in primates. *J. Comp. Neurol.* 457, 133–158. doi: 10.1002/cne.10539

Kumar, V. J., van Oort, E., Scheffler, K., Beckmann, C. F., and Grodd, W. (2017). Functional anatomy of the human thalamus at rest. *NeuroImage* 147,678–691. doi: 10.1016/j.neuroimage.2016.12.071

Le Gros Clark, W. E. (1933). The medial geniculate body and the nucleus isthmi. *J Anat*. 67, 536–548.

Lenz, F. A., Casey, K. L., Jones, E. G., and Willis, W. D. (2010). *The Human Pain System, Experimental and Clinical Perspectives*. Cambridge: University Press. doi: 10.1017/CBO9780511770579

Lima, R. R., Pinato, L., Nascimento, R. B., Engelberth, R. C., Nascimento, E. S., Cavalcante, J. C., et al. (2012). Retinal projections and neurochemical characterization of the pregeniculate nucleus of the common marmoset (*Callithrix jacchus*). *J. Chem. Neuroanatomy*. 44, 34–44. doi: 10.1016/j.jchemneu.2012.04.001

Macchi, G., and Jones, E. G. (1997). Toward an agreement on terminology of nuclear and subnuclear divisions of the motor thalamus. *J. Neurosurg*. 86, 670–685. doi: 10.3171/jns.1997.86.4.0670

Mai, J. K., and Forutan, F. (2012). "Thalamus," in *The Human Nervous System, 3rd Edn*, eds J. K Mai and G. Paxinos (San Diego, CA: Academic Press/Elsevier), 618–677.

Mai, J. K., and Majtanik, M. (2017). *Human Brain in Standard MNI Space: A Comprehensive Pocket Atlas*. San Diego, CA: Academic Press/Elsevier.

Mai, J. K., Majtanik, M., and Paxinos, G. (2016). *Atlas of the Human Brain*, *4th Edn*., San Diego, CA: Academic Press/Elsevier.

Mai, J. K., Stephens, P. H., Hopf, A., and Cuello, A. C. (1986). Substance P in the human brain. *Neuroscience* 17, 709–739. doi: 10.1016/0306-4522(86)90041-2

Mai, J. K., Winking, R., and Ashwell, K. W. S. (1999). Transient CD15 expression reflects stages of differentiation and maturation in the human subcortical central auditory pathway. *J. Comp. Neurol.* 404:197–211. doi: 10.1002/(SICI)1096-9861(19990208)404:23.3.CO;2-Z

Malmierca, M. M., and Hackett, T. A. (2010). "Structural and functional organization of the auditory brain," in *The Auditory Brain, OUP Handbook of Auditory Science,* Vol. 2, eds A. R Palmer and A. Rees (Oxford: Elsevier), 9–42.

Mehler, W. R. (1971). Idea of a new anatomy of the thalamus. *J. Psychiat. Res.* 8, 203–217. doi: 10.1016/0022-3956(71)90019-7

Meynert, T. (1872). "Vom Gehirn der Säugetiere," in *Handburch der Lehre von den Geweben des Menschen und Tiere,* Vol. 2, ed S. Stricker (Leipzig, Engelmann), 694–808.

Mitra, P. P. (2014). The circuit architecture of whole brains at the mesoscopic scale. *Neuron* 83, 1273–1283. doi: 10.1016/j.neuron.2014.08.055

Morel, A. (2007). *Stereotactic Atlas of the Human Thalamus and Basal Ganglia*. Boca Raton, FL: CRC Press. doi: 10.3109/9781420016796

Morel, A., Magnin, M., and Jeanmonod, D. (1997). Multiarchitectonic and stereotactic atlas of the human thalamus. *J. Comp. Neurol.* 387, 588–630.

Morest, D. K. (1964). The neuronal architecture of the medial geniculate body of the cat. *J. Anat. Lond*. 98, 611–680.

Münkle, M. C., Walvogel, H. J., and Faull, R. L. (2000). The distribution of calbindin, calretinin, and parvalbumin immunoreactivity in the human thalamus. *J. Chem. Neuroanat*. 19, 155–173. doi: 10.1016/S0891-0618(00)00060-0

Namba, M. (1958). The finer structures of the medio-dorsal supranucleus and lamella medialis of the thalamus in the human. *J. Hirnforsch* 4, 1–42.

Nieuwenhuys, R., Voogd, J., and van Huijzen, C. (2008). *The Human Central Nervous System, 3rd Edn*. Berlin: Springer.

Niimi, K. (1949). Zur vergleichenden Cytoarchitektonik der vorderen, medianen und medialen Kerngruppe des Sehhügels des Menschen. *Acta Scholae Med. Univ. Kyoto* 27, 116–131.

Niimi, K., and Kuwahara, E. (1973). The dorsal thalamus of the cat and comparison with monkey and man. *J. Hirnforsch* 14, 303–325.

Ohye, C. (1990). "Thalamus," in The Human Nervous System, ed G. Paxinos (New York, NY: Academic Press), 439–468. doi: 10.1016/B978-0-12-547625-6.50022-2

Ohye, C., and Narabayashi, H. (1979). Physiological study of the presumed ventralis intermedius neurons in the human thalamus. *J. Neurosurg.* 50, 290–297. doi: 10.3171/jns.1979.50.3.0290

Olszewski, J. (1952). *The Thalamus of the Macaca mulatta. An Atlas for Use with the Stereotaxic Instrument*. Basel: Karger.

Percheron, G. (1997). Neurosurgical forum: the motor thalamus. *J. Neurosurg*. 87, 981–982.

Percheron, G. (2004). "Thalamus," in *The Human Nervous System*, eds G. Paxinos and J. K. Mai (San Diego, CA: Elsevier/Academic Press), 439–468. doi: 10.1016/B978-012547626-3/50021-1

Percheron, G., François, C., Talbi, B., Yelnik, J., and Fénelon, G. (1996). The primate motor thalamus. *Brain Res. Brain Res. Rev.* 22, 93–181 doi: 10.1016/0165-0173(96)00003-3

Percheron, G., François, C., Yelnik, J., Talbi, B., Meder, J. F., and Fénelon, G. (1993). "The pallidal and nigral thalamic territories and the problem of the anterior part of the lateral region in primates," in Thalamic Networks for Relay and Modulation, eds D. Minciacchi, M. Molinari, G. Macchi, E. G. Jones (Oxford: Pergamon Press), 145–154. doi: 10.1016/B978-0-08-042274-9.50019-5

Pinto, F. R., Melo-Cristino, J., and Ramirez, M. (2008). A confidence interval for the Wallace coefficient of concordance and its application to microbial typing methods. *PLoS ONE* 3:e3696. doi: 10.1371/journal.pone.0003696

Pritchard, T. C. (2012). "Gustatory System" in *The Human Nervous System, 3rd Edn,* J.K. Mai and G. Paxinos (San Diego, CA: Academic Press/Elsevier), 1187–1218. doi: 10.1016/B978-0-12-374236-0.10033-1

Puelles, L., and Rubenstein, J. L. (2003). Forebrain gene expression domains and the evolving prosomeric model. *Trends Neurosci.* 26, 469–476. doi: 10.1016/S0166-2236(03)00234-0

Riley, H. A. (1960). *An Atlas of the Basal Ganglia, Brain Stem, and Spinal Cord*. New York, NY: Hafner Publ. Co.

Rioch, D. M. (1929). Studies on the diencephalon of carnivora: Part, I. The nuclear configuration of the thalamus, epithalamus and hypothalamus of the dog and the cat. *J. Comp. Neurol.* 49, 1–119. doi: 10.1002/cne.900490102

Rose, J. E. (1942). The thalamus of the sheep: cellular and fibrous structure and comparison with pig, rabbit and cat. *J. Comp. Neurol.* 77, 469–523. doi: 10.1002/cne.900770303

Schnopfhagen, F. (1877). Beiträge zur Anatomie des Sehhügels und dessen nächster Umgebung. Sitzungsber. Akad. Wiss. *Wien Math.-naturw. Klasse Anat. usw. Abt. III* 76, 315–326.

Sheps, J. G. (1945). The nuclear configuration and cortical connections of the human thalamus. *J. Comp. Neurol*. 83, 1–56. doi: 10.1002/cne.900830102

Swanson, L. W. (2015). Brain maps online: toward open access atlases and a pan-mammalian nomenclature. *J. Comp. Neurol.* 523, 2272–2276. doi: 10.1002/cne.23788

Swanson, L. W., and Bota, M. (2010). Foundational model of nervous system structural connectivity with a schema from wiring diagrams, connectome, and basic plan architecture. *Proc. Natl. Acad. Sci. U.S.A*. 107, 20610–20617. doi: 10.1073/pnas.1015128107

TNA (2017). *Terminologia Neuroanatomica. FIPAT.library.dal.ca.* Federative International Programme for Anatomical Terminology.

Van Buren, J. M., and Borke, R. C. (1972). *Variations and Connections of the Human Thalamus.* Berlin: Springer.

Vogt, C. (1909). La myéloarchitecture du thalamus du cercopithèque. *J. Psychol. Neurol* 12, 285–324.

Vogt, C., and Vogt, O. (1941/1942). Thalamusstudien I-II. *J. Psychol. Neurol*. 50, 3–74.

Walker, A. E. (1938). *The Primate Thalamus*. Chicago, Chicago University Press.

Walker, A. E. (1966). "Internal structure and afferent-efferent relations of the thalamus," in *The Thalamus,* eds D. P. Purpura and M. D. Yahr (New York, NY: Columbia University Press), 1–11.

Wallace, D. L. (1983). A method for comparing two hierarchical clusterings: comment. *J. Am. Stat. Assoc.* 78, 569–576. doi: 10.2307/2288118

Welker, W. I. (1973). Principles of organization of the ventrobasal complex in mammals. *Brain Behav. Evol*. 7, 253–336. doi: 10.1159/000124417

Winer, J. A. (1984). The human medial geniculate body. *Hearing Res.* 15, 225–247. doi: 10.1016/0378-5955(84)90031-5

Winer, J. A. (1992). "The functional architecture of the medial geniculate body and the primary auditory cortex," in *Springer Handbook of Auditory Research, Vol. 1. The Mammalian Auditory Pathway: Neuroanatomy*, eds D. B. Webster, A. N. Popper, and R. R. Fay (New York, NY: Springer Verlag), 222–409. doi: 10.1007/978-1-4612-4416-5_6

Conflict of Interest Statement: JM is CEO of MRX-Brain GmbH, MM is data analyst and AI developer for MRX-Brain GmbH.

Copyright © 2019 Mai and Majtanik. This is an open-access article distributed under the terms of the Creative Commons Attribution License (CC BY). The use, distribution or reproduction in other forums is permitted, provided the original author(s) and the copyright owner(s) are credited and that the original publication in this journal is cited, in accordance with accepted academic practice. No use, distribution or reproduction is permitted which does not comply with these terms.

frontiers in Neuroanatomy

PERSPECTIVE
published: 13 December 2018
doi: 10.3389/fnana.2018.00102

The Representation of White Matter in the Central Nervous System

Robert Baud[1,2]*, *Pierre Sprumont*[1] *and Hans J. ten Donkelaar*[3]

[1] *Anatomy, Section of Medicine, Faculty of Science and Medicine, University of Fribourg, Fribourg, Switzerland,* [2] *SIB Data mining, Swiss Institute for Bioinformatics, Geneva, Switzerland,* [3] *Department of Neurology, Radboud University Medical Center and Donders Center for Medical Neuroscience, Nijmegen, Netherlands*

The white matter of the central nervous system (CNS) is difficult to represent in anatomy because it is located predominantly "between" other anatomical entities. In a classic presentation, like a cross section of a brain segment, white matter is present and can be labeled adequately. Several appearances of the same entity are feasible on successive cross section views. The problem is the absence of a global view on long tracts, and more generally, the lack of a comprehensive classification of white matter pathways. Following the recent revision of the *Terminologia Anatomica* (TA, 1998), in particular the chapter on the nervous system, resulting in the *Terminologia Neuroanatomica* (TNA, 2017), the authors have developed a new schema for the representation of white matter. In this approach, white matter is directly attached to the CNS, and no longer considered as part of the brain segments. Such a move does not affect the content but redistributes the anatomical entities in a more natural fashion. This paper gives an overall description of this new schema of representation and emphasizes its benefits. The new classification of white matter tracts is developed, selecting the origin as the primary criterion and the type of tract as the secondary criterion.

Keywords: neuroanatomy, terminology, white matter, ontology, knowledge representation

OPEN ACCESS

Edited by:
Kathleen S. Rockland,
Boston University, United States

Reviewed by:
Trygve B. Leergaard,
University of Oslo, Norway
Richard Jarrett Rushmore,
Boston University, United States

***Correspondence:**
Robert Baud
robert.baud@unifr.ch

Received: *30 July 2018*
Accepted: *15 November 2018*
Published: *13 December 2018*

Citation:
Baud R, Sprumont P and ten Donkelaar HJ (2018) The Representation of White Matter in the Central Nervous System. Front. Neuroanat. 12:102. doi: 10.3389/fnana.2018.00102

INTRODUCTION

At large, white matter coordinates communication between regions of the brain and the spinal cord. It is described by several nouns such as *tract, funiculus, fasciculus, commissure, lemniscus, fibers, decussation*, and *stria*. For convenience, in this article, they will be referred to as *tract* or alternatively as *pathway*. However, the above-mentioned specific names will continue to be used in the terminology, because they eventually bring some additional information to the named entity. There is a permanent discussion when building a terminology: how much a term should contribute to the definition of its referred entity. Short terms or longer versatile terms? Both have their advantages.

Any tract has an origin located in a cortical region or in a nucleus (or a group of nuclei). It has terminations in one or more locations of gray matter in the *central nervous system* (CNS), where it synapses, the locations are not always well-known. A tract is made of several bundles of fibers, possibly not completely identified. Between the origin and the termination, the path may be short between near structures or long between brain segments, either crossing the midline or not.

Our description of tracts is in line with other studies such as the Foundational Model of Connectivity (FMC) developed by Swanson and Bota (2010) which is the basis of the representation of white matter tracts in the Terminologia Neuroanatomica (TNA, 2017). The TNA is a recent

revision of the terminology on the CNS, the peripheral nervous system (PNS) and the sensory organs. These were abstracted from the Terminologia Anatomica (TA, 1998) and the Terminologia Histologica (TH, 2008) and were extensively updated by the Neuroanatomy Working Group of the Federative International Programme for Anatomical Terminology (FIPAT) of the International Federation of Anatomical Associations (IFAA), and was merged to form the TNA (ten Donkelaar et al., 2017; TNA, 2017), which currently stands alone. The FMC presentation of the connectome, with its three levels of connections—macroconnections (white matter tracts), mesoconnections (dealing with neuron types), and microconnections (dealing with individual neurons of a neuron type)—is a pertinent schema of representation, totally compatible with our approach. Most of the tract names in the TNA refer to macroconnections, because they reveal enough knowledge for naming a tract, whether the type of cells is reported or not. But there is no doubt that the documentation of mesoconnections in the future will help to differentiate new structures with consequent updates in the terminology.

Today, anatomical terminologies are challenged by the emergence of ontology and its formal approach. There was a time for the atlas of anatomy (and this approach is still valid), and there is a time for computer-based presentations. The basis of modern terminology for the biomedical sciences is the Basic Formal Ontology 2.0 (Smith et al., 2015), on which the FMA and our model are grounded. As seen in **Table 2** below, we adopt the taxonomy developed by the FMA (Rosse and Mejino, 2003). The rules governing the taxonomy and the partonomy have been made explicit and they are imperative. An expected benefit is to favor the exchange of data between computer applications. But the overall goal is a precise definition of anatomical entities. This will allow a better understanding among people living in distinct communities, with a specific background, while communicating in different languages. The past terminologies are the initial background for future developments, while modern terminologies are now ready to take the lead. This paper positions itself as a contribution to the advent of a modern terminology.

We have observed that anatomists may be reluctant to ontologies and related formal approaches.

> *"Terminologies should not be developed by reference to a system of preferred terms, rather they should be developed in such a way that their individual nodes and relations amongst these nodes are modeled on an underlying formal ontology, where the linguistic content of these nodes will be filled in based on a system of terms and synonyms (from many different languages) that is associated with each node based on the intended ontological interpretation of that node."*

(see Baud et al., 2007, where additional references may be found). Indeed, there is no opposition: ontologies are the necessary support of terminologies.

In a classic view of anatomical terminology, white matter is considered as a part of the brain segment where it appears. For example, in the Terminologia Anatomica (TA, 1998), the *posterior spinocerebellar tract* is described as a part of the *myelencephalon*. This entity is also present as a part of the *spinal cord*, but it is absent as part of the *cerebellum* where it terminates. Many tracts are mentioned several times in other segments, as if they are a part of it. The benefit of this approach was to document cross section views of brain segments and to make the path followed by the different tracks more explicit. This is an important aspect, but, hopefully, it is not lost in our new schema of presentation (see discussion below, see **Table 5**). The problem with such a presentation is that we depart from the rules of partonomy.

This is a classical error: it is well-known that the relation *CONTAINED_IN* differs from *PART_OF*. The *blood* is contained in the *vessels*, but not a part of them. The fact that a tract is crossing a brain segment does not makes this tract a part of it. If it did, because it crosses several segments, it would simultaneously be part of several brain segments. That is incompatible with the general statement of single inheritance in the partonomy: no entity can be a part of two entities. Therefore, it is formally incorrect to represent white matter tracts as part of the brain segments. The consequence is an ambiguous representation making it difficult to navigate in the knowledge base, as reported by several authors (Martin et al., 2001; Rosse, 2001; Rosse and Mejino, 2003; Bota and Swanson, 2008; Swanson and Bota, 2010; Swanson, 2014).

This classic view is widespread and shared by the TA (TA, 1998), the Foundational Model of Anatomy (FMA; Rosse and Mejino, 2003) and NeuroNames (Bowden and Martin, 1995; Martin et al., 2001; Bowden et al., 2012). Other initiatives generally claim to be compatible with any of these former studies. In the TA, the *pyramidal tract* is present as part of the *myelencephalon* and the *mesencephalon* with different codes. In the FMA, the *pyramidal tract* has no partonomic information so far. In NeuroNames, the *pyramidal tract* is part of the *medulla* or *myelencephalon*. Those statements are incomplete, because the pyramidal tract passes from the *cerebral cortex* to the *spinal cord*: only some segments of the pyramidal tract could be considered

TABLE 1 | Generic partonomy of tracts.

Nervous system	Systema nervosum
Central nervous system	Systema nervosum centrale
Tracts of central nervous system	Tractus systematis nervosi centralis
Tracts of origin	Tractus originis
Tracts of origin in segment 1	Tractus originis segmenti 1
Central roots	Radices centrales
Commissural tracts	Tractus commissurales
Intrinsic tracts	Tractus associationis; tractus proprii
Long tracts	Tractus longi
Ascending tracts	Tractus ascendentes
Descending tracts	Tractus descendentes
Tracts of origin in segment 2	Tractus originis segmenti 2
Mixed tracts	Tractus mixti

The numbers represent specific segments of the CNS. Plural terms represent sets of entities and the hierarchical relation between two plural terms is subset_of interpreted as a specialization of part_of.

as part of the brain segments as stated above. But is it acceptable to state that *myelencephalic segment of pyramidal tract PART_OF myelencephalon* instead of *myelencephalic segment of pyramidal tract PART_OF pyramidal tract*? Certainly not. It is time to adjust our representation of tracts.

NEW VIEW ON TRACTS

On the contrary, as a general statement, the tracts are not a part of any segment, but should rather be considered in a separate section of the CNS as previously advocated in the Jenaer Nomina Anatomica (JNA, 1936), which contains the collection of all tracts and only those. This places a direct focus on the connections running through the white matter. The current number of tracts is about 100 items, but this number may grow in the coming years due to new discoveries.

What we propose is that tracts form directly part of the CNS (see **Table 1**). When concentrating all tracts in a single section, it is necessary to classify these tracts based on natural acceptable criteria. The origin of a tract is finally considered as the primary criterion, because it is always known and relatively well-localized to a single location, in contrast to terminations of tracts that are numerous and not always completely documented. On this basis, the tracts of the CNS are classified by their origin in the following 9 segments: *telencephalon (pallium), telencephalon (subpallium), hypothalamus, diencephalon, mesencephalon, cerebellum, rostral rhombencephalon*, *caudal rhombencephalon,* and *spinal cord*.

In the TNA, a more natural hierarchical classification of brain structures is used for the prosencephalon (forebrain) as implemented in the revised version of the Terminologia Embryologica (TE2, 2017). The forebrain is subdivided into the caudal prosencephalon, giving rise to the diencephalon (pretectum, thalamus with epithalamus, prethalamus, and the prerubral or diencephalic tegmentum), and a rostral or secondary prosencephalon, giving rise to the hypothalamus and the entire telencephalon. The telencephalon is divided into the pallium and the subpallium (striatum, pallidum, basal forebrain, and preoptic area).

The diencephalon in its classic, columnar view (Herrick, 1910) was divided into four dorsoventrally arranged columns separated by ventricular sulci, i.e., the epithalamus, the dorsal thalamus, the ventral thalamus and the hypothalamus. It should be noted that NeuroNames and the FMC still follow this doctrine. Extensive embryological studies (see Puelles et al., 2013; ten Donkelaar et al., 2017, 2018) made it clear that the thalamic "columns" are derived from transversely oriented zones, the prosomeres which, from caudal to rostral, contain, in their alar domains, the pretectum (prosomere 1 or P1), the epithalamus and the thalamus (P2), and the prethalamus and the eminentia thalami (P3). The diencephalic basal plate contains the diencephalic part of the substantia nigra–VTA complex, the interstitial nucleus of Cajal, the nucleus of Darkschewitsch and the fields of Forel, collectively known as the prerubral or diencephalic tegmentum. The entire hypothalamus arises from the alar and basal components of the secondary prosencephalon. The preoptic region arises from the subpallium, but for practical reasons it is listed preceding the hypothalamus. The Kuhlenbeck (1967-1978) terms "interbrain" for diencephalon, and "afterbrain" for myelencephalon, as advocated in the FMC, are not widely recognized.

The term "pons," as used in colloquial neuroanatomy for the rostral part of the hindbrain, is replaced by the term rostral rhombencephalon, keeping the term pons for the pons proper (the basilar part of the pons in most studies). For the caudal part of the hindbrain, the myelencephalon, the term caudal rhombencephalon is suggested.

Our choice of origin as the primary classification criterion is in accordance with the FMC. The first level or macroconnection is based on the region including the origin of a tract, whereas the second level, mesoconnection, is based on cell types. Therefore, our first criterion corresponds to the FMC first level.

A second criterion was necessary for the classification within a segment. The type of tract was selected for this purpose. The following subdivision was used (see **Tables 1**, **2**):

(1) *Central roots*, defined as the white matter tracts of the CNS that contribute (a) to cranial nerve roots within the brain stem, including the genu of the facial nerve, the decussation

TABLE 2 | Taxonomy of tract.

- Anatomical entity
  - Physical anatomical entity
    - Material anatomical entity
      - Anatomical structure
        - Postnatal anatomical structure
          - Cell part cluster
            - Cell part cluster of central nervous system
              - Tract of central nervous system
                - Tract of brain
                  - Tract of origin in telencephalon
                    - Central root of telencephalon
                    - Commissural tract of origin in telencephalon
                    - Association tract of origin in telencephalon
                    - Descending tract of origin in telencephalon
                  - Tract of origin in hypothalamus
                  - Tract of origin in diencephalon
                    - Central root of diencephalon
                    - Commissural tract of origin in diencephalon
                    - Association tract of origin in diencephalon
                    - Long tract of origin in diencephalon
                      - Ascending tract of origin in diencephalon
                      - Descending tract of origin in diencephalon
                  - Tract of origin in mesencephalon
                  - Tract of origin in cerebellum
                  - Tract of origin in rostral rhombencephalon
                  - Tract of origin in caudal rhombencephalon
                - Tract of spinal cord
                  - Tract of origin in spinal cord

This is a partial expansion of the global taxonomy. All indentations in the hierarchy represent the ISA relation.

of the trochlear nerve, the spinal and mesencephalic tracts of the trigeminal nerve, and the solitary tract; and (b) the central projections of the dorsal roots of the spinal cord, forming the gracile and cuneate fasciculus. The optic tract may also be viewed as a central root.

(2) *Intrinsic tracts*, restricted to a particular part of the brain, include: (a) *association tracts*, the association pathways of the telencephalon; (b) *intrinsic tracts* of other parts of the brain; and (c) the *intrinsic*, *propriospinal tracts* of the spinal cord.

(3) *Commissural tracts*, connecting left and right parts of the brain or spinal cord segment, including the corpus callosum, the anterior, habenular, posterior and supraoptic commissures, and commissural connections in the spinal cord.

(4) *Long tracts* connect various segments of the CNS and can be divided into (a) *ascending tracts*; (b) *cerebellar efferent tracts*; and (c) *descending tracts*, irrespective of whether they cross the midline or not.

In order to illustrate the use of the two criteria, three examples of partonomy are presented here:

1) **long tracts of origin in telencephalon > descending tracts of origin in telencephalon >** pyramidal tract > corticorubral fibers.

TABLE 3 | Tracts of origin in the diencephalon.

Tracts of origin in diencephalon	Tractus originis diencephali
Central roots of diencephalon	**Radices centrales diencephali**
Optic tract	Tractus opticus
Lateral root	Radix lateralis
Medial root	Radix medialis
Retinohypothalamic tract	Tractus retinohypothalamicus
Commissural tracts of origin in diencephalon	**Tractus commissurales originis diencephali**
Habenular commissure	Commissura habenulae
Posterior commissure	Commissura posterior
Intrinsic tracts of origin in diencephalon	**Tractus proprii originis diencephali**
External medullary lamina	Lamina medullaris lateralis
Internal medullary lamina	Lamina medullaris medialis
Intrathalamic fibers	Fibrae intrathalamicae
Periventricular fibers	Fibrae periventriculares
Long tracts of origin in diencephalon	**Tractus longi originis diencephali**
Ascending tracts of origin in diencephalon	**Tractus ascendentes originis diencephali**
Thalamostriatal fibers	Fibrae thalamostriatales
Subthalamopallidal fibers	Fibrae subthalamopallidales
Thalamic radiations	Radiationes thalamicae
Anterior thalamic radiation; anterior radiation	Radiatio anterior thalami
Thalamofrontal fibers	Fibrae thalamofrontales
Central thalamic radiation; central radiation	Radiatio centralis thalami
Thalamoparietal fibers	Fibrae thalamoparietales
Inferior thalamic radiation; inferior radiation	Radiatio inferior thalami
Thalamotemporal fibers	Fibrae thalamotemporales
Posterior thalamic radiation; posterior radiation	Radiatio posterior thalami
Acoustic radiation	Radiatio acustica
Optic radiation; geniculocalcarine fibers	Radiatio optica; fibrae geniculocalcarinae
Anterior bundle	Fasciculus anterior
Central bundle	Fasciculus centralis
Dorsal bundle	Fasciculus dorsalis
Ascending peduncular fasciculus	Fasciculus pedunculares ascendens
Descending tracts of origin in diencephalon	**Tractus descendentes originis diencephali**
Habenulointerpeduncular tract; fasciculus retroflexus	Tractus habenulointerpeduncularis; fasciculus retroflexus
Medial tegmental tract	Tractus tegmentalis medialis
Pretectoolivary tract	Tractus pretectoolivaris
Prerubroolivary tract	Tractus prerubroolivaris
Descending medial longitudinal fasciculus	Fasciculus longitudinalis medialis descendens
Interstitiospinal tract	Tractus interstitiospinalis

2) **tracts of origin in hypothalamus > efferent tracts of hypothalamus >** hypothalamohypophysial tracts > paraventriculohypophysial tract.
3) **long tracts of origin in spinal cord > ascending tracts of origin in spinal cord >** anterolateral tract > spinoreticular tract.

Once a tract has been classified according to its origin, it is possible to give more information on its path through different brain segments. To do that, it is possible in a partonomic view to present the path of this tract, decomposed in ipsilateral and contralateral segments and decussations as well. These parts of a track may be referenced in the partonomic presentation of the white matter of the brain segments.

An open question remains: how will this model evolve when new discoveries are made? In the domain of TNA, massive data are collected, and new investigation tools are available. There is no doubt that integration of new information will be necessary in the future. There are two open solutions. (1) the origin of tracts may be further defined, and the tract could be split up into subtracts corresponding to detailed origins; (2) different types of cells (mesoconnection) at the origin of a tract may be used to differentiate the tract into several tracts. This paper does not answer this question, however, the new schema formally improves the approach relative to the traditional approach and is consequently better adapted to the evolution of knowledge.

INTEGRATION IN TAXONOMY

Today, there is a single valid taxonomy for the domain of human anatomy, provided by the FMA (Rosse and Mejino, 2003). The emergence of an alternate taxonomy, although theoretically possible, has little chance, because such an enterprise has a workload of several years, currently not available, with no promise of an improved solution. The scientific community must therefore concentrate on the existing FMA taxonomy, and create collaborations to accommodate further improvements. And indeed, the actual FMA taxonomy is of significant value.

The role of the taxonomy is important in a modern ontology. The traditional presentation by the anatomists is the atlas of anatomy, inspired by the partonomic hierarchy. The atlas paradigm is convenient for the inventory of the relevant anatomical entities. Because past terminologies essentially were inventories of the domain, this approach was convenient. But today, a modern terminology must include a classification schema. The taxonomy, based on the genus and differentia principle of Aristotle, is the answer of choice to this need. Consequently, any anatomical entity is positioned in both hierarchies: partonomy and taxonomy. For example: *humerus isa long bone* and *humerus partof free upper limb*.

Apparently, the FMA taxonomy was not recently updated to correspond with the many new developments in neuroanatomy. Therefore, a revision of the neuroanatomical subdivision, based largely on NeuroNames, would be welcome. The present study offers a contribution to such a revision. Currently, the white matter that is essentially made of axons is classified (see **Table 2**) as a *cell part cluster of central nervous system* and its main child is *tract of central nervous system* that contains the majority of tracts. There are roughly 100 tracts classified into two groups: *tract of brain* and *tract of spinal cord*. Because this figure may be considerably augmented in the future, such a long flat list is no longer acceptable: further subdivisions must be created. Here, the above criterion may be inserted.

TABLE 4 | Mixed tracts.

Mixed tracts of central nervous system	Tractus mixti systematis nervosi centralis
Peduncular fasciculus	Fasciculus pedunclaris
>Ascending peduncular fasciculus	>Fasciculus peduncularis ascendens
>Descending peduncular fasciculus	>Fasciculus peduncularis descendens
Ansa peduncularis	Ansa peduncularis
>Thalamotemporal fibers	>Fibrae thalamotemporales
>Corticothalamic fibers	>Fibrae corticothalamicae
>Ventral amygdalofugal tract	>Tractus amygdalofugalis ventralis
Medial fasciculus of prosencephalon	Fasciculus prosencephali medialis
>Ascending medial fasciculus of prosencephalon	>Fasciculus prosencephali medialis ascendens
>Descending medial fasciculus of prosencephalon	>Fasciculus prosencephali medialis descendens
Posterior longitudinal fasciculus; dorsal longitudinal fasciculus	Fasciculus longitudinalis posterior; fasciculus longitudinalis dorsalis
>Ascending posterior longitudinal fasciculus	> Fasciculus longitudinalis posterior ascendens
>Descending posterior longitudinal fasciculus; descending dorsal longitudinal fasciculus	>Fasciculus longitudinalis posterior descendens; fasciculus longitudinalis dorsalis descendens
Medial longitudinal fasciculus	Fasciculus longitudinalis medialis
>Ascending medial longitudinal fasciculus	>Fasciculus longitudinalis medialis ascendens
>Descending medial longitudinal fasciculus	>Fasciculus longitudinalis medialis descendens

The sign ">" means a reference to another table of which the tract is a part. The present list is not exhaustive and limited to the main mixed tracts.

OVERVIEW OF THE TRACTS

Making an exhaustive inventory of tracts is not the goal of the terminology of today, when our knowledge of the CNS must be permanently updated by new discoveries. Therefore, the presentation of tracts is made of open lists. There are basically two conditions to fulfill before a new tract may enter the tables: (1) it should be recognized as important; and (2) it should have reached a significant level of agreement in the domain. These criteria are obviously subjective: it is the responsibility of the authors of the terminology to decide what is present or not. These two conditions should obviously be updated permanently, making the terminology subject to continual changes.

As seen above, tracts are grouped into 9 segments. In this paper, only tracts originating in the diencephalon are presented. An extended version of this paper, including all segments, is available by the authors.

The tables related to each segment are exclusively partonomic: each indentation means a *part_of* relation between the father entity and the indented entity. Plural terms refer to a set of entities. The link from a plural to a plural term must be understood as a *subset_of* and from a plural to a singular term as a *member_of*, both being a specialization of a *part_of*.

TABLE 5 | White matter of cerebellum.

White matter of cerebellum	Substantia alba cerebelli
Arbor vitae	Arbor vitae
Medullary body of cerebellum	Corpus medullare cerebelli
Medullary lamella of cerebellum	Lamella medullaris cerebelli
Cerebellar cortical afferent fibers	Neurofibrae afferentes corticis cerebelli
Mossy fibers	Neurofibrae muscosae
Climbing fibers	Neurofibrae ascendentes
Multilayered fibers; monoaminergic fibers	Neurofibrae multistratificatae
Cerebellar cortical efferent fibers	Neurofibrae efferentes corticis cerebelli
Axons of Purkinje cell	Axones neuri purkinjensis
>Commissural tracts of origin in the cerebellum	>Tractus commissurales originis cerebelli
>Cerebellar commissure	>Commissura cerebelli
Cerebellar peduncles	Pedunculi cerebellares
Superior cerebellar peduncle	Pedunculus cerebellaris superior
Brachium conjunctivum	Brachium conjunctivum
Ascending branch	Ramus ascendens
>Cerebellorubral tract	>Tractus cerebellorubrale
>Cerebellothalamic tract	>Tractus cerebellothalamicum
Descending branch	Ramus descendens
>Uncinate fasciculus of cerebellum	> Fasciculus uncinatus cerebelli
>Fastigiobulbar fibers	> Fibrae fastigiobulbares
>Fastigiospinal tract	> Tractus fastigiospinalis
>Interpositospinal tract	> Tractus interpositospinalis
>Anterior spinocerebellar tract; ventral spinocerebellar tract	>Tractus spinocerebellaris anterior; tractus spinocerebellaris ventralis
Middle cerebellar peduncle	Pedunculus cerebellaris medius
>Pontocerebellar fibers	>Fibrae pontocerebellares
Inferior cerebellar peduncle	Pedunculus cerebellaris inferior
Restiform body	Corpus restiforme
>Cerebelloolivary fibers; nucleoolivary fibers	>Fibrae cerebelloolivares; fibrae nucleoolivares
>Posterior spinocerebellar tract; dorsal spinocerebellar tract	>Tractus spinocerebellaris posterior; tractus spinocerebellaris dorsalis
>Cuneocerebellar fibers	>Fibrae cuneocerebellares
>Trigeminocerebellar fibers	>Fibrae trigeminocerebellares
>Olivocerebellar tract	>Tractus olivocerebellaris
>Nucleocerebellar fibers	>Fibrae nucleocerebellares
>Raphecerebellar fibers	>Fibrae raphecerebellares
Juxtarestiform body	Corpus juxtarestiforme
>Vestibulocerebellar fibers	>fibrae vestibulocerebellares
>Cerebellovestibular fibers	>Fibrae cerebellovestibulares
Peduncle of flocculus	Pedunculus flocculi

The sign ">" means a reference to another table of which the tract is a part.

THE TRACTS OF ORIGIN IN THE DIENCEPHALON

The *tracts of origin in diencephalon* (*tractus originis diencephali*) include a central root, commissural, intrinsic and long tracts, ascending as well as descending (**Table 3**). The unique *central root* in the diencephalon is the *optic tract* (*tractus opticus*) with three distinct parts, the *lateral root* (*radix lateralis*), the *medial root* (*radix medialis*), and the *retinohypothalamic tract* (*tractus hypothalamicus*). Since the optic tract, arising from the retinal ganglion cells, mainly terminates in the lateral geniculate body, it is defined as a diencephalic central root. There are two crossing bundles of fibers, the *habenular commissure* (*commissura habenulae*), connecting the epithalami, and the *posterior commissure* (*commissura posterior*), a commissure of the pretectum. Intrinsic to the diencephalon are four tracts, the *external medullary lamina* (*lamina medullaris lateralis),* the *internal medullary lamina* (*lamina medullaris medialis*), *intrathalamic fibers* (*fibrae intrathalamicae*), and *periventricular fibers* (*fibrae periventriculares*).

There are three groups of *ascending fibers*: the *thalamostriatal fibers* (*fibrae thalamostriatales*), the *subthalamopallidal fibers* (*fibrae subthalamopallidales*), and the extensive connections of the thalamus to the cerebrum, known by the generic name *thalamic radiations* (*radiationes thalamicae*). These radiations, anterior, central, inferior and posterior (see **Table 3**) reach each lobe of the cerebrum. The *acoustic radiation* (*radiatio acustica*) projects to the temporal lobe, the *optic radiation* (*radiatio optica*) to the occipital lobe, whereas the *ascending peduncular fasciculus* (*fasciculus peduncularis ascendens*) connects the thalamus to the claustrum. This mixed tract (see **Table 4**) also contains fibers from the claustrum to the thalamus (the *descending peduncular fasciculus*).

The descending fibers arising in the diencephalon include: (1) the *habenulointerpeduncular tract* or *fasciculus retroflexus* (*tractus habenulointerpeduncularis* or *fasciculus retroflexus*) from the habenular nuclei to the mesencephalic interpeduncular nucleus; (2) the *medial tegmental tract* (*tractus tegmentalis medialis*), arising in the pretectum and the prerubral tegmentum, projecting to the inferior olivary complex, and composed of the *pretectoolivary tract* (*tractus pretectoolivaris*) from the pretectum, and the *prerubroolivary tract* (*tractus prerubrolivaris*) from the elliptic nucleus (the nucleus of Darkschewitsch) in the prerubral tegmentum; (3) the *descending medial longitudinal fasciculus* (*fasciculus longitudinalis medialis descendens*), containing the *interstitiospinal tract* (*tractus interstitiospinalis*), arising in the interstitial nucleus of Cajal.

MIXED TRACTS

Mixed tracts have ascending and descending components, using the same tract, exemplified by the *medial fasciculus of the prosencephalon*, also known as the *medial forebrain bundle*. See **Table 4** for a list of mixed tracts.

ROSTROCAUDAL SEQUENCING

A general rule has been adopted for the sequence of entities, when there are several children from a father entity. In general, in a partonomic hierarchy, the order of children is open. It was decided to always sequence the tracts from the most rostral to the most caudal, when this sequence is significant. In other situations, like the *spinal laminae*, the sequence is determined by the current usage, here from posterior to anterior position.

BRAIN SEGMENT WHITE MATTER

It was also necessary to make explicit the links between the white matter representation in a segment and the tracts originating, terminating and traversing this segment. Because the representation is done by a partonomy, and the tracts are no more a part of the segment, we used a convention, named a *reference*. In a brain segment, we were concerned with tracts of several origins. We had to point to all of them in a specific order, proper to the segment. A reference is a pointer to an anatomical entity located elsewhere in the partonomic hierarchy. It is here represented by the sign ">."

Typically, in the representation of the white matter of the cerebellum, we would point to the tracts running in the *brachium conjunctivum* using references. The long tracts using this pathway to enter or exit the cerebellum are not part of it and can only be revealed by a reference. See **Table 5** about the white matter of the cerebellum.

CONCLUSION

The new schema for white matter gives a direct focus on the several tracts of the central nervous system. It brings a formally correct representation that is necessary for further developments of a highly developing domain.

The need to improve the formal aspect of a modern terminology has been underlined. The dual approach with two facets–the partonomy and the taxonomy–becomes evidence. Multiple computer applications are developed today, and they will exchange their data only on the condition that they have a common background: the taxonomy plays this role. The terminological aspect remains a predominant source of problems and a universal consensus has not yet been reached. However, sound principles as exemplified in this paper contribute to the solutions of tomorrow.

AUTHOR CONTRIBUTIONS

All authors listed have made a substantial, direct and intellectual contribution to the work, and approved it for publication.

ACKNOWLEDGMENTS

Thanks to Jose Leonardo V. Mejino Jr., M.D., for reviewing the manuscript of this paper.

REFERENCES

Baud, R., Ceusters, W., Ruch, P., Rassinoux, A. M., Lovis, C., and Geissbühler, A. (2007). Reconciliation of ontology and terminology to cope with linguistics. *Stud. Health Technol. Inform.* 29(Pt. 1):796–801.

Bota, M., and Swanson, L. W. (2008). BAMS neuroanatomical ontology: design and implementation. *Front. Neuroinform.* 2:8. doi: 10.3389/neuro.11.002.2008

Bowden, D. M., and Martin, R. F. (1995). NeuroNames brain hierarchy. *Neuroimage* 2, 63–83. doi: 10.1006/nimg.1995.1009

Bowden, D. M., Song, E., Kosheleva, J., and Dubach, M. F. (2012). neuronames: an ontology for the braininfo portal to neuroscience on the web. *Neuroinformatics* 10, 97–114. doi: 10.1007/s12021-011-9128-8

Herrick, C. J. (1910). The morphology of the forebrain in amphibia and reptilia. *J. Comp. Neurol.* 20, 413–547 doi: 10.1002/cne.920200502

JNA, Jenaer Nomina Anatomica (1936). *Approved June 1935 by the Anatomische Gesellschaft in Jena, Published Early 1936 by H.Stieve*. Jena: Fischer

Kuhlenbeck, H. (1967-1978). *The Central Nervous System of Vertebrates*, Vol 5. Basel: Karger.

Martin, R. F., Mejino, J. L. V. Jr, Bowden, D. M., Brinkley, J. F., and Rosse, C. (2001). Foundational model of neuroanatomy: implications for the human brain project. *Proc. AMIA Symp.* 2001, 438–442.

Puelles, L., Harrison, M., Paxinos, G., and Watson, C. (2013). A developmental ontology for the mammalian brain based on the prosomeric model. *Trends Neurosci.* 36, 570–578. doi: 10.1016/j.tins.2013.06.004

Rosse, C. (2001). Terminologia Anatomica: considered from the perspective of next-generation knowledge sources. *Clin. Anat.* 14, 120–133. doi: 10.1002/1098-2353(200103)14:2<120::AID-CA1020>3.0.CO;2-V

Rosse, C., and Mejino, J. L. V Jr. (2003). A reference ontology for biomedical informatics: the foundational model of anatomy. *J. Biomed. Inform.* 36, 478–500. doi: 10.1016/j.jbi.2003.11.007

Smith, B., Almeida, M., Bona, J., Brochhausen, M., Ceusters, W., Courtot, M., et al. (2015). *BFO 2.0 Specification and User's Guide*. Available online at: https://raw.githubusercontent.com/BFO-ontology/BFO/v2.0/BFO2-Reference.docx

Swanson, L. W. (2014). *Neuroanatomical Terminology. A Lexicon of Classical Origins and Historical Foundations*. New York, NY: Oxford University Press.

Swanson, L. W., and Bota, M. (2010). Foundational model of structural connectivity in the nervous system with a schema for wiring diagrams, connectome, and basic plan architecture. *Proc. Natl. Acad. Sci. U. S. A.* 107, 20610–20617. doi: 10.1073/pnas.1015128107

TA (1998) *Terminologia Anatomica. Federative Committee on Anatomical Terminology*. Stuttgart: Thieme.

TE2 (2017) *Terminologia Embryologica. FIPAT.Library.dal.ca.* Federative International Programme for Anatomical Terminology.

ten Donkelaar, H. J., Broman, J., Neumann, P. E., Puelles, L., Riva, A., Tubbs, R. S., et al. (2017). Towards a terminologia neuroanatomica. *Clin. Anat.* 30, 145–155. doi: 10.1002/ca.22809

ten Donkelaar, H. J., Kachlík, D., and Tubbs, S. T. (2018). *An Illustrated Terminologia Neuroanatomica: A Concise Encyclopedia of Human Neuroanatomy*. Heidelberg: Springer.

TH (2008) *Terminologia Histologica. Federative Committee on Anatomical Terminology*. Philadelphia, PA: Lippincott, Williams & Wilkins.

TNA (2017) *Terminologia Neuroanatomica. FIPAT.Library.dal.ca.* Federative International Programme for Anatomical Terminology.

Conflict of Interest Statement: The authors declare that the research was conducted in the absence of any commercial or financial relationships that could be construed as a potential conflict of interest.

The reviewer RR and handling Editor declared their shared affiliation at the time of review.

Copyright © 2018 Baud, Sprumont and ten Donkelaar. This is an open-access article distributed under the terms of the Creative Commons Attribution License (CC BY). The use, distribution or reproduction in other forums is permitted, provided the original author(s) and the copyright owner(s) are credited and that the original publication in this journal is cited, in accordance with accepted academic practice. No use, distribution or reproduction is permitted which does not comply with these terms.

frontiers in Neuroanatomy

REVIEW
published: 06 November 2018
doi: 10.3389/fnana.2018.00094

The Nomenclature of Human White Matter Association Pathways: Proposal for a Systematic Taxonomic Anatomical Classification

Emmanuel Mandonnet[1]*†, *Silvio Sarubbo*[2†] *and Laurent Petit*[3]*

[1]*Department of Neurosurgery, Lariboisière Hospital, Paris, France,* [2]*Division of Neurosurgery, Structural and Functional Connectivity Lab, Azienda Provinciale per i Servizi Sanitari (APSS), Trento, Italy,* [3]*Groupe d'Imagerie Neurofonctionnelle, Institut des Maladies Neurodégénératives—UMR 5293, CNRS, CEA University of Bordeaux, Bordeaux, France*

The heterogeneity and complexity of white matter (WM) pathways of the human brain were discretely described by pioneers such as Willis, Stenon, Malpighi, Vieussens and Vicq d'Azyr up to the beginning of the 19th century. Subsequently, novel approaches to the gross dissection of brain internal structures have led to a new understanding of WM organization, notably due to the works of Reil, Gall and Burdach highlighting the fascicular organization of WM. Meynert then proposed a definitive tripartite organization in association, commissural and projection WM pathways. The enduring anatomical work of Dejerine at the turn of the 20th century describing WM pathways in detail has been the paramount authority on this topic (including its terminology) for over a century, enriched sporadically by studies based on blunt Klingler dissection. Currently, diffusion-weighted magnetic resonance imaging (DWI) is used to reveal the WM fiber tracts of the human brain *in vivo* by measuring the diffusion of water molecules, especially along axons. It is then possible by tractography to reconstitute the WM pathways of the human brain step by step at an unprecedented level of precision in large cohorts. However, tractography algorithms, although powerful, still face the complexity of the organization of WM pathways, and there is a crucial need to benefit from the exact definitions of the trajectories and endings of all WM fascicles. Beyond such definitions, the emergence of DWI-based tractography has mostly revealed strong heterogeneity in naming the different bundles, especially the long-range association pathways. This review addresses the various terminologies known for the WM association bundles, aiming to describe the rules of arrangements followed by these bundles and to propose a new nomenclature based on the structural wiring diagram of the human brain.

Keywords: white matter anatomy, association pathways, nomenclature, human brain, dissection, tractography

OPEN ACCESS

Edited by:
Hans J. ten Donkelaar, Radboud University Nijmegen, Netherlands

Reviewed by:
Robert Turner, Max-Planck-Institut für Kognitions- und Neurowissenschaften, Germany
Francesco Sammartino, The Ohio State University, United States
Giorgio Innocenti, Karolinska Institutet (KI), Sweden

***Correspondence:**
Emmanuel Mandonnet
emmanuel.mandonnet@aphp.fr
Laurent Petit
laurent.petit@u-bordeaux.fr

†These authors share co-first authorship

Received: *30 July 2018*
Accepted: *17 October 2018*
Published: *06 November 2018*

Citation:
Mandonnet E, Sarubbo S and Petit L (2018) The Nomenclature of Human White Matter Association Pathways: Proposal for a Systematic Taxonomic Anatomical Classification. Front. Neuroanat. 12:94. doi: 10.3389/fnana.2018.00094

INTRODUCTION

> *"Unfortunately, nature seems unaware of our intellectual need for convenience and unity, and very often takes delight in complication and diversity."*
>
> *— Ramón y Cajal (1906).*

In 1695, Ijsbrand Van Diemerbroeck wrote the following in the second volume of *L'anatomie du corps humain*: "*Descartes in his Traité de l'Homme (1648) tried to establish by several probable*

conjectures, that the substance of the brain is necessarily all fibrous, and composed of an infinity of filaments which Willis calls small pipes, or flutings. What Descartes saw from the mind's eyes, Malpighi in his Epistola anatomica de cerebro ad Fracassatum (1665) has demonstrated it by those of the body. Actually, he writes that by means of the microscope he has very often observed in the brains of oxen, and other animals, both raw and boiled, that the whole white portion of the brain is, of course, divided into very small, round, and somewhat flat fibrils, and so evidently visible in the brains of the fish, that if we look at them through the daylight they will look like an ivory comb, or church organs. He says that the tip or head of these fibrils sinks into the cortex (that is, in the outer gray part of the brain) as to extract the matter from which they must be fed" (Van Diemerbroeck, 1695).

Three and a half centuries later, there is less mystery regarding such a fibrous composition of the brain. Among the neurons inhabiting the gray matter (GM), there are two groups: interneurons and long-projection neurons. The first group includes neurons that remain more or less confined in the GM to connect the other neurons of the GM together. Long-projection neurons have their cell bodies and their dendritic arborization within the GM, but their axons project their information long distances from the cell body. In addition, long-projection neurons are relatively dispersed in the GM. However, when subsequently emerging from the GM, they arrange themselves in fibers, fan out and then regroup themselves to form bundles of fibers. These axons are myelinated all along their path, which gives the path a whitish color. Consequently, white matter (WM) comprised the parts of the nervous tissue that essentially contain long-range bundles of fibers (axons) sheathed with myelin.

Despite the fact that the brain is made up of billions of neurons, and therefore as many axons with a large number of long-range projections, the spatial organization of such a large number of axons that compose the brain WM is far from being anarchic but is composed of densely packed axons organized into fiber tracts, also named bundles or fascicles. These tracts form a complex but well-organized tridimensional architecture within the hemispheres, the brainstem and the spinal cord.

A detailed knowledge of the anatomy of the WM fascicles is crucial for neurosurgical decision-making and is also of great interest for neuroscience studies in light of the emergence of diffusion-weighted magnetic resonance imaging (DWI) and tractography techniques to reveal the structural connectome of the human brain (Sporns, 2013; Jbabdi et al., 2015). Despite numerous algorithmic developments, diffusion tractography still faces important challenges to properly reconstruct WM tracts for the whole brain (Maier-Hein et al., 2017). Previous studies have demonstrated that even when diffusion tractography is combined with the gold standard anatomical tracer injection technique, tractography parameters (Thomas et al., 2014; Aydogan et al., 2018; Sinke et al., 2018), the superficial fiber system (Reveley et al., 2015) and anatomical constraints (Donahue et al., 2016; Aydogan et al., 2018) strongly bias the tractography results. The most current statement about diffusion tractography is the lack of precise ground-truth anatomical knowledge. Such a lack of trajectories of fiber tracts and their origins as well as terminations in the GM makes it difficult to reconstruct reliable whole brain tractograms, which may encompass the entirety of the tract-based WM organization of the human brain.

Therefore, there is a crucial need to benefit from exact definitions of the trajectories and endings of all WM fascicles. Beyond such definitions, questioning the human WM anatomy with DWI-based tractography has mostly revealed a strong heterogeneity in naming the different bundles, especially the long-range association pathways.

In this review, we propose a comprehensive description of the terminology of the main long-range association pathways of the human brain. Then, we propose a new nomenclature, mainly based on a set of rules of topographical organization of these long-range association pathways.

A Brief History of the Description of the Fascicular Organization of the WM

From an historical point of view, the human WM pathways were discretely described by pioneers from the 16th century up to the beginning of the 19th century. In *Anatomia capitis humani* Dryander (1536), (also known as Johann Eichmann (1500–1560)) illustrated the different steps of human head dissection. **Figure 1A** (Figure 6 from Dryander, 1536) is considered one of the first representations of cerebral circumvolution superficial to the WM (Dryander, 1536). Vesalius provided the same description in *De humani corporis fabrica*, which was published 7 years later (**Figure 1B**; Vesalius, 1543), and Piccolomini followed by describing a clear distinction between the GM of the cortex and the white medulla (Piccolomini, 1586). Improvements in the specimen preparation during the 17th century allowed finer descriptions (Malpighi, 1665; Steno, 1669; Vieussens, 1684). Steno was one of those who distinguished fiber trajectories within the WM, while as mentioned above, Malpighi also described its fibrous aspect. A significant advance was then made twenty years later when Vieussens found that boiling the brain in oil before dissecting it rendered the WM fibers harder and therefore easier to separate. He discovered that the corpus callosum (**Figure 1C**) was not a single structure but rather an intricate bundle of fibers that could be separated from the rest of the WM located in each hemisphere.

Due to its unformed appearance upon inspection with the naked eye, the cerebral WM was logically described in terms of large regional patterns (e.g., *centrum semiovale, corona radiata, sagittal stratum, internal, external and extreme capsules*). Vieussens described the WM region located above the lateral ventricles and the corpus callosum, the *centrum semiovale* in relation to its semioval shape (**Figure 1D**). The *corona radiata*, often referenced as the ventral continuum of the *centrum semiovale*, was considered by Reil as the "longitudinal" component of the WM with a radiating aspect in the sagittal view, in contrast to the "transverse" corpus callosum (Reil, 1809). Mayo translated the Reil description of the corona radiata as follows: "*The fibers derived from the crus cerebri, which diverge at the upper margin of the thalamus towards the circumference of either hemisphere, form the fibrous cone (English term used by*

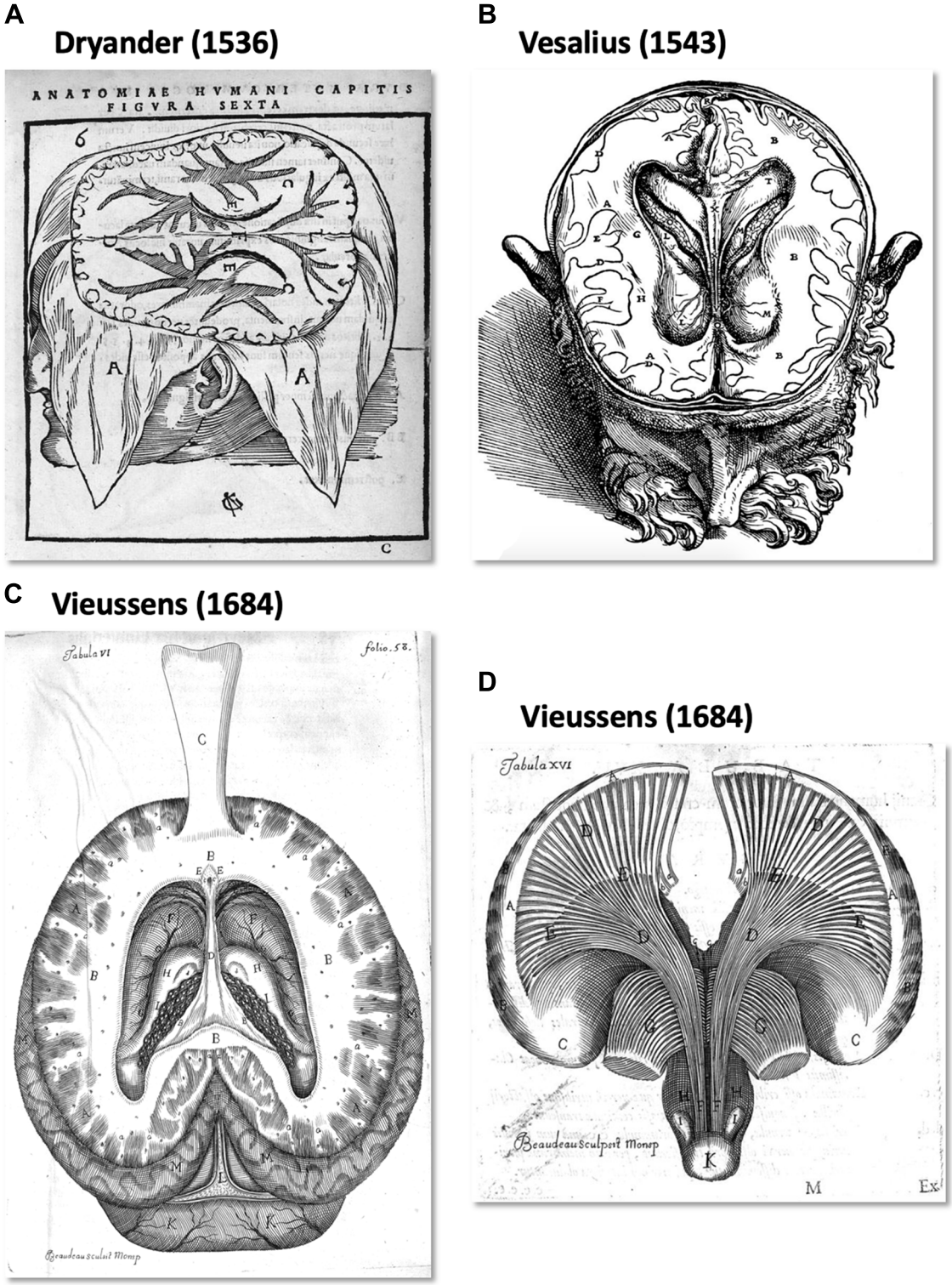

FIGURE 1 | The first illustration of brain anatomy reveals the gross white matter (WM) organization. **(A)** One of the first representations of cerebral circumvolution superficial to the WM in *Anatomica Capitis Humani* (Dryander, 1536). **(B)** Horizontal slice of a human head showing the lateral ventricles, the WM and (less precisely) the gray matter (GM) in *De Humani Corporis Fabrica Libri Septem* (Vesalius, 1543). **(C,D)** Tabula VI and XV of Vieussens's (1684) *Nevrographia universalis*, respectively. **(C)** A superior section of the human brain at the level of the *centrum ovale* (B) after exposing and folding forward the corpus callosum (C) and **(D)**, the WM tracts projecting from the *centrum ovale* (A) through the *corpora striata* (C,E).

Mayo for corona radiata"; Mayo, 1823). Currently, the *corona radiata* is described as a WM sheet composed of ascending and descending projection fibers, namely, the corticopontine, corticobulbar and corticospinal tracts and the different thalamo-cortical peduncles.

The term "capsule" was also introduced to refer to the bands of WM that pass between cortical and subcortical structures. The internal capsule was first denominated by Burdach (1822) but inspired by Reil (1809), who used the term "*inner wall of capsule*." It is located between the caudate nucleus and the lenticular nucleus (anterior limb or *crus anterius*) and between the thalamus and the lenticular nucleus (posterior limb or *crus posterius*). The external capsule (EC) is located between the lenticular nucleus and the claustrum, while the extreme capsule is located between the insula and the claustrum (Burdach, 1822).

Beyond this regional terminology, Vicq d'Azir introduced the French term "*faisceau*" (in Latin, "*fasciculus*," and in English, "*fascicle*" or "*bundle*") as a cluster of fibers or filaments (Vicq d'Azyr, 1786). Therefore, novel approaches to the gross dissection of brain internal structures led to a new understanding of the WM organization, notably thanks to the works published in the 1800s by Reil (1809), Gall and Spurzheim (1810–1819) and Burdach (1822), highlighting the fascicular organization of the WM. The blunt dissection of fiber bundles performed by Gall and Spurzheim remarkably showed that the WM consists of tracts connecting cortical GM regions that these researchers considered to be the organ of mental activity (Gall and Spurzheim, 1810–1819). It was finally Burdach who defined and designated clearly, through gross dissection studies between 1819 and 1826, the main association pathways, namely, the cingulum, the uncinate fascicle (UF), the arcuate/superior longitudinal fascicle and the inferior longitudinal fascicle (ILF; Burdach, 1819–1826). Subsequently, Meynert made the final distinction between the fibers of association connecting intrahemispheric cortical regions, the fibers of projection connecting a cortical region to a subcortical GM nucleus and the commissural fibers connecting similar regions between both hemispheres (Meynert, 1888).

The enduring anatomical work of Dejerine and Dejerine-Klumpke at the turn of the 20th century describing the WM pathways in detail has therefore been the preeminent authority for over a century (Dejerine and Dejerine-Klumpke, 1895, 1901). Additional association bundles missing in Dejerines' work were also described early in the 20th century, such as the inferior fronto-occipital fascicle (IFOF; Trolard, 1906; Curran, 1909). The association tract description has therefore been sporadically enriched thanks to the technique of fiber dissection in postmortem human brains, first described by Klingler (Ludwig and Klingler, 1956) and more recently improved (Martino et al., 2011). Based on the freezing of the brains during the fixation process, the cortex-sparing Klingler blunt dissection technique is currently the only technique capable of directly studying the fiber tracts in the human brain at the macroscopic level.

The Current Status of WM Terminology

Some debates are still ongoing regarding the terminology of the different gyri and sulci of the human cerebral cortex (see in this Research Topic, ten Donkelaar et al., 2018b). However, there is a better consensus for describing the human cortex in terms of gyri and sulci than for describing the WM fiber tracts that link the cortical structures.

The gross dissection, myelin-stained or degeneration techniques used in the 1800s and early 1900s allowed descriptions of the fascicular organization of the WM and the naming of some of the major association bundles either in relation to the cortical structure they connect (e.g., *IFOF, corticospinal tract*) or in relation to their shape (e.g., *UF, arcuate fascicle, cingulum*) and/or their location (e.g., *superior and ILFs*). **Table 1** shows how the standard terms used to describe the different bundles have numerous early synonyms and translations that have added to the confusion regarding their description. Although there is still intense debate even about their existence, all these fascicles are named in a confusing way in the current literature, especially with the emergence of DWI-based tractography and the resultantly tremendous increase in WM tract descriptions in the last decade.

Also appearing during the second half of the 19th century but truly emerging as the gold standard for studying brain neuroanatomy at the beginning of the 1970s, the tracing of neural pathways is considered to provide access to the ground truth of structural brain connectivity. Tracer studies inject compounds into the live brain and allow the compounds to disperse by means of axonal transport, marking individual axons over long-range distances. However, these studies can map only a fraction of a neural pathway and are not feasible in humans. A great deal of work has been achieved by such invasive tracing studies in monkeys (Schmahmann and Pandya, 2006). However, a first drift was committed by using the knowledge of the wiring diagram from tract tracing in the monkey as a basis for the classification and functional significance of WM pathways of the human brain (see, for example, Chapter 28 in Schmahmann and Pandya, 2006). A second drift was literally terminological, as some bundles first named in humans based on their shape were also named in the same manner in nonhuman primates but did not show the same shape. In fact, the arcuate fasciculus (AF) was first described and named in humans with regard to the arcuate shape of its fibers connecting the inferior frontal cortex to the caudal superior temporal and middle temporal cortices (Burdach, 1819–1826; Dejerine and Dejerine-Klumpke, 1895). The bundle carrying the fibers from the homologous cortical areas in the macaque monkey has also been denominated the AF but does not show a so-arched shape due to the location and orientation of the temporal lobe in the monkey (Schmahmann and Pandya, 2006; Yeterian et al., 2012). The lack of a consistent connection between the caudal temporal cortex and the inferior frontal cortex in the macaque monkey even led to questioning the existence of the AF in the monkey (Dick and Tremblay, 2012). In fact, as it is now well recognized that, although showing strong similarities, WM pathways in the macaque monkey cannot be considered as the ground truth of human neuroanatomy, especially regarding the association pathways that connect frontal territories, which have undergone a considerably more recent phylogenetic development in humans (Thiebaut de Schotten et al., 2012). As a direct consequence of

TABLE 1 | Synonyms and translation of the terms used to describe the main associated fascicles, adapted from Swanson (2015) *Neuroanatomical terminology—A lexicon of Classical Origins and Historical Foundations*.

General name and definition	Earlier synonyms and/or translation
Cingulum (Cing)	- *tenia tecta* (Reil, 1809), Latin form of the term in German, *bedeckten Bänder*, used by Reil; also translated in English as *covered band* (Mayo, 1823); - *lateral longitudinal striae* (Meckel, 1817); - *fillet of the great commissure* (Mayo, 1823); - *peripheral part of the fornix* (Arnold, 1838); - *external fornix* (Arnold, 1838);
External capsule (EC)	- *capsula externa* (Burdach, 1822), original Latin form of the EC first clearly illustrated by Vesalius (1543); - *corporis striati limbus anterior* (Willis, 1672); - *exterior smaller medullary tract of the anterior process of the medulla oblongata* (Vieussens, 1684); - *medullary capsule of the lentiform nucleus* (Arnold, 1838);
Inferior fronto-occipital fascicle (IFOF)	- *inferior longitudinal fascicle* (Trolard, 1906);
Inferior longitudinal fascicle (ILF)	- *fasciculus longitudinalis inferior* (Burdach, 1822), original Latin form of the ILF, perhaps first clearly delineated by Reil (1809); - *longitudinal fascicle arising from the inferior part of the corona radiata* (Arnold, 1838); - *temporo-occipital fasciculus* (Trolard, 1906);
Superior longitudinal fascicle—Arcuate fascicle (SLF/AF)	- *intermediate white matter* (Reil, 1809), first description of a macrodissected adult human SLF; in the original German, *intermediäre Marksubstanz*; - *arcuate fasciculus* (Burdach, 1822); - *longitudinal striae of Reil* (Rolando, 1831); - *lateral longitudinal striae* (Rolando, 1831); - *superior longitudinal commissure* (Solly, 1836); - *longitudinal fascicle of the corona radiata* (Arnold, 1838);
Uncinate fascicle (UF)	- *unciform fascicle* (Reil, 1809), first description of a macrodissected adult human UF; in the original German, *haakenförmige Markbundel*; - *fasciculi unciformes* (Burdach, 1822); - *hamular fasciculus* (Mayo, 1823); - *white nucleus of the Sylvian fossa* (Treviranus and Treviranus, 1816–1821); - *anteromedial arch* (Rolando, 1831); - *olfactory arch* (Rolando, 1831);

the odyssey in WM neuroanatomical knowledge and interspecies analogy, many historical denominations of the different bundles are today more confusing than ever. Depending on whether a bundle coexists in monkeys and humans, different names can be used for labeling the same pathways in monkeys and humans, e.g., the extreme capsule vs. the inferior fronto-occipital fasciculus (Schmahmann and Pandya, 2006; Makris and Pandya, 2009). Some previously described association pathways have also been more recently shown to potentially be methodological artifacts. For example, the superior fronto-occipital fasciculus is now considered to not exist in the human brain after having inherited several terminologies from animal studies, namely, the Muratoff or subcallosal fasciculus (Forkel et al., 2014; Meola et al., 2015; Bao et al., 2017). In the same vein, the initial name of a bundle has sometimes been generalized to describe an extension of the initial pathway, without a semantic relationship with the genuine pathway. Indeed, the "vertical portion of the superior longitudinal fasciculus" may be considered as an oxymoron (Bartsch et al., 2013; Martino and García-Porrero, 2013). Finally, new classifications or nomenclatures based on functional rather than anatomical criteria have led to a confusing description of the same anatomical structures. For example, the joint description of the peri-sylvian language pathways vs. the tripartite superior longitudinal fascicles (SLFI, II, III) is more often used to describe WM pathways related to visuo-spatial functions (Catani et al., 2007; Thiebaut de Schotten et al., 2011a,b). The former introduced the description of an anterior segment of the AF (AFas), which carries fronto-parietal fibers that are also considered part of the SLFIII. This led to a confusing situation in which different studies alternatively described their results in terms of AFas or SLFIII depending on whether they dealt with language or spatial functions (Gharabaghi et al., 2009). The AF has also been renamed for some time as the fourth subdivision of the superior longitudinal fasciculi (SLF IV, Makris et al., 2005) but does not have a longitudinal trajectory like those of the three other SLF branches. Hence, progress in our understanding of WM has been hampered by a nomenclature using a wealth of different rules, methods and different species, leading to contradictions and inevitable confusion (see for example the terminology used in the Terminologia Neuroanatomica (TNA; ten Donkelaar et al., 2018a)).

General Features of the Organization of the Association Pathways of the Human Brain

Association fibers interconnect different cortical areas within the same hemisphere. They are usually subdivided into short and long association fibers. Short association fibers remain within the cortical GM or only pass through the superficial WM between neighboring cortical areas by forming U-shaped fibers around the sulci. Meynert's pioneering work on WM pathways was the first to differentiate short U-shaped fibers and long association fibers (Meynert, 1892). As specified by

the Dejerine" the direction of the U-shaped fibers is always perpendicular to the main axis of the sulcus they cover (Dejerine and Dejerine-Klumpke, 1895). They later reported the following: "*The U-shaped fibers are not generally referred to by a specific name: if, however, for the sake of clarity of the description of a microscopic anatomo-pathological examination, we wish to designate them more especially, it seems to us that the name of the sulcus or the fissure which they cover is the best*." From a quantitative point of view, the number of U-shaped fibers appears to overwhelm the one of the long-range association fibers in the human brain by at least a factor of 10 (Schuz and Braitenberg, 2002). Although such counts have been estimated based on several assumptions that need confirmation, these authors suggest that only approximately 2% of the total intrahemispheric number of cortico-cortical fibers corresponds to long-rang association fibers, which is the same number as that in the callosal system.

General rules, likely resulting from the biophysics of brain development at the individual level and/or genetic evolution at the species level, have been observed that can help to unravel the complex organization of WM pathways. A debate about the existence of sheet structures in the brain pathways has recently received much attention from the neuroscience and diffusion magnetic resonance imaging communities (Catani et al., 2012a; Wedeen et al., 2012a,b). Wedeen et al. (2012b) proposed that WM fibers form a regular grid by crossing almost orthogonally and uniformly in the entire brain. Although presented as consistent with embryogenesis, such a geometric structure was more mathematically specific than a real characteristic of the brain pathways, and the brain grid theory has not been supported by the evidence (Galinsky and Frank, 2016; Tax et al., 2017). In the same vein, a recent study showed that a dMRI finding thought to be caused by fiber crossings may rather result from sharp turns and/or arborization of fibers than a true crossing between two types of fibers (Mortazavi et al., 2018). Interestingly, and somehow contradicting this claim, Galinsky and Frank (2016) have shown that the overall fiber tract structures of the human brain appear to be more consistent with a small angle treelike branching of tracts forming a lamellar vector field. At the mesoscopic level, this finding is consistent with the laminar origin of cortico-cortical connections demonstrated in nonhuman primates (Barbas, 1986). At the macroscopic level, this propensity for lamellarity in human brain fiber pathways is reminiscent of what the dissectionists "*à la Klingler*" know, and they progress sequentially in a lateromedial direction (Martino et al., 2011). Dissectionists first expose the shorter U-shaped fibers between adjacent gyri, then layer after layer they remove longer fibers between more distant gyri up to the longest bundles (De Benedictis et al., 2012, 2014; Sarubbo et al., 2013, 2016; Fernández-Miranda et al., 2015; Wang et al., 2016; Hau et al., 2017).

Such a practice leads to the consideration of some reliable organizational rules that are useful to apprehend the whole organization of association fibers. One rule is to consider that the long-range fascicles can be defined by their "stem" (Sarubbo et al., 2013; Hau et al., 2016, 2017). The stem is the bottleneck where fibers converge, running all together densely packed over a few centimeters, before fanning in a dispersed manner towards their cortical sites of destination. The stem-based approach applied to diffusion MRI allows virtually dissecting a specific bundle at its densest part, where there are no crossings or too-sharp turns of fibers. In fact, almost all WM regions consist of interdigitated fibers that cross, bend and fan out (Jeurissen et al., 2013; Jones et al., 2013).

Another rule is to consider that the position of the different long association fibers follows a lateromedial organization depending on their length, e.g., the deeper the fibers in the core of the WM, the more distant the two interconnected areas (Curran, 1909; Sarubbo et al., 2016).

TOWARDS A COMMON TERMINOLOGY FOR LONG-RANGE ASSOCIATION FIBERS IN HUMANS

From a general point of view, we propose to classify the long-range association bundles in a hierarchical manner based on the way in which the different distant parts of the same hemisphere can be connected to each other. Due to obvious anatomic constraints, such as the presence of lateral ventricles and subcortical gray nuclei, association fibers connecting one cortical region to another cannot pass anywhere. In fact, both efferent and afferent long-range association fibers connecting the frontal lobe with the parietal, occipital and temporal cortices have only two options of passage, either superiorly at the level of the corona radiata above the superior limiting sulcus of the insula or inferiorly at the level of the inferior limiting sulcus of the insula, within the external/extreme capsule. This situation leads the present stem-based nomenclature to define two major longitudinal systems (superior longitudinal system (SLS), inferior longitudinal system (ILS)) aligned along an antero-posterior axis. Applying the same type of reasoning between each major part of the brain allows us to gather tracts in different systems, according to the global location and orientation of their stems. A second numerical attribute will complement the first level of the hierarchy to more precisely identify the cortical areas connected by the fasciculi. Following this principle, we made an inventory of seven systems that are illustrated in **Figures 2**, **3** and summarized in **Figure 4**:

- The superior longitudinal system (SLS)
- The inferior longitudinal system (ILS)
- The middle longitudinal system (MidLS)
- The basal longitudinal system (BLS)
- The mesial longitudinal system (MesLS)
- The anterior transverse system (ATS)
- The posterior transverse system (PTS).

Each of these systems will be now detailed and put in perspective with the current terminology.

Superior Longitudinal System (SLS, Figure 2)

The SLS gathers the fibers connecting the frontal cortex to the parietal, occipital and temporal cortices by passing through the

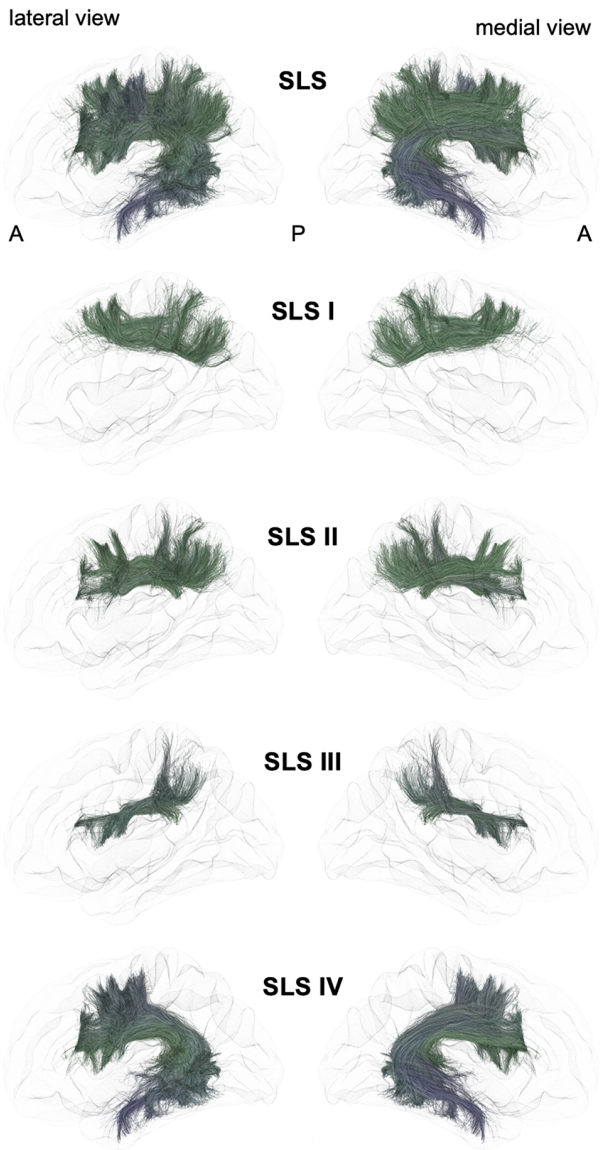

FIGURE 2 | Schematic lateral and medial views of the superior longitudinal system (SLS) and its four different branches. A: anterior, P: posterior. Note that the schematic bundle views were derived from the diffusion tractography data of 42-year-old right-hander male participants of the BIL&GIN database (Mazoyer et al., 2016). Diffusion imaging and whole brain tractography have been detailed in De Benedictis et al. (2016). Briefly, fiber tracking was performed using particle-filter tractography with anatomical priors (Girard et al., 2014) and seeding initiated from the WM/GM interface (10 seeds/voxel). The different association bundles were therefore segmented manually with regions of interest (ROIs) based on the guidelines provided in previous studies (Zhang et al., 2010; Hau et al., 2016, 2017; Rojkova et al., 2016).

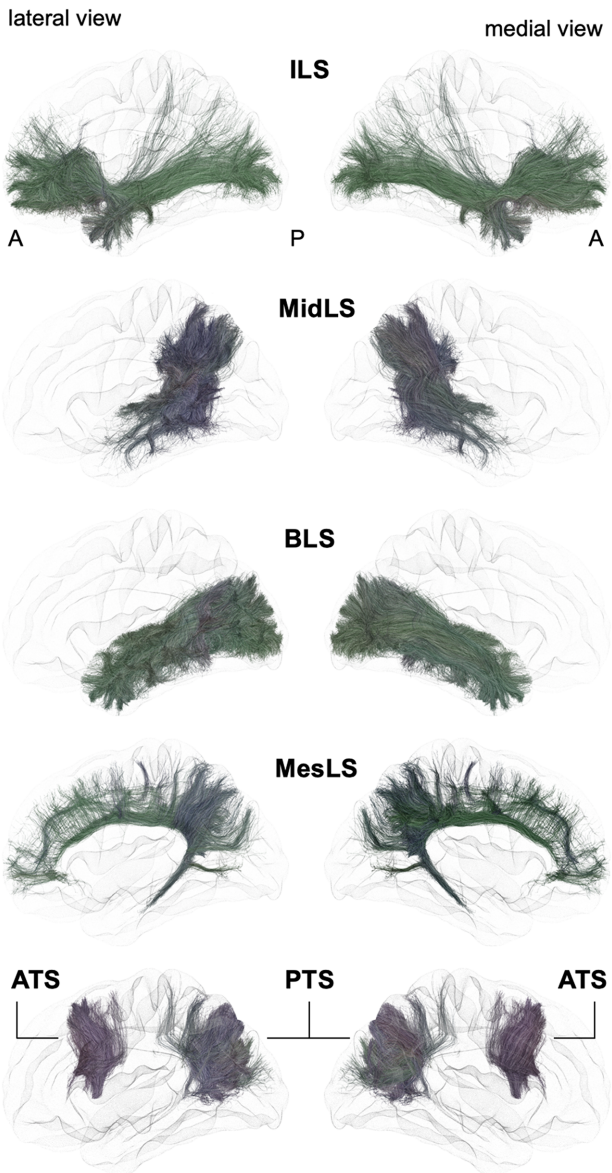

FIGURE 3 | Schematic lateral and medial views of the inferior longitudinal system (ILS), middle longitudinal system (MidLS), basal longitudinal system (BLS), mesial longitudinal system (MesLS), anterior transverse system (ATS) and posterior transverse system (PTS). A: anterior, P: posterior. See **Figure 2** for details.

corona radiata above the superior limiting sulcus of the insula. The SLS comprises the three superior longitudinal fasciculi (SLF I–III) and the AF. Because its stem also belongs to the SLS, the AF is considered to be part of the SLS, albeit the connections of the AF are exclusively fronto-temporal. The fronto-parietal part of the SLS, classically named the "superior longitudinal fasciculus," has been first described by tracing studies in monkeys (Schmahmann and Pandya, 2006) and described as topographically organized in a very similar way in humans (Thiebaut de Schotten et al., 2011a, 2012; Rojkova et al., 2016; Wang et al., 2016; Parlatini et al., 2017). We will successively detail these fronto-parietal connections of the SLS and then the fronto-temporal connections.

The First Branch of the SLS (SLS I)

A dorso-mesial branch of the SLS (**Figures 2**, **4**), joining the superior frontal gyrus with the superior parietal lobe and previously referred to as the first branch of the superior

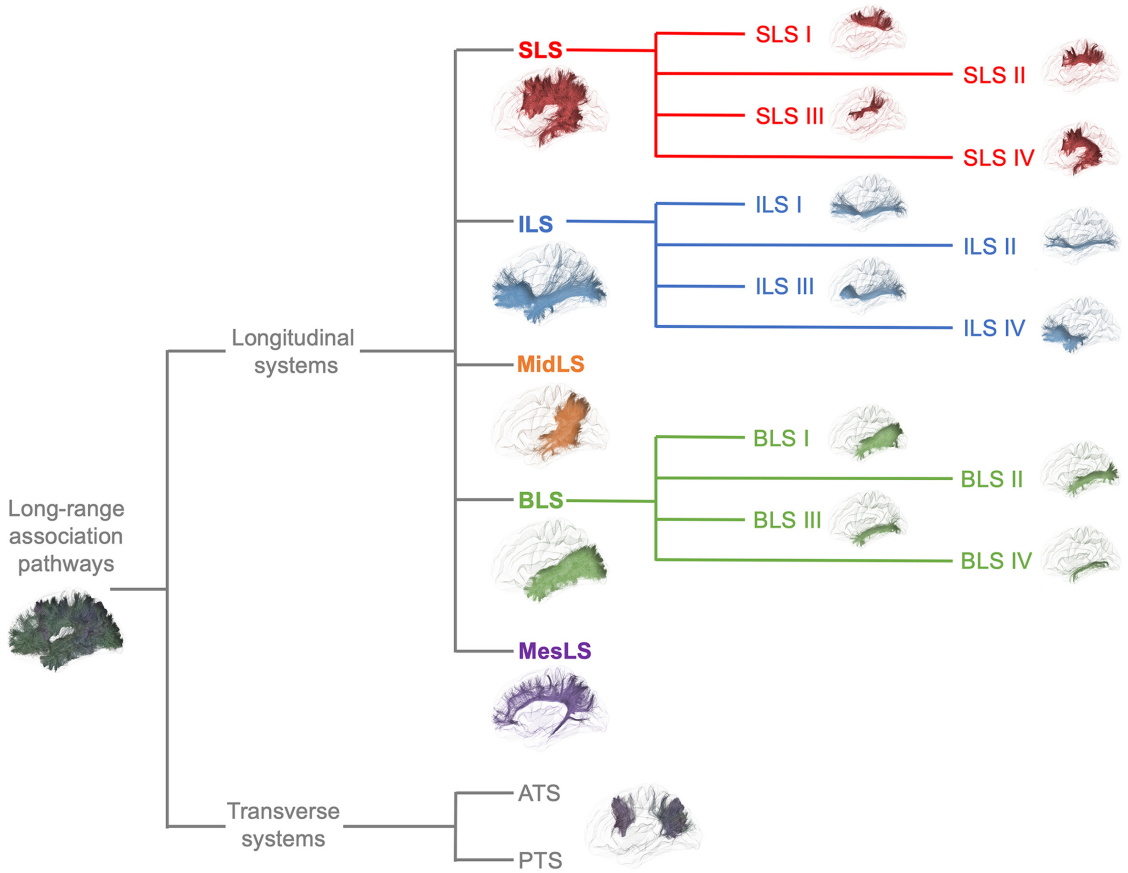

FIGURE 4 | Summary of the proposed nomenclature of the seven main systems of human WM association pathways. The schematic left lateral views of the different systems and sub-systems were derived from the same diffusion tractography data that in **Figures 2**, **3**. See text for details about the terminology and its numbering.

longitudinal fasciculus (SLF I), was first manually delineated on colored-fractional anisotropy maps (Makris et al., 2005). This work was largely inspired by the knowledge coming from monkey tracing studies. However, the described trajectory, running within the gyral WM of the superior frontal gyrus, was shown to be unrealistic (Maldonado et al., 2012). The SLS I was finally defined as the more dorsal and mesial branches of the SLS (Thiebaut de Schotten et al., 2012), connecting the superior frontal gyrus with the superior parietal lobule but running across the corona radiata above the cingulate sulcus. These characteristics allowed differentiating the SLS I from the cingulum, located medially to the corona radiata, below the cingulate sulcus. Hence, the importance of analyzing coronal views when depicting the SLS I cannot be overemphasized: for example, in the study of Kamali et al. (2014), the trajectory of the SLS I corresponds to a branch of the cingulum (Kamali et al., 2014), as also found by Wang et al. (2016). Many other studies are inconclusive regarding the accurate anatomical trajectory of the SLS I, as no coronal slices were provided (Jang and Hong, 2012; Vallar et al., 2014; Yagmurlu et al., 2016; Wang et al., 2016; Fitzgerald et al., 2018). Of note, the stem should also pass below the central sulcus, another property that can be properly analyzed only in the coronal view.

The Second Branch of the SLS (SLS II)

The second branch of the SLS (**Figures 2**, **4**) links the middle frontal gyrus with the angular gyrus and posterior part of the supramarginal gyrus and corresponds to the SLF II (Makris and Pandya, 2009; Thiebaut de Schotten et al., 2011a; Wang et al., 2016). Such connectivity is in very good agreement with the findings of electrophysiological connectivity studies relying on the methodology of cortico-cortical evoked-potentials (Matsumoto et al., 2012).

The Third Branch of the SLS (SLS III)

The third branch of the SLS (**Figures 2**, **4**) is the most ventral and lateral branch and corresponds to SLF III. It is also the shortest branch, as it links the anterior part of the supramarginal gyrus with the ventral part of the precentral gyrus and the posterior end of the inferior frontal gyrus (Makris and Pandya, 2009; Thiebaut de Schotten et al., 2011a; Wang et al., 2016).

The Arcuate Branch of the SLS (SLS IV)

The AF belongs to the SLS because of its stem, which runs parallel and ventrally to the other branches of the SLS (**Figures 2**, **4**). However, the posterior endings of the AF in the temporal lobe dictate its curvature around the posterior insular point, from

which its name was derived by pioneering anatomists from Burdach (1822) to Dejerine and Dejerine-Klumpke (1895).

The advent of virtual dissection by diffusion MRI tractography led some authors to gather some short-distance fronto-parietal and parieto-temporal connections under the arcuate terminology. Indeed, a very confusing tractographic study coined the terms "direct" and "indirect" pathways (Catani et al., 2005), both being assigned to the arcuate nomenclature. In fact, the so-called anterior short indirect horizontal segment is none other than the SLF III also defined by the same authors (Thiebaut de Schotten et al., 2011a). It would be anatomically irrelevant to keep the posterior short indirect vertical segment within the arcuate or SLS taxonomy. It should be more naturally referred to as the vertical temporo-parietal fasciculus (VTPF) at the anterior part of the PTS (see below).

A combined fiber dissection and tractography study further subdivided the AF according to the cortical endpoints at both ends (Fernández-Miranda et al., 2015).

The Case of the Superior Occipito-Frontal Fasciculus

Finally, to the best of our knowledge, fronto-occipital connections have not been reported within the SLS, except for one study showing SLF connections extending to the most anterior and superior part of the occipital lobe (Forkel et al., 2014). There has been a longstanding controversy regarding the existence of a superior occipito-frontal fasciculus in humans, whose putative stem would have been located, by analogy with the monkey anatomy, at the angle between the corpus callosum and the caudate nucleus, in close relationship with the cortico-striatal tract (also called the subcallosal fasciculus or Muratoff bundle; Schmahmann and Pandya, 2007). The putative SOF has never been evidenced by any dissection studies (Ture et al., 1997; Meola et al., 2015; Bao et al., 2017), but the controversy is still ongoing, and a recent tractographic study suggested that if such a tract existed, it would, rather, be a fronto-parietal one (Bao et al., 2017). In fact, it seems that such a bundle could be a remnant of a fetal pathway that could play a role in axonal guidance during a specific temporal window of brain development, explaining its involution in postnatal brain development and the difficulty in identifying this remnant in adult brains by dissection and tractographic studies (Vasung et al., 2011).

Inferior Longitudinal System (ILS)

Following the terminology of the SLS, we designate the ILS (**Figures 3**, **4**) as the connections between the frontal cortex and the parietal, occipital and temporal cortices that pass below the level of the inferior limiting sulcus of the insula, within the floor of the external/extreme capsule. This system thus comprises the uncinate fasciculus and the currently named inferior fronto-occipital fasciculus. While the former name was chosen purposely by Reil (1809) to describe the three-dimensional hooked shape of the pathway, the latter inherited a misnomer from its first description. Indeed, in its seminal description, Curran (1909) wrote the following: "*The fasciculus occipito-frontalis inferior is a large associating bundle of fibers uniting, as its name indicates, the occipital with the frontal lobe. It also contains fibers that join the frontal lobe with the posterior part of the temporal and parietal lobes*." Of note, three years before, the very same fasciculus was coined the "inferior longitudinal fasciculus" by the French anatomist Trolard (1906), who preferred to call the 'temporo-occipital fasciculus" what is currently termed the "inferior longitudinal fasciculus" (see below the description of the BLS). It should be mentioned that because occipito-frontal connections running through the floor of the external/extreme capsule have never been described in monkeys, the existence of the IFOF has been questioned by authors extrapolating the human anatomy from the monkey anatomy. However, there may be a terminological misunderstanding, and by shedding light on the exact nature of fibers under different names, we may reconcile the two worlds. As mentioned by Curran, the so-misnamed IFOF also includes branches from the frontal lobe towards the caudal part of the temporal cortex. The trajectory of such fibers through the floor of the external/extreme capsule corresponds exactly to the connections named "extreme capsule fiber systems" in monkeys, which are made of fibers joining the frontal and temporal lobes. Moreover, some connections assigned to the middle longitudinal fasciculus in monkeys have been shown to link the frontal and parietal lobes by running through the extreme capsule (Schmahmann and Pandya, 2006), thus making such connections very similar to the fronto-parietal branches of the IFOF. In sum, it seems that the extreme capsule fiber system in monkeys may be conceptually and anatomically part of the IFOF described in humans. However, it must be acknowledged that the existence of true direct occipito-frontal connections in humans remains to be proven by cortico-cortical evoked-potentials, or by any other methodology that would not be subject to false positives, as is the case for gross fiber dissections and tractography in the region lateral to the optic radiations, where it is almost impossible to separate the middle longitudinal fasciculus, inferior longitudinal fasciculus and occipital branches of the presumed IFOF with reliability. From a functional point of view, it is tempting to point out the specific existence of very posterior branches of the IFOF (i.e., in the basal part of the temporo-occipital junction in the fusiform gyrus and in the occipital lobe) in humans as one of the key factors that laid the foundation for the emergence of the human ability to manipulate formal concepts, such as semantic knowledge and its verbal embodiment in language.

In sum, we propose relinquishing the confusing terminology of IFOF and extreme capsule fibers and subsuming under the term "ILS" all fibers coming from the temporal, parietal or occipital lobes, converging at the level of the anterior floor of the external/extreme capsule, and then spreading all over the frontal lobe.

The Different Branches of the ILS

For the medio-lateral SLS numerical organization, we propose to distinguish four parts, ILS I–IV, by dividing the frontal terminations of the ILS into four medio-lateral portions (**Figure 4**).

ILS I–III would encompass the longest fibers connecting ventrally the frontal lobe with the parietal, occipital and temporal cortices, namely, the fibers referred to as the IFOF (Hau et al.,

2016; Panesar et al., 2017). The most medial branch with frontal terminations in the most medial third of the frontal lobe would delineate ILS I, while ILS II would comprise the fibers of the inner third of the frontal lobe and ILS III the branches with frontal terminations in the most lateral third of the frontal lobe. There is no current agreement on the posterior terminations of ILS I, II and III (Caverzasi et al., 2014; Hau et al., 2016; Wu et al., 2016; Panesar et al., 2017). Again, this is due to the high degree of overlapping of the posterior terminations of the ILS with the optic radiations, ILF and middle longitudinal fasciculus (MdLF). Moreover, there is also a crossing with the temporo-basal endings of the arcuate fibers.

The fourth branch of the ILS is more commonly referred to as the UF. Most studies agree on its anatomical trajectory, arching around and above the vallecula of the sylvian fissure. Fiber dissection revival started with the work of Ebeling and von Cramon (1992), who detailed different subcomponents, which have also been demonstrated more recently in combined dissection and diffusion tractography studies (Leng et al., 2016; Hau et al., 2017; Panesar et al., 2017).

Middle Longitudinal System (MidLS, Figure 3)

Contrary to the main association bundles originally macrodissected in humans, the MdLF was first characterized in monkeys. Tracing studies have demonstrated this bidirectional tract, linking the anterior temporal lobe with the inferior parietal lobule. In their monography, Schmahmann and Pandya (2006) also include within the MdLF some fibers linking the lateral and orbital prefrontal cortices with the temporo-parieto-occipital (TPO) area and passing through the extreme capsule. Anatomically speaking, it would have been more coherent to associate such connections with the extreme capsule fiber system, and we assign such connections to the ILS in the new nomenclature (see above).

A diffusion tractography study first reported the existence of the MdLF in humans (Makris et al., 2009, 2013), soon after confirmation by its first dissection (Maldonado et al., 2013) and diffusion tractography studies (Menjot de Champfleur et al., 2013; Wang et al., 2013). The anterior part runs within the WM of the superior temporal gyrus. When reaching the level of the AF posteriorly, the MdLF changes its orientation from the axial plane to the sagittal plane. In its posterior part, the MdLF merges with the deepest fibers of the ILS, rendering both dissection and diffusion tracking complicated. Thus, it is not surprising that there are some discrepancies regarding the posterior cortical terminations of this tract. Most authors agree on the connections with the angular gyrus, while others mainly report connections with the superior parietal lobule and parieto-occipital region (Wang et al., 2013). Interestingly, six different branches of fiber connections of the human MdLF have been recently described, four of which are temporo-parietal and two of which are temporo-occipital (Makris et al., 2017). Following the current nomenclature, they may be considered as different middle longitudinal system (MidLS) branches, but further studies including specific microdissection of these different branches are required before their full description.

Basal Longitudinal System (BLS, Previously Named "ILF", Figure 3)

There is a longstanding controversy regarding the so-called "inferior longitudinal fasciculus," a long association pathway running in the ventral part of the temporal and occipital lobes. Its first description dates back to 1809 by anatomist Reil, but the term "inferior longitudinal fasciculus" was coined by Burdach (1822). Subsequently, in 1906, Trolard coined the term "occipito-temporal pathway." The existence of this pathway was questioned a few years later (Davis, 1921). Another study combining dissections in humans and radiographic studies in monkeys further argues that the long fibers of the ILF belonging to the external sagittal stratum are nothing but optic radiations (Tusa and Ungerleider, 1985). These authors introduced the concept of the occipito-temporal *system*, which consists of successive series of U-fibers. The first tractographic study focusing on occipito-temporal connections provided evidence for the coexistence of both a series of U-fiber systems and a direct link between the temporal pole to the occipital pole (Catani et al., 2003). At the same time, a fiber dissection study located such direct connections rather inferiorly to the external sagittal stratum, almost within the WM of the fusiform gyrus (Peuskens et al., 2004). Finally, the most recent dissection and tractographic studies subdivided the long-range connections of the occipito-temporal system into several components, according to their posterior occipital terminations (Sarubbo et al., 2016; Latini et al., 2017; Panesar et al., 2018), which follow a multilayered functional organization (Herbet et al., 2018). We thus propose that the present BLS may be subdivided into four branches (BLS I–IV, **Figure 4**):

- BLS I, linking the temporal cortex to the lateral occipital gyri;
- BLS II, linking the temporal cortex to the cuneus;
- BLS III, linking the temporal cortex to the lingual gyrus;
- BLS IV, linking the temporal cortex within the fusiform gyrus.

Mesial Longitudinal System (MesLS, Figure 3)

The mesial longitudinal system (MesLS) comprises connections all along the medial surface of the hemisphere, arching from the frontal pole up to the amygdala area. It may essentially comprise two branches:

- Its first branch (MesLS I or "inner cingulum") corresponds to the cingulum *per se*. There is a wide agreement on the trajectory of this long associative tract, running in the WM of the cingulate gyrus, arching around the splenium of the corpus callosum at the level of the cingulate isthmus, and joining at this level the parahippocampal gyrus, within which it continues its course towards the amygdala.
- The second branch (MesLS II or "outer cingulum") remains hypothetical. It would correspond to an "outer" part of the anterior cingulum. It has been recently discovered by a diffusion tractography study, which needs additional confirmation from postmortem dissection (David et al., 2018). In essence, such connections are very similar to what some authors call the supracingulate pathway (Wang et al., 2016).

Anterior Transverse System (ATS, Previously Named "Aslant", Figure 3)

In 2008, a DTI tractography study described for the first time an associative fiber complex, which interconnects the SMA/pre-SMA of the medial superior frontal cortex to the sus-sylvian precentral gyrus, and the *pars triangularis* and *opercularis* of the inferior frontal gyrus (Lawes et al., 2008). Following this seminal report, this fiber system was further described (Ford et al., 2010; Kinoshita et al., 2012; Vergani et al., 2014a) and finally named the frontal aslant tract (FAT; Catani et al., 2012b; Thiebaut de Schotten et al., 2012). In this latter study, it was also shown that the posterior end of the superior, middle and inferior frontal gyrus constituted a network, with the FAT and U-fibers linking any two pairs of these 3 cortical sites. Following the hierarchical principle of the proposed nomenclature, the ATS can be subdivided into several branches (ATS I–IV), from anterior to posterior, as evidenced by Ford et al. (2010):

- ATS I, first branch of the ATS joining the mesial frontal area to the most anterior part of the pars triangularis;
- ATS II, second branch of the ATS joining the mesial frontal area to the posterior part of the pars triangularis;
- ATS III, third branch of the ATS joining the pre-SMA to the pars opercularis;
- ATS IV, fourth branch of the ATS joining the SMA to the precentral gyrus.

Posterior Transverse System (PTS, Figure 3)

Mirroring the ATS, the PTS refers to the vertically oriented connectivity, linking the posterior temporo-occipital cortex to the parietal and occipital areas.

The PTS would be composed of two branches (PTS I-II):

- PTS I, located anteriorly, would correspond to connections between the middle temporal gyrus and the supramarginal and angular gyri. PTS I may also be referred to as the *VTPF*, but its inherited name from its first description (Catani et al., 2005), namely, the "posterior short vertical branch of AF," should not be used anymore. Even if it is indeed located laterally to the temporal part of the arcuate fibers, referring to this tract as a vertical portion of the AF seems rather incoherent. Moreover, recent tractographic studies have revealed some slightly deeper connections, joining the inferior temporal gyrus with the superior parietal lobule (Kamali et al., 2014; Wu et al., 2016). These deeper connections run side by side not only with the vertical part of the deepest arcuate fibers but also with the posterior end of the MdLF.
- PTS II is located more posteriorly and is intralobar. The name *vertical occipital fasciculus* (VOF) could be kept (as it perfectly describes its location and shape), while the historical name of "fasciculus of Wernicke" should no longer be mentioned. This tract has been nicely depicted by fiber dissections (Curran, 1909; Vergani et al., 2014b), as well as by tractographic studies (Yeatman et al., 2014; Wu et al., 2016). It connects the ventral temporo-occipital regions with the transverse occipital sulcus and posterior end of the intraparietal sulcus.

CONCLUSION

We propose a new hierarchical nomenclature of long associative intrahemispheric pathways, grouping the tracts into seven main systems designed according to their location and orientation as follows: superior longitudinal, inferior longitudinal, middle longitudinal, basal longitudinal, mesial longitudinal, anterior transverse and posterior transverse (**Figure 4**). Within each system, the different branches corresponding to distinct cortical endings are listed numerically. However, for some branches, their historical name may be difficult to change (SLS IV, aka AF; ILS IV, aka uncinate fasciculus; MesLS I, aka cingulum; and PTS II aka VOF). We hope that compliance with this new terminology will facilitate the clarity of future studies, especially for newcomers to the field. Finally, the existence of some of the aforementioned branches still needs to be well demonstrated, which will be accomplished by improving the current diffusion tractography tools (Maier-Hein et al., 2017) and combining them with improved cortex-sparing Klingler dissection approaches (De Benedictis et al., 2018), polarized light imaging (Axer et al., 2011), advanced techniques for labeling axon tracts (Brainbow (Weissman and Pan, 2015), and CLARITY (Chang et al., 2017); iDISCO (Renier et al., 2014)) as well as by developing unbiased new methodologies, such as cortico-cortical evoked-potentials (Matsumoto et al., 2012; Mandonnet et al., 2016).

AUTHOR CONTRIBUTIONS

EM, SS and LP co-wrote the manuscript.

ACKNOWLEDGMENTS

We are grateful to Michel Thiebaut de Schotten (Brain Connectivity and Behaviour Group, Sorbonne Universities, Paris; Frontlab, Institut du Cerveau et de la Moelle épinière (ICM), UPMC UMRS 1127, Inserm U 1127, CNRS UMR 7225, Paris, France) for his constructive reading of this manuscript.

REFERENCES

Arnold, F. (1838). *Tabulae Anatomicae. Fasciculus I. Continens Icones cerebri et Medullae Spinalis.* Turici, Impensis Orelii, Fuesslini et sociorum. 1–47.

Axer, M., Grässel, D., Kleiner, M., Dammers, J., Dickscheid, T., Reckfort, J., et al. (2011). High-resolution fiber tract reconstruction in the human brain by means of three-dimensional polarized light imaging. *Front. Neuroinform.* 5:34. doi: 10.3389/fninf.2011.00034

Aydogan, D. B., Jacobs, R., Dulawa, S., Thompson, S. L., Francois, M. C., Toga, A. W., et al. (2018). When tractography meets tracer injections: a systematic study of trends and variation sources of diffusion-based connectivity. *Brain Struct. Funct.* 223, 2841–2858. doi: 10.1007/s00429-018-1663-8

Bao, Y., Wang, Y., Wang, W., and Wang, Y. (2017). The superior fronto-occipital fasciculus in the human brain revealed by diffusion spectrum imaging tractography: an anatomical reality or a methodological

artifact? *Front. Neuroanatomy* 11:119. doi: 10.3389/fnana.2017.00119

Barbas, H. (1986). Pattern in the laminar origin of corticocortical connections. *J. Comp. Neurol.* 252, 415–422. doi: 10.1002/cne.902520310

Bartsch, A. J., Geletneky, K., and Jbabdi, S. (2013). The temporoparietal fiber intersection area and wernicke perpendicular fasciculus. *Neurosurgery* 73, E381–E382. doi: 10.1227/01.neu.0000430298.25585.1d

Burdach, K. F. (1819–1826). *Vom Baue und Leben Des Gehirns und Rückenmark.* Leipzig: Dyk.

Burdach, K. F. (1822). *Vom Baue und Leben des Gehirns.* Leipzig: Dyk.

Catani, M., Allin, M. P. G., Husain, M., Pugliese, L., Mesulam, M. M., Murray, R. M., et al. (2007). Symmetries in human brain language pathways correlate with verbal recall. *Proc. Natl. Acad. Sci. U S A* 104, 17163–17168. doi: 10.1073/pnas.0702116104

Catani, M., Bodi, I., and Dell'Acqua, F. (2012a). Comment on "the geometric structure of the brain fiber pathways". *Science* 337:1605. doi: 10.1126/science.1223425

Catani, M., Dell'Acqua, F., Vergani, F., Malik, F., Hodge, H., Prasun, R., et al. (2012b). Short frontal lobe connections of the human brain. *Cortex* 48, 273–291. doi: 10.1016/j.cortex.2011.12.001

Catani, M., Jones, D. K., Donato, R., and Ffytche, D. H. (2003). Occipito-temporal connections in the human brain. *Brain* 126, 2093–2107. doi: 10.1093/brain/awg203

Catani, M., Jones, D. K., and Ffytche, D. H. (2005). Perisylvian language networks of the human brain. *Ann. Neurol.* 57, 8–16. doi: 10.1002/ana.20319

Caverzasi, E., Papinutto, N., Amirbekian, B., Berger, M. S., and Henry, R. G. (2014). Q-ball of inferior fronto-occipital fasciculus and beyond. *PLoS One* 9:e100274. doi: 10.1371/journal.pone.0100274

Chang, E. H., Argyelan, M., Aggarwal, M., Chandon, T.-S. S., Karlsgodt, K. H., Mori, S., et al. (2017). The role of myelination in measures of white matter integrity: combination of diffusion tensor imaging and two-photon microscopy of CLARITY intact brains. *Neuroimage* 147, 253–261. doi: 10.1016/j.neuroimage.2016.11.068

Curran, E. J. (1909). A new association fiber tract in the cerebrum with remarks on the fiber tract dissection method of studying the brain. *J. Comp. Neurol. Psychol.* 19, 645–656. doi: 10.1002/cne.920190603

David, S., Heemskerk, A. M., Corrivetti, F., Thiebaut de Schotten, M., Sarubbo, S., Petit, L., et al. (2018). Superoanterior Fasciculus (SAF): novel fiber tract revealed by diffusion MRI fiber tractography. *bioRxiv* doi: 10.1101/319863

Davis, L. E. (1921). An anatomic study of the inferior longitudinal fasciculus. *Arch. Neurol. Psychiat.* 5, 370–381. doi: 10.1001/archneurpsyc.1921.02180280011002

De Benedictis, A., Duffau, H., Paradiso, B., Grandi, E., Balbi, S., Granieri, E., et al. (2014). Anatomo-functional study of the temporo-parieto-occipital region: dissection, tractographic and brain mapping evidence from a neurosurgical perspective. *J. Anat.* 225, 132–151. doi: 10.1111/joa.12204

De Benedictis, A., Nocerino, E., Menna, F., Remondino, F., Barbareschi, M., Rozzanigo, U., et al. (2018). Photogrammetry of the human brain: a novel method for 3D the quantitative exploration of the structural connectivity in neurosurgery and neurosciences. *World Neurosurg.* 115, e279–e291. doi: 10.1016/j.wneu.2018.04.036

De Benedictis, A., Petit, L., Descoteaux, M., Marras, C. E., Barbareschi, M., Corsini, F., et al. (2016). New insights in the homotopic and heterotopic connectivity of the frontal part of the human corpus callosum revealed by microdissection and diffusion tractography. *Hum. Brain Mapp.* 37, 4718–4735. doi: 10.1002/hbm.23339

De Benedictis, A., Sarubbo, S., and Duffau, H. (2012). Subcortical surgical anatomy of the lateral frontal region: human white matter dissection and correlations with functional insights provided by intraoperative direct brain stimulation. *J. Neurosurg.* 117, 1053–1069. doi: 10.3171/2012.7.jns12628

Dejerine, J., and Dejerine-Klumpke, A. (1895). *Anatomie des Centres Nerveux. Tome 1.* Paris: Rueff et Cie.

Dejerine, J., and Dejerine-Klumpke, A. (1901). *Anatomie des Centres Nerveux. Tome 2.* Paris: Rueff et Cie.

Dick, A. S., and Tremblay, P. (2012). Beyond the arcuate fasciculus: consensus and controversy in the connectional anatomy of language. *Brain* 135, 3529–3550. doi: 10.1093/brain/aws222

Donahue, C. J., Sotiropoulos, S. N., Jbabdi, S., Hernandez-Fernandez, M., Behrens, T. E., Dyrby, T. B., et al. (2016). Using diffusion tractography to predict cortical connection strength and distance: a quantitative comparison with tracers in the monkey. *J. Neurosci.* 36, 6758–6770. doi: 10.1523/JNEUROSCI.0493-16.2016

Dryander, J. (1536). *Anatomica Capitis Humani.* Marburg: Eucharium Ceruicoznum.

Ebeling, U., and von Cramon, D. (1992). Topography of the uncinate fascicle and adjacent temporal fiber tracts. *Acta Neurochir.* 115, 143–148. doi: 10.1007/bf01406373

Fernández-Miranda, J. C., Wang, Y., Pathak, S., Stefaneau, L., Verstynen, T., and Yeh, F. C. (2015). Asymmetry, connectivity, and segmentation of the arcuate fascicle in the human brain. *Brain Struct. Funct.* 220, 1665–1680. doi: 10.1007/s00429-014-0751-7

Fitzgerald, J., Leemans, A., Kehoe, E., O'Hanlon, E., Gallagher, L., and McGrath, J. (2018). Abnormal fronto-parietal white matter organisation in the superior longitudinal fasciculus branches in autism spectrum disorders. *Eur. J. Neurosci.* 47, 652–661. doi: 10.1111/ejn.13655

Ford, A., McGregor, K. M., Case, K., Crosson, B., and White, K. D. (2010). Structural connectivity of Broca's area and medial frontal cortex. *Neuroimage* 52, 1230–1237. doi: 10.1016/j.neuroimage.2010.05.018

Forkel, S. J., Thiebaut de Schotten, M., Kawadler, J. M., Dell'Acqua, F., Danek, A., and Catani, M. (2014). The anatomy of fronto-occipital connections from early blunt dissections to contemporary tractography. *Cortex* 56, 73–84. doi: 10.1016/j.cortex.2012.09.005

Galinsky, V. L., and Frank, L. R. (2016). The lamellar structure of the brain fiber pathways. *Neural Comput.* 28, 2533–2556. doi: 10.1162/neco_a_00896

Gall, F. J., and Spurzheim, J. K. (1810–1819). *Anatomie et Physiologie du Système Nerveux en Général et du Cerveau en Particulier.* Paris: Schoell.

Gharabaghi, A., Kunath, F., Erb, M., Saur, R., Heckl, S., Tatagiba, M., et al. (2009). Perisylvian white matter connectivity in the human right hemisphere. *BMC Neurosci.* 10:15. doi: 10.1186/1471-2202-10-15

Girard, G., Whittingstall, K., Deriche, R., and Descoteaux, M. (2014). Towars quantitative connectivity analysis: reducing tractography biaises. *Neuroimage* 98, 266–278. doi: 10.1016/j.neuroimage.2014.04.074

Hau, J., Sarubbo, S., Houde, J. C., Corsini, F., Girard, G., Deledalle, C., et al. (2017). Revisiting the human uncinate fasciculus, its subcomponents and asymmetries with stem-based tractography and microdissection validation. *Brain Struct. Funct.* 222, 1645–1662. doi: 10.1007/s00429-016-1298-6

Hau, J., Sarubbo, S., Perchey, G., Crivello, F., Zago, L., Mellet, E., et al. (2016). Cortical terminations of the inferior fronto-occipital and uncinate fasciculi: stem-based anatomical virtual dissection. *Front. Neuroanat.* 10:58. doi: 10.3389/fnana.2016.00058

Herbet, G., Zemmoura, I., and Duffau, H. (2018). Functional anatomy of the inferior longitudinal fasciculus: from historical reports to current hypotheses. *Front. Neuroanat.* 12:77. doi: 10.3389/fnana.2018.00077

Jang, S. H., and Hong, J. H. (2012). The anatomical characteristics of superior longitudinal fasciculus I in human brain: diffusion tensor tractography study. *Neurosci. Lett.* 506, 146–148. doi: 10.1016/j.neulet.2011.10.069

Jbabdi, S., Sotiropoulos, S. N., Haber, S. N., Van Essen, D. C., and Behrens, T. E. (2015). Measuring macroscopic brain connections *in vivo*. *Nat. Neurosci.* 18, 1546–1555. doi: 10.1038/nn.4134

Jeurissen, B., Leemans, A., Tournier, J. D., Jones, D. K., and Sijbers, J. (2013). Investigating the prevalence of complex fiber configurations in white matter tissue with diffusion magnetic resonance imaging. *Hum. Brain Mapp.* 34, 2747–2766. doi: 10.1002/hbm.22099

Jones, D. K., Knösche, T. R., and Turner, R. (2013). White matter integrity, fiber count, and other fallacies: the do's and don'ts of diffusion MRI. *Neuroimage* 73, 239–254. doi: 10.1016/j.neuroimage.2012.06.081

Kamali, A., Flanders, A. E., Brody, J., Hunter, J. V., and Hasan, K. M. (2014). Tracing superior longitudinal fasciculus connectivity in the human brain using high resolution diffusion tensor tractography. *Brain Struct. Funct.* 219, 269–281. doi: 10.1007/s00429-012-0498-y

Kinoshita, M., Shinohara, H., Hori, O., Ozaki, N., Ueda, F., Nakada, M., et al. (2012). Association fibers connecting the Broca center and the lateral superior frontal gyrus: a microsurgical and tractographic anatomy. *J. Neurosurg.* 116, 323–330. doi: 10.3171/2011.10.jns11434

Latini, F., Mårtensson, J., Larsson, E.-M., Fredrikson, M., Åhs, F., Hjortberg, M., et al. (2017). Segmentation of the inferior longitudinal fasciculus in the human brain: a white matter dissection and diffusion tensor tractography study. *Brain Res.* 1675, 102–115. doi: 10.1016/j.brainres.2017.09.005

Lawes, I. N. C., Barrick, T. R., Murugam, V., Spierings, N., Evans, D. R., Song, M., et al. (2008). Atlas-based segmentation of white matter tracts of the human brain using diffusion tensor tractography and comparison with classical dissection. *Neuroimage* 39, 62–79. doi: 10.1016/j.neuroimage.2007.06.041

Leng, B., Han, S., Bao, Y., Zhang, H., Wang, Y., Wu, Y., et al. (2016). The uncinate fasciculus as observed using diffusion spectrum imaging in the human brain. *Neuroradiology* 58, 595–606. doi: 10.1007/s00234-016-1650-9

Ludwig, E., and Klingler, J. (1956). *Atlas Cerebri Humani.* Basel: S. Karger.

Maier-Hein, K. H., Neher, P. F., Houde, J. C., Côté, M. A., Garyfallidis, E., Zhong, J., et al. (2017). The challenge of mapping the human connectome based on diffusion tractography. *Nat. Commun.* 8:1349. doi: 10.1038/s41467-017-01285-x

Makris, N., Kennedy, D. N., McInerney, S., Sorensen, A. G., Wang, R., Caviness, V. S., et al. (2005). Segmentation of subcomponents within the superior longitudinal fascicle in humans: a quantitative, *in vivo*, DT-MRI study. *Cereb. Cortex* 15, 854–869. doi: 10.1093/cercor/bhh186

Makris, N., and Pandya, D. (2009). The extreme capsule in humans and rethinking of the language circuitry. *Brain Struct. Funct.* 213, 343–358. doi: 10.1007/s00429-008-0199-8

Makris, N., Papadimitriou, G. M., Kaiser, J. R., Sorg, S., Kennedy, D. N., and Pandya, D. N. (2009). Delineation of the middle longitudinal fascicle in humans: a quantitative, *in vivo*, DT-MRI study. *Cereb. Cortex* 19, 777–785. doi: 10.1093/cercor/bhn124

Makris, N., Preti, M., Asami, T., Pelavin, P., Campbell, B., Papadimitriou, G., et al. (2013). Human middle longitudinal fascicle: variations in patterns of anatomical connections. *Brain Struct. Funct.* 218, 951–968. doi: 10.1007/s00429-012-0441-2

Makris, N., Zhu, A., Papadimitriou, G. M., Mouradian, P., Ng, I., Scaccianoce, E., et al. (2017). Mapping temporo-parietal and temporo-occipital cortico-cortical connections of the human middle longitudinal fascicle in subject-specific, probabilistic, and stereotaxic Talairach spaces. *Brain Imaging Behav.* 11, 1258–1277. doi: 10.1007/s11682-016-9589-3

Maldonado, I. L., de Champfleur, N. M., Velut, S., Destrieux, C., Zemmoura, I., and Duffau, H. (2013). Evidence of a middle longitudinal fasciculus in the human brain from *in vitro* dissection. *J. Anat.* 223, 38–45. doi: 10.1111/joa.12055

Maldonado, I. L., Mandonnet, E., and Duffau, H. (2012). Dorsal fronto-parietal connections of the human brain: a fiber dissection study of their composition and anatomical relationships. *Anat. Rec.* 295, 187–195. doi: 10.1002/ar.21533

Malpighi, M. (1665). "De cerebro," in *Tetras Anatomicarum Epistolarum de Lingua, et Cerebro*, (Bologna: Benati), 1–46. Available online at: https://babel.hathitrust.org/cgi/pt?id=ucm.530944685x;view=1up;seq=1

Mandonnet, E., Dadoun, Y., Poisson, I., Madadaki, C., Froelich, S., and Lozeron, P. (2016). Axono-cortical evoked potentials: a proof-of-concept study. *Neurochirurgie* 62, 67–71. doi: 10.1016/j.neuchi.2015.09.003

Martino, J., De Witt Hamer, P. C., Vergani, F., Brogna, C., de Lucas, E. M., Vázquez-Barquero, A., et al. (2011). Cortex-sparing fiber dissection: an improved method for the study of white matter anatomy in the human brain. *J. Anat.* 219, 531–541. doi: 10.1111/j.1469-7580.2011.01414.x

Martino, J., and García-Porrero, J. A. (2013). Wernicke perpendicular fasciculus and vertical portion of the superior longitudinal fasciculus: in reply. *Neurosurgery* 73, E382–E383. doi: 10.1227/01.neu.0000430303.56079.0e

Matsumoto, R., Nair, D. R., Ikeda, A., Fumuro, T., Lapresto, E., Mikuni, N., et al. (2012). Parieto-frontal network in humans studied by cortico-cortical evoked potential. *Hum. Brain Mapp.* 33, 2856–2872. doi: 10.1002/hbm.21407

Mayo, H. (1823). *Anatomical and Physiological Commentaries, Number II.* London: Underwood.

Mazoyer, B., Mellet, E., Perchey, G., Zago, L., Crivello, F., Jobard, G., et al. (2016). BIL&GIN: a neuroimaging, cognitive, behavioral, and genetic database for the study of human brain lateralization. *Neuroimage* 124, 1225–1231. doi: 10.1016/j.neuroimage.2015.02.071

Meckel, J. F. (1817). *Handbuch der Menschlichen Anatomie.* Halle und Berlin: der Buchhandlung des Hallischen Waisenhauses. 1–800.

Menjot de Champfleur, N., Lima Maldonado, I., Moritz-Gasser, S., Machi, P., Le Bars, E., Bonafé, A., et al. (2013). Middle longitudinal fasciculus delineation within language pathways: a diffusion tensor imaging study in human. *Eur. J. Radiol.* 82, 151–157. doi: 10.1016/j.ejrad.2012.05.034

Meola, A., Comert, A., Yeh, F. C., Stefaneanu, L., and Fernandez-Miranda, J. C. (2015). The controversial existence of the human superior fronto-occipital fasciculus: connectome-based tractographic study with microdissection validation. *Hum. Brain Mapp.* 36, 4964–4971. doi: 10.1002/hbm.22990

Meynert, T. (1888). *Psychiatrie: Clinique des Maladies du Cerveau Antérieur Basée sur sa Structure, ses Fonctions et sa Nutrition. Trans. G. Cousot.* Bruxelles: A. Manceaux.

Meynert, T. (1892). Neue studien über die associations-bündel des hirnmantels. *Mathnat. Sci. Class* 101, 361–380.

Mortazavi, F., Oblak, A. L., Morrison, W. Z., Schmahmann, J. D., Stanley, H. E., Wedeen, V. J., et al. (2018). Geometric navigation of axons in a cerebral pathway: comparing dMRI with tract tracing and immunohistochemistry. *Cereb. Cortex* 28, 1219–1232. doi: 10.1093/cercor/bhx034

Panesar, S. S., Yeh, F.-C., Deibert, C. P., Fernandes-Cabral, D., Rowthu, V., Celtikci, P., et al. (2017). A diffusion spectrum imaging-based tractographic study into the anatomical subdivision and cortical connectivity of the ventral external capsule: uncinate and inferior fronto-occipital fascicles. *Neuroradiology* 59, 971–987. doi: 10.1007/s00234-017-1874-3

Panesar, S. S., Yeh, F.-C., Jacquesson, T., Hula, W., and Fernandez-Miranda, J. C. (2018). A quantitative tractography study into the connectivity, segmentation and laterality of the human inferior longitudinal fasciculus. *Front. Neuroanat.* 12:47. doi: 10.3389/fnana.2018.00047

Parlatini, V., Radua, J., Dell'Acqua, F., Leslie, A., Simmons, A., Murphy, D. G., et al. (2017). Functional segregation and integration within fronto-parietal networks. *Neuroimage* 146, 367–375. doi: 10.1016/j.neuroimage.2016.08.031

Peuskens, D., van Loon, J., Van Calenbergh, F., van den Bergh, R., Goffin, J., and Plets, C. (2004). Anatomy of the anterior temporal lobe and the frontotemporal region demonstrated by fiber dissection. *Neurosurgery* 55, 1174–1184. doi: 10.1227/01.neu.0000140843.62311.24

Piccolomini, A. (1586). *Anatomicae Praelectiones, Archangeli Piccolhomini, Ferrariensis, Civisque Romani, Explicantes Mirificam Corporis Humani Fabriquam.* Rome: Bodfadinus.

Ramón y Cajal, S. (1906). "The structure and connexions of neurons—nobel lecture, December 12, 1906," in *Nobel Lectures, Physiology or Medicine 1901–1921*, (Amsterdam, New York, NY: Elsevier Publishing Company). Available online at: https://www.nobelprize.org/prizes/medicine/1906/cajal/lecture/

Reil, J. C. (1809). Die Sylvische Grube oder das Thal, das gestreifte grobe hirnganglium, dessen kapsel und die seitentheile des grobn gehirns. *Archiv. Physiol.* 9, 195–208.

Renier, N., Wu, Z., Simon David, J., Yang, J., Ariel, P., and Tessier-Lavigne, M. (2014). iDISCO: a simple, rapid method to immunolabel large tissue samples for volume imaging. *Cell* 159, 896–910. doi: 10.1016/j.cell.2014.10.010

Reveley, C., Seth, A. K., Pierpaoli, C., Silva, A. C., Yu, D., Saunders, R. C., et al. (2015). Superficial white matter fiber systems impede detection of long-range cortical connections in diffusion MR tractography. *Proc. Natl. Acad. Sci. U S A* 112, E2820–E2828. doi: 10.1073/pnas.1418198112

Rojkova, K., Volle, E., Urbanski, M., Humbert, F., Dell'Acqua, F., and Thiebaut de Schotten, M. (2016). Atlasing the frontal lobe connections and their variability due to age and education: a spherical deconvolution tractography study. *Brain Struct. Funct.* 221, 1751–1766. doi: 10.1007/s00429-015-1001-3

Rolando, L. (1831). Della struttura degli emisferi cerebrali. *R. Accad. Delle Sci. Torino* 35, 1–46.

Sarubbo, S., De Benedictis, A., Maldonado, I. L., Basso, G., and Duffau, H. (2013). Frontal terminations for the inferior fronto-occipital fascicle: anatomical dissection, DTI study and functional considerations on a multi-component bundle. *Brain Struct. Funct.* 218, 21–37. doi: 10.1007/s00429-011-0372-3

Sarubbo, S., De Benedictis, A., Merler, S., Mandonnet, E., Barbareschi, M., Dallabona, M., et al. (2016). Structural and functional integration between dorsal and ventral language streams as revealed by blunt dissection and direct electrical stimulation. *Hum. Brain Mapp.* 37, 3858–3872. doi: 10.1002/hbm.23281

Schmahmann, J. D., and Pandya, D. N. (2006). *Fiber Pathways of the Brain.* New York, NY: Oxford University Press.

Schmahmann, J. D., and Pandya, D. N. (2007). The complex history of the fronto-occipital fasciculus. *J. Hist. Neurosci.* 16, 362–377. doi: 10.1080/09647040600620468

Schuz, A., and Braitenberg, V. (2002). "The human cortical white matter: quantitative aspects of cortico-cortical long-range connectivity," in *Cortical Areas: Unity and Diversity*, eds A. Schuz and R. Miller (London: Taylor & Francis), 377–386.

Sinke, M. R. T., Otte, W. M., Christiaens, D., Schmitt, O., Leemans, A., van der Toorn, A., et al. (2018). Diffusion MRI-based cortical connectome reconstruction: dependency on tractography procedures and neuroanatomical characteristics. *Brain Struct. Funct.* 223, 2269–2285. doi: 10.1007/s00429-018-1628-y

Solly, S. (1836). *The Human Brain, its Configuration, Structure, Development, and Physiology.* London: Longman, Rees, Orme, Brown, Green and Longman. 1–492.

Sporns, O. (2013). The human connectome: origins and challenges. *Neuroimage* 80, 53–61. doi: 10.1016/j.neuroimage.2013.03.023

Steno, N. (1669). *Discourse de Monsieur Stenon sur l'anatomie du Cerveau.* Paris: Ninville.

Swanson, L. W. (2015). *Neuroanatomical Terminology: A Lexicon of Classical Origins and Historical Foundations.* New York, NY: Oxford University Press.

Tax, C. M. W., Westin, C. F., Dela Haije, T., Fuster, A., Viergever, M. A., Calabrese, E., et al. (2017). Quantifying the brain's sheet structure with normalized convolution. *Med. Image Anal.* 39, 162–177. doi: 10.1016/j.media.2017.03.007

ten Donkelaar, H. J., Kachlik, D., and Tubbs, R. S. (2018a). *An Illustrated Terminologia Neuroanatomica.* Cham: Springer.

ten Donkelaar, H. J., Tzourio-Mazoyer, N., and Mai, J. K. (2018b). Towards a common terminology for the gyri and sulci of the human Cerebral cortex. *Front. Neuroanat.* 12:93. doi: 10.3389/fnana.2018.00093.

Thiebaut de Schotten, M., Dell'Acqua, F., Forkel, S. J., Simmons, A., Vergani, F., Murphy, D. G. M., et al. (2011a). A lateralized brain network for visuospatial attention. *Nat. Neurosci.* 14, 1245–1246. doi: 10.1038/nn.2905

Thiebaut de Schotten, M., Ffytche, D., Bizzi, A., Dell'Acqua, F., Allin, M., Walshe, M., et al. (2011b). Atlasing location, asymmetry and inter-subject variability of white matter tracts in the human brain with MR diffusion tractography. *Neuroimage* 54, 49–59. doi: 10.1016/j.neuroimage.2010.07.055

Thiebaut de Schotten, M., Dell'Acqua, F., Valabregue, R., and Catani, M. (2012). Monkey to human comparative anatomy of the frontal lobe association tracts. *Cortex* 48, 82–96. doi: 10.1016/j.cortex.2011.10.001

Thomas, C., Ye, F. Q., Irfanoglu, M. O., Modi, P., Saleem, K. S., Leopold, D. A., et al. (2014). Anatomical accuracy of brain connections derived from diffusion MRI tractography is inherently limited. *Proc. Natl. Acad. Sci. U S A* 111, 16574–16579. doi: 10.1073/pnas.1405672111

Treviranus, G. R., Treviranus, L. C. (1816–1821). *Vermischte Schriften Anatomischen und Physiologischen Inhalts. Göttingen*: Röwer.

Trolard, P. (1906). Le faisceau longitudinal inférieur du cerveau. *Rev. Neurol.* 14, 440–446.

Ture, U., Yasargil, M. G., and Pait, T. G. (1997). Is there a superior occipitofrontal fasciculus? A microsurgical anatomic study. *Neurosurgery* 40, 1226–1232. doi: 10.1097/0006123-199706000-00022

Tusa, R. J., and Ungerleider, L. G. (1985). The inferior longitudinal fasciculus: a reexamination in humans and monkeys. *Ann. Neurol.* 18, 583–591. doi: 10.1002/ana.410180512

Vallar, G., Bello, L., Bricolo, E., Castellano, A., Casarotti, A., Falini, A., et al. (2014). Cerebral correlates of visuospatial neglect: a direct cerebral stimulation study. *Hum. Brain Mapp.* 35, 1334–1350. doi: 10.1002/hbm.22257

Van Diemerbroeck, I. (1695). *L'anatomie du Corps Humain.* Lyon: Anisson & Posuel.

Vasung, L., Jovanov-Milosevic, N., Pletikos, M., Mori, S., Judas, M., and Kostovic, I. (2011). Prominent periventricular fiber system related to ganglionic eminence and striatum in the human fetal cerebrum. *Brain Struct. Funct.* 215, 237–253. doi: 10.1007/s00429-010-0279-4

Vergani, F., Lacerda, L., Martino, J., Attems, J., Morris, C., Mitchell, P., et al. (2014a). White matter connections of the supplementary motor area in humans. *J. Neurol. Neurosurg. Psychiatry* 85, 1377–1385. doi: 10.1136/jnnp-2013-307492

Vergani, F., Mahmood, S., Morris, C. M., Mitchell, P., and Forkel, S. J. (2014b). Intralobar fibers of the occipital lobe: a post mortem dissection study. *Cortex* 56, 145–156. doi: 10.1016/j.cortex.2014.03.002

Vesalius, A. (1543). *De Humani Corporis Fabrica Libri Septem.* Basel: Oporinus.

Vicq d'Azyr, F. (1786). *Traité D'anatomie et de Physiologie avec des Planches Coloriées.* Paris: Imrpimerie de François Amb Didot l'Ainé.

Vieussens, R. (1684). *Neurographia Universalis.* Lyons: Certe.

Wang, Y., Fernández-Miranda, J. C., Verstynen, T., Pathak, S., Schneider, W., and Yeh, F.-C. (2013). Rethinking the role of the middle longitudinal fascicle in language and auditory pathways. *Cereb. Cortex* 23, 2347–2356. doi: 10.1093/cercor/bhs225

Wang, X., Pathak, S., Stefaneanu, L., Yeh, F. C., Li, S., and Fernandez-Miranda, J. C. (2016). Subcomponents and connectivity of the superior longitudinal fasciculus in the human brain. *Brain Struct. Funct.* 221, 2075–2092. doi: 10.1007/s00429-015-1028-5

Wedeen, V. J., Rosene, D. L., Wang, R., Dai, G., Mortazavi, F., Hagmann, P., et al. (2012a). Response to comment on "the geometric structure of the brain fiber pathways". *Science* 337:1605. doi: 10.1126/science.1223493

Wedeen, V. J., Rosene, D. L., Wang, R., Dai, G., Mortazavi, F., Hagmann, P., et al. (2012b). The geometric structure of the brain fiber pathways. *Science* 335, 1628–1634. doi: 10.1126/science.1215280

Weissman, T. A., and Pan, Y. A. (2015). Brainbow: new resources and emerging biological applications for multicolor genetic labeling and analysis. *Genetics* 199, 293–306. doi: 10.1534/genetics.114.172510

Willis, T. (1672). *De Anima Brutorum.* London: Gulielm Wells & Robertum Scott. 1–638.

Wu, Y., Sun, D., Wang, Y., and Wang, Y. (2016). Subcomponents and connectivity of the inferior fronto-occipital fasciculus revealed by diffusion spectrum imaging fiber tracking. *Front. Neuroanat.* 10:88. doi: 10.3389/fnana.2016.00088

Yagmurlu, K., Middlebrooks, E. H., Tanriover, N., and Rhoton, A. L. Jr. (2016). Fiber tracts of the dorsal language stream in the human brain. *J. Neurosurg.* 124, 1396–1405. doi: 10.3171/2015.5.JNS15455

Yeatman, J. D., Weiner, K. S., Pestilli, F., Rokem, A., Mezer, A., and Wandell, B. A. (2014). The vertical occipital fasciculus: a century of controversy resolved by *in vivo* measurements. *Proc. Natl. Acad. Sci. U S A* 111, E5214–E5223. doi: 10.1073/pnas.1418503111

Yeterian, E. H., Pandya, D. N., Tomaiuolo, F., and Petrides, M. (2012). The cortical connectivity of the prefrontal cortex in the monkey brain. *Cortex* 48, 58–81. doi: 10.1016/j.cortex.2011.03.004

Zhang, Y., Zhang, J., Oishi, K., Faria, A. V., Jiang, H., Li, X., et al. (2010). Atlas-guided tract reconstruction for automated and comprehensive examination of the white matter anatomy. *Neuroimage* 52, 1289–1301. doi: 10.1016/j.neuroimage.2010.05.049

Conflict of Interest Statement: The authors declare that the research was conducted in the absence of any commercial or financial relationships that could be construed as a potential conflict of interest.

Copyright © 2018 Mandonnet, Sarubbo and Petit. This is an open-access article distributed under the terms of the Creative Commons Attribution License (CC BY). The use, distribution or reproduction in other forums is permitted, provided the original author(s) and the copyright owner(s) are credited and that the original publication in this journal is cited, in accordance with accepted academic practice. No use, distribution or reproduction is permitted which does not comply with these terms.

frontiers in Neuroanatomy

GENERAL COMMENTARY
published: 11 June 2019
doi: 10.3389/fnana.2019.00061

Commentary: The Nomenclature of Human White Matter Association Pathways: Proposal for a Systematic Taxonomic Anatomical Classification

*Sandip S. Panesar and Juan Fernandez-Miranda**

Department of Neurosurgery, Stanford University, Stanford, CA, United States

Keywords: tractography, association tracts, white matter, neuroanatomy, arcuate fasciculus

A Commentary on

The Nomenclature of Human White Matter Association Pathways: Proposal for a Systematic Taxonomic Anatomical Classification
by Mandonnet, E., Sarubbo, S., and Petit, L. (2018). Front. Neuroanat. 12:94. doi: 10.3389/fnana.2018.00094

OPEN ACCESS

Edited by:
Hans J. ten Donkelaar, Radboud University Nijmegen, Netherlands

Reviewed by:
Michela Ferrucci, University of Pisa, Italy
Giorgio Innocenti, Karolinska Institute (KI), Sweden

****Correspondence:***
Juan Fernandez-Miranda
drjfm@stanford.edu

Received: *13 November 2018*
Accepted: *24 May 2019*
Published: *11 June 2019*

Citation:
Panesar SS and Fernandez-Miranda J (2019) Commentary: The Nomenclature of Human White Matter Association Pathways: Proposal for a Systematic Taxonomic Anatomical Classification. Front. Neuroanat. 13:61. doi: 10.3389/fnana.2019.00061

The anatomical study of mammalian white matter structure and arrangement has evolved over the past two centuries. There have been three major revolutions facilitating neuroanatomical study of white matter: Early development of post-mortem preparation techniques like Klingler's (Ludwig and Klingler, 1956) to readily visualize the gross orientation of larger white fibers in dissection specimens; introduction of neurochemical tracing techniques to permit cortical-connectivity analysis in non-human primates in the second half of the twentieth century (Lanciego and Wouterlood, 2011); and most recently, development of *in vivo* diffusion magnetic resonance (MR) tractography in the 1990's, which has grown to become the premier white matter research technique. Unfortunately, and for varying reasons, the anatomical classification and nomenclature of white matter architecture, particularly of the association fasciculi, has been subject to considerable heterogeneity, conflicting theories, and disagreements between researchers. Nevertheless, attempts have been made to unify the classification and nomenclature of the human white matter fasciculi.

Recently, Mandonnet et al. (2018) proposed a global classification for the long-range human association fasciculi on a hierarchical basis, using the insular sulcus as a demarcating boundary of larger dorsal and ventral systems (Mandonnet et al., 2018). Each system contained particular, well-known bundles interconnecting cortical areas, which received novel numerical classification e.g., the arcuate fasciculus is known as the superior longitudinal system IV. Though this attempt to unify the anatomy is commendable, we believe, however, that their proposal potentially adds more confusion to the current scenario. From our perspective, the major shortcoming of this nomenclature is that it does not adequately dispel the archaic, conflicting notions of white matter anatomy compounded over the years, but rather "paints over" them while leaving the fundamental controversies unaddressed, or possibly causing greater confusion.

Though it is unfeasible to discuss every association tract discussed in the current classification, we use our own recently published data regarding several relevant tracts (Fernández-Miranda et al., 2015; Wang et al., 2016; Panesar et al., 2017, 2018a,b) to argue our point: The superior longitudinal fascicle (SLF) was first divided into 4 subsegments (SLF I to IV) based on primate neurochemical tracer data (Petrides and Pandya, 1984), and later reinforced by a diffusion tensor imaging (DTI) study (Makris et al., 2005). These initial studies included the arcuate fasciculus (AF) as the "SLF-IV" or "perisylvian-SLF," a proposal later propagated by others (Catani et al., 2005; Martino et al., 2013). The present authors propose the AF to be considered as the "superior longitudinal system (SLS) IV." In our view, this is problematic: The AF cannot be regarded as a longitudinal tract as it is an "arcuate-shaped" tract; in fact, the AF is a lateral fronto-temporal fascicle with no parietal connections (Fernández-Miranda et al., 2015), while the SLF is a lateral fronto-parietal fascicle with no temporal connections (Wang et al., 2016). From an anatomical (morphological and topographical) perspective, defining an "arcuate" tract as a "longitudinal" tract is misleading.

Furthermore, the literature generally shows that the AF has strong leftward-lateralization in terms of its subdivisions, volume, and connectivity profiles, while the "superior longitudinal fasciculus proper" (excluding AF) (Thiebaut de Schotten et al., 2011; Wang et al., 2016), is rightward-lateralized in terms of subdivision, connectivity, and volume. Based upon comparisons between human and simian AF morphology, Rilling et al. (2008) proposed the human AF to be evolutionarily differentiated to sub-serve lexical-semantic functionality (Rilling et al., 2008). This view was further elaborated upon and reinforced with our dedicated tractographic and dissection study (Fernández-Miranda et al., 2015). As the structural characteristics of white matter likely reflect evolutionary divergence, underpinned by functional specialization (Glasser and Rilling, 2008; Rilling et al., 2008), this adds further evidence that these anatomo-functionally differentiated should not be grouped together.

In our advanced fiber tractography study of the SLF (Wang et al., 2016), we were unable to find the so-called SLF-I, which in theory travels adjacent to SLF-II to interconnect the superior frontal gyrus with the superior parietal lobule. We did find fibers interconnecting these two regions, but they were traveling medial to the corona radiata in the mesial aspect of the hemisphere. We subsequently proposed these fibers to be part of the cingulum fiber system rather than the SLF. However, multiple authors have continued preserving the inappropriate nomenclature derived from primate studies for no good reason. Our study showed that the SLF can be practically classified in dorsal and ventral components, which correlate with the SLF-II and III, but offer additional anatomical information in their description while adhering to modern anatomical nomenclature systems.

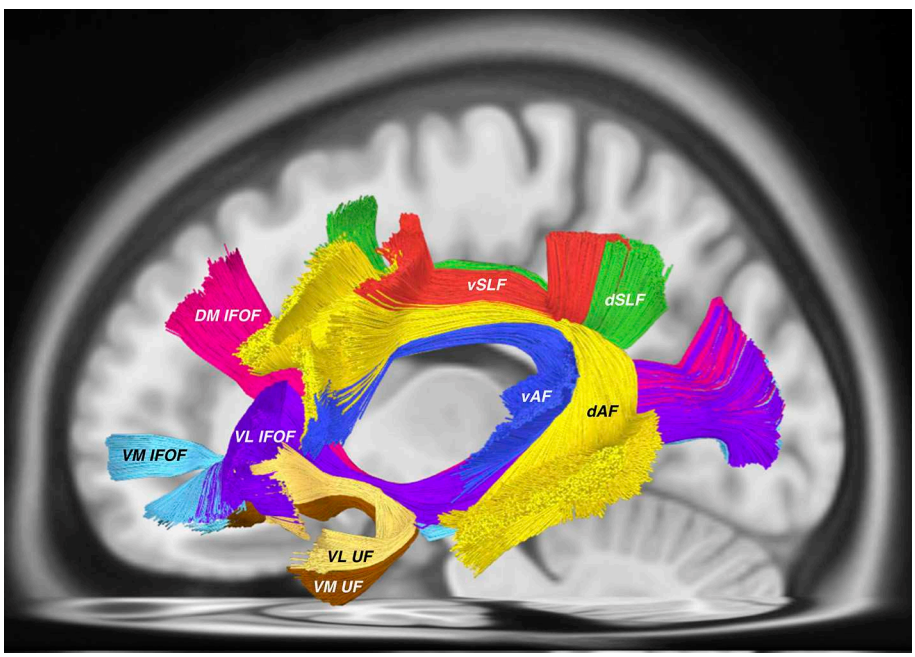

FIGURE 1 | All tractography conducted in DSI studio (http://dsi-studio.labsolver.org) using the HCP 842 atlas (Yeh et al., 2018) as a template. AF tracts were created according to the method described in (Fernández-Miranda et al., 2015), while SLF tracts were created according to the methodology used by Wang et al. (2016). IFOF and UF tracts were created using the method from Panesar et al. (2017). This tractography template represents "averaged" healthy white matter tractographic anatomy of 842 subjects from the Human Connectome Project. Visible in this picture are the dorsal (dAF) and ventral (vAF) AF components, the dorsal (dSLF) and ventral (vSLF) SLF components. Deep and ventral to these tracts are the IFOF consisting of the dorsomedial (DM IFOF), ventromedial (VM IFOF) and ventrolateral (VL) subfascicles. The UF also traverses through the ventral external capsule and is comprised of the ventrolateral (VL UF) and ventromedial (VM UF) sub-fascicles.

The same issues arise when considering the proposed nomenclature for the "inferior longitudinal system (ILS)" which includes both the inferior fronto-occipital fasciculus (IFOF) and the uncinate fasciculus (UF). According to the authors, the "ILS IV" is synonymous with the UF. Recent tractographic studies have demonstrated a unique, subdivided morphology of the UF (Hau et al., 2016, 2017; Panesar et al., 2017). According to the proposed "ILS" nomenclature, the various subcomponents of the IFOF, in concordance with our previous findings (Panesar et al., 2017) are accounted for, yet the subdivisions of the UF are not (**Figure 1**).

Fiber tracts should not be grouped with other fasciculi on the sole basis of spatial proximity, but on the basis of distinct connectivity. In addition, the present proposal carries on with tract sub-classifications that originated from animal studies and were later "validated" with DTI studies. The classifications, from our point of view, are inaccurate and inappropriate for human brain anatomy, especially in light of new tractography findings. We strongly recommend against the use of numerical subsegments (I to IV), and we favor using a topographic classification (dorsal-ventral, medial-lateral), which has a long tradition and is better understood by neuroanatomists as the names themselves provide anatomical information, as opposed to numeric classifications that provide no additional information.

Finally, we highlight technical factors that may potentially confound this classification proposal. At this point, the differences between DTI and more advanced white matter tractography modalities such as high-angular resolution diffusion imaging (HARDI) or generalized Q-sampling imaging (GQI) are well-recognized. In a recent dissection and tractography study into the short vertical association tracts of the posterior hemisphere, we demonstrated that GQI-based tractography could reliably demonstrate the unique spatial separation between the two components within what Mandonnet et al. refer to as the posterior transverse system, and which we refer to as the "temporo-parietal aslant tract" (temporo-parietal course) and vertical occipital fasciculus (occipito-occipital course), respectively (Panesar et al., 2018a). Yeatman et al. (2014) first questioned whether these two fasciculi were indeed separated, a discrete "band of fibers" or whether they appeared unified due to shortcomings of the DTI method. In our study, we demonstrated that the temporo-parietal aslant tract and vertical occipital fasciculus were indeed spatially separated. The band of fibers bridging the two fascicles may be comprised of U-fibers or may be comprised of false continuities from other fasciculi, arising from tensor-based tractography.

In conclusion, we congratulate the authors for the efforts toward a unified classification of the white matter tracts, but at the same time we encourage them and all other experts in the field to consider the points of concern raised here, and to utilize a more practical, anatomically-oriented, and academically-accurate classification of the human fiber tracts.

AUTHOR CONTRIBUTIONS

Both authors SP and JF-M contributed equally to the manuscript: JF-M: main idea and editing. SP: writing and figure creation.

REFERENCES

Catani, M., Jones, D. K., and ffytche, D. H. (2005). Perisylvian language networks of the human brain. *Ann. Neurol.* 57, 8–16. doi: 10.1002/ana.20319

Fernández-Miranda, J. C., Wang, Y., Pathak, S., Stefaneau, L., Verstynen, T., and Yeh, F.-C. (2015). Asymmetry, connectivity, and segmentation of the arcuate fascicle in the human brain. *Brain Struct. Funct.* 220, 1665–1680. doi: 10.1007/s00429-014-0751-7

Glasser, M. F., and Rilling, J. K. (2008). DTI tractography of the human brain's language pathways. *Cereb. Cortex* 18, 2471–2482. doi: 10.1093/cercor/bhn011

Hau, J., Sarubbo, S., Houde, J. C., Corsini, F., Girard, G., Deledalle, C., et al. (2017). Revisiting the human uncinate fasciculus, its subcomponents and asymmetries with stem-based tractography and microdissection validation. *Brain Struct. Funct.* 222, 1645–1662. doi: 10.1007/s00429-016-1298-6

Hau, J., Sarubbo, S., Perchey, G., Crivello, F., Zago, L., Mellet, E., et al. (2016). Cortical terminations of the inferior fronto-occipital and uncinate fasciculi: anatomical stem-based virtual dissection. *Front. Neuroanat.* 10:58. doi: 10.3389/fnana.2016.00058

Lanciego, J. L., and Wouterlood, F. G. (2011). A half century of experimental neuroanatomical tracing. *J. Chem. Neuroanat.* 42, 157–183. doi: 10.1016/j.jchemneu.2011.07.001

Ludwig, E., and Klingler, J. (1956). "Atlas Cerebri Humani," in *Der Innere Bau des Gehirns Dargestellt auf Grund Makroskopischer Präparate: The Inner Structure of the Brain Demonstrated on the Basis of Macroscopical Preparations: La Structure Interne du Cerveau Démontrée sur les Préparations Macroscopiques: La Arquitectura Interna del Cerebro Demostrada Mediante Preparaciones Macroscópicas* (Boston, MA: Little, Brown and Company), 1–6. doi: 10.1159/000389712

Makris, N., Kennedy, D. N., McInerney, S., Sorensen, A. G., Wang, R., Caviness, V. S., et al. (2005). Segmentation of subcomponents within the superior longitudinal fascicle in humans: a quantitative, *in vivo*, DT-MRI study. *Cereb. Cortex* 15, 854–869. doi: 10.1093/cercor/bhh186

Mandonnet, E., Sarubbo, S., and Petit, L. (2018). The nomenclature of human white matter association pathways: proposal for a systematic taxonomic anatomical classification. *Front. Neuroanat.* 12:94. doi: 10.3389/fnana.2018.00094

Martino, J., De Witt Hamer, P. C., Berger, M. S., Lawton, M. T., Arnold, C. M., de Lucas, E. M., et al. (2013). Analysis of the subcomponents and cortical terminations of the perisylvian superior longitudinal fasciculus: a fiber dissection and DTI tractography study. *Brain Struct. Funct.* 218, 105–121. doi: 10.1007/s00429-012-0386-5

Panesar, S. S., Belo, J. T. A., Yeh, F.-C., and Fernandez-Miranda, J. C. (2018a). Structure, asymmetry, and connectivity of the human temporo-parietal aslant and vertical occipital fasciculi. *Brain Struct. Funct.* 224, 907–923. doi: 10.1007/s00429-018-1812-0

Panesar, S. S., Yeh, F.-C., Deibert, C. P., Fernandes-Cabral, D., Rowthu, V., Celtikci, P., et al. (2017). A diffusion spectrum imaging-based tractographic study into the anatomical subdivision and cortical connectivity of the ventral external capsule: uncinate and inferior fronto-occipital fascicles. *Neuroradiology* 59, 971–987. doi: 10.1007/s00234-017-1874-3

Panesar, S. S., Yeh, F.-C., Jacquesson, T., Hula, W., and Fernandez-Miranda, J. C. (2018b). A quantitative tractography study into the connectivity, segmentation and laterality of the human inferior longitudinal fasciculus. *Front. Neuroanat.* 12:47. doi: 10.3389/fnana.2018.00047

Petrides, M., and Pandya, D. N. (1984). Projections to the frontal cortex from the posterior parietal region in the rhesus monkey. *J. Comp. Neurol.* 228, 105–116.

Rilling, J. K., Glasser, M. F., Preuss, T. M., Ma, X., Zhao, T., Hu, X., et al. (2008). The evolution of the arcuate fasciculus revealed with comparative DTI. *Nat. Neurosci.* 11, 426–428. doi: 10.1038/nn2072

Thiebaut de Schotten, M., Ffytche, D. H., Bizzi, A., Dell'Acqua, F., Allin, M., Walshe, M., et al. (2011). Atlasing location, asymmetry and inter-subject variability of white matter tracts in the human brain with MR diffusion tractography. *Neuroimage* 54, 49–59. doi: 10.1016/j.neuroimage.2010.07.055

Wang, X., Pathak, S., Stefaneanu, L., Yeh, F.-C., Li, S., and Fernandez-Miranda, J. C. (2016). Subcomponents and connectivity of the superior longitudinal fasciculus in the human brain. *Brain Struct. Funct.* 221, 2075–2092. doi: 10.1007/s00429-015-1028-5

Yeatman, J. D., Weiner, K. S., Pestilli, F., Rokem, A., Mezer, A., and Wandell, B. A. (2014). The vertical occipital fasciculus: a century of controversy resolved by *in vivo* measurements. *Proc. Natl. Acad. Sci. U.S.A.* 111, E5214–E5223. doi: 10.1073/pnas.1418503111

Yeh, F. C., Panesar, S., Fernandes, D., Meola, A., Yoshino, M., Fernandez-Miranda, J. C., et al. (2018). Population-averaged atlas of the macroscale human structural connectome and its network topology. *NeuroImage* 178, 57–68. doi: 10.1016/j.neuroimage.2018.05.027

Conflict of Interest Statement: The authors declare that the research was conducted in the absence of any commercial or financial relationships that could be construed as a potential conflict of interest.

Copyright © 2019 Panesar and Fernandez-Miranda. This is an open-access article distributed under the terms of the Creative Commons Attribution License (CC BY). The use, distribution or reproduction in other forums is permitted, provided the original author(s) and the copyright owner(s) are credited and that the original publication in this journal is cited, in accordance with accepted academic practice. No use, distribution or reproduction is permitted which does not comply with these terms.

frontiers in Neuroanatomy

MINI REVIEW
published: 23 November 2018
doi: 10.3389/fnana.2018.00099

Auditory Nomenclature: Combining Name Recognition With Anatomical Description

Bernd Fritzsch and Karen L. Elliott*

Department of Biology, The University of Iowa, Iowa City, IA, United States

The inner ear and its two subsystems, the vestibular and the auditory system, exemplify how the identification of distinct cellular or anatomical elements ahead of elucidating their function, leads to a medley of anatomically defined and recognition oriented names that confused generations of students. Past attempts to clarify this unyielding nomenclature had incomplete success, as they could not yet generate an explanatory nomenclature. Building on these past efforts, we propose a somewhat revised nomenclature that keeps most of the past nomenclature as proposed and follows a simple rule: Anatomical and explanatory terms are combined followed, in brackets, by the name of the discoverer (see **Table 1**). For example, the "organ of Corti" will turn into the spiral auditory organ (of Corti). This revised nomenclature build as much as possible on existing terms that have explanatory value while keeping the recognition of discoverers alive to allow a transition for those used to the eponyms. Once implements, the proposed terminology should help future generations in learning the structure-function correlates of the ear more easily. To facilitate future understanding, leading genetic identifiers for a given structure have been added wherever possible.

Keywords: ear, development, sensory epithelia, sensory neurons, auditory nuclei

OPEN ACCESS

Edited by:
Hans J. ten Donkelaar, Radboud University Nijmegen, Netherlands

Reviewed by:
Robert Joel Ruben, Montefiore Medical Center, United States
Robert H. Baud, Université de Fribourg, Switzerland

****Correspondence:***
Bernd Fritzsch
bernd-fritzsch@uiowa.edu

Received: *27 July 2018*
Accepted: *05 November 2018*
Published: *23 November 2018*

Citation:
Fritzsch B and Elliott KL (2018) Auditory Nomenclature: Combining Name Recognition With Anatomical Description. Front. Neuroanat. 12:99. doi: 10.3389/fnana.2018.00099

INTRODUCTION

The ear was recognized as the organ for hearing since antiquity, but its function could only be understood mechanistically after Corti (1851) described some of the cells on the basilar membrane of what Kölliker soon referred to as the organ of Corti (Kölliker, 1852, 1867). Nearly overlapping in time, Reissner (1851) described the membrane separating the scala media from the scala vestibuli, now bearing his name (Reissner's membrane) to identify three distinct channels in the cochlear canal instead of two as previously identified based on ever improving anatomical work. With the event of better preservation, decalcification and histological sections, many new features were discovered in the second half of 19th century. Naming those novel ear structures in the 1850-70 time frame continued a tradition of eponyms that dates back to Falloppio's canal [now known as facial nerve canal (Politzer, 1907, 1981)] and followed the rational that names of first identifiers were associated with the structure they identified (Claudius, 1856; Boettcher, 1859; Hensen, 1863). Since discovery of new cell types outpaced for many years any reasonable understanding of their function, this approach was the most logical way forward to avoid over speculating on unclear function. In parallel to anatomical discoveries, functional ideas were proposed by Willis (1672). He believed that sound enters with movement of the stapes footplate through the oval window, is reflected and amplified in the semicircular canals before it is received by the "acoustic nerve"

in the cochlea. Duverney (1730) noticed the different diameters of the cochlea duct and used his anatomical insights to invoke a resonance theory of hearing only much later elaborated on by Helmholtz (1859) and ultimately demonstrated as tonotopic organization of the cochlea by Békésy (1930). Neither name is in any way associated with their insights as eponyms, emphasizing the lopsided distribution of credit given by the somewhat random use of eponyms.

For example, it was only in 1789 that Scarpa (1800) surpassed the detailed description of Duverney (1730) and fully described the membranous labyrinth of the inner ear. And yet Scarpa's name is only used as an eponym of the vestibular (or Scarpa's ganglion; **Table 1**). The excellent illustrative work of von Sömmering (1806) which laid the foundation of much of the histology and comparative work of the 19th century, including the comparative work of Retzius (1881, 1884) never earned him any eponym. Even Retzius' name was not associated with the amphibian papilla he described but is only associated with the Retzius' bodies in the outer hair cells (Lim, 1986). After the foundation of the histology of the mammalian organ of Corti was established, details that were added later through more refined histological analysis did not earn eponyms such the newly described border cells for Held (1902, 1926). This contrasts sharply with the fact that Held's earlier description of large contacts in brainstem auditory nuclei are now known under the eponym "endbulbs" and "calyx" of Held (1893).

Many years of continued insight into the cellular and subcellular details of the organ of Corti, organization and function allow now to go beyond the purely descriptive and initially disputed original work. Today, the entrenched use of eponyms in otolaryngology confuses students and blocks understanding through enforced learning of eponyms that have no meaning beyond honoring the original descriptor and conserve an anatomical terminology that is in part unrelated to the function that was mostly unclear at the time the structures were first described. Eponyms were less fashionable from 1880 to today, novel features nevertheless received trivial names that do not convey the level of understanding detailed anatomy, physiology and molecular development of the ear now allows. Inconsistencies abound, such as the inner border cells [Grenzzelle (Held, 1902)] are not called Held's cells whereas the outer border cells are now referred to as Hensen's (1863) cells . Likewise, the outer phalangeal cells are now mostly referred to as Deiters (1860) cells whereas the inner phalangeal cells have no eponym. Complicating cochlear nomenclature even further, some trivial names are redundant and confusing such as type 1 and 2 hair cells in the vestibular system and Type I and II spiral ganglion neurons in the cochlea, evoking false associations in students new to the ear nomenclature. And some names were differently translated such as the German "Pfeilerzelle" is now referred to in US English as "pillar cells" but in United Kingdom English as "pilar cells," with only the former presenting a translation according to the German meaning. Some of these issues have been partially rectified by taking traditional/scientific terms, multilingual discrepancies, role of Latin terms, usage of adjectives vs. genitive, usage of poorly defined words, usage of eponyms into account in previous nomenclature revisions (FCOA, 1998; FIPAT, 2017). The motivation for the present revision is to build on these past considerations reflected in the most recently proposed nomenclature (**Table 1**) while taking a more novel molecular and functional considerations into account.

Obviously, eponyms avoided associating mistaken functions to various parts of the ear (Politzer, 1907, 1981; Lustig et al., 1998; Mudry, 2001) and isolated the morphological description from functional speculations, certainly an important consideration at a time when vestibular and auditory function of the ear were mostly unknown and in many cases simply misinterpreted. Adding to this confusion in the more recent literature were mistranslations [the border cells of Held are now mostly referred to as "inner border cells" (Held, 1902) due to a mistake in one summary image] that identified what appears to be the same cell by different names. It was only later that hearing and vestibular function could be associated with different parts of the ear through the works of Mach (1865a,b), Breuer (1873), Barany (1906), Békésy (1930) and Helmholtz (1859). Both the function of the ear as a gravistatic and angular motion detection system and the function of the cochlea as a frequency and intensity monitoring system have been clarified as distinct functions of the mammalian ear (Hudspeth, 1989). The detailed understanding of the organ of Corti was advanced by modern techniques beyond the excellent description of Held (1902, 1926) using electron microscopy, summarized by Lim (1986) and Slepecky (1996) and quantitative ratios of different cell types of the organ of Corti (Jahan et al., 2015). We now know that hair cells function as polarized mechanotransducers (Hudspeth, 1989) with a distinctly different function of the inner and outer hair cells in amplification and reception of sound (Zheng et al., 2000). For example, sound stimulation of the organ of Corti was long been depicted as a simple up-down movement that directly caused shearing forces of the tectorial membrane on the inner hair cell stereocilia (Lewis et al., 1985). In contrast, more recent work suggest that the adult inner hair cell is not connected to the tectorial membrane (Lim, 1986) but acts as a hydrodynamic receptor monitoring endolymph flow in and out of the subtectorial space (Elliott et al., 2018).

More recent work on early development using gene expression and functional assessments of afferent, efferent, and hair cell proteins provides novel ways of identifying cells of the ear not only based on their topology and function but on their molecular signature (Liu et al., 2014). Unsurprisingly, such molecular data open again issues of identification of cell types and regrouping previous anatomical distinctions into smaller subgroups. For example, spiral ganglion neurons were initially described as homogenous (Corti, 1851) or as multiple types (De No, 1981), regrouped eventually into just two types based on diameters and innervation (Spoendlin, 1971), but subsequently again expanded to three types based on physiological properties (Merchan-Perez and Liberman, 1996; Rutherford and Moser, 2016). The latter suggestions are now supported by their molecular signatures (Petitpré et al., 2018; Shrestha et al., 2018; Sun et al., 2018). While all papers agree on the major expression they use inconsistent, albeit similar nomenclature: for example, what is Type Ia in two papers (Shrestha et al., 2018; Sun et al., 2018) is Type Ic in the third paper (Petitpré et al., 2018). The solution to this

TABLE 1 | Terminology for the inner ear.

Latin terms (TNA, 2017)	English terms (US spelling, proposed terms)	English terms (UK spelling; TNA, 2017)	Molecular signature	Related terms and Eponyms
Cochlea	**Cochlea**	Cochlea		
	Inner spiral sulcus			
	Outer spiral sulcus			
Modiolus cochleae	Modiolus	Modiolus		
Canalis spiralis modioli	Spiral canal of Rosenthal	Spiral canal of modiolus		Canal of **Rosenthal**
Canales longitudinales modioli	Longitudinal canals of modiolus	Longitudinal canals of modiolus		
Scala vestibuli	Vestibular scala	Scala vestibuli		
Helicotrema	Helicotrema	Helicotrema		Orifice of **Scarpa**
Scala tympani	Tympanic scala	Scala tympani		
Ductus endolymphaticus	**Endolymphatic duct**	Endolymphatic duct		
Saccus endolymphaticus	Endolymphatic sac	Endolymphatic sac		
Ductus reuniens	Ductus reuniens	Ductus reuniens		Duct of **Hensen**
Ductus cochlearis	**Middle duct**	**Cochlear duct**		Canal of **Reissner**
Membrana vestibularis	Vestibular membrane of Reissner	Vestibular membrane		Membrane of **Reissner**
Lamina basilaris	Basilar membrane	Basal lamina		Spiral membrane of **Duverney**
Membrana tectoria	Tectorial membrane	Tectorial membrane		
Organum spirale	**Spiral organ of Corti**	**Spiral organ**		Organ of **Corti**
Cochleocytus	**Hair cells**	**Hair cells**		Hair cells of **Corti**
Cochleocytus internus	Inner hair cell	Inner hair cell	*Fgf8*	
Cochleocytus externus	Outer hair cell	Outer hair cell	*Prestin*	
Cellulae ductus cochlearis		**Cells of cochlear duct**		
Epitheliocyti limitantes sulcus internus	Inner sulcus cells	Cuboidal inner sulcus cells		
Epitheliocytus limitans internus	Cnner border cell	Inner border cell	*GLAST, S100*	Inner border cell of **Held**
Epitheliocytus limitans externus	Outer border cell	Outer border cell		Outer border cell of **Hensen**
Epitheliocytus glandularis externus basalis	Outer glandular cell	Basal external glandular cell		Glandular cell of **Boettcher**
Epitheliocytus cuboideus sulcus externus	Outer sulcus cells	Cuboidal external sulcus cells	*BMP4*	Epithelial cell of **Claudius**
Epitheliocyti sustenantes	**Supporting cells**	**Supporting cells**		
Epitheliocytus internus pilae	Inner pillar cell	Internal pilar epithelial cell	*p75, Prox1*	Inner pillar cell of **Corti**
Epitheliocytus phalangeus internus	Inner phalangeal cell	Internal phalangeal epithelial cell	*GLAST, S100*	Inner phalangeal cells
Epitheliocytus externus pilae	Outer pillar cell	External pilar epithelial cell	*Prox1*	Outer pillar cell of **Corti**
Epitheliocytus phalangeus externus	Outer phalangeal cell	External phalangeal epithelial cell	*Prox1, S100, GLAST*	Epithelial cell of **Deiters**
Membrana reticularis	Reticular membrane	Reticular membrane		Reticular membrane of **Koelliker**
Cuniculi		**Tunnels**		
Cuniculus externus	Outer tunnel of Held	External tunnel		Tunnel of **Held**
Cuniculus internus	Pillar tunnel	Inner tunnel		Tunnel of **Corti**
Cuniculus intermedius	Outer phalangeal space	Intermediate tunnel		Space of **Nuel**
Ganglion cochleare	**Spiral ganglion**	**Cochlear ganglion**	*Neurod1, NeuN, TrkB, TrkC*	Ganglion cochleare of **Corti**
Perikaryon nonmyelinatum	Outer spiral ganglion neuron (oSGN)	Nonmyelinated perikaryon	*Peripherin, Th, Cgrp*	Type II neuron **of Spoendlin**

(Continued)

TABLE 1 | Continued

Latin terms (TNA, 2017)	English terms (US spelling, proposed terms)	English terms (UK spelling; TNA, 2017)	Molecular signature	Related terms and Eponyms
Perikaryon myelinatum	Inner spiral ganglion neuron (iSGNa,b,c)	Myelinated perikaryon	iSGNa = *Calb2* iSGNb = *Calb1* iSGNc = *Pou4f1*	Type I neuron **of Spoendlin**
Gliocytus ganglionicus ganglii cochlearis	Satellite cell of spiral ganglion	Satellite cell of cochlear ganglion	*Sox10, ErbB2*	
Neurofibra radialis ganglii cochlearis	Radial fiber of spiral ganglion	Radial fiber of cochlear ganglion		Mix of afferents and efferents
Fasciculus spiralis internus	Inner spiral bundle	Inner spiral bundle		
Fasciculus intraganglionicus	Intraganglionic spiral bundle	Intraganglionic spiral bundle	*AChE, Chna9, Chna 10*	Intraganglionic efferent bundle
Fasciculus spiralis externus	Outer spiral bundle	Outer spiral bundle		
Ganglion vestibulare	**Vestibular ganglion**	**Vestibular ganglion**		
Neuron bipolare ganglii vestibularis		Bipolar neuron of vestibular ganglion	*Neurod1, Pou4f1, TrkB*	Ganglion of **Scarpa (**with variable neuron size)
Gliocytus ganglionicus ganglii vestibularis		Satellite cell of vestibular ganglion	*Sox10, ErbB2*	
Nervus vestibulocochlearis	**Vestibulocochlear nerve**	**Vestibulocochlear nerve**		
Nervus vestibularis	**Vestibular nerve**	**Vestibular nerve**		
Ramus communicans cochlearis	Vestibulocochlear anastomosis	Cochlear communicating branch	*AChE, Chna9*	Vestibulocochlear anastomosis of **Oort**
Pars superior	Utriculoampullary nerve	Superior part		**Related term:** Nervus vestibularis superior.
Nervus utricularis	Utricular nerve	Utricular nerve		
Nervus ampullaris anterior	Anterior ampullary nerve	Anterior ampullary nerve		
Nervus ampullaris lateralis	Lateral ampullary nerve	Lateral ampullary nerve		
Pars inferior	Inferior part	Inferior part		
Nervus ampullaris posterior	Posterior ampullary nerve	Posterior ampullary nerve		**Related term:** Nervus vestibularis inferior.
Nervus saccularis	Saccular nerve	Saccular nerve		**Related term:** Nervus vestibularis posterior.
Nervus cochlearis	**Auditory nerve**	**Cochlear nerve**		**Related term:** Nervus auditus.

This table was modified after (FCOA, 1998; FIPAT, 2017).

emerging nomenclature problem is to adopt a more meaningful nomenclature such as inner Spiral Ganglion Neurons, subtype a (iSGNa) as proposed in **Table 1**. It is to be expected that further single cell sequencing will likely lead to subdivisions of vestibular ganglion neurons as well given their cellular heterogeneity.

While some genes such as Sox2 are associated early in development with all neurosensory cells of the ear, they later become restricted to supporting cells following upregulation of high levels of Atoh1 in hair cells (Dabdoub et al., 2008). Interestingly enough, such gene expression over time depends on the level of expression of other transcription factors, as inner pillar cells show only limited expression of Atoh1 that does not affect Sox2 expression (Matei et al., 2005). Thus, while anatomical features and their physiological implications are largely settled, molecular signatures are still in flux due to technical advances that permit cell specific expression profile assessment to understand the complex cell type development and maintenance (Booth et al., 2018) as well as the gene expression profiles leading to specific structures such a stereocilia development (Ellwanger et al., 2018). Past research has stepwise improved the understanding of how sound moves the basilar membrane/organ of Corti/tectorial membrane complex to provide topology specific amplification (Ren et al., 2016; Dewey et al., 2018), including a detailed understanding of the function of the cochlear amplifier in the three rows of outer hair cells (Xia et al., 2018). Increasingly detailed insights into the function of the various sections of the organ of Corti have revealed major distinctions as an outer section playing a role in sound amplification and an inner section playing a role in sound conversion (Elliott et al., 2018). Molecular signatures that highlight nearly all outer section cells, including the inner pillar cells, such as Prox1, have been described (Fritzsch et al., 2010) that set the organ of Corti apart from vestibular sensory epithelia (Bermingham-McDonogh et al., 2006). Other transcription factors are uniquely found in a single cell type of the organ of Corti such as Fgf8 in inner hair cells that is found in many vestibular hair cells (Jahan et al., 2018) or the p75 neurotrophin receptor in inner pillar cells but also in sensory neurons (Von Bartheld et al., 1991). As more single cell

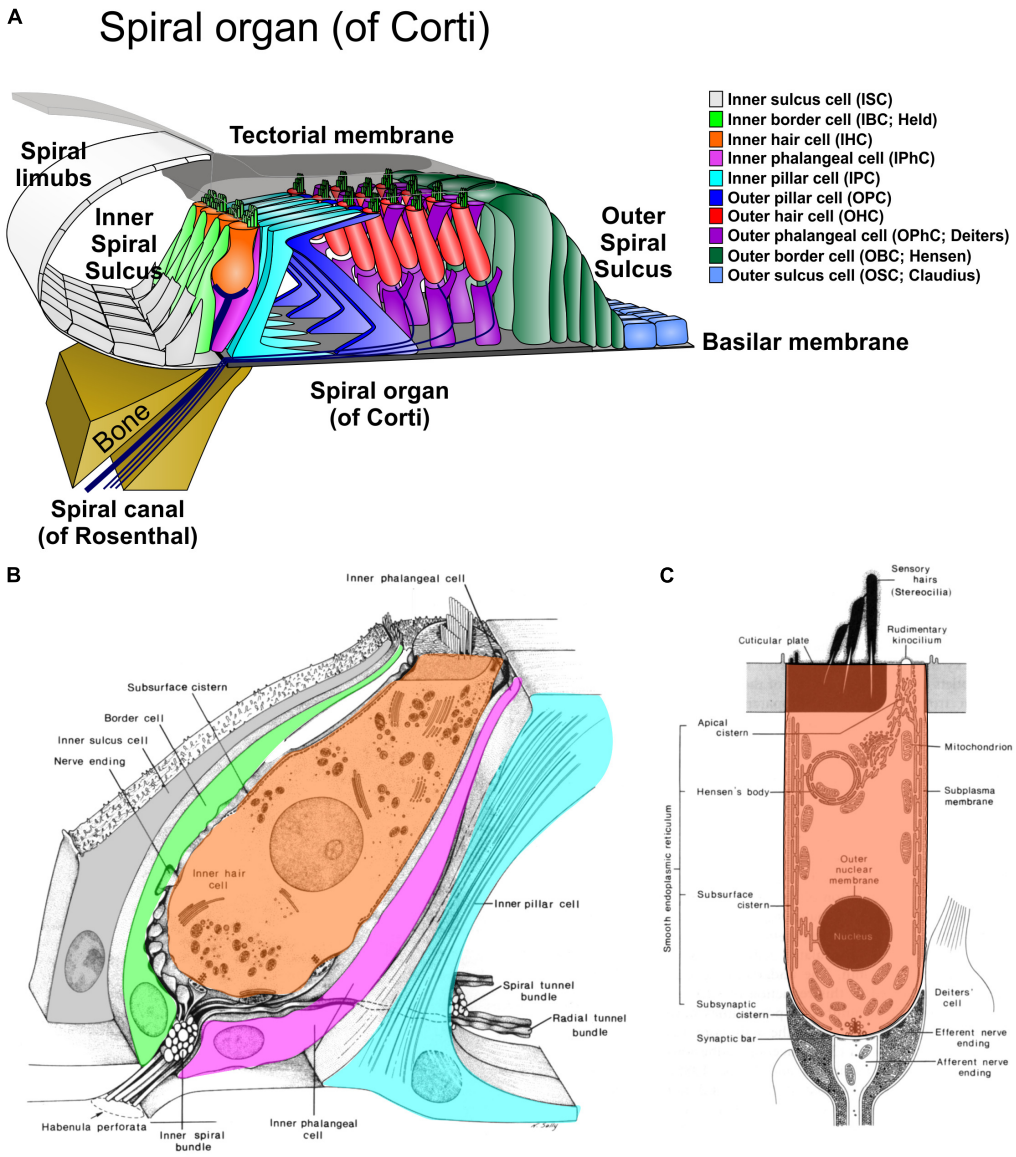

FIGURE 1 | The cellular organization of the organ of Corti is shown in a radial section **(A)** and the details of the inner hair cell **(B)** and outer hair cell **(C)** as revealed by transmission electron microscopy. Radial sections suggest a simple numerical relationship of cells of the inner section (1IBC, 1IHC, 1IPhC, 1 IPC) and other section (1OPC, 3 OHC, 3 OPhC, 3+ OBC). Note that the inner pillar cell (IPC) sits on the bony lip of the spiral canal (of Rosenthal). Equivalent cells of the outer and inner section are in different shades of the same color. Modified after Elliott et al. (2018) and Lim (1986).

transcriptome analyses are published, the current insights will likely be supplemented by both better characterization of unique expression profiles but will likely also end up indicating that some specificity is only a matter of thresholds of detection inherent to applied techniques.

GOALS OF THE PROPOSED REVISION

With this caveat of some future refinement based on deeper molecular understanding in mind, we propose here a revision of the most recent nomenclature (FCOA, 1998; FIPAT, 2017) that primarily builds on topology, physiology and, wherever possible, unique molecular signature (**Figures 1**, **2** and **Table 1**), taken ultrastructural details and their functional significance revealed over the last 70 years into account (Engström et al., 1964; Kimura, 1975; Lim, 1986; Slepecky, 1996). We propose to divide the spiral auditory organ (of Corti) into an **inner and an outer section** with appropriate expansion of the existing nomenclature to name each element accordingly:

The inner section is the sound receiving section. We propose to expand the already partially consistent nomenclature (inner spiral sulcus, inner hair cell, inner pillar cell, inner phalangeal cells (FCOA, 1998; FIPAT, 2017)) that excludes

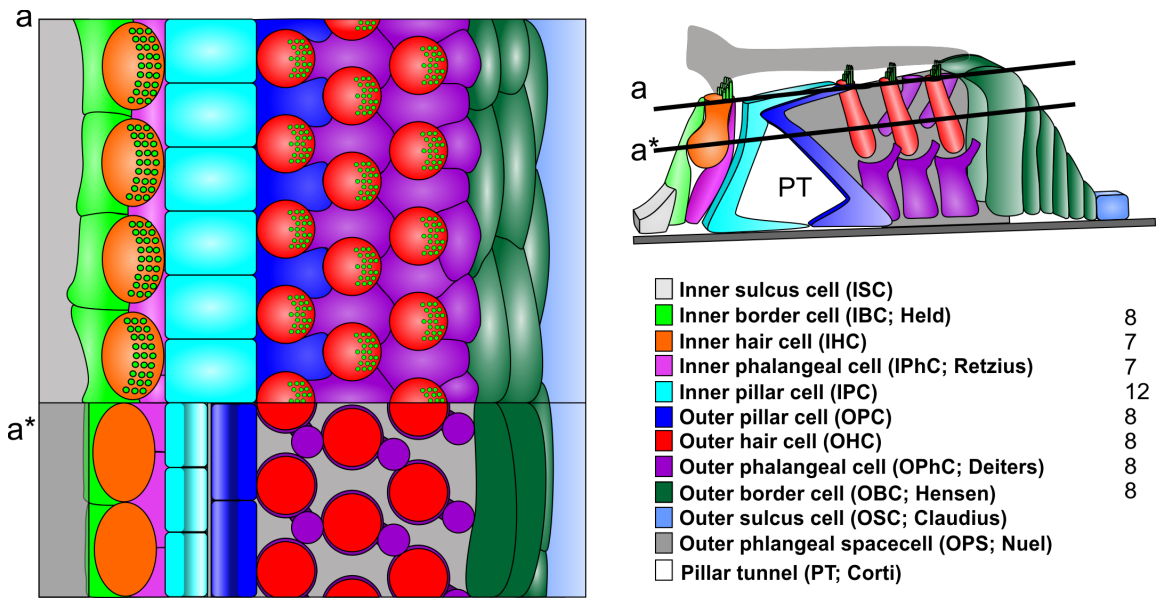

FIGURE 2 | In contrast to radial sections, top views on the reticular lamina **(a)** or horizontal sections below the reticular lamina **(a*)** indicate a different numerical ration between the cells of the inner section and outer section (right). Note that the largest number of cells are the iIPC with no clear numeric ratio to any of the adjacent cells. Note that the outer section has a simple 1:1 ratio between all elements of a given row also the details of most cells differ. For example, the reticular lamina is formed by the out rudder of the OPC between the first row of OHC (blue) but by the 1+2 second rows of OPhCs between the 2+3 row of OHC. The third row of OPhCs forms a continuous boundary along the reticular lamina flanking OBCs. IHC are in direct contact to IPCs only at the reticular lamina **(a)** whereas they are in contact with each other below the reticular lamina and are completely separated from IPC by the IPhC. Modified after Jahan et al. (2015).

some other relevant features. For example, it is now clear that the two major types of spiral ganglion neurons, type I and II, innervate the inner and outer hair cells, respectively. We therefore propose to use a new nomenclature of inner spiral ganglion neuron and outer spiral ganglion neuron instead of type I and type II. With the exception of transient expansion of some inner spiral neurons into the outer section during development (Druckenbrod and Goodrich, 2015; Goodrich, 2016) and under certain conditions of hair cell disorganization (Jahan et al., 2018), these neuronal processes of type 1 spiral ganglion neurons remain within the inner section and are named inner spiral ganglion neurons. Beyond possible transient developmental expansions to outer hair cells, the so-called lateral olivo-cochlear (LOC) system of inner ear efferents (Simmons et al., 2011) remains also restricted to the inner section and should thus be referred to as the inner (olivo-cochlear) efferents. Past use was also inconsistent with respect to (inner) border cells, dating back to the original description of this cell (Held, 1902) and extending into more detailed histology (Lim, 1986; Slepecky, 1996). We propose to use inner border cells to highlight these transitional cell type from the inner sulcus cells and propose to use the term outer border cells for the transitional cell type to outer sulcus cells, both with appropriate eponyms [inner border cells (of Held), outer border cells (of Hensen)].

The outer section is the sound amplifying section. The nomenclature of this section is less consistent overall (FCOA, 1998; FIPAT, 2017). The outer pillar cells (of Corti) and outer sulcus cells (of Claudius) are in the existing nomenclature as well as outer phalangeal cells (of Deiters). Neither the Hensen cells (here referred to as outer border cells of Hensen) nor the Boettcher cells (restricted to the basal turn) have been included into a consistent nomenclature. As with the inner section, both afferent and efferent innervation can be renamed to reflect their exclusive projection to outer hair cells in the adult organ (Rubel and Fritzsch, 2002; Goodrich, 2016). With this exclusive connection in normal adult mammals in mind, type II spiral ganglion neurons should be renamed as outer spiral ganglion neurons. Likewise, the clear exclusive connection of the medial olivo-cochlear neurons to outer hair cells (Simmons et al., 2011) necessitates to rename them as outer (olivo-cochlear) efferents. Note that this nomenclature proposal for afferent and efferent neurons reflects to terminals in spiral auditory organ (of Corti) and not the distribution of their cell bodies near the superior olivary complex as in the past.

Adopting this nomenclature would help to entrench the functional differences of the two sections in the context of their topology: the **inner section is the "hearing" section** that has all the inner hair cells with associated inner supporting cells, inner afferents and inner efferents needed for hearing. In contrast, the **outer section is the "amplifier" section** with the contractile outer hair cells innervated predominantly by the outer efferents with outer spiral afferents playing a role only in very loud sound hearing related to damage (Liu et al., 2015). Both sections are mirror symmetric with respect to cell type distribution.

The **inner section** cell types progresses from medial (modiolar) to lateral as follows: inner sulcus cells (ISC), inner

border cells (IBC), inner hair cells (IHC), inner phalangeal cells (IPhC), inner pillar cells IPC (**Figure 1**).

The **outer section** cell types progresses (in reverse cellular order) from lateral to medial as follows: outer sulcus cells (OSC), outer border cells (OBC), outer hair cells (OHC), outer phalangeal cells (OPhC), and outer pillar cells (OPC; **Figure 1**). The pillar tunnel (of Corti) divides the numerical and organizationally distinct (Jahan et al., 2015) inner and outer section.

While the two sections have similar overall numbers of cell types (excluding the basal outer border cells [of Boettcher] in the apex, the total numbers of cellular units to each section vary dramatically. For example, the inner section receives the vast majority of afferents (∼95%) and efferents (∼60%) but has overall fewer units of each cell type in a radial section (one IBC as compared to 2–4 OBC, one IPhC as compared to three OPhC, one IHC compared to three OHC [except for reduced numbers in the base and increased numbers in the apex]. The only symmetry in terms of numbers of elements are IPC and OPC. However, this apparent symmetry even of these cells is a consequence of the radial section perspective (**Figure 1**). Viewed from the reticular lamina, the OHC and OphC/OPC form a nearly perfectly alternating cellular network (**Figure 2**). In contrast, near the basal lamina, all supporting cells in the outer section are in broad contact with each other without any outer hair cell in between. Interestingly enough, while IPC and OPC are in broad contact both basally and apically (Lim, 1986; Slepecky, 1996), the numbers of IPC and OPC cells are in a 3:2 ratio (Held, 1902). Whereas OHC are never in contact with each other, IHC are in very broad contact with each other being separated only at the reticular lamina by the IPhC and IBC [Lim, 1986; Held, 1902; Slepecky, 1996] and touching only at the reticular lamina the IPC (**Figures 1**, **2**). Thus, while lateral inhibition with the delta–notch interaction may explain the formation of the outer section mosaic it fails to explain the inner section cell assembly. In fact, the real numerical relationship of each cell type for a given stretch of the spiral auditory organ (of Corti) for humans is: IBC = 8; IHC = 7; IPhC = 7; IP = 12; OP = 8; IHC = 8 × 3 rows; OPhC = 8 × 3 rows; OBC = 8 × 3 − 4 rows (Jahan et al., 2015).

While some of these odd numerical relationships have been known since Retzius (1884) and Held (1902) counted them, their implication for developmental biology in terms of regulating their differential numbers has been nearly universally ignored. Various studies have revealed that this ratio is extremely dependent on diffusible factors and cell–cell interactions (Groves and Fekete, 2012, 2017; Jahan et al., 2018). More recent emphasis on effects of gene replacement on these cellular numeric ratios and their distribution have re-emphasized these differences between the two sections that need to be understood for any forward looking strategy to restore a functional spiral auditory organ (of Corti) and thus hearing from a flat epithelium (Jahan et al., 2018). Restoring an outer section will certainly not restore hearing but an inner section associated with proper amplification might be beneficial to maintain most afferent innervation through neurotrophic support (Fritzsch et al., 2016) and might be useful for hearing with proper amplification to offset the loss of the outer section. Overall, our proposal takes much of the existing nomenclature (FCOA, 1998; FIPAT, 2017) into account but provides a more uniform description of cellular elements around the now understood functional sections of the spiral auditory organ (of Corti), the mammalian hearing organ.

AUTHOR CONTRIBUTIONS

BF conceived and wrote the initial draft. KE reviewed the draft and prepared the illustrations.

FUNDING

This work was supported by a grant from NIH (RO1 AG060504).

REFERENCES

FCOA (1998). *Terminology, Terminologia Anatomica*. London: Georg Thieme Verlag.

Barany, R. (1906). *Untersuchungen über den vom Vestibularapparat des Ohres Reflektorisch Ausgelösten Rhythmischen Nystagmus und seine Begleiterscheinungen*. Washington, DC: Oscar Coblentz.

Békésy, G. V. (1930). Uber das Fechnersche Gesetz und seine Bedeutung für die Theorie der akustischen Beobachtungsfehler und die Theorie des Hörens. *Annalen der Physik* 399, 329–359. doi: 10.1002/andp.19303990305

Bermingham-McDonogh, O., Oesterle, E. C., Stone, J. S., Hume, C. R., Huynh, H. M., and Hayashi, T. (2006). Expression of Prox1 during mouse cochlear development. *J. Comp. Neurol.* 496, 172–186. doi: 10.1002/cne.20944

Boettcher, A. (1859). Weitere beiträge zur anatomie der schnecke. *Arch. Pathol. Anatom. Physiol. klinische Med.* 17, 243–281.

Booth, K. T., Azaiez, H. R., Smith, J. H., Jahan, I., and Fritzsch, B. (2018). Intracellular regulome variability along the organ of Corti: evidence, approaches, challenges and perspective. *Front. Genet.* 9:156. doi: 10.3389/fgene.2018.00156

Breuer, J. (1873). Ueber die Bogengänge des Labyrinths. *Allgemeine Wiener Med. Zeitung* 18, 598.

Claudius, M. (1856). Bemerkungen uber den Bau der hautigen Spiralleiste der Schnecke. *Z. wiss. Zool.* 7, 154–161.

Corti, A. (1851). Recherches sur l'organe de l'ouie des mammiferes. *Z. Wiss. Zool.* III , 3–63.

Dabdoub, A., Puligilla, C., Jones, J. M., Fritzsch, U., Cheah, X. K. S., Pevny, L. H., et al. (2008). Sox2 signaling in prosensory domain specification and subsequent hair cell differentiation in the developing cochlea. *Proc. Natl. Acad. Sci. U.S.A.* 105, 18396–18401. doi: 10.1073/pnas.0808175105

De No, R. L. (1981). *The Primary Acoustic Nuclei*. Newark, NJ: Raven Press.

Deiters, O. (1860). Beitrage zur Kenntniss der Lamina spiralis membranacea der Schnecke. *Z. Wissensch. Zool.* 10, 1–14.

Dewey, J. B., Xia, A., Müller, U., Belyantseva, I. A., Applegate, B. E., and Oghalai, J. S. (2018). Mammalian auditory hair cell bundle stiffness affects frequency tuning by increasing coupling along the length of the cochlea. *Cell Rep.* 23, 2915–2927. doi: 10.1016/j.celrep.2018.05.024

Druckenbrod, N. R., and Goodrich, L. V. (2015). Sequential retraction segregates SGN processes during target selection in the cochlea. *J. Neurosci.* 35, 16221–16235. doi: 10.1523/JNEUROSCI.2236-15.2015

Duverney, G. (1730). Traité de l'Organe de l'Ouïe. *Paris. English Ed.* 76, 83–104.

Elliott, K. L., Fritzsch, B., and Duncan, J. S. (2018). Evolutionary and developmental biology provide insights intot he regeneration of organ of corti hair cells. *Front. Cell. Neurosci.* 12:252. doi: 10.3389/fncel.2018.00252

Ellwanger, D. C., Scheibinger, M., Dumont, R. A., Barr-Gillespie, P. G., and Heller, S. (2018). Transcriptional dynamics of hair-bundle morphogenesis revealed with cell trails. *Cell Rep.* 23, 2901–2914. doi: 10.1016/j.celrep.2018.05.002

Engström, H., Ades, H. W., and Hawkins, J. E. (1964). Cytoarchitecture of the organ of Corti. *Acta Otolaryngol.* 57, 92–99. doi: 10.3109/00016486409134545

FIPAT (2017). *Terminologia Neuroanatomica*. Halifax, NS: FIPAT.

Fritzsch, B., Dillard, M., Lavado, A., Harvey, N. L., and Jahan, I. (2010). Canal cristae growth and fiber extension to the outer hair cells of the mouse ear require Prox1 activity. *PLoS One* 5:e9377. doi: 10.1371/journal.pone.0009377

Fritzsch, B., Kersigo, J., Yang, T., Jahan, I., and Pan, N. (2016). "Neurotrophic factor function during ear development: expression changes define critical phases for neuronal viability," in *The Primary Auditory Neurons of the Mammalian Cochlea*, eds A. Dabdoub, B. Fritzsch, A. N. Popper, and R. R. Fay (New York, NY: Springer), 49–84.

Goodrich, L. V. (2016). *Early Development of the Spiral Ganglion, The Primary Auditory Neurons of the Mammalian Cochlea*. Berlin: Springer, 11–48.

Groves, A. K., and Fekete, D. M. (2012). Shaping sound in space: the regulation of inner ear patterning. *Development* 139, 245–257. doi: 10.1242/dev.067074

Groves, A. K., and Fekete, D. M. (2017). "New directions in cochlear development," in *Understanding the Cochlea*, Vol. 62, eds G. Manley, A. Gummer, A. Popper, and R. Fay (Cham: Springer), 33–73. doi: 10.1007/978-3-319-52073-5_3

Held, H. (1893). *Die centrale Gehörleitung, Arch. Anat. Physiol; Anatomische Abteilung*. Frankfurt: Universitätsbibliothek Johann Christian Senckenberg, 201–248.

Held, H. (1902). *Untersuchungen über den feineren Bau des Ohrlabyrinthes der Wirbeltier*. Leipzig: BG Teubner.

Held, H. (1926). *Die Cochlea der Säuger und der Vögel, ihre Entwicklung und ihr Bau, Receptionsorgane I*. Berlin: Springer, 467–534.

Helmholtz, H. V. (1859). Ueber die Klangfarbe der Vocale. *Annalen Physik* 184, 280–290. doi: 10.1002/andp.18591841004

Hensen, V. (1863). Zur Morphologie der Schnecke des Menschen und der Saugetiere. *Z. Wiss. Zool.* 13, 481–512.

Hudspeth, A. J. (1989). How the ear's works work. *Nature* 341:397. doi: 10.1038/341397a0

Jahan, I., Elliott, K. L., and Fritzsch, B. (2018). Understanding molecular evolution and development of the organ of Corti can provide clues for hearing restoration. *Integr. Comp. Biol.* 58, 351–365. doi: 10.1093/icb/icy019

Jahan, I., Pan, N., Elliott, K. L., and Fritzsch, B. (2015). The quest for restoring hearing: understanding ear development more completely. *Bioessays* 37, 1016–1027. doi: 10.1002/bies.201500044

Kimura, R. S. (1975). *The Ultrastructure of the Organ of Corti1, International Review of Cytology*. Amsterdam: Elsevier, 173–222.

Kölliker, A. (1852). *Mikroskopische Anatomie, Bd. II, S.* 409. Leipzig: Universität Basel.

Kölliker, A. (1867). *Handbuch der Gewebelehre des Menschen: Für Aerzte und Studirende*. Leipzig: Wilhelm Engelmann.

Lewis, E. R., Leverenz, E. L., and Bialek, W. S. (1985). *The Vertebrate Inner ear*. Boca Raton, FL: CRC PressI Llc.

Lim, D. J. (1986). Functional structure of the organ of Corti: a review. *Hear. Res.* 22, 117–146. doi: 10.1016/0378-5955(86)90089-4

Liu, C., Glowatzki, E., and Fuchs, P. A. (2015). Unmyelinated type II afferent neurons report cochlear damage. *Proc. Natl. Acad. Sci. U.S.A.* 112, 14723–14727. doi: 10.1073/pnas.1515228112

Liu, H., Pecka, J. L., Zhang, Q., Soukup, G. A., Beisel, K. W., and He, D. Z. (2014). Characterization of transcriptomes of cochlear inner and outer hair cells. *J. Neurosci.* 34, 11085–11095. doi: 10.1523/JNEUROSCI.1690-14.2014

Lustig, L., Jackler, R. R. K., and Mandelcorn, R. (1998). The history of otology through its eponyms I: anatomy. *Otol. Neurotol.* 19, 371–389.

Mach, E. (1865a). Bemerkungen über den Raumsinn des Ohres. *Annalen Physik* 202, 331–333. doi: 10.1002/andp.18652021010

Mach, E. (1865b). *Zwei Populäre Vorlesungen über Musikalische Akustik*. Leipzig: Leuschner & Lubensky.

Matei, V., Pauley, S., Kaing, S., Rowitch, D., Beisel, K., Morris, K., et al. (2005). Smaller inner ear sensory epithelia in Neurog1 null mice are related to earlier hair cell cycle exit. *Dev. Dyn.* 234, 633–650. doi: 10.1002/dvdy.20551

Merchan-Perez, A., and Liberman, M. C. (1996). Ultrastructural differences among afferent synapses on cochlear hair cells: correlations with spontaneous discharge rate. *J. Comp. Neurol.* 371, 208–221. doi: 10.1002/(SICI)1096-9861(19960722)371:2<208::AID-CNE2>3.0.CO;2-6

Mudry, A. (2001). The origin of eponyms used in cochlear anatomy. *Otol. Neurotol.* 22, 258–263. doi: 10.1097/00129492-200103000-00024

Petitpré, C., Wu, H., Sharma, A., Tokarska, A., Fontanet, P., Wang, Y., et al. (2018). Neuronal heterogeneity and stereotyped connectivity in the auditory afferent system. *Nat. Commun.* 9:3691. doi: 10.1038/s41467-018-06033-3

Politzer, A. (1907). *Geschichte der Ohrenheilkunde*. Stuttgart: Eke Verlag.

Politzer, A. (1981). *History of Otology: From Earliest Times to the Middle of the Nineteenth Century*. Ann Arbor, MI: Columella Press.

Reissner, E. (1851). *De Auris Internae Formatione: Dissertatio Inauguralis: Accedit Tabula Lithographica*. Tartu: Dorpati Livonorum Laakmann.

Ren, T., He, W., and Kemp, D. (2016). Reticular lamina and basilar membrane vibrations in living mouse cochleae. *Proc. Natl. Acad. Sci. U.S.A.* 113, 9910–9915. doi: 10.1073/pnas.1607428113

Retzius, G. (1881). *Das Gehörorgan der Wirbelthiere: Morphologisch-Histologische Studien. 1, Das Gehörorgan der Fische und Amphibien*. Stockholm: Samson & Wallin in Commission.

Retzius, G. (1884). *Das Gehörorgan der Wirbelthiere: Morphologisch-Histologische Studien. 2, Das Gehörorgan der Reptilien, der Vögel und der Säugethiere*. Stockholm: Samson & Wallin in Commission.

Rubel, E. W., and Fritzsch, B. (2002). Auditory system development: primary auditory neurons and their targets. *Annu. Rev. Neurosci.* 25, 51–101. doi: 10.1146/annurev.neuro.25.112701.142849

Rutherford, M. A., and Moser, T. (2016). The ribbon synapse between type I spiral ganglion neurons and inner hair cells. *Prim. Audit. Neurons Mamm. Cochlea* 52, 117–156. doi: 10.1007/978-1-4939-3031-9_5

Scarpa, A. (1800). *Anatomische Untersuchungen des Gehörs und Geruchs. Aus dem Lat*. Nürnberg: Verlag.

Shrestha, B. R., Chia, C., Wu, L., Kujawa, S. G., Liberman, M. C., and Goodrich, L. V. (2018). Sensory neuron diversity in the inner ear is shaped by activity. *Cell* 174, 1229–1246. doi: 10.1016/j.cell.2018.07.007

Simmons, D., Duncan, J., de Caprona, D. C., and Fritzsch, B. (2011). *Development of the Inner ear Efferent System, Auditory and Vestibular Efferents*. Berlin: Springer, 187–216. doi: 10.1007/978-1-4419-7070-1_7

Slepecky, N. B. (1996). *Structure of the Mammalian Cochlea, The Cochlea*. Berlin: Springer, 44–129.

Spoendlin, H. (1971). Degeneration behaviour of the cochlear nerve. *Arch. klinische Exp. Ohren* 200, 275–291. doi: 10.1007/BF00373310

Sun, S., Babola, T., Pregernig, G., So, K. S., Nguyen, M., Su, S. M., et al. (2018). Hair cell mechanotransduction regulates spontaneous activity and spiral ganglion subtype specification in the auditory system. *Cell* 174, 1247–1263. doi: 10.1016/j.cell.2018.07.008

Von Bartheld, C. S., Patterson, S. L., Heuer, J. G., Wheeler, E. F., Bothwell, M., and Rubel, E. W. (1991). Expression of nerve growth factor (NGF) receptors in the developing inner ear of chick and rat. *Development* 113, 455–470.

von Sömmerring, S. T. (1806). *Abbildungen des Menschlichen Hörorgans*. Wenner: Varrentrapp u.

Willis, T. (1672). *De Anima Brutorum Quae Hominis Vitalis ac Sensitiva Est, Exercitationes Duae*. Davis, CA: E Theatro Sheldoniano, impensis Ric.

Xia, A., Udagawa, T., Raphael, P. D., Cheng, A. G., Steele, C. R., Applegate, B. E., et al. (2018). "Basilar membrane vibration after targeted removal of the third row of OHCs and Deiters cells," in *AIP Conference Proceedings, AIP Publishing*, (Hamburg), 020004.

Zheng, J., Shen, W., He, D. Z., Long, K. B., Madison, L. D., and Dallos, P. (2000). Prestin is the motor protein of cochlear outer hair cells. *Nature* 405:149. doi: 10.1038/35012009

Conflict of Interest Statement: The authors declare that the research was conducted in the absence of any commercial or financial relationships that could be construed as a potential conflict of interest.

Copyright © 2018 Fritzsch and Elliott. This is an open-access article distributed under the terms of the Creative Commons Attribution License (CC BY). The use, distribution or reproduction in other forums is permitted, provided the original author(s) and the copyright owner(s) are credited and that the original publication in this journal is cited, in accordance with accepted academic practice. No use, distribution or reproduction is permitted which does not comply with these terms.

frontiers in Neuroanatomy

MINI REVIEW
published: 06 December 2018
doi: 10.3389/fnana.2018.00104

Neural Progenitor Cell Terminology

Verónica Martínez-Cerdeño[1,2]* *and Stephen C. Noctor*[2,3]*

[1]*Department of Pathology and Laboratory Medicine, Institute for Pediatric Regenerative Medicine and Shriners Hospitals for Children of Northern California, UC Davis School of Medicine, Sacramento, CA, United States,* [2]*UC Davis Medical Center, MIND Institute, Sacramento, CA, United States,* [3]*Department of Psychiatry and Behavioral Sciences, UC Davis School of Medicine, Sacramento, CA, United States*

Since descriptions of neural precursor cells (NPCs) were published in the late 19th century, neuroanatomists have used a variety of terms to describe these cells, each term reflecting contemporary understanding of cellular characteristics and function. As the field gained knowledge through a combination of technical advance and individual insight, the terminology describing NPCs changed to incorporate new information. While there is a trend toward consensus and streamlining of terminology over time, to this day scientists use different terms for NPCs that reflect their field and perspective, i.e., terms arising from molecular, cellular, or anatomical sciences. Here we review past and current terminology used to refer to NPCs, including embryonic and adult precursor cells of the cerebral cortex and hippocampus.

Keywords: stem cell, neural precursor cell, central nervous system, radial glial cell, intermediate progenitor cell, neurogenesis, proliferation, terminology

OPEN ACCESS

Edited by:
Hans J. ten Donkelaar, Radboud University Nijmegen, Netherlands

Reviewed by:
Christoph Viebahn, Georg-August-Universität Göttingen, Germany
Richard S. Nowakowski, Florida State University College of Medicine, United States

***Correspondence:**
Verónica Martínez-Cerdeño
vmartinezcerdeno@ucdavis.edu
Stephen C. Noctor
scnoctor@ucdavis.edu

Received: *09 August 2018*
Accepted: *15 November 2018*
Published: *06 December 2018*

Citation:
Martínez-Cerdeño V and Noctor SC (2018) Neural Progenitor Cell Terminology. Front. Neuroanat. 12:104. doi: 10.3389/fnana.2018.00104

INTRODUCTION

"Stem cells" have the capacity to undergo self-renewing divisions that produce additional stem cells with the same properties and potential, and divisions that produce daughter cells that differentiate into multiple cell types. Stem cells can be "pluripotent precursor cells" that give rise to all cell types within an organism, or "multipotent precursor cells" that have the capacity to differentiate into a subset of cell types. The embryonic stem cells that are present in the inner cell mass of the blastocyst are an example of pluripotent stem cells. Many types of multipotent stem cells exist and can also be referred to as "progenitor cells." The embryonic layers and each specific tissue, such as the central nervous system (CNS) tissue, develop from cellular divisions of progenitor cells.

"Neural progenitor cells (NPCs)" are the progenitor cells of the CNS that give rise to many, if not all, of the glial and neuronal cell types that populate the CNS. NPCs do not generate the non-neural cells that are also present in the CNS, such as immune system cells. NPCs are present in the CNS of developing embryos but are also found in the neonatal and mature adult brain, and therefore are not strictly embryonic stem cells. "Embryonic NPCs" may ultimately give rise to "adult NPCs," as in the cerebral cortex (Merkle et al., 2004). NPCs are characterized based on their location in the brain, morphology, gene expression profile, temporal distribution and function. In general, embryonic NPCs have more potential than NPCs in the adult brain. NPCs can be generated *in vitro* by differentiating embryonic stem cells or "induced pluripotent stem cells (iPSC)." iPSCs are derived from adult cells, most often from fibroblasts or blood cells, and programmed into an embryonic-like pluripotent state.

EMBRYONIC NEURAL PROGENITOR CELLS

Embryonic NPCs were first described in the fetal spinal cord by Camillo Golgi in 1885 (see Rakic, 2003). Neuroanatomists in the 19th century began to identify and characterize basic properties of NPCs and the proliferative zones in the developing brain (Kölliker, 1882; Magini, 1888; His, 1889; Lenhossek, 1891; Retzius, 1894; Schaper, 1897; Ramón y Cajal, 1911; Rakic, 2003). Work in the late 19th and early 20th century revealed mitotic cells dividing near the telencephalic ventricle and concluded these were the "germinal cells" that produced cortical neurons (His, 1889). Hamilton (1901) conducted what in our knowledge is the first developmental study of NPC distribution in the developing cortex. She plotted the location of mitotic precursor cells in the cerebral cortex and spinal cord at several stages of prenatal and postnatal development in the rat and showed that mitoses were positioned in two basic locations: at the lumen of the ventricle and away from the ventricle, which she termed "ventricular" and "extra-ventricular" mitoses (Hamilton, 1901). Hamilton found that there was a shift in the location of mitoses during development, with most precursor cells dividing at the ventricle during early stages of development, and the majority of precursor cells dividing away from the ventricle at later stages of development (Hamilton, 1901). In addition, Hamilton reported morphological differences among precursor cells that correlated with the position of the dividing cell—in other words that precursor cells at the ventricle and away from the ventricle were morphologically distinct (Hamilton, 1901).

Embryonic Neural Proliferative Zones

Two proliferative zones in the developing cerebral cortex are commonly recognized today and using the terminology that was established in 1970 by the Boulder Committee (Angevine et al., 1970). The "ventricular zone (VZ)" is the primary proliferative zone that appears first during development and is adjacent to the ventricle, and the "subventricular zone (SVZ)" is the secondary proliferative zone that appears during later stages of development and is superficial to the VZ (Boulder Committee: Angevine et al., 1970). The only significant revision to Boulder Committee terminology in recent years stems from the work by Iain Smart and Henry Kennedy showing that the SVZ in rhesus monkeys is further subdivided into an "outer SVZ (oSVZ)" and an "inner SVZ (iSVZ)" (Smart et al., 2002). Subsequent work showed that the oSVZ is more prominent in the fetal human cortex (Fietz et al., 2010; Hansen et al., 2010), appears to be present in the developing cortex of most gyrencephalic mammals (Fietz et al., 2010; Reillo and Borrell, 2012), and is even present in the lissencephalic rat cortex during later stages of embryonic neurogenesis (Martínez-Cerdeño et al., 2012). The realization that the SVZ comprises distinct proliferative zones has stimulated significant lines of research into whether these different zones are populated by distinct NPC subtypes.

The terms that have been used to refer to NPCs in the developing cerebral cortex have varied over the past 100 years. These NPCs were initially referred to as "spongioblasts" and "fetal glia," reflecting their presumed non-neuronal nature and non-mature glial cell morphology. The names of these cells changed over the course of time to reflect not only personal perspective but also appreciation of features that were newly revealed through application of new scientific technology. The morphology of NPCs in human and non-human primates were first characterized through whole-cell impregnation techniques such as Golgi staining, and were more fully characterized after the introduction of electron microscopy (Rakic, 1972) and immunohistochemistry (Levitt and Rakic, 1980). Because VZ cells in many species persist beyond birth and are arranged in a radial orientation in the telencephalon and other structures including the diencephalon and spinal cord, the combined term "radial glia (RG)" was introduced (Rakic, 1971a), and remains the most commonly used term for primary NPCs in the VZ.

Embryonic Neural Progenitor Cells

RG cells appear through differentiation of precursor cells known as "neuroepithelial cells" that initially form the walls of the neural tube. Neuroepithelial precursor cells arise from the ectoderm early in development and are recognizable by their radial alignment and bipolar morphology—one process of the cell contacts the lumen of the ventricle, and the second process usually contacts the pial meninges. Neuroepithelial cells have the potential to undergo self-renewing symmetric divisions that increase the size of the precursor cell pool in early stages of development while forming the neural plate. After closure of the neural tube, neuroepithelial cells begin to upregulate glial specific factors, at which point they are thought to transform into RG cells and acquire the potential to generate neurons and glia (Aaku-Saraste et al., 1996; Morest and Silver, 2003). This cellular transformation is apparent at the morphological level by the lengthening of the cellular process that contacts the pial meninges, which we refer to as "pial fiber," and which is also referred to as "basal process."

RG cells located in the VZ are now considered to be the primary NPC in many regions of the developing brain. In the dorsal forebrain primary RG cells in the VZ can be identified by expression of the nuclear transcription factor Pax6 (Götz et al., 1998) and lack of expression for additional transcription factors such as Tbr2 (Englund et al., 2005). RG cells have been shown to exhibit several patterns of division and generate multiple cell types *in vitro* and *in vivo* during cortical histogenesis. RG cells initially undergo symmetric divisions that produce additional RG cells and expand the proliferative population in the VZ (Takahashi et al., 1995, 1996; Cai et al., 2002). *In vitro* experiments successfully replicate this feature of NPC behavior in the developing cerebral cortex (Noctor et al., 2008). At the onset of cortical neurogenesis, RG cells begin undergoing asymmetric divisions (Caviness et al., 2003), which produce a self-renewed RG cell and a neuronal daughter cell (Malatesta et al., 2000; Hartfuss et al., 2001; Miyata et al., 2001; Noctor et al., 2001; Tamamaki et al., 2001).

Embryonic Neural Progenitor Cells in the Cerebral Cortex

Later work demonstrated that asymmetric RG cell divisions appear to produce most neuronal daughter cells indirectly in the cerebral cortex, by first generating an NPC daughter cell that migrates to the SVZ, where it divides symmetrically to produce a pair of daughter neurons (Haubensak et al., 2004; Miyata et al., 2004; Noctor et al., 2004, 2008). Mitotic NPCs that divide in the SVZ have been identified by various terms, such as "extraventricular cells" (Hamilton, 1901), "subependymal cells" (Allen, 1912; Smart, 1961), "cells that divide away from the ventricle near blood vessels (BVs)" (Sauer, 1935), "SVZ cells" (Angevine et al., 1970), "non-surface progenitor cells" (Miyata et al., 2004), and some researchers have also used the term "abventricular mitoses." Currently, two interchangeable terms are used for mitotic NPCs in the SVZ: "intermediate progenitor (IP) cells" (Noctor et al., 2004), and "basal progenitor cells" (Haubensak et al., 2004). IP cells are generally multipolar and can therefore be distinguished from bipolar RG cells based on morphology (Noctor et al., 2004, 2008). IP cells can often be distinguished from RG cells based on location of division and, in the cerebral cortex, by expression of the Tbr2 transcription factor (Englund et al., 2005). Evidence gathered to date from rodents suggests that cortical neurogenesis involves a series of amplifying divisions that can be characterized as a two-step process in which: (1) RG cells divide in the VZ to produce IP cells; and (2) IP cells divide in the SVZ to produce pairs of daughter neurons (Kriegstein et al., 2006; Martínez-Cerdeño et al., 2006). As a result of this pattern of division, each RG cell division produces two daughter neurons, and potentially more, depending on how many times each IP cell divides (Hansen et al., 2010). Similar patterns of amplifying divisions have been identified in the ventral forebrain (Lim and Alvarez-Buylla, 2014) and in the adult germinal niches (Seri et al., 2004; **Figure 1**).

In the 1970s evidence was presented on the detachment of RG cells from the ventricle and subsequent translocation toward the pial surface. The translocation of these cells is more frequent toward the end of the cortical neurogenic period, and their existence was hinted in early studies of the developing cortex that examined Golgi stained material (see Schmechel and Rakic, 1979). Translocating RG cells have been reported in fixed fetal tissue obtained from human (Choi and Lapham, 1978; deAzevedo et al., 2003), macaque (Schmechel and Rakic, 1979), ferret (Voigt, 1989) and rat (Noctor et al., 2004, 2008). As in

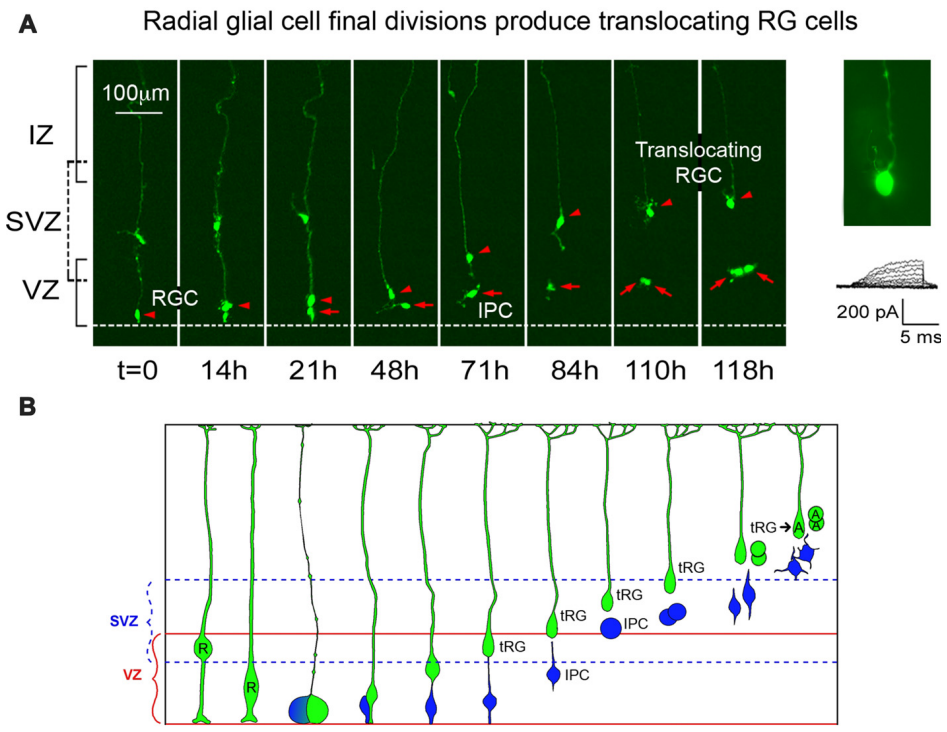

FIGURE 1 | Adapted from Noctor et al. (2004) Nature Neuroscience with permission of Nature publishing group—Springer Nature. Radial glial (RG) cells divide at the surface of the ventricle to produce translocating RG (tRG) daughter cells. Panel **(A)** presents images from an organotypic slice culture prepared from embryonic rat. A time-lapse series began on E18 and showed a single RG cell (red arrowhead) that divided at the ventricle to produce a translocating daughter cell, which maintained the pial process (red arrowhead) and translocated toward the pia. A second daughter cell (red arrow) divided away from the surface (t = 110 h). Electrophysiological recording from the translocating cell at 118 h demonstrated an absence of the voltage-dependent inward current that is typical of astroglial cells. Panel **(B)** summarizes findings from multiple time-lapse series performed in embryonic rat. Following their final division at the ventricle, radial glial cells (R) translocate and begin transformation into astrocytes (A). One daughter cell is an intermediate progenitor (IP) cell (blue) that divides in the subventricular zone (SVZ). The tRG also continues dividing and electrophysiological recordings obtained from the newborn daughter cells show that they have the membrane properties of astroglial cells.

the case of IP cells, multiple terms have been used to describe translocating RG cells, including "transitional RG" (Choi and Lapham, 1978; deAzevedo et al., 2003), "transitional astroglial cells" (Schmechel and Rakic, 1979), "transforming astroglial cells" (Voigt, 1989), "transforming RG cells" (Noctor et al., 2002), "translocating cells" (Noctor et al., 2004), "intermediate RG cells" (Reillo et al., 2011; Borrell and Reillo, 2012) and "translocating RG cells" (Martínez-Cerdeño et al., 2012). These cells are now referred to as "outer RG (oRG) cells" (Hansen et al., 2010) and "basal RG cells" (e.g., Fietz et al., 2010). *In vivo* and *in vitro* experiments in embryonic rat neocortex showed that translocating RG cells express glial fibrillary acidic protein (GFAP; Noctor et al., 2004), are mitotic, and generate glial cells (Noctor et al., 2008; Martínez-Cerdeño et al., 2012). More recent evidence shows that the translocating RG retain expression of the RG cell marker Pax6 (Fish et al., 2008; Fietz et al., 2010; Hansen et al., 2010; Reillo et al., 2011; Wang et al., 2011; Martínez-Cerdeño et al., 2012; Betizeau et al., 2013; Gertz et al., 2014; Poluch and Juliano, 2015), and may produce daughter neurons (Wang et al., 2011). Evidence gathered to date support the concept that translocating RG cells contribute to the population of astrocytes that are located in the cerebral cortex, including direct observations of *in vivo* data from sequential developmental stages (Voigt, 1989), live imaging of translocating cells followed by analysis through immunohistochemistry and electrophysiological recordings (Noctor et al., 2008), and data from early clonal lineage studies that provided evidence for mixed neuronal/astrocyte clones (Walsh and Cepko, 1990; **Figure 1**).

Non-cortical Structures

Evidence suggests that at very early stages of development primary precursor cells across a number of CNS structures share fundamental characteristics. For example, mitotic precursor cells in the developing pineal gland express the nuclear transcription factor Pax6, express vimentin, undergo division at the ventricle and express phosphorylated vimentin during mitosis, as in the cortex (Ibañez-Rodriguez et al., 2016). In the pineal gland the primary precursor cells acquire distinct characteristics as development proceeds, at which point they no longer resemble cortical NPCs. These data support the idea of regional specialization of common NPC phenotypes that facilitate the generation of distinct cell types across the CNS.

Human Brain

Nomenclature for NPCs in the human brain has largely been adopted from experimental animal models, in particular non-human primates (Smart et al., 2002). However, examination of developing human brain tissue has strengthened the case for unique features and characteristics of NPCs in human brain (Fietz et al., 2010; Hansen et al., 2010; Gertz et al., 2014; Otani et al., 2016). This may reflect functional adaptations of NPCs in the human brain that facilitate the production of more neurons and glia that are required to populate larger brain structures or may result from the evolution of functionally unique precursor cells that are not present in other mammals. Recent work examining single cell genomics of NPCs in the developing human brain will undoubtedly provide many answers for these questions (Nowakowski et al., 2017; Kosik and Nowakowski, 2018).

Non-mammalian Vertebrates

Data from non-mammalian vertebrates, for example lizard, turtle and chicken points to NPCs that share features across a broad spectrum of vertebrates. For example, primary NPCs in the forebrain of developing lizards, turtles and chicken express Pax6 as in mammals. Furthermore, a dense band of Tbr2 cells is arranged in what appears to be an SVZ in the pallium of developing chick, and in the dorsal ventricular ridge of turtles (Martínez-Cerdeño et al., 2016). These data suggest that the evolution of NPC phenotypes is not recent or restricted to certain classes of mammals.

ADULT NEURAL PROGENITOR CELLS

NPC are recognized as residing within two well-characterized niches in the adult mammalian brain: the "subgranular zone (SGZ)" of the dentate gyrus, and the "adult SVZ" surrounding the lateral ventricles of the mature cerebral cortex. The concept that neurons could be generated in the CNS of adult animals began with reports in the 1960s that neurons were generated in the postnatal rodent brain. Smart injected thymidine-H^3 in 3-day old and adult mice, and found newborn neurons near the subependymal layer in neonatal mice (Smart, 1961). Smart also reported evidence of neuron production in the adult brain but did not find surviving neurons in the cerebral cortex and concluded that newborn neurons in the adult degenerated (Smart, 1961). Postnatal neurogenesis also takes place within the external granular layer (EGL) of the cerebellum. Precursor cells in these proliferative zones are derived from precursor cells in the prenatal brain. Sidman and colleagues showed that the cerebellar EGL arises from the embryonic cerebellar VZ/SVZ, and produces neurons during postnatal development (Miale and Sidman, 1961; Sidman and Rakic, 1973). Similarly, NPC in the dentate SGZ derive from the embryonic VZ (Nowakowski and Rakic, 1981). These data provide evidence that adult neural progenitor cells derive, at least in part, from embryonic precursor cells that seed the adult proliferative zones.

Adult Neural Progenitor Cells in the Subgranular Zone

Adult NPCs in the dentate gyrus share fundamental properties with the RG cells and are therefore, referred to as "RG-like (RGL) cells" or "Type 1 cells." Type 1 cells are located in the SGZ, have a complex radial process that extends through the granule cell layer to the molecular layer where its end-feet terminate on synapses and vasculature (Moss et al., 2016). Type 1 cells express nestin, GFAP, and Sox2, and generate adult granule neurons (Seri et al., 2001). Type 1 cells can be quiescent or proliferative, and when mitotically active can divide symmetrically and asymmetrically. During neurogenic divisions the Type 1 NPCs give rise to IP cells called "Type 2 cells" that, as in the developing cerebral cortex, express Tbr2, exhibit a multipolar morphology, and

undergo a limited round of divisions that give rise to newborn neuronal cells that express doublecortin. The newborn daughter cells migrate radially into the granular cell layer where they mature into Prox1+ dentate granule neurons (Sun et al., 2015). Adult neurogenesis in the dentate gyrus has been observed in all mammals studied to date including humans (Eriksson et al., 1998; Ming and Song, 2011; Spalding et al., 2013; Hevner, 2016). The degree of adult neurogenesis in the dentate gyrus has been linked to crucial affective and cognitive behaviors, including learning, memory retention, pattern recognition and memory clearance (Sahay et al., 2011; Akers et al., 2014; Kitamura and Inokuchi, 2014; Anacker and Hen, 2017; for review see Berg et al., 2018).

Neural Progenitor Cells in the Adult Subventricular Zone

New born cells generated in the adult cortical SVZ migrate rostrally to the olfactory bulb where they disperse and differentiate into interneurons (**Figure 2**). Adult NPCs in the SVZ also generate glial cells. Adult NPC are referred to as "B1 cells." B1 cells are identified by location, expression of GFAP, GLAST and BLBP, and by endfeet that contact blood vessels (Doetsch et al., 1997; García-Verdugo et al., 1998). B1 cells can be

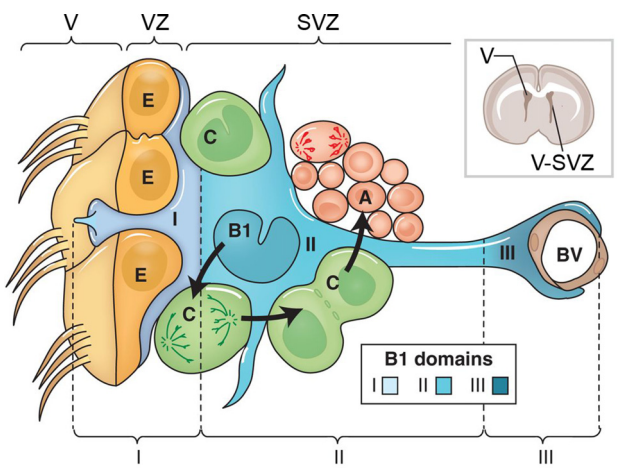

FIGURE 2 | This figure adapted from Lim and Alvarez-Buylla (2016) with permission of Cold Spring Harbor Laboratory Press. The cellular composition of the ventricular zone (VZ) and SVZ that line the lateral ventricle (V) of the adult brain. The drawing at upper right shows the location of the lateral ventricle and the VZ and SVZ in a coronal section from an adult rat brain. The VZ and SVZ region is enlarged at the left. Type B1 cells (blue) are astrocytes that serve as the VZ/SVZ stem cell. B1 cells divide to produce Type C cells (green). C cells are rapidly dividing transit amplifying cells that produce to Type A cells (red), which are migratory neuroblasts. B1 cells contact blood vessels (BVs, brown). The apical surface of B1 cells makes contact with the ventricle and has a primary cilium. The apical surfaces of the B1 cells are found at the center of a "pinwheel" composed of multiciliated ependymal cells (Type E cells, yellow). The apical process of the B1 cells, and the multiciliated processes of the Type E ependymal cells extend from their respective cell bodies into the lateral ventricle. The boundary between the ventricle (V) and VZ is indicated by the brackets at top, and by the solid line in each Type E cell. The VZ/SVZ is subdivided into three domains: domain I contains the B1 cell apical processes and ependymal cells; domain II contains the cell body of B1 cells; and domain III contains the B1 cell contact with BVs.

in a quiescent or proliferative state. Proliferative B1 cells undergo asymmetric divisions to generate a self-renewed B1 cells and transient progenitor cells that acts as a transit amplifying cell known as "C cells" (Ortega et al., 2013). C cells subsequently undergo divisions that generate daughter cells referred as "A cells," which migrate into the olfactory bulb. C cells express the transcription factors Ascl1 and Dlx2, while A cells express DCX and PSA-CAM (Doetsch et al., 1997; for review see Lim and Alvarez-Buylla, 2016).

Adult Neural Progenitor Cells in the Third Ventricle, Fourth Ventricle, and Cerebral Aqueduct

Tanycytes are a subpopulation of ependymal cells that are located in the third ventricle surrounding the circumventricular organs. Tanycytes participate in the regulation of energy balance, energy homeostasis and chemosensitivity (Langlet et al., 2013; Langlet, 2014). Recent studies on the ultrastructural and molecular characterization of tanycytes in mouse identified these cells as E2 ependymal cells. E2 cells comprise a continuous epithelium along the floor of the cerebral aqueduct and fourth ventricle (Mirzadeh et al., 2017). Molecular properties of tanycytes in the third ventricle suggest that these cells are floor-plate derivatives (Mirzadeh et al., 2017). Proliferation of tanycytes located in the wall of the third ventricle is very limited under normal conditions in the adult rat brain, but can be induced *in vivo* (Mirzadeh et al., 2017; Hendrickson et al., 2018). More recently, it has been shown that the adult human hypothalamus contains four distinct populations of cells that express neuronal progenitor markers, each of these cell types, with the exception of tanycytes, are human-specific (Pellegrino et al., 2018).

Adult Radial Glia Cells

Some RG cells in specific regions of the developing CNS differentiate into distinct RG cell types that persist into adulthood. These include "Müller glia" in the retina, "Bergmann glia (BG)" in the cerebellum (Guo et al., 2013; Surzenko et al., 2013), and RG cells in the adult spinal cord. BG derive from transformed RG cells and share many properties including radial alignment, multiple branching endfeet (Rakic, 1971b), vimentin expression, neuronal migration guidance (Schmechel and Rakic, 1979; Levitt and Rakic, 1980; Voigt, 1989), and mitotic activity (Bascó et al., 1977). Müller glia in the retina also derive from transformed RG cells and stain for vimentin and GFAP (Bignami, 1984; Pixley and de Vellis, 1984). In the adult retina, and specifically under conditions of stress, the RG derived Müller glia retain the potential to dedifferentiate, proliferate and generate newborn retinal neurons (Fischer and Reh, 2001).

CONCLUSIONS

The variety of terms used by neuroscientists to describe NPCs have often reflected contemporary concepts arising from techniques that were prevalent at a given time to label, identify and view CNS cells. This is also true today to some degree. Research into CNS development has gained considerable

knowledge in recent years through a combination of technical advances and individual insight. The terminology describing NPCs has evolved to incorporate newly revealed information about cellular characteristics and functions. While there has been a trend toward consensus and streamlined terminology, different terms for NPCs persist. The combined effect of research coming from diverse perspectives serves to increase our knowledge of what is ultimately most important: understanding NPC function in the developing and adult CNS.

AUTHOR CONTRIBUTIONS

Both authors wrote the manuscript.

FUNDING

This work was supported by National Institute of Mental Health 2R01MH094681 and Shriners Hospitals for Children funding to VM-C and R01MH101188 to SN.

REFERENCES

Aaku-Saraste, E., Hellwig, A., and Huttner, W. B. (1996). Loss of occludin and functional tight junctions, but not ZO-1, during neural tube closure—remodeling of the neuroepithelium prior to neurogenesis. *Dev. Biol.* 180, 664–679. doi: 10.1006/dbio.1996.0336

Akers, K. G., Martinez-Canabal, A., Restivo, L., Yiu, A. P., De Cristofaro, A., Hsiang, H. L., et al. (2014). Hippocampal neurogenesis regulates forgetting during adulthood and infancy. *Science* 344, 598–602. doi: 10.1126/science.1248903

Allen, E. (1912). Cessation of mitosis in central nervous system of the albino rat. *J. Comp. Neurol.* 22, 547–568.

Anacker, C., and Hen, R. (2017). Adult hippocampal neurogenesis and cognitive flexibility—linking memory and mood. *Nat. Rev. Neurosci.* 18, 335–346. doi: 10.1038/nrn.2017.45

Angevine, J. B., Bodian, D., Coulombre, A. J., Edds, M. V., Hamburger, V., Jacobson, M., et al. (1970). Embryonic vertebrate central nervous system: revised terminology. *Anat. Rec.* 166, 257–261. doi: 10.1002/ar.1091660214

Bascó, E., Hajós, F., and Fülöp, Z. (1977). Proliferation of Bergmann-glia in the developing rat cerebellum. *Anat. Embryol.* 151, 219–222. doi: 10.1007/bf00297482

Berg, D. A., Bond, A. M., Ming, G. L., and Song, H. (2018). Radial glial cells in the adult dentate gyrus: what are they and where do they come from? *F1000Res.* 7:277. doi: 10.12688/f1000research.12684.1

Betizeau, M., Cortay, V., Patti, D., Pfister, S., Gautier, E., Bellemin-Ménard, A., et al. (2013). Precursor diversity and complexity of lineage relationships in the outer subventricular zone of the primate. *Neuron* 80, 442–457. doi: 10.1016/j.neuron.2013.09.032

Bignami, A. (1984). Glial fibrillary acidic (GFA) protein in Müller glia. Immunofluorescence study of the goldfish retina. *Brain Res.* 300, 175–178. doi: 10.1016/0006-8993(84)91355-6

Borrell, V., and Reillo, I. (2012). Emerging roles of neural stem cells in cerebral cortex development and evolution. *Dev. Neurobiol.* 72, 955–971. doi: 10.1002/dneu.22013

Cai, L., Hayes, N. L., Takahashi, T., Caviness, V. S. Jr., and Nowakowski, R. S. (2002). Size distribution of retrovirally marked lineages matches prediction from population measurements of cell cycle behavior. *J. Neurosci. Res.* 69, 731–744. doi: 10.1002/jnr.10398

Caviness, V. S. Jr., Goto, T., Tarui, T., Takahashi, T., Bhide, P. G., and Nowakowski, R. S. (2003). Cell output, cell cycle duration and neuronal specification: a model of integrated mechanisms of the neocortical proliferative process. *Cereb. Cortex* 13, 592–598. doi: 10.1093/cercor/13.6.592

Choi, B. H., and Lapham, L. W. (1978). Radial glia in the human fetal cerebrum: a combined Golgi, immunofluorescent and electron microscopic study. *Brain Res.* 148, 295–311. doi: 10.1016/0006-8993(78)90721-7

deAzevedo, L. C., Fallet, C., Moura-Neto, V., Daumas-Duport, C., Hedin-Pereira, C., and Lent, R. (2003). Cortical radial glial cells in human fetuses: depth-correlated transformation into astrocytes. *J. Neurobiol.* 55, 288–298. doi: 10.1002/neu.10205

Doetsch, F., García-Verdugo, J. M., and Alvarez-Buylla, A. (1997). Cellular composition and three-dimensional organization of the subventricular germinal zone in the adult mammalian brain. *J. Neurosci.* 17, 5046–5061. doi: 10.1523/JNEUROSCI.17-13-05046.1997

Englund, C., Fink, A., Lau, C., Pham, D., Daza, R. A., Bulfone, A., et al. (2005). Pax6, Tbr2, and Tbr1 are expressed sequentially by radial glia, intermediate progenitor cells, and postmitotic neurons in developing neocortex. *J. Neurosci.* 25, 247–251. doi: 10.1523/JNEUROSCI.2899-04.2005

Eriksson, P. S., Perfilieva, E., Björk-Eriksson, T., Alborn, A. M., Nordborg, C., Peterson, D. A., et al. (1998). Neurogenesis in the adult human hippocampus. *Nat. Med.* 4, 1313–1317. doi: 10.1038/3305

Fietz, S. A., Kelava, I., Vogt, J., Wilsch-Bräuninger, M., Stenzel, D., Fish, J. L., et al. (2010). OSVZ progenitors of human and ferret neocortex are epithelial-like and expand by integrin signaling. *Nat. Neurosci.* 13, 690–699. doi: 10.1038/nn.2553

Fischer, A. J., and Reh, T. A. (2001). Muller glia are a potential source of neural regeneration in the postnatal chicken retina. *Nat. Neurosci.* 4, 247–252. doi: 10.1038/85090

Fish, J. L., Dehay, C., Kennedy, H., and Huttner, W. B. (2008). Making bigger brains-the evolution of neural-progenitor-cell division. *J. Cell Sci.* 121, 2783–2793. doi: 10.1242/jcs.023465

García-Verdugo, J. M., Doetsch, F., Wichterle, H., Lim, D. A., and Alvarez-Buylla, A. (1998). Architecture and cell types of the adult subventricular zone: in search of the stem cells. *J. Neurobiol.* 36, 234–248. doi: 10.1002/(sici)1097-4695(199808)36:2<234::aid-neu10>3.0.co;2-e

Gertz, C. C., Lui, J. H., Lamonica, B. E., Wang, X., and Kriegstein, A. R. (2014). Diverse behaviors of outer radial glia in developing ferret and human cortex. *J. Neurosci.* 34, 2559–2570. doi: 10.1523/JNEUROSCI.2645-13.2014

Götz, M., Stoykova, A., and Gruss, P. (1998). Pax6 controls radial glia differentiation in the cerebral cortex. *Neuron* 21, 1031–1044. doi: 10.1016/s0896-6273(00)80621-2

Guo, Z., Wang, X., Xiao, J., Wang, Y., Lu, H., Teng, J., et al. (2013). Early postnatal GFAP-expressing cells produce multilineage progeny in cerebrum and astrocytes in cerebellum of adult mice. *Brain Res.* 1532, 14–20. doi: 10.1016/j.brainres.2013.08.003

Hamilton, A. (1901). The division of differentiated cells in the central nervous system of the white rat. *J. Comp. Neurol.* 11, 297–322. doi: 10.1002/cne.910110403

Hansen, D. V., Lui, J. H., Parker, P. R., and Kriegstein, A. R. (2010). Neurogenic radial glia in the outer subventricular zone of human neocortex. *Nature* 464, 554–561. doi: 10.1038/nature08845

Hartfuss, E., Galli, R., Heins, N., and Götz, M. (2001). Characterization of CNS precursor subtypes and radial Glia. *Dev. Biol.* 229, 15–30. doi: 10.1006/dbio.2000.9962

Haubensak, W., Attardo, A., Denk, W., and Huttner, W. B. (2004). Neurons arise in the basal neuroepithelium of the early mammalian telencephalon: a major site of neurogenesis. *Proc. Natl. Acad. Sci. U S A* 101, 3196–3201. doi: 10.1073/pnas.0308600100

Hendrickson, M. L., Zutshi, I., Wield, A., and Kalil, R. E. (2018). Nestin expression and *in vivo* proliferative potential of tanycytes and ependymal cells lining the walls of the third ventricle in the adult rat brain. *Eur. J. Neurosci.* 47, 284–293. doi: 10.1111/ejn.13834

Hevner, R. F. (2016). Evolution of the mammalian dentate gyrus. *J. Comp. Neurol.* 524, 578–594. doi: 10.1002/cne.23851

His, W. (1889). Die neuroblasten und deren entstehung im embryonalen mark. *Abh. Kgl. sachs. Ges. Wissensch. math. phys. Kl.* 15, 311–372.

Ibañez-Rodriguez, M. P., Noctor, S. C., and Muñoz, E. M. (2016). Cellular basis of pineal gland development: emerging role of microglia as phenotype regulator. *PLoS One* 11:e0167063. doi: 10.1371/journal.pone.0167063

Kitamura, T., and Inokuchi, K. (2014). Role of adult neurogenesis in hippocampal-cortical memory consolidation. *Mol. Brain* 7:13. doi: 10.1186/1756-6606-7-13

Kölliker, A. (1882). *Embryologie ou Traité Complet du Développement de L'homme et Des Animaux Superieurs.* Paris: Oxford University.

Kosik, K. S., and Nowakowski, T. (2018). Evolution of new miRNAs and cerebrocortical development. *Annu. Rev. Neurosci.* 41, 119–137. doi: 10.1146/annurev-neuro-080317-061822

Kriegstein, A., Noctor, S. C., and Martínez-Cerdeño, V. (2006). Patterns of neural stem and progenitor cell division may underlie evolutionary cortical expansion. *Nat. Rev. Neurosci.* 7, 883–890. doi: 10.1038/nrn2008

Langlet, F. (2014). Tanycytes: a gateway to the metabolic hypothalamus. *J. Neuroendocrinol.* 26, 753–760. doi: 10.1111/jne.12191

Langlet, F., Mullier, A., Bouret, S. G., Prevot, V., and Dehouck, B. (2013). Tanycyte-like cells form a blood-cerebrospinal fluid barrier in the circumventricular organs of the mouse brain. *J. Comp. Neurol.* 521, 3389–3405. doi: 10.1002/cne.23355

Lenhossek, M. (1891). Zur kenntnis der neuroglia des menschlichen ruckenmarkes. *Verh. Anat. Ges.* 5, 193–221.

Levitt, P., and Rakic, P. (1980). Immunoperoxidase localization of glial fibrillary acidic protein in radial glial cells and astrocytes of the developing rhesus monkey brain. *J. Comp. Neurol.* 193, 815–840. doi: 10.1002/cne.901930316

Lim, D. A., and Alvarez-Buylla, A. (2014). Adult neural stem cells stake their ground. *Trends Neurosci.* 37, 563–571. doi: 10.1016/j.tins.2014.08.006

Lim, D. A., and Alvarez-Buylla, A. (2016). The adult ventricular-subventricular zone (V-SVZ) and olfactory bulb (OB) neurogenesis. *Cold Spring Harb. Perspect. Biol.* 8:a018820. doi: 10.1101/cshperspect.a018820

Magini, G. (1888). Sur la neuroglie et les cellules nerveuses cerebrales chez les foetus. *Arch. Ital. Biol.* 9, 59–60.

Malatesta, P., Hartfuss, E., and Götz, M. (2000). Isolation of radial glial cells by fluorescent-activated cell sorting reveals a neuronal lineage. *Development* 127, 5253–5263.

Martínez-Cerdeño, V., Cunningham, C. L., Camacho, J., Antczak, J. L., Prakash, A. N., Cziep, M. E., et al. (2012). Comparative analysis of the subventricular zone in rat, ferret and macaque: evidence for an outer subventricular zone in rodents. *PLoS One* 7:e30178. doi: 10.1371/journal.pone.0030178

Martínez-Cerdeño, V., Cunningham, C. L., Camacho, J., Keiter, J. A., Ariza, J., Lovern, M., et al. (2016). Evolutionary origin of Tbr2-expressing precursor cells and the subventricular zone in the developing cortex. *J. Comp. Neurol.* 524, 433–447. doi: 10.1002/cne.23879

Martínez-Cerdeño, V., Noctor, S. C., and Kriegstein, A. R. (2006). The role of intermediate progenitor cells in the evolutionary expansion of the cerebral cortex. *Cereb. Cortex* 16, i152–i161. doi: 10.1093/cercor/bhk017

Merkle, F. T., Tramontin, A. D., García-Verdugo, J. M., and Alvarez-Buylla, A. (2004). Radial glia give rise to adult neural stem cells in the subventricular zone. *Proc. Natl. Acad. Sci. U S A* 101, 17528–17532. doi: 10.1073/pnas.0407893101

Miale, I. L., and Sidman, R. L. (1961). An autoradiographic analysis of histogenesis in the mouse cerebellum. *Exp. Neurol.* 4, 277–296. doi: 10.1016/0014-4886(61)90055-3

Ming, G. L., and Song, H. (2011). Adult neurogenesis in the mammalian brain: significant answers and significant questions. *Neuron* 70, 687–702. doi: 10.1016/j.neuron.2011.05.001

Mirzadeh, Z., Kusne, Y., Duran-Moreno, M., Cabrales, E., Gil-Perotin, S., Ortiz, C., et al. (2017). Bi- and uniciliated ependymal cells define continuous floor-plate-derived tanycytic territories. *Nat. Commun.* 8:13759. doi: 10.1038/ncomms13759

Miyata, T., Kawaguchi, A., Okano, H., and Ogawa, M. (2001). Asymmetric inheritance of radial glial fibers by cortical neurons. *Neuron* 31, 727–741. doi: 10.1016/s0896-6273(01)00420-2

Miyata, T., Kawaguchi, A., Saito, K., Kawano, M., Muto, T., and Ogawa, M. (2004). Asymmetric production of surface-dividing and non-surface-dividing cortical progenitor cells. *Development* 131, 3133–3145. doi: 10.1242/dev.01173

Morest, D. K., and Silver, J. (2003). Precursors of neurons, neuroglia, and ependymal cells in the CNS: what are they? Where are they from? How do they get where they are going? *Glia* 43, 6–18. doi: 10.1002/glia.10238

Moss, J., Gebara, E., Bushong, E. A., Sánchez-Pascual, I., O'Laoi, R., El M'Ghari, I., et al. (2016). Fine processes of Nestin-GFP-positive radial glia-like stem cells in the adult dentate gyrus ensheathe local synapses and vasculature. *Proc. Natl. Acad. Sci. U S A* 113, E2536–E2545. doi: 10.1073/pnas.1514652113

Noctor, S. C., Flint, A. C., Weissman, T. A., Dammerman, R. S., and Kriegstein, A. R. (2001). Neurons derived from radial glial cells establish radial units in neocortex. *Nature* 409, 714–720. doi: 10.1038/35055553

Noctor, S. C., Flint, A. C., Weissman, T. A., Wong, W. S., Clinton, B. K., and Kriegstein, A. R. (2002). Dividing precursor cells of the embryonic cortical ventricular zone have morphological and molecular characteristics of radial glia. *J. Neurosci.* 22, 3161–3173. doi: 10.1523/JNEUROSCI.22-08-03161.2002

Noctor, S. C., Martínez-Cerdeño, V., Ivic, L., and Kriegstein, A. R. (2004). Cortical neurons arise in symmetric and asymmetric division zones and migrate through specific phases. *Nat. Neurosci.* 7, 136–144. doi: 10.1038/nn1172

Noctor, S. C., Martínez-Cerdeño, V., and Kriegstein, A. R. (2008). Distinct behaviors of neural stem and progenitor cells underlie cortical neurogenesis. *J. Comp. Neurol.* 508, 28–44. doi: 10.1002/cne.21669

Nowakowski, T. J., Bhaduri, A., Pollen, A. A., Alvarado, B., Mostajo-Radji, M. A., Di Lullo, E., et al. (2017). Spatiotemporal gene expression trajectories reveal developmental hierarchies of the human cortex. *Science* 358, 1318–1323. doi: 10.1126/science.aap8809

Nowakowski, R. S., and Rakic, P. (1981). The site of origin and route and rate of migration of neurons to the hippocampal region of the rhesus monkey. *J. Comp. Neurol.* 196, 129–154. doi: 10.1002/cne.901960110

Ortega, F., Berninger, B., and Costa, M. R. (2013). Primary culture and live imaging of adult neural stem cells and their progeny. *Methods Mol. Biol.* 1052, 1–11. doi: 10.1007/7651_2013_22

Otani, T., Marchetto, M. C., Gage, F. H., Simons, B. D., and Livesey, F. J. (2016). 2D and 3D stem cell models of primate cortical development identify species-specific differences in progenitor behavior contributing to brain size. *Cell Stem Cell* 18, 467–480. doi: 10.1016/j.stem.2016.03.003

Pellegrino, G., Trubert, C., Terrien, J., Pifferi, F., Leroy, D., Loyens, A., et al. (2018). A comparative study of the neural stem cell niche in the adult hypothalamus of human, mouse, rat, and gray mouse lemur *(Microcebus murinus)*. *J. Comp. Neurol.* 526, 1419–1443. doi: 10.1002/cne.24376

Pixley, S. K., and de Vellis, J. (1984). Transition between immature radial glia and mature astrocytes studied with a monoclonal antibody to vimentin. *Brain Res.* 317, 201–209. doi: 10.1016/0165-3806(84)90097-x

Poluch, S., and Juliano, S. L. (2015). Fine-tuning of neurogenesis is essential for the evolutionary expansion of the cerebral cortex. *Cereb. Cortex* 25, 346–364. doi: 10.1093/cercor/bht232

Rakic, P. (1971a). Guidance of neurons migrating to the fetal monkey neocortex. *Brain Res.* 33, 471–476. doi: 10.1016/0006-8993(71)90119-3

Rakic, P. (1971b). Neuron-glia relationship during granule cell migration in developing cerebellar cortex. A Golgi and electronmicroscopic study in Macacus rhesus. *J. Comp. Neurol.* 141, 283–312. doi: 10.1002/cne.901410303

Rakic, P. (1972). Mode of cell migration to the superficial layers of fetal monkey neocortex. *J. Comp. Neurol.* 145, 61–83. doi: 10.1002/cne.901450105

Rakic, P. (2003). Elusive radial glial cells: historical and evolutionary perspective. *Glia* 43, 19–32. doi: 10.1002/glia.10244

Ramón y Cajal, S. (1911). *Histologie du Système Nerveux de L'homme et Des Vertébrés.* Paris: Maloine.

Reillo, I., and Borrell, V. (2012). Germinal zones in the developing cerebral cortex of ferret: ontogeny, cell cycle kinetics, and diversity of progenitors. *Cereb. Cortex* 22, 2039–2054. doi: 10.1093/cercor/bhr284

Reillo, I., de Juan Romero, C., García-Cabezas, M. Á., and Borrell, V. (2011). A role for intermediate radial glia in the tangential expansion of the mammalian cerebral cortex. *Cereb. Cortex* 21, 1674–1694. doi: 10.1093/cercor/bhq238

Retzius, G. (1894). Die neuroglia des gehirns beim menschen und bei Säugetieren. *Biol. Untersuchun.* 6, 1–24.

Sahay, A., Scobie, K. N., Hill, A. S., O'Carroll, C. M., Kheirbek, M. A., Burghardt, N. S., et al. (2011). Increasing adult hippocampal neurogenesis is sufficient to improve pattern separation. *Nature* 472, 466–470. doi: 10.1038/nature09817

Sauer, F. C. (1935). Mitosis in the neural tube. *J. Comp. Neurol.* 62, 377–405. doi: 10.1002/cne.900620207

Schaper, A. (1897). Die frühesten differenzierungsvorgänge im centralnervensystem. Kritische studie und versuch einer geschichte der entwicklung nervöser substanz. *Arch. Entwicklungsmech* 5, 81–132. doi: 10.1007/bf02153233

Schmechel, D. E., and Rakic, P. (1979). A Golgi study of radial glial cells in developing monkey telencephalon: morphogenesis and transformation

into astrocytes. *Anat. Embryol.* 156, 115–152. doi: 10.1007/bf00300010

Seri, B., García-Verdugo, J. M., Collado-Morente, L., McEwen, B. S., and Alvarez-Buylla, A. (2004). Cell types, lineage, and architecture of the germinal zone in the adult dentate gyrus. *J. Comp. Neurol.* 478, 359–378. doi: 10.1002/cne.20288

Seri, B., García-Verdugo, J. M., McEwen, B. S., and Alvarez-Buylla, A. (2001). Astrocytes give rise to new neurons in the adult mammalian hippocampus. *J. Neurosci.* 21, 7153–7160. doi: 10.1523/JNEUROSCI.21-18-07153.2001

Sidman, R. L., and Rakic, P. (1973). Neuronal migration, with special reference to developing human brain: a review. *Brain Res.* 62, 1–35. doi: 10.1016/0006-8993(73)90617-3

Smart, I. H. (1961). The subependymal layer of the mouse brain and its cell production as shown by radioautography after thymidine-H3 injection. *J. Comp. Neurol.* 116, 325–345. doi: 10.1002/cne.901160306

Smart, I. H., Dehay, C., Giroud, P., Berland, M., and Kennedy, H. (2002). Unique morphological features of the proliferative zones and postmitotic compartments of the neural epithelium giving rise to striate and extrastriate cortex in the monkey. *Cereb. Cortex* 12, 37–53. doi: 10.1093/cercor/12.1.37

Spalding, K. L., Bergmann, O., Alkass, K., Bernard, S., Salehpour, M., Huttner, H. B., et al. (2013). Dynamics of hippocampal neurogenesis in adult humans. *Cell* 153, 1219–1227. doi: 10.1016/j.cell.2013.05.002

Sun, G. J., Zhou, Y., Stadel, R. P., Moss, J., Yong, J. H., Ito, S., et al. (2015). Tangential migration of neuronal precursors of glutamatergic neurons in the adult mammalian brain. *Proc. Natl. Acad. Sci. U S A* 112, 9484–9489. doi: 10.1073/pnas.1508545112

Surzenko, N., Crowl, T., Bachleda, A., Langer, L., and Pevny, L. (2013). SOX2 maintains the quiescent progenitor cell state of postnatal retinal Muller glia. *Development* 140, 1445–1456. doi: 10.1242/dev.071878

Takahashi, T., Nowakowski, R. S., and Caviness, V. S. Jr. (1995). The cell cycle of the pseudostratified ventricular epithelium of the embryonic murine cerebral wall. *J. Neurosci.* 15, 6046–6057. doi: 10.1523/JNEUROSCI.15-09-06046.1995

Takahashi, T., Nowakowski, R. S., and Caviness, V. S. Jr. (1996). The leaving or Q fraction of the murine cerebral proliferative epithelium: a general model of neocortical neuronogenesis. *J. Neurosci.* 16, 6183–6196. doi: 10.1523/JNEUROSCI.16-19-06183.1996

Tamamaki, N., Nakamura, K., Okamoto, K., and Kaneko, T. (2001). Radial glia is a progenitor of neocortical neurons in the developing cerebral cortex. *Neurosci. Res.* 41, 51–60. doi: 10.1016/s0168-0102(01)00259-0

Voigt, T. (1989). Development of glial cells in the cerebral wall of ferrets: direct tracing of their transformation from radial glia into astrocytes. *J. Comp. Neurol.* 289, 74–88. doi: 10.1002/cne.902890106

Walsh, C., and Cepko, C. L. (1990). Cell lineage and cell migration in the developing cerebral cortex. *Experientia* 46, 940–947. doi: 10.1007/bf01939387

Wang, X., Tsai, J. W., Lamonica, B., and Kriegstein, A. R. (2011). A new subtype of progenitor cell in the mouse embryonic neocortex. *Nat. Neurosci.* 14, 555–561. doi: 10.1038/nn.2807

Conflict of Interest Statement: The authors declare that the research was conducted in the absence of any commercial or financial relationships that could be construed as a potential conflict of interest.

Copyright © 2018 Martínez-Cerdeño and Noctor. This is an open-access article distributed under the terms of the Creative Commons Attribution License (CC BY). The use, distribution or reproduction in other forums is permitted, provided the original author(s) and the copyright owner(s) are credited and that the original publication in this journal is cited, in accordance with accepted academic practice. No use, distribution or reproduction is permitted which does not comply with these terms.

frontiers in Neuroanatomy

HYPOTHESIS AND THEORY
published: 21 March 2019
doi: 10.3389/fnana.2019.00025

Neuron Names: A Gene- and Property-Based Name Format, With Special Reference to Cortical Neurons

Gordon M. Shepherd[1,2], Luis Marenco[1,2], Michael L. Hines[1], Michele Migliore[1,3], Robert A. McDougal[1,2], Nicholas T. Carnevale[1], Adam J. H. Newton[1,4], Monique Surles-Zeigler[1,2] and Giorgio A. Ascoli[5]*

[1] Department of Neuroscience, Yale School of Medicine, New Haven, CT, United States, [2] Yale Center for Medical Informatics, New Haven, CT, United States, [3] Institute of Biophysics, National Research Council, Palermo, Italy, [4] Department of Physiology and Pharmacology, SUNY Downstate Medical Center, Brooklyn, NY, United States, [5] Bioengineering Department and Center for Neural Informatics, Krasnow Institute for Advanced Study, George Mason University, Fairfax, VA, United States

Precision in neuron names is increasingly needed. We are entering a new era in which classical anatomical criteria are only the beginning toward defining the identity of a neuron as carried in its name. New criteria include patterns of gene expression, membrane properties of channels and receptors, pharmacology of neurotransmitters and neuropeptides, physiological properties of impulse firing, and state-dependent variations in expression of characteristic genes and proteins. These gene and functional properties are increasingly defining neuron types and subtypes. Clarity will therefore be enhanced by conveying as much as possible the genes and properties in the neuron name. Using a tested format of parent-child relations for the region and subregion for naming a neuron, we show how the format can be extended so that these additional properties can become an explicit part of a neuron's identity and name, or archived in a linked properties database. Based on the mouse, examples are provided for neurons in several brain regions as proof of principle, with extension to the complexities of neuron names in the cerebral cortex. The format has dual advantages, of ensuring order in archiving the hundreds of neuron types across all brain regions, as well as facilitating investigation of a given neuron type or given gene or property in the context of all its properties. In particular, we show how the format is extensible to the variety of neuron types and subtypes being revealed by RNA-seq and optogenetics. As current research reveals increasingly complex properties, the proposed approach can facilitate a consensus that goes beyond traditional neuron types.

Keywords: neuron classification, terminology, axons, dendrites, brain regions, genomics

OPEN ACCESS

Edited by:
Hans J. ten Donkelaar, Radboud University Nijmegen, Netherlands

Reviewed by:
Kathleen S. Rockland, Boston University, United States
Mihail Bota, University of Southern California, United States
Robert H. Baud, Université de Fribourg, Switzerland

****Correspondence:***
Gordon M. Shepherd
gordon.shepherd@yale.edu

Received: *30 October 2018*
Accepted: *07 February 2019*
Published: *21 March 2019*

Citation:
Shepherd GM, Marenco L, Hines ML, Migliore M, McDougal RA, Carnevale NT, Newton AJH, Surles-Zeigler M and Ascoli GA (2019) Neuron Names: A Gene- and Property-Based Name Format, With Special Reference to Cortical Neurons. Front. Neuroanat. 13:25. doi: 10.3389/fnana.2019.00025

INTRODUCTION

Accurate terminology for neurons is increasingly needed for communication of research on the nervous system and the establishment of databases that can give access to data about neurons and their properties. Here we show how this effort can be enhanced by combining neuron databases based on traditional names with new research on genes and neuron properties, in a format in which multidisciplinary properties are part of the name. This extended format facilitates the investigation

of a given neuron type within the context of all its properties, while at the same time providing an orderly listing of neurons within databases of neurons of different brain regions. This is particularly advantageous in support of studies of the complex properties of neurons in different regions of the cerebral cortex.

Most terms for neurons are holdovers from the nineteenth century, when it was discovered that nerve cells appear as distinct types based on the structure and location of their axons, dendrites and cell bodies. The terms varied in an idiosyncratic way among investigators, based on personal impression and imagination. Small cells were often called "granules," and large cells sometimes given the discoverer's name, such as "Purkinje cell" or "Betz cell." All attempts to bring order into this daunting terminological jungle originate in the vast overview contained in Ramón y Cajal's (1911) great work *Histologie du système nerveux de l'homme & des vertébrés*.

The pace of modern neuroscience research is now carrying us far beyond this strictly anatomical base. In particular it is providing new properties based on gene expression and functional characteristics. We have been developing archives of neurons and their properties, in which the names are listed separately from their properties. However, the properties are increasingly central to the identity of a neuron type. Incorporating these multimodal properties in the neuron name will have distinct advantages, so that a neuron can be readily searched and recognized, to facilitate research into increasingly complex types. The present aim is to outline a framework for achieving this.

Background

The SenseLab[1] suite of databases, initiated in 1993 and building on publications on synaptic organization of local regions, contains NeuronDB, which has focused on the terminology and properties of many of the most highly investigated neurons[2] (Mirsky et al., 1998; Crasto et al., 2007). As stated at the outset (Shepherd et al., 1998, p. 466):

> ". . . NeuronDB . . . is a tool for enabling the user to understand the significance of a molecular property within the context of other properties contributing to the functions at a particular site within a particular neuron. This is a goal, not only for neuroscientists, but also for molecular biologists studying gene function in the emerging fields of functional genomics and pharmacogenomics."

With this approach, a neuron name is closely related to its multimodal properties, a principle that will be used in expanding to a systematic, properties-based, terminology outlined in this paper.

An early effort in developing a systematic neuron terminology occurred within a Brain Architecture Knowledge Management System (BAMS) (Bota and Swanson, 2007, 2008, 2010), which has been later related to rat and mouse connectomes (Bota et al., 2012a,b). The NeuronDB approach was greatly expanded by an effort sponsored by the Society for Neuroscience with the Neuroscience Information Framework (NIF) (Gardner et al., 2008), a web-based data and knowledge archive, with a section entitled Neurolex Neuron aimed at providing a list of all the known neurons in vertebrates and invertebrates, including those in BAMS. Accompanying the list were entries for each neuron containing further information on such properties as axon myelination, dendritic branching, soma site, neurotransmitters, etc., A series of articles related to this effort developed an ontological approach to the terminology of the neurons and their properties (Bug et al., 2008; Hamilton et al., 2012; DeFelipe et al., 2013; Larson and Martone, 2013; Polavaram and Ascoli, 2017). Many of these principles have been tested for neuron types from the rodent hippocampal formation in Hippocampome.org (Wheeler et al., 2015; Hamilton et al., 2017), which is closely related to the present account. Detailed coverage of neurons has been available in *The Synaptic Organization of the Brain* (Shepherd, 1974, 2004), and from the perspective of organization of neurons into microcircuits in the *Handbook of Brain Microcircuits* (Shepherd and Grillner, 2018).

The new era based on the methods of single cell transcriptomics and optogenetics is revealing the genes expressed by, and the electrophysiological properties of, morphologically identified neuron types. Here we build on the multimodal representation of neurons in several databases: NeuronDB, which started with representations of morphology, neurotransmitters, neurotransmitter receptors, and ion channels; ModelDB, which contains realistic neuron models reproducing the firing properties; and NeuroMorpho.Org (Ascoli et al., 2007; Akram et al., 2018), which contains reconstructions of the morphology of the cell types.

It is now timely to incorporate the new data on multimodal properties. The aim of the BRAIN Initiative Cell Census Consortium (Ecker et al., 2017) is "developing, validating, and scaling up emerging genomic and anatomical mapping technologies for creating a complete inventory of neuronal cell types and their connections in multiple species and during development." The present proposal goes beyond genomics and anatomy, with the ultimate aim of the Consortium: a hierarchical organization of multimodal features in neuron names:

> "Finally, the importance of establishing a common cell type nomenclature across species cannot be overstated .... The nomenclature could follow a hierarchical order, starting at the highest level: the species, then the brain region annotated based on a unified anatomical reference atlas system with cross-correlations among species, and then the *cell type as defined by a multimodal feature set (including locational, molecular, morphological, physiological, and ontological features)* (ed. italics).... The nomenclature should be a culmination of knowledge gained about the cellular organization of the nervous system." (Ecker et al., 2017, p. 551)

A similar initiative is reported in "The NIF ontology: brain parcels, cell types, and methods" (Gillespie et al., 2018). It recognizes the need for multiple techniques to reach a consensus "about even a single aspect of a cell type." It also aims to provide a knowledge base for neuron types "characterized by accumulated knowledge" regarding multiple phenotypes including "species,

[1] https://senselab.med.yale.edu/

[2] https://senselab.med.yale.edu/NeuronDB/

anatomical, molecular, morphological, physiological, synaptic and projection targets."

Finally, a major new initiative by the Allen Brain Institute (see Tasic et al., 2018) uses single cell RNA-seq, stochastic neighbor embedding (SNE) and connectivity methods to establish neuron identities on the combined basis of genes, markers, laminar localization and hodology. As will be shown, the format for reporting these results fits well with the present proposal. The multidisciplinary aims of these initiatives are thus shared with the current databases, underlying the timeliness of combining them in the present proposal.

INITIAL CONSIDERATIONS

With regard to the format of the neuron nomenclature, the approach used in NeuronDB and the NIF is to anchor the neuron in the region containing its cell nucleus (for most purposes the cell body). This sets up a parent-child relation for all neurons belonging to this region. In listing neurons in the brain, neuron types are thus all contained in alphabetical order within their appropriate region. This avoids any confusion about the identity of disparate neurons with similar names, such as granule cell, stellate cell, or pyramidal cell.

After the region, the neuron needs to be situated in its subregion, followed by its properties. In general, as indicated above, a consensus is emerging on the main categories of multimodal properties. As outlined in **Table 1**, the general order begins with defining the anatomical location and neuron morphology, followed by gene and molecular markers, physiological properties, and neurotransmitter. These are all properties of the neuron itself ("intrinsic").

An inconvenience for any nomenclature scheme is that many exceptions arise. Some regions are organized in a relatively simple fashion, whereas in others, like the cerebral cortex, there are many key factors to consider. Even more confusing, knowledge about different factors is often incomplete or lacking altogether. The interaction between morphology and molecular expression unavoidably adds a further level of complexity, because in neurons proteins may be expressed not only in the soma but in distant axonal or dendritic compartments. Another problem is that RNA-seq can show that a gene is expressed, but does not guarantee that it produces a protein.

Any nomenclature format must also take account of the fact that a given property may not always be present. As will be discussed, current research is showing that the properties that define a neuron are dependent on many dynamic factors, reflecting different functional states that can include differences in gene expression. These can be regarded in sum as the context within which a given name is applied. The solution here is to include the contextual factors in the name, so that the name is transparent in the context of other properties. We will discuss examples later in the multimodal cells of the cerebral cortex.

Including all of these factors in completely spelled out form can become cumbersome. It can be useful therefore to use abbreviations. This is already being done for a number of factors, such as cortical area and neuropeptides (M1 for primary motor area, SOM for somatostatin, etc.). We generally use abbreviations only when traditionally established.

PRINCIPLES FOR A SYSTEMATIC NEURON TERMINOLOGY

In general, it may be useful to distinguish three conceptual levels of description: a common term (the label), a definition (a combination of key properties), and additional features (other non-essential properties). Consider for example the entity associated with the term "neuronal dendrite." The NeuroLex definition is "A protoplasmic process of a neuron that receives and integrates signals from other neurons and conveys the resulting signal to the cell body." This definition identifies the unique set of necessary and sufficient properties of dendrites. Additional descriptive properties may be useful to identify a dendrite (branch length, tapering, microtubule-associated protein expression, presence of post-synaptic densities etc.), but

TABLE 1 | Categories of multimodal properties, for example, of a neocortical pyramidal neuron and interneuron in the primary motor area M1.

	Anatomical Properties					Functional Properties			
Naming system	**Region**	**Subreg**	**Layer**	**Conn**	**Name**	**Genes**	**Peptides**	**Physiol**	**Trans**
Pyramidal neurons									
Traditional	Neocortex	MI	L2/3		Pyramid				
NIF/NeuronDB	Neocortex	M1	L2/3	IT	Pyramid			{non-adapt	GLU}
Proposed	Neocortex	M1	L2/3	IT	Pyramid			{non-adapt	GLU}
Interneurons									
Traditional	Neocortex	M1	L2/3		Basket				
NIF/NeuronDB	Neocortex	M1	L2/3	INT	Basket		{SST	burst	GABA}
Proposed	Neocortex	M1	L2/3	INT	Basket	*Pvalb*	{SST	burst	GABA}

The table compares the formats for the relatively stable (anatomical) properties and functional properties used in the nomenclature in traditional use, NeuronDB/NIF NeuroLex, and the present proposal. Brackets { } indicate that in most current schemes the functional properties are stored in a separate database; in the present proposal they are part of the neuron name itself. Subreg, subregion; Conn, connectivity; Physiol, physiology; Trans, transmitter; L, layer; IT, intratelencephalic; INT, interneuron; non-adapt, non-adapting impulse firing; GLU, glutamate; GABA, gamma-amino butyric acid. References will be added to document critical properties.

are not part of the definition. The problem with existing common neuron names is that proper definitions are lacking in the vast majority of cases, and the label often reflects non-essential descriptive properties (such as "bistratified" or "horizontal").

A comprehensive attempt was made by the "Petilla Conference" to list the most common properties used to classify the inhibitory interneurons of the cerebral cortex, all the way to quantitative measurements of cell processes and features (Petilla Interneuron Nomenclature Group [PING] et al., 2008). In practice, the investigator seldom has access to all of these measurements and properties. A practical approach is therefore needed that provides a format for including properties that are usually available, especially ones that are the most relevant to critical functions that may be under investigation. That will be the approach taken here. Issues related to formal ontology are covered by authors cited previously.

Synapses are a cardinal feature of neurons, expressing and determining their interactions with other neurons and cells to generate the behavior of the organism (Shepherd, 2004). A systematic approach to describing the synaptic organization of neurons is therefore a logical basis for formulating a terminology that defines a given neuron type in terms of its function. It needs to start with the morphology of the neuron, the classical basis for neuron names. Especially for the cortex, it must include localization in relation to lamination and to projections, as well as potential connectivity (with input/output directionality) within the circuit (Ascoli and Wheeler, 2016; Rees et al., 2017).

This classical unimodal anatomical approach based on structure, however, is not enough in a molecular era. One must be able to add other properties that may be judged as essential for the identity and specific function of that neuron type. These may include, for example, biophysical properties, such as ionic currents critically involved in distinct functional features, such as action potential generation and firing patterns. They must include synaptic pharmacology, such as neurotransmitter receptors and neurotransmitters or neuromodulators released, and they must include data on cell markers identified by antibody staining and, increasingly, data on gene expression.

How detailed should the morphology be in identifying a neuron type? The Petilla terminology provided the option to account for quantitative measurements of dendritic branch sizes and branching patterns. NeuronDB introduced the concept of canonical dendritic branching types in which these branching details are considered not necessary to the basic identity of the neuron. Similarly, dendritic spines are important subcellular structures for synaptic connections in certain types of neurons, for example cerebellar Purkinje cells, olfactory granule cells, neostriatal medium spiny cells, and cortical pyramidal cells. However, except for neostriatal medium spiny cells, which are otherwise defined by their connectivity and output sites, neuron identity can presently be made without relying on the spines. This situation is likely to change as more is learned about the critical properties of these important structures.

All of this needs to be provided within a framework of overall data about the subject: we assume therefore that each full name technically would begin by indicating the species (and where applicable the strain), gender, and age (**Table 2**).

TABLE 2 | Basic features that apply to all neuron nomenclatures.

a. Species	mouse
b. Strain	see e.g., jax.org/mouse-search and purl.obolibrary.org/obo/NCBITaxon_10090
c. Gender	m/f
d. Age	embryo, newborn, young, adolescent, adult, old

*The embryo phase, with its many stages of neurogenesis and migration underlying early development, warrants its own expanded nomenclature (cf **Figure 9**).*

To simplify, in this review we will focus on the terminology for mouse (strain unspecified, gender unspecified, and age adolescent to mature adult).

This may seem to be a large amount of data to include in a name, which is why names and properties have until now been listed separately in NeuronDB, NeuroLex Neuron, Hippocampome.org, BAMS, NeuroMorpho.Org, and most other databases.

APPLICATION OF PRINCIPLES TO SPECIFIC EXAMPLES

We assume a consensus of common names as contained in the NIF, BAMS, synaptic organization of well-studied regions (Shepherd, 2004) and microcircuits in over 50 brain regions (Shepherd and Grillner, 2018). We start with this traditional name that captures the essential features of the distinct morphology of neurons, and add to it the combination of properties that defines a unique neuron type. We focus on methods of specifying names of neurons that identify neurons in research reports and databases containing information derived from or supplemental to those reports. Every neuron name has the flexibility of being augmented (to select subsets) or diminished (selecting supersets) to match the study. It will be for future neuroscientists to continue to work toward a consensus on the ontology of the names for unambiguous retrieval by arbitrarily combinatorial digital search.

IMPORTANCE OF REGION

Central nervous systems are characteristically organized in terms of regions where neurons interact with each other, and pathways which carry connections between the regions. We recognize that whereas for most of us it is sufficient in practice to refer to a standard text or atlas (e.g., Paxinos and Franklin, 2001; Allen Mouse Brain Atlas[3]), many regional boundaries are controversial. When the region is a part of the name, as proposed here, it makes it that much more important. Many feel that anatomical boundaries are better replaced by three-dimensional coordinates in a consensus brains atlas. For present purposes we assume the reader will identify the region from their own atlas. See also the discussion of relating neurons to regions in Ecker et al. (2017).

Two issues are important to recognize here. The first is that the required granularity with which anatomical regions

[3]http://mouse.brain-map.org/static/atlas

are delineated is hardly agreed upon in the community. Even for an intensely scrutinized neural system such as the hippocampal formation, the most up-to-date version of the Common Coordinate Framework (CCF) of the Allen Mouse Brain Atlas (arguably the most widely accepted freely available scholarly resource for this purpose) is rather non-uniform: it divides the dentate gyrus in three layers (molecular, granular, and polymorphic), but it leaves areas CA3 and CA1 undivided. The dentate laminar distinction is justified because different neuron types reside in different layers: granule cells in granular layer, mossy cells in hilus (polymorphic), and distinct types of GABAergic interneurons in each of the three parcels. Moreover, this lamination reflects the input/output organization of the principal cells and thus of the whole local circuit, as the axons and dendrites of the granule cells extend into the molecular layer and the hilus, respectively. These same reasons, however, also apply to areas CA3 and CA1, which should therefore be divided into layers as well. At the same time, many argue that the dentate gyrus molecular layer should be subdivided further since "semilunar" granule cells are only found in the inner one-third (Williams et al., 2007) while neurogliaform cells are only found in the outer two-thirds (Armstrong et al., 2011). Meanwhile, at the circuit level, the input from the entorhinal cortex is exclusively limited to the outer molecular layer while the feedback from hilus is limited to the inner molecular layer.

The second issue is that the order of priority in dividing a neural system into regions is not always straightforward. For example, different researchers may wish to specify the location of a pyramidal cell within the principal layer of area CA1 by depth (deep vs. superficial), by transversal position (closer to CA2 or to subiculum), or along longitudinal axis (from septal to temporal). Distinct properties appear to be organized along those dimensions, such as (among several others): phase-locking to distinct rhythms (Valero et al., 2015), separate axonal targeting (Tamamaki and Nojyo, 1990), and differential gene expression (Cembrowski et al., 2016), respectively. Thus, depending on the focus of a study, one and the same CA1 pyramidal cell might be described as placed "in the superficial layer," "near the subicular border," or "towards the septal pole," but these descriptors are complementary and not indicative of mutually exclusive types.

Within a region (identified with the above caveats) are a set of different types of neurons that are characteristic for that region. The first basic rule for terminology of neuron types recognizes that they are extraordinarily diverse across all regions, and that each type is usually unique in its soma-dendritic morphology, which is traditionally the main criterion for naming. The first requirement for the name is therefore that it begin with the region in which the neuron is located. This is in line with much of common usage. For example, we refer to a "cerebellar Purkinje cell" to discriminate between it and a cardiac Purkinje cell, though we can drop the adjective when the distinction is clear. Similarly we refer to a "cerebellar granule cell" to discriminate between it and quite different neurons named granule cells in other regions. This enabled the NIF NeuroLex list of over three hundred names to be organized coherently on an easily searchable regional basis. Similar considerations will apply to neuron databases using the proposed format.

NUCLEAR REGIONS: NEURON NAMES FOLLOW PARENT-CHILD FORMAT

We begin by considering examples of brain regions for applying the proposed terminology format in order to test the general validity of the approach. Regions may vary from simple, in which the set of different neurons is relatively homogeneous throughout a region, to complex, containing subregions, laminae, clusters, etc.; these delineations are not always agreed upon, as mentioned above. The simplest case is often called a "nucleus." Examples are the ventral horn of the spinal cord containing the motor neurons projecting to the muscles; the caudate and putamen of the neostriatum; and the many "nuclei" that characterize the central nervous system of the avian brain. This homogeneity implies that the entire region is organized to generate a specific set of functions, combining that with operations on its inputs to send outputs to other regions.

Spinal Cord

As an example we take the ventral horn of the spinal cord. The cord occurs in four main groups of segments: cervical, thoracic, lumbar and sacral. The lumbar ventral horn contains two types of neurons: large cells, motor neurons, which have long axons that innervate the skeletal muscles and muscle spindles, and small cells, which have short axons that stay within the anterior horn (**Figure 1**). Golgi was the first to differentiate between long axon cells and short axon cells, and that distinction remains fundamental. The current convention is to call those with long axons principal cells and those with short axons interneurons. In the NeuronDB list, the nomenclature is simplified by indicating principal neurons in dark green, and interneurons slightly indented and in light green. For present purposes, in order to make the terminology as efficient as possible, any neuron type not labeled interneuron is assumed to be a principal neuron without adding "principal ('P')," unless it is needed for clarity.

Traditionally "interneuron ('int, INT')" has been used rather loosely, sometimes referring to any cell that connects to other cells, but it is much more useful to use this term to designate the type of cell whose direct actions are entirely local. This will include a cell that lacks an axon as well (as in the retina and olfactory bulb). We note that a short axon cell can have inputs coming from long axons, and long axon cells may give off collaterals that stay within the local region. We will also note later that interneurons have been found whose axons connect local arborizations in different regions.

With these distinctions, we have "Spinal cord ventral horn motor neuron" and "Spinal cord ventral horn interneuron" as traditional names for these two types of cell in the vertebrate spinal cord. However, because the spinal cord contains several regions, we need to clarify which region contains these cells. We thus have expanded terms for region, subregion, and axon type as: "Spinal cord lumbar ventral horn motor neuron" and "Spinal

cord lumbar ventral horn interneuron" (**Figure 1**). Note how the inversion of the adjectival "lumbar" is necessary to keep all that follows under the common term "Spinal cord."

Ventral horn motor neurons come in two sizes with different connectivity: large alpha and smaller gamma. Interneurons may be of several types: Renshaw, Ia, Ib, etc. The controlling rule for adding these to the names is that in order to maintain the alphabetical order they must be modifiers of the main types, i.e., they must satisfy a parent-child relation, giving "Spinal cord lumbar ventral horn motor neuron alpha" and "Spinal cord lumbar ventral horn interneuron Renshaw." These examples are fully consistent with the format used in NeuronDB and NeuroLex Neuron.

The terminology builds directly on the chapter on "Spinal Cord" by Robert Burke in *The Synaptic Organization of the Brain*, ed. 5 (2004). The structured terminology ensures that the neurons are listed together in logical parent-child relations for easy visual review. Note that the principal neurons are differentiated on the basis of size, but also more distinctively on connectivity to completely different targets, alpha motor neurons to skeletal muscle and gamma motor neurons to muscle spindles. We will see that morphology and connectivity will vie for priority in defining neurons in many regions; together, they are in fact usually enough to specifically define the cell type. In ventral horn neurons, differentiating between motor neurons and interneurons, and between subtypes of each, is relatively easily possible because of their relation to specific reflex pathways that experimentally can be differentially activated.

With regard to the functional properties in our classification, alpha motor neurons express RNA for *Err3* (Friese et al., 2009); firing may be adapting or non-adapting, and acetylcholine (ACh) is the transmitter, which is excitatory at skeletal (skel) muscle endplates. Renshaw cells are known to be bursting, releasing glycine which is inhibitory to motor neurons. More complete names for the alpha motor neuron and the Renshaw interneuron are thus (*Err3*: Friese et al., 2009):

Region	Subreg	Layer	Conn	Trad. Name
Spinal cord	lumbar	VH	skel	MN alpha
Spinal cord	lumbar	VH	INT	Renshaw

Genes	Peptides	Physiol	Trans
Err3		adapt	ACh
		burst	GLY

If data on properties is missing, as for genes and peptides in this case, the category may be omitted and the name can be written in succinct form; the abbreviations are standard and therefore need no explanation:

Spinal cord lumbar VH INT Renshaw burst GLY

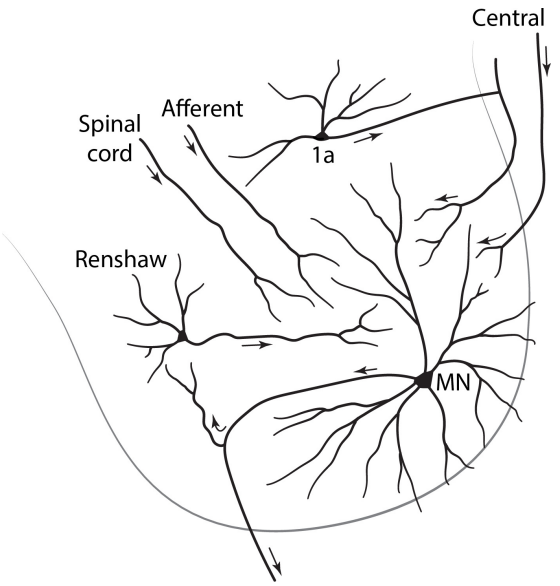

FIGURE 1 | Cross section of the lumbar spinal cord, showing in the ventral horn a principal neuron (alpha motor neuron: MN) with long motor axon to a distant target, a skeletal muscle; and interneurons with short axons that remain within their region of origin.

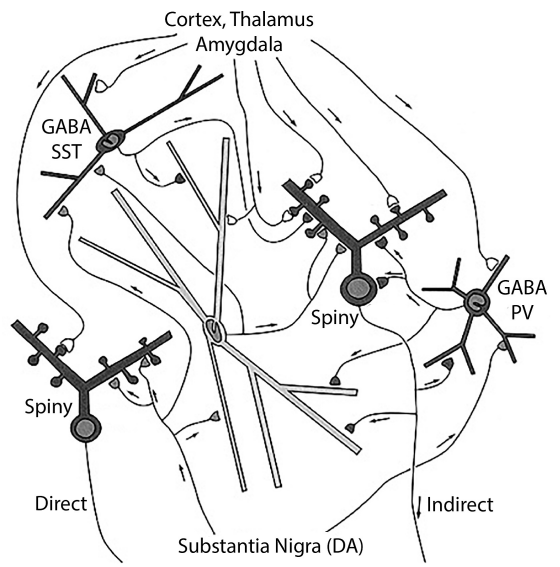

FIGURE 2 | Neostriatum, showing the direct and indirect principal neuron projections to the globus pallidus interna by the medium spiny neurons, and the several types of interneurons, including the large cholinergic interneuron [see text, adapted from Wilson (2004)].

Neostriatum

The neostriatum consists of the caudate and putamen nuclei, which are very similar in neuronal constituents (Doig and Bolam, 2018): one set of output (principal) neurons, the medium spiny neuron (spiny), is divided into two subtypes depending on the external target. Some (spiny indirect) connect indirectly to the globus pallidus pars interna through a relay in the pars externa, while others (spiny direct) connect directly to the pars interna (**Figure 2**). Within the neostriatum the main type of interneuron is the large cholinergic interneuron. In traditional terms:

"neostriatal direct medium spiny neuron"; "neostriatal indirect medium spiny neuron"; and "neostriatal large cholinergic interneuron," terminology consistent with NeuronDB and NeuroLex Neuron. In contrast to the ventral horn, the medium spiny neurons are relatively homogeneous in appearance, so differentiation between direct and indirect subtypes requires further physiological or molecular approaches (see below).

In this context, a problem arises if an experimental study is carried out reporting properties of medium spiny neurons in which the differentiation between direct and indirect connectivity is not known. Where do the properties get assigned? One possibility is a third category of "Undifferentiated medium spiny neuron." Another possibility is to enter the property into both types, with an asterisk or other sign that indicates differentiation unknown.

The neostriatum has also been characterized in terms of an organization of the medium spiny neurons into patches (striosomes: strio) within a continuous matrix (Graybiel, 2018). The medium spiny neurons have both direct and indirect projections from these entities. For some purposes, striosome and matrix locations of the cell bodies may be more important for the identities of the medium spiny neurons under investigation. A cell type with a given soma and dendritic morphology may therefore have a multiple identity depending on whether it is being characterized by its soma location or its axonal projections. This multiple identity is contained within the hierarchically organized name.

Data on genes include an early marker *DARPP-32* (Ouimet and Greengard, 1990) and differential expression of dopamine receptors 1 and 2 in direct and indirect medium spiny neurons, respectively. Thus, at present, we have, as examples for database entries, for a principal neuron and the large cholinergic interneuron (choline acetyltransferase: CHAT):

Region	Subreg	Layer	Conn	Trad. Name
Striatum	caudate	strio	direct	med spiny
Striatum	caudate	strio	INT	cholinergic
Genes	Peptides	Physiol	Trans	
Ppp1r1b, Drd1		non-adapt	GABA	
CHAT		burst	ACh	

APPLICATION TO CORTICAL NEURONS: THE CHALLENGE OF CORTICAL LAYERS AND CORTICAL AREAS

The approach thus far indicates that developing a systematic nomenclature for even apparently simple brain regions has many issues; nevertheless, we can develop and refine methods which can then apply to the complexities of cortical regions. In the same way, an approach through simpler types of cortex may also be effective. In recent years there has been increasing interest in the evolution from three-layer cortex, as exemplified in the olfactory and hippocampal cortices, to six-layer neocortex (Shepherd, 2011; Aboitiz and Montiel, 2015; Brunjes and Osterberg, 2015; Fournier et al., 2015; Luzzati, 2015; Diodato et al., 2016; Rowe and Shepherd, 2016; Klingler, 2017; Naumann and Laurent, 2017; Shepherd and Rowe, 2017). A nomenclature for cortical neurons should therefore be consistent with an evolutionary perspective. An exciting possibility is that the proposed approach to the nomenclature could ultimately reflect, and give insight into, the evolutionary processes that formed the neocortex and its neurons. For this purpose, the cortex of the present day turtle has become of interest as providing a lens into the forerunner of the earliest mammalian neocortex over 200 million years ago. We diverge to consider it briefly.

Turtle Dorsal Cortex

The dorsal cortex of the turtle has a single layer of pyramidal cells. As the name suggests, it lies dorsally, between the lateral olfactory cortex and the medial hippocampal cortex (ten Donkelaar, 1998). It is referred to as a "three-layer" cortex: a layer of pyramidal neuron bodies, between a deep layer of fibers and a superficial layer of dendrites, interneurons, and fibers (Smith et al., 1980; Kriegstein and Connors, 1986). As shown in **Figure 3**, the "pyramidal" name refers to the shape of the cell body. The cell has basal dendrites and a single apical dendrite, both covered in dendritic spines where excitatory synapses are made. The axon gives off collaterals which provide for excitation of itself and neighboring cells, and excitation of interneurons that provide for feedback and lateral inhibition of itself and neighboring cells.

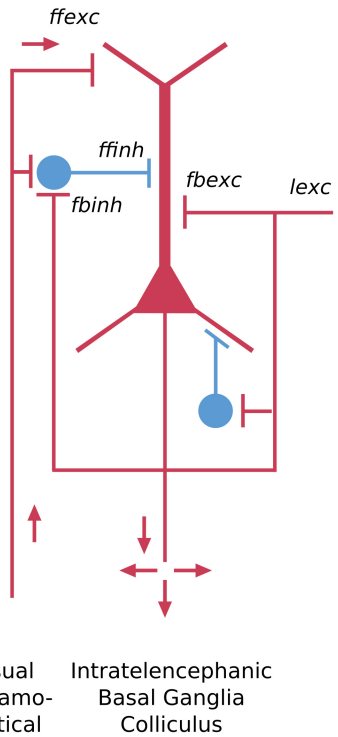

FIGURE 3 | Basic pyramidal cell (principal cell) forms the cortical circuit module of three-layer cortex in the turtle dorsal cortex. Red indicates excitatory, blue indicates inhibitory cell. *ffexc*, feedforward excitatory; *fbexc*, feedback excitatory; *lexc*, lateral excitatory; *ffinh*, feedforward inhibition; *fbinh*, feedback inhibition [Adapted from Shepherd and Rowe (2017)].

The axon then exits to target other cortical regions as well as the basal ganglia. We adopt current terminology for the neocortex in referring to this type of connectivity remaining mainly within the forebrain cortex and basal ganglia as "intratelencephalic (IT)" (Reiner et al., 2010; Harris and Shepherd, 2015; Shepherd and Rowe, 2017). There is also a projection to the superior colliculus.

The key features of this neuron type include the pyramidal-shaped cell body, the basal and apical dendrites, their dendritic spines, the recurrent and axon collaterals providing for feedback and lateral excitation and inhibition, and the projections to other "intratelencephalic" regions (see Shepherd, 2011). From an evolutionary perspective, this cell type can be traced back past the reptiles to the earliest vertebrate ancestors in fish and lamprey (Suryanarayana et al., 2017), where it appears in more generalized forms.

Applying the nomenclature rules thus far, assuming turtle instead of mouse for species, this neuron would be designated in full as:

Species	Region	Subregion	Connect
turtle	forebrain	cortex dorsal	IT
Name	**Physiol**	**Trans**	
pyramidal	non-adapting	GLU	

Further data on gene expression and cell markers are under investigation. Comparisons with simple piriform cortex and layers of neocortex are discussed below.

Piriform "Olfactory" Cortex

The piriform cortex is often referred to as olfactory cortex because it receives the output fibers of the olfactory bulb, and is an essential link to the neocortex where olfactory perception arises. This cortex arose in fish, amphibians and reptiles. Like dorsal cortex, it is usually referred to as a "three-layer" cortex. Closer observation shows that the cellular layer is actually composed of three distinct types of principal neuron in three layers: a most superficial layer of pyramidal semilunar (SL) cells; a middle layer of superficial (spc) pyramidal cells; and a layer of deep (dpc) pyramidal cells (Neville and Haberly, 2004; Wilson and Barkai, 2018) (see **Figure 4**). The piriform cortex is also divided into anterior and posterior parts.

The semilunar cell, though lacking basal dendrites and a single apical dendrite, is usually classified as a variant of a pyramidal neuron because of its extensive association fiber connections within the olfactory cortex, with the olfactory bulb and with the endopiriform (EN) nucleus, as well as its glutamate transmitter. Applying the nomenclature rules, the semilunar cell in a mammal would thus be designated in full:

Region	Subreg	Layer	Conn	Trad. Name
Piriform	anterior	supfl	IT	semilunar
Genes	**Peptides**	**Physiol**	**Trans**	
		non-adapt	GLU	

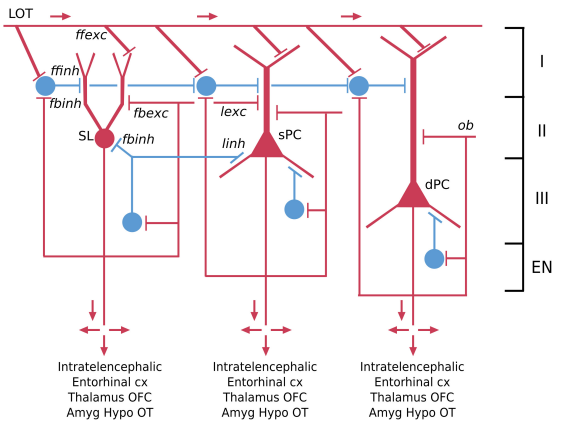

FIGURE 4 | Basic pyramidal cell (principal cell) circuit modules of the piriform (olfactory) cortex. Red indicates excitatory neurons, blue indicates inhibitory neurons. SL, semilunar pyramidal cell; sPC, superficial pyramidal cell; dPC, deep pyramidal cell [Adapted from Shepherd and Rowe (2017)].

Similarly, a second type, the superficial pyramidal cell, also has axon collaterals within the olfactory cortex, providing both the excitatory and, through an interneuron, inhibitory feedback. We also have data on functional properties. RNA-seq shows expression of several genes such as cux1 in this layer, but it is not at the single cell level (Brunjes and Osterberg, 2015). Action potential firing tends to be non-adapting and the neurotransmitter is glutamate. The name would thus be:

piriform anterior supfl IT pyramidal Cux1 non-adapt GLU

Similar rules apply to the deep pyramidal neuron and the pyramidal neurons in the posterior cortex.

The corresponding interneurons are classified as superficial, middle and deep (see **Figure 4**). Their full names follow the usual rule: for example:

piriform anterior supfl INT superficial burst GABA

Hippocampus

A third type of three-layer cortex in the mouse is the hippocampus. The olfactory cortex has provided examples of principal neurons arranged in different layers (**Figure 4**); the hippocampus particularly provides examples of principal neurons organized into distinctly different areas.

Classical studies identified a region in the temporal lobe that had a coiled structure remindful of a seahorse (hippo, horse; campus, monster) and a ram's horn (cornu ammonis: CA). The hippocampal complex is divided into a dentate gyrus and the hippocampus proper, the latter of which is further divided, in rodents, into three areas (CA1-3). We focus here on neurons of the dentate, CA3, and CA1 (see **Figure 5**). Classically, the cell

bodies all appear to be localized in a single layer within each area (granule cell layer in the dentate; pyramidal cell layer in CA3 and CA1). Some studies find it useful to separate further CA1 pyramidal cells into superficial and deep subtypes (see Slomianka et al., 2011; Valero and de la Prida, 2018). The dentate principal neurons are called granule cells, a name which arose only because they appeared very small in early microscopic studies; they have no necessary relation to granule cells in other parts of the nervous system. The parent-child format of region-name ensures there is no confusion. They have bushy spiny dendrites extending into a molecular layer where they receive input from stellate neurons in the medial and lateral entorhinal cortices. Their mossy fiber (MF) axon extends in a curving arc through the polymorphic layer (also known as the hilus) to terminate in large "mossy"-appearing terminals onto specialized sites (thorny excrescences) on proximal apical dendrites of pyramidal cells in area CA3. The CA3 pyramidal neuron in turn projects its axon through "Schaffer collaterals" mainly to the mid-apical dendrites of CA1 pyramidal neurons. CA1 pyramidal neurons project to the subiculum. All three of these principal neurons release glutamate as their neurotransmitter and are excitatory.

Recent studies are beginning to provide evidence for the richness of gene expression in hippocampal neurons. Examples for the principal neurons from Cembrowski et al. (2016) can be summarized in the names by following the canonical "three-synapse circuit," dentate to CA3 to CA1:

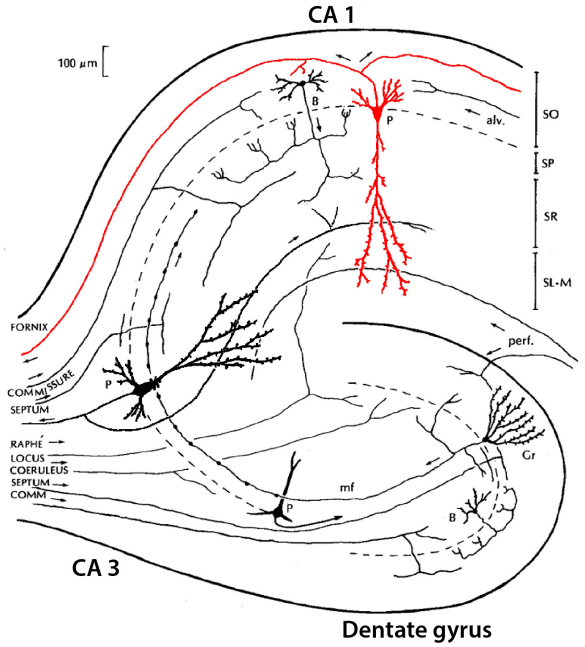

FIGURE 5 | Simplified summary of neurons in the hippocampus, showing the three main subregions: dentate gyrus (DG), CA3, and CA1, with their three main principal neurons: granule cell (Gr), and pyramidal (P) cells in CA3 and CA1. Examples of interneurons are shown for basket (B) cells in dentate gyrus and CA1 [Adapted from NeuronDB: (https://senselab.med.yale.edu/FunctionalConnectomeDB/realisticdiagram/diagram.py?id=154765)].

Region	Subreg	Layer	Conn	Trad. Name
Hippocampus	dentate	gran	MF	granule
Hippocampus	CA3	pyr	Sc	pyramidal
Hippocampus	CA1	pyr	sub	pyramidal
Genes	**Peptides**	**Physiol**	**Trans**	
Math-2, Tox3		non-adapt	GLU	
Math-2, Coch		non-adapt	GLU	
Math-2, Wfs1		non-adapt	GLU	

Similar considerations apply to names for the CA2 principal neurons.

The Problem of Interneurons

With regard to interneurons, a common type found in all hippocampal areas is the basket cell, with long superficial and deep dendrites, and an axon that innervates the soma and nearby dendritic shafts. The common name for this cell in the dentate gyrus is therefore "hippocampus dentate interneuron basket cell." In CA3, a basket cell interneuron would be "hippocampus CA3 interneuron basket cell," and similarly for a basket cell in CA1. As in the rest of the hippocampus and neocortex, two mutually exclusive types of morphologically identified GABAergic basket cells are clearly distinguished in the granule layer of the dentate: those expressing the calcium-binding protein parvalbumin (PV), which are fast-spiking, and those expressing the neuropeptide cholecystokinin (CCK), which are regular-spiking. Their formatted names according to the current proposal would then be:

Region	Subreg	Layer	Conn	Trad. Name
Hippocampus	dentate	gran	INT	basket
Hippocampus	dentate	gran	INT	basket
Genes	**Peptides**	**Physiol**	**Trans**	
Pvalb		fast-spk	GABA	
	CCK	reg-spk	GABA	

Interneurons in the hippocampus, however, are not simple. Somogyi and Klausberger (2018) have reviewed evidence indicating 28 different interneuron types across the dentate, CA3 and CA1 (see their **Table 17.1**), but even this is seen by themselves as an over-simplification. For instance, distilling a rich literature spanning over two decades (Freund and Buzsáki, 1996; Pelkey et al., 2017), Hippocampome.org reports experimental evidence for as many as 71 distinct interneurons in these three areas, based on the laminar location of their axons and dendrites, the specificity of their post-synaptic targets, and clearly distinct combinations of molecular and physiological properties.

This overwhelming number of interneuron types presents several problems that are special for the nervous system and its cellular nomenclature. First is relating the neuron types to many genes and proteins and other cell markers. Second is to include their functional properties. And third is to incorporate them into the neuron nomenclature. Although it may seem that this is a problem that must somehow be minimized, this large

number must rather be telling us something very important about the function of the hippocampus. Since the function of the hippocampus is crucial for understanding mechanisms of episodic memory as well as of spatial navigation and learning, the different types of interneurons are obviously critical to that understanding. This makes it all the more important to provide an efficient nomenclature system to facilitate studies at whatever level of detail is needed.

A solution to providing this support within the context of the larger nomenclature database is to compartmentalize it as a knowledge base of its own, and this has been the approach pursued by Hippocampome.org (Wheeler et al., 2015), which contains the full details of all interneuron types currently identified and is continuously updated with further types that may be revealed by future research. A start toward similar types of specialized databases for highly complex neuronal populations in the retina and the neocortex has been made in NeuronDB and in collaboration with NeuroLex Neuron (Larson and Martone, 2013). For general purposes, the main nomenclature database will include the key principal neurons and such interneurons that have particular importance for functions of general interest, as indicated above, such as generation of theta waves, long-term memory, and spatial orientation and learning.

Hippocampal interneurons are revealing yet a further complexity with neuron identities and nomenclature. In a study of transcriptomes of many hippocampal inhibitory cells, Harris et al. (2018) confirmed the presence of discrete classes, but also cells that show continuous variation in gene expression. As discussed above (see Cembrowski et al., 2016), this can mean that neuron classes based on gene expression may vary continuously with space or with activity states of the neurons.

We have focused on the adult mouse, but much interest is directed toward development for the insights it can give into how cortical neuron diversity is established (Wamsley and Fishell, 2017). Evidence is now rapidly accumulating on the subsets of transcription and related factors responsible for determining neuron types. We will return to this question in discussing neocortex below.

TERMINOLOGY FOR NEOCORTICAL NEURONS

The neocortex is believed to have arisen in the earliest mammals around 250 mya, combining features of the three-layer olfactory cortex and reptilian dorsal cortex to form the characteristic six layers in the adult (Shepherd, 2011; Aboitiz and Montiel, 2015; Brunjes and Osterberg, 2015; Fournier et al., 2015; Luzzati, 2015; Diodato et al., 2016; Rowe and Shepherd, 2016; Klingler, 2017; Naumann and Laurent, 2017; Shepherd and Rowe, 2017). At the beginning, the neocortex was a small part of the forebrain cortex, which was dominated by a large olfactory area (Molnar et al., 2014). During mammalian evolution the olfactory area continued to dominate in the opossums, while the neocortical area expanded greatly in most other species. Thus arose the fundamental forces that formed the expanded neocortex: the multiple intracortical layers of neurons and fibers; the multiple regions reflecting differences in the layers of neurons and fibers; and the multiple input and output connections unique for the neurons of each region.

We apply the same nomenclature rules used for other parts of the nervous system, focusing on the adult mouse. No major differences in cortical regions have been reported on the basis of mouse strain or gender, so this will be unspecified.

Principal Neurons of the Neocortex

Our nomenclature will begin as usual with the region in which it is located. There are some 42 regions in the mouse neocortex (Paxinos and Franklin, 2001; Allen Mouse Brain Atlas) (over 180 in human, another reason to begin with the mouse). Among these regions, one of the most easily recognized is the primary motor area (MOp or M1), defined as containing the neurons whose axons project directly into the pyramidal tract. The name thus begins with "Neocortex M1."

In the neocortex the basic cellular building block is the same as for other cortical regions we have discussed: the pyramidal neuron basic module, with basal and apical dendrites and recurrent and lateral excitatory and inhibitory feedback (Pyr in **Figure 6**). Since there are five layers containing pyramidal neurons (layer 1 lacks them), a traditional approach has been to name the pyramidal neurons in relation to the layer containing their cell bodies, which may be summarized as (Pyr L2/6). This has the advantage of relating to the cells the investigator sees under the microscope, but gives little information on their structural or functional significance.

A better alternative from that point of view is in terms of the hodology, the connectivity. In this approach, three basic connectivity profiles of pyramidal cells have been identified (reviewed in Harris and Shepherd, 2015). Some pyramidal cells have axons whose connections are entirely within the neocortex or the basal ganglia just under it; they are called "intratelencephalic" (IT) ("within the forebrain"). These are equivalent to all of the three-layer cortices we have discussed, whose output axons also are confined within the forebrain. A second type is the pyramidal tract "PT" neuron, whose axon descends to carry output from the neocortex to the brain stem and in some species all the way into the spinal cord. The third type is the cortico-thalamic ("CT") cell, which as the name implies, connects to the thalamus, in a way that completes the loop from thalamo-cortical cells to the cortex.

These three types have different relations to the layers. IT cells can be found in all layers from L2/6, although especially in superficial layers 2/3. PT cells are found specifically in L5b, whereas CT cells are found in L6. It should be emphasized that a layer may contain cells with different axonal targets (cf Thomson, 2010). This approach to classifying neocortical neurons is illustrated in **Figure 6**. Thus the traditional name for intratelencephalic neurons in primary motor cortex is: "neocortex M1 L2/5 IT pyramidal cell." Adding known functional properties (N. Sestan, personal communication for genes) gives, respectively:

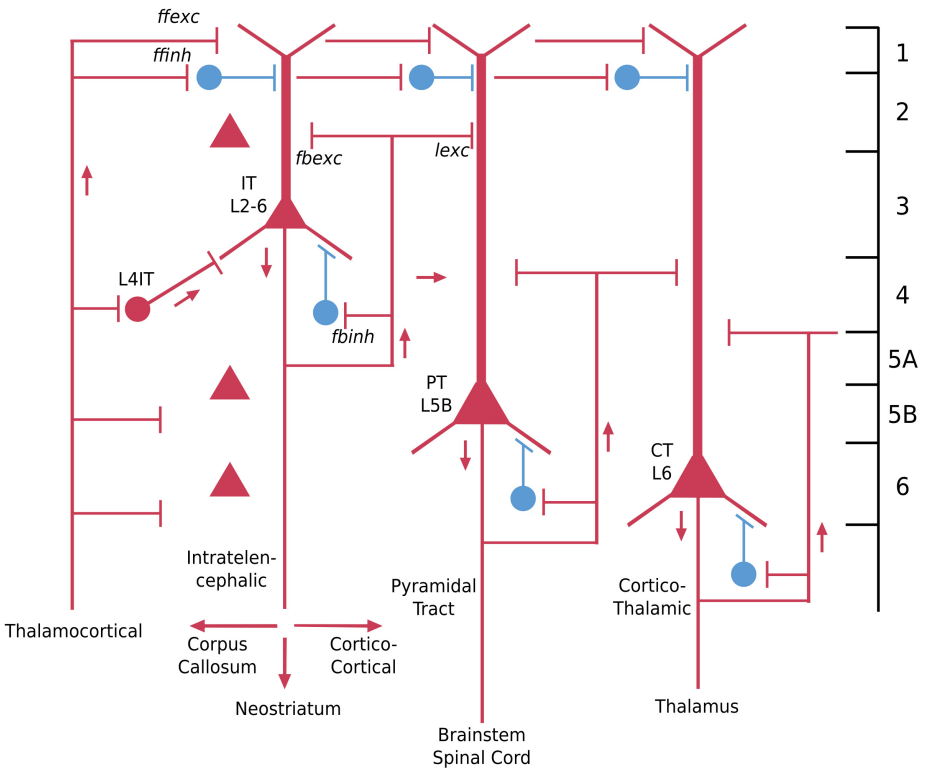

FIGURE 6 | Basic pyramidal cell (principal neuron) types (in red) in the adult neocortex in relation to the six layers and to the three connectivity types: intratelencephalic (IT), pyramidal tract (PT) and corticothalamic (CT). Interneuron examples (in blue) are superficial cells in layer 1, and basket-cell types in relation to pyramidal cell bodies. Red color indicates excitatory neurons, blue indicates inhibitory neurons [Adapted from Shepherd and Rowe (2017)].

Region	Subreg	Layer	Conn	Trad. Name
Neocortex	M1	L2/6	IT	pyramidal
Neocortex	M1	L5b	PT	pyramidal
Neocortex	M1	L6	CT	pyramidal

Genes	Peptides	Physiol	Trans
Cux1, Satb2		non-adapt	GLU
Sox5-Fezf2		non-adapt	GLU
Zfpm2		non-adapt	GLU

Note that cux1 is also expressed in olfactory cortex (see above). Identifying genetic or molecular markers at the single cell level for these principal neurons is now beginning (Shibata et al., 2015; Gillespie et al., 2018; Gouwens et al., 2018; Tasic et al., 2018), as discussed below.

Interneurons of the Neocortex

We have seen that in the case of the hippocampus, there is to a certain extent only a single type of pyramidal neuron for each area CA1-3, but many types of interneurons. The situation is similar in the neocortex where, although numerically 80% of the cells are glutamatergic pyramidal cells and 20% gabaergic interneurons, so far a greater diversity has been discovered in interneurons. From a circuit viewpoint, neocortical interneurons can be divided into three main families: perisomatic (whose axon targets largely the cell body, the proximal dendrites, and the axonal initial segment), which are mainly responsible for controlling the output of pyramidal cells; axo-dendritic (largely targeting the intermediate and distal dendrites), which are responsible for controlling the input to pyramidal cells; and interneuron-specific (mainly targeting other gabaergic cells), which are responsible for controlling disinhibition. As an example of the first family, there are chandelier cells connecting to pyramidal neurons in most layers; parvalbumin (*Pvalb*) has become a marker for this cell type, so we can incorporate that in the name: thus "neocortex M1 L1/6 interneuron chandelier PV cell." Similarly, Martinotti cell containing somatostatin (an instance of the second interneuron family) may be named: "neocortex M1 L2/6 interneuron Martinotti SOM cell." A main type of the third family is the bipolar interneuron containing vasoactive intestinal peptide: "neocortex M1 L2/6 interneuron bipolar VIP cell."

neocortex	M1	L1/6	INT	chandelier
neocortex	M1	L2/6	INT	Martinotti
neocortex	M1	L2/6	INT	bipolar
Pvalb		burst	GABA	
	SOM	burst	GABA	
	VIP	burst	GABA	

Note that these three types are also found in all other regions of the cortex, including visual (Jiang et al., 2015) and somatosensory (Markram et al., 2004). This emphasizes the importance of attaching each neuron type to its brain region, to track whether the cell properties and functions are similar or different across regions.

We have focused on three main types of interneurons in the neocortex, but as in the hippocampus there are many more. For example, Markram et al. (2004) described a basic set of 12 in their analysis of neuropeptides (see below). Schuman et al. (2019) describe 4 unique interneuron populations in layer 1 alone, each with unique morphology, gene expression and physiology.

Finally, the basic distinction between a principal, long-axon, cell projecting to other regions, and interneurons projecting only within their region, is beginning to yield to findings of gabaergic interneurons with long projecting axons. For example, optogenetic activation of a somatostatin-containing interneuron in mouse neocortex has been shown to modulate spike-timing through gabaergic inhibition of medium spiny output neurons in the striatum (Rock et al., 2016), a specific function controlled by a genetically defined type of interneuron in a distant cortical region. This balance between the excitatory PT and IT cells and inhibitory cortical somatostatin interneurons is believed to shape the timing of motor control output from the striatum in response to sensory stimuli. Further examples of long-range interneuron inhibition are cited in Yamawaki et al. (2019). We thus have examples of long range axon collaterals involved in local circuits and short-range axons also involved in long-range circuits. Our terminology can accommodate these variations by indicating an interneuron connecting to two or more regions as a combined interneuron and principal neuron (INT/P):

Necortex M1 L2/3 INT/P basket SOM burst GABA

The Problem of Large Numbers of Cortical Neuron Types

In NeuroLex Neuron, a start was made (G. Shepherd, S. Larson, M. Martone and K. Rockland) to building a specialized database for neocortical neurons. This consisted, briefly, of separate sections for principal neurons and interneurons, each arranged to contain different cell types in individual layers of distinct cortical areas. In the current approach this would at least be simplified to the extent of covering only mouse. However, even then, in terms of layers, one would potentially have a minimum of IT pyramidal cells in all 5 cell layers, plus PT in layer 5b and CT in layer 6, for a total of 7 types, plus at least 3 interneuron types in each of the 6 layers, for a total of 25 neuron types in one cortical area; considering 42 areas makes a total of over 1,000 different neuron types, by layer and connectivity, in the neocortex of an adult mouse. Humans with over 180 neocortical areas must have many times more.

These numbers likely underestimate the number of neuron types in the neocortex. The IT type of pyramidal cell potentially makes connections to the ipsilateral and contralateral neocortex, and different targets within the basal ganglia (Shepherd, 2013; Harris and Shepherd, 2015). Not every cell projects in exactly the same manner to every target neuron within these regions. Left largely undetermined is how different the projections are to different combinations of cells, but recent findings in this regard potentially point to a combinatorial explosion of possibilities (Economo et al., 2018), which will likely greatly diversify the IT cell population. Similar considerations would appear to apply to PT neurons, which in aggregate project to many regions within the subcortical neuraxis; different PT neurons are known to end on different subpopulations of target neurons (Kita and Kita, 2012), greatly amplifying the combinatorial possibilities.

These many potential types might suggest that we should try to lump as many as possible together to make our database more manageable. However, a better conclusion is that this approach to neuron terminology is revealing one of the essential features of the neocortex: the uniquely large number of different neuron types, each potentially able to process information in ways that differ either slightly or radically in generating enhanced behavior of the animal.

ADDING PROPERTIES TO NEURON NAMES: INCREASING THE CHAIN

We next discuss in more detail the multiple neuron properties that can be added to the name. In NeuronDB, NIF, Hippocampome.org, and NeuroMorpho.Org, the name for most neurons is succinct, and the properties that characterize the neuron are contained in a separate section. However, the present approach enables most characterizing properties to be incorporated into the name itself. As has been emphasized, this has two advantages: the properties of a given neuron are more obvious in the name, and in a listing of all neurons the properties are quickly accessible to search.

Gene Expression

In some cases the properties naturally become part of the name as research correlates morphology with marker molecules; see the interneurons in the hippocampus and neocortex. This trend will strongly increase in the future, especially for gene expression in specific neuron types. Single cell PCR with RNA-seq and related methods are already adding many genes expressed in single identified neurons. In our notation scheme the gene names can be added beside the marker labels. We will discuss problems with identifying genes with high throughput RNA-seq methods, combining the genes with functional methods and neurotransmitters, and finally incorporating the most recent data into our naming format.

An advantage of including a specific expressed gene or RNA in the name is that it can then be searched for across different regions and neuron types. We have noted a study comparing gene expression between three-layer olfactory cortex and six-layer neocortex (Brunjes and Osterberg, 2015) that found expression of cux1 in the layers containing both the superficial

pyramidal neurons of anterior piriform cortex and presumed IT pyramidal neurons of superficial neocortex. These findings could be incorporated into the names when established at the single cell level. This would greatly facilitate the study of gene expression and neuron identity in these two cell types, a study which may also give insight into the evolution of the neocortex as noted above.

A problem will be what to do as dozens and hundreds of genes are identified that could be added to the name. The key will be to focus on the genes that are essential to differentiating that cell's identity. At this point there is no consensus answer. We can suggest several possibilities (see also below under Physiology). First, genes can be related to a given neuron in a separate specialized database, as noted above for the hippocampus. Second, a specific gene or several genes may be of special interest in a given context. Third, in the primary database the genes may be retrieved by hovering over a single characteristic gene to reveal all the genes expressed in that cell. This is challenge for the future.

A further problem for the whole idea of specific names for neuron types is the recent study mentioned above of hippocampal interneurons by Harris et al. (2018), which found continuous variation in classes of properties:

> "A division into discrete classes, however, was not sufficient to describe the diversity of these cells, as continuous variation also occurred between and within classes. Latent factor analysis revealed that a single continuous variable could predict the expression levels of several genes, which correlated similarly with it across multiple cell types. Analysis of the genes correlating with this variable suggested it reflects a range from metabolically highly active faster-spiking cells that proximally target pyramidal cells to slower-spiking cells targeting distal dendrites or interneurons. These results elucidate the complexity of inhibitory neurons in one of the simplest cortical structures and show that characterizing these cells requires continuous modes of variation as well as discrete cell classes."

The authors conclude:

> "Our data suggest a common genetic continuum exists between and within classes, from faster-firing cells targeting principal cell somata and proximal dendrites, to slower-firing cells targeting distal dendrites or interneurons. Several classes previously described as discrete represent ranges along this continuum of gene expression."

We will further discuss this variation in physiological properties in the next section.

Physiology

As already indicated, incorporating physiological properties into the classification of a neuron has turned out to be surprisingly difficult. Whereas agreement on the morphology of a neuron is relatively straightforward, there is little agreement on how to include physiological properties. Many electrophysiologists argue that it cannot be done: physiological properties by their very nature are exquisitely dependent on many factors affecting the state of the recorded neuron, including age, anesthetic, animal treatment, temperature, duration of the experiment, *in vitro* recording, slice methodology, behavioral setup, solution composition, type of recording electrode, damage by the recording electrode, identification of the recorded neuron, activity due to injected current or stimulation of inputs, to name a few. Few classifications of neurons therefore include physiological properties among criteria for neuron identification.

Despite these multiple variables, many neurons do show clear types of properties that must be crucial for their function. One type of property is the basic biophysics of the cell as tested by intracellular recordings: its input resistance, membrane resistance, membrane time constant, spike half-width, after-hyperpolarization, etc. These are essential, when combined with the morphology, for constructing a model of the neuron that can simulate how it carries out its input-output operations. Such data from the publications that reported them are now available for over 70 neuron types at NeuroElectro.org, the most specialized database for electrophysiological properties. Data on membrane properties are also archived in CellPropDB for whole neurons and for neuronal compartments in NeuronDB; the models that combine these properties with the morphology are archived in ModelDB. Moreover, Hippocampome.org reports all known biophysical parameters for morphologically identified neurons in the hippocampal formation.

An important general conclusion from comparing the properties in these databases is that, in general, many properties, such as Na_t in axons and GLU receptors in dendrites, are found in most neurons. Differentiation of function occurs through localization of precise combinations of properties (often reflecting selective receptor subunit expression) in specific axon, soma, and dendritic compartments, as archived in NeuronDB, and demonstrated by the models in ModelDB. For most purposes the genetic basis of these properties will be reflected in the physiology; the genes responsible can be included in the name when they are relevant to a particular investigation.

Specific impulse firing patterns are necessary for giving insight into the neural basis of behavior. This information is obtained by a variety of recording methods, including extracellular single- and multi-electrodes in anesthetized or behaving animals, field potentials, and functional imaging, to name the most important. The Blue Brain Project has been leading the effort to identify these "morphoelectric" cortical neuron types. Firing properties are characterized by responses to injected current: the main response types are a burst (burst) of impulses; a steady non-adapting (non-adapt) impulse train; a rapidly adapting firing (rapidadapt); and fast spiking (fastspike) (see the different neuron types). **Figure 7** shows an example of the relations between cell morphology, impulse firing pattern, cell layer, and connectivity for excitatory pyramidal neurons, from the study of Gouwens et al. (2018) at the Allen Brain Institute.

Figure 7 might suggest that a given morphological cell type is always associated with a given functional property, but as usual, biology isn't that simple. As an example, Markram et al. (2004) identified eight morphological types of neocortical inhibitory interneurons. They found that all types expressed not just one, but several tags of calcium-binding proteins and neuropeptides.

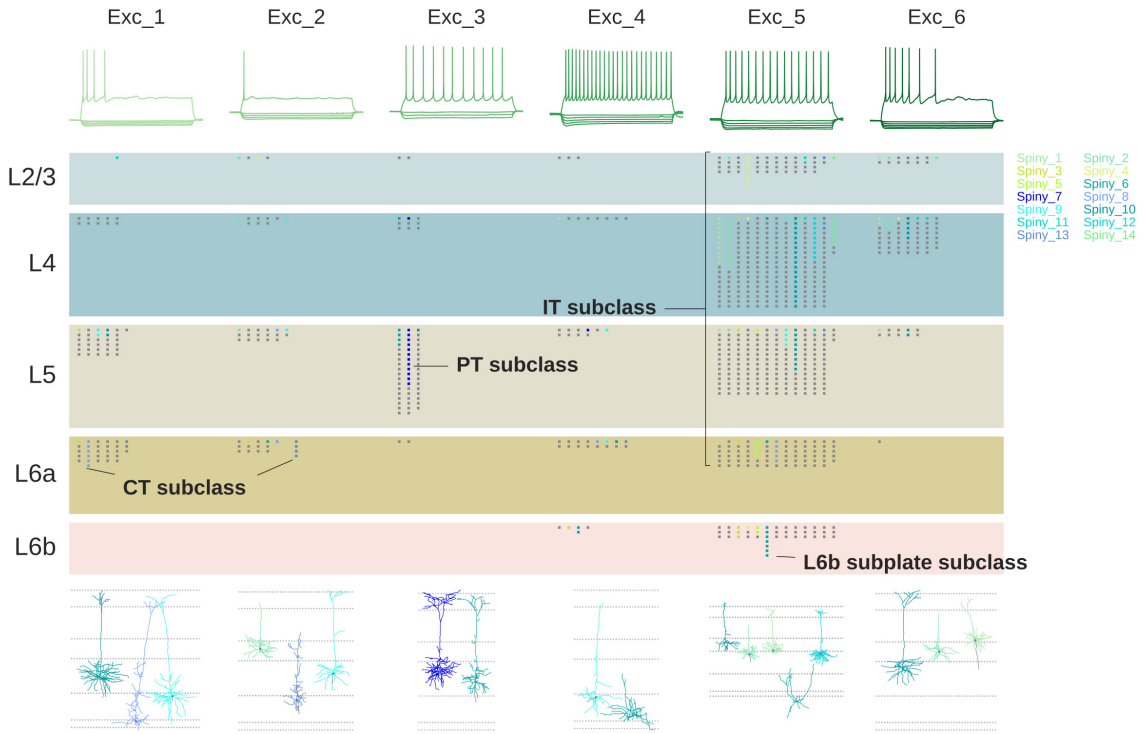

FIGURE 7 | Relations between firing patterns, laminar localization, connectivity and morphology of pyramidal cells. Types of firing patterns at top are aligned with representative cell morphologies giving the patterns at bottom. Laminar localization is shown (each dot a recorded cell) in the middle separated into IT, PT and CT categories; colors indicate the reconstructed cells at bottom [Adapted from Gouwens et al., 2018].

They went further and characterized the physiological properties in terms of 9 different impulse firing patterns. In about half the cases a given firing pattern was associated with more than one molecular tag and more than one morphological type. As can be seen in **Figure 8**, this made for a complex combinatorial pattern of associations between morphology, molecular identity, and firing pattern.

These complex patterns raise the question of whether neocortical interneurons contain a continuum of different combinations of properties or are divided into distinct classes. Markram et al. (2004, p. 804) note: "... only a few transcription factors, expressed in different combinations, might give rise to a finite number of distinct classes of interneuron. So, most interneurons probably lie in distinct electrical, morphological and molecular classes. The observed diversity is several orders of magnitude smaller than expected for a continuum of electrical types using more than 100 ion-channel genes, indicating powerful constraints on diversity. Understanding these constraints is also key to resolving the class-versus-continuum debate."

Unique physiological properties are the most difficult to characterize as a neuron class; Markram et al. (2004) note:

> "The proof that these responses represent distinct classes and that each class maps onto anatomically and molecularly distinct types of interneuron is still lacking ... The fundamental question now is how microcircuits in different species, different brain

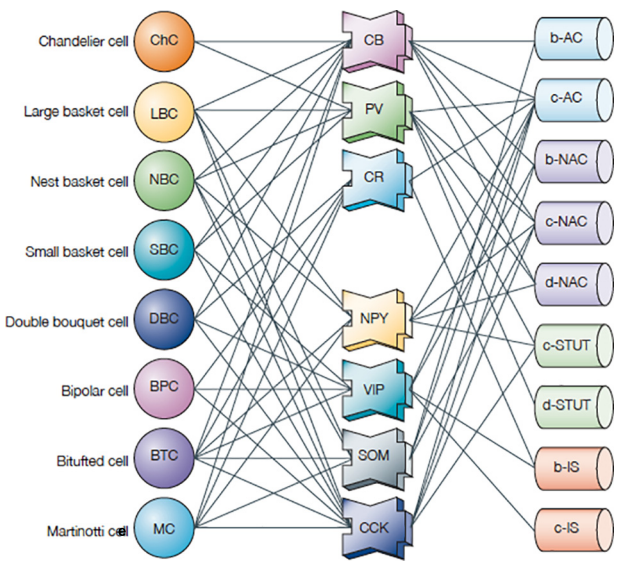

FIGURE 8 | Interneurons (left column) in the neocortex: correlation of expression of calcium-binding proteins (CBPs: middle column: CB, calbindin; PV, parvalbumin; CR, calretinin NPY) and neuropeptides (NPY, neuropeptide Y; VIP, vasoactive intestinal peptide; SOM, somatostatin; CCK, cholecystokinin) with different morphological and electrophysiological classes (right column: AC, accommodating; b, burst; c, classic burst; d, delay burst; iS, irregular spiking; NAC, non-accommodating; STUT, stuttering) [Adapted from Markram et al. (2004)].

regions of the same species, different layers and even different neurons in the same layer are driven to diversify to form countless variations of the microcircuit template – in particular, whether stimulus diversity is the ultimate driving force behind interneuron diversity."

How does one name a neuron in which these issues have not yet been resolved? The parent-child approach may be useful. If a combination of gene expression, neuropeptides and functional properties is found to define a subset of neurons, it can be identified as such, either by its most dominant characteristic(s), by a single characteristic noted by an asterisk, or by a new symbol. For example, a basket cell in M1 L2/6, drawing on **Figure 8**, could be named:

Region	Subreg	Layer	Conn	Trad. Name	Genes
neocortex	M1	L2/6	INT	basket	*Pvalb*

Peptides	Physiol	Trans
NPY SOM CCK	burst	GABA

It should be remembered that a known property carries with it the caution that it does not exclude the possibility that further research will reveal the expression of other properties, an important condition on any neuron name.

Neurotransmitters

The functional properties of the neuron drive the output through synapses on other neurons. Chemical synapses are the primary means for communication between neurons. There are several types of neurotransmitter molecules: the main actors are glutamate (GLU), gamma-amino-butyric acid (GABA), acetylcholine (ACh), and dopamine (DA). As we have shown, these can easily be added to the name. The excitatory action of glutamate is of course not a property of the releasing neuron but of the receptors on its cell target; its inclusion in the name could be optional if it is relevant. Similarly, cortical interneurons are mostly GABAergic and inhibitory. More slowly acting modulators such as neuropeptides and neurohormones can also be added. Including these among the functional properties in the neuron name greatly facilitates identifying the neurotransmitter, neuropeptide and neurohormone families across the database, as has been done in NIF NeuroLex and NeuronDB.

The other main type of synapse is the gap junction (electrical synapse). It consists of a scaffold of proteins that connect cells to form pores allowing small molecules and electric current to flow between them. They are common in many cells; for example, between INTs in the neocortex. They can be indicated by "gap" added to the name, as in:

Neocortex	M1	L2/6	INT	basket	burst
GABA	gap				

THE PROPOSED FORMAT IS SUPPORTED BY RECENT GENE STUDIES

A summary of the naming format for the neurons considered here is provided in **Table 3**. The advantages for investigations of single cells are evident in displaying both the relatively stable (anatomical) and functional properties, together with the most important genes for the identity of the cell type, without having to search a separate database. The advantages for listing cells from different regions in the same database are evident in the strict lineup of categories, facilitating comparison of a given cell type with other types within the same region and between different regions. The names shown for principal (pyramidal) cells and interneurons will apply to neurons in most cortical areas.

It may seem that the inventory for cortical pyramidal cells is unnecessarily repetitious because they all appear to have the same properties. However, they should be specific for each area because of the distinct connectivity of input fibers from different brain regions to each area, and the different output targets of the principal neurons of each area. Although differences in properties between neurons in different areas may not be apparent now, future research will test the extent to which they may be similar or different.

The format appears marred by the lack of data for genes and peptides for most of the cell types depicted, suggesting those categories could be deleted. The absences are in fact useful because they make specific the need for those data for those cells. The naming scheme can thus serve as a stimulus for investigations of those cell types, providing at the same time the context of what is known in the other cell types.

The table has the further advantage that it allows us to compare the approach used in this proposal with the approach used in the recent studies of gene expression that we have mentioned. As shown at the bottom of the table, the format for the expressed genes reported by Tasic et al. (2018) in fact fits precisely with the properties as far as they go into the proposed scheme. This applies to the properties for both pyramidal cells and interneurons. Similarly, the properties reported by Gillespie et al. (2018) and Gouwens et al. (2018) also fit very closely. These recent results show that the proposed naming format can also be applied to data-driven classifications of neuron types. While the name cannot capture the structure of the classifier, it still retains several of the salient features.

When we began our review these data were not available; the fact that the new data fit so well indicates that the format is likely to prove effective for future work. These new reports enter the era of high throughput RNA-seq, generating up to hundreds of genes, which obviously do not fit into the name. The focus should be on the expression of those genes most essential to the identity of that neuron type. An example would be the Sox5 – Fezf2 transcription factor regulatory network expressed in subcerebral (PT) pyramidal cells (see **Table 3**). Otherwise there needs to be a link to a database of these high capacity studies. Databases are being constructed for this purpose.

TABLE 3 | Summary of formats for anatomical and functional properties of different neuron types covered in the text.

	Anatomical Properties				Functional Properties			
Region	**Subreg**	**Layer**	**Conn**	**Trad. Name**	**Genes**	**Peptides**	**Physiol**	**Trans**
Spinal cord	lumbar	VH	Skel	MN alpha	*Err3*		adapt	ACh
Spinal cord	lumbar	VH	INT	Renshaw			burst	GLY
Striatum	caudate	strio	direct	m. spiny	*Ppp1r1b*		non-adapt	GABA
Striatum	caudate	strio	INT	cholinergic	*CHAT*		burst	ACh
Piriform	anterior	supfl	af	pyramidal	*Cux1*		non-adapt	GLU
Piriform	anterior	supfl	INT	superfl int			burst	GABA
Hippocampus	dentate		MF	granule	*Math-2, Tox3*		non-adapt	GLU
Hippocampus	CA3		Sc	pyramidal	*Math-2, Coch*		non-adapt	GLU
Hippocampus	CA1		Sub	pyramidal	*Math-2, Wfs1*		non-adapt	GLU
Neocortex	M1	L2/6	IT	pyramidal	*Cux1, Satb2*		non-adapt	GLU
Neocortex	M1	L5b	PT	pyramidal	*Sox5-Fezf2*		non-adapt	GLU
Neocortex	M1	L6	CT	pyramidal	*Zfpm2*		non-adapt	GLU
Neocortex	M1	L2/3	INT	basket	*Pvalb*	SOM	burst	GABA
Neocortex	M1	L2/3	INT/P	basket	*Pvalb*	SOM	burst	GABA
Tasic et al., 2018								
Neocortex	M1	L5	IT	pyramidal	*Tnc*		non-adapt	GLU
Neocortex	M1	L2/6	INT	basket	*Reln, Itm2, Pvalb*		burst	GABA
Gillespie et al., 2018								
Neocortex	S1		INT	L basket	*Pvalb*	+VIP -SOM	fast spiking	GABA
Gouwens et al., 2018								
Neocortex	VISp	L4	IT	pyramidal	*Rorb*		adapt	GLU

Single entries for genes and peptides are examples from larger populations which may be archived in separate databases. At the bottom for comparison are formats for current studies covered in the text of RNA-seq gene expression. The comparison shows the close similarity between the approaches, indicating that the format can accommodate new data regarding genes and peptides revealed by RNA-seq and other methods. Leaving blank the entries for genes and peptides when not yet available makes clear where new studies are needed, while also providing comparisons with what is known in other neuron types (see text). Abbreviations for Gouwens et al. (2018): VISp, VI S posterior; spiney 1 cluster, gene group; for other abbreviations, see previous nomenclature entries for these neurons.

MULTIMODAL SEARCHES FOR FAMILIES OF PROPERTIES

We have focused on the unique set of properties shared by all members of a given neuron morphological type. However, neurons can also be classified by their shared functional properties independent of their anatomical shape.

Exploring this possibility is analogous to identifying families in sequence databases using the powerful tool in bioinformatics called Basic Local Alignment Search Tool (BLAST). This enables a search of a gene or protein database for any arbitrary sequence of nucleotides or amino acids, to identify families with shared properties that otherwise are unknown. This constitutes a single modality BLAST search.

A novel multimodal tool has been created by SenseLab to enable an analogous search of different neuron properties, by membrane currents, neurotransmitters, and neurotransmitter receptors that are contained in CellPropDB and NeuronDB. In analogy with BLAST, this can be termed a Multimodal Alignment Search Tool (MAST). The power of a MAST search is that one can take an arbitrary combination of currents, receptors and/or transmitters found in a cell of interest and search CellPropDB or NeuronDB for the family of neurons containing the same properties. An obvious example is the family of all the neurons that express glutamate or gaba. This is also possible in the NIF Neurolex. Even more precisely, in NeuronDB one can search for the families of currents, receptors and/or transmitters found in a specific axon, soma or dendritic compartment. Such across-neuron families imply that these morphologically distinct neurons and neuron compartments carry out similar processing operations, as has been shown in a previous study (Migliore and Shepherd, 2002). Understanding these common functional motifs across morphologically different neurons and neuron compartments will become increasingly important with increasing research on functional properties at the cellular and subcellular level. It is an additional reason to have these properties be explicit in the neuron name alongside the traditional morphological features. Effective use of this tool depends on population of the searched databases, which is in progress.

STATE DEPENDENCE OF NEURONAL PROPERTIES

The functional properties of a brain region are state dependent: they vary depending on the behavioral state of the animal. When the focus is on anatomical features as the basis of nomenclature this fact is usually overlooked. However, when the nomenclature reflects functional properties they must be taken into consideration. A typical example; zebrafish fast motor neurons may secrete glutamate plus ACh during forced exercise

(Bertuzzi et al., 2018). Thus, the functional properties of a pyramidal cell are different whether the animal is active or resting; awake or sleeping; hungry or sated; sexually active or not; an alpha or beta male; estrous or menopausal; normal or addicted; responding to injury; and so on. This also applies to gene expression; the expression of individual genes in individual cells also varies with many of these behavioral or cognitive states. A nomenclature must regard these added complexities not as problems but as opportunities to reflect the nervous system as it really is.

DEVELOPMENT

We have seen that during evolution there was continuity of the three main types of cortical pyramidal neurons when characterized in terms of connectivity: intratelencephalic, pyramidal tract and corticothalamic. It remains to ask how these types emerge during early development and are maintained into adulthood, a field of increasingly intense activity. Cortical neurogenesis and cell type specification and maintenance depend on networks of transcription factors, regulatory elements, synaptic interactions and modulatory signals. In the summary diagram of **Figure 9** from Shibata et al. (2015), different types of pyramidal neurons are sequentially generated by the same lineage of progenitor cells in the ventricular and subventricular zones (VZ and SVZ, respectively) and migrate into the emerging cortical plate in "inside first, out last" manner. Birthdating and lineage studies have shown that the earliest ascending cells form the large deep layer pyramidal cells shown on the right, whose axons constitute the subcerebral projections to the pyramidal tract (PT) and the thalamus (CT). In contrast, later ascending cells differentiate into pyramidal cells which distribute themselves mainly in the upper layers but also throughout; these become the intracerebral (intratelencephalic: IT) pyramidal cells. The proposed cortical pyramidal cell nomenclature is thus consistent through early development (this figure), adult connectivity (**Figure 6**), and evolution (IT cells in **Figure 3**) (cf also **Table 3**). Our review of cortical names has thus taken us to the earliest mechanisms for when and how the different neuron types arise.

In summary, complex gene networks, varying with activity and developmental stage, arise early in development to construct a neuron's identity as reflected in its name.

DISCUSSION

In conclusion, we summarize the advantages of moving toward a systematic format for neuron names in which traditional names based on structure are extended to include genes and functional properties.

First, the format builds directly on classical terminology and on current initiatives in terminology, knowledge bases, and databases as in NeuronDB, NeuroMorpho.Org, Hippocampome.org, NIF, and BAMS. Most of the traditional names are still identifiers for each main neuron type.

Second, it anchors each neuron type to the region in which its cell body is localized. There is no ambiguity, for example, about whether a "granule cell" is in the cerebellum, olfactory bulb, neocortex, dorsal cochlear nucleus, or dentate gyrus. This enhances archival listing in a database because it enables easy alphabetical order by "parent-child relation," grouping all cells in a given region instead of distributing them throughout the database due to spelling of modifying terms. This approach is already established in NeuronDB and the NIF. The format also enhances research on an individual neuron type by making all properties visible so that new properties can readily define new neuron subtypes.

Third, the approach differentiates long-axon "principal" cells from short-axon "interneuron" cells, a distinction going back to Golgi and in wide use today, crucial to understanding the distinctive functions that these two types have in information processing. Both types carry out local processing; the long axons also transmit specific information between regions while the short axons function mainly as modifiers within regions.

Fourth, in cortical areas, the pyramidal cell functions as the core of a basic cortical module in cortical evolution, with recurrent and lateral excitation and inhibition, together with modulatory interneurons, laid down during development and present across the vertebrate series.

Fifth, the neocortical pyramidal cells, as principal neurons carrying cortical output, can be characterized in two ways within the neuron name. One is by the location of their cell body in one of the different cortical layers, recognizing that a layer may contain different cell types. The other is by the connectivity of their axons, of which there are three main types: intratelencephalic (IT), connecting to ipsilateral and/or basal ganglia and neocortex; pyramidal tract (PT), connecting to the pyramidal tract and the neuraxis; and corticothalamic (CT), connecting to the thalamus. The relevance of this dual characteristic is seen in its current use in identifying the expression of genes in cortical pyramidal cells.

Sixth, genes and functional properties fit naturally into the expanded name for a neuron. These should include labels for the neurotransmitter released by the neuron; neuropeptide neuromodulators that are markers for the neuron type; significant genes expressed by that type; and characteristic impulse firing patterns associated with that type. Including these in the name for the neuron makes its multiple properties immediately and unambiguously recognizable. As a result, the multimodal properties that define a specific neuron type are present in the name itself, making its anatomical, genetic and functional identity immediately obvious.

Seventh, a succinct terminology format is suggested in which the basic properties are indicated, beginning with the general and relatively more stable defining anatomical characteristics of region, subregion, and connectivity, and adding more detailed functional properties including neuropeptides, gene markers, physiological firing patterns, and neurotransmitters.

Eighth, with functional properties carried transparently in the name across different anatomical neuron types, there will be an enhanced ability to identify functional motifs that carry out similar processing steps despite different morphologies and

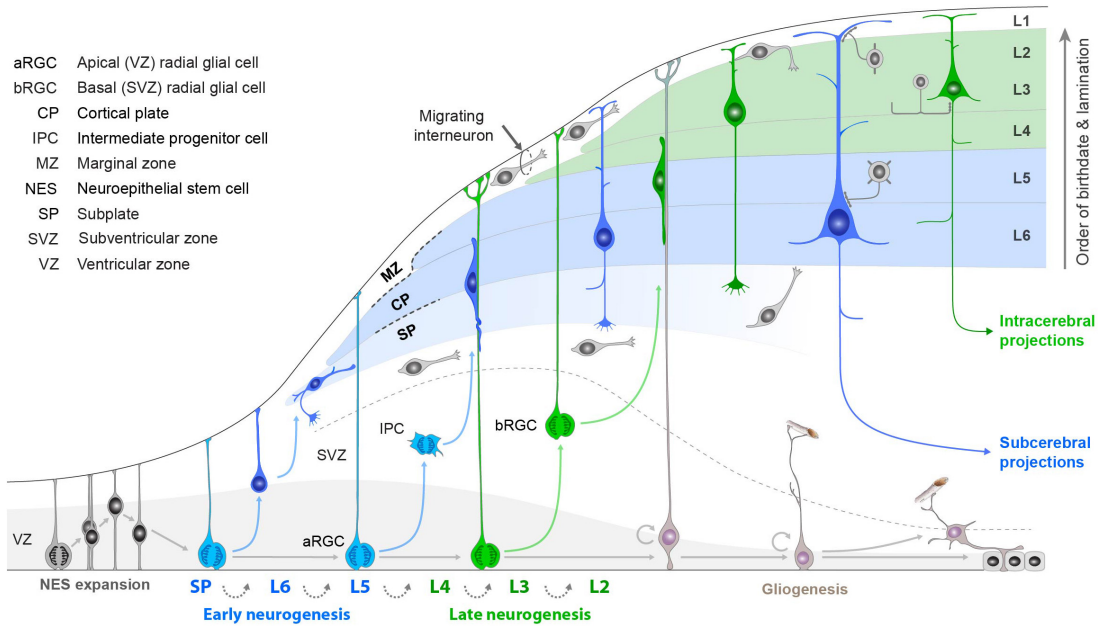

FIGURE 9 | Summary of steps in neurogenesis and differentiation of the main types of neocortical pyramidal cells based on intracerebral (intratelencephalic IT) and subcerebral (pyramidal tract PT, corticothalamic CT) connectivity, as described in the text. Note the consistency of these types with the adult pyramidal cell types in **Figures 3**, **4**, and **6**. [Adapted from Shibata et al. (2015); see also Rakic (2009)].

connectivities. These functional families should go far beyond the present recognition of glutamatergic excitatory and GABAergic inhibitory cells, for example, and reveal similar or contrasting basic processing steps carried out by different neurons and their subcellular compartments at all stages of development and aging.

Ninth, in a rapidly evolving field such as neuroscience, one of the challenges is having names for neurons remain stable despite new research constantly revealing new functional properties. One way this is accomplished is by having the category of relatively stable, anatomically based neuron types provide the basic family identity, so that when new research expands the number of functional subtypes they are all children of the same parent, i.e., they form an extended family.

Tenth, the neocortex presents a special problem in that, because of the multiple cortical areas, multiple layers, and multiple output connections, the number of distinct neuron types could exceed 1,000 for just the adult mouse, and many times that for the human. This uniquely large number reflects one of the essential features of the neocortex: the multiple neuron types within a cortical region are potentially able to process information in many different ways, inborn or learned, in generating the rich behavioral repertoire of the animal. Special databases will be required to give adequate recognition to the especially complex neuron populations in the neocortex, and for other complex regions such as the retina, similarly to recent and ongoing progress for the hippocampus.

Finally, the new era of high-throughput RNA-seq and its related methods is yielding massive data sets of gene expression that go far beyond previous characterizations of neuron types. Separate databases will obviously be needed for these gene data. In addition, variation of gene expression within a type is challenging the very concept of a neuron type, as we have documented and is summarized well by Cembrowski and Menon (2018):

> "Next-generation RNA sequencing (RNA-seq) is becoming increasingly popular in the deconstruction of this complexity into distinct classes of 'cell types' . . . the technology has also begun to illustrate that continuous variation can be found within narrowly defined cell types. Here we summarize the evidence for graded transcriptomic heterogeneity being present, widespread, and functionally relevant in the nervous system. We explain how these graded differences can map onto higher-order organizational features and how they may reframe existing interpretations of higher-order heterogeneity. Ultimately, a multimodal approach incorporating continuously variable cell types will facilitate an accurate reductionist interpretation of the nervous system."

AUTHOR CONTRIBUTIONS

GS developed the idea in discussions with LM, MH, MM, RM, NC, AN, MS-Z, and GA. GS wrote the first draft of the manuscript. GS and GA finalized the manuscript after approval by the co-authors.

ACKNOWLEDGMENTS

We thank M. E. Martone, S. D. Larson, and D. J. Hamilton for valuable discussions related to nomenclature in the development of the Neuroscience Information Framework; G. M. G. Shepherd, S. Hill, S. Tripathy, M. Harwylycz, T. M. Morse, and C. J.

Wilson for valuable discussions relating to cortical neurons; and M. E. Martone, T. Gillespie, Q. Li, and N. Sestan for critical feedback in developing the manuscript. We also thank M. E. Martone for pointing out the consistency between the goal of the BRAIN consortium and the approach we have been developing at SenseLab and are proposing in this article. R. Wang provided the essential structuring of the NeuronDB neuron list. Our Editor HtD provided patient support for the extended development of the manuscript. We are grateful to the Editor and the reviewers for many valuable suggestions and for keeping the focus on the proposed neuron names. We are also grateful to the National Institute for Deafness and Other Communicative Disorders for long-term support of SenseLab (R01 DC 009977); as well as to the National Institute of Neurological Disorders and Stroke and the National Institute of Mental Health for continuous support of NeuroMorpho.Org (U01 MH 114829) and Hippocampome.org (R01 NS 039600).

REFERENCES

Aboitiz, F., and Montiel, J. F. (2015). Olfaction, navigation, and the origin of isocortex. *Front. Neurosci.* 9:402. doi: 10.3389/fnins.2015.00402

Akram, M. A., Nanda, S., Maraver, P., Armañanzas, R., and Ascoli, G. A. (2018). An open repository for single-cell reconstructions of the brain forest. *Sci. Data* 5:180006. doi: 10.1038/sdata.2018.6

Armstrong, C., Szabadics, J., Tamas, G., and Soltesz, I. (2011). Neurogliaform cells in the molecular layer of the dentate gyrus as feed-forward gamma-aminobutyric acidergic modulators of entorhinal-hippocampal interplay. *J. Comp. Neurol.* 519, 1476–1491. doi: 10.1002/cne.22577

Ascoli, G. A., Donohue, D. E., and Halavi, M. (2007). NeuroMorpho.Org: a central resource for neuronal morphologies. *J. Neurosci.* 27, 9247–9251. doi: 10.1523/JNEUROSCI.2055-07.2007

Ascoli, G. A., and Wheeler, D. W. (2016). In search of a periodic table of the neurons: axonal-dendritic circuitry as the organizing principle - Patterns of axons and dendrites within distinct anatomical parcels provide the blueprint for circuit-based neuronal classification. *Bioessays* 38, 969–976. doi: 10.1002/bies.201600067

Bertuzzi, M., Chang, W., and Ampatzis, K. (2018). Adult spinal motoneurons change their neurotransmitter phenotype to control locomotion. *Proc. Natl. Acad. Sci. U.S.A.* 115, E9926–E9933. doi: 10.1073/pnas.1809050115

Bota, M., Dong, H. W., and Swanson, L. W. (2012a). Combining collation and annotation efforts toward completion of the rat and mouse connectomes in BAMS. *Front. Neuroinform.* 6:2. doi: 10.3389/fninf.2012.00002

Bota, M., Sporns, O., and Swanson, L. W. (2012b). Neuroinformatics analysis of molecular expression patterns and neuron populations in gray matter regions: the rat BST as a rich exemplar. *Brain Res.* 1450, 174–193. doi: 10.1016/j.brainres.2012.02.034

Bota, M., and Swanson, L. W. (2007). The neuron classification problem. *Brain Res. Rev.* 56, 79–88. doi: 10.1016/j.brainresrev.2007.05.005

Bota, M., and Swanson, L. W. (2008). BAMS neuroanatomical ontology: design and implementation. *Front. Neuroinform.* 2:2. doi: 10.3389/neuro.11.002.2008

Bota, M., and Swanson, L. W. (2010). Collating and curating neuroanatomical nomenclatures: principles and use of the Brain Architecture Knowledge Management System (BAMS). *Front. Neuroinform.* 4:3. doi: 10.3389/fninf.2010.00003

Brunjes, P. C., and Osterberg, S. K. (2015). Developmental markers expressed in neocortical layers are differentially exhibited in olfactory cortex. *PLoS One* 10:e0138541. doi: 10.1371/journal.pone.0138541

Bug, W. J., Ascoli, G. A., Grethe, J. S., Gupta, A., Fennema-Notestine, C., Laird, A. R., et al. (2008). The NIFSTD and BIRNLex vocabularies: building comprehensive ontologies for neuroscience. *Neuroinformatics* 6, 175–194. doi: 10.1007/s12021-008-9032-z

Cembrowski, M. S., Bachman, J. L., Wang, L., Sugino, K., Shields, B. C., and Spruston, N. (2016). Spatial gene-expression gradients underlie prominent heterogeneity of CA1 pyramidal neurons. *Neuron* 89, 351–368. doi: 10.1016/j.neuron.2015.12.013

Cembrowski, M. S., and Menon, V. (2018). Continuous variation within cell types of the nervous system. *Trends Neurosci.* 41, 337–348. doi: 10.1016/j.tins.2018.02.010

Crasto, C. J., Marenco, L. N., Liu, N., Morse, T. M., Cheung, K. H., Lai, P. C., et al. (2007). SenseLab: new developments in disseminating neuroscience information. *Brief. Bioinform.* 8, 150–162. doi: 10.1093/bib/bbm018

DeFelipe, J., López-Cruz, P. L., Benavides-Piccione, R., Bielza, C., Larrañaga, P., Anderson, S., et al. (2013). New insights into the classification and nomenclature of cortical GABAergic interneurons. *Nat. Rev. Neurosci.* 14, 202–216. doi: 10.1038/nrn3444

Diodato, A., Ruinart de Brimont, M., Yim, Y. S., Derian, N., Perrin, S., Pouch, J., et al. (2016). Molecular signatures of neural connectivity in the olfactory cortex. *Nat. Commun.* 7:12238. doi: 10.1038/ncomms12238

Doig, N. M., and Bolam, J. P. (2018). "Microcircuits of the striatum," in *Handbook of Brain Microcircuits*, 2nd Edn, eds G. M. Shepherd and S. Grillner (New York, NY: Oxford University Press), 121–132.

Ecker, J. R., Geschwind, D. H., Kriegstein, A. R., Ngai, J., Osten, P., Polloudakis, D., et al. (2017). The BRAIN initiative cell census consortium: lessons learned toward generating a comprehensive brain cell atlas. *Neuron* 96, 542–567. doi: 10.1016/j.neuron.2017.10.007

Economo, M. N., Viswanathan, S., Tasic, B., Bas, E., Winnubst, J., Menon, V., et al. (2018). Distinct descending motor cortex pathways and their roles in movement. *Nature* 563, 79–84. doi: 10.1038/s41586-018-0642-9

Fournier, J., Muüller, C. M., and Laurent, G. (2015). Looking for the roots of cortical sensory computation in three-layer cortices. *Curr. Opin. Neurobiol.* 31, 119–126. doi: 10.1016/j.conb.2014.09.006

Freund, T. F., and Buzsáki, G. (1996). Interneurons of the hippocampus. *Hippocampus* 6, 347–470. doi: 10.1002/(SICI)1098-1063(1996)6:4<347::AID-HIPO1>3.0.CO;2-I

Friese, A., Kaltschmidt, J. A., Ladle, D. R., Sigrist, M., Jessell, T. M., and Arber, S. (2009). Gamma and alpha motor neurons distinguished by expression of transcription factor Err3. *Proc. Natl. Acad. Sci. U.S.A.* 106, 13588–13593. doi: 10.1073/pnas.0906809106

Gardner, D., Akil, H., Ascoli, G. A., Bowden, D. M., Bug, W., Donohue, D. E., et al. (2008). The neuroscience information framework: a data and knowledge environment for neuroscience. *Neuroinformatics* 6, 149–160. doi: 10.1007/s12021-008-9024-z

Gillespie, T., Brandrowski, A. E., Grethe, J. S., and Martone, M. E. (2018). "The NIF ontology: brain parcels, cell types, and methods," in *Proceedings of the Society for Neuroscience Abstracts: Program No. 254.10. Neuroscience Meeting Planner* (San Diego, CA: Society for Neuroscience).

Gouwens, N. W., Sorensen, S. A., Berg, J., Lee, C., Jarsky, T., Ting, J., et al. (2018). Classification of electrophysiological and morphological types in mouse visual cortex. *bioRxiv* [Preprint]. doi: 10.1101/368456

Graybiel, A. M. (2018). "Templates for neural dynamics in the striatum: striosomes and matrisomes," in *Handbook of Brain Microcircuits*, 2nd Edn, eds G. M. Shepherd and S. Grillner (New York, NY: Oxford University Press), 133–142.

Hamilton, D. J., Shepherd, G. M., Martone, M. E., and Ascoli, G. A. (2012). An ontological approach to describing neurons and their relationships. *Front. Neuroinform.* 6:15. doi: 10.3389/fninf.2012.00015

Hamilton, D. J., Wheeler, D. W., White, C. M., Rees, C. L., Komendantov, A. O., Bergamino, M., et al. (2017). Name-calling in the hippocampus (and beyond): coming to terms with neuron types and properties. *Brain Inform.* 4, 1–12. doi: 10.1007/s40708-016-0053-3

Harris, K. D., Hochgerner, H., Skene, N. G., Magno, L., Katona, L., Bengtsson Gonzales, C., et al. (2018). Classes and continua of hippocampal CA1 inhibitory neurons revealed by single-cell transcriptomics. *PLoS Biol.* 16:e2006387. doi: 10.1371/journal.pbio.2006387

Harris, K. D., and Shepherd, G. M. G. (2015). The neocortical circuit: themes and variations. *Nat. Neurosci.* 18, 170–181. doi: 10.1038/nn.3917

Jiang, X., Shen, S., Cadwell, C. R., Berens, P., Sinz, F., Ecker, A. S., et al. (2015). Principles of connectivity among morphologically defined cell types in adult neocortex. *Science* 350:aac9462. doi: 10.1126/science.aac9462

Kita, T., and Kita, H. (2012). The subthalamic nucleus is one of multiple innervation sites for long-range corticofugal axons: a single-axon tracing study in the rat. *J. Neurosci.* 32, 5990–5999. doi: 10.1523/JNEUROSCI.5717-11.2012

Klingler, E. (2017). Development and organization of the evolutionarily conserved three-layered olfactory cortex. *eNeuro* 4:ENEURO.0193-16.2016. doi: 10.1523/ENEURO.0193-16.2016

Kriegstein, A. R., and Connors, B. W. (1986). Cellular physiology of the turtle visual cortex: synaptic properties and intrinsic circuitry. *J. Neurosci.* 6, 178–191. doi: 10.1523/JNEUROSCI.06-01-00178.1986

Larson, S. D., and Martone, M. E. (2013). NeuroLex.org: an online framework for neuroscience knowledge. *Front. Neuroinform.* 7:18. doi: 10.3389/fninf.2013.00018

Luzzati, F. (2015). A hypothesis for the evolution of the upper layers of the neocortex through co-option of the olfactory cortex developmental program. *Front. Neurosci.* 9:162. doi: 10.3389/fnins.2015.00162

Markram, H., Toledo-Rodriguez, M., Wang, Y., Gupta, A., Silberberg, G., and Wu, C. (2004). Interneurons of the neocortical inhibitory system. *Nat. Rev. Neurosci.* 10, 793–807. doi: 10.1038/nrn1519

Migliore, M., and Shepherd, G. M. (2002). Emerging rules for the distributions of active dendritic conductances. *Nat. Rev. Neurosci.* 3, 362–370. doi: 10.1038/nrn810

Mirsky, J. S., Nadkarni, P. M., Healy, M. D., Miller, P. L., and Shepherd, G. M. (1998). Database tools for integrating and searching membrane property data correlated with neuronal morphology. *J. Neurosci. Methods* 82, 105–121. doi: 10.1016/S0165-0270(98)00049-1

Molnar, Z., Kaas, J. H., de Carlos, J. A., Hevner, R. F., Lein, E., and Nımec, P. (2014). Evolution and development of the mammalian cerebral cortex. *Brain Behav. Evol.* 83, 126–139. doi: 10.1159/000357753

Naumann, R. K., and Laurent, G. (2017). "Function and evolution of the reptilian cerebral cortex," in *Evolution of Nervous Systems 2*, Vol. 1, ed. J. Kaas (Amsterdam: Elsevier), 491–518.

Neville, K. R., and Haberly, L. B. (2004). "Olfactory cortex," in *The Synaptic Organization of the Brain*, ed. G. M. Shepherd (New York, NY: Oxford University Press), 415–454. doi: 10.1093/acprof:oso/9780195159561.003.0010

Ouimet, C. C., and Greengard, P. (1990). Distribution of DARPP-32 in the basal ganglia: an electron micro scopic study. *J. Neurocytol.* 19, 39–52. doi: 10.1007/BF01188438

Paxinos, G., and Franklin, K. B. J. (2001). *The Mouse Brain in Stereotaxic Coordinates*, 2nd Edn. San Diego, CA: Academic Press.

Pelkey, K. A., Chittajallu, R., Craig, M. T., Tricoire, L., Wester, J. C., and McBain, C. J. (2017). Hippocampal GABAergic inhibitory interneurons. *Physiol. Rev.* 97, 1619–1747. doi: 10.1152/physrev.00007.2017

Petilla Interneuron Nomenclature Group [PING], Ascoli, G. A., Alonso-Nanclares, L., Anderson, S. A., Barrionuevo, G., Benavides-Piccione, R., et al. (2008). Petilla terminology: nomenclature of features of GABAergic interneurons of the cerebral cortex. *Nat. Rev. Neurosci.* 9, 557–568. doi: 10.1038/nrn2402

Polavaram, S., and Ascoli, G. A. (2017). An ontology-based search engine for digital reconstructions of neuronal morphology. *Brain Inform.* 4, 123–134. doi: 10.1007/s40708-017-0062-x

Rakic, P. (2009). Evolution of the neocortex: a perspective from developmental biology. *Nat. Rev. Neurosci.* 10, 724–735. doi: 10.1038/nrn2719

Ramón y Cajal's S. (1911). *Histologie du Système Nerveux de L'homme & des Vertébrés*, Vol. II. Paris: Maloine.

Rees, C. L., Moradi, K., and Ascoli, G. A. (2017). Weighing the evidence in peters' rule: does neuronal morphology predict connectivity? *Trends Neurosci.* 40, 63–71. doi: 10.1016/j.tins.2016.11.007

Reiner, A., Hart, N. M., Lei, W., and Deng, Y. (2010). Corticostriatal projection neurons – dichotomous types and dichotomous functions. *Front. Neuroanat.* 4:142. doi: 10.3389/fnana.2010.00142

Rock, C., Zurita, H., Wilson, C., and Apicella, A. J. Jr. (2016). An inhibitory corticostriatal pathway. *eLife* 5:e15890. doi: 10.7554/eLife.15890

Rowe, T. B., and Shepherd, G. M. (2016). The role of ortho-retronasal olfaction in mammalian cortical evolution. *J. Comp. Neurol.* 524, 471–495. doi: 10.1002/cne.23802

Schuman, B., Machold, R. P., Hashikawa, Y., Fuzik, J., Fishell, G. J., and Rudy, B. (2019). Four unique interneuron populations reside in neocortical layer 1. *J. Neurosci.* 39, 125–139. doi: 10.1523/JNEUROSCI.1613-18.2018

Shepherd, G. M. (1974). *The Synaptic Organization of the Brain*. New York, NY: Oxford University Press.

Shepherd, G. M., Mirsky, J. S., Healy, M. D., Singer, M. S., Skoufos, E., Hines, M. S., et al. (1998). The Human Brain Project: neuroinformatics tools for integrating, searching and modeling multidisciplinary neuroscience data. *Trends Neurosci.* 21, 460–468. doi: 10.1016/S0166-2236(98)01300-9

Shepherd, G. M. (2011). The microcircuit concept applied to cortical evolution: from three-layer to six-layer cortex. *Front. Neuroanat.* 5:30. doi: 10.3389/fnana.2011.00030

Shepherd, G. M. (ed.) (2004). *The Synaptic Organization of the Brain*, 5th Edn. New York, NY: Oxford University Press. doi: 10.1093/acprof:oso/9780195159561.001.1

Shepherd, G. M., and Grillner, S. (eds). (2018). *Handbook of Brain Microcircuits*, 2nd Edn. New York, NY: Oxford University Press.

Shepherd, G. M., and Rowe, T. B. (2017). Neocortical lamination: insights from neuron types and evolutionary precursors. *Front. Neuroanat.* 11:100. doi: 10.3389/fnana.2017.00100

Shepherd, G. M. G. (2013). Corticostriatal connectivity and its role in disease. *Nat. Rev. Neurosci.* 14, 278–291. doi: 10.1038/nrn3469

Shibata, M., Gulden, F. O., and Sestan, N. (2015). From trans to cis: transcriptional regulatory net- works in neocortical development. *Trends Genet.* 31, 77–87. doi: 10.1016/j.tig.2014.12.004

Slomianka, L., Amrein, I., Knuesel, I., Sørensen, J. C., and Wolfer, D. P. (2011). Hippocampal pyramidal cells: the reemergence of cortical lamination. *Brain Struct. Funct.* 216, 301–317. doi: 10.1007/s00429-011-0322-0

Smith, L. M., Ebner, F. F., and Colonnier, M. (1980). The thalamocortical projection in Pseudemys turtles: a quantitative electron microscopic study. *J. Comp. Neurol.* 190, 445–461. doi: 10.1002/cne.901900304

Somogyi, P., and Klausberger, T. (2018). "Hippocampus: intrinsic organization," in *Handbook of Brain Microcircuits*, 2nd Edn, eds G. M. Shepherd and S. Grillner (New York, NY: Oxford University Press), 199–216.

Suryanarayana, S. M., Robertson, B., Wallén, P., and Grillner, S. (2017). The lamprey pallium provides a blueprint of the mammalian layered cortex. *Curr. Biol.* 27, 3264–3277. doi: 10.1016/j.cub.2017.09.034

Tamamaki, N., and Nojyo, Y. (1990). Disposition of the slab-like modules formed by axon branches originating from single CA1 pyramidal neurons in the rat hippocampus. *J. Comp. Neurol.* 291, 509–519. doi: 10.1002/cne.902910403

Tasic, B., Yao, Z., Graybuck, L. T., Smith, K. A., Nguyen, T. N., Bertagnolli, D., et al. (2018). Shared and distinct transcriptomic cell types across neocortical areas. *Nature* 563, 72–78. doi: 10.1038/s41586-018-0654-5

ten Donkelaar, H. J. (1998). "Reptiles," in *The Central Nervous System of Vertebrates*, Vol. 2, eds R. Nieuwenhuys, H. J. ten Donkelaar, and C. Nicholson (Berlin: Springer), 1315–1524. doi: 10.1007/978-3-642-18262-4_20

Thomson, A. (2010). Neocortical layer 6, a review. *Front. Neuroanat.* 4:13. doi: 10.3389/fnana.2010.00013

Valero, M., Cid, E., Averkin, R. G., Aguilar, J., Sanchez-Aguilera, A., Viney, T. J., et al. (2015). Determinants of different deep and superficial CA1 pyramidal cell dynamics during sharp-wave ripples. *Nat. Neurosci.* 18, 1281–1290. doi: 10.1038/nn.4074

Valero, M., and de la Prida, L. M. (2018). The hippocampus in depth: a sublayer-specific perspective of entorhinal-hippocampal function. *Curr. Opin. Neurobiol.* 52, 107–114. doi: 10.1016/j.conb.2018.04.013

Wamsley, B., and Fishell, G. (2017). Genetic and activity-dependent mechanisms underlying interneuron diversity. *Nat. Rev. Neurosci.* 18, 299–309. doi: 10.1038/nrn.2017.30

Wheeler, D. W., White, C. M., Rees, C. L., Komendantov, A. O., Hamilton, D. J., and Ascoli, G. A. (2015). Hippocampome.org: a knowledge base of neuron types in the rodent hippocampus. *eLife* 4:e09960. doi: 10.7554/eLife.09960

Williams, P. A., Larimer, P., Gao, Y., and Strowbridge, B. W. (2007). Semilunar granule cells: glutamatergic neurons in the rat dentate gyrus with axon collaterals in the inner molecular layer.

J. Neurosci. 27, 13756–13761. doi: 10.1523/JNEUROSCI.4053-07.2007

Wilson, C. J. (2004). "Basal ganglia," in *The Synaptic Organization of the Brain*, ed. G. M. Shepherd (New York, NY: Oxford University Press).

Wilson, D. A., and Barkai, E. (2018). "Olfactory cortex," in *Handbook of Brain Microcircuits*, 2nd Edn, eds G. M. Shepherd and S. Grillner (New York, NY: Oxford University Press), 323–332.

Yamawaki, N., Li, X., Lambot, L., Ren, L. Y., Radulovic, J., and Shepherd, G. M. G. (2019). Long-range inhibitory intersection of a retrosplenial thalamocortical circuit by apical tuft-targeting CA1 neurons. *Nat. Neurosci.* 1–12 (in press).

Conflict of Interest Statement: The authors declare that the research was conducted in the absence of any commercial or financial relationships that could be construed as a potential conflict of interest.

Copyright © 2019 Shepherd, Marenco, Hines, Migliore, McDougal, Carnevale, Newton, Surles-Zeigler and Ascoli. This is an open-access article distributed under the terms of the Creative Commons Attribution License (CC BY). The use, distribution or reproduction in other forums is permitted, provided the original author(s) and the copyright owner(s) are credited and that the original publication in this journal is cited, in accordance with accepted academic practice. No use, distribution or reproduction is permitted which does not comply with these terms.

frontiers in Neuroanatomy

ORIGINAL RESEARCH
published: 02 November 2018
doi: 10.3389/fnana.2018.00082

Navigating the Murine Brain: Toward Best Practices for Determining and Documenting Neuroanatomical Locations in Experimental Studies

*Ingvild E. Bjerke, Martin Øvsthus, Krister A. Andersson, Camilla H. Blixhavn, Heidi Kleven, Sharon C. Yates, Maja A. Puchades, Jan G. Bjaalie and Trygve B. Leergaard**

Department of Molecular Medicine, Institute of Basic Medical Sciences, University of Oslo, Oslo, Norway

In experimental neuroscientific research, anatomical location is a key attribute of experimental observations and critical for interpretation of results, replication of findings, and comparison of data across studies. With steadily rising numbers of publications reporting basic experimental results, there is an increasing need for integration and synthesis of data. Since comparison of data relies on consistently defined anatomical locations, it is a major concern that practices and precision in the reporting of location of observations from different types of experimental studies seem to vary considerably. To elucidate and possibly meet this challenge, we have evaluated and compared current practices for interpreting and documenting the anatomical location of measurements acquired from murine brains with different experimental methods. Our observations show substantial differences in approach, interpretation and reproducibility of anatomical locations among reports of different categories of experimental research, and strongly indicate that ambiguous reports of anatomical location can be attributed to missing descriptions. Based on these findings, we suggest a set of minimum requirements for documentation of anatomical location in experimental murine brain research. We furthermore demonstrate how these requirements have been applied in the EU Human Brain Project to optimize workflows for integration of heterogeneous data in common reference atlases. We propose broad adoption of some straightforward steps for improving the precision of location metadata and thereby facilitating interpretation, reuse and integration of data.

Keywords: best practice, brain atlas, data mining, data sharing, FAIR, reproducibility, location metadata, rodent brain

OPEN ACCESS

Edited by:
Hans J. ten Donkelaar, Radboud University Nijmegen, Netherlands

Reviewed by:
Piotr Majka, Nencki Institute of Experimental Biology (PAS), Poland
Robert P. Vertes, Florida Atlantic University, United States

****Correspondence:***
Trygve B. Leergaard
t.b.leergaard@medisin.uio.no

Received: *13 July 2018*
Accepted: *19 September 2018*
Published: *02 November 2018*

Citation:
Bjerke IE, Øvsthus M, Andersson KA, Blixhavn CH, Kleven H, Yates SC, Puchades MA, Bjaalie JG and Leergaard TB (2018) Navigating the Murine Brain: Toward Best Practices for Determining and Documenting Neuroanatomical Locations in Experimental Studies. Front. Neuroanat. 12:82. doi: 10.3389/fnana.2018.00082

INTRODUCTION

Over last decades, considerable effort has been invested in large-scale the production of neuroscience data (see, e.g., Stopps et al., 2004; Boy et al., 2006; Lein et al., 2007; Zakiewicz et al., 2011; Hintiryan et al., 2012; Ragan et al., 2012; Oh et al., 2014). With increasingly efficient data production pipelines the number of scientific reports and amount of available data is steadily growing (Hey and Trefethen, 2003). To organize, compare and integrate such large amounts of

data into new knowledge and understanding about the brain, new computational approaches have emerged (Amari et al., 2002; Bjaalie et al., 2005; Koslow and Subramaniam, 2005; Bjaalie, 2008; Tiesinga et al., 2015; Bjerke et al., 2018) to make data discoverable, accessible, interpretable and re-usable, as outlined in the widely endorsed FAIR Guiding Principles (Findability, Accessibility, Interoperability, and Re-usability; Wilkinson et al., 2016). However, these integration efforts face the challenge that neuroscience data span multiple spatial and temporal scales (see, e.g., Amunts et al., 2016), and that results are commonly reported in journal articles as narratives supported with documentation in selected figures and tables that are difficult to compare. A prerequisite for data integration is that the nature and relationships of data parameters are well defined and easily comparable, hence integration efforts will have to incorporate methods for dealing with these differences.

Interpretation of observations collected from the brain depends critically on specific information about anatomical location (see, e.g., Bjaalie, 2002): e.g., from which cortical area, cell layer, or nucleus were measurements or observations obtained? Comparison of results across studies, or replication of experimental findings, necessitates that the specific anatomical position of a measurement, observation, or experimental perturbation, is well-defined. Such anatomical descriptions in experimental reports are of variable quality and are prone to ambiguity, since anatomical terms can be interpreted in a number of ways, and alternative anatomical parcellation schemes often uses different boundary definitions (see, e.g., Van De Werd and Uylings, 2014). Thus, the lack of universally accepted and well-defined descriptions of neuroanatomical location, defining the precise location being studied, is a major challenge when attempting to compare and integrate data from different investigations.

In response to this challenge, open access, three-dimensional (3-D) brain atlases have been developed for murine brains (Hjornevik et al., 2007; Lein et al., 2007; Johnson et al., 2010; Hawrylycz et al., 2011; Veraart et al., 2011; Oh et al., 2014; Papp et al., 2014; Kjonigsen et al., 2015) to serve as spatial frameworks for data sharing and integration (Boline et al., 2008; Amunts et al., 2014; Zaslavsky et al., 2014). Building upon a new generation of 3-D brain atlases, the EU Human Brain Project develops tools and workflows for integrating, sharing and analyzing brain data that have been defined within a common anatomical framework. The project has established workflows for mapping diverse types of murine and human image data to common spatial reference atlas frameworks, building on tools for spatial registration of two-dimensional (2-D) histological image data to a 3-D reference volume (Papp et al., 2016; Puchades et al., 2017), and use of organized collections of metadata describing basic features of data, including descriptions of the anatomical location from which the data originate. These tools and workflows are currently routinely used in the Human Brain Project, but their wider adoption outside the project requires a better understanding of the presently used approaches for describing and documenting neuroanatomical location in experimental studies of murine brains.

To first assess how anatomical location is reported in the neuroscience literature, we evaluated and compared current practices for interpreting and documenting the location of measurements in different disciplines of neuroscience that typically deal with invasive techniques or extraction of tissue. Our observations indicate substantial differences in approach, interpretation and reproducibility of anatomical location between different categories of experimental research, as well as a potential for improvement with relatively simple measures. Based on these observations, we have adjusted and optimized the Human Brain Project tools and workflows to accommodate the type of data and documentation typically used in different domains of experimental research on murine brains. We propose step-wise practical implementations that can improve current practices, and argue that these procedures increase reproducibility and facilitate integration of neuroscience data. We finally discuss costs and benefits of increasingly elaborate approaches.

MATERIALS AND METHODS

Survey of Current Practices for Assignation and Reporting of Anatomical Location

We performed a literature study to explore current practices for reporting anatomical information in different categories of experimental neuroscientific studies in murine brains.

We focused on experimental studies involving invasive procedures or tissue extraction, and classified publications into the following seven methodological categories based on the principal methodology employed: (1) cytoarchitectonic staining techniques, including immunohistochemistry (IHC) and *in situ* hybridization (ISH); (2) axonal tract tracing; (3) transmission electron microscopy (TEM); (4) immunoblotting; (5) *in vitro* electrophysiology with slice preparations and microscopic visualization of recorded cells; (6) *in vivo* electrophysiology, and (7) two-photon and optogenetic imaging. Studies involving tomographic whole-brain imaging and trans-cranial measurements were not included.

Individual search strings were made for each methodological category, and a search was performed in Ovid MEDLINE. Except for the terms related to the specific methods, the criteria used for building the search strings were consistent across searches and contained the following: ((exp mice/or exp rats/) OR (mouse or mice or rat or rats).tw,kf.) AND ((brain or brains or neuroscien* or neuroanatom* or neuro anatom* or neuron or neurons).mp.). Strings related to the specific methodologies of interest (see above) were added to this:

(1) (immunohistochemistry/or immunohistochemistry.tw,kf.) OR ((in situ hybridization).tw,kf.)
(2) ((retrograde or anterograde) adj trac*.tw,kf.) for axonal tract tracing
(3) ((Microscopy, Electron, Transmission/) OR (transmission adj (electronmicroscop* or electron microscop*)).tw,kf.)
(4) ((western blot* or immunoblot*).tw,kf.)

(5) ((((invitro or in vitro) adj2 (electrophysiolog* or electro physiolog* or cell recording)) or cell recording).tw,kf.)
(6) ((invivo or in vivo) adj2 (electrophysiolog* or electro physiolog*)).tw,kf
(7) ((optogenetics/or optogenetics or optogenetic*.tw,kf.)) OR ((((twophoton or two photon or two-photon or 2 photon or 2-photon) adj2 (microscop* or imaging)).tw,kf.))

Filters were then added to limit results to those with journal article format and publication data from 2012 through 15.02.2017. The search returned 9839 entries related to immunohistochemistry and *in situ* hybridization, 547 related to axonal tract tracing, 949 related to electron microscopy, 7004 related to immunoblotting, 95 related to *in vitro* electrophysiology, 213 related to *in vivo* electrophysiology, and 2023 related to optogenetic or two-photon microscopy.

Papers (n = 120; 20 for each methodological category) were chosen from the selection of search entries by use of a random number generator and evaluated using the following inclusion criteria: (a) contained murine brain data; (b) presented original data; and (c) were published within the last 5 years. Papers not meeting these criteria were excluded and a new random paper selected.

For each paper in the survey, we evaluated the descriptions of anatomical locations with respect to: (1) any additional information provided beyond the structure name (e.g., by citing an anatomical reference atlas, illustration of the region of interest by use of a schematic drawing or reference atlas plate, or description of the general histological, cytoarchitectonic or electrophysiological features of the region); (2) use of histological sections (without counterstaining); (3) use of (immuno-)histochemical staining to visualize anatomical features; (4) specification of spatial coordinates (e.g., stereotaxic coordinates observed during experimental surgery or by comparison with a reference atlas); (5) documentation using images that show anatomical landmarks suitable for identifying location in addition to features of interest (see below); (6) annotation of anatomical landmarks or boundaries in images from the material; (7) images from multiple (serial) sections through a region of interest; and (8) spatial registration of images to a reference atlas.

Some papers reported results obtained using several methodologies, but for each paper we only assessed the documentation related to the specific methodology for which the paper was selected. Documentation of anatomical location with images was only considered sufficient if images gave a reasonable overview of the regions of interest, allowing the reader to identify the position of the image relative to a reference atlas. We set the minimum standard to be that images should show the region of interest *and* at least one other distinct anatomical landmark, such as a part of the ventricular system, a major white matter tract, or a distinct gray matter structure. Consequently, high-power images showing structural details of a smaller region, e.g., a part of the cerebral cortex with visible layers, were not considered sufficient to allow interpretation of anatomical location in this context.

Most commonly, the region of interest was an *observation site* in which some analysis had been performed (e.g., cell counting, immunoreactivity observations, cell reconstructions). Alternatively, the region of interest may have been a site of an experimental procedure, or *perturbation* (e.g., a lesion, an electrode implantation or a virus injection). In the case of multiple regions of interest of the same type, e.g., cell counting in several regions or multi-site electrode recordings, we assumed the same level of effort had been undertaken to determine the location of each site, and we evaluated the paper according to the best documented region. In the case of multiple regions of interest of different types, we evaluated both types of regions separately. In tract tracing studies, for example, there are sites of perturbation (injection of tracer) and observation (labeled features). For tracing studies we therefore assessed injection sites and terminal fields as individual reports of regions of interest. Thus, while 20 papers from each of the seven methodological categories were surveyed, the total number of papers used was 120, because each tract tracing paper was included in two of the categories (tract tracing injection site and tract tracing terminal fields). References to these 120 papers are given in **Supplementary Table 1**, which also provides an overview of the observations extracted from 162 different reports of anatomical observations found in these papers.

Tools Used to Facilitate Documentation of Anatomical Locations

We aimed to demonstrate how new tools and procedures can be applied in order to map and co-visualize data spanning several methodological categories, and to identify key strategies in this process that should influence how data are acquired and documented.

We used the Human Brain Project software tool QuickNII (Puchades et al., 2017) to register single or serial section images to a 3-D reference atlas template by positioning and slicing the atlas in user-defined planes of sectioning. The QuickNII tool is bundled either with the Waxholm Space atlas of the Sprague-Dawley rat brain (version 2, Papp et al., 2014; Kjonigsen et al., 2015)[1] or the Allen Mouse Common Coordinate Framework (version 3, downloaded June 17, 2016; Oh et al., 2014)[2]. We furthermore used the Human Brain Project tool LocaliZoom for extraction of coordinates from annotated points of interest. The coordinates representing the location of these points in reference atlas space were exported as x, y, z coordinates to MeshView, a Human Brain Project web-viewer tool for visualization of 3-D mesh-data (structural atlas parcellations) together with the point coordinates extracted with LocaliZoom.

Data Used to Demonstrate Workflows

To demonstrate workflows for spatial integration of different types of data, we used existing or publicly available data sets from the following four methodological categories: (1) *in vivo* electrophysiology; (2) transmission electron microscopy; (3) cytoarchitectonic staining techniques; and (4) *in vitro* electrophysiology with cell reconstruction. These categories

[1]https://www.nitrc.org/projects/whs-sd-atlas

[2]http://download.alleninstitute.org/informatics-archive/current-release/mouse_ccf/annotation/ccf_2015/

represent four of the seven methodologies included in our literature survey, and the workflows used to map these data to anatomical space can easily be extended to the remaining categories.

Electron microscopy data showing parvalbumin positive neurons in the rat medial entorhinal cortex (Berggaard et al., 2018), was generously made available to the present study by Nina Berggaard (Norwegian University of Science and Technology, Norway). *In vivo* electrophysiology recording data from the rat hippocampal region were produced by Debora Ledergerber (Norwegian Institute of Science and Technology, Norway; Puchades et al., 2017). Immunohistological material showing parvalbumin positive neurons across a horizontally cut hemisphere (Boccara et al., 2015) was shared through the Human Brain Project by Menno P. Witter (Norwegian University of Science and Technology, Norway). A 3-D reconstruction of a mouse striatal cholinergic interneuron was performed by Alexander Kozlov, Johanna Frost Nylén and Sten Grillner (Karolinska Institutet, Sweden) and shared via the Human Brain Project[3]. Lastly, a series of sagittal sections from the Allen Institute for Brain Science repository of *in situ* hybridization data (Lein et al., 2007)[4] was downloaded through their API.

For each data set, section images were spatially registered to a reference atlas template using the QuickNII tool. The first three data sets (*in vivo* electrophysiology, immunohistochemistry, and electron microscopy data) were registered to the Waxholm Space atlas of the rat brain. Section material from the *in vitro* electrophysiology with cell reconstruction and *in situ* hybridization was mapped to the Allen Mouse Common Coordinate Framework of the mouse brain. Following spatial registration to atlas, images with associated atlas information were exported to LocaliZoom for visualization and retrieval of spatial coordinates.

[3]https://www.humanbrainproject.eu/en/explore-the-brain/search/

[4]http://mouse.brain-map.org/experiment/show/75457579

Ethical Considerations

This study used animal data acquired in accordance with European Union and International legislation regarding use of animal subjects. For data shared by the Human Brain Project, verification of compliance with European legal and regulatory requirements is provided with the data. For other data, statements regarding ethical conduct care are found in the original papers (Lein et al., 2007; Berggaard et al., 2018).

RESULTS

Survey of Anatomical Descriptions and Metadata Provided in Original Neuroscientific Reports

We surveyed anatomical descriptions and documentation provided in 120 scientific original reports (published within the last 5 years) involving different types of experimental methods, and evaluated their inclusion of tissue sectioning and histological staining, specification of spatial coordinates, documentation with images (with or without annotations) and the use of spatial registration to anatomical reference atlases. We found systematic variations across methodological categories regarding the degree to which anatomical locations were described and documented (summarized in **Table 1**). Below, we first summarize our findings of anatomical documentation per methodological category, and secondly compare the use of anatomical descriptions and different types of documentation across the methodological categories.

Tract-tracing studies generally provide more anatomical documentation than studies using other methods (**Table 1**). In 85% of the papers investigated, the location of tracer injection

TABLE 1 | Overview of anatomical metadata elements provided in the publications investigated.

	Description of ROI	Sectioning	Staining	Coordinates	Image documentation	Annotations	>1 section image	Atlas registration
Tract tracing (injection site)	100	100	80	85	80	50	20	5
Tract tracing (terminal fields)	80	100	95	45	60	45	15	0
Cytoarchitectonic studies	45	95	95	30	60	30	10	0
In vivo electrophysiology	95	45	25	65	30	10	0	5
In vitro electrophysiology	70	100	30	15	20	15	0	0
Advanced imaging	86	64	32	50	18	14	0	0
Electron microscopy	30	25	10	10	5	0	0	0
Western blot	20	5	0	0	0	0	0	0
Average	66	67	46	38	34	21	6	1

Percentage of papers (n = 120), sorted by methodological category (rows), using different approaches (columns) to document anatomical location selected articles. Employed practices to identify and document anatomical location vary across the categories of investigations. Most studies describe location semantically, while the use of image documentation and spatial registration of images to reference atlases is limited.

sites was given by the perioperatively recorded stereotaxic coordinates used when placing the tracer injections, and 35% of these further documented injection sites with section coordinates upon verification of position. Injection sites were often documented with images showing anatomical location of the injection (80%), and in 60% of cases the regions of interest containing neuronal labeling were also documented with images (**Table 1**). Contrary to our expectation, we found that in most of the investigated papers reporting on tract tracing experiments (17 of 20 papers, 85%), the anatomical location of tracer injection sites was more thoroughly described and documented than the location of transported neuronal labeling in one or more remote brain regions (see **Table 1** for details).

While all reports from cytoarchitectonic investigations used histological techniques and almost all (18 of 20, 90%) presented images of microscopic observations, only 60% provided images with visible anatomical landmarks (**Table 1**), and very few (10%) included images showing their region(s) of interest across multiple sections. In several of the papers investigated we found it difficult to interpret and reproduce the investigated regions in a reference atlas.

Our results also show that *in vivo* electrophysiological experiments typically provide better documentation of anatomical location than most other study types, mainly as the location of the recording electrodes (in 65% of cases, **Table 1**) is usually defined by perioperatively recorded stereotaxic coordinates. In 38% of these papers, implantation sites were further documented by providing histologically verified section coordinates. Of the publications reporting on *in vitro* electrophysiological studies with microscopic visualization of recorded cells, 30% used histological staining to reveal anatomical landmarks, but only 20% included overview images documenting anatomical boundaries or landmarks (**Table 1**).

Studies using advanced *in vivo* optogenetic or two-photon microscopic imaging techniques often (in 85% of cases, **Table 1**) contained some form of description of the region of interest, and coordinates were provided in approximately half of the papers. Somewhat surprisingly, we found that the microscopic images of the analyzed material rarely (in 18% of the papers investigated, **Table 1**) included anatomical landmarks suitable for documenting anatomical locations.

Lastly, we found that documentation of anatomical location was, to a small degree, provided in reports of electron microscopy and immunoblot studies. 20–30% of such studies contained anatomical descriptions of regions of interest, while use of additional documentation was minimal or absent (**Table 1**). These types of studies were the least likely to include sufficient anatomical information of all the assessed methods.

Our results thus show that of all 120 papers surveyed only 66% included some form of anatomical descriptions of regions of interest, beyond mention of the region name (**Table 1**). In the remaining 34% of papers, we found no descriptions of the region of interest apart from the name of the region. A further breakdown of the 66% papers providing anatomical descriptions is summarized in **Table 2**. This breakdown showed that 29% of the papers providing a description of a region of interest did so by using a reference to a specific anatomical atlas. Notably, we also found that anatomical reference atlases were most frequently cited in reports of tract tracing injection sites (60%, **Table 2**), while none of the immunoblot reports providing anatomical descriptions related these to a reference atlas. Interestingly, among the anatomical descriptions provided in reports of neural labeling observed in tract-tracing studies, or advanced imaging studies, only 44 or 11%, respectively, included reference to a specific anatomical atlas. We further found that among the 66% of papers including anatomical descriptions, 76% included illustrations or line drawing of anatomical features, 42% indicated measurements of distances to specific anatomical landmarks, and 13% related their descriptions to observed microscopic or electrophysiological features (**Table 2**).

Although stereotaxic atlases are widely used and stereotaxic coordinates provide precise indications of location, we found

TABLE 2 | Overview of the types of descriptions and coordinate based information provided the publications investigated.

	Tract tracing injection site	Tract tracing terminal fields	Cytoarchitectonic studies	*In vivo* electrophysiology	*In vitro* electrophysiology	Advanced imaging	Electron microscopy	Western blot	Average
Descriptions	**100**	**80**	**45**	**95**	**70**	**86**	**30**	**20**	**66**
Based on distance to landmark	90	13	22	84	0	68	33	25	42
Based on reference atlas	60	44	22	53	21	11	17	0	29
Based on illustration	55	100	89	58	71	89	67	75	76
Based on cellular features	20	19	0	26	36	5	0	0	13
Coordinates	**85**	**45**	**30**	**65**	**15**	**50**	**10**	**0**	**38**
Point coordinates	100	0	0	100	0	91	50	0	43
Section coordinates	35	45	100	38	100	27	50	0	49

Percentage of papers (n = 120) from different methodological categories (columns) providing different types of documentation (rows) as descriptions or point coordinates.

that coordinate-based information was presented in only 38% of the papers surveyed (**Table 1**). Further breakdown showed that of the 38% of papers that included spatial coordinates, 49% provided positions of sections or slices reported as distances from skull landmarks or the midline (**Table 2**), while 43% specified points of interest as x, y, z coordinates (**Table 2**) targeted perioperatively and/or identified by *post hoc* analyses. Of the publications reporting tract tracing or *in vivo* electrophysiological experiments, 65% included spatial coordinates, while none of the publications reporting immunoblotting results contained such information.

While most studies included high-power image documentation of observed features, only 34% included images showing anatomical landmarks and/or boundaries suitable for interpretation of anatomical locations, while 21% of studies provided images with anatomical annotations superimposed (**Table 1**). Most of the images showing anatomical landmarks were restricted to one brain region of interest; in fact, only ∼9% of all studies provided overview images showing a whole, half or smaller part of a brain section. None of the papers examined included images from macroscopic dissection. Only 6% of the papers used more than a single section image to document the same region of interest (**Table 1**).

Only two of the surveyed papers (1%) used spatial registration tools to map the position of their experimental images to anatomical reference atlases (**Table 1**). We thus found systematic differences in the documentation of anatomical regions of interest provided in original research papers that varied across methodological subfields of neuroscience. Our findings indicate that most studies lack elementary descriptions and documentation of anatomical location that in principle should be straightforward to include in scientific reports, regardless of the type of methodology used.

Minimum Requirements for Documentation of Locations in Experimental Murine Brain Research

Based on the above findings, we considered how anatomical descriptions from different methodological traditions could be improved to achieve more consistent and reproducible descriptions of anatomical locations. A key principle underlying empirical scientific research is that original publications should contain sufficient descriptions of materials and methods used to allow peers to reproduce experimental results. Extrapolating from this, an obvious minimum requirement for the reporting of anatomical location is that anatomical regions of interest should be specifically and unambiguously reported, with sufficient documentation to allow interpretation and replication of described anatomical positions. However, our survey of the current literature above revealed that the location of data is often poorly described and documented, making reported anatomical positions hard to replicate. Combining the findings summarized in **Table 1** and accumulated experiences with interpretation and validation of anatomical locations in a wide range of materials measurements collected in context of the Human Brain Project (see e.g., Bjerke et al., 2018), we identified some key documentation elements that we found to be of particular importance for our ability to unequivocally specify anatomical locations for different data sets. We also formulate a set of method-independent recommendations for a minimum documentation practice that could alleviate the ambiguity observed in many research papers (see above), and facilitate interpretation of anatomical positions and comparison of research findings. Thus, to achieve more unambiguous and reproducible descriptions of anatomical locations in neuroscientific reports we propose that adherence to at least one and preferably several of the following recommendations should be set as a minimum requirement:

(1) Employ and refer to a specific anatomical parcellation scheme
(2) Provide precise semantic descriptions relating observations to anatomical landmarks or features
(3) Define points or regions of interest using an anatomical illustration or diagram
(4) Provide annotated images showing distinct anatomical landmarks
(5) Report spatial coordinates

Below, we specify and exemplify these recommendations in further detail.

Referring to a Defined Parcellation Scheme

Several parcellation schemes exist for the whole mouse and rat brain, including the widely used 2-D stereotaxic reference atlases (Swanson, 2004; Paxinos and Franklin, 2012; Paxinos and Watson, 2013), and 3-D reference atlas templates (Johnson et al., 2010; Hawrylycz et al., 2011; Papp et al., 2014). More detailed parcellation schemes have also been defined for parts of the brain, such as the hippocampus (Kjonigsen et al., 2011; Witter, 2012; Boccara et al., 2015). Anatomical parcellation schemes should preferably include graphical representations of the boundaries defining anatomical structures specified in a nomenclature list. Use of standardized schemes that are widely used in the community will facilitate comparison of anatomical locations. To be unambiguous, a description based on a parcellation scheme should include (1) the name of the region of interest exactly *as it appears* in the reference atlas, and (2) appropriate citation of the reference atlas (and version) employed. Reference to 3-D atlas templates, e.g., the Allen Mouse Common Coordinate Framework (Lein et al., 2007; Oh et al., 2014) or Waxholm Space (Hawrylycz et al., 2011; Papp et al., 2014), that can be sliced in any orientation provides superior anatomical precision for both volumetric data and 2-D sectioned data (**Figure 1**). For observations or measurements that are sampled from an entire brain region, for example describing populations of labeled cells distributed across a given brain region, reference to the region name will usually be unambiguous. However, if observations or measurements only pertain to a small subset of a region of interest, e.g., for a single cell reconstruction or a tissue sample processed for electron microscopy, information about parcellation scheme should be supplemented with one of the other recommendations listed above to more clearly specify

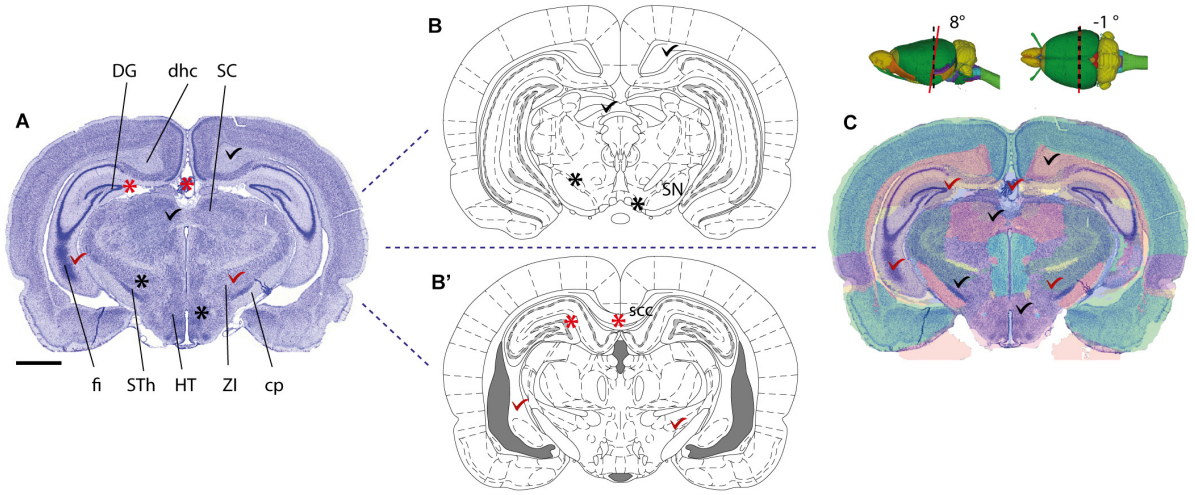

FIGURE 1 | Mapping a coronal rat brain section with a slight tilt to a reference atlas**. (A)** Image of a thionine stained coronal rat brain section, cut with a slight deviation from the standard plane of orientation. A slight left-right asymmetry is visible in the fimbria of the hippocampus (fi), and when comparing the section with a standard reference atlas, reference plates from different anteroposterior levels match the dorsal and ventral parts of the section, respectively. **(B,B')** Atlas diagrams 78 **(B)** and 68 **(B')**, reproduced from Paxinos and Watson (2005) with permission, separated by ∼1.5 mm. In both diagrams, anatomical structures that are consistent (check marks) or inconsistent (asterisks) with corresponding regions in the histological section are seen. Regions located dorsally in **(A)**, such as the dentate gyrus (DG), dorsal hippocampal commissure (dhc) and the superior colliculus (SC) correspond with plate 78 **(B)**, but not plate 68 **(B')**, while regions located ventrally in **(A)**, such as the fimbria (fi), subthalamic nucleus (STh), hypothalamic region (HT), zona incerta (ZI), and cerebral peduncle (cp) correspond with plate 68 **(B')**, but not with plate 78 **(B)**. **(C)** A custom generated transparent atlas overlay from the 3-D Waxholm Space atlas of the rat brain (v2, Papp et al., 2014; Kjonigsen et al., 2015) superimposed onto the thionine section shows better overall anatomical correspondence of structures in both dorsal and ventral parts of the section. The location and tilt of the custom atlas plate is indicated by red lines in the inset 3-D figures. Scale bar, 2 mm.

location within the region of interest, e.g., using an image or anatomical illustration.

Semantically Describing Spatial Relation to Distinct Anatomical Landmarks or Architectonic Features

In some cases, a region of interest might be described by defining its relation to structural or cellular landmarks. This is a particularly relevant form of description when regions are defined differently or with more detail than in standard atlas frameworks. See, for example, Insausti et al. (1997, pp. 151–155), where subregional boundaries of the entorhinal cortex are described both in terms of cytoarchitectonic features, and in relation to anatomical landmarks. It should be emphasized that while such description can be elaborate and detailed, they can also be challenging to interpret without expert knowledge. Anatomical illustrations or annotated images can facilitate easier interpretation for the reader.

Indicating the Location in an Anatomical Illustration

Anatomical locations can be graphically defined using reference atlas diagrams, schematic summary drawings or other figures. Indication of sampling position within such illustrations (see, e.g., Akhter et al., 2014, their **Figure 2**) can serve as supplements to semantic descriptions, or alternative to spatial coordinates.

Providing (Annotated) Images

Images of experimental material may depict sections or macroscopic dissections. Low-resolution images are generally as useful for the purpose of visualizing location as high-resolution ones, even images obtained with a standard cell phone camera. Section images should show structural landmarks outside the region of interest, if possible more than one. Suggestions for anatomical landmarks that can be consistently identified in volumetric material of the rodent brain are provided in Sergejeva et al. (2015). For sectioned material, the size and shape of prominent gray and white matter regions (e.g., the hippocampus, caudoputamen, pontine nucleus, anterior commissure, and corpus callosum) are also highly useful in order to interpret location in the brain. Ideally, images should cover entire sections. A simple evaluation of the influence of the coverage of a section image on spatial registration accuracy (**Figure 2**) confirms that the more information an image contains, the more likely are two independent and equally experienced researchers to interpret the anatomical position of a region of interest consistently. For procedures not involving histological processing and tissue sections, macroscopic images of the whole brain or tissue sample(s) before and after dissection of tissue samples can improve the interpretation of the anatomical location of the investigated sample considerably (**Figure 3A**). Annotations defining regional boundaries and specifying locations sampled or measured increase precision considerably (see, e.g., Dobi et al., 2013; their **Figure 9**).

Using Spatial Coordinates

Spatial coordinates defined in relation to unique skull features or anatomical landmarks effectively communicate exact positions within the brain, independent of parcellation schemes. Descriptions based on spatial coordinates must specify the

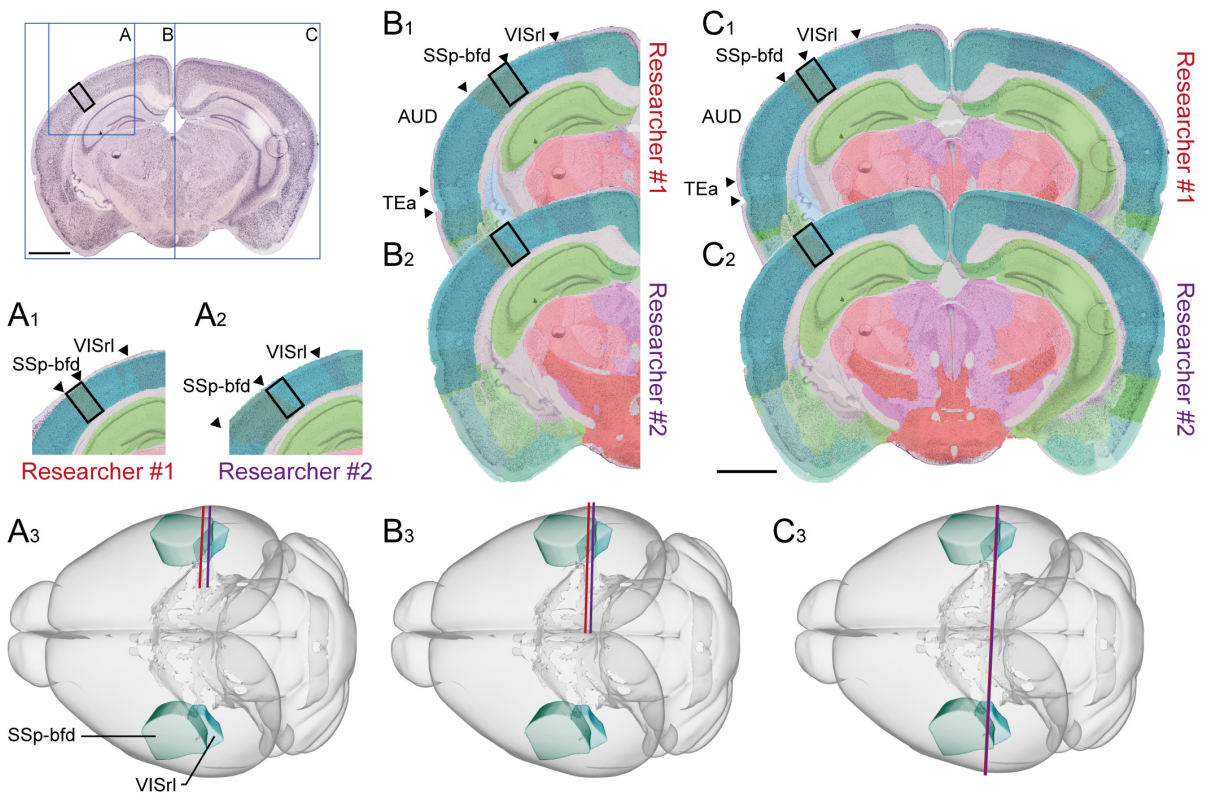

FIGURE 2 | Documenting anatomical location at varying levels of coverage. Illustration showing the influence of image coverage on the spatial accuracy of registration to a reference atlas. Upper left inset: image of a coronal, thionine stained mouse brain section, the black rectangle indicates an arbitrary region of interest in the cerebral cortex, blue rectangles indicate the size of the image used in examples **(A–C)**. **(A–C)** Images with increasing anatomical coverage were shown to two experienced researchers, who independently registered the images to the Allen Mouse Common Coordinate Framework using the QuickNII tool. **(A)** With only a small part of the section image available, the two researchers interpreted the location of the image differently, as the primary somatosensory cortex, barrel field (SSP-bfd, **A1**) by Researcher #1, and as the rostrolateral visual area (VISrl, **A2**) by the Researcher #2. (**A3**) Shows the positions of the section image assigned by Researcher #1 (red line) and Researcher #2 (purple line) in atlas space. **(B)** With an image showing half of the section, the researchers' interpretations of the position become more similar **(B1–B3)**, and when the entire section image was available, both researchers interpreted the region of interest to be located in SSp-bfd **(C1–C3)**. This illustrates that access to images covering more anatomical landmarks is important to provide reproducible information about anatomical positions. Scale bars: 2 mm.

reference space used (e.g., reference atlas or local coordinate system). Coordinates may indicate the level or distance of a section or slice from an anatomical landmark (e.g., bregma or the midline of the brain) or specific points defined by x, y, z coordinates. The method used to define coordinates should be specified and additional validation steps, such as e.g., histological confirmation of perioperative stereotaxic measurements supplemented with documentation using image(s) or illustrations, can improve precision.

Combining Different Types of Data in Reference Atlas Space

A considerable challenge for efforts toward integration of different types of neuroscience data is the heterogeneity in the spatial scale and modality of data. In context of the ambition of the Human Brain Project to make heterogeneous brain data accessible for integrative analyses and computational modeling (Bjerke et al., 2018), we have explored ways to assign location to disparate categories of murine neuroscience data. Using the minimum requirements for documentation of anatomical location proposed above as a starting point, and having the ambition to optimize anatomical descriptions of different types of neuroscience data, we established workflows to relate data sets acquired by *in vivo* electrophysiology, immunohistochemistry, *in situ* hybridization, transmission electron microscopy and *in vitro* electrophysiology with cell reconstruction to a common spatial atlas framework. The core workflow, used to spatially combine features of interest from different types of data sets, involves three steps. We first link the data to the same anatomical reference framework, secondly extract spatial coordinates representing features of interest from each of the data sets and thirdly co-visualize the extracted features in a 3-D atlas viewer as a starting point for various analytic approaches. The workflow is implemented using a suite of digital atlas and viewer tools developed in the Human Brain Project. The QuickNII tool is developed for registering 2-D (serial) images to a reference atlas by mapping a spatially corresponding, customized atlas image onto images (Puchades et al., 2017). The LocaliZoom viewer tool provides an overlay of custom

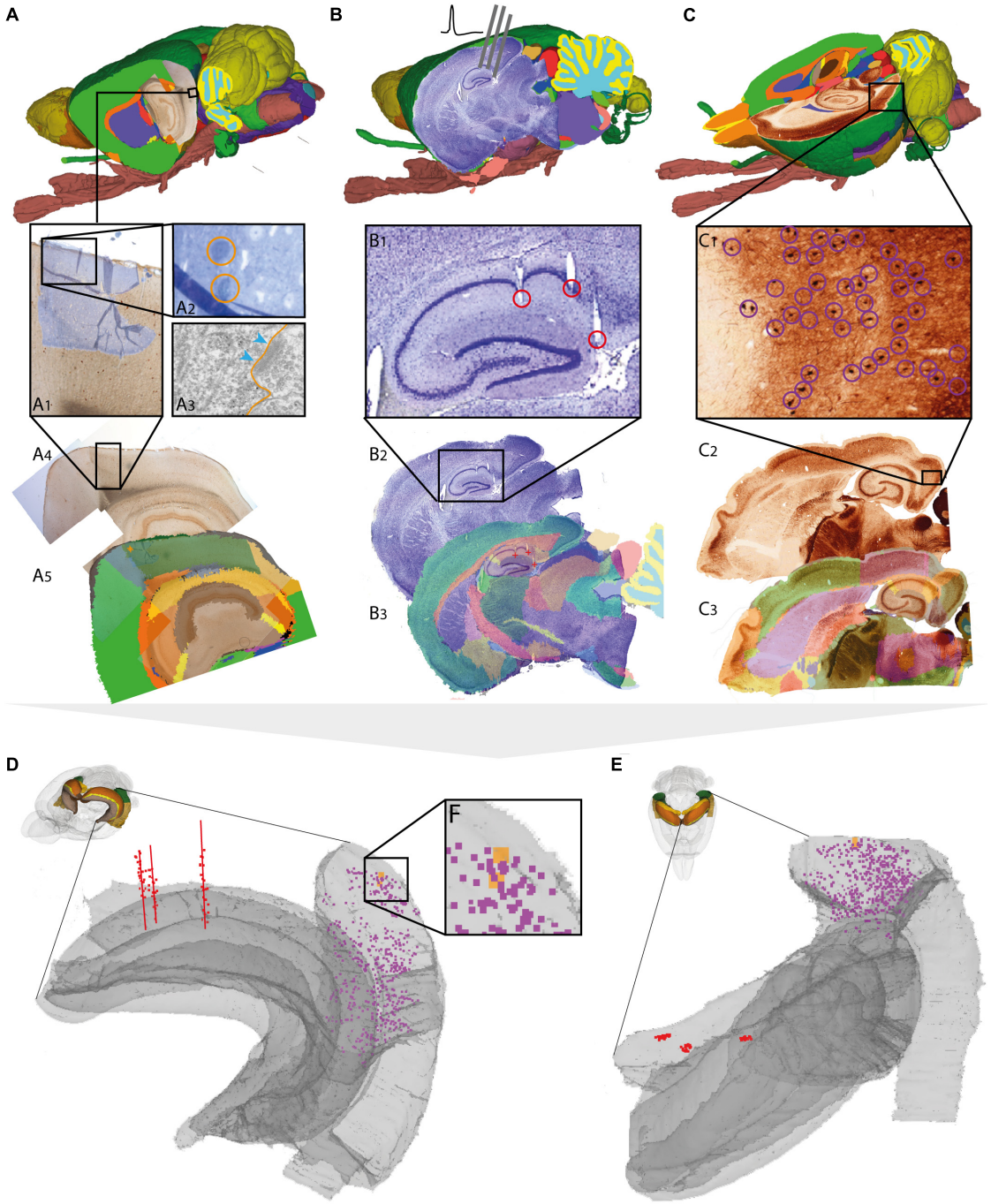

FIGURE 3 | Assigning anatomical location and integrating data using 3-D atlas and new workflows: Examples showing rat brain data. **(A–C)** Data from experimental studies using **(A)** transmission electron microscopy (Berggaard et al., 2018), **(B)** *in vivo* electrophysiology (Puchades et al., 2017), and **(C)** histochemical visualization of chemoarchitecture (Boccara et al., 2015), are mapped to the Waxholm Space atlas of the rat brain (v2, Papp et al., 2014; Kjonigsen et al., 2015). **(A1–A5)** Show the stepwise procedure used to define the location of an electron microscopy (EM) image in atlas space, by mapping an image of semithin, toluidine blue-stained section onto a low-power image showing a larger part of the brain **(A1)**. In this way the location of the parvalbumin stained cell (encircled in **A2**) shown in the EM image **(A3)** is determined in different images. By mapping the overview image **(A4)** in atlas space **(A5)**, the location of the paravalbumin positive cells shown in **(A3)** can be defined by 3-D atlas coordinates (orange crosses in **A5**). **(B1–B3)** Show how tracks of recording electrodes (encircled in **B1**), visible in a thionine stained section cut obliquely halfway between the coronal and sagittal plane **(B2)**, are mapped in atlas space by registration to the reference atlas (red crosses in **B3**). **(C1–C3)** show how positions of parvalbumin positive cells (encircled in **C1**), visualized by immunolabelling of horizontal rat brain sections **(C2)** can be determined by spatially registering section images to a reference atlas **(C3)**. **(D,E)** 3-D co-visualization of point coordinates extracted from the three data sets (**A**, orange dots; **B**, red dots, **C**, purple dots) together with gray surfaces of the right hippocampal and entorhinal regions, shown from an anterolateral **(D)** and dorsal **(E)** view. **(F)** Magnified view of data points representing the location of the cells shown in example **(A)**.

made reference atlas maps and allows extraction of spatial coordinates representing features of interest. The 3-D viewer tool MeshView was used to co-visualize the color coded coordinates from different data sets together with selected elements from the 3-D reference atlas. With this core workflow as a basis, we identified specific strategies for determining anatomical location and extracting spatial coordinates for features of interest from each methodological category. The step-wise implementation of these workflows are exemplified below for different types of data, illustrating how descriptions of location can be improved and used for data integration purposes with relatively simple steps.

For *electron microscopy* data, spatial coordinates were obtained for two parvalbumin positive cells from the medial entorhinal cortex, imaged under a transmission electron microscope (**Figure 3A3**). The ultrathin sections used for electron microscopy were sectioned from a small tissue sample dissected from a sagittal vibratome rat brain section from the temporal cortex, stained for parvalbumin by immunohistochemistry. Prior to ultrathin sectioning, semithin sections were obtained and counterstained using toluidine blue (Berggaard et al., 2018) for orientation and identification of immunopositive cells. To determine the location of the cells viewed by electron microscopy in a 3-D reference atlas, three main steps were followed (**Figures 3A1–3A5**). First, an image of the entire sagittal brain section taken prior to removal of the tissue sample was mapped to the reference atlas using QuickNII (**Figure 3A5**). Secondly, a transparent image of the semithin, toluidine blue-stained section was manually registered to the larger image of the sagittal section, by aligning specific features visible in both images, including blood vessels, labeled cells, outer surface and boundary between gray and white matter (**Figure 3A1**). Finally, the location of the parvalbumin positive cells was identified both in the semithin and ultrathin sections, and coordinates were extracted from the vibratome section (**Figure 3A5**), thus allowing identification of cells across all spatial scales. The above procedure can in principle be applied to any method involving small tissue samples, such as immunoblotting and related methods.

For *electrophysiological recording* data, spatial coordinates were extracted from the bottom of individual electrode track throughout a series of sections cut in a non-standard plane and stained to reveal cytoarchitecture (**Figure 3B**; Puchades et al., 2017). While the location of electrophysiological recordings is usually reported by use of perioperatively determined stereotaxic coordinates (**Table 1**; see above), a key step to improve precision is to determine the location of electrode tracks in histological sections. In our example, a non-standard oblique section plane was used to identify electrode tracks, which is very difficult to compare with a traditional 2-D atlas framework. Using the QuickNII tool, the section image could nevertheless be mapped to atlas space, thus allowing the location of electrode tracks to be annotated and visualized (**Figures 3B1–3B3**; Puchades et al., 2017; see also similar example shown in Bjerke et al., 2018).

For *histological material* used in microscopic studies of brain architecture, the strategy for extracting coordinates for labeled features of interest is straightforward compared to the examples above. In our example (**Figure 3C**), we used images of serial histological sections immunostained for parvalbumin (Boccara et al., 2015). After mapping the serial section images to the reference atlas, we recorded point coordinates representing immunopositive cells located within the medial entorhinal cortex in sections sampled at 200 μm intervals through the entire left entorhinal cortex (**Figure 3C1**). A similar example is shown in **Figure 4A**, using section images (downloaded from the Allen Institute for Brain Science, Lein et al., 2007)[5] showing parvalbumin positive cells visualized by *in situ* hybridization. The spatial registration of these images to the Allen Mouse Common Coordinate Framework was adjusted using the QuickNII tool, and point coordinates representing parvalbumin positive cells in the left caudoputamen were extracted from all sections (**Figure 4A2**).

For *neuron reconstructions*, a slightly different approach was used. The data included coordinate lists created by 3-D reconstruction of neurons (intracellularly filled with neurobiotin) using the Neurolucida software tool (MBF Bioscience, Williston, VT, United States), together with low-power images of sagittal sections images in which the labeled somata were visible. The sagittal section images were registered to the mouse brain atlas using QuickNII, following which the atlas coordinates corresponding to the center of the neuronal soma (seen in the histological section, cf. **Figure 4B2**) were extracted using LocaliZoom. Having determined the center point of the soma and the position and orientation of the histological section image in atlas space, we spatially translated the local (Neurolucida) coordinates representing the complete neuronal arbors of the 3-D reconstructed cell to atlas coordinates.

Thus, by mapping very different types of data to a common anatomical reference atlas, it became possible to extract point coordinates for key data features and co-visualize these in atlas space (**Figures 3D,E**, **4C–E**).

Improving Location Metadata Using New Tools and Workflows for Anatomical Localization

Based on the strategies and documentation elements used above to connect different types of data to a common anatomical framework, and extending on the minimum practice recommendations proposed above, we suggest the following additional method-independent documentation steps to improve precision and facilitate data integration: (1) document features of interest in relation to cellular or regional characteristics; (2) register images to a 3-D reference atlas framework; and, if possible (3) acquire multiple serial histological (or tomographical) images covering several anatomical landmarks.

Document Features of Interest in Relation to Cellular or Regional Characteristics

The anatomical boundaries of brain regions are usually defined by characteristic structural or functional features. These can be visualized by (immuno-)histological staining, such as the thionine or parvalbumin staining shown in **Figure 3**, or other cellular properties such as autoradiographic visualization of

[5]http://mouse.brain-map.org/experiment/show/75457579

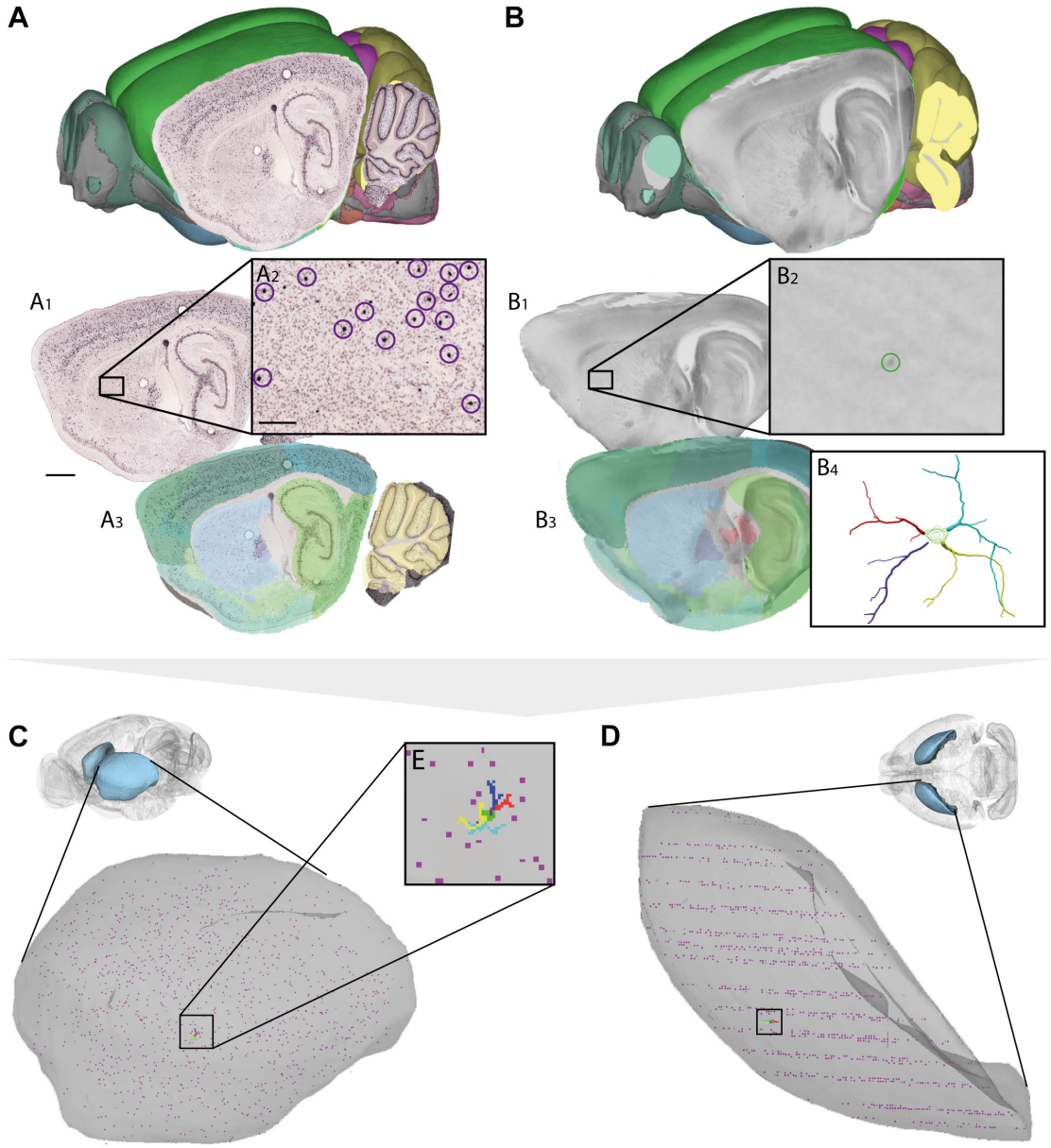

FIGURE 4 | Assigning anatomical location and integrating data using 3-D atlas and new workflows: Examples showing mouse brain data. **(A,B)** Data from experiments using **(A)** *in situ* hybridization (Lein et al., 2007) and **(B)** *in vitro* electrophysiology with single-cell reconstruction (Kozlov et al., unpublished data) mapped to the Allen Mouse Common Coordinate Framework. **(A1–A3,B1–B4)** show the stepwise procedures used to map overview images covering sagittal sections **(A1,B1)**, showing labeled cells of interest (encircled in **A2,B2**), to reference atlas space **(A3,B3)**. **(B4)** shows the 3-D reconstruction of the neuron shown in **(B2)**. **(C,D)** 3-D co-visualization of point coordinates extracted from the two data sets (**A**, purple dots; **B**, red, green, blue, and yellow dots) together with the surface of the caudoputamen, shown in view from anterolateral **(C)** and dorsal **(D)**. **(E)** Magnified view of data points representing the location of the 3-D cell reconstruction shown in example **(B)**. Scale bars: 1 mm **(A1)**, 200 μm **(A2)**.

receptors (Schubert et al., 2016) or enzyme based visualization of chemical properties (e.g., patches of cytochrome oxidase positive cell groups in the sensory whisker barrel cortex; Land and Simons, 1985). Additional approaches used to pinpoint anatomical location include, e.g., visualization of specific well-known cellular architectures or connectivity, electrophysiological measures of sensory receptive fields (Chapin and Lin, 1984) or motor-related activity (Neafsey et al., 1986), or any combination of the above. Use of such measurements can allow more fine-grained and precise anatomical descriptions of location.

Spatial Registration of Images to Reference Atlas

As shown in the examples provided in **Figures 3**, **4**, spatial registration of brain images to an anatomical atlas provides

specific evidence of location in a standard anatomical reference space. If images have been acquired with orientations matching the standard coronal, sagittal and horizontal planes used in reference atlases, such registration can simply be done by mapping 2-D diagrams from any standard reference atlases on section images. However, to correct for deviations in the angle of orientations commonly seen in histological sections, and to more directly relate positions in the experimental images to a spatial 3-D reference framework, we recommend mapping images to a 3-D atlas (Lein et al., 2007; Hawrylycz et al., 2011; Oh et al., 2014; Papp et al., 2014). Depending on the properties of the experimental material used, several software tools are available for such purposes (Majka and Wójcik, 2016; Puchades et al., 2017; **Figures 3**, **4**), allowing more accurate determination of the anatomical position and section angle in experimental material (**Figure 1B**).

Use of Serial Sections

Interpretation of anatomical location, particularly for the purpose of spatial registration, can be improved with use of serial section images that display multiple anatomical landmarks. Inclusion of more sections is particularly useful when determining deviations of section angles from the standard plane. The precision of such a registration can therefore be improved by including more section images than the ones used for analysis.

Regardless of the atlas used and the methods for relating data to it, the anatomical information as extracted from the atlas (region names, coordinates of points or sections) for the entire analyzed region(s) should be clearly communicated in publications and collections of metadata.

DISCUSSION

We have here reviewed anatomical location metadata provided in recent neuroscience publications, and found considerable differences across subfields of neuroscience. We have proposed a set of method-independent, easily adopted practices (minimum requirements) that can significantly improve reproducibility of neuroanatomical locations reported in publications. Furthermore, we have shown that re-usability and integration of data can be improved with additional steps using new software tools and workflows developed through the Human Brain Project, and that these procedures are applicable to data obtained by a range of methods.

Factors contributing to inconsistency and ambiguity in location metadata included (1) variable use of reference atlases, (2) lack of specification regarding nomenclatures, terms, and definitions used, (3) limited use of coordinate-based information, and (4) use of highly magnified image material without sufficient annotation as the only graphical display of data location. The amount of location metadata found in publications depended on the methodology with which the data had been obtained, likely pointing to different approaches and traditions having evolved as common practice within subfields of neuroscience.

The minimum requirements presented here are intended to be flexible and easily applicable to any neuroscientific method. They essentially state that descriptions of locations should be complete, and precisely define the relationship of sites of interest to anatomical landmarks, by use of semantics, coordinates or graphical representations, and preferably a combination of these. Appropriate reference to a specific nomenclature and citation of the reference atlases consulted is an obvious requirement, which is easy to implement regardless of the method used, but as our results show, often overlooked. We claim that adherence to the minimum recommendations requires little additional effort by researchers, and can substantially improve the precision of anatomical descriptions and data interpretation in neuroscience publications. Our examples specify how this can be implemented for different types of data.

However, comparison of descriptions based on text, reference atlases and image material remains dependent on substantial human interpretation. The second part of our work therefore demonstrate that data obtained by several methodologies, spanning spatial and temporal scales, may be thoroughly and accurately located in space using novel tools and workflows, and that the output of these procedures can be used to co-visualize data.

The workflows tested here for mapping data to atlas space can be implemented for any neuroscience method, provided that image material showing features of interest in relation to anatomical landmarks is available. For methods where such features are readily seen in histological section images, the procedures are quite easily applicable, as seen in our examples using immunohistochemical and *in situ* hybridization material, as well as *in vivo* electrophysiological recordings. In the case of electron microscopy data, the spatial correlation of features seen at the microscopic and ultrastructural levels is essential in order to map specific objects imaged at the electron microscopic level to a reference atlas. This was achieved here using low-power overview images acquired during tissue processing and images of semithin sections stained to show cytoarchitecture. Some steps could have been improved, e.g., by imaging the whole brain section before and after sectioning, and by keeping track of the location within the ultrathin section from which the electron microscopy images were obtained. An alternative approach would be to extract coordinates representing the perimeters of the data set, e.g., the corners of a block of tissue dissected from a vibratome section and prepared for electron microscopic imaging. Whether highly specific information about the position of individual cellular elements is desirable and attainable for a data set will depend on the research question and the methods of tissue preparation. Nevertheless, our example shows that even minor additions to common protocols (e.g., acquiring images of sections from which electron microscopic samples have been dissected) can give major improvements of precision of location metadata. For neuronal reconstruction data, we show that spatial coordinates recorded with a 3-D reconstruction software can be translated to atlas coordinates by using reference points visible in macroscopic section images. For mapping of more complex neuronal arbors in atlas space, annotation of at least four (and preferably more) reference points representing key landmarks in the neuronal reconstruction will increase precision. Again, access to low-power overview images documenting soma locatio

relative to visible landmarks was critical for translating the location of reconstructed neurons to atlas space.

We lastly summarized the workflows developed through these examples as a set of improved practices, aimed to facilitate efforts to compare and integrate neuroscience data. Mapping data to a common anatomical framework is an effective means to allow comparison and facilitate integration of disparate data types, a key goal within the Human Brain Project (Bjerke et al., 2018). Adherence to the improved practice recommendations proposed here ensures that heterogeneous data can be organized and shared in databases, with location metadata suitable for conducting queries based on location, either by using semantic strings and anatomical ontologies or by use of more fine-grained 3-D spatial queries for coordinate locations in atlas space.

Additional documentation and more extensive interpretation of anatomical locations, as exemplified above, requires additional efforts including production of additional material and documentation, as well as analytical efforts. Depending on the size of the data set, type and quality of images and the features to be extracted, the process of registering data, extracting and visualizing coordinates requires from a couple of days to a week. The workflows used to extract spatial coordinates for different data features in our examples, were based on manual annotations performed with the tool LocaliZoom. The advantage of this approach is that atlas coordinates are directly exported, but it can be tedious to apply to larger data sets. New tools and workflows are currently being developed in the Human Brain Project that will allow (semi-)automated extraction of labeled features from serial images (Kreshuk et al., 2014; Papp et al., 2016; Yates et al., 2017).

We argue that costs of such additional efforts are outweighed by improved precision of anatomical location metadata, and the added value gained by making data easier to compare across studies. Today, finding and comparing data in the literature based on a region of interest is a time-consuming task that often reveals inconsistencies in results. Indeed, flexible use of definitions has been related to poor reproducibility in science (Ioannidis, 2005). Concepts of brain regions are examples of such fluid definitions (Van De Werd and Uylings, 2014), and inaccurate reporting of location is likely to amplify the challenge caused by these changes. However, the coordinate systems that embed concepts of brain regions are static. Mapping current data to such coordinate frameworks will make data more robust in the face of evolving concepts of brain regions and is thus necessary to ensure long-term relevance of findings. Furthermore, following the improved practice recommendations outlined here can facilitate data integration and re-use of data, as the output of spatial registration procedures is structured metadata about anatomical locations that can accompany data to be shared. We therefore consider the benefits of performing these methods to outweigh the costs in the long term. New practices for data sharing in neuroscience (Ferguson et al., 2014; Leitner et al., 2016; Ascoli et al., 2017) will likely lead to augmented focus on high-quality metadata as a tool for increasing the value and impact of data, and thus also establish more prominent short-term incentives for mapping data to reference atlas space.

DATA AND SOFTWARE AVAILABILITY STATEMENT

The data sets generated for the literature survey of this study are available from the corresponding author upon request. The data sets used for testing procedures for spatial registration were obtained from public sources (Allen Institute for Brain Science repository, the Human Brain Project), or from generous colleagues as specified in the methods section. Requests to access these data sets can be directed to t.b.leergaard@medisin.uio.no. Software tools are available from the Human Brain Project (www.humanbrainproject.eu), requests for access to these tools can be directed to j.g.bjaalie@medisin.uio.no.

AUTHOR CONTRIBUTIONS

IB contributed to conceiving the study, performed analyses, contributed to development of workflows, and co-authored the manuscript. MØ and KA contributed to conceiving the study, performed analyses, and contributed to development of workflows. CB, HK, SY, and MP contributed to the analyses and development of workflows. JB supervised development of tools, infrastructure, and workflows and contributed to writing the paper. TL conceived and supervised the study, and co-authored the manuscript. All the authors reviewed and approved the manuscript.

FUNDING

This research has received funding from the European Union's Horizon 2020 Framework Programme for Research and Innovation under the Specific Grant Agreement No. 720270 (Human Brain Project SGA1) and Specific Grant Agreement No. 785907 (Human Brain Project SGA2). Funding was also received from The Research Council of Norway under Grant Agreement No. 269774 (INCF National Node).

ACKNOWLEDGMENTS

We thank Gergely Csucs, Dmitri Darine, Hong Qu, and Grazyna Babinska for expert technical assistance, and Hilde Flaatten and Leiv Sandvik for helpful bibliographical advice. Histological section images were acquired at the Norbrain Slidescanning Facility at the Institute of Basic Medical Sciences, University of Oslo.

SUPPLEMENTARY MATERIAL

The Supplementary Material for this article can be found online at: https://www.frontiersin.org/articles/10.3389/fnana.2018.00082/full#supplementary-material

REFERENCES

Akhter, F., Haque, T., Sato, F., Kato, T., Ohara, H., Fujio, T., et al. (2014). Projections from the dorsal peduncular cortex to the trigeminal subnucleus caudalis (medullary dorsal horn) and other lower brainstem areas in rats. *Neuroscience* 266, 23–37. doi: 10.1016/j.neuroscience.2014.01.046

Amari, S.-I., Beltrame, F., Bjaalie, J. G., Dalkara, T., De Schutter, E., Egan, G. F., et al. (2002). Neuroinformatics: the integration of shared databases and tools towards integrative neuroscience. *J. Integr. Neurosci.* 1, 117–128. doi: 10.1142/S0219635202000128

Amunts, K., Ebell, C., Muller, J., Telefont, M., Knoll, A., and Lippert, T. (2016). The human brain project: creating a European research infrastructure to decode the human brain. *Neuron* 92, 574–581. doi: 10.1016/J.NEURON.2016.10.046

Amunts, K., Hawrylycz, M. J. J., Van Essen, D. C. C., Van Horn, J. D. D., Harel, N., Poline, J.-B. B., et al. (2014). Interoperable atlases of the human brain. *Neuroimage* 99, 525–532. doi: 10.1016/j.neuroimage.2014.06.010

Ascoli, G. A., Maraver, P., Nanda, S., Polavaram, S., and Armananaz, R. (2017). Win-win data sharing in neuroscience. *Nat. Methods* 14, 112–116. doi: 10.1038/nmeth.4152

Berggaard, N., Bjerke, I. E., Paulsen, A. E. B., Hoang, L., Skogaker, N. E. T., Menno, P., et al. (2018). Development of Parvalbumin-expressing basket terminals in layer II of the rat medial entorhinal cortex. *eNeuro* 5:ENEURO.0438-17.2018 doi: 10.1523/ENEURO.0438-17.2018

Bjaalie, J. G. (2002). Opinion: localization in the brain: new solutions emerging. *Nat. Rev. Neurosci.* 3, 322–325. doi: 10.1038/nrn790

Bjaalie, J. G. (2008). Understanding the brain through neuroinformatics. *Front. Neurosci.* 2, 19–21. doi: 10.3389/neuro.01.022.2008

Bjaalie, J. G., Leergaard, T. B., Lillehaug, S., Odeh, F., Moene, I. A., Kjode, J. O., et al. (2005). Database and tools for analysis of topographic organization and map transformations in major projection systems of the brain. *Neuroscience* 136, 681–695. doi: 10.1016/j.neuroscience.2005.06.036

Bjerke, I. E., Øvsthus, M., Papp, E. A., Yates, S. C., Silvestri, L., Fiorilli, J., et al. (2018). Data integration through brain atlasing: human brain project tools and strategies. *Eur. Psychiatry* 50, 70–76. doi: 10.1016/j.eurpsy.2018.02.004

Boccara, C. N., Kjonigsen, L. J., Hammer, I. M., Bjaalie, J. G., Leergaard, T. B., and Witter, M. P. (2015). A three-plane architectonic atlas of the rat hippocampal region. *Hippocampus* 25, 838–857. doi: 10.1002/hipo.22407

Boline, J., Lee, E.-F., and Toga, A. W. (2008). Digital atlases as a framework for data sharing. *Front. Neurosci.* 2, 100–106. doi: 10.3389/neuro.01.012.2008

Boy, J., Leergaard, T. B., Schmidt, T., Odeh, F., Bichelmeier, U., Nuber, S., et al. (2006). Expression mapping of tetracycline-responsive prion protein promoter: digital atlasing for generating cell-specific disease models. *Neuroimage* 33, 449–462. doi: 10.1016/j.neuroimage.2006.05.055

Chapin, J. K., and Lin, C.-S. (1984). Mapping the body representation in the SI cortex of anesthetized and awake rats. *J. Comp. Neurol.* 229, 199–213. doi: 10.1002/cne.902290206

Dobi, A., Sartori, S. B., Busti, D., Van Der Putten, H., Singewald, N., Shigemoto, R., et al. (2013). Neural substrates for the distinct effects of presynaptic group III metabotropic glutamate receptors on extinction of contextual fear conditioning in mice. *Neuropharmacology* 66, 274–289. doi: 10.1016/j.neuropharm.2012.05.025

Ferguson, A. R., Nielson, J. L., Cragin, M. H., Bandrowski, A. E., and Martone, M. E. (2014). Big data from small data: data-sharing in the "long tail" of neuroscience. *Nat. Neurosci.* 17, 1442–1447. doi: 10.1038/nn.3838

Hawrylycz, M., Baldock, R. A., Burger, A., Hashikawa, T., Johnson, G. A., Martone, M., et al. (2011). Digital atlasing and standardization in the mouse brain. *PLoS Comput. Biol.* 7:e1001065. doi: 10.1371/journal.pcbi.1001065

Hey, T., and Trefethen, A. (2003). "The data deluge: an e-science perspective," in *Grid Computing - Making the Global Infrastructure a Reality*, eds F. Berman, G. Fox, and T. Hey (Hoboken, NJ: Wiley), 809–824.

Hintiryan, H., Gou, L., Zingg, B., Yamashita, S., Lyden, H. M., Song, M. Y., et al. (2012). Comprehensive connectivity of the mouse main olfactory bulb: analysis and online digital atlas. *Front. Neuroanat.* 6:30. doi: 10.3389/fnana.2012.00030

Hjornevik, T., Leergaard, T. B., Darine, D., Moldestad, O., Dale, A. M., Willoch, F., et al. (2007). Three-dimensional atlas system for mouse and rat brain imaging data. *Front. Neuroinform.* 1:4. doi: 10.3389/neuro.11.004.2007

Insausti, R., Herrero, M. T., and Witter, M. P. (1997). Entorhinal cortex of the rat: cytoarchitectonic subdivisions and the origin and distribution of cortical efferents. *Hippocampus* 7, 146–183. doi: 10.1002/(SICI)1098-1063(1997)7:2<146::AID-HIPO4>3.0.CO;2-L

Ioannidis, J. P. A. (2005). Why most published research findings are false. *PLoS Med.* 2:e124. doi: 10.1371/journal.pmed.0020124

Johnson, G. A., Badea, A., Brandenburg, J., Cofer, G., Fubara, B., Liu, S., et al. (2010). Waxholm space: an image-based reference for coordinating mouse brain research. *Neuroimage* 53, 365–372. doi: 10.1016/J.NEUROIMAGE.2010.06.067

Kjonigsen, L. J., Leergaard, T. B., Witter, M. P., and Bjaalie, J. G. (2011). Digital atlas of anatomical subdivisions and boundaries of the rat hippocampal region. *Front. Neuroinform.* 5:2. doi: 10.3389/fninf.2011.00002

Kjonigsen, L. J., Lillehaug, S., Bjaalie, J. G., Witter, M. P., and Leergaard, T. B. (2015). Waxholm Space atlas of the rat brain hippocampal region: three-dimensional delineations based on magnetic resonance and diffusion tensor imaging. *Neuroimage* 108, 441–449. doi: 10.1016/j.neuroimage.2014.12.080

Koslow, S. H., and Subramaniam, S. (eds). (2005). *Databasing the Brain: From Data to Knowledge*. New York, NY: John Wiley & Sons, Inc.

Kreshuk, A., Koethe, U., Pax, E., Bock, D. D., and Hamprecht, F. A. (2014). Automated detection of synapses in serial section transmission electron microscopy image stacks. *PLoS One* 9:e87351. doi: 10.1371/journal.pone.0087351

Land, P. W., and Simons, D. J. (1985). Cytochrome oxidase staining in the rat smI barrel cortex. *J. Comp. Neurol.* 238, 225–235. doi: 10.1002/cne.902380209

Lein, E. S., Hawrylycz, M. J., Ao, N., Ayres, M., Bensinger, A., Bernard, A., et al. (2007). Genome-wide atlas of gene expression in the adult mouse brain. *Nature* 445, 168–176. doi: 10.1038/nature05453

Leitner, F., Bielza, C., Hill, S. L., and Larrañaga, P. (2016). Data publications correlate with citation impact. *Front. Neurosci.* 10:419. doi: 10.3389/fnins.2016.00419

Majka, P., and Wójcik, D. K. (2016). Possum—a framework for three-dimensional reconstruction of brain images from serial sections. *Neuroinformatics* 14, 265–278. doi: 10.1007/s12021-015-9286-1

Neafsey, E. J., Bold, E. L., Haas, G., Hurley-Gius, K. M., Quirk, G., Sievert, C. F., et al. (1986). The organization of the rat motor cortex: a microstimulation mapping study. *Brain Res.* 396, 77–96. doi: 10.1016/0165-0173(86)90011-1

Oh, S. W., Harris, J. A., Ng, L., Winslow, B., Cain, N., Mihalas, S., et al. (2014). A mesoscale connectome of the mouse brain. *Nature* 508, 207–214. doi: 10.1038/nature13186

Papp, E. A., Leergaard, T. B., Calabrese, E., Johnson, G. A., and Bjaalie, J. G. (2014). Waxholm space atlas of the sprague dawley rat brain. *Neuroimage* 97, 374–386. doi: 10.1016/j.neuroimage.2014.04.001

Papp, E. A., Leergaard, T. B., Csucs, G., and Bjaalie, J. G. (2016). Brain-wide mapping of axonal connections: workflow for automated detection and spatial analysis of labeling in microscopic sections. *Front. Neuroinform.* 10:11. doi: 10.3389/fninf.2016.00011

Paxinos, G., and Franklin, K. (2012). *The Mouse Brain in Stereotaxic Coordinates*, 4th Edn, San Diego, CA: Academic Press.

Paxinos, G., and Watson, C. (2005). *The Rat Brain in Stereotaxic Coordinates*, 5th Edn, San Diego, CA: Elsevier.

Paxinos, G., and Watson, C. (2013). *The Rat Brain in Stereotaxic Coordinates*, 7th Edn, Burlington, NJ: Elsevier Inc.

Puchades, M. A., Csucs, G., Checinska, M., Øvsthus, M., Bjerke, I. E., Andersson, K., et al. (2017). *QuickNII: Neuroinformatics Tool and Workflow for Anchoring of Serial Histological Images in Rodent Brain 3D Space. Abstract no. 532.12 in Neuroscience Meeting Planner*. Washington, DC: Society for Neuroscience.

Ragan, T., Kadiri, L. R., Venkataraju, K. U., Bahlmann, K., Sutin, J., Taranda, J., et al. (2012). Serial two-photon tomography for automated ex vivo mouse brain imaging. *Nat. Methods* 9, 255–258. doi: 10.1038/nmeth.1854

Schubert, N., Axer, M., Schober, M., Huynh, A.-M., Huysegoms, M., Palomero-Gallagher, N., et al. (2016). 3D reconstructed Cyto-, Muscarinic M2 receptor, and fiber architecture of the rat brain registered to the waxholm space atlas. *Front. Neuroanat.* 10:51. doi: 10.3389/fnana.2016.00051

Sergejeva, M., Papp, E. A., Bakker, R., Gaudnek, M. A., Okamura-Oho, Y., Boline, J., et al. (2015). Anatomical landmarks for registration of experimental image data to volumetric rodent brain atlasing templates. *J. Neurosci. Methods* 240, 161–169. doi: 10.1016/j.jneumeth.2014.11.005

Stopps, M., Allen, N., Barrett, R., Choudhury, H. I., Jarolimek, W., Johnson, M., et al. (2004). Design and application of a novel brain slice system that permits independent electrophysiological recordings from multiple slices. *J. Neurosci. Methods* 132, 137–148. doi: 10.1016/j.jneumeth.2003.08.015

Swanson, L. (2004). *Brain Maps: Structure of the Rat Brain*, 3rd Edn, Amsterdam: Elsevier.

Tiesinga, P., Bakker, R., Hill, S., and Bjaalie, J. G. (2015). Feeding the human brain model. *Curr. Opin. Neurobiol.* 32, 107–114. doi: 10.1016/j.conb.2015.02.003

Van De Werd, H. J., and Uylings, H. B. (2014). Comparison of (stereotactic) parcellations in mouse prefrontal cortex. *Brain Struct. Funct.* 219, 433–459. doi: 10.1007/s00429-013-0630-7

Veraart, J., Leergaard, T. B., Antonsen, B. T., Van Hecke, W., Blockx, I., Jeurissen, B., et al. (2011). Population-averaged diffusion tensor imaging atlas of the Sprague Dawley rat brain. *Neuroimage* 58, 975–983. doi: 10.1016/j.neuroimage.2011.06.063

Wilkinson, M. D., Dumontier, M., Aalbersberg, I. J., Appleton, G., Axton, M., Baak, A., et al. (2016). The FAIR Guiding Principles for scientific data management and stewardship. *Sci. Data* 3, 1–9. doi: 10.1038/sdata.2016.18

Witter, M. (2012). "Hippocampus," in *The Mouse Nervous System*, ed. L. Puelles (Amsterdam: Elsevier), 112–139. doi: 10.1016/B978-0-12-369497-3.10005-6

Yates, S. C., Puchades, M. A., Coello, C., Kreshuk, A., Hartlage-Rübsamen, M., Rossner, S., et al. (2017). *Workflow for Automated Quantification and Spatial Analysis of Labeling in Microscopic Rodent Brain Sections. Abstract no. 44.15 in Neuroscience Meeting Planner*. Washington, DC: Society for Neuroscience.

Zakiewicz, I. M., van Dongen, Y. C., Leergaard, T. B., and Bjaalie, J. G. (2011). Workflow and atlas system for Brain-Wide mapping of axonal connectivity in rat. *PLoS One* 6:e22669. doi: 10.1371/journal.pone.0022669

Zaslavsky, I., Baldock, R. A., and Boline, J. (2014). Cyberinfrastructure for the digital brain: spatial standards for integrating rodent brain atlases. *Front. Neuroinform.* 8:74. doi: 10.3389/fninf.2014.00074

Conflict of Interest Statement: The authors declare that the research was conducted in the absence of any commercial or financial relationships that could be construed as a potential conflict of interest.

Copyright © 2018 Bjerke, Øvsthus, Andersson, Blixhavn, Kleven, Yates, Puchades, Bjaalie and Leergaard. This is an open-access article distributed under the terms of the Creative Commons Attribution License (CC BY). The use, distribution or reproduction in other forums is permitted, provided the original author(s) and the copyright owner(s) are credited and that the original publication in this journal is cited, in accordance with accepted academic practice. No use, distribution or reproduction is permitted which does not comply with these terms.

Advantages of publishing in Frontiers

OPEN ACCESS
Articles are free to read for greatest visibility and readership

FAST PUBLICATION
Around 90 days from submission to decision

HIGH QUALITY PEER-REVIEW
Rigorous, collaborative, and constructive peer-review

TRANSPARENT PEER-REVIEW
Editors and reviewers acknowledged by name on published articles

Frontiers
Avenue du Tribunal-Fédéral 34
1005 Lausanne | Switzerland

Visit us: www.frontiersin.org
Contact us: info@frontiersin.org | +41 21 510 17 00

REPRODUCIBILITY OF RESEARCH
Support open data and methods to enhance research reproducibility

DIGITAL PUBLISHING
Articles designed for optimal readership across devices

FOLLOW US
@frontiersin

IMPACT METRICS
Advanced article metrics track visibility across digital media

EXTENSIVE PROMOTION
Marketing and promotion of impactful research

LOOP RESEARCH NETWORK
Our network increases your article's readership